

SEISMIC MICROZONATION OF ERBAA (TOKAT-TURKEY) LOCATED  
ALONG EASTERN SEGMENT OF  
THE NORTH ANATOLIAN FAULT ZONE (NAFZ)

A THESIS SUBMITTED TO  
THE GRADUATE SCHOOL OF NATURAL AND APPLIED SCIENCES  
OF  
MIDDLE EAST TECHNICAL UNIVERSITY

BY

MÜGE AKIN

IN PARTIAL FULFILLMENT OF THE REQUIREMENTS  
FOR  
THE DEGREE OF DOCTOR OF PHILOSOPHY  
IN  
GEOLOGICAL ENGINEERING

DECEMBER 2009

Approval of the thesis:

**SEISMIC MICROZONATION OF ERBAA (TOKAT-TURKEY) LOCATED ALONG  
EASTERN SEGMENT OF  
THE NORTH ANATOLIAN FAULT ZONE (NAFZ)**

submitted by **MÜGE AKIN** in partial fulfillment of the requirements for the degree of **Doctor of Philosophy in Geological Engineering Department, Middle East Technical University** by,

Prof. Dr. Canan Özgen  
Dean, Graduate School of **Natural and Applied Sciences**

\_\_\_\_\_

Prof. Dr. Zeki Çamur  
Head of Department, **Geological Engineering**

\_\_\_\_\_

Prof. Dr. Tamer Topal  
Supervisor, **Geological Engineering Dept., METU**

\_\_\_\_\_

**Examining Committee Members:**

Prof. Dr. Vedat Doyuran  
Geological Engineering Dept., METU

\_\_\_\_\_

Prof. Dr. Tamer Topal  
Geological Engineering Dept., METU

\_\_\_\_\_

Prof. Dr. Steven L. Kramer  
Civil and Environmental Eng. Dept.,  
University of Washington

\_\_\_\_\_

Prof. Dr. Reşat Ulusay  
Geological Engineering Dept., Hacettepe University

\_\_\_\_\_

Prof. Dr. K. Önder Çetin  
Civil Engineering Dept., METU

\_\_\_\_\_

**Date:** December 14, 2009

**I hereby declare that all information in this document has been obtained and presented in accordance with academic rules and ethical conduct. I also declare that, as required by these rules and conduct, I have fully cited and referenced all material and results that are not original to this work.**

Name, Last name: Müge Akın

Signature :

## **ABSTRACT**

### **SEISMIC MICROZONATION OF ERBAA (TOKAT-TURKEY) LOCATED ALONG EASTERN SEGMENT OF THE NORTH ANATOLIAN FAULT ZONE (NAFZ)**

Akın, Müge

Ph.D., Department of Geological Engineering

Supervisor : Prof. Dr. Tamer Topal

December 2009, 416 pages

Turkey is one of the most earthquake prone countries in the world. The study area, Erbaa, is located in a seismically active fault zone known as North Anatolian Fault Zone (NAFZ). Erbaa is one of the towns of Tokat located in the Middle Black Sea Region. According to the Earthquake zoning map of Turkey, the study area is in the First Degree Earthquake Zone. The city center of Erbaa (Tokat) was previously settled on the left embankment of Kelkit River. After the disastrous 1942 Niksar-Erbaa earthquake ( $M_w = 7.2$ ), the settlement was moved southwards. From the period of 1900s, several earthquakes occurred in this region and around Erbaa. The 1942 earthquake is the most destructive earthquake in the center of Erbaa settlement.

In this study, the geological and geotechnical properties of the study area were investigated by detailed site investigations. The Erbaa settlement is located on alluvial and Pliocene deposits. The Pliocene clay, silt, sand, and gravel layers exist in the southern part of Erbaa. Alluvium in Erbaa region consists of gravelly, sandy, silty, and clayey layers. The alluvial deposits are composed of stratified materials of heterogeneous grain sizes, derived from various geological units in the vicinity.

The main objective of this study is to prepare a seismic microzonation map of the study area for urban planning purposes since it is getting more essential to plan new settlements considering



safe development strategies after the disastrous earthquakes. In this respect, seismic hazard analyses were performed to deterministically assess the seismic hazard of the study area. Afterwards, the essential ground motions were predicted regarding near fault effects as the study area is settled on an active fault zone. 1-D equivalent linear site response analyses were carried out to evaluate the site effects in the study area. Amplification values obtained from site response analyses reveal that the soil layers in the study area is quite rigid. Furthermore, liquefaction potential and post liquefaction effects including lateral spreading and vertical settlement were also delineated for the study area. The above-mentioned parameters were taken into account in order to prepare a final seismic microzonation map of the study area. The layers were evaluated on the basis of overlay methodologies including Multi-Criteria Decision Analysis (MCDA). Two different MCDA techniques, Simple Additive Weighting (SAW) and Analytical Hierarchical Process (AHP), were carried out in GIS environment. The seismic microzonation maps prepared by SAW and AHP methods are compared to obtain a final seismic microzonation map. Finally, the map derived from the AHP method is proposed to be the final seismic microzonation map of Erbaa.

As an overall conclusion, the northwestern part of the study area where the loose alluvial units exist is found to be vulnerable to earthquake-induced deformations. On the other hand, the Pliocene units in the southern and alluvial units in the northeastern part are quite resistant to earthquake effects. In addition, the proposed final seismic microzonation map should be considered by urban planners and policy makers during urban planning projects in Erbaa.

**Keywords:** Seismic Microzonation, Erbaa, North Anatolian Fault Zone, Site Response Analysis, Liquefaction, GIS, MCDA

## ÖZ

### KUZHEY ANADOLU FAY ZONU DOĞU SEGMENTİNDE YER ALAN ERBAA (TOKAT)' NİN SİSMİK MİKROBÖLGELEMESİ

Akın, Müge

Doktora, Jeoloji Mühendisliği Bölümü

Tez Yöneticisi : Prof. Dr. Tamer Topal

Aralık 2009, 416 sayfa

Türkiye, dünyadaki depreme duyarlı olan en önemli ülkelerden biridir. Çalışma alanı, Erbaa, Kuzey Anadolu Fay Zonu (KAFZ) olarak bilinen sismik olarak aktif bir fay zonu içinde yer almaktadır. Tokat şehrinin bir ilçesi olan Erbaa, Orta Karadeniz Bölgesi'nde yer alır. Çalışma alanı, Türkiye Deprem Bölgeleri Haritası'na göre 1. Derece Deprem Bölgesi içinde bulunmaktadır. Erbaa ilçe merkezi, daha önceden Kelkit Nehri'nin sol sahilinde kurulmuştur. Ancak bu merkez, 1942 Niksar-Erbaa ( $M_w = 7.2$ ) depreminden sonra daha güneye taşınmıştır. Bölgede 1900'lü yıllardan sonra birçok deprem meydana gelmiştir. 1942 depremi, Erbaa ilçe merkezine en hasar verici depremlerden biridir.

Bu çalışmada ayrıntılı saha incelemeleri yapılarak çalışma alanının jeolojik ve jeoteknik özellikleri ortaya konmuştur. Erbaa yerleşimi alüvyon ve Pliyosen yaşlı çökeller üzerine kurulmuştur. Erbaa'nın güneyinde Pliyosen yaşlı kil, silt, kum ve çakıl seviyelerine rastlanılmaktadır. Erbaa bölgesindeki alüvyon ise çakıllı, kumlu, siltli ve killi birimlerden oluşmaktadır. Alüvyon çökeller heterojen tane boyuna sahip olup, çevrede yer alan çeşitli jeolojik birimlerden gelen malzemeleri içermektedir.

Bu çalışmanın başlıca amacı, çalışma alanı için kentsel planlamaya yönelik bir sismik mikrobölgeleme haritasının hazırlanmasıdır. Çünkü yıkıcı depremlerden sonra yeni yerleşim

alanlarının daha güvenli şekilde planlamasına verilen önem giderek artmıştır. Bu doğrultuda, sismik tehlikenin belirlenmesi için deterministik sismik tehlike analizi gerçekleştirilmiştir. Daha sonra gerekli yer hareketi değerlendirmeleri, çalışma alanının aktif fay zone içinde yer alması sebebiyle yakın fay etkileri de göz önüne alınarak yapılmıştır. Tek boyutlu dinamik davranış analizleri ile zemin koşulları ortaya konmuştur. Dinamik zemin davranış analizleri ile belirlenen büyütme değerleri çalışma alanındaki zemin birimlerinin genelde katı özellikte olduğunu göstermektedir. Bununla birlikte, inceleme alanı için sıvılaşma potansiyeli ile oturma ve yanal yayılma gibi sıvılaşma sonrası etkiler de belirlenmiştir. Çalışma alanına ait nihai mikrobölgeleme haritasının hazırlanması için yukarıda belirtilen parametreler dikkate alınmıştır. Oluşturulan katmanlar Çok Ölçütlü Karar Analizi (ÇÖKA) kullanılarak değerlendirilmiştir. Basit Ağırlıklı Toplam (BAT) ve Analitik Aşamalı Sistem (AAS) olmak üzere iki farklı analiz, Coğrafi Bilgi Sistemi (CBS) tabanında uygulanmıştır. Oluşturulan BAT ve AAS 'ye dayalı haritalar, nihai sismik mikrobölgeleme haritasının belirlenmesi için karşılaştırılmıştır. Sonuç olarak, AAS yöntemine dayalı olarak hazırlanmış olan harita, Erbaa için nihai sismik mikrobölgeleme haritası olarak önerilmiştir.

Genel bir sonuç olarak, çalışma alanının kuzeybatısındaki, gevşek alüvyon birimlerinin de bulunduğu bölge, deprem kaynaklı deformasyonlara karşı hassasiyet göstermektedir. Öte yandan, güneydeki Pliyosen birimleri ile kuzeydoğudaki alüvyon birimleri deprem etkilerine karşı daha dayanımlıdır. Ek olarak, önerilen nihai sismik mikrobölgeleme haritası Erbaa'da şehir plancıları ve yerel yetkililerce yeni yerleşim planlamalarında dikkate alınmalıdır.

Anahtar Kelimeler: Sismik Mikrobölgeleme, Erbaa, Kuzey Anadolu Fay Zonu, Yanıt Spektrumu, Sıvılaşma, CBS, ÇÖKA

To My Family

## ACKNOWLEDGEMENTS

First of all, I would like to express my deepest appreciation to my honorific supervisor Prof. Dr. Tamer Topal, without whom I would not be able to complete my dissertation. His continuous and unconditional guidance and support encouraged me at every step of this study. His unlimited assistance, advice, criticism, patience, motivation, and tolerance throughout the research should never be forgotten.

I really owe further thanks to Prof. Dr. Steven L. Kramer for his positive approach and considerable support during my studies in the Department of Civil and Environmental Engineering at University of Washington as a visiting scholar. I will never forget his valuable guidance on Geotechnical Earthquake Engineering. He is like a co-supervisor not only during my studies at the University of Washington, but also during the preparation stage of my dissertation.

I also appreciate the advice of the committee members, Prof. Dr. Vedat Doyuran and Prof. Dr. Reşat Ulusay for their constructive suggestions and objective comments throughout this research period. I would like to also thank Prof. Dr. K. Önder Çetin for his encouraging comments during my academic life in METU. I would like to express my appreciation to Assoc. Prof. Dr. M. Lütfi Süzen for his support in the evaluation stage of GIS and MCDA methods as well.

I would like to also express my appreciation for honorary J. William Fulbright scholarship for supporting my studies in the University of Washington in Seattle as a visiting scholar.

I would like to gratefully acknowledge four different financial supports provided by Middle East Technical University Research Funding Projects (BAP-2007-03-09-03 and BAP-2009-03-09-01); State Planning Organization (DPT) (CUBAP M-359/DPT 2006K-120220), and The Scientific and Technological Research Council of Turkey (TUBITAK 107Y068).

I want to acknowledge the support and proofreading of my dear friend Dr. Samad Joshani-Shirvan. Special thanks go to Dr. Emine Sütçü and Yavuz Sütçü for their assistance on the use of GIS and geological interpretations.

The author would like to thank the chairman of Erbaa Municipality and the staff for their assistance during field studies and for providing essential maps.

I am grateful to Dr. Serhat Ataktürk and Nicholas Burmeister from the University of Washington and Ulaş Canatalı from Middle East Technical University for technical support as IT members. I am also grateful to my friends Zeynep Seviner, Reyhan Yıldız, Dr. Şebnem Arslan, Burcu Ertaş Deniz, Erkan Yılmaz, and my officemates in METU and in University of Washington, Ceren Küçükuysal and Tyler Stephens for their support and friendship. The friendship of Oğuz Tüfenkci and Dr. Aykan Mert is also gratefully acknowledged.

I owe thanks to Prof. Dr. Kudret Ekiz from GATA (Gülhane Military Medical Academy) and Prof. Dr. Nezih Erverdi from Medical Faculty of Ankara University for their medical diagnostics and treatments during my illnesses in this study period.

I am sincerely grateful to my family for their immeasurable support and love. They never left me alone. My mother Asuman Kıvanç and my father Ersin Kıvanç deserve many thanks for always being with me and for their efforts that encouraged me to realize my goals. I also want to thank my sisters Bilge Kıvanç and Özge Özkan. I would like to express my deepest thanks to my father in law Prof. Dr. Galip Akın for his academic supports, and my mother in law Gülderen Akın and my sister in law, Sinem Akın for being with me.

Last but not least, Dr. Mutluhan Akın, my beloved husband, who inspired and believed in me, deserves more thanks for his endless support, encouragement, friendship, assistance, and patience for not only during this limited time period but also throughout my entire life.

## TABLE OF CONTENTS

ABSTRACT.....	iv
ÖZ.....	vi
ACKNOWLEDGEMENTS.....	ix
TABLE OF CONTENTS.....	xi
LIST OF TABLES.....	xv
LIST OF FIGURES.....	xviii
CHAPTERS	
1 INTRODUCTION.....	1
1.1 Purpose and Scope.....	1
1.2 Historical Background.....	3
1.3 Geographical Setting and Accessibility.....	4
1.4 Climate.....	7
1.5 Methodology.....	9
1.5.1 Data production.....	9
1.5.2 Evaluation.....	10
2 BACKGROUND INFORMATION ON SEISMIC MICROZONATION.....	13
2.1 Definition of Seismic Microzonation.....	13
2.2 Previous Works on Seismic Microzonation.....	15
2.2.1 Single criteria-based seismic microzonation.....	16
2.2.1.1 Seismic hazard-based seismic microzonation.....	17
2.2.1.2 Liquefaction-based seismic microzonation.....	19
2.2.1.3 Site effects/response-based seismic microzonation.....	21
2.2.2 Multi criteria-based seismic microzonation.....	29
2.3 Microzonation Methodologies and Mapping Techniques.....	36
3 GEOLOGY, TECTONIC ACTIVITY, AND SEISMICITY OF ERBAA.....	42
3.1 Regional Geology and Previous Studies.....	42
3.2 Stratigraphy.....	43
3.2.1 Paleozoic units.....	44
3.2.1.1 Turhal group.....	44
3.2.2 Mesozoic units.....	44
3.2.2.1 Seyfe formation.....	44
3.2.2.2 Doğdu formation.....	44
3.2.2.3 Yumaklı formation.....	44
3.2.3 Tertiary units.....	45
3.2.3.1 Akveren formation.....	45
3.2.3.2 Kusuri formation.....	45
3.2.3.3 Tekkeköy formation.....	45
3.2.3.4 Çerkeş formation.....	45
3.2.4 Quaternary units.....	46

3.3	Tectonics.....	49
3.4	Seismic Activity of Erbaa and Close Vicinity.....	54
3.5	Geology of the Study Area.....	59
3.6	Concluding Remarks.....	70
4	FIELD AND LABORATORY STUDIES.....	71
4.1	Field and Laboratory Data.....	71
4.2	Previous Studies.....	71
4.2.1	DSI Groundwater Research Project.....	71
4.2.2	Ankara University Research Project.....	75
4.2.3	Geotechnical investigations for industrial area and water treatment plant.....	85
4.3	Recent Field Studies.....	86
4.4	Recent Laboratory Studies.....	98
4.5	Recent Geophysical Studies.....	106
4.5.1	Resistivity survey.....	106
4.5.2	Seismic refraction.....	115
4.5.3	SPT (Standard Penetration Test)-based uphole.....	122
4.5.4	Microtremor measurements.....	125
4.5.5	Downhole measurements.....	128
4.5.5.1	Refraction Microtremor survey at 3 downhole borehole locations.....	135
4.5.5.2	Microtremor survey at 3 downhole borehole locations... ..	140
4.5.5.3	Resistivity survey at 3 downhole borehole locations....	144
4.5.5.4	Seismic refraction survey at 3 downhole borehole locations.....	145
4.6	SCPTU Applications.....	146
4.7	Concluding Remarks.....	150
5	SEISMIC HAZARD ANALYSIS AND GROUND MOTION PREDICTION.....	151
5.1	Introduction.....	151
5.2	Seismic Hazard Analysis.....	152
5.2.1	Probabilistic seismic hazard analysis (PSHA).....	152
5.2.2	Deterministic seismic hazard analysis (DSHA).....	154
5.2.3	Seismic hazard analysis for Erbaa.....	156
5.3	Ground Motion Prediction.....	159
5.3.1	Ground motion models (attenuation relationships).....	161
5.3.1.1	Boore and Atkinson (2008) NGA relationship.....	164
5.3.1.2	Campbell and Bozorgnia (2008) NGA relationship.....	171
5.3.2	Ground motion models for Erbaa.....	176
5.3.3	Selection of real earthquake records for Erbaa.....	179
5.3.4	Spectral matching (scaling) of ground motions.....	184
5.3.5	Scaling and prediction of ground motion for Erbaa.....	187
5.4	Concluding Remarks.....	194
6	DYNAMIC SOIL PROPERTIES, SITE RESPONSE, AND AMPLIFICATION.....	195
6.1	Introduction.....	195
6.2	Dynamic Soil Properties.....	196
6.3	Estimation of $V_s$ for Erbaa.....	206
6.3.1	Measured shear wave velocity ( $V_s$ ).....	207



6.3.2	Empirical calculations of the shear wave velocity.....	209
6.3.3	Comparison of measured and empirical shear wave velocity.....	226
6.3.4	Site classification based on $V_s$ soil profiles and determination of $V_{s30}$ for Erbaa.....	235
6.4	Site Response Analyses.....	241
6.4.1	1-D equivalent linear site response analyses.....	243
6.4.1.1	Soil parameters used for site response analyses.....	244
6.4.1.2	Modeling of soil profiles for site response analyses.....	249
6.4.1.3	Ground motions used for site response analyses.....	250
6.4.1.4	Input and output formats in ProShake (v.1.12) software.....	250
6.5	Site Effects and Amplification.....	253
6.5.1	Amplification of soil deposits in Erbaa.....	257
6.5.2	Amplification factors determined from shear wave velocity.....	265
6.5.3	Amplification factors determined from Stewart et al. (2003) equation.....	267
6.5.4	Amplification values from microtremor measurements.....	279
6.5.5	Comparison of the estimated site effects for Erbaa based on amplification values.....	280
6.6	Concluding Remarks.....	284
7	LIQUEFACTION AND POST-LIQUEFACTION EFFECTS.....	285
7.1	Introduction.....	285
7.2	Liquefaction Definition.....	286
7.2.1	Flow liquefaction.....	287
7.2.2	Cyclic mobility.....	288
7.3	Liquefaction Susceptibility.....	290
7.3.1	Susceptibility criteria.....	291
7.3.2	Liquefaction potential.....	293
7.3.3	Liquefaction susceptibility of Erbaa.....	295
7.3.4	Liquefaction potential of Erbaa.....	299
7.4	Evaluation of Initiation of Liquefaction.....	302
7.4.1	Liquefaction initiation models of Erbaa.....	305
7.5	Post-liquefaction Effects.....	306
7.5.1	Lateral spreading displacements.....	307
7.5.1.1	Youd et al. (2002) lateral spreading model.....	308
7.5.1.2	Zhang et al. (2004) lateral spreading model.....	310
7.5.1.3	Kramer and Baska (2006) lateral spreading model.....	311
7.5.1.4	Idriss and Boulanger (2008) lateral spreading model....	312
7.5.2	Evaluation of lateral spreading displacements for Erbaa.....	313
7.5.3	Post liquefaction settlements.....	315
7.5.3.1	Tokimatsu and Seed (1984) post- liquefaction settlement model.....	316
7.5.3.2	Ishihara and Yoshimine (1992) post- liquefaction settlement model.....	317
7.5.3.3	Shamoto et al. (1998) post-liquefaction settlement model.....	318
7.5.3.4	Wu and Seed (2004) post-liquefaction settlement model.....	319
7.5.4	Evaluation of post liquefaction settlements for Erbaa.....	319

7.5.5	Ground deformation models.....	324
7.5.6	Evaluation of ground deformation model maps for Erbaa.....	326
7.6	Evaluation of Liquefaction and Post-Liquefaction Maps of Erbaa.....	327
7.7	Concluding Remarks.....	330
8	<b>MULTI-CRITERIA DECISION ANALYSES FOR SEISMIC MICROZONATION OF ERBAA.....</b>	331
8.1	Introduction.....	331
8.2	Seismic Microzonation Using GIS-Based MCDA.....	332
8.2.1	Simple Additive Weighting (SAW).....	334
8.2.2	Analytical Hierarchical Process (AHP).....	335
8.3	Data Production and Analyses for Seismic Microzonation.....	337
8.3.1	Input data.....	337
8.3.1.1	Elevation map.....	337
8.3.1.2	Slope map.....	339
8.3.1.3	Aspect map.....	341
8.3.1.4	Lithology map.....	343
8.3.1.5	Depth to groundwater table map.....	344
8.3.2	Evaluated input data.....	345
8.3.2.1	Distance to fault map.....	345
8.3.2.2	$V_{s30}$ -based site classification map.....	346
8.3.2.3	Amplification map.....	348
8.3.2.4	Liquefaction-induced ground deformation map.....	349
8.4	Multi-Criteria Decision Analyses.....	350
8.4.1	Classification of settlement zones.....	350
8.4.2	Multi-Criteria Decision Analyses using Simple Additive Weighting (SAW) method.....	352
8.4.3	Multi-Criteria Decision Analyses using Analytical Hierarchical Process (AHP) method.....	356
8.5	Comparison of Seismic Microzonation Maps.....	359
8.6	Concluding Remarks.....	361
9	<b>DISCUSSION.....</b>	362
9.1	Data Production.....	362
9.2	Data Evaluation.....	365
10	<b>CONCLUSIONS AND RECOMMENDATIONS.....</b>	367
10.1	Conclusions.....	367
10.2	Recommendations.....	369
	REFERENCES.....	370
	VITA.....	414

## LIST OF TABLES

### TABLES

Table 1.1. Variation of population in Erbaa through years (Erbaa Municipality, 2007)...	4
Table 2.1. Use of data for three levels of zonation (after ISSMGE-TC4, 1999).....	37
Table 3.1. Nine earthquakes occurred along the NAFZ from 1939 to 1999 (modified from Lorenzo-Martin, 2006).....	51
Table 3.2. Seismic activity of Erbaa and its vicinity.....	60
Table 4.1. General properties of 46 boreholes in Ankara University Scientific Research Project (Canik and Kayabali, 2000).....	75
Table 4.2. Summary of the laboratory test results of Ankara University Scientific Research Project (Canik and Kayabali, 2000).....	78
Table 4.3. General results of the resistivity measurements in Ankara University Scientific Research Project (Canik and Kayabali, 2000).....	80
Table 4.4. General results of the seismic refraction measurements in Ankara University Scientific Research Project (Canik and Kayabali, 2000).....	84
Table 4.5. General properties of boreholes in the industrial area and water treatment plant projects.....	85
Table 4.6. Summary of the laboratory test results of the industrial area and water treatment plant projects.....	86
Table 4.7. General properties of recent boreholes drilled in this study.....	87
Table 4.8. Statistical distribution of water content for alluvium and Pliocene soils.....	99
Table 4.9. Statistical distribution of grain size for alluvium and Pliocene soils.....	99
Table 4.10. Statistical distribution of Atterberg limits for alluvium and Pliocene soils...	102
Table 4.11. Statistical distribution of natural unit weight, dry unit weight, specific gravity, void ratio, porosity, and saturation ratio for alluvium soils.....	104
Table 4.12. Statistical distribution of undrained cohesion and internal friction angle, swelling ratio, and swelling pressure for alluvial soils.....	105
Table 4.13. Statistical distribution of natural unit weight, dry unit weight, specific gravity, effective cohesion and internal friction angle for Pliocene soils.....	105
Table 4.14. Total number of geophysical applications.....	106
Table 4.15. Summary of the resistivity survey results.....	109
Table 4.16. Results of seismic refraction surveys.....	117
Table 4.17. Seismic downhole survey results.....	129
Table 4.18. Dynamic properties of soils obtained from seismic downhole survey.....	129
Table 4.19. Summary of REMI results for 3 downhole borehole locations.....	136

Table 4.20. Seismic refraction measurements near 3 downhole boreholes.....	146
Table 4.21. General properties of SCPTU locations in the study area.....	148
Table 5.1. Historical earthquakes around Erbaa.....	157
Table 5.2. Summary of ground motion parameters and related characteristic (after Kramer, 1996).....	161
Table 5.3. Summary of attenuation relationships in literature (modified from Douglas, 2001).....	162
Table 5.4. Parameters used in the NGA models.....	163
Table 5.5. Style of faulting class for the NGA models (after Abrahamson and Silva, 2008).....	164
Table 5.6. Aleatory uncertainties for different periods for Boore and Atkinson GMPE...	166
Table 5.7. Distance-scaling coefficients ( $M_{ref}=4.5$ and $R_{ref}=1.0$ km for all periods, except $R_{ref}=5.0$ km for pga4nl).....	167
Table 5.8. Magnitude-scaling coefficients.....	168
Table 5.9. Period-independent site-amplification coefficients.....	170
Table 5.10. Period-dependent site-amplification coefficients.....	170
Table 5.11. Coefficients for Campbell and Bozorgnia (2008) NGA model ( $c_1$ - $c_{12}$ ).....	174
Table 5.12. Coefficients for Campbell and Bozorgnia (2008) NGA model ( $k_1$ - $p$ ).....	175
Table 5.13. Parameters employed in NGA relationships.....	177
Table 5.14. Calculated rock PGA values from NGA relationships for different distance zones in the study area.....	177
Table 5.15. Selection criterion of ground motions from Baker (2007) database.....	181
Table 5.16. Selected earthquake ground motion records from Baker (2007) database....	182
Table 5.17. Selected earthquake records with minimum scaling factors from Baker (2007) database.....	188
Table 5.18. Distance dependent PGA values for different earthquake ground motions...	194
Table 6.1. Different techniques for the determination of dynamic soil properties (after Brandes, 2003).....	197
Table 6.2. Overconsolidation ratio exponent ( $k$ ) (after Hardin and Drnevich, 1972).....	198
Table 6.3. $G_{max}/s_u$ value based on OCR and plasticity index (after Weiler, 1988).....	199
Table 6.4. Effect of various factors on $G/G_{max}$ and $D$ of normally consolidated and moderately overconsolidated clays (Dobry and Vucetic, 1987).....	201
Table 6.5. Depth ranges for dynamic curves and the representative depth (EPRI, 1993).....	203
Table 6.6. Coefficients for Darendeli (2001) model.....	205
Table 6.7. Summary of empirical correlations based on SPT-N vs. $V_s$ .....	211
Table 6.8. Site categories in NEHRP and CGS Provisions for the design of new structures....(modified from Bozorgnia and Campbell, 2004).....	236
Table 6.9. Summary of regression coefficients for Equation 6.28.....	237
Table 6.10. Power-law relationships for SPT-based uphole boreholes.....	239
Table 6.11. Calculated $V_{s30}$ values for each borehole in the study area.....	240
Table 6.12. Softwares used for site response analyses (after Arduino and Kramer, 2009).....	243

Table 6.13. Results of site response analysis for BH-4.....	259
Table 6.14. Correlations of relative amplification factors with average shear wave velocity (after TCEGE, 1999).....	265
Table 6.15. Amplification factors based on Midorikawa (1987) shear wave velocity relation.....	266
Table 6.16. Criteria used for surface geology classification (Stewart et al., 2003).....	268
Table 6.17. Geotechnical site categories proposed by Rodriguez-Marek et al. (2001).....	268
Table 6.18. Site categories in NEHRP Provisions (Martin, 1994).....	269
Table 6.19. Surface geology categories (modified from Stewart et al., 2003).....	271
Table 6.20. NEHRP and Geotechnical Categories (after Stewart et al., 2003).....	272
Table 6.21. Comparison of amplification and predominant periods based on different methods.....	281
Table 7.1. Probability of liquefaction-induced ground failure (after Li et al., 2006).....	294
Table 7.2. Liquefaction index categories proposed by Iwasaki et al. (1982).....	299
Table 7.3. Liquefaction index categories proposed by Sonmez (2003).....	299
Table 7.4. Liquefaction index categories proposed by Sonmez and Gokceoglu (2005).....	299
Table 7.5. Coefficients for Youd et al. (2002) lateral spreading model.....	309
Table 7.6. Coefficients for Kramer and Baska (2006) lateral spreading model.....	311
Table 7.7. Variation of earthquake magnitude and volumetric strain ratio for dry sands (after Tokimatsu and Seed, 1987).....	323
Table 7.8. Weights assigned to the classes of each layer during the preparation of liquefaction-induced deformation map.....	327
Table 8.1. Scale for pairwise comparison (after Saaty, 1980).....	336
Table 8.2. RI values with respect to the number of layers (n) (after Saaty, 1980).....	337
Table 8.3. Classification of slope angle.....	340
Table 8.4. Classification of aspect layer.....	341
Table 8.5. Classification of lithological units.....	343
Table 8.6. Classification of depth to groundwater level.....	344
Table 8.7. Classification of distance to fault map.....	346
Table 8.8. Classification of $V_{s30}$ -based site classification map.....	347
Table 8.9. Classification of amplification factor based map.....	348
Table 8.10. Classification of liquefaction-induced ground deformation.....	349
Table 8.11. Assigned rank and weight values for the layers/classes in SAW method.....	352
Table 8.12. Normalized rank and weight values for the layers/classes in SAW method.....	354
Table 8.13. Comparison matrix developed for AHP-based seismic microzonation map.....	356
Table 8.14. Assigned weight and rank values to the layers/classes in AHP method.....	357
Table 8.15. Pairwise comparison matrix for liquefaction-induced ground deformation map.....	357
Table 8.16. Consistency ratios (CR) for each layer.....	358

## LIST OF FIGURES

### FIGURES

Figure 1.1. Location map of the study area.....	5
Figure 1.2. Panoramic view of Erbaa.....	6
Figure 1.3. Temperature variations in Erbaa (1976-2006) (Turkish State Meteorological Service, 2006).....	7
Figure 1.4. Precipitation variations in Erbaa (1976-2006) (Turkish State Meteorological Service, 2006).....	8
Figure 1.5. Relative humidity variations in Erbaa (1976-2006) (Turkish State Meteorological Service, 2006).....	8
Figure 1.6. Flow chart of the methodology.....	12
Figure 2.1. Preparation steps of microzonation maps (after Anbazhagan and Sitharam, 2008).....	16
Figure 3.1. Regional geology of the study area (modified from Aktimur et al., 1989).....	47
Figure 3.2. Stratigraphic columnar section of the study area and its vicinity (modified from Aktimur et al., 1989).....	48
Figure 3.3. Simplified tectonic map of Turkey showing major neotectonic structures and regimes (from Şengör et al., 1985; Barka, 1992; Bozkurt, 2001b).....	50
Figure 3.4. North Anatolian Fault Zone and some important surface ruptures occurred during different earthquakes (from USGS, 2007).....	50
Figure 3.5. North Anatolian Fault Zone and its earthquake history (a,b,c) (from Stein et al., 1997).....	51
Figure 3.6. (A) Map of Turkey showing location of the North Anatolian (NAFZ) and the East Anatolian (EAFZ) Fault Zones..... from Barka et al., 2000).....	52
Figure 3.7. Simplified map showing major structural elements of east Central Anatolia (modified from Koçyiğit and Erol, 2001; .....; Bozkurt, 2001b)...	53
Figure 3.8. Seismicity of the eastern Mediterranean region for the period of 1964-2001 with magnitudes, $M > 4.0$ (modified from Taymaz et al., 2001)...	54
Figure 3.9. GPS horizontal velocities and their 95% confidence ellipses in a Eurasia-fixed reference ..... (modified from Taymaz et al., 2001).....	55
Figure 3.10. Seismic gaps for the North Anatolian Fault Zone (modified from Demirtaş and Yılmaz, 1996).....	56
Figure 3.11. Rupture zones for large historical earthquakes (modified from	

Stein et al., 1997).....	56
Figure 3.12. Stress distributions based on important earthquakes on the NAFZ (Stein et al., 1997).....	57
Figure 3.13. Allocation of seismic zones for the city of Tokat and its towns (after General Directorate of Disaster Affairs, 2008).....	58
Figure 3.14. Earthquake zoning map of Turkey (from Çağatay, 2005).....	59
Figure 3.15. Geological map of Erbaa (modified from Aktimur et al., 1989).....	61
Figure 3.16. Sectional sketch of the NAFZ with the Esiñçay Fault segment (from Stein et al, 1997).....	62
Figure 3.17. Geological map of Erbaa (modified from Canik and Kayabalı, 2000).....	64
Figure 3.18. A general view of Pliocene units.....	64
Figure 3.19. A close-up view of Pliocene units.....	65
Figure 3.20. A general view of Imbat River bed.....	65
Figure 3.21. Revised geological map of the study area.....	66
Figure 3.22. A sectional view of alluvial units in the study area.....	67
Figure 3.23. Alternation of different grain sizes in the alluvial units.....	68
Figure 3.24. A close-up view of gravelly layers.....	68
Figure 3.25. Gravel lenses in the alluvial sequence.....	69
Figure 3.26. Sandy layers very close to the Kelkit River.....	69
Figure 3.27. Shallow groundwater level very close to the Kelkit River.....	69
Figure 4.1. Location of DSI groundwater boreholes in the study area (modified from DSI, 1971).....	73
Figure 4.2. A general cross section of Erbaa (B-B') (modified from Barka et al., 2000)...	74
Figure 4.3. General distribution of previous projects' boreholes.....	76
Figure 4.4. Distribution of geophysical survey points in Ankara University Scientific Research Project (modified from Canik and Kayabalı, 2000).....	79
Figure 4.5. A-A' resistivity cross-section of Ankara University Scientific Research Project (modified from Canik and Kayabalı, 2000).....	81
Figure 4.6. B-B' resistivity cross-section of Ankara University Scientific Research Project (modified from Canik and Kayabalı, 2000).....	82
Figure 4.7. C-C' resistivity cross-section of Ankara University Scientific Research Project (modified from Canik and Kayabalı, 2000).....	83
Figure 4.8. General distribution of recent and previous borehole locations considered in this study.....	88
Figure 4.9. Depth to groundwater level map.....	89
Figure 4.10. A general view of drilling application in the study area.....	90
Figure 4.11. General views from SPT application (a) and SPT disturbed sample (b).....	90
Figure 4.12. Variation of SPT-N <sub>30</sub> blow counts in alluvium and Pliocene layers based on the data from six boreholes.....	91
Figure 4.13. Alignment of cross section lines (I-I', II-II', III-III', IV-IV', V-V').....	92

Figure 4.14. Cross section I-I'.....	93
Figure 4.15. Cross section II-II'.....	94
Figure 4.16. Cross section III-III'.....	95
Figure 4.17. Cross section IV-IV'.....	96
Figure 4.18. Cross section V-V'.....	97
Figure 4.19. A close-up view of UD and SPT samples.....	98
Figure 4.20. Examples of sieve and hydrometer analyses graphics for alluvium soil samples from BH-4, BH-20, and BH-39.....	100
Figure 4.21. Examples of sieve and hydrometer analyses graphics for Pliocene soil samples from BH-12, BH-24, and BH-33.....	101
Figure 4.22. Plasticity chart for alluvial soils.....	103
Figure 4.23. Plasticity chart for Pliocene soils.....	103
Figure 4.24. Distribution of geophysical survey points.....	107
Figure 4.25. Schlumberger electrode configuration.....	108
Figure 4.26. Application of resistivity measurement in the study area.....	109
Figure 4.27. A-A' resistivity cross section.....	111
Figure 4.28. B-B' resistivity cross section.....	112
Figure 4.29. C-C' resistivity cross section.....	113
Figure 4.30. D-D' resistivity cross section.....	114
Figure 4.31. Seismic refraction test (modified from ASTM D 5777-00, 2006).....	115
Figure 4.32. Application of seismic refraction survey at the field.....	116
Figure 4.33. A-A' seismic refraction cross section.....	118
Figure 4.34. B-B' seismic refraction cross section.....	119
Figure 4.35. C-C' seismic refraction cross section.....	120
Figure 4.36. D-D' seismic refraction cross section.....	121
Figure 4.37. A schematic diagram of SPT-based uphole method (after Bang and Kim, 2007).....	123
Figure 4.38. Installation of geophones before SPT-based uphole application.....	123
Figure 4.39. Installation of trigger cable below the hammer anvil.....	124
Figure 4.40. A sample SPT-based uphole record including 7 different geophones.....	124
Figure 4.41. Predominant period values at microtremor measurement locations (after Dikmen et al., 2009).....	126
Figure 4.42. Amplification ratios at microtremor measurement locations (after Dikmen et al., 2009).....	126
Figure 4.43. Location of REMI-MASW and microtremor measurement points.....	127
Figure 4.44. $V_s$ values obtained from REMI-MASW measurements.....	128
Figure 4.45. A schematic diagram of seismic downhole test.....	128
Figure 4.46. Seismic downhole measurement at the field, a) geophone, b) lowering of geophone into borehole.....	129
Figure 4.47. Depth versus travel time graphics for (a) DBH-1 (b) DBH-2 (c) DBH-3 downhole boreholes.....	130
Figure 4.48. Variation of P and S wave velocity in (a) DBH-1 (b) DBH-2	



(c) DBH-3 downhole boreholes.....	131
Figure 4.49. Variation of Young's modulus (in kPa) in (a) DBH-1 (b) DBH-2 (c) DBH-3 downhole boreholes.....	132
Figure 4.50. Variation of Poisson's ratio in (a) DBH-1 (b) DBH-2 (c) DBH-3 downhole boreholes.....	133
Figure 4.51. Variation of Shear modulus (in kPa) in (a) DBH-1 (b) DBH-2 (c) DBH-3 downhole boreholes.....	134
Figure 4.52. Variation of Bulk modulus (in kPa) in (a) DBH-1 (b) DBH-2 (c) DBH-3 downhole boreholes.....	135
Figure 4.53. Variation of shear wave velocity based on REMI measurement for DBH-1 downhole borehole location.....	137
Figure 4.54. Variation of shear wave velocity based on REMI measurement for DBH-2 downhole borehole location.....	138
Figure 4.55. Variation of shear wave velocity based on REMI measurement for DBH-3 downhole borehole location.....	139
Figure 4.56. Microtremor measurement results for DBH-1 location.....	141
Figure 4.57. Microtremor measurement results for DBH-2 location.....	142
Figure 4.58. Microtremor measurement results for DBH-3 location.....	143
Figure 4.59. Resistivity survey result for DBH-1 location.....	144
Figure 4.60. Resistivity survey result for DBH-2 location.....	144
Figure 4.61. Resistivity survey result for DBH-3 location.....	145
Figure 4.62. A schematic view of SCPTU system.....	146
Figure 4.63. An example record of SCPTU (CPT-16).....	147
Figure 4.64. Distribution of the SCPTU locations in the study area.....	149
Figure 4.65. An example of seismic record for a certain depth (CPT-30, 9 meter depth).....	149
Figure 4.66. An example of evaluated seismic record, depth versus shear wave velocity ( $V_s$ ) (CPT-30).....	150
Figure 5.1. Comparison of deterministic and probabilistic approaches for different projects (after McGuire, 1995).....	155
Figure 5.2. Parallel zonation with respect to fault surface rupture in the study area.....	158
Figure 5.3. Boore and Atkinson (2008) target spectrum model for different distances....	178
Figure 5.4. Campbell and Bozorgnia (2008) target spectrum model for different distances.....	178
Figure 5.5. Comparison of BA08 and CB08 models for 0 km distance.....	179
Figure 5.6. Ground motion scaling in time domain (Nikolau, 1998).....	186
Figure 5.7. Example of scaling of 42 motions with a target spectrum.....	189
Figure 5.8. Time history of ground motion 9.....	190
Figure 5.9. Time history of ground motion 10.....	190
Figure 5.10. Time history of ground motion 16.....	191
Figure 5.11. Time history of ground motion 19.....	191
Figure 5.12. Time history of ground motion 34.....	192

Figure 5.13. Time history of ground motion 40.....	192
Figure 5.14. Time history of ground motion 42.....	193
Figure 5.15. Scaled ground motions with target spectrum (for BA-08 with 0 km zone) and the average ground motion.....	193
Figure 6.1. Modulus reduction and damping curves based on the hyperbolic relation of Hardin and Drnevich (1972).....	201
Figure 6.2. Modulus reduction and damping curves based on the experimental study of Idriss (1990).....	202
Figure 6.3. Empirical curves for modulus reduction and damping (Vucetic and Dobry, 1991).....	202
Figure 6.4. Empirical modulus reduction (a) and damping curves (b) for different soil types (EPRI, 1993).....	203
Figure 6.5. Empirical modulus reduction (a) and damping curves (b) for different confining pressures (EPRI, 1993).....	204
Figure 6.6. Modulus reduction and damping curves based on Darendeli model (2001).....	206
Figure 6.7. Comparison of shear wave velocity determined from CPT, SCPTU, seismic refraction, and SPT-based uphole for BH-10 location.....	207
Figure 6.8. Shear wave velocity distribution for all geophones (BH-4).....	209
Figure 6.9. Shear wave velocity profiles obtained from SPT-based uphole tests; a: alluvial soils, b: Pliocene soils.....	210
Figure 6.10. SPT-N and $V_s$ correlations for all soils in BH-4 with respect to different researchers.....	212
Figure 6.11. SPT-N and $V_s$ empirical relations for all alluvial soils in Erbaa.....	213
Figure 6.12. SPT-N and $V_s$ empirical relations for alluvial sand in Erbaa.....	214
Figure 6.13. SPT-N and $V_s$ empirical relations for alluvial clay in Erbaa.....	214
Figure 6.14. SPT-N and $V_s$ empirical relations for all Pliocene soils in Erbaa.....	215
Figure 6.15. SPT-N and $V_s$ empirical relations for Pliocene sand in Erbaa.....	215
Figure 6.16. SPT-N and $V_s$ empirical relations for Pliocene clay in Erbaa.....	216
Figure 6.17. Proposed relationship for all alluvial soils in Erbaa.....	217
Figure 6.18. Comparison of measured and predicted shear wave velocity for all alluvial soils.....	217
Figure 6.19. Proposed relationship for alluvial sand in Erbaa.....	218
Figure 6.20. Comparison of measured and predicted shear wave velocity for alluvial sand.....	218
Figure 6.21. Proposed relationship for alluvial clay in Erbaa.....	219
Figure 6.22. Comparison of measured and predicted shear wave velocity for alluvial clay.....	219
Figure 6.23. Proposed relationship for all Pliocene soils in Erbaa.....	220
Figure 6.24. Comparison of measured and predicted shear wave velocity for all Pliocene soils.....	220
Figure 6.25. Proposed relationship for Pliocene sand in Erbaa.....	221

Figure 6.26. Comparison of measured and predicted shear wave velocity for Pliocene sand.....	221
Figure 6.27. Proposed relationship for Pliocene clay in Erbaa.....	222
Figure 6.28. Comparison of measured and predicted shear wave velocity for Pliocene clay.....	222
Figure 6.29. Effect of soil type on SPT- $N_{30}$ - $V_s$ relationships for alluvial soils in Erbaa.....	223
Figure 6.30. Effect of soil type on SPT- $N_{30}$ - $V_s$ relationships for Pliocene soils in Erbaa.....	223
Figure 6.31. Distribution of $V_s$ determined by Ohta and Goto (1976) relationship.....	225
Figure 6.32. Comparison between measured and empirical $V_s$ for BH-4.....	227
Figure 6.33. Linear relationship between measured and empirically calculated $V_s$ for alluvial sand (A-2).....	227
Figure 6.34. Linear relationship between measured and empirically calculated $V_s$ for Pliocene sand (P-2).....	228
Figure 6.35. Variation of new $\alpha$ coefficient with depth for alluvial sands.....	229
Figure 6.36. Variation of new $\alpha$ coefficient with depth for Pliocene sands.....	229
Figure 6.37. Variation of vertical effective stress using constant and variable $\alpha$ coefficients for alluvial sands.....	230
Figure 6.38. Variation of vertical effective stress using constant and variable $\alpha$ coefficients for Pliocene sands.....	231
Figure 6.39. Comparison between measured and empirically calculated $V_s$ with new $\alpha$ coefficient for BH-4.....	232
Figure 6.40. Linear relationship between measured and empirically calculated $V_s$ with new $\alpha$ coefficient for alluvial sand (A-2).....	233
Figure 6.41. Linear relationship between measured and empirically calculated $V_s$ with new $\alpha$ coefficient for Pliocene sand (P-2).....	233
Figure 6.42. Comparison of SPT $N_{30}$ and $N_{1,60}$ based empirical formulas with measured $V_s$ values.....	234
Figure 6.43. Relationship between shear wave velocity and depth for BH-4.....	238
Figure 6.44. $V_{s30}$ map of the study area.....	241
Figure 6.45. Effects of ground motion in soil layers.....	242
Figure 6.46. Modified modulus reduction curves for alluvium clay (A-1).....	245
Figure 6.47. Modified damping curves for alluvium clay (A-1).....	245
Figure 6.48. Modified modulus reduction curves for alluvium sand (A-2).....	246
Figure 6.49. Modified damping curves for alluvium sand (A-2).....	246
Figure 6.50. Modified modulus reduction curves for Pliocene clay (P-1).....	247
Figure 6.51. Modified damping curves for Pliocene clay (P-1).....	247
Figure 6.52. Modified modulus reduction curves for Pliocene sand (P-2).....	248
Figure 6.53. Modified damping curves for Pliocene sand (P-2).....	248
Figure 6.54. Grid system used for site response analysis in this study.....	249
Figure 6.55. Input summary table in ProSHAKE (v.1.12) software.....	251

Figure 6.56. A soil profile in ProSHAKE (v.1.12) software.....	251
Figure 6.57. Assigning input motions for each profile in ProSHAKE (v.1.12) software.....	252
Figure 6.58. Output of ProShake (v.1.12) software representing the variations in motions.....	252
Figure 6.59. An amplification during 1989 Loma Prieta earthquake (after Kramer 2009a).....	253
Figure 6.60. An illustration of wave propagation from rupture zone to surface.....	254
Figure 6.61. General description of the Standard Spectral Ratio Technique (SSR) (after Pitilakis, 2004).....	255
Figure 6.62. Description of the Horizontal to Vertical Spectral Ratio Technique (HVSr) (after Pitilakis, 2004).....	256
Figure 6.63. Input response spectra of BH-4 based on Boore and Atkinson (2008) model for 0 km distance zone.....	258
Figure 6.64. Surface response spectra of BH-4 based on Boore and Atkinson (2008) model for 0 km distance zone.....	258
Figure 6.65. Amplification ratio of BH-4 based on Boore and Atkinson (2008) model for 0 km distance zone.....	259
Figure 6.66. Variation of PGA values along depth for alluvium units in BH-9.....	260
Figure 6.67. Variation of PGA values along depth for Pliocene units in BH-14.....	261
Figure 6.68. Peak ground acceleration (PGA) (surface) map of the study area based on Boore and Atkinson (2008) model.....	262
Figure 6.69. Peak ground acceleration (PGA) (surface) map of the study area based on Campbell and Bozorgnia (2008) model.....	262
Figure 6.70. Amplification map of the study area based on Boore and Atkinson (2008) model (for 0.001 sec).....	263
Figure 6.71. Amplification map of the study area based on Campbell and Bozorgnia (2008) model (for 0.001 sec).....	263
Figure 6.72. Predominant period map of the study area (for BA08 model).....	264
Figure 6.73. Predominant period map of the study area (for BA08 model).....	264
Figure 6.74. Comparison of amplification factors according to different relationships (after TCEGE, 1999).....	266
Figure 6.75. Amplification factor map of the study area based on Midorikawa (1987) shear wave velocity relationship.....	267
Figure 6.76. Amplification factor based on surface geology for Pliocene soils with BA08 model.....	273
Figure 6.77. Amplification factor based on surface geology for alluvial soils with BA08 model.....	273
Figure 6.78. Amplification factor based on geotechnical classification for Pliocene soils with BA08 model.....	274
Figure 6.79. Amplification factor based on geotechnical classification for alluvial soils with BA08 model.....	274

Figure 6.80. Amplification factor based on surface geology for Pliocene soils with CB08 model.....	275
Figure 6.81. Amplification factor based on surface geology for alluvial soils with CB08 model.....	275
Figure 6.82. Amplification factor based on geotechnical classification for Pliocene soils with CB08 model.....	276
Figure 6.83. Amplification factor based on geotechnical classification for alluvial soils with CB08 model.....	276
Figure 6.84. Amplification factor map based on geological classification with BA08 model.....	277
Figure 6.85. Amplification factor map based on geological classification with CB08 model.....	277
Figure 6.86. Amplification factor map based on geotechnical classification with BA08 model.....	278
Figure 6.87. Amplification factor map based on geotechnical classification with CB08 model.....	278
Figure 6.88. Amplification map of the study area based on microtremor results.....	279
Figure 6.89. Predominant period map of the study area based on microtremor results....	280
Figure 6.90. Comparison of amplification factors for alluvial soils.....	282
Figure 6.91. Comparison of amplification factors for Pliocene soils.....	283
Figure 7.1. Flow chart for evaluation of liquefaction (after Robertson, 1994).....	287
Figure 7.2. Flow liquefaction mechanism.....	288
Figure 7.3. Mechanism of cyclic mobility.....	289
Figure 7.4. Mechanism of cyclic liquefaction.....	289
Figure 7.5. Combination of two phenomena in cyclic softening (modified from Rauch, 1997).....	290
Figure 7.6. Atterberg limits chart showing representative values for soils exhibiting clay-like, sand-like, and intermediate stress-strain behaviors (after Boulanger and Idriss, 2005).....	291
Figure 7.7. Ranges of $w_p/LL$ and plasticity index for various susceptibility categories according to Bray and Sancio (2006).....	292
Figure 7.8. Introduction page of WSliq liquefaction evaluation software.....	296
Figure 7.9. Data entry into the input files of WSliq software for BH-7.....	296
Figure 7.10. Liquefaction susceptibility evaluation in WSliq software for BH-7.....	298
Figure 7.11. Liquefaction susceptibility map of Erbaa.....	298
Figure 7.12. Liquefaction potential map of the study area based on Iwasaki et al. (1982) LPI method.....	300
Figure 7.13. Liquefaction potential map of the study area based on Sonmez (2003) LPI method.....	301
Figure 7.14. Liquefaction potential map of the study area based on Sonmez and Gokceoglu (2005) LSI method.....	301
Figure 7.15. (a) Recommended probabilistic standard penetration	

test-based liquefaction triggering correlation (b) recommended “deterministic” standard penetration test-based liquefaction triggering correlation (after Cetin et al., 2004).....	305
Figure 7.16. Liquefaction initiation models of Erbaa based on NCEER (Youd et al., 2001), Boulanger and Idriss (2006), and Cetin et al. (2004) models.....	306
Figure 7.17. Schematic examples of (a) liquefaction-induced lateral translation and (b) liquefaction-induced vertical displacements (after Seed et al., 2001).....	307
Figure 7.18. Notations for slope geometry (after Youd et al., 2002).....	308
Figure 7.19. Recommended values for the Youd et al. (2002) predictive equation.....	309
Figure 7.20. Relationship between $\gamma_{\max}$ and FS for different $D_r$ for clean sands (after Zhang et al., 2004).....	310
Figure 7.21. Limiting strain curves (after Kramer, 2008).....	313
Figure 7.22. Lateral spreading map of the study area based on Youd et al. (2002) method (lateral spreading in meters).....	314
Figure 7.23. Lateral spreading map of the study area based on Kramer and Baska (2006) method (lateral spreading in meters).....	314
Figure 7.24. Lateral spreading map of the study area based on Idriss and Boulanger (2008) method (lateral spreading in meters).....	315
Figure 7.25. Variation of volumetric strain with corrected SPT resistance and cyclic stress ratio (after Tokimatsu and Seed, 1987).....	316
Figure 7.26. Variation of volumetric strain with relative density, SPT or CPT resistance, and factor of safety against liquefaction (after Ishihara and Yoshimine, 1992).....	317
Figure 7.27. Variation of maximum residual volumetric strain with corrected SPT resistance and cyclic stress ratio for sands with different percent fines content (0, 10, 20 %) (after Shamoto et al., 1998).....	318
Figure 7.28. Variation of volumetric strain with corrected SPT-N and CSR (after Wu and Seed, 2004).....	319
Figure 7.29. Post-liquefaction vertical settlement map of the study area based on Tokimatsu and Seed (1984) method (settlement in meters).....	320
Figure 7.30. Post-liquefaction vertical settlement map of the study area based on Ishihara and Yoshimine, (1992) method (settlement in meters).....	321
Figure 7.31. Post-liquefaction vertical settlement map of the study area based on Shamoto et al. (1998) method (settlement in meters).....	321
Figure 7.32. Post-liquefaction vertical settlement map of the study area based on Wu and Seed (2004) method (settlement in meters).....	322
Figure 7.33. Relationship between volumetric shear strain and cyclic shear strain in terms of (a) relative density and (b) standard penetration resistance (after Tokimatsu and Seed, 1987).....	323

Figure 7.34. (a) the evaluation guide of the thickness of liquefiable layer and overlying liquefiable layer, and (b) the boundary curves for liquefaction induced damage (after Ishihara, 1985).....	325
Figure 7.35. The chart proposed for discriminating between occurrence and non-occurrence of surface effects of liquefaction (after Sonmez et al., 2008).....	325
Figure 7.36. Liquefaction-induced ground surface disruption zoning map based on Sonmez et al. (2008) model.....	326
Figure 7.37. Different weight combinations for the production of liquefaction-induced ground deformation map.....	328
Figure 7.38. Final liquefaction-induced ground deformation map of Erbaa.....	329
Figure 8.1. Classification of GIS-MCDA (after Malczewski, 2006).....	333
Figure 8.2. Contour map of the study area.....	338
Figure 8.3. Digital Elevation Model (DEM) of the study area.....	339
Figure 8.4. Distribution of slope angle in the study area.....	340
Figure 8.5. Slope map of the study area.....	341
Figure 8.6. Distribution of aspect values in the study area.....	342
Figure 8.7. Aspect map of the study area.....	342
Figure 8.8. Lithology map of the study area.....	343
Figure 8.9. Depth to groundwater table map of the study area.....	344
Figure 8.10. Distance to fault map of the study area.....	346
Figure 8.11. $V_{s30}$ -based site classification map of the study area.....	347
Figure 8.12. Amplification factor based map of the study area.....	348
Figure 8.13. Liquefaction-induced ground deformation map of the study area.....	350
Figure 8.14. Histogram showing the boundaries of three zones of seismic microzonation map based on SAW method.....	355
Figure 8.15. Seismic microzonation map of the study area based on SAW method.....	355
Figure 8.16. Histogram showing the boundaries of three zones of seismic microzonation map based on AHP method.....	358
Figure 8.17. Seismic microzonation map of the study area based on AHP method.....	359
Figure 8.18. Comparison map of SAW and AHP-based seismic microzonation maps....	360

## CHAPTER 1

### INTRODUCTION

#### 1.1 Purpose and Scope

Urban areas with an increasing population require new and appropriate residential places. Moreover, the urban planning is a crucial topic to deal with the expansion of the urban areas and the application of the zonation for the landuse management. As historically observed in the earlier concepts of urban planning, controlling the development of this hierarchy mostly depends on the population including different criteria such as visual satisfaction and agriculture. However, having understood the important role of natural hazards in the selection of residential areas, new planning techniques are implemented with safety concerns.

Selection of settlement areas for urban planning purposes is a significant issue for the authorities. The alluvial basins are the most preferred places regarding easy transportation and economical activities. Nonetheless, from the natural hazard point of view, these areas are generally the most vulnerable places for earthquake-related hazards, especially in Turkey which is an earthquake-prone country. Thousands of fatalities were recorded after 1999 Adapazarı ( $M_w=7.4$ ) and Düzce ( $M_w=7.1$ ) earthquakes. Adapazarı basin, where the downtown is located on, is a sedimentary alluvial basin like Düzce basin. Therefore, it became more essential to improve construction quality and to plan new settlements depending on the newer and safer development strategies. That is why seismic microzonation should be considered to improve existing settlement areas and to distinguish safer sites for the future residential in urban planning.

Preparation of the seismic microzonation maps is the main aspect for the evaluation of natural hazard related effects. Seismic microzonation requires multi-disciplinary contributions and combinations of the effects of earthquake generated ground motions on man-made structures (De Mulder, 1996; Ansal et al., 2004a). Furthermore, it can be



considered as the process of response of soils under earthquake ground motion characteristics using geological, geotechnical and geophysical explorations. Additionally, geological and geotechnical data are crucial factors to identify, control, and prevent geological natural hazards (Bell et al., 1987; Legget, 1987; Hake, 1987; Rau, 1994; Dai et al., 1994, 2001; GDDA, 1996; 2000; Van Rooy and Stiff, 2001; Ansal et al., 2001a; 2004a; Topal et al., 2003). By means of seismic microzonation maps generated from different layers should be evaluated the slope, aspect and digital elevation models of the study area to point out the topographic conditions for processing the geographical spatial data (Dai et al., 2001). The key issue affecting the applicability and thus feasibility of any microzonation study is the suitability and reliability of the parameters selected for zonation (Ansal et al., 2004a). Accordingly, seismic microzonation studies should be performed in different areas to prove how applicable these procedures in the development stage of landuse and urban plans are.

Turkey is one of the most earthquake-prone countries in the world with major seismic and active fault zones. These faults represent orogenic belts as well as tectonic movements along these zones. One of the major seismic sources for this tectonic activity is the North Anatolian Fault Zone (NAFZ) which has a dextral strike-slip movement with an approximately 1600 km long surface rupture (Allen, 1969; Ketin, 1969; Ambraseys, 1970; Şengör, 1979; Şengör et al., 1985; Barka, 1992; Armijo, et al., 1999; Bozkurt, 2001a). The seismic origin of the 1999 Adapazarı and Düzce earthquakes is related to the western segment of this fault zone with high magnitudes ( $M_w = 7.4$  and  $7.1$ ). Besides, the eastern segment has also the similar capability of these types of active tectonic movements since similar and higher magnitude earthquakes occurred in 1940s.

Erbaa (Tokat), located on the eastern part of the North Anatolian Fault segment, has a critical place from the construction and development aspects. This town has fertile lands for agriculture with its warm climate conditions. There were high magnitude (7.2 and 7.3) earthquakes occurred in 1942 and 1943 in Erbaa and its close vicinity which led to move the settlement to the south of old Erbaa (Figure 1.1). The authorities initiated possible locations for new settlements due to the rapid increase in population of Erbaa. Although some of the residential areas were moved to southern part of alluvium-Pliocene contact after the disastrous earthquakes, there is still huge quantity of residential places settled on alluvial deposits at the time of this study. Moreover, there is an increasing trend and pressure to expand the settlement areas towards Kelkit River where alluvium exists.

In this study, it is aimed to prepare a seismic microzonation map considering different conditions containing a variety of geological, geotechnical and geophysical data since such a type of seismic microzonation study for Erbaa will also be the first seismic microzonation research. Therefore, field and laboratory surveys are utilized to collect data from the site and they are analyzed to obtain geological-geotechnical and geophysical data.

The thesis organization is briefly summarized in this section. All the studies based on microzonation are summarized with a review of the previous works on Seismic microzonation in Chapter 2. The methodologies for seismic microzonation and applications are explained in the following chapters as well. The geology of the area including field observation with the revised geological map of the area is given in Chapter 3. The data including geotechnical and geophysical studies are pointed out in Chapter 4. Possible ground motions obtained from the seismic hazard analyses and previous earthquake records are discussed in Chapter 5. Chapters 6 and 7 include the possible earthquake-related hazards such as site response and liquefaction for the settlement areas. The entire layers prepared for GIS-based overlay analyses are given in Chapter 8. They include different approaches for multi-criteria decision analyses. Two decision analyses techniques named as Simple Additive Weighting (SAW) and Analytical Hierarchy Process (AHP) are employed and the result maps are prepared to represent the finalized seismic microzonation map. The comparison of these maps and final suggestions are summarized in Chapter 8 as well. Discussions and conclusions including the future recommendations of all chapters are given in Chapters 9 and 10, respectively.

## **1.2 Historical Background**

Several archeological studies confirm that Erbaa settlement dates back to B.C. 2000 – 600 with a prehistoric data. Additionally, the Hittites and Phrygians were settled along the Kelkit Valley at the ancient times. In 1892, during the Ottoman Empire period, Erbaa head official was jointed to Tokat.

Erbaa was also famous with the use of minerals in the history of civilizations (Özgüç, 1964; Kaptan, 1990). Since one of the oldest underground minings from 5000 years ago was discovered in Erbaa, an urban archaeological site called “Horoztepe” was also explored in the southeastern part of Erbaa (Figure 1.1). This historical area reveals high quality examples

of copper, lead, gold, silver, bronze (coppertin), and electrum (gold-silver) pieces (Kaptan, 1990).

### 1.3 Geographical Setting and Accessibility

The study area (Erbaa) is located in the Middle Black Sea Region. Erbaa is one of the biggest towns of Tokat. The coordinates of the area are 40° 40' 0" N -Latitude, 36° 34' 0" - Longitude with an average altitude of 248 m. The district is in the zone of 37 North and Universal Transverse Mercator projection (UTM) coordinates are 4504602N, 294316E. In addition, it is in the quadrangle of G37d1 in 1/25000 scale topographical map. Erbaa basin covers approximately 1111 km<sup>2</sup> land including Kelkit River plains. The study area is approximately 25 km<sup>2</sup> with a dimension of 6.5 km long and 4.1 km wide. There are several towns around Erbaa; in the western part Taşova (Amasya); in the eastern part Niksar (Tokat) and in the southern part Turhal (Tokat) as seen in Figures 1.1 and 1.2. The city center of Erbaa is located on the left embankment of the Kelkit River. After the disastrous 1942 earthquake (M=7.2) and 1943 earthquake (M=7.3), the settlement was shifted southwards. New and old settlements are shown in Figure 1.1. Moreover, many residential buildings started to be located near the Kelkit River embankment towards old town area.

The variation of Erbaa population is summarized in Table 1.1 (Erbaa, 2007 and Erbaa Municipality, 2007). As seen from Table 1.1, the population increases rapidly in Erbaa downtown. Therefore, the necessity of new residential places becomes more significant concerning migration to the town as well as rapid increase in the population.

Table 1.1. Variation of population in Erbaa through years (Erbaa Municipality, 2007)

Year	Town population	Village population	Total
1980	28 840	66 020	91 263
1990	33 554	66 042	99 596
1997	43 132	56 633	99 765
2008	57 210	38 849	96 059

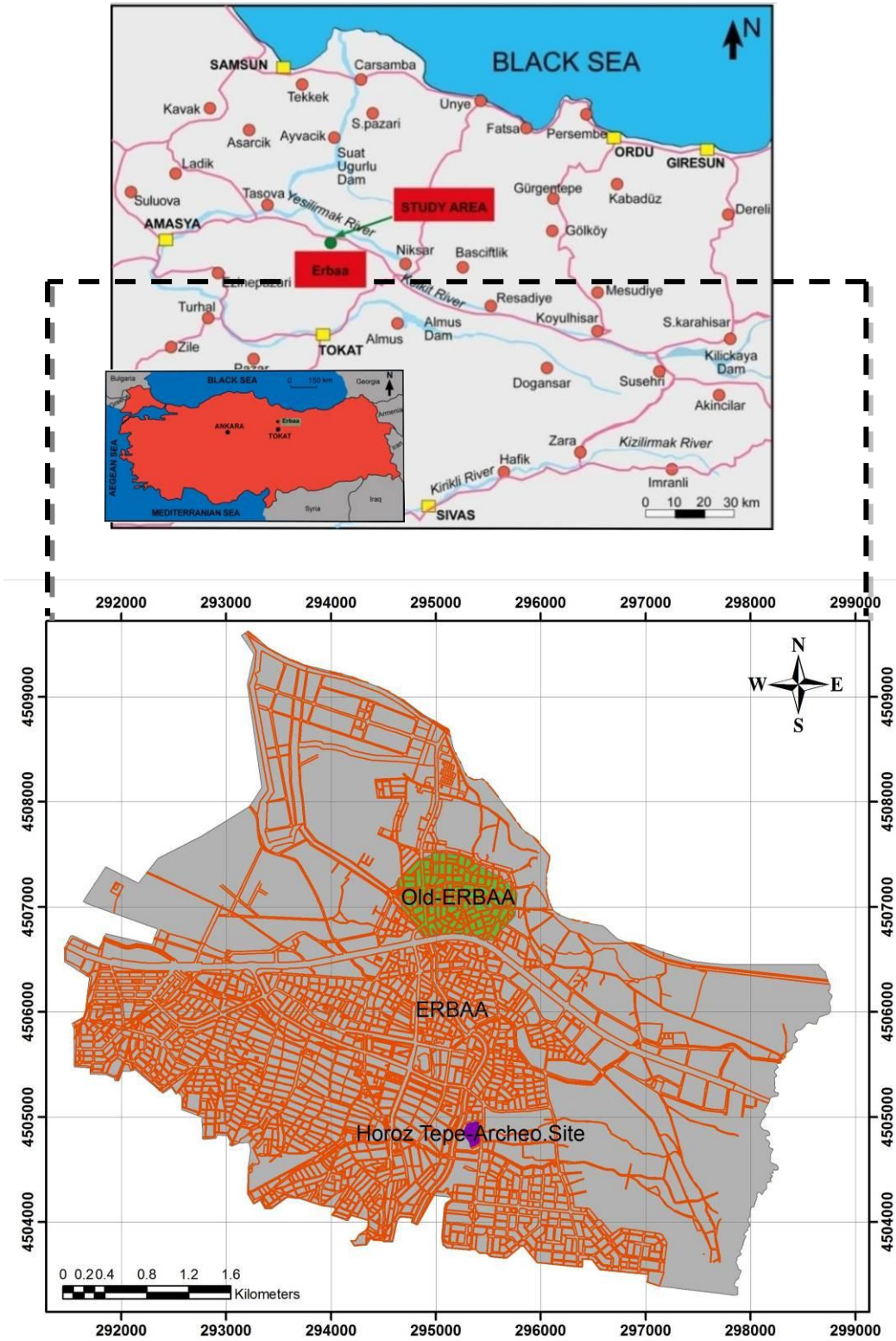


Figure 1.1. Location map of the study area



Figure 1.2. Panoramic view of Erbaa

## 1.4 Climate

The Erbaa meteorological station is located on 40° 67'N and 36° 57'E with an altitude of 920 m. It is the only meteorological station in the close vicinity. The climatic conditions around Erbaa resemble a transition between The Black Sea and continental climates. Generally, the summers are hot and dry, the winters are rainy and warm based on the meteorological data. The meteorological data of Erbaa with minimum, maximum and average temperature values are given in Figure 1.3. The average lowest and highest temperatures at the station are 4°C and 23°C in January and July, respectively. The minimum precipitation is measured in August as 9 mm and the maximum precipitation in May as 68 mm. The monthly temperatures, precipitation, and relative humidity between 1976 and 2006 at Erbaa meteorological station are shown in Figures 1.3 and 1.4, respectively.

Precipitation occurs almost in every month and especially spring and winter seasons are rainy. Total precipitation value reaches up to 70 mm per month in spring. The variation of precipitation can be seen in Figure 1.4. Due to the amount of the precipitation, relative humidity in Erbaa and its vicinity is high as seen in Figure 1.5.

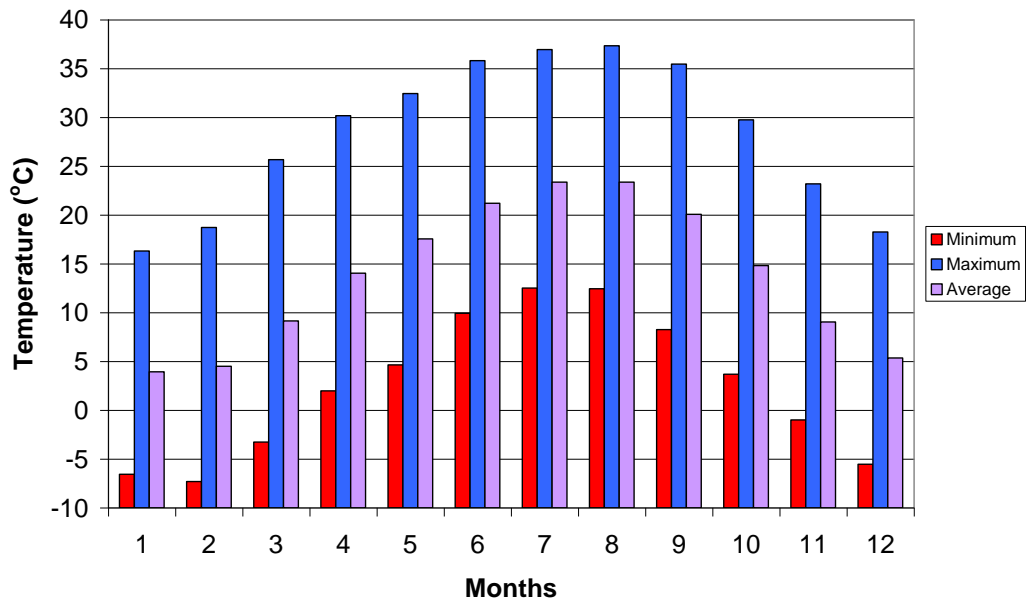


Figure 1.3. Temperature variations in Erbaa (1976-2006) (Turkish State Meteorological Service, 2006)

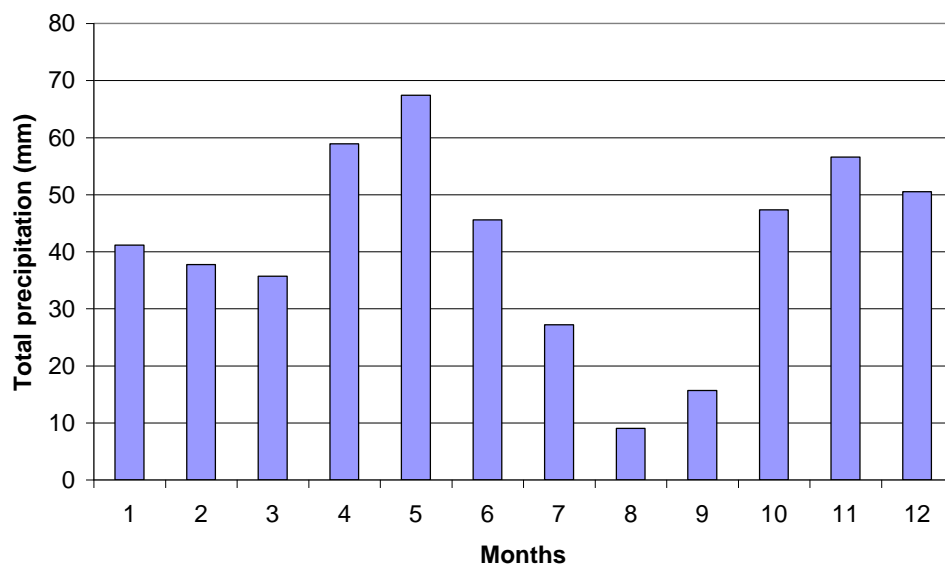


Figure 1.4. Precipitation variations in Erbaa (1976-2006) (Turkish State Meteorological Service, 2006)

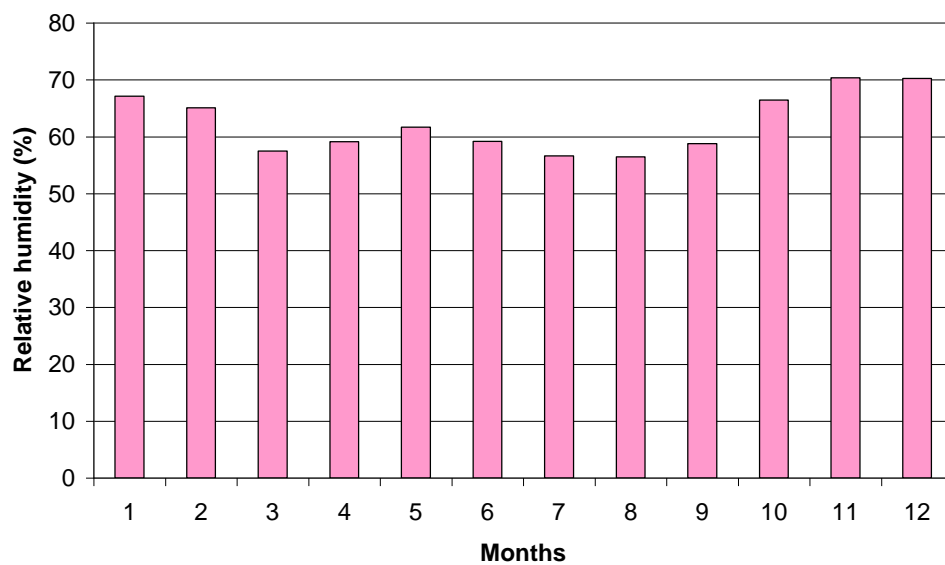


Figure 1.5. Relative humidity variations in Erbaa (1976-2006) (Turkish State Meteorological Service, 2006)



## **1.5 Methodology**

The methodology used in this dissertation can be divided into two steps. The first parts include data production with different methods of analyses and the second parts cover all evaluation and comparison sections as seen in Figure 1.6. The details of procedures are summarized in the following chapters.

### **1.5.1 Data production**

The data production is the main section for seismic microzonation of Erbaa. In addition, a review of literature for each chapter and related background information are explained at the beginning of every section. More details of these approaches are given in the related chapters.

As a preliminary intention for the geological data production, geological mapping of the study area (Erbaa-Tokat) including faults and seismic activity is considered. The historical earthquake data are also summarized in this section.

The geotechnical data production is mainly conducted through of the implementation of boreholes and the collection of samples is carried out using two different sampling techniques. During drilling, Standard Penetration Tests (SPT) and Undisturbed (UD) sampling are utilized at 1 m interval. These samples are used for soil classification purposes with respect to sieve and hydrometer analyses, Atterberg limits, and definition of strength parameters. Besides, various seismic cone penetration tests with pore pressure measurements (SCPTU) are recorded in the study area. Considering the geophysical data production, seismic refraction and resistivity surveys are performed in different locations separately. Furthermore, several microtremor and refraction microtremor (REMI) measurements are obtained in the study area. As a new method for Turkey, SPT-based uphole tests are utilized in the study area as well. Based on these data, engineering soil classifications and cross sections of the geological units are assembled.

Afterwards, the new and existing data, as well as the maps for detailed site characterization are combined including geophysical analyses based on bedrock elevation and depth-to bedrock maps. Depending on the groundwater level (GWL) measurements, a GWL map is prepared. During the clustering of these soil properties, it is aimed to determine dynamic soil



characteristics of this area to define sub-soil layers. Firstly, shear wave velocity ( $V_s$ ) values are calculated with different formulas on the basis of SPT-N versus  $V_s$  relationships. In this section, field and laboratory database are also considered for specific formulas. These calculations are correlated with the field measurements of the shear wave velocity by means of geophysical data. Secondly, the soil layers are differentiated and classified according to the shear wave velocity for site characterization. Finally, these results are shown in the related maps and these evaluations are used for the other steps.

Before dealing with the site response analyses, it is aimed to identify ground motion parameters for this specific area. For this reason, some of the proper attenuation relationships newly adapted in NGA (Next Generation Attenuation) project are considered as an empirical approach and ground motion parameters. Before this assumption, deterministic seismic hazard analyses are performed for the study area. Afterwards, recorded earthquake ground motions from essential ground motion databases are investigated. The proper motions are selected and scale with target spectra obtained from NGA ground models. As a result, the ground motions used in site response analyses are clarified.

Site response analyses and amplification factors including different parameters are evaluated for the geological, geotechnical and shear wave velocity aspects. On the basis of these parameters, essential maps and response spectra are combined for equivalent linear analyses using ProSHAKE software. During the calculation stage in the program, the ground motion and the other previous data are considered to explain the site response of the study area.

As the last step for data production part, one of the possible earthquake-related hazards, liquefaction, is investigated for the study area including susceptibility, initiation and post-liquefaction models. Throughout this evaluation process, software called WSLiq is used and different approaches are considered for this step to produce a final liquefaction map of the area.

### **1.5.2 Evaluation**

The evaluation part covers different methodologies for seismic microzonation. In this section, the produced data are combined and evaluated for different overlay analyses.

The layers applied to different weight and ranking criteria are firstly grouped into several maps. This group of maps is evaluated for the degree of importance which gives an idea for decision making. Then, these maps and the database of this system are prepared in ARC-GIS (version 9.2) (ESRI, 2006) program which is a Geographical Information System (GIS) based-software.

The methodology of Multi-Criteria Decision Analysis (MCDA) is assigned to each layer by means of using different approaches. Two of decision analyses namely Simple Additive Weighting (SAW) and Analytical Hierarchy Process (AHP) as the most preferable MCDA methods in the literature especially for land-use planning are applied to obtain the final maps from these produced layers.

In the last part, two seismic microzonation maps based on different MCDA techniques are produced. These maps are compared with each another and then, the final seismic microzonation map of the study area is proposed.

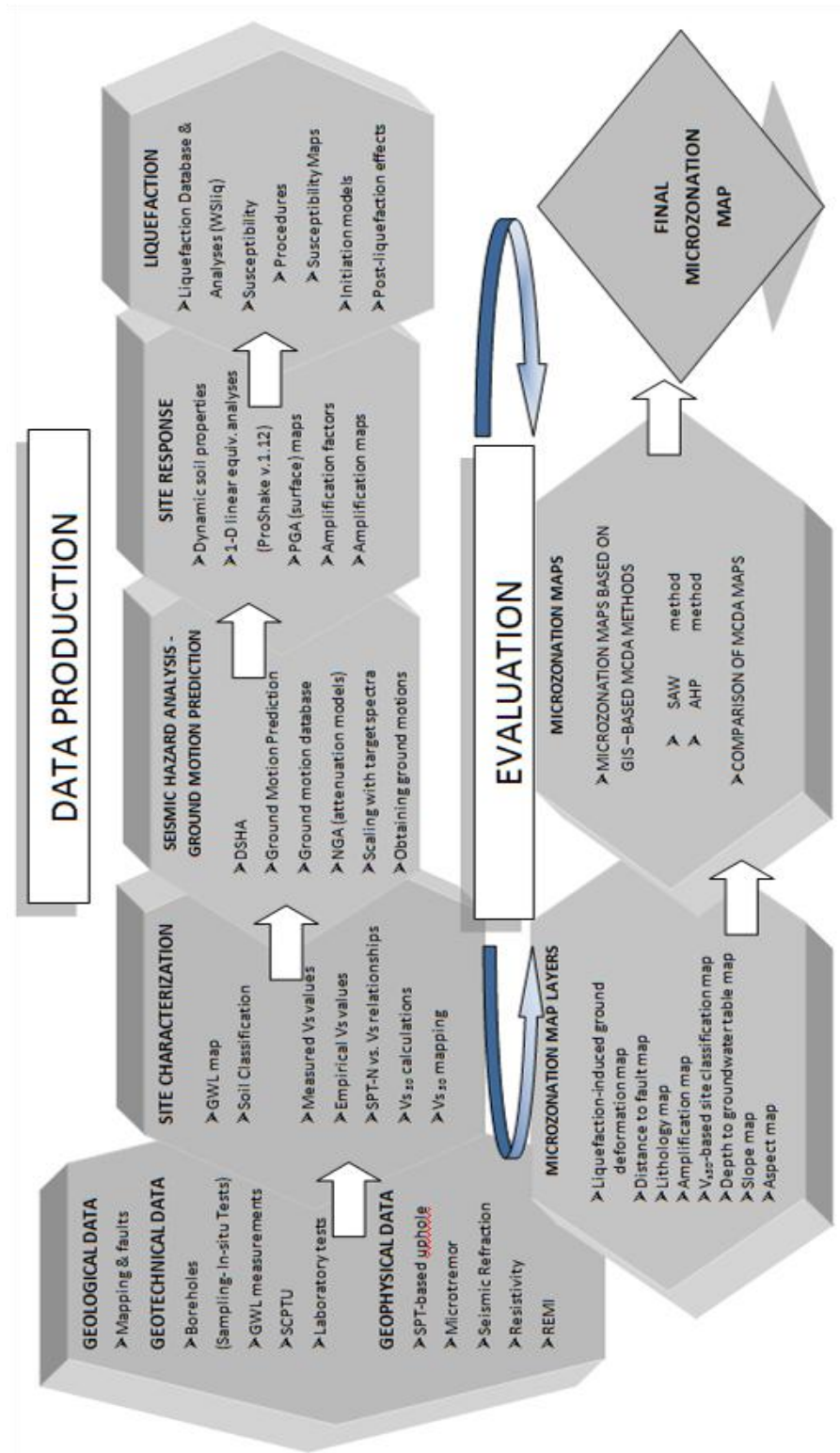


Figure 1.6. Flow chart of the methodology

## **CHAPTER 2**

### **BACKGROUND INFORMATION ON SEISMIC MICROZONATION**

#### **2.1 Definition of Seismic Microzonation**

Preparation of the seismic hazard zoning and seismic microzonation maps are effective solutions for evaluating the effects of natural hazards in urban planning and earthquake resistant design of constructions. Seismic hazard zoning consists of expected possible earthquakes at any location regarding to active faults. Microzonation is an application of subdivision of urban areas considering the direct and indirect effects of natural events and applying the zonation principles in regional scale. Seismic microzonation also known as zonation and /or seismic zonation is the procedure of the evaluation of soil/rock layers under earthquake loading conditions with ground motion properties. There have been several types of methodologies and definitions for the seismic microzonation subject in the literature. The most recent literature is summarized in the following paragraphs.

Wang and Law (1994) defined the microzonation by means of two criteria. The first criterion is based on seismic intensity which is the result of different microzones connected with different hazards. The second criterion is defined in terms of response spectrum. The writers mentioned that microzonation is the subdivision of a seismic zone into smaller zones (microzones) according to these two criteria.

Finn and Ventura (1995) stated that mapping of seismic hazard at local scales to integrate the effects of soil conditions is called microzonation for seismic hazard. Ansal et al. (2001a) stated that seismic microzonation can be considered as the process of estimating the response of soil layers under earthquake loading and the variations of earthquake ground motion characteristics on the ground surface.

Seismic microzonation includes the identification and mapping at local or site scales of areas having different potentials for hazardous earthquake effects, such as ground-shaking intensity, liquefaction, or landslide potential (Lee et al., 2003).

Seismic microzonation is defined as geographic segregation of variations in the earthquake hazard potential. This segregation is meaningful when all the parameters affecting the ground motions which are taken into account the effects of local site conditions including the soil profile and the topographic structures (Sharma et al., 2003). In most cases, the required data are occasionally available for the microzonation studies of the area. In these situations, seismic zonation can be significantly accomplished on the basis of expected bedrock ground motion. A similar definition for seismic microzonation was made by Yağcı (2005). The writer is of the opinion that microzonation is an inter-disciplinary approach to obtain soil characteristics considering earthquake source and mechanism rupture distance and the site response of urban areas.

Seismic microzonation requires multi-disciplinary contributions and arrangements for the effects of earthquake-based ground motions on the structures (De Mulder, 1996; Ansal et al., 2004b; 2005; Pitilakis, 2004; Dan, 2005). In addition, it can be considered as the process of response of soils under earthquake ground motion characteristics using geological, geotechnical and geophysical explorations. Additionally, geological and geotechnical data are considered as important issues for identifying and suggesting mitigation procedures of natural hazards (Bell et al., 1987; Legget, 1987; Hake, 1987; Rau, 1994; Dai et al., 1994, 2001; GDDA, 1996, 2000; Van Rooy and Stiff, 2001; Ansal et al., 2001a, 2004a, 2004b; JICA, 2002; Topal et al., 2003; Laue et al., 2004; DRM, 2004; Lebrun et al., 2004).

The seismic microzonation maps generated from different layers should also consider the slope, aspect, and digital elevation models of the study area to point out the topographic conditions for processing geographical spatial data (Dai et al., 2001). The reason is that it is getting more important to consider both what can safely be performed with a given piece of land, and what type of optimum methods can be applied for the future settlement areas. The key issue affecting the applicability and feasibility of any seismic microzonation study is the precision and consistency of the parameters selected for zonation (Abeki et al., 1995; Ansal et al., 2004b). Seismic microzonation studies should be conducted in different areas to prove how applicable of these procedures in the development stage of landuse and urban plans are (Bademli, 2001).

Urban planning becomes a significant issue where urban areas expand as a result of an increase in the population. The purpose of urban planning is to improve the proper settlement areas in terms of environmental and geological effects (Bell et al., 1987; Bell, 1998). Therefore, the obtained geological and geotechnical data in microzonation projects are crucial to identify and mitigate the geological hazards (Legget, 1987; Hake, 1987; Rau, 1994; Dai et al., 1994, 2001; Bademli, 2001; Van Rooy and Stiff, 2001).

## **2.2 Previous Works on Seismic Microzonation**

In the literature, numerous microzonation studies using single or multiple parameters and / or layers were conducted. Anbazhagan and Sitharam (2008) proposed the preparation steps of ideal seismic microzonation and seismic hazard maps with its essential layers (Figure 2.1). The input data and output layers are illustrated in the same figure.

Some of the researchers considered single parameter such as microtremor measurements, liquefaction potential evaluation, amplification, or earthquake induced-landslides for seismic microzonation studies (Lav, 1994; Finn and Ventura, 1995; Gaull et al., 1995; Abeki et al., 1995; Panza et al., 1996; Regnier et al., 2000; Trifunac and Todorovska, 2000; Hitchcock et al., 2000; Ayday et al., 2001; Marinos et al., 2001; Teves-Costa et al., 2001; Mirzaoglu and Dikmen, 2003; Cetin, 2004; Signanini et al., 2004; Alvarez et al., 2005; Papathanassiou et al., 2005; Gizzi, 2006; Hasançebi and Ulusay, 2006; Parolai et al., 2007; Ulanış and Kılıç, 2008; Koçkar et al., 2009). As a particular note, the seismic microzonation related to landsliding for the preparation of seismically-induced landslide hazard maps are generally not so advanced as liquefaction mapping due to diversity of physical processes in the landslide category. Landslides can be triggered by many mechanisms rather than only seismic loading.

On the contrary, the usage of multi-parameters in seismic microzonation is expanding its popularity in multi-disciplinary works. The multiple parameters considered in seismic microzonation should be part of the seismic hazard analysis, site characterization, site response, liquefaction analysis and earthquake related direct and indirect hazard analysis as well as the evaluation of geographical spatial data for the topographic conditions. Therefore, the selection of these parameters should be realistic and also be consistent with site-specific conditions. The previous works about microzonation are distinguished and summarized in this part of the dissertation.

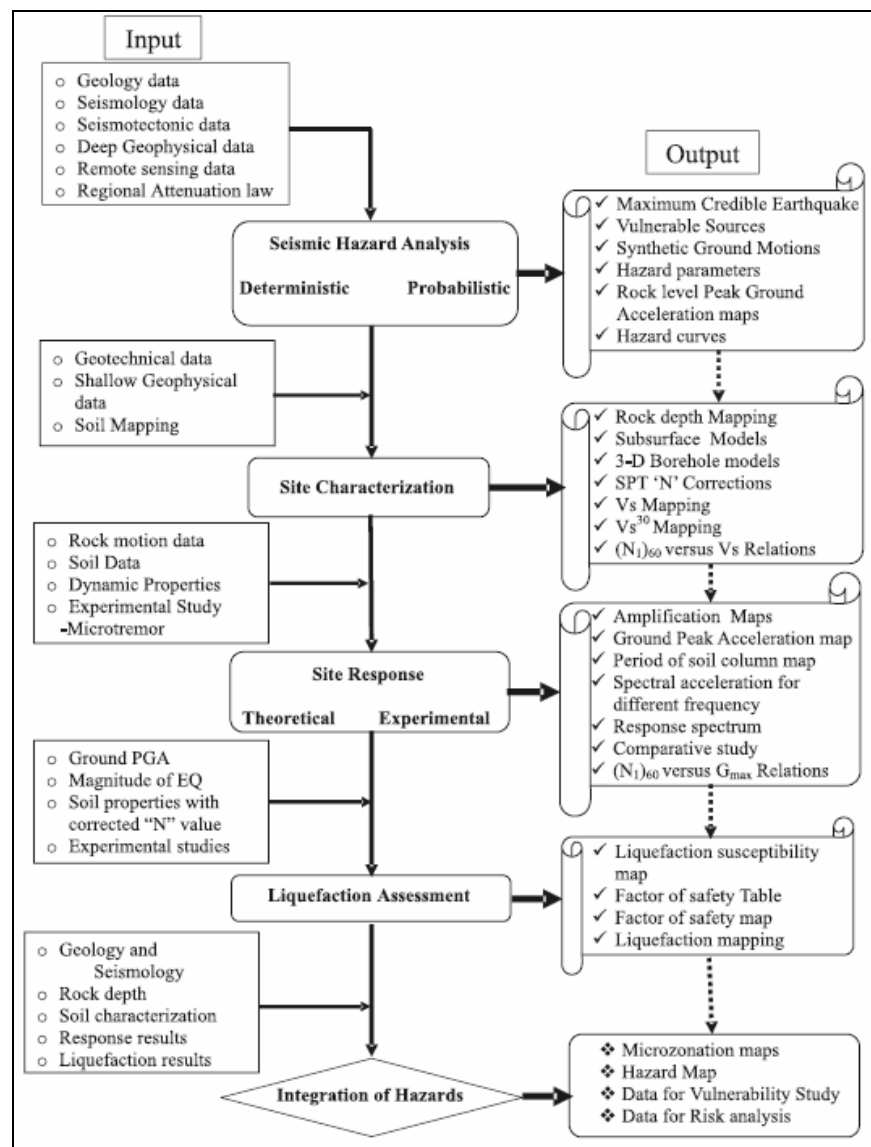


Figure 2.1. Preparation steps of microzonation maps (after Anbazhagan and Sitharam, 2008)

### 2.2.1 Single criteria-based seismic microzonation

The parameters based on the earthquake risks and geological/geotechnical characteristics of the soil material were generally considered during microzonation studies. However, a specific parameter was also preferred in many studies (such as seismic hazard, liquefaction or site response-based studies). The parameters used for seismic microzonation are grouped under single parameter-based studies.

### **2.2.1.1 Seismic hazard-based seismic microzonation**

Seismic hazard analyses involve quantitative evaluation of ground shaking hazards at a specific site. Seismic hazards may be analyzed deterministically, once a particular earthquake scenario is considered. They can also be analyzed in terms of probability, in which uncertainties in earthquake size, location and time of occurrence are evaluated (Kramer, 1996).

The first scientific and technical methods developed for zoning were deterministic and based on the observation of spatial damage distribution and the physical properties of underlying layers. The construction of probabilistic seismic zoning maps was started in 1970s in urban microzoning scale. The use of zoning in seismic risk management revealed that the destruction caused by an earthquake is the result of different factors such as seismic source, local site-specific soil conditions, the quality of constructions and social, economic and political system in a world-wide extent (Panza et al., 1996).

Finn and Ventura (1995) stated that the analysis for calculating the probability of exceeding different levels of the mapped ground motion parameter is called as seismic hazard analysis. Seismic hazard analysis is the major component of microzonation for seismic hazard and seismic risk.

Crespellani et al. (1997) defined the hazardous problems (landsliding, ground shaking effects, etc.) for the northern region of Tuscany and surrounding area in Italy, and the study area was zoned using the criteria of Manual for Zonation on Seismic Geotechnical Hazards (MZSGH) (ISSMGE-TC4, 1999). The application of MZGSH in this region offered many opportunities to evaluate the methods and their applications for the similar sites. They have also concluded that the return period for evaluating seismic hazard, the soil classes for the design spectra and the dynamic effects of earthquakes should be considered for these types of zonation and classification guidelines.

Balassanian et al. (1997a) proposed a new deterministic seismic zonation map for a province of Armenia. This map includes the active faults which are the main seismic source zones in the region. The calculation of seismic effect from the seismic source zones was performed in order to analyze the western and eastern standards of seismic hazard assessment in the study of Balassanian et al. (1997a).



Priolo (2001) used the deterministic approach in the microzonation of Fabriano (Italy) situated in the Marche Region at the foothills of the Apennine chain. Marcellini and Pagani (2004) considered deterministic, stochastic and probabilistic approaches for the same area. They concluded that the probabilistic approach is more suitable for the microzonation of a municipality in an area subjected to moderate seismicity. In addition, deterministic approach can also be used to assume the upper boundary of the expected motion in case of a strong earthquake considering the importance of the directivity effects. The deterministic approach assists in estimating the motion in long period and plays an important role in the design of industrial plant areas (Marcellini et al., 2001; Marcellini and Pagani, 2004).

Bommer et al. (2000) expressed that in many cases it is impossible to define a single earthquake scenario that is well-matched with the results of probabilistic seismic hazard assessment where the hazard is influenced by more than one seismic source. For this reason, it is extremely recommended to use deterministic hazard analysis in highly seismic areas.

In the study of McGuire (2001), the advantages and disadvantages of both probabilistic and deterministic methods which have a role in seismic hazard and risk analyses performed for decision-making purposes for seismic hazards were evaluated. One method will have priority over the other; depending on how quantitative are the decisions to be made, depending on the seismic location, and depending on the extent of the project (single site or a region).

Marinos et al. (2001) revealed that in the absence of systematic geotechnical investigations, the site should be classified by assessing the geological and geotechnical data according to the seismic code criteria. For instance, the damage distribution of 1999 Athens earthquake ( $M_s=5.9$ ) with its seismic hazard analyses was considered in the proposed microzonation for Athens (Greece).

Marcellini et al. (2001) analyzed and compared three different approaches (probabilistic, stochastic and deterministic) to evaluate input motion in a microzonation project. The researchers expressed that evaluated seismic hazard potential at a regional scale should consider the soil effects of a site-specific area and the integration of seismic codes and seismic hazard analyses should be taken into account for microzonation studies. In general, these seismic codes were produced to be based on probabilistic approaches for structural designs. Moreover, microzonation studies point out the expected ground motion given site condition as well as input motion.

Alvarez et al. (2005) compared the results of previous probabilistic seismic zoning and the recent deterministic seismic zoning of Cuba. The deterministic seismic zonation of eastern Cuba was performed in accordance with two alternative hypotheses: The maximum possible magnitudes of earthquakes in each seismic zone were determined by the known seismic history ( $M_{obs}$ ) and seismotectonical criteria ( $M_{max}$ ). Expected ground motion values range in the intervals were defined by means of these two variants.

Parolai et al. (2007) measured seismic noise in 20 different locations in the Cologne area (Germany) where the region is aligned nearly perpendicular to a graben structure. The H/V spectral noise ratio was applied to derive realistic S-wave velocity profiles down to the bedrock by means of a genetic algorithm inversion at each site. The site-specific values from response spectral ratios were modified to obtain attenuation functions entering the logic-tree algorithm of the probabilistic seismic hazard assessment (PSHA). Afterwards, a detailed seismic hazard analysis was re-performed in the Cologne area. The previous results and the combination of the previous approaches were considered to obtain engineering parameters for PSHA and microzonation of Cologne.

Pace et al. (2008) presented the results of a PSHA and disaggregation analysis which were aimed to understand the dominant magnitudes and source-to-site distances of earthquakes that control the hazard at the Celano site in the Abruzzo region of central Italy. The results indicated the percentage contribution to the Celano hazard of the various seismogenic sources for different expected peak ground acceleration classes. It is a common practice in seismic microzonation studies to use “scenario earthquakes” which are well-known historical or instrumentally recorded significant earthquakes, possibly occurred near the area of interest or having seismotectonic similarity with the region where the area is located. Thus, they proposed three different scenario earthquakes that are useful seismic microzonation study. The probabilistic and time-dependent approach to define the scenario earthquakes apparently changes the results in comparison to traditional deterministic analysis in terms of engineering design and seismic risk reduction as mentioned in the same study.

#### **2.2.1.2 Liquefaction-based seismic microzonation**

Liquefaction is one of the most disastrous earthquake-related phenomena which may occur in the susceptible soils during earthquakes. It is essential to define susceptible areas and

liquefaction potential in the microzonation maps depending on the susceptibility, initiation and effects of the liquefaction hazards.

Widespread liquefaction and associated sand boils, ground fissures and ground deformations occurred during a moderate earthquake ( $M_s = 6.2$ ) due to lateral spreading in Ceyhan town (Adana, Turkey) on 27 June 1998. In the study of Ulusay and Kuru (2004), the main characteristics of Ceyhan earthquake were presented and the liquefaction potential of the site was evaluated to establish preliminary microzonation maps for Ceyhan using the data from liquefaction susceptibility analyses. The liquefaction assessments were performed using the field performance data in terms of factor of safety against liquefaction and liquefaction potential index. In addition, the effect of the thickness of non-liquefiable cap soil was explored. Preliminary assessments indicated that the liquefaction potential of thin sand layers tends to diminish at around 5 m depth. A moderate earthquake ( $M_s = 6.2$ ) resulted in widespread liquefaction, liquefaction-induced lateral spreading and more damage than would be expected for an event of this magnitude. Comparison of the expected liquefiable zones and observed liquefaction-induced ground surface deformations revealed that the amount of liquefaction susceptible layers in the soil profile was reduced to considerable extent when the effect of overlying liquefaction resistant layers were considered (Ulusay and Kuru, 2004).

Selçuk and Çiftçi (2007) studied the Yüzüncü Yıl University (YYU/Van-Turkey) campus area in order to delineate the liquefaction-prone areas on the basis of the Liquefaction Potential Index ( $I_L$ ) to propose a microzonation map. Three main geotechnical seismic zones were identified within the campus area to reflect the potential damage to structures. The study highlighted the importance of proper design of buildings constructed in this area, and the necessity to undertake the appropriate geotechnical assessments of particular geological environments which have sediments prone to be liquefied.

According to the study of Papathanassiou et al. (2005), the most characteristic macro-seismic effects were extensive typical ground failures like rockfalls, soil liquefactions, subsidence, densification, ground cracks and landslides. An attempt was also made to establish a preliminary microzonation map for Lefkada town (Greece) using the data from Liquefaction Potential Index (LPI) analyses. The prepared map was validated by the occurrence of liquefaction phenomena inside the town. The ability of a soil element to resist liquefaction is defined as liquefaction factor of safety ( $F_s$ ), and two variables were required for its calculation: the cyclic resistance ratio CRR and the earthquake induced cyclic stress ratio

CSR at a specific depth for a given design earthquake in this study. Layers with factors of safety greater than 1.2 and between 1.0 and 1.2 were considered as non-liquefied and marginally liquefiable on the basis of the previous studies (e.g. Tosun and Ulusay, 1997; Ulusay and Kuru, 2004).

Sonmez and Ulusay (2008) presented a microzonation map along the southern coast of Izmit Bay (Turkey) using the data obtained from liquefaction susceptibility analyses and liquefaction severity index (LSI), which was proposed by Sonmez and Gokceoglu (2005). Furthermore, Sonmez et al. (2008) compared two sites (the southern shore of Izmit Bay, Turkey and Yuanlin, Taiwan) where the liquefaction was observed within the framework of a proposed LSI-based microzonation map, and recommended a chart to assess liquefaction-induced surface manifestation.

### **2.2.1.3 Site effects/response-based seismic microzonation**

Source, travel path and local site effects mainly involve earthquake-related ground motions at a particular site. Site effects are caused by various processes related to the local topography, near-surface geology, hydrogeology and subsurface geometry (Field, 1996; Bard, 1999). These processes influence ground motion in the form of impedance changes, resonant modes, focusing and defocusing effects, basin-edge effects, and non-linear behavior (Pitilakis, 2004; Kienzle et al., 2006).

Site effects and the importance of site response analyses are well understood by the previous catastrophic examples of the strong earthquakes. Numerous remarkable examples of this phenomenon occurred during the Mexico City earthquake in 1985 (Singh et al., 1988), the Armenian (Spitak) earthquake in 1988 (Borcherdt et al., 1989), the Loma Prieta earthquake in 1989 (e.g. Hough et al., 1990), the Northridge earthquake in 1994 and the Hyogo-ken Nanbu (Kobe) earthquake in 1995. The site response analysis determines the main frequencies and amplification at the ground surface. The site effects related to soil amplification and a measurement technique which are commonly used for the site-specific analyses of seismic microzonation are distinguished in this part. Generally, the comparison of different techniques with microtremor measurements has been made in the literature (Lermo and Chavez-Garcia, 1994; Duval et. al, 1994; Field and Jacob, 1995; Gaull et al., 1995; Chavez-Garcia and Cuenca, 1998; Bour et al., 1998; Cid et al., 2001; Dikmen and Mirzaoglu, 2005, Hasançebi and Ulusay, 2006).

In terms of simple qualitative and quantitative estimation of site effects is often expressed by the amplification factors (Stewart et al., 2003). These factors can be obtained from different approaches such as theoretical methods, linear and/or non-linear software programs (Shake91, ProSHAKE, EERA, D-MOD 2000, NERA, etc.) and/or field measurements.

A reliable seismic response in terms of both peak ground acceleration and spectral amplification is necessary to define actions required to mitigate the seismic hazard. Seismic response evaluation can be carried out either theoretically or empirically. Theoretical approach allows making a parametric study for a large sample of possible input motions; however, detailed geotechnical and seismic information and sophisticated computing algorithms are required. Empirical approach is based on the analysis of weak and strong ground motion recorded on sites with different geological conditions to assume the differences in the response of soft soil sites to a firm rock site. The empirical approach can be applied in regions of high seismicity whereas the theoretical approach is required in regions of moderate to low seismicity (Nunziata, 2007).

The microtremor measurement and analysis have been widely used for microzoning in many places around the world. This fast and easy measurement is a popular tool to evaluate the effect of soil conditions, ground motion characteristics due to an earthquake and site response parameters such as site amplification and predominant soil periods (Bour et al., 1998). Engineering application of microtremors was initially proposed by Kanai and Tanaka (1961). Microtremors are very low amplitude oscillations of the ground surface produced by natural sources such as wind, ocean waves, geothermal reactions and small magnitude earth tremors. In other words, microtremors are ground vibrations with displacement amplitude about 0.1-1 micron, and velocity amplitude about 0.001-0.01cm/s that can be detected by seismograph with high magnification. There are two types of microtremors on the basis of period range: Short-period microtremors with periods less than 1 second and long-period microtremors with periods longer than 1 second. Short-period microtremors are related to shallow subsurface structures with several tens of meters thick. On the contrary, long-period microtremors are related to deeper soil structure up to hard rock depth with an S-wave velocity of 3 km/s. Ohta et al. (1978a) proposed that the predominant ground periods (2.5 second) in both microtremors and strong ground motion records were attributed to the existence of deep alluvial deposits.

The microtremor (ambient seismic noise) measurement which evaluates the site response was used in many studies in different areas such as Japan (Ohta et al., 1978a), the San Fernando Valley (Kagami et al., 1986), Mexico (Lermo et al., 1988; Gutierrez and Singh, 1992; Chavez-Garcia and Cuenca, 1998), Italy (Rovelliet et al., 1991, Hough et al., 1992, Malagnini et al., 1993), New York (Field et al., 1990), Australia (Gauill et al., 1995; Kagami et al., 1986), and Colombia (Cardona and Yamin, 2000).

Kagami et al. (1986) employed two dimensional approaches to revise the site effects in San Fernando Valley and prepared an amplification map for the study area. Possible site amplification during 1985 Michoacan earthquake near Mexico City was studied by Singh et al. (1988). The results revealed that the amplification factors in the lake bed zone are 8-50 times higher than the hilly zone. Masaki et al. (1988) exhibited the predominant periods at several sites in Mexico City applying microtremors and the results were consistent with those obtained from the strong ground motion at the same site during the earthquake. Kagami et al. (1982) and Yamanaka et al. (1994) studied the simultaneous observation of long period microtremors which were appropriate for the evaluation of the amplification due to deep soil deposits.

Microtremor records have been widely used by many researchers to estimate site response under earthquake excitations (Lu et al., 1992; Lermo and Chavez-Garcia, 1994; Duval et al., 1994; Gauill et al., 1995). The method proposed by Nakamura (1989) guided the extensive use of microtremor measurements to evaluate site conditions. However, general experience among scientists and engineers indicates that the predominant site periods determined from spectral ratios are more reliable than site amplifications (Mucciarelli, 1998). One possible reason for this conclusion may be the differences among spectral accelerations and spectral amplifications since the latter is partially independent from peak ground accelerations.

In the study of Bodle (1992), a statistical microzonation tool was proposed for a region susceptible to strong spectral amplification of earthquake accelerations within 2-4 Hertz range. The tool was introduced within the framework of Modified Mercalli Intensity (MMI) surveys and surface geology. A case study for Olympia (Washington-US) area was considered as a practical application. It was concluded that the Quaternary glacial recessional outwash sands were the dominant surface geologic unit associated with the strongest amplification of earthquake motions within 2-4 Hz frequency range.

A new microzonation map of Perth, Western Australia was proposed by utilizing microtremor spectral ratios by Gaull et al. (1995). The earthquake spectral ratios were correlated with the microtremor equivalent in the same study. It was found that the low-strain vibrations can provide a preliminary approach for strong motion during earthquakes. It was also stated that microtremors can be a very useful tool in measuring seismic ground amplification for earthquake hazard assessment.

In the study of Ansal et al. (1997), a preliminary microzonation study was conducted using the Manual for Zonation on Seismic Geotechnical Hazards (MZSGH) for Dinar (Turkey). The variation of soil profile was defined by means of in-situ penetration tests, microtremor measurements as well as shear wave velocity measurements. The results were compared with the damage distribution in Dinar by representing the effect of soil conditions and soil amplification obtained from geological and geotechnical profiles. They indicated that the evaluation of microtremor recordings using the reference point method (Kanai and Tanaka, 1961) or the spectral ratio method (Nakamura, 1989) is dependent to existing site conditions. In general, the reference point method is preferable on stiff and hard soil layers while spectral ratios may yield more realistic site amplifications on soft soil conditions (Ansal et al., 1997; 2001b). Additionally, site amplifications were estimated from microtremor spectral ratios, and microzonation was performed applying a GIS methodology in Dinar by Güllü (2001) and Ansal et al. (2001b).

Fah et al. (1997) proposed the ambient seismic noise measurements and the one and two-dimensional numerical modeling to estimate the expected seismic ground motion during the strong earthquakes. However, due to the limited resources only quantitative estimates were presented for selected sites and cross-sections. In order to incorporate entire results from the geotechnical site characterization and the ambient noise measurements, the researchers developed a rating system to achieve a qualitative microzonation map of the centre of Basel (Switzerland). Their microzonation study includes the geology of the area, measurements, modelling and interpretation of ambient noise data, and numerical modeling of expected ground motion during earthquakes.

Seht and Wohlenberg (1999) mentioned that the microtremor measurements can be used to determine the thickness of soft cover layers by applying Nakamura's technique (Nakamura, 1989). This Nakamura technique relies on the interpretation of microtremors as Rayleigh waves propagating in single layer over a half-space. Nakamura's technique provides a

reliable estimation of the resonance frequency for sites where site amplification is significant. This method is mainly criticized when it is executed for estimating the amplification level (Regnier et al., 2000). In addition, Bour et al. (1998) mentioned that many theoretical and experimental studies have revealed that the spectral ratio, also called as H/V spectral ratio, enables an adequate determination of site fundamental frequency. However, Nakamura's method might not provide all the information required for a reliable estimation of the amplification of surface ground motion.

Regnier et al. (2000) focused on site effects and seismic hazard by providing a detailed microzonation map which considers site effects in terms of resonance and amplification factors.

Cid et al. (2001) studied the seismic zonation of Barcelona (Spain) based on the complete soil transfer functions. The obtained frequencies of maximum amplification were compared with those derived from microtremor measurements. It was then recommended not to base microzoning only on experimental Nakamura's technique without comparing with other methods for amplification calculations.

Teves-Costa et al. (2001) compared the 1-D theoretical modeling (using the Thompson-Haskell 1-D approach) to the results obtained in previous studies conducted applying microtremor analysis. According to their study, 1-D theoretical modeling approach can be used for microzonation purposes. They presented their results as contour maps of peak frequencies and corresponding amplification factors. The estimation of amplification factors is an advantage of this method over the microtremor analysis as it allows estimating the relative amplitude at different sites. However, they concluded that the microtremor analysis is more sensitive to both alluvial valleys and topographical irregularities.

Ojeda et al. (2002) stated that a total of 32 stations were operated in the metropolitan area for the accelerographic network of Santa Fe de Bogota (Colombia) since 1999. The spectral amplification levels reach up to a factor of 5. The predominant periods obtained by the amplification spectra from different stations in the city vary from 0.3 to 3.0 s. A comparison was also made between the predominant periods obtained by H/V spectral ratios of microtremors and those using weak motion. In order to evaluate the potential use of microtremors in future investigations as a tool for estimation of soil dynamic behavior, measurements and analysis of microtremors were performed at each station of the



accelerographic network. Microtremors were recorded in time windows of 60 s at different times of the day. For each station, a minimum of four records were taken and every record was processed using Nakamura technique. A good correlation among soil types, weak motion periods, and microtremors were achieved. As a result of this study, microtremors were considered to be a useful tool for refining a future isoperiod map of the city.

Mirzaoglu and Dikmen (2003) presented an experimental study of 114 microtremors for the investigation of ground characteristics in Shin-Yokohama area in Japan to prepare a microzoning map. A map showing the distribution of the site predominant periods and strong motion records was developed for microzonation purposes. The employed parameters are predominant period, classification of soil conditions, H/V spectral ratio and amplification ratio in this study. As a result of Mirzaoglu and Dikmen (2003) study, it should be noted that the characteristics of microtremors are dependent on the type of soil deposits. Site effect plays an important role in microtremors measurements. The authors proposed experimental methods using microtremor recordings to establish a seismic microzonation by comparing long period, predominant and H/V period distribution maps. H/V spectral ratio approach provides a simple means of determining the predominant frequency of a soil site. In other words, the H/V spectral ratio technique ensured making a better distribution map of predominant frequency.

The study conducted by Dikmen and Mirzaoglu (2005), seismic noise measurements were performed at 151 locations to obtain seismic microzonation maps at Yenişehir-Bursa (Turkey). Two maps were prepared showing the spatial variations of the predominant period and seismic amplification according to Nakamura's technique for the investigated area. The analyses indicated that the north and south edges of the Yenişehir basin have relatively high predominant periods and high seismic amplification compared to the centre of the basin. This result is coherent with the theory of topographic effects on seismic amplification and also confirms the suitability of the H/V spectral ratio of ambient noise as a geophysical exploration tool in seismic hazard assessment.

Moreover, Hasançebi and Ulusay (2006) compared microtremor measurements with the soil amplification in Yenişehir (Bursa). Three different methods (shear wave velocity based empirical relationships, 1-D site response program SHAKE, and microtremor data) were evaluated to propose a microzonation map. Site periods obtained by SHAKE modeling were presented and compared with the obtained microtremor data. Nakamura's technique was

considered for the evaluation of microtremor measurements in the investigated area. A microzonation map was proposed derived from amplification factors and site periods for Yenişehir town (Bursa).

The soft soil deposits amplify certain frequencies of ground motion thereby increasing earthquake damage. The 1985 Michoacan earthquake (Mexico City) was the well-known example of amplification phenomena. Mexico City is settled on the former bed of a drained lake over a soft soil deposition of lacustrine sediments, known as Mexico clay. The fault rupture distance in this earthquake was around 350 km away from the city center. However, a catastrophic damage occurred in Mexico City due to strong amplification of the ground motion by soft soil deposits (Seed et al., 1988; Lermo et al., 1988).

Although Bangkok, the capital city of Thailand, is located in a low seismic hazard area, there is a potential hazard from distant earthquakes due to the ability of underlying soft clay to amplify ground motions (Warnitchai et al., 2000). In the study of Tuladhar et al. (2004), a seismic microzonation map for the greater Bangkok area was constructed using 150 microtremor measurements. The predominant periods of the ground were determined from the horizontal-to-vertical (H/V) spectral ratio technique. A microzonation map was then prepared for the study area based on the observations. Besides, the transfer functions were calculated for the soil profile at eight sites using the computer program SHAKE91 to validate the results from microtremor analysis. The area near the Gulf of Thailand is underlain by a thick soft clay layer and found to have long natural periods ranging from 0.8s to 1.2s. However, the areas outside the lower central plain have shorter predominant periods less than 0.4 s. The study conducted by Tuladhar et al. (2004) revealed that there is a great possibility of long-period ground vibration in Bangkok, especially in the areas near the Gulf of Thailand. This may have severe effects on long-period structures such as high-rise buildings and long-span bridges.

Measurements of background noise at Al Hoceima city (Morocco) and its extension zones allocated a seismic microzonation map as a first survey of seismic microzonation by Mourabit et al. (2000). Talhaoui et al. (2004) aimed to undertake a study for the site effects covering both Al Hoceima city and its extension zones using the Nakamura (1989) method which is based on the measurements of background noise. A strong correlation between the dominant periods and the topography was determined. Moreover, larger dominant periods in

the areas with higher topography were specified in the northern and southern region of the city.

Sharma et al. (2003) carried out seismic hazard analysis using complete and extreme part of the seismicity data for Delhi based on six different seismogenic sources. They suggested that the seismic zonation map of Delhi region generated from PGA values at the bedrock level can be used directly as input for the microzonation of ground motion at the surface by incorporating the local site conditions. Additionally, the seismic hazard microzonation for ground shaking site effects has been determined from 75 microtremor measurements in and around Delhi, India by Mukhopadhyay and Bormann (2004). The data set showed that the resonance frequency varies within a short distance in Delhi. The resonance frequency of a site becomes lower when the basement depth increases and vice versa. The resonance frequency is lower in areas which have younger alluvial deposits. The amplification of ground vibration has been determined in terms of lower bound estimate of the level of amplification. It was concluded that the microtremor data are very useful for low cost microzonation studies although they tend to underestimate the level of ground motion amplification when compared to earthquake records. Furthermore, Iyengar and Ghosh (2004) discussed the usage of seismic hazard microzonation map which was based on the quantified hazard in terms of the rock level peak ground acceleration value mapped on a grid size of 1 km x 1 km for a return period of 2500 years for further site-specific studies at soft soil deposits.

Two seismic microzonation maps of iso-frequency and iso-amplification factor were prepared in the study of Motamed et al. (2007). Regarding iso-frequency map, soil type in Bam (Iran) is mainly stiff and shear wave velocity reaches up to 750 m/s at the depth of 7.5 m in most areas. However, the amplification factor map presents relatively large values. The sediment depth was estimated from microtremor results as a preliminary tool for microzonation studies.

A microzonation study was performed as a part of Zeytinburnu Pilot Project within the framework of the Earthquake Master Plan for Istanbul to determine the effects of local soil conditions on the earthquake forces that will act on structures by Kılıç et al. (2006). In order to explore the effects of local soil conditions on the dynamic behavior, site response analyses were performed with the computer code EERA employing the results of field and laboratory explorations. The study area was divided into approximately 250 m×250 m grids to

determine the necessary parameters for microzonation. For each grid, representative soil profiles and site conditions were determined and the site was classified in accordance with three different criteria: Turkish Earthquake Code TEC (1998), NEHRP (2000) and equivalent shear wave velocities (MERM, 2003; Ansal et al., 2004a; 2004b; Studer and Ansal, 2003).

Kamalian et al. (2008) conducted a site effect microzonation study as an important step in effectively reducing seismic risk and the vulnerability of the city of Qom (Iran). The study area was divided into a grid of 1 km×1 km elements and the sub-surface ground conditions were represented by 59 different geotechnical profiles. Site response analyses were carried out on each representative profile using 30 different base rock input motions. Besides, the maps of site periods and peak ground acceleration distributions for the city were developed providing a useful basis for land-use planning.

### **2.2.2 Multi criteria-based seismic microzonation**

The combination of different parameters (layers) such as liquefaction, amplification, slope-aspect maps for seismic microzonation purposes are grouped as multi-criteria based studies. GIS (Geographical Information System) and its softwares have functional capabilities to support the development of spatial geo-environmental evaluation especially in microzonation projects. Seismic microzonation studies have been conducted in all earthquake-prone areas of the world (Chavez-Garcia and Cuenca 1998; Faccioli et al. 1999; Fah et al. 1997, 2000; Topal et al., 2003; Destegül, 2005; Nath, 2004, 2005; Mohanty et al., 2009; Walling and Mohanty, 2009; Grasso and Maugeri, 2009) and are continuously being executed with the use of GIS. The advantage of using GIS for seismic hazard mapping and seismic microzonation confirms its ability to calculate areas and lengths of geometric features in a spatial environment. The seismic microzonation maps created in GIS environment are both useful and powerful for land use planning or making hazard mitigation decisions in site-specific analysis. It is also getting a common practice to create a seismic microzonation map by incorporating a variety of factors including geology, topography, subsoil condition, building morphology, earthquake ground motion amplification, etc. (Lee et al., 2003; Nath, 2004; DRM, 2004; Kolat et al., 2006).

Jimenez et al. (2000) studied the GIS based seismic zonation of Barcelona (Spain) considering the soil effects. It was the first application of an integrated GIS environment to mapping soil effects for Barcelona.

In the study of Dai et al. (2001), a GIS-based geo-environmental evaluation for urban land-use planning in Lanzhou City and its vicinity in Northwest China was performed by multi-criteria analysis. Topography, surface and bedrock geology, groundwater conditions and geological hazards were included in the analyses. A suitability map for each parameter was developed using an algorithm which merges factors in weighted linear combinations. It was concluded that GIS methodology has an important impact for geo-environmental evaluation, and it is capable of supplying a degree of precision to evaluate the suitability of land parcels for urban growth.

Site amplifications were estimated from microtremor spectral ratios and a microzonation study was carried out using GIS methodology in the study of Ansal et al. (2001b) for Dinar (Afyon, Turkey). The results of in-situ penetration tests and seismic wave velocity measurements as well as the damage distribution were compared with the amplification zonation obtained from microtremor records. The results indicated the applicability of microtremor spectral ratios for assessing the local site conditions and site amplifications.

Anastasiadis et al. (2001) presented the results of large-scale geophysical and geotechnical survey in order to determine and validate the geometrical as well as dynamic properties of main soil formations in the Thessaloniki area (Greece). The synthesis and combination of recent results considering dynamic properties obtained from the elaboration of a large database of classical geotechnical tests led to the design of a detailed geotechnical map and the design of various 1-D profiles, 2-D cross-sections and 3-D thematic maps for the main soil formations. These soil profiles and maps were oriented to site effect studies and provided a comprehensive picture that could be easily adapted to GIS for planning and design purposes. The results of this study were correlated with macroseismic observations and previous preliminary microzoning studies. It was also concluded that topographic irregularities, lateral variations, possible discontinuities and a variety of soil types may induce complex site effects.

Topal et al. (2003) considered a number of different parameters for microzonation such as geological, geotechnical, seismotectonic and hydrogeological conditions in Yenişehir (Bursa,

Turkey) town to obtain the subsurface conditions of present and future settlement areas. Two geotechnical zones were distinguished in accordance with liquefaction potential, cohesive soils of high expansion behavior, slope and aspects maps.

The seismic ground motion hazard was mapped in Sikkim Himalaya through a GIS model considering local and regional site conditions by Nath (2004). Topographical maps, the geographical boundary of the State of Sikkim, surface geological maps, soil classification map in 1:50,000 scale and seismic refraction profiles, the seismological and geological thematic (SR, PGA, PF, lithology, soil class, slope, drainage, and landslide) layers were generated at the beginning of the study. The seismological themes were assigned normalized weights and feature ranks following a pair-wise comparison hierarchical approach. Afterwards, all seismological parameters were integrated to develop a seismic hazard map. Finally, a GIS-based microzonation map was prepared considering all topographic, geologic, and seismic parameters. Therefore, it was concluded that it is essential to develop seismic microzonation maps of earthquake hazard prone areas by incorporating site effects, soil class, lithological conditions, topographic effects, and seismological parameters (site amplification, peak ground acceleration and predominant frequency of ground motion). Additionally, overlaying, union and integration of various geologic and seismologic layers are complicated spatial operations which are optimally performed in GIS environment.

The study of Nath (2004) was modified by Nath (2005). Six major hazard zones were differentiated using different percentages of probability index values for the geological, seismological hazard and microzonation maps of Sikkim Himalaya region. Seismic microzonation consists of several subtasks such as the study of the seismotectonic setting of a region, ground failure susceptibility analysis, geotechnical parameterization, spatial variation of ground motion using both weak and strong motion recordings, estimation of site amplification factors, study of attenuation relations, seismological simulation of source and propagation effects, and thematic mapping in this study. The researcher also mentioned that producing a microzonation map should consider site effects, a digital map of the lithological and soil conditions, a digital map showing the topographic effect (% slope), peak ground acceleration (PGA) and the resonance/predominant frequency (RF) of ground motion at different sites.

Moldoveanu et al. (2004) proposed the first-order microzonation of Bucharest (Romania). They evaluated the existing database of structural and geotechnical parameters, and revised

previous studies concerning the seismicity of the Vrancea region considering the site conditions of the city, the characterization of the building stock, and the codes of practice which regulate the earthquake resistant design in Bucharest. Their seismic microzonation study revealed important information for detailed urban planning that establishes an appropriate level of awareness to earthquake threat. Cioflan et al. (2004) also projected a new seismic microzonation map for the Vrancea region in Bucharest where five different zones were identified by their characteristic response spectra. The employed hybrid technique enables the study of local soil effects even at long distances from the source considering the characteristics of seismic source and the effects of seismic wave propagation. The applied technique by Cioflan et al. (2004) provides realistic estimates of spectral amplifications when strong motion recordings are not existent for the target site.

Ansal et al. (2004b) developed a methodology for adoption as a guideline for seismic microzonation investigations within the framework of the pilot microzonation studies conducted for Adapazarı and Gölcük regions in Turkey. The proposed methodology is based on the regional estimation of the earthquake hazard, detailed investigation of geological and geotechnical site conditions and analysis of the ground motion characteristics based on a grid layout. The pilot areas were divided into cells by a grid system of 500 m  $\times$  500 m for estimating the effects of site conditions at a scale of 1:5000 by assigning representative soil profiles at the centre of each grid. These soil profiles were classified in accordance with the Turkish Earthquake Code (1998), NEHRP (2000) site classification, and equivalent shear wave velocity used for site response analyses. Even though the peak spectral amplifications calculated from microtremor H/V ratios were not considered as very reliable, they seem consistent with the ground shaking zonation map of Adapazarı. As a result, the average of spectral accelerations and peak spectral amplifications can be preferred for the zonation criteria in ground shaking microzonation maps.

Teramo et al. (2005) introduced a seismic site response-based seismic microzonation in their study. A seismic site response characterization was proposed with regards to geomorphological conditions, geotechnical and geophysical parameters such as slope, average shear-wave velocity, maximum expected acceleration on bedrock, and depth of groundwater table. An empirical relationship was presented for these parameters and the same relationship was applied to determine ground motion amplification coefficients to be used in specific programs of land use or town planning dedicated to the mitigation of seismic risk in seismic microzonation project.

One methodology was presented to evaluate the local seismic response of an urbanized site and to establish cost-effective seismic microzoning studies on a quantitative basis providing more insights for the choice of risk mitigation measures by Romeo and Bisiccia (2006). Deterministic and probabilistic seismic hazard analyses were carried out to select the reference earthquake and the related ground motion used to assess the local seismic response. The resulting seismic microzonation map was used for the adoption of risk mitigation measures such as the seismic retrofitting of buildings and the formulation of emergency plans for civil protection purposes in the same project.

Kienzle et al. (2006) presented a research concerning the development of an original approach for the earthquake microzonation of densely populated urban areas considering the city of Bucharest (Romania) as an example. In case of the absence of a sufficient dense network of ground motion recording stations in the study area, the only possible way to comprehend a complete microzonation is to correlate detailed subsurface geological data at instrumented sites with the macroseismic intensities and to extrapolate the results to non-instrumented areas in GIS environment. Transfer functions and dynamic ground responses were calculated using the linear modeling software ProSHAKE utilizing soil profiles taken from discrete locations in the developed model as well as shear wave velocities and densities characteristic for each Quaternary unit. The distribution of computed spectral amplifications and spectral accelerations were interpolated for the ground surface of Bucharest city. A GIS method was applied to produce a 3-D digital geological model (DGM) from existing analogue geological data. It was concluded that the GIS-based approach is a helpful tool for modeling local site effects in urban areas where strong motion registrations exist only at limited sites. Nevertheless, they mentioned that in regions where many strong motion registrations exist, the existing method can be applied as a complementary tool for an improved interpolation of site effects between the strong motion stations by correlation with the local geology.

Kolat (2004) and Kolat et al. (2006) proposed a geotechnical microzonation map integrating GIS and Multicriteria Decision Analysis (MCDA) techniques for Eskisehir (Turkey). During the preparation of microzonation map, slope, flood susceptibility, soil classification, groundwater table depth, swelling potential, and liquefaction potential maps were assigned different weights and rank values in GIS-based multicriteria decision making or spatial MCDA. It was concluded that the use of GIS-based; is an essential method for the preparation of geotechnical microzonation maps due to the large amount of spatial



geographical and geotechnical data. This study reveals the advantage of MCDA techniques with GIS for the preparation of geotechnical microzonation maps regarding the suitability of urban areas (Carver, 1991; Jankowski, 1995). Moreover, many real world spatial planning and management problems including microzonation projects are growing through GIS-based multicriteria decision making or spatial Multicriteria Decision Analysis (MCDA) (Malczewski, 1999; Belton and Stewart, 2002).

A first order GIS-based seismic microzonation map of Delhi was prepared using five thematic layers; Peak Ground Acceleration (PGA) contour, different soil types at 6 m depth, geology, groundwater fluctuation and bedrock depth integrated on GIS environment by Mohanty et al. (2007). The integration was performed following a pair-wise comparison of Analytical Hierarchy Process (AHP) which is a multi-criteria mathematical evaluation method in decision making process. Each thematic map was assigned weight in the order of 5 to 1 scale depending on its contribution to seismic hazard. On the microzonation theme, the Delhi region has been classified into four broad zones of vulnerability to the seismic hazard.

The seismic microzonation of the Bengal Basin, Haldia region, India was carried out using the Analytical Hierarchy Process (AHP) in GIS environment by Mohanty and Walling (2008). A first-order seismic microzonation map of Haldia was prepared in which four hazard zones (very high, high, moderate, and less) have been broadly classified for Haldia.

İnce et al. (2008) investigated the geological and geotechnical conditions of old Istanbul settlement area (Fatih and Eminönü provinces) in a detailed seismic microzonation study. Microzonation maps were prepared based on ground shaking intensity, liquefaction hazard and seismic landslide hazard according to the procedures proposed in the new seismic microzoning handbook prepared by the World Institute for Disaster Risk Management (DRM) for mitigation of earthquake hazards (MERM, 2003). The output data obtained from the analyses were evaluated by means of GIS techniques, and ground shaking, liquefaction susceptibility and landslide hazard maps were prepared. The study area was divided into 250 m x 250 m cells, and representative soil profiles were created for each cell compatible with geological maps and cross sections. Furthermore, considering the importance of the shear wave velocity on the behavior of soil layers during earthquakes, the shear wave velocity profiles were also prepared for each cell. The procedure recommended in the MERM (2003) manual prepared by DRM was used to prepare microzonation maps with respect to soil amplification. In order to evaluate the region in terms of seismic slope stability hazard, the

computer code KoeriSlope v1.0 (Fahjan et al. 2003; Siyahi and Fahjan, 2004) which is based on the slope stability analysis method proposed by Siyahi and Ansal (1993) was used, and microzonation maps were prepared in accordance with the computed factor of safety values. For each cell, dynamic site response analysis was carried out to determine the expected behavior during a probable earthquake. It was concluded that ground-shaking intensity varies across the historical peninsula, which can affect the distribution of structural damage during an earthquake.

Anagnostopoulos et al. (2008) summarized the development of a GIS scenario-based system, called SEISMOCARE, for the regional damage and loss estimation due to the earthquake of Chania (Greece). The proposed system allows users to perform ‘if–then’ scenarios to analyze the sensitivity of its estimations and to optimize the decisions for the planning process of existing cities as well as their future developments.

Nath et al. (2008) studied a comprehensive analytical and numerical treatment of seismological, geological, geomorphological, and geotechnical models which were employed through microzonation projects representing contrasting geological backgrounds (a hilly terrain and a predominantly alluvial basin) in the northeast Indian provinces of Sikkim Himalaya and Guwahati city. Seismic microzonation was completed with respect to the integration of thematic layers compatible to the various hazard components following a multi-criteria evaluation technique called Analytical Hierarchical Process (AHP) introduced by Saaty (1980) in that study. The geomorphological factors for Sikkim Himalaya including surface geology, soil cover, slope, rock outcrop and landslide and the seismological factors (surface peak ground acceleration and predominant frequency) were chosen to prepare a seismic hazard microzonation map. Besides, the microzonation study of Guwahati city considered eight topics for geological and geomorphological, basement or bedrock, landuse, landslide, factor of safety for soil stability, shear wave velocity, predominant frequency, and surface peak ground acceleration. As a result, both study areas were classified into low, moderate, high, moderate high and very high hazard level zones.

Sun et al. (2008) developed an integrated GIS-based tool (GTIS) which was constructed to estimate site effects related to the earthquake hazards in the Gyeongju area of Korea. The GTIS was used to estimate site effects associated with the amplification of ground motion. The seismic microzonation maps of characteristic site period and mean shear wave velocity to a depth of 30 m were created and presented as a regional synthetic strategy addressing

earthquake-induced hazards. Various seismic microzonation maps for short and mid-period amplification potentials were prepared for the study area based on one-dimensional site response analyses. The effectiveness of the GTIS for predicting seismic hazards in the region was verified by the previous seismic microzonation case studies performed in the Gyeongju area.

Papadimitriou et al. (2008) presented an automated methodology for performing GIS-aided seismic microzonation studies for Athens (Greece). It was concluded that a common, user-friendly automated methodology for GIS-aided microzonation studies is possible without loss of accuracy at least for a preliminary estimation of seismic risk and for depicting high-risk locations where further geotechnical investigations should be performed and more detailed (possibly numerical) analyses should be implemented.

Antoniou et al. (2008) also proposed a GIS approach which manages geotechnical data obtained from detailed geotechnical surveys and in-situ observations in Athens (Greece). This methodology for an automated GIS-aided seismic microzonation study is outlined and being employed considering the aforementioned geotechnical, engineering geological information and existing seismological data to estimate the variability of seismic ground motion for the southern part of Athens.

### **2.3 Microzonation Methodologies and Mapping Techniques**

In this part, several previous microzonation methodologies were summarized. In the 1990s, some researchers proposed fundamental steps for the awareness of future events and the mitigation of earthquake risk involved in a microzonation study. The evaluation of the local soil conditions and the estimation of their influence on seismic ground motion in a three-step approach were presented in order to obtain site response of the study area by Fah et al. (1997). In the first step, all available geological and geotechnical data were collected, interpreted and mapped. In the second step, ambient seismic noise measurements were carried out and interpreted in order to predict the dominant site periods of the unconsolidated sediments. Together with the evaluation of standard penetration tests (SPT), the estimates of shear-wave velocities were obtained. Finally, one and two-dimensional numerical modeling were completed to interpret the local site conditions. In addition, the Technical Committee on Earthquake Geotechnical Engineering of the International Society of Soil Mechanics and Foundation Engineering (ISSMGE-TC4, 1999) highlighted that the first grade (Level I) map

can be prepared with a scale of 1:1.000.000-1:50.000, and the ground motion is assessed based on the historical earthquakes and the existing information of geological and geomorphological maps as given in Table 2.1. Furthermore, if the scale of mapping is 1:100.000-1:10.000 and ground motion is assessed with respect to microtremor and simplified geotechnical studies then it is called second grade (Level II) map. In the third grade (Level III) map ground motion is assessed by means of complete geotechnical investigations and ground response analysis with a scale of 1:25.000-1:5.000 to include proposed seismic microzonation maps (Sitharam and Anbazhagan, 2008).

In a detailed urban planning, the earthquake effects on ground surface are defined by seismic zoning and seismic microzonation which are based on the proper knowledge of:

1. regional geology and tectonics
2. regional seismicity and earthquake catalogues
3. seismic ground motion and zoning
4. faulting and permanent ground deformations
5. engineering aspects of disastrous earthquakes (Moldoveanu et al., 2004)

Table 2.1. Use of data for three levels of zonation (after ISSMGE-TC4, 1999)

	Grade-1	Grade-2	Grade-3
Ground motions	Historical earthquakes and existing information Geological maps Interviews with local residents	Microtremor Simplified geotechnical study	Geotechnical investigation Ground response analysis
Slope instability	Historical earthquakes and existing information Geological and geomorphological maps	Air photos and remote sensing Field studies Vegetation and precipitation data	Geotechnical investigation Analyses
Liquefaction	Historical earthquakes and existing information Geological and geomorphological maps	Air photos and remote sensing Field studies Interview with local residents	Geotechnical investigation Analysis
Mapping scale	1:1.000.000-1:50.000	1:100.000-1:10.000	1:25.000-1:5.000

The optimal development of the realistic estimation of site effects based on the scenario modeling approaches should be used to predict the seismic strong motion. In fact, the results

of microzoning are used by end users, such as local authorities, city planners, land-use specialists and civil engineers, whose background is very different and for whom the recommendations must be clear and understandable (Moldoveanu et al., 2004, Pitilakis, 2004).

In the manual of Seismic Microzonation for Municipalities in Turkey, the literature was reviewed and the main parameters were summarized for an ideal seismic microzonation. In practice, it was suggested that the seismic microzonation should involve five different phases: site characterization, evaluation of the seismic hazard; estimation of the ground motion characteristics on the ground surface, assessment of liquefaction susceptibility and assessment of landslide hazard (DRM, 2004).

Ansal et al. (2004b) considered the seismic microzonation with the variation of earthquake ground motion and the earthquake source and path characteristics, as well as geological and geotechnical site conditions in a probabilistic manner. Due to the damage distributions observed during past earthquakes, it was understood that the earthquake zonation maps prepared at small scales do not obtain necessary information for risk mitigation at a city scale. According to these scientific and technical experiences, it is more feasible to conduct seismic zonation studies at regional scale and microzonation at local levels with continuously increasing scales (Lachet et al., 1996; Marcellini et al., 1995). The main objective is to estimate precisely the ground motion characteristics during possible earthquakes with the main controlling factors in the seismic microzonation studies.

Natural, engineering and social sciences contribute to the evaluation of earthquake impact on urban areas (Dan, 2005). Accordingly, the integration of seismology and urbanism can be classified into three different stages:

- a. The assessment techniques like seismic microzonation
- b. Planning instruments for visualization and for the strategy development/implementation in both pre- and post-disaster interference like urban zoning
- c. Shared models between the experts involved in decision making for risk management

Local site conditions such as near surface geological conditions or topography, and distance effects can amplify/reduce the peak ground acceleration (PGA) site value (Pitilakis, 2004). Long distance earthquakes can have disastrous effects on high-density urban settlements,

once alluvial soil deposits amplify the ground motion. The microzonation studies increasingly contribute to seismic risk evaluation in urban areas (Dan, 2005). Urban seismic microzonation was researched by Parvez et al. (2004), Moldoveanu et al. (2004), Panza et al. (2001), Ansal (2002), and Faccioli and Pessina (2001). Parvez et al. (2004) initiated a project for an integrated expert system to use seismic microzonation parameters together with information about the earth, environmental, socio-economic and political systems in urban planning processes and to provide well-defined seismic inputs for earthquake resistant building design.

Dan (2005) classified urban microzonation system into three main parts:

1. The earth system consists of regional geologic factors, seismic source and seismic wave propagation and the conditions of local physical geology in seismic microzonation using geological, geophysical and geotechnical data. Pre-event seismic microzonation can be extrapolated in time and location depending on the seismic records for urban planning and building design.
2. The social, economic and political system includes periods given in building codes and disaster regulations.
3. The human-based system (buildings and infrastructure) accounts by vulnerability studies and seismic planning.

Kılıç et al. (2006) divided the investigated area (Zeytinburnu, İstanbul) into 250 m×250 m cells in order to analyze and evaluate the available geotechnical information in terms of microzonation studies. Moreover, representative soil profiles were defined up to bedrock level for each cell based on soil borings conducted at the site. The grid approach in this study has two advantages in terms of microzonation;

- a. To utilize all available data in each cell in order to gain more complete information about the soil profile.
- b. To eliminate the effects of different distances among the site investigation points during GIS mapping procedure.

Representative soil profiles in each grid can be created by considering one or more available borehole data whereas hypothetical soil profiles can be constructed employing the available data in neighboring grids for the grids with no borehole information (Kılıç, 2006).

The obtained results were mapped using GIS techniques applying linear interpolation among the grid points, thus enabling a smooth transition of the selected parameters. The behavior of region during a probable earthquake was investigated through one dimensional response analysis, and microzonation maps were prepared with respect to ground shaking intensity in accordance with the new microzonation manual (Ansal et al., 2004b; Studer and Ansal, 2003).

A methodology for a risk-oriented seismic microzonation (SM) of an urban settlement was presented by Romeo and Bisiccia (2006). Although most SM studies focus on the local seismic response (LSR), the importance of assessing the entire response of the built-up area and providing a set of information for technical purposes were emphasized in this study. Thus, a SM based on the expected damage is more informative than a microzoning based on the expected seismic actions, especially for already urbanized areas according to the study conducted by Romeo and Bisiccia (2006).

Nunziata (2007) mentioned that a reliable seismic response in terms of both peak ground acceleration and spectral amplification is necessary to mitigate the seismic hazard, and explained the best use of noise measurements in four steps:

1. A detailed knowledge of the physical properties of the sub-soil, mostly the Vs velocities, available from the non-linear inversion of Rayleigh group velocities.
2. A realistic estimation of the expected ground motion which takes into account the complete wave-field and the lateral heterogeneities.
3. Evaluation of site amplification effects through the ratio of response spectrum computed at a site in 2-D structural model and the response spectrum computed for 1-D average reference model.
4. Measurement of H/V noise ratios and comparison with computed spectral amplification at the resonance frequency.

As a conclusion, the best use of noise measurements is a rapid, detailed mapping of the spectral amplifications and average physical properties of the sub-soil as mentioned in this study.

Seismic microzonation studies generally involve three stages according to Ince et al. (2008): a) the assessment of seismicity and regional seismic hazard, b) identification of geological structure and fault features, c) the determination of the effects of local geotechnical conditions in the region.

The methodology applied by Irsyam et al. (2008) depends on one-dimensional (1-D) shear wave propagation method for ground response analysis. 1-D method is based on an assumption that all boundaries are horizontal and the response of a soil layers is mostly caused by vertical shear wave propagation from the underlying bedrock. Although the soil layers are sometimes inclined or bended, they are mostly considered as horizontal in previous case studies.

An attempt was made to evaluate the seismic hazard considering local site effects by carrying out detailed geotechnical and geophysical site characterization in Bangalore, India to develop microzonation maps by Anbazhagan and Sitharam (2008). Seismic hazard analysis and the microzonation of Bangalore were introduced in three parts. Firstly, the estimation of seismic hazard was performed using seismotectonic and geological information. Secondly, site characterization using geotechnical and shallow geophysical techniques was conducted. Finally, local site effects were assessed by carrying out 1-D ground response analysis using SHAKE 2000 software (Ordonez, 2004). The methodology for complete seismic microzonation of the study area was formulated by considering the topology, geology, geomorphology and possible hazards during earthquakes in the same study. According to Anbazhagan and Sitharam (2008), the earthquake damage basically depends on three groups of factors: earthquake source and path characteristics, local geological and geotechnical site conditions, structural design and construction features. Seismic microzonation should deal with the assessment of first two groups of factors. For the present investigation, the seismic microzonation was subdivided into three major items: a) evaluation of the expected input motion, b) Local site effects and ground response analysis, and c) preparation of microzonation maps.



## CHAPTER 3

### GEOLOGY, TECTONIC ACTIVITY, AND SEISMICITY OF ERBAA

#### 3.1 Regional Geology and Previous Studies

The sedimentological and structural evolution of sedimentary sequences exposed in the Niksar and Taşova-Erbaa basins have been studied by a number of scientists in order to understand their relationships with the North Anatolian Fault Zone (e.g. Irrlitz, 1972; Tatar, 1975; Barka and Hancock, 1984; Barka, 1984; Barka and Gülen, 1989; Koçyiğit, 1988; 1989; 1990; 1991; Toprak, 1989; Keçer, 1990; Aktimur et al., 1992; Tatar and Park, 1992; Dirik, 1993; Over et al., 1993; Rojay, 1993; Tatar et al., 1995; Andrieux et al., 1995; Bellier et al., 1997; Barka et al., 2000).

The first important study related to the Erbaa basin and its vicinity was performed by Blumenthal (1950) who prepared a 1/100.000 scaled geologic map for the northern part of Kelkit Valley. In addition, Göksu (1960) organized a geologic map covering this area with a scale of 1/500.000. Typical traces of NAFZ including Erbaa basin were studied by Ambraseys (1970). Seymen (1975) divided the units into northern and southern part and concluded that the movement in NAFZ started in Miocene. Öztürk (1979) was the first scientist to name the limestone in Ladik-Destek region as the Doğdu formation. The basement geology of the area between NAFZ and Kırşehir was considered by Özcan et al. (1980). Tutkun and İnan (1982) determined that basement units consist of Paleozoic Turhal group metamorphic rocks and added that they are covered by Doğdu formation with an unconformity. Arpat and Şaroğlu (1975) studied the recent tectonic activities, and Şaroğlu et al. (1987) investigated the active faults in Erbaa basin and their earthquake potential. Barka (1984) stated that Erbaa became a basin within the mountains as a result of compressional regime of northern and southern part of NAFZ. Temiz (1989) and İnan and Temiz (1991) studied the litho- and bio-stratigraphic sections of Niksar-Erbaa region and correlated the geological units with the development of NAFZ movements. On behalf of the General Directorate of Mineral Research and Exploration, Aktimur et al. (1989; 1990; 1992)

investigated the geology of Niksar, Erbaa and Destek areas, and prepared a Tokat D-23 geological map revision with a scale of 1 / 100.000. According to this study, rock-soil units are classified from Permian to Cenozoic ages with different sublayers.

In Yılmaz (1998), preliminary studies for a HPP (hydro-electrical power plant) project in the northern part of Erbaa were presented. In this study, the general geology of Erbaa was revised by Yılmaz (1998). In addition, Yılmaz and Karacan (2002) divided the Erbaa basin into six geological units ranging from Late Jurassic-Early Cretaceous to Quaternary age. From oldest to youngest, they are the Doğdu formation, Kırandağ formation, Eocene volcanic series, Ohtap formation, debris and alluvium.

Furthermore, two different investigations were performed to show the geographical and geomorphological characteristics of Erbaa and Niksar Basins (Yürüdür, 1991; Şahin, 1998). Both researchers investigated the geomorphological depressions and their effects to the formation of topographic units around Erbaa. The tectonic movements and the lithological units were evaluated by the topographic changes in the area. Şahin (1998) confirmed that tectonic subsidence was the main cause of the deposition of the sediments with clastics in these basins and was followed by the erosion of these deposits by the river.

### **3.2 Stratigraphy**

Briefly, rocks of Permian to Cenozoic age can be observed in the close vicinity of Erbaa basin. Turhal group metamorphic rocks (Permian to Triassic) form the basement units. (Figure 3.1) (Aktimur et al., 1990). Lower-Middle Jurassic agglomerate-sandstone and Late Jurassic-Early Cretaceous limestone units overlay basement formations with an unconformity. The Yumaklı formation, which is younger than the former geological units, consists of conglomerate, sandstone, mudstone, shale and marl alternations. The age of the formation is assigned as Late Cretaceous. This formation is overlain by two different Tertiary formations; Akveren and Kusuri. Tertiary units are covered by the Çerkeş formation which represents a detrital environment with an unconformity. The recent geological unit in the Erbaa basin is Quaternary alluvium which can be found in the basement of valleys (Aktimur et al., 1990) (Figures 3.1 and 3.2).

### **3.2.1 Paleozoic units**

#### **3.2.1.1 Turhal group (Ttg)**

Blumenthal (1950) named the basement rock group in the Erbaa basin as Tokat formation. The same basement rocks were described as undifferentiated metamorphic units by Göksu (1960). Özcan et al. (1980) named the basement rocks as Turhal group. The basement rocks crop out in the southern part of Erbaa. Turhal rock group includes an alternation of sandstone, siltstone, limestone, schist and shale with a low-degree of metamorphism. This group is characterized by meta-detritics with a yellowish to grayish color. The age of the basement rock units is assigned as Permian-Triassic by Özcan et al. (1980).

### **3.2.2 Mesozoic units**

#### **3.2.2.1 Seyfe formation (Js)**

The Seyfe formation contains conglomerate, grey to greenish sandstone, mudstone, tuff, and agglomerate, and marl alternation. Some outcrops of these rock types can be observed in the northern part of Kelkit Valley; starting from the eastern part of Çeçkırı Hill to the eastern part of Kelkit River. The thickness of the formation is approximately 400 m and Özcan et al. (1980) pointed out the age of this formation as Early-Middle Jurassic.

#### **3.2.2.2 Doğdu formation (Jkd)**

The Doğdu formation can be observed 5 km away from the eastern part of Erbaa. It contains limestone with interbedded pinkish claystone and marl. The thickness of this formation is almost 400-500 m. The typical outcrops of this formation can be observed along the Erbaa-Niksar road and in the Kelkit Valley. Aktimur et al. (1989) aged the formation as Late Jurassic-Early Cretaceous.

#### **3.2.2.3 Yumaklı formation (Ky)**

The Yumaklı formation consists of an alternation of conglomerate, sandstone, marl, tuff, agglomerate and clayey limestone. The age of the formation is Cenomanian to Campanian

(Aktimur et al., 1989). This formation has 200 m thickness with typical exposures in Karakaya region.

### **3.2.3 Tertiary units**

#### **3.2.3.1 Akveren formation (KPa)**

Akveren formation is exposed in the northern part of the Kelkit Valley. It was first defined by Ketin and Gümüş (1963). The Akveren formation contains limestone, sandstone, marl and tuff. The thickness of the formation reaches up to 500 m. Its age is Late Maastrichtian-Paleocene.

#### **3.2.3.2 Kusuri formation (Tk)**

The Kusuri formation crops out in the northern part of Kelkit Valley. A relationship cannot be observed with the Akveren formation at the site. It is a flysch unit with an alternation of limestone, claystone and marl. The age of the formation was defined as Middle Eocene by Aktimur et al. (1989).

#### **3.2.3.3 Tekkeköy formation (Tt)**

The Tekkeköy formation is partly a combination of volcanic rock groups that contain basalt, andesite, agglomerate, tuff and the alternation of sandstone-siltstone. Its age is Middle-Late Eocene with a thickness of 600 m.

#### **3.2.3.4 Çerkeş formation (Tç)**

The activity of the North Anatolian Fault affects the formation of pull-apart basins (Taşova-Erbaa-Niksar). These basins have been filled with gravelly, sandy, silty and clayey detritics. Especially after Pliocene, the thickness of these layers reached approximately 500 m. Some of the gravelly layers are cemented by  $\text{CaCO}_3$ . In the middle of the basins, fine-grained material can also be seen with the combination of reddish clay and silt which are still used in the brick industry (Canik and Kayabalı, 2000). This formation is observed all around Erbaa, Niksar, Taşova and Destek areas and was first defined by Öztürk (1979). Its thickness can be

as great as 600 m in some areas. The age of the formation is Pliocene and it is overlain by alluvium units with an unconformity.

#### **3.2.4 Quaternary units (Qal, Qk, Qt)**

Gravel, sand, silt, and clay terraces (Qal) exist in the areas along the Kelkit Valley. In addition, the deposition of sand and gravel in river beds is getting thicker, and is joining with alluvial cone (Qk) near the Kelkit River. Quaternary units are characterized by old and new (recent) alluvial deposits by Canik and Kayabalı (2000). Quaternary travertine deposits (Qt) can also be observed in the close vicinity of fault zones.

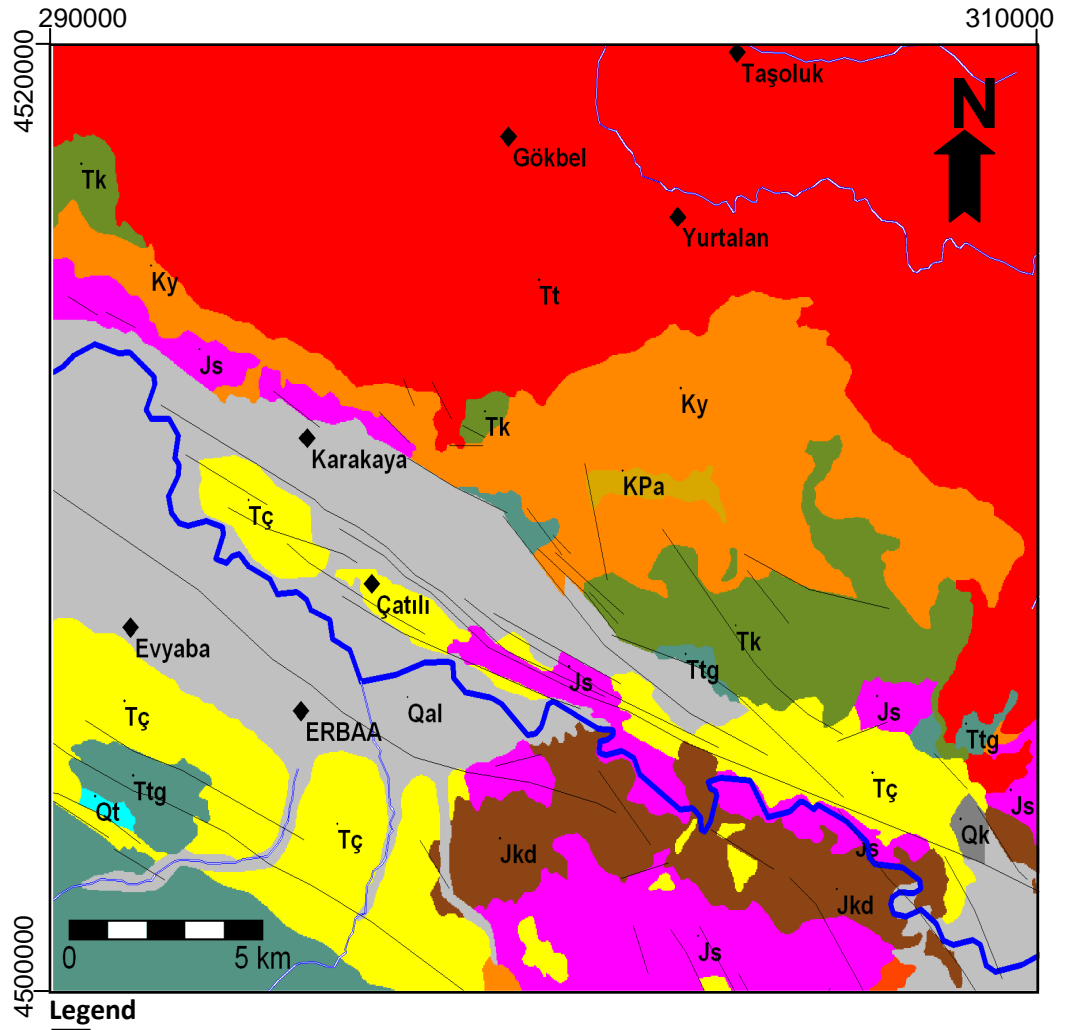


Figure 3.1. Regional geology of the study area (modified from Aktimur et al., 1989)

PERIOD	EPOCH	GROUP	FORMATION	MEMBER	THICKNESS (m)	SYMBOL	LITHOLOGY	EXPLANATION
QUATERNARY						Qal, Qk, Qt		Alluvium, alluvium cone, travertine
TERTIARY		PLIOCENE		Yolüstü basalt		TQy		Basalt
			Çerkeş		500	Tç		Gravel, sand, silt and clay
		EOCENE				Tt		Basalt, andesite, tuff, agglomerate, sandstone
			Tekkeköy Çekerek		650	Tçe		Basalt, andesite, tuff, agglomerate, sandstone
		PALEOCENE				Tk		Volcano-clastics
			Kurşun		750	Tk		Conglomerate, sandstone, claystone, marl
		Upp. Mast. Paleocene				KPa		Marl, claystone, clayey limestone
			Akveren Çatalçeşme		500	KPa		Limestone
		Mast.				Kt		Volcano-clastics - flisch
			Tersakan		500	Kt		Volcano-clastics - flisch
CRETACEOUS		UPPER CRETACEOUS				Kk		Ophiolitic melange thrust
			Artova ophiolitic Yumaklı melange			Kk		Ophiolitic melange thrust
		Cenomanien-Campanien				Kyk		Micrite
			Gökçebel Kapanboğazı Harmankaya		2000	Kyk		Turbiditic flisch
						Kyh		Crystallised tuff
						Kyg		Sandstone, claystone, tuff
		LOWER CRETACEOUS				Jkd		Limestone
			Doğdu		450	Jkd		Limestone
		SEYFE				Js		Agglomerate, tuff, sandstone
			Seyfe		400	Js		Agglomerate, tuff, sandstone
PERMIAN	TRIASSIC					Ttg		Limestone
PERMO-TRIASSIC	PERMO-TRIASSIC							Recrystallised limestone, marble, metamorphics

Figure 3.2. Stratigraphic columnar section of the study area and its vicinity (modified from Aktimur et al., 1989)

### 3.3 Tectonics

The North Anatolian Fault Zone (NAFZ) is one of the best known strike-slip faults in the world, and has a number of pull-apart basins with different origins along its trace. NAFZ is a 1500 km long, seismically active, right lateral strike slip fault that takes up to the relative motion between Anatolian Plate and Black Sea Plate (Şengör et al., 1985). This right-lateral motion has been interpreted as a consequence of the westward motion of Anatolia away from compressive zones in eastern Turkey (McKenzie, 1972; Şengör, 1979). This zone extends from eastern Turkey to Greece (Şengör, et al., 1985; Ketin, 1968; 1969; Ambraseys, 1970; McKenzie, 1972; Dewey, 1976; Kiratzi, 1993, Bozkurt, 2001a). It forms a broad arc separating the tectonically active Northern Turkey province from the Anatolian plate (Figure 3.3). It is one of the major tectonic regimes of Turkey that forms a continental triple junction with the other strike slip fault (East Anatolian Fault Zone-EAFZ) in the eastern part and this zone connects with the EAFZ at the Karlıova-triple junction (Ketin, 1948; Ambraseys, 1970; Şengör et al., 1985; Bozkurt, 2001a). Tchalenk (1977) emphasizes that this fault zone also continues towards the southeast region. In the western part it splays into several strands near the Marmara Sea that covers an area approximately 40 km wide (Taymaz et al., 1991; Barka, 1992).

According to the study conducted by Bozkurt (2001b), the age and cause of dextral (right-lateral) movement along NAFZ are controversial, and there are different approaches for this topic. In brief, the age of this fault zone is estimated to be Late Middle Miocene - Early Pliocene (~5 Ma) (Barka and Kadinsky-Cade, 1988).

The total offset on the fault zone has been estimated to be as high as 350 km by Pavoni (1961). However, most studies estimate the total offset of the NAFZ in the western part as ranging from  $85 \pm 5$  km to 20-25 km depending on the different geological approaches (Şengör, 1979; Şengör et al., 1985; Barka, 1992; Armijo, et al., 1999). Seymen (1975) suggested an  $85 \pm 5$  km offset by correlating two ends of the Neothetian suture zone. Barka and Gulen (1989) and Barka (1992) reported that the total offset of the lithological boundaries is more likely to be 25– 45 km. More recently, Armijo et al. (1999) pointed out that the offset along the fault in the Marmara Sea region is about 85 km. The rate of motion is assumed as 10 mm-40 mm per year (Taymaz et al., 1991; Barka, 1992; Westaway, 1994). Conversely; GPS measurements indicated that these rates change between 15 and 25 mm in a year (Taymaz et al., 1991; Ayhan et al., 1995; Reilinger et al., 1997).



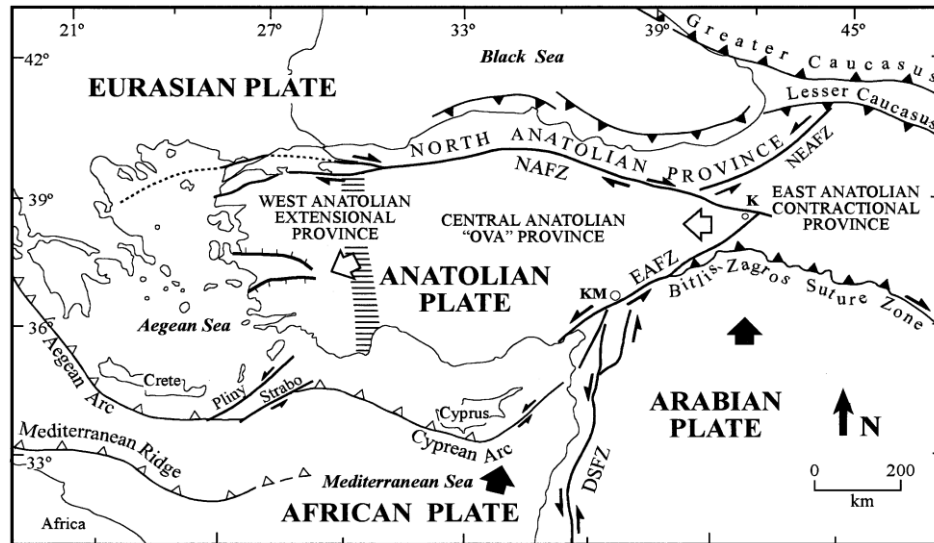


Figure 3.3. Simplified tectonic map of Turkey showing major neotectonic structures and regimes (from Şengör et al., 1985; Barka, 1992; Bozkurt, 2001b) (K – Karlıova, KM – Kahramanmaraş, DSFZ – Dead Sea Fault Zone, EAFZ – East Anatolian Fault Zone, NAFZ – North Anatolian Fault Zone, NEAFZ – Northeast Anatolian Fault Zone)

Between 1939 and 1967, the NAFZ ruptured by a westward propagating series of nine large earthquakes that had magnitudes greater than 6.7, and formed almost 1000 km long surface rupture (Allen, 1969; Ketin, 1969; Ambraseys, 1970; Bozkurt, 2001b) (Figure 3.4) (Table 1).

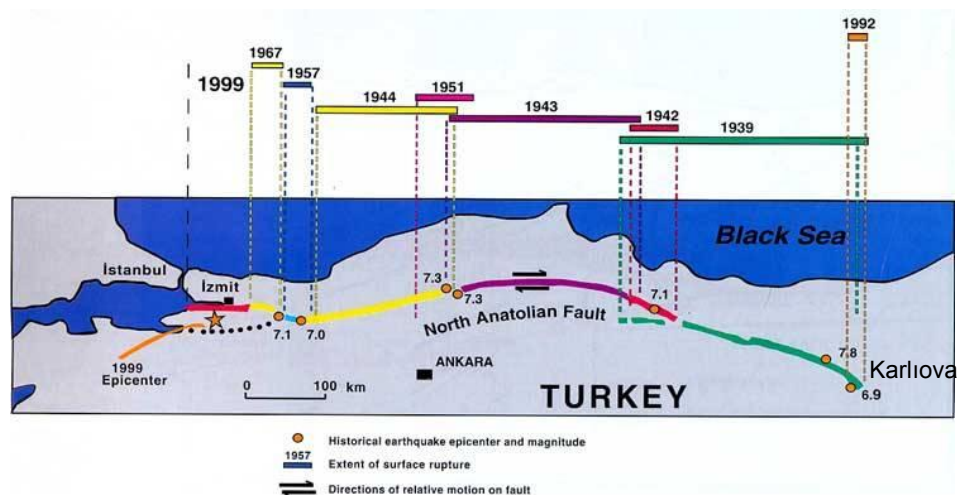


Figure 3.4. North Anatolian Fault Zone and some important surface ruptures occurred during different earthquakes (from USGS, 2007)

Table 3.1. Nine earthquakes occurred along the NAFZ from 1939 to 1999 (modified from Lorenzo-Martin, 2006)

Earthquake	Location	Magnitude $M_s$	Surface rupture (km)*	References
26 December 1939	Erzincan	8.0	360	2, 3, 5, 7
20 December 1942	Erbaa-Niksar	7.2	50	2, 3, 5, 7
26 November 1943	Tosya	7.6	280	2, 3, 5, 7
1 February 1944	Bolu–Gerede	7.3	165	2, 3, 5, 7
26 May 1957	Abant	7.0	30	2, 3, 5, 7
22 July 1967	Mudurnu valley	7.1	80	1, 2, 3, 5, 7, 13
13 March 1992	Erzincan	6.8	-	4, 5, 6, 8, 9
17 August 1999	Kocaeli	7.4	125 <sup>#</sup>	11, 12, 13
12 November 1999	Düzce	7.1	43 <sup>#</sup>	10, 11, 14, 15
1 Ambraseys and Zatopek, 1969;		10 Ayhan et al., 2001;		
2 Ambraseys, 1970;		11 Tibi et al., 2001;		
3 Dewey, 1976;		12 Wright et al., 2001;		
4 Barka and Kadinsky-Cade, 1988;		13 Barka et al., 2002;		
5 Saroglu et al., 1992;		14 Utkucu et al., 2003;		
6 Pinar et al., 1994;		15 Umutlu et al., 2004.		
7 Barka, 1996		*approximately given in USGS (2008)		
8 Nalbant et al., 1996;		# Herece, 1999; Arpat et al., 2001;		
9 Grosser et al., 1998;		Herece and Uysal, 1999		

According to Stein et al. (1997) study, four westward mitigating earthquakes from 1939 to 1944 caused totally 725km surface rupture with an extension to both directions and the mitigation progress are still alive for two directions (Figure 3.5).

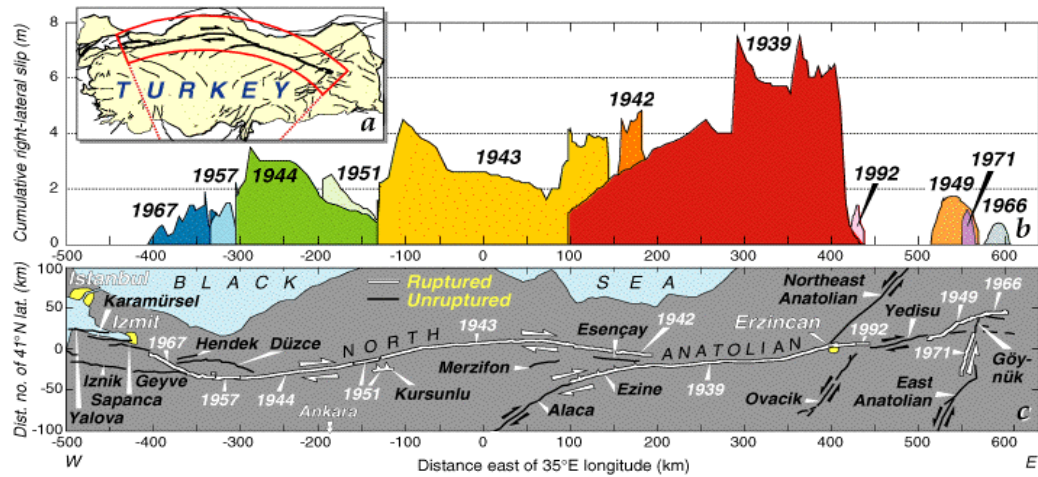


Figure 3.5. North Anatolian Fault Zone and its earthquake history (a,b,c) (from Stein et al., 1997)

The stratigraphy and structures of the pull-apart basins formed by NAFZ have been studied by numerous scientists (Barka and Hancock, 1984; Barka, 1984; Barka and Gülen, 1989; Koçyigit, 1989, 1990; Tatar and Park, 1992; Andrieux et al., 1995; Bellier et al., 1997), to point out their relationships with the North Anatolian Fault. These studied adjacent pull-apart basins, the Taşova-Erbaa and Niksar basins, which had destructive earthquakes in 1939 and 1942, were also explored by different researchers (Tatar et al., 1990; Tatar and Park, 1992; Barka et al., 2000). These two pull-apart basins are narrowly connected and sometimes defined as two different formations and sometimes grouped as a single unit (Figure 3.6).

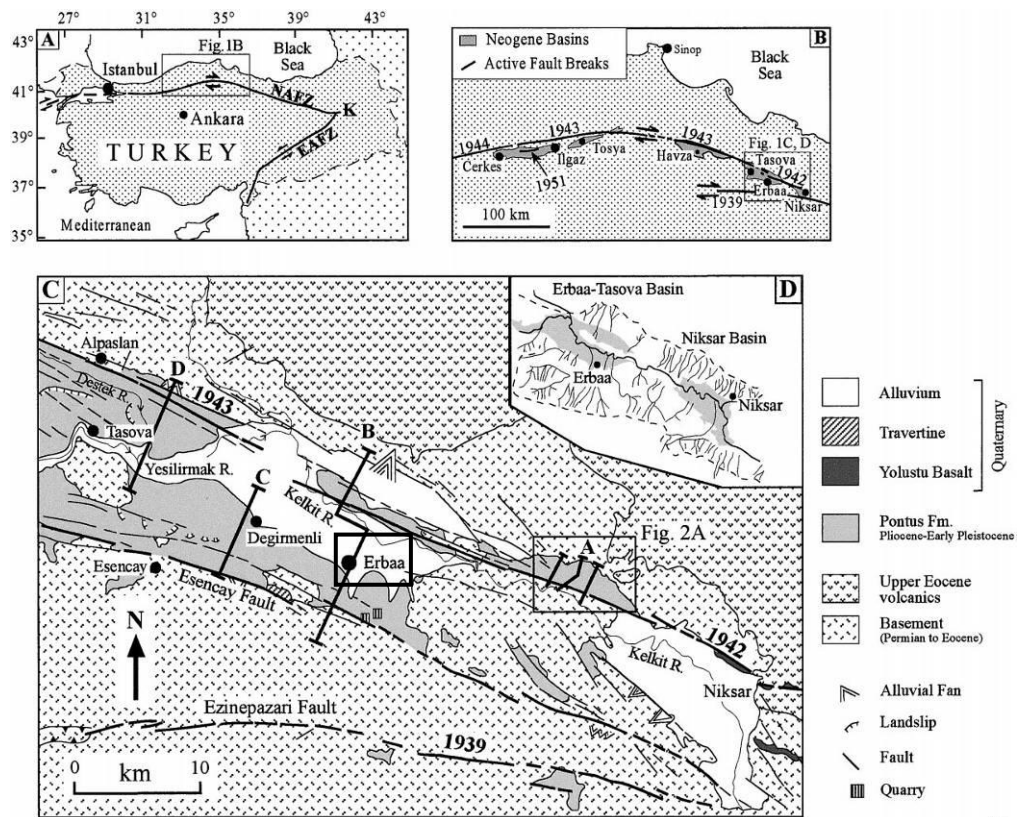


Figure 3.6. (A) Map of Turkey showing location of the North Anatolian (NAFZ) and the East Anatolian (EAFZ) Fault Zones. (B) Central portion of the NAFZ with locations of major Neogene and Recent basins. (C) Simplified geological map of the Taşova-Erbaa and Niksar basins showing basement units and positions of modern-day basins (modified from Aktimur et al., 1992). Neogene sediments of basins are grouped together as the Pliocene-Early Pleistocene Pontus Formation. Positions of structural cross-sections in subsequent figures are indicated by thick black lines. (D) Present-day drainage basins of the Taşova-Erbaa and Niksar basins (from Barka et al., 2000)

The present study area, Erbaa basin, is located on the eastern part of the NAFZ and is bounded near its northern margin by fault segments that ruptured in the 1942 and 1943 earthquakes. Surface ruptures of 1939, 1942 (M=7.2) and 1943 (M=7.6) earthquakes occurred in Taşova-Erbaa and Niksar basins (Barka et al., 2000). Barka et al. (2000) emphasized that Taşova-Erbaa basin is a present-day morphological depression, asymmetrically bounded by historically active fault traces and approximately 65 km long and 15-18 km wide (Figure 3.6). Neogene-Recent sediments of this basin are currently being cut into by the drainage systems, and are therefore exposed at the surface. The southern margin is bounded by the Esencay fault, which has a distinct morphological expression; however, no instrumental and/or historical earthquakes have been reported, yet.

Many researchers have studied the fault strands that occur around Erbaa (Koçyiğit, 1989; 1990; Bozkurt and Koçyiğit, 1995; 1996; Westaway, 1998; Toprak, 1994; Dirik and Göncüoğlu, 1996; Koçyiğit and Beyhan, 1998; Kaymakçı, 2000). Various fault zones (Almus, Yağmurlu- Ezinepazarı, Taşova - Çorum, Göksun - Yazıyurdu, Malatya - Ovacık and Central Anatolian Fault Zone) splayed from NAFZ can be seen in Figure 3.7. The historical and instrumental earthquake records show that the eastern parts of Central Anatolia are seismically less active than the NAFZ (Bozkurt, 2001b).

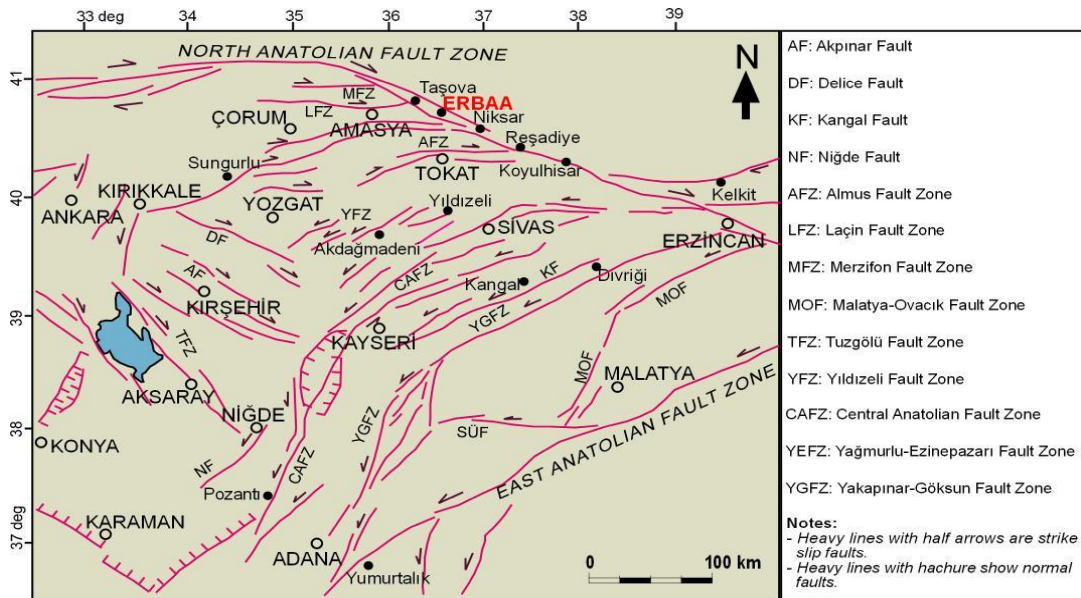


Figure 3.7. Simplified map showing major structural elements of east Central Anatolia (modified from Koçyiğit and Erol, 2001; Bozkurt and Koçyiğit, 1996; Şaroğlu et al., 1992; Dirik and Göncüoğlu, 1996; Bozkurt, 2001b)

### 3.4 Seismic Activity of Erbaa and Close Vicinity

The tectonic evolution of the Eastern Mediterranean region is dominated by the effects of subduction along the Hellenic (Aegean) arc and of continental collision in eastern Turkey (Anatolia) (Sato et al., 2004; Taymaz, 1990; Taymaz et al., 1991). The Anatolian plate locates in the upper part of the Arabian and African plates (Figures 3.8 and 3.9). Therefore, the movement of these plates causes seismic activity in Turkey. As a result, Turkey is known as one of the earthquake-prone countries in the world. Two important fault zones in Turkey, the North Anatolian Fault and the East Anatolian Fault Zones formed as a result of this tectonic activity. A combination of topography, bathymetry and earthquake epicenter distributions for Turkey and its vicinity can be observed through the broad period with magnitudes,  $M > 4.0$  (Figures 3.8 and 3.9). In addition, GPS movement vectors completely support the exact structure and movement among the different plates.

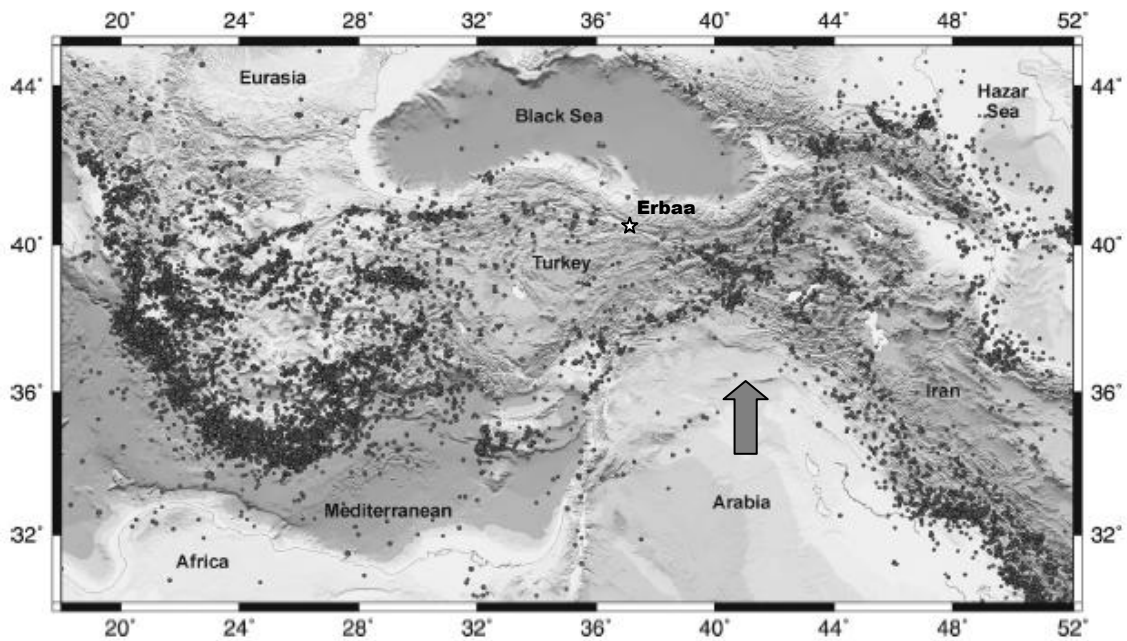


Figure 3.8. Seismicity of the eastern Mediterranean region for the period of 1964-2001 with magnitudes,  $M > 4.0$  (modified from Taymaz et al., 2001)

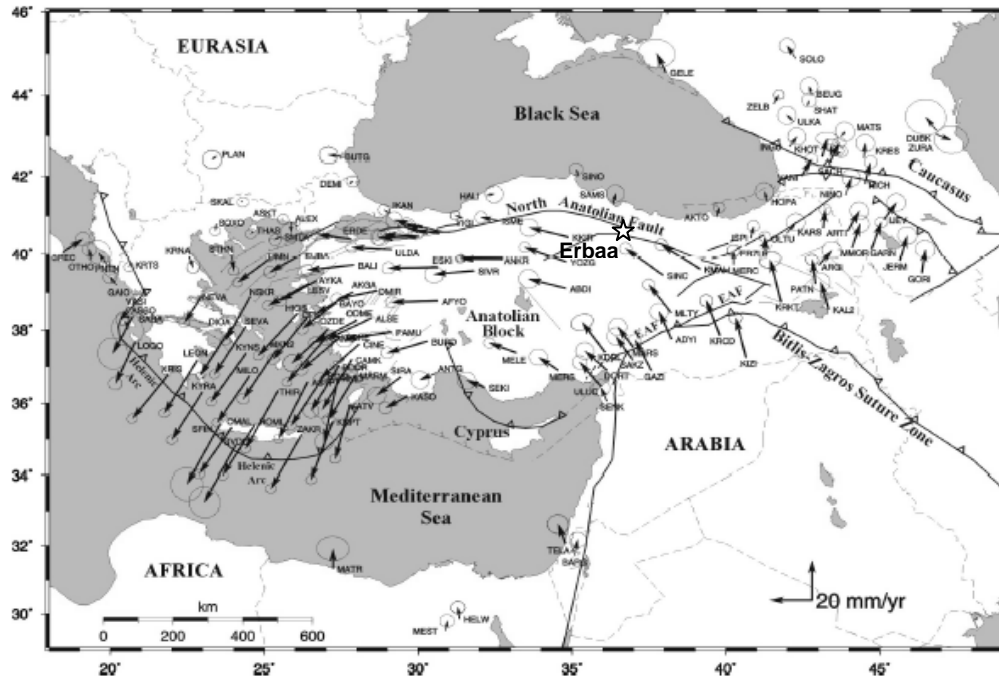


Figure 3.9. GPS horizontal velocities and their 95% confidence ellipses in a Eurasia-fixed reference frame for the period 1988-1997 at 189 sites extending east-west from the Caucasus mountains to the Adriatic Sea and north-south from the southern edge of the Eurasian plate to the northern edge of the African plate (modified from Taymaz et al., 2001)

Between 1939 and 1999, nine large fault ruptures formed a westward-migrating sequence of events along a 1000-km long nearly continuous portion of the North Anatolian fault (as mentioned in Table 3.1). The migration of earthquake sequences was evaluated by Demirtaş and Yılmaz (1996) and Stein, et al. (1997). These studies showed that seismic gaps occurred on the North Anatolian Fault Zone with the inventory of several earthquakes, and that fault segments could be differentiated. These gaps with the North Anatolian Fault Zone surface ruptures can be observed in Figure 3.10.

According to Demirtaş and Yılmaz (1996), the relationship between the possible seismic gaps and active segments can be defined. Thick solid lines represent the segments of active fault zone and the circles filled with horizontal solid lines show the possible seismic gaps for this fault zone (Figure 3.10). So, the active tectonic regime on the North Anatolian Fault Zone can give possible evidences for the area of seismic gap.



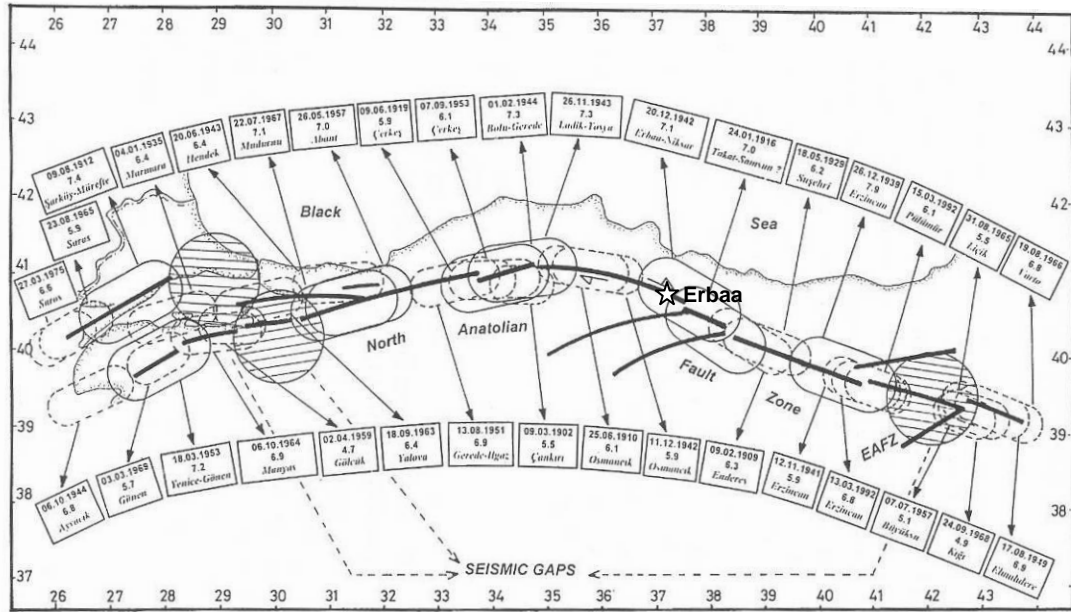


Figure 3.10. Seismic gaps for the North Anatolian Fault Zone (modified from Demirtaş and Yılmaz, 1996)

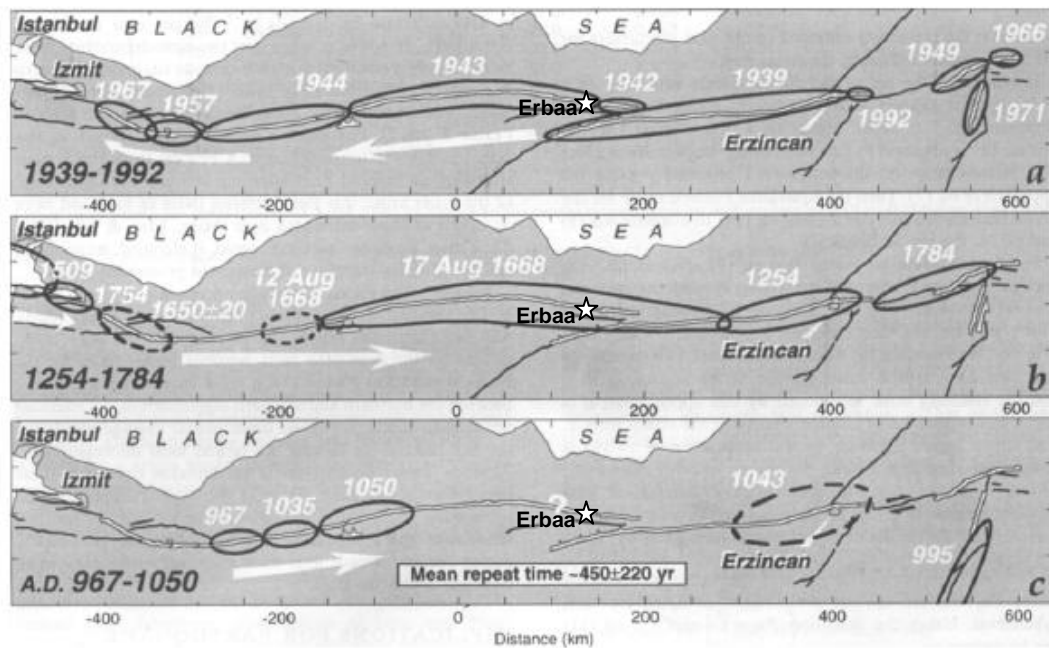


Figure 3.11. Rupture zones for large historical earthquakes (modified from Stein et al., 1997)

Besides, Stein et al. (1997) mentioned that stress distribution depending on the propagation of earthquakes is changing from time to time, which can be explained with some gaps or some of the big earthquake activities. The important rupture zones for large historical earthquakes are shown in Figure 3.11. The sequences of earthquakes indicated by white arrows occurred in different directions on NAFZ. The migration of these earthquakes can be related to their cumulative stress changes with the Coulomb stress calculations (Figure 3.12) (Stein et al., 1997).

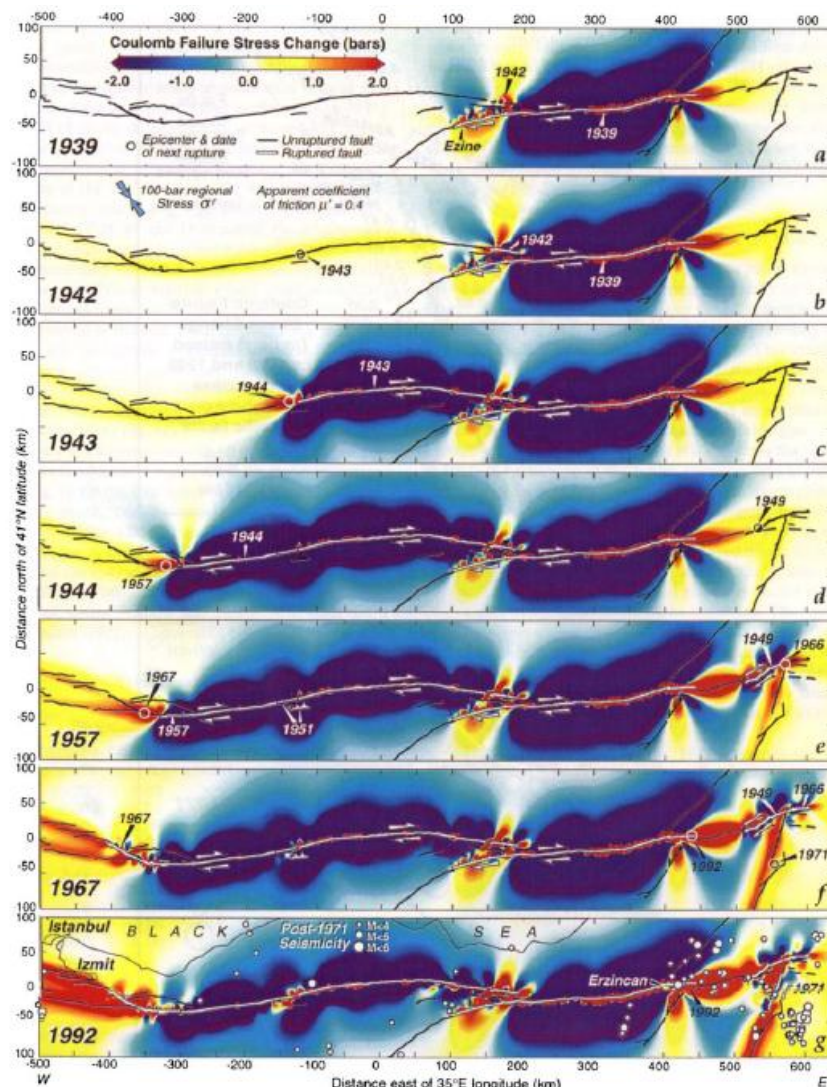


Figure 3.12. Stress distributions based on important earthquakes on the NAFZ (Stein et al., 1997)



During the 1900s, several earthquakes occurred in this region. Erbaa is considered in the First Degree Earthquake Zone of Turkey (General Directorate of Disaster Affairs, 2008) (Figure 3.13 and Figure 3.14). As mentioned previously, Erbaa is one of the important seismic areas on the North Anatolian Fault Zone with past seismic activity. 1942 Niksar-Erbaa earthquake is the most destructive earthquake for the Erbaa region. Because of this earthquake, the city had to be moved to the southern part of the old settlement. Furthermore, three of the seismic gaps mentioned in the study of Demirtaş and Yılmaz (1996) along the North Anatolian Fault Zone can be observed in Figure 3.11. Although three seismic gap zones are indicated for the NAFZ in this figure, Erbaa and its close vicinity can also be questioned as an additional seismic gap if the return period of 1942 Erbaa-Niksar earthquake is considered. As evidence, no seismic activity is recorded since 1942 Erbaa-Niksar earthquake in this region.

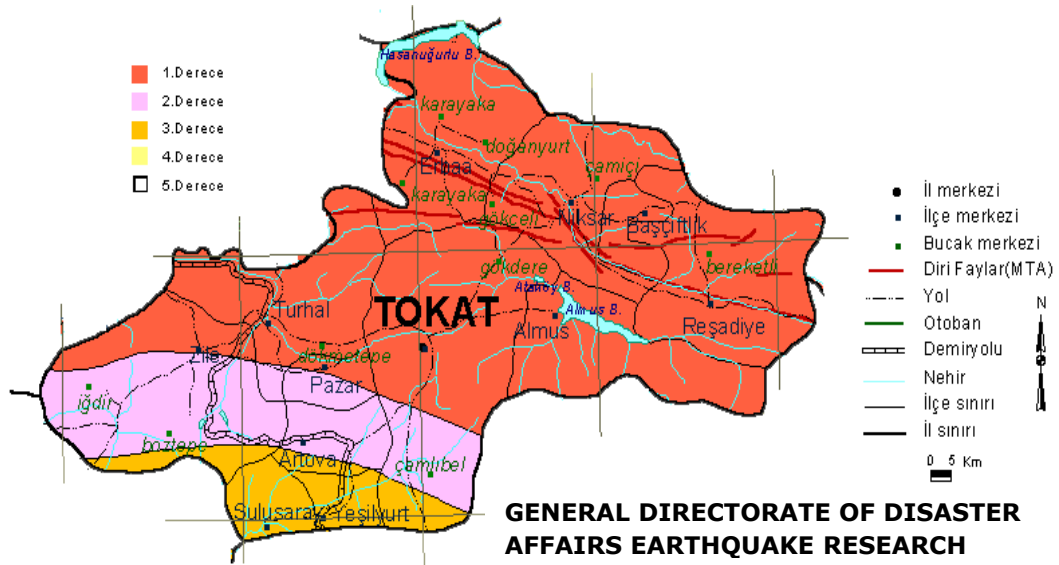


Figure 3.13. Allocation of seismic zones for the city of Tokat and its towns (after General Directorate of Disaster Affairs, 2008)

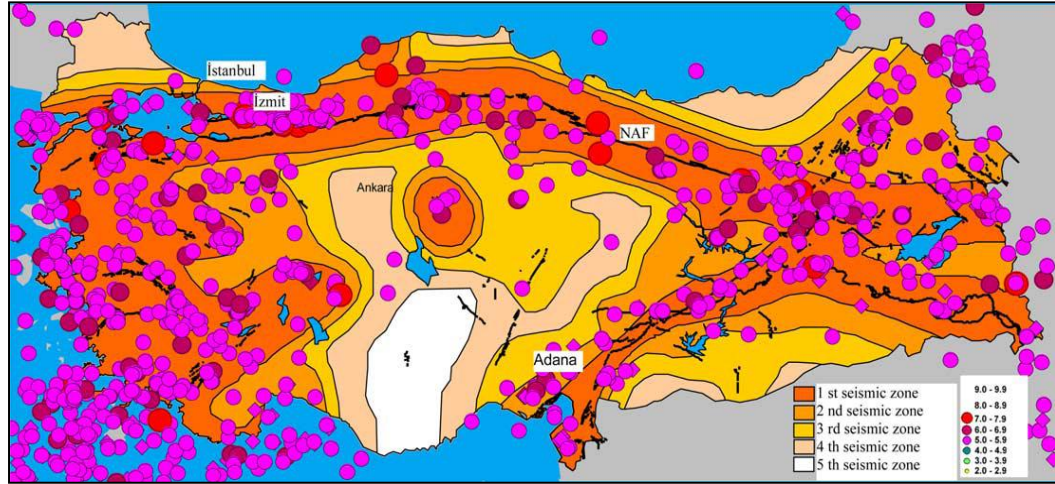


Figure 3.14. Earthquake zoning map of Turkey (Gulkan et al. (1993) (The zones in the map are classified as being apt to acceleration values characteristic of 1st, 2nd, 3rd, 4th, and 5th degree earthquakes: higher than 0.4 g, between 0.3 and 0.4 g, between 0.2 and 0.3 g, between 0.2 and 0.1 g, lower than 0.1 g ( $g = 981 \text{ cm/s}^2$ ), respectively.  $M_w \geq 5$ ) (from Çağatay, 2005)

Seismic activities of Erbaa and vicinity through broad period with magnitudes,  $M > 5.5$  are summarized in Table 3.2.

### 3.5 Geology of the Study Area

The study area and its close vicinity contain mainly Pliocene and alluvial deposits. Kecer (1990) classified the Pliocene (Neogene) units as combinations of gravel, sand, clay, marl and uncemented sandstone as well as conglomerate in the study area. Although the Pliocene deposits consist of coarse clastic materials, fine content is increasing through the southern part of the Erbaa plain. According to Aktimur et al. (1989), the alluvial units mostly cover half of the 1/25000 scale map (Figure 3.15). Pliocene units ( $T_c$ ) named as Çerkeş formation consists of clay, silt, sand, gravel and uncemented sandstone layers. Turhal group sedimentary and metamorphic rocks crop out in the southern part of the study area under the Pliocene units with an unconformity. The other geological units shown in Figure 3.16 are exposed in the northern part of the Kelkit River valley, and are considered to be beyond the scope of this study.

The fault zones shown in Figure 3.15 indicate surface ruptures of the NAFZ (Tatar et al., 2006; 2007). There are two different rupture zones that can be distinguished in the Pliocene

and alluvial deposits. One branch of 1942 Niksar-Erbaa earthquake surface rupture is quite close to the old settlement of Erbaa. The other surface ruptures mapped in the southern part of Erbaa are represented as the Esençay Fault Zone (Tatar et al., 2006). The same fault zone is also mentioned in Stein et al. (1997) without describing any surface rupture (Figure 3.16).

Table 3.2. Seismic activity of Erbaa and its vicinity

<b>Date</b>	<b>Location</b>	<b>M<sub>w</sub> ≥ 5.5</b>	<b>Northing</b>	<b>Easting</b>
04.04.1543 <sup>(1)</sup>	Tokat and Erzincan	?	?	?
1688 <sup>(1)</sup>	Amasya-Niksar	?	?	?
1909 <sup>(2,4)</sup>	Erbaa & its vicinity	6.3	40,0	38,0
1909 <sup>(2)</sup>	Erbaa & its vicinity	5.8	40,0	38,0
1909 <sup>(2,4)</sup>	Erbaa & its vicinity	5.7	40,0	38,0
24.01.1916 <sup>(2,4)</sup>	Tokat	7.1	40,27	36,83
1923 <sup>(2)</sup>	Erbaa & its vicinity	5.9	40,07	36,43
1929 <sup>(2,3,4)</sup>	Erbaa & its vicinity	6.1	40,2	37,9
1935 <sup>(2,3)</sup>	Erbaa & its vicinity	5.5	33,99	38,14
1939 <sup>(2)</sup>	Erbaa & its vicinity	5.7	40,47	37,0
26.12.1939 <sup>(2)</sup>	Erzincan	7.9	39,80	39,51
1940 <sup>(2)</sup>	Erbaa & its vicinity	6.2	39,64	35,25
1941 <sup>(2,4)</sup>	Erbaa & its vicinity	5.7	39,68	35,31
20.12.1942 <sup>(2)</sup>	Niksar-Erbaa	7.1-7.2	40,87	36,47
26.11.1943 <sup>(2,3,4)</sup>	Tosya-Ladik	7.2-7.3	41,05	33,72
1943 <sup>(2)</sup>	Erbaa & its vicinity	5.6	41,0	37,9
1944 <sup>(2)</sup>	Erbaa & its vicinity	5.5	41,1	34,87
1960 <sup>(2,4)</sup>	Erbaa & its vicinity	5.9	40,19	38,75
13.03.1992 <sup>(1,2,3)</sup>	Erzincan	6.8	39,72	39,63
15.03.1992 <sup>(2,4)</sup>	Erzincan	5.8	39,53	39,93

References:

- 1) Ambraseys and Finkel, 2006
- 2) Özmen et al., 1997
- 3) Ayhan et al., 1984
- 4) İnan et al., 1996



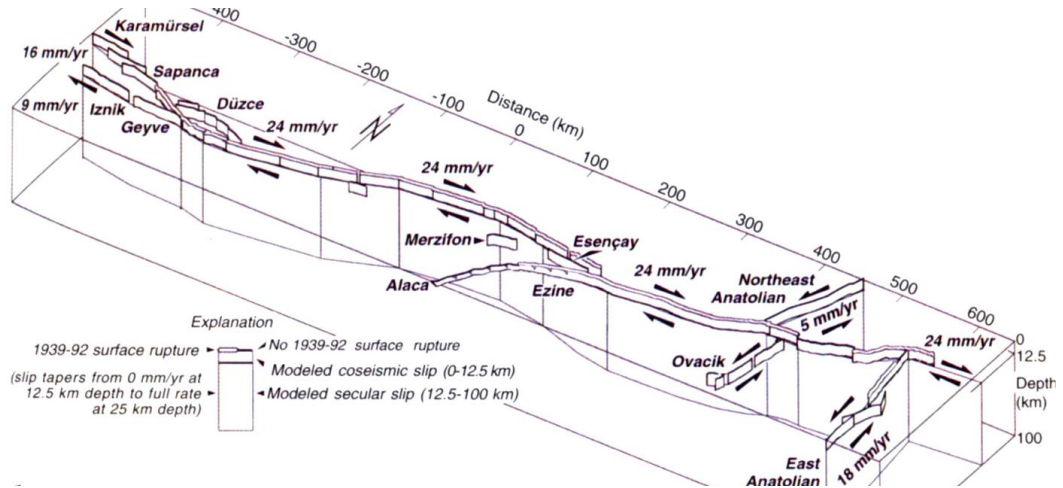


Figure 3.16. Sectional sketch of the NAFZ with the Esençay Fault segment (from Stein et al, 1997)

The geographical and geomorphological variations in the study area were investigated by two different studies (Yurudur, 1991; Sahin, 1998). The researchers mainly studied the Erbaa plain and the effects of the NAFZ. In the study of Yurudur (1991), the alluvial units are described as random alternation of gravel, sand, silt and clay materials. As a result, the alluvial plains are formed by the deposition from the Kelkit River and/or other creeks of Yesilirmak River sediments. Moreover, terrace units are also mentioned in these two studies. According to Yurudur study, (1991), the terrace units can be observed in the Kelkit and Yesilirmak River beds with three different stages. One of the places where these stages of the terrace deposits can be seen is in the old Erbaa settlement called “Dedembahçe Region”. The geological units in Erbaa are evaluated from the point of geomorphological changes in Sahin (1998). Contrary to Yurudur’s findings (1991), more general explanation is given for the terrace deposits instead of a detailed differentiation. It is stated that the northern part of Erbaa was mostly affected by subsidence mechanism caused by the NAFZ ruptures. Therefore, the depositional variations can be observed around river beds.

The Erbaa settlement area was studied by Canik and Kayabalı (2000) from the seismicity point of view. Owing to their study, geological and geotechnical evaluations are performed and it is concluded that the Quaternary alluvial units and the Pliocene aged detritics most extensively cover the study area (Figure 3.17). While the northern part of the settlement area is positioned on the alluvial units; the Pliocene aged clay, silt, sand, gravel and sandstone

layers dominate in the southern part. It should also be noted that the same Pliocene units are also mapped by Aktimur et al. (1989) as Çerkeş formation. They mentioned that there are gravel and sand terrace deposits in areas along Kelkit River Valley. In addition, the deposition of sand and gravel in the river beds is becoming thicker and is joining with an alluvial fan near the Kelkit River. On the basis of the study by Canik and Kayabalı (2000), the Quaternary alluvial units can be differentiated as old and recent deposits (Figure 3.17). They defined that old alluvium is divided into Upper and Middle Terraces which were formed by the Kelkit River. The Upper Terrace level contains mostly river material with loose sediments such as gravel, sand, silt and clay layers and these materials merge with Imbat river deposits around old Erbaa settlement. The Middle Terrace level consists of gravel, sand, clay and silt detritics along the embankments of the Kelkit River. Lower Terrace level involves recent alluvial deposits, alluvial fan and river alluviums in Kelkit River bed. Lower Terrace is not well compacted and it is below 1-3 m lower level of the Middle Terrace. Alluvial fan consists of gravel, sand and silts in the downstream of the Imbat river and the river alluvium is defined as gravelly-sandy loose material. Moreover, the thickness of the river alluvium is given as less than 1-2 m (Canik and Kayabalı, 2000). The surface ruptures or segments of the North Anatolian Fault Zone could not be noticed in the geological map of Canik and Kayabalı (2000) (Figure 3.17).

In this thesis study, Erbaa settlement is also evaluated from geological perspective considering the previous studies, field observations and in-situ field tests. Erbaa settlement is mainly located on the Erbaa Basin which consists of Pliocene deposits and Quaternary deposits (Figure 3.18). Eventually, the geological map of the Erbaa region is revised. The revised map of the study area is taken into consideration in overlay analyses as a final geological map.

One of the main geological units observed in the Erbaa region is Pliocene deposits (Figure 3.18). First of all, these deposits can be distinguished by their densities. The field tests represent that they have a denser structure than the other alluvial units. They mainly consist of uncemented gravel, sand and occasionally uncompact sandstone layers. The groundwater level is assumed to be deeper, since 30 m deep boreholes opened during the thesis study in this geological unit are all dry. The Pliocene deposits are mainly observed towards the hills in the southern part of the settlement. The properties of this unit can easily be discriminated from the alluvium by physical appearance and density characteristics as well (Figures 3.18 and 3.19).



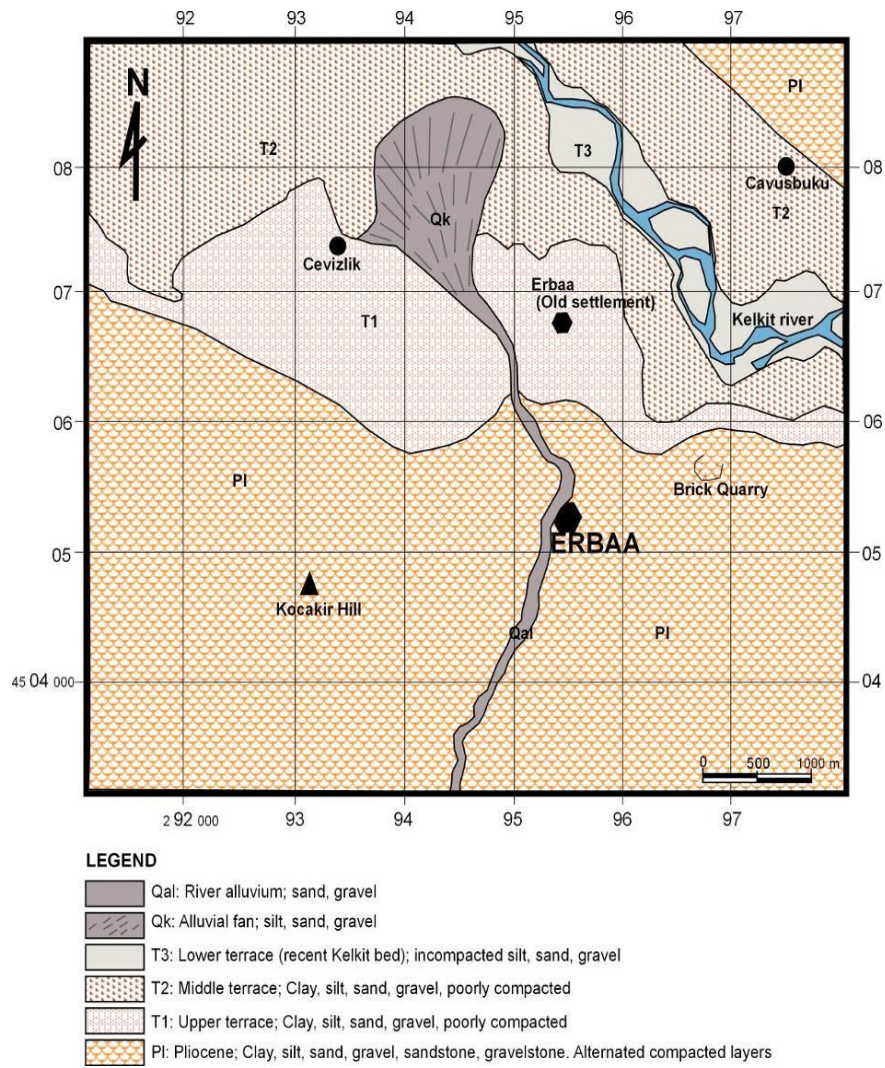


Figure 3.17. Geological map of Erbaa (modified from Canik and Kayabali, 2000)



Figure 3.18. A general view of Pliocene units

Alluvial fans are not very common in the study area and can only be observed in the Imbat River and its surrounding. They are related to the depositional energy of the river. They can be easily seen around flood channels that have been built by the authorities to prevent flooding problems (Figure 3.20). The alluvial fans do not spread over a wide area in the Erbaa Basin (Figure 3.21).



Figure 3.19. A close-up view of Pliocene units



Figure 3.20. A general view of Imbat River bed



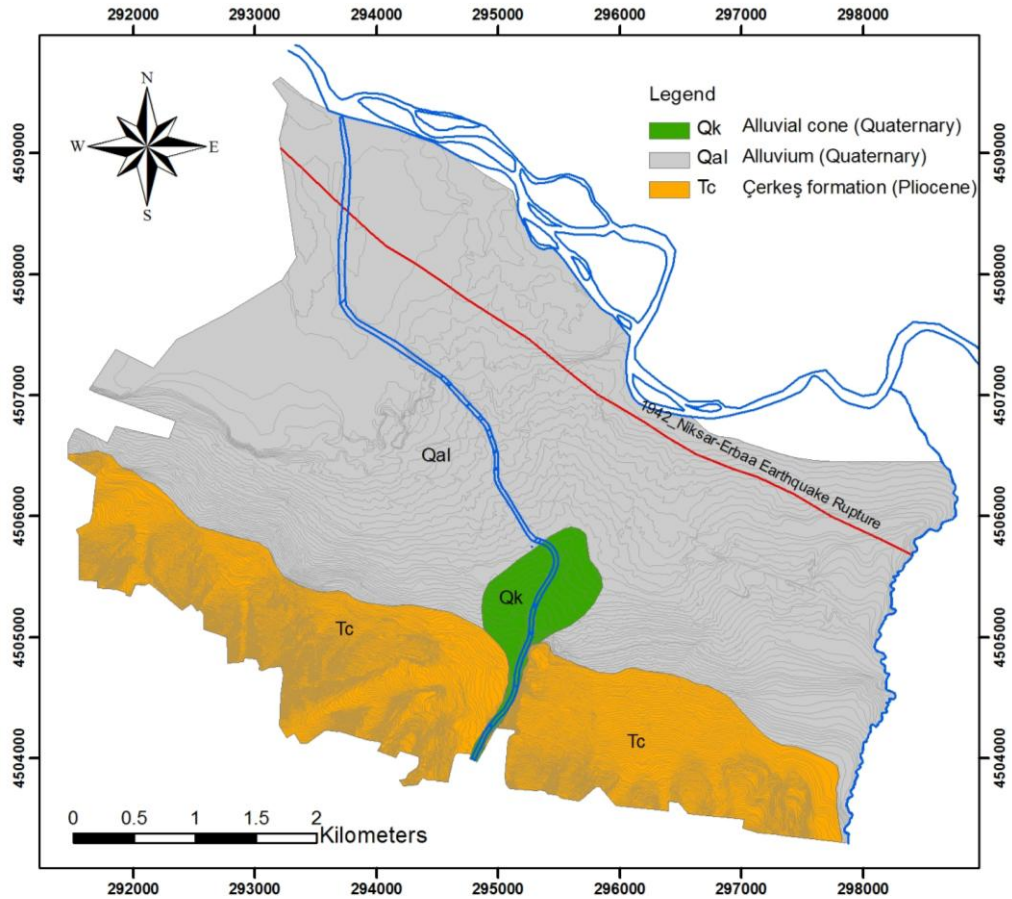


Figure 3.21. Revised geological map of the study area

The alluvium represents the main deposits that widely cover the study area as shown in Figure 3.21. The thickness of the alluvium nearby the northern part (Kelkit River part) is greater than that of the southern part. A variety of sediments with different grain size in this unit can be observed depending on the flow energy and regimes of the Kelkit River (Figures 3.22-3.25). For this reason, vertical or horizontal variations, sometimes from coarse material to fine material or vice versa, are quite common in the same unit. The alluvium contains stratified materials of heterogeneous grain sizes, derived from various geological units in the vicinity. The alluvium in the Erbaa region consists of gravelly, sandy, silty, clayey layers (Figure 3.23). The gravel size generally ranges between 2 and 5 cm. The gravels are well-rounded in shape and well-graded with grey color. Their continuities cannot be recognized laterally and vertically, as wedges and lenses are locally observed. The sandy layers occasionally include small gravels and they are rounded shape. They are light brown, medium dense to dense with poorly-well graded particles (Figure 3.26). The density of the

layers varies with distance to the river; the sandy layers start to lose their densities towards the river. The silty layers also include some clay and sand particles, and they are medium plastic with brown color. The clay layers are medium-high plastic with dark green to light brown in color. The alluvium has a generally shallow groundwater level, especially in the northern part of Erbaa towards the Kelkit River (Figure 3.27).

According to the field study, the terrace deposits defined by previous researchers were rarely recognized around the Kelkit River bed. However, the terrace units cannot be continuously traced in the field. Therefore, they are included into alluvial deposits regarding similar geotechnical properties obtained from in-situ tests and test samples in the study area.



Figure 3.22. A sectional view of alluvial units in the study area

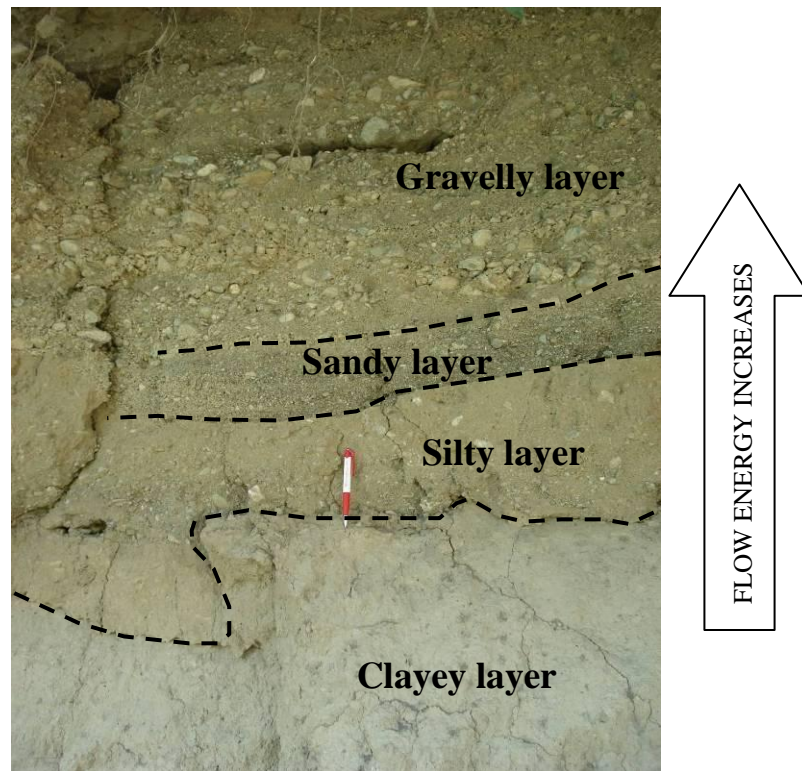


Figure 3.23. Alternation of different grain sizes in the alluvial units

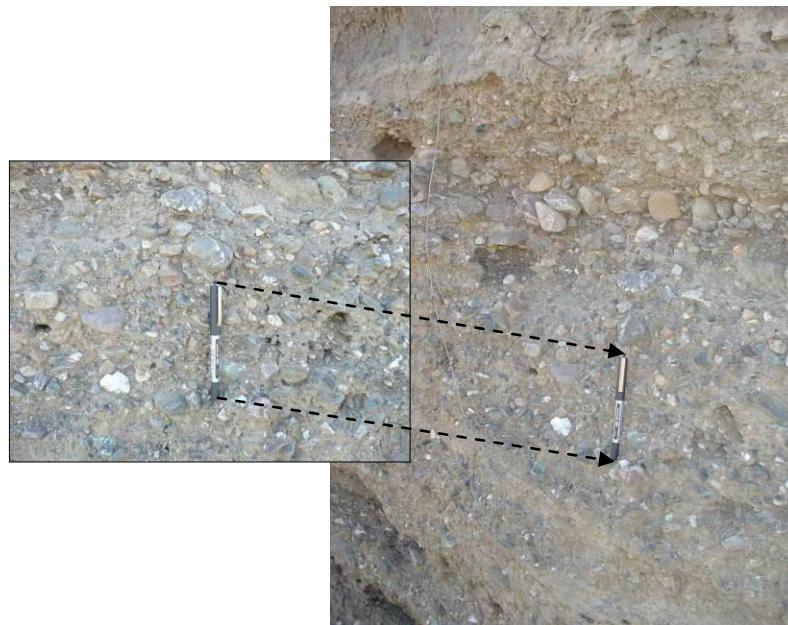


Figure 3.24. A close-up view of gravelly layers





Figure 3.25. Gravel lenses in the alluvial sequence



Figure 3.26. Sandy layers very close to the Kelkit River



Figure 3.27. Shallow groundwater level very close to the Kelkit River

### **3.6 Concluding Remarks**

The study area, the Erbaa basin, is located on the eastern part of the NAFZ and is surrounded by fault segments that ruptured in the 1942 and 1943 earthquakes. The district was firstly located on the Quaternary alluvium and the alluvial fan nearby the Kelkit River before these disastrous earthquakes. After the destructive 1942 earthquake with a magnitude of 7.1, the settlement had to be moved towards the Pliocene deposits on the southern hills. There are still some possible seismic gap zones mentioned by different researchers near the study area, since no instrumental records have been taken until today.

The tectonic mechanism of the NAFZ and geological setting of the basin increase its importance for investigation. Erbaa settlement is mainly located on the Quaternary deposits and rarely on the Pliocene units. Pliocene units consist of uncemented gravel, sand, clay and occasionally uncompacted sandstone layers. Alluvium is the dominant deposit in the study area and the depth of alluvium becomes thicker towards the Kelkit River. Due to different and variable flow regimes of the Kelkit River in the past, there is a variety of soil materials with different grain sizes. Alluvial sequence mainly consists of gravelly, sandy, silty, and clayey layers. Furthermore, the transition in horizontal-vertical directions is quite common in these deposits. The alluvial layers are quite loose particularly near the embankments of the Kelkit River.

## **CHAPTER 4**

### **FIELD AND LABORATORY STUDIES**

#### **4.1 Field and Laboratory Data**

In this section, the field and laboratory tests and their results are introduced. The field studies mainly involve drilling and geophysical applications in the study area. In addition, seismic cone penetration tests (SCPTU) with pore pressure measurements are conducted as well. Laboratory tests were performed on the samples obtained from drillings to characterize the geotechnical properties of geological units in Erbaa. The previous works including different projects and this recent study are summarized with the details of geotechnical, geophysical, and laboratory studies.

#### **4.2 Previous Studies**

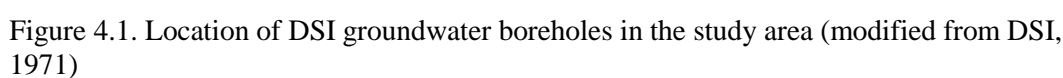
In order to classify the foundation soils in the Erbaa Basin, previous geological and geotechnical studies in the study area are considered as a preliminary step. In the previous years, a total of 56 boreholes were drilled for different projects in Erbaa and its close vicinity. Previously, the first investigation in Erbaa was held in 1971 by the General Directorate of Hydraulic Works (DSI) to investigate the hydrogeological properties of the area (DSI, 1971). Moreover, three additional geotechnical investigations were carried out. One of the projects was Ankara University Research Project held by Canik and Kayabali (2000). The other geotechnical investigations were performed for industrial area and water treatment plant areas by Akademi Geotechnical Company (2002) and Metropol Geotechnical Company (2005), respectively. The details of these previous projects are given in the following paragraphs.

##### **4.2.1 DSI Groundwater Research Project**

The first detailed investigation in Erbaa was held in 1971 by the General Directorate of Hydraulic Works (DSI). In this project, it was aimed to investigate the hydrogeological

properties of the area including the locations, depth, reserve and quality of groundwater at the right embankment of Kelkit River (DSI, 1971). At that time, the left embankment of the river, where the old Erbaa settlement was also located, was in the project of irrigation of surface water. Therefore, there were several groundwater boreholes in the close vicinity of the study area. One of these boreholes (borehole 4025) was drilled in 1963 with a total depth of 220 m (Figure 4.1). The static groundwater level in the same borehole was measured as 4 m. The aquifer layers in the aforementioned well reaches down to 106m depth which can be accepted as the boundary between alluvium and Pliocene units in that location. The second borehole, borehole 4217, is located in the east side of the study area near Bolucek town with a 186 m total depth and 4 m static groundwater level.

The DSI borehole (BH4025) was also considered in the study of Barka et al. (2000). The depth of alluvial deposit was mentioned as 106 m near Kelkit River with respect to BH-4025 as presented in the cross section of Barka et al. (2000) (Figure 4.2). The cross section line (BB') was also depicted in Figure 4.1. Furthermore, the DSI borehole 91/6 (shown as 916 in Figure 4.1) was also evaluated by Barka et al. (2000). The total depth of borehole 91/6 is 144 m and the Alluvium-Pliocene boundary was encountered at 55 m depth (Barka et al., 2000) (Figure 4.2). It should be noted that the whole length of BB' cross section cannot be depicted in Figure 4.1 as Barka et al. (2000) studied a longer area in the basin.





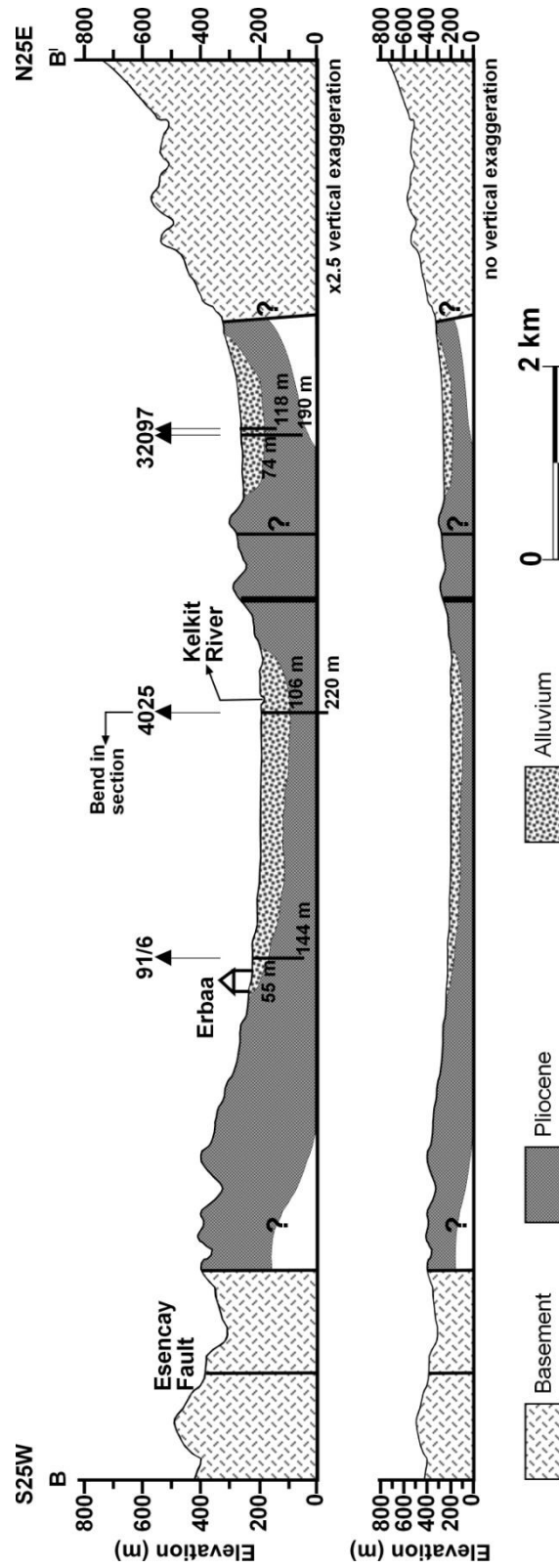


Figure 4.2. A general cross section of Erbaa (B-B') (modified from Barka et al., 2000)  
 (Note: The entire length of the cross section cannot be presented in Figure 4.1.)

#### 4.2.2 Ankara University Research Project

A limited number of geotechnical projects were performed in Erbaa in the past. Ankara University Scientific Research Project was one of the main geotechnical studies carried out in Erbaa settlement by Canik and Kayabalı (2000). In this project, the geotechnical properties of subsurface layers were investigated by means of several boreholes and geophysical methods. A total of 46 boreholes with varying depths from 5 m to 50 m were drilled and almost 845 m drilling was performed in that project. The general properties (coordinates, depths, and depth to GWL) of these boreholes are presented in Table 4.1 and the distribution of these boreholes is depicted with other projects' boreholes in Figure 4.3. It should be noted that the number of the previous boreholes are given in two different columns in Table 4.1. The first column (Old BH No) represents the original number of previous borehole, whereas the second column (New BH No) defines the new number of the same borehole assigned in this study.

Table 4.1. General properties of 46 boreholes in Ankara University Scientific Research Project (Canik and Kayabalı, 2000) \*(The borehole was not considered in the analyses due to shallow depth)

Old BH No	New BH No	Coordinates		Depth (m)	Depth to GWL (m)	Old BH No	New BH No	Coordinates		Depth (m)	Depth to GWL (m)
		Easting	Northing					Easting	Northing		
1	AU-49	294703	4508398	15	1,5	24	AU-72	297368	4504717	15	12
2	AU-50	294983	4506534	15	5	25	AU-73	294910	4504583	15	-
3	AU-51	294986	4507017	15	9	26	AU-74	295416	4504848	15	-
4	AU-52	295715	4503932	32	-	27	AU-75	293136	4504795	15	-
5	AU-53	295074	4566258	15	7	28	AU-76	745211	4465756	15	-
6	AU-54	294224	4506372	15	12	29	AU-77	294558	4504624	15	-
7	AU-55	294908	4506156	15	7	30	AU-78	295295	4504018	10	-
8	AU-56	294674	4505618	15	-	31	AU-79	294151	4504333	15	-
9	AU-57	294963	4505722	15	-	32	AU-80	295406	4503916	15	-
10	AU-58	293324	4506004	15	11	33	AU-81	Not given	Not given	15	-
11	AU-59	293800	4505787	15	6	34	AU-82	294553	4508405	47	4
12	AU-60	295210	4505786	11	-	35	AU-83	294352	4505693	47	-
13	AU-61	293003	4505633	15	-	36	AU-84	294798	4505211	15	-
14	AU-62	294745	4505645	15	-	37	AU-85	294558	4504208	35	-
15	AU-63	293087	4504695	15	-	38	AU-86	292222	4505806	44	-
16*	AU-64	295584	4505230	5	-	39	AU-87	295627	4506252	13	-
17	AU-65	746378	4464570	15	-	40	AU-88	294808	4507617	15	5
18	AU-66	295157	4505278	10	-	41	AU-89	294477	4505760	50	-
19	AU-67	293008	4505092	15	-	42	AU-90	294718	4505749	20	-
20	AU-68	293033	4505178	15	-	43	AU-91	294011	4505954	15	6
21	AU-69	294513	4504200	15	-	44	AU-92	295381	4504414	15	-
22	AU-70	295117	4505768	15	-	45	AU-93	292883	4506116	20	-
23	AU-71	293001	4504752	15	-	46	AU-94	294729	4504687	15	-

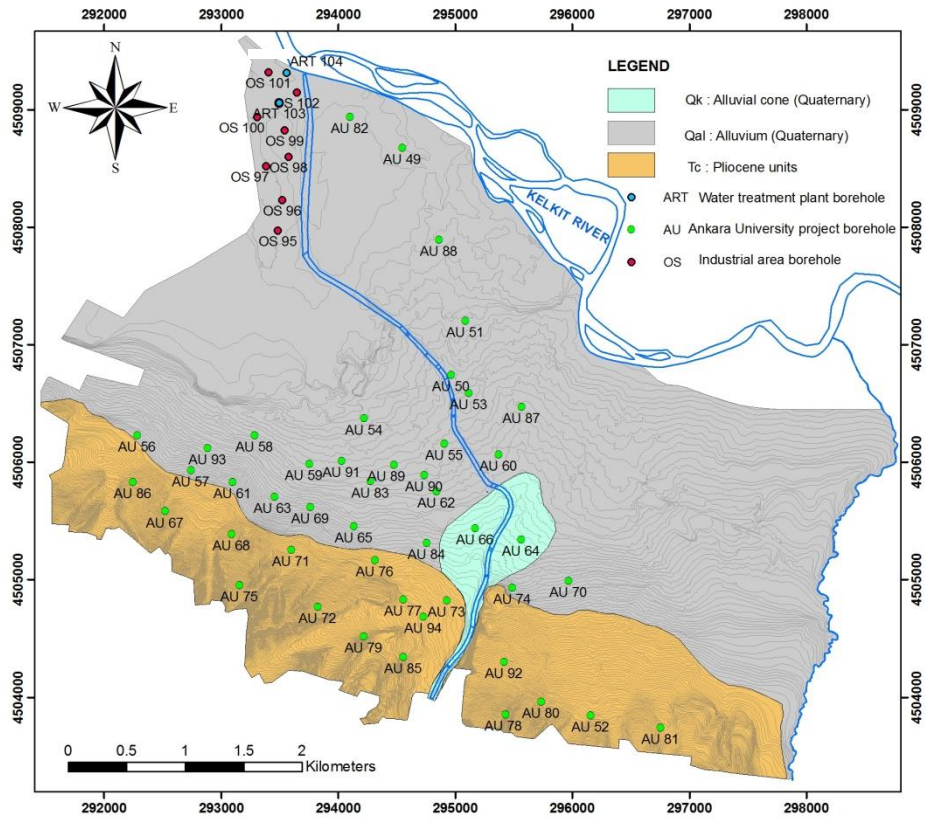


Figure 4.3. General distribution of previous projects' boreholes

Most of the boreholes in Ankara University Scientific Research Project are relatively shallow (about 15 m). The groundwater level varies between 1.5 and 12 m in 12 boreholes of Canik and Kayabalı (2000) study. Approximately 150 disturbed samples were collected from Standard Penetration Tests (SPT). Moreover, SPT- $N_{30}$  values change between 5 to >50 (refusal values) as given in the Ankara University Scientific Research Project. In addition to disturbed sampling, 80 undisturbed samples were also taken to characterize the physical and mechanical properties of soil units. In the same project, DSI groundwater borehole (91/6) was considered to assess the depth of alluvium. The soil layers in these two groundwater boreholes were defined as an alternation of clay and sandy, and gravelly clay layers with a total depth of 70 m and 144 m, respectively (Canik and Kayabalı, 2000). The static groundwater level of both boreholes was indicated as 16.8 m. The locations of these two DSI boreholes are also shown in Figure 4.1.

Several laboratory tests were performed to classify the soil layers in the study area in Ankara University Scientific Research Project. Based on the grain size distributions of 225 samples, most of the soil layers in the study area are represented by clay with low plasticity. There is also a great amount of poorly graded sand, clayey sand and silt with low plasticity in the region. The water content of these samples is varying between 4% and 38%. Generally, the water content of clayey layers is greater than 10%. The natural unit weight of undisturbed clay samples is between 18.72 - 20.87 kN/m<sup>3</sup>. A total of 22 triaxial and uniaxial compressive strength tests were carried out on undisturbed samples. According to undrained triaxial tests, cohesion and internal friction angle of CL (clay with low plasticity) and ML (silt with low plasticity) type soils are ranging between 4 and 202 kPa, and 4° and 38°, respectively. Furthermore, unconfined compressive strength is between 147 and 481 kPa. The laboratory test results of Ankara University Scientific Research Project are summarized in Table 4.2. It should be noted that the soil samples were not differentiated on the basis of alluvium and Pliocene units in laboratory tests.

In addition to field and laboratory studies, liquefaction analyses were also performed using the available data. A peak ground acceleration of 0.3 g and a magnitude of 7.5 were considered as a scenario earthquake by Canik and Kayabali (2000) in the project. The data from 12 boreholes with varying groundwater levels were employed in liquefaction analyses. As a result, the sequence at 6 borehole locations (AU-51, AU-54, AU-55, AU-59, AU-82, AU-88) have the liquefaction potential in Erbaa, since the abovementioned boreholes are generally located in loose and sandy alluvial layers (Canik and Kayabali, 2000). It was also pointed out that the soil characteristics of the settlement area are compatible with the field-laboratory tests and geophysical measurements.

Table 4.2. Summary of the laboratory test results of Ankara University Scientific Research Project (Canik and Kayabali, 2000)

Soil type		W <sub>n</sub> (%)	γ <sub>n</sub> (kN/m <sup>3</sup> )	Sieve analyses (%)		Atterberg limits (%)			q <sub>u</sub> (kPa)
				Sieve #4	Sieve #200	LL	PL	PI	
CL	Data #	117	28	117		112			7
	Minimum	4	18.72	0	50.3	20	11	4	147
	Maximum	40.4	20.87	16.8	95.7	48	25	29	481
	Average	17.38	19.99	3.2	69.4	33	19	14	311
	Std. dev.	6.09	0.59	3.8	12.4	6.5	3.1	5	124
ML	Data #	7	3	7		7			1
	Minimum	10.90	19.70	0.00	51.30	28	17	4	363
	Maximum	27.40	20.58	5.50	94.70	41	30	15	-
	Average	19.24	20.29	1.51	75.04	36	25	10	-
	Std. dev.	6.07	0.49	2.36	16.40	4.08	4.00	3.69	-
SC-SM	Data #	25	1	25		25			-
	Minimum	3.50	20.68	0.00	20.70	21	9	4	-
	Maximum	22.10	-	28.60	49.90	37	21	18	-
	Average	10.72	-	10.65	40.02	26	16	10	-
	Std. dev.	4.16	-	5.75	7.56	3.40	2.94	3.82	-
SW-SP	Data #	52	1	52					-
	Minimum	4.30	20.19	0.00	8.70	NP	NP	NP	-
	Maximum	26.40	-	36.70	49.10				-
	Average	10.64	-	13.33	26.50				-
	Std. dev.	5.35	-	9.71	12.30				-
GC	Data #	1	-	1		1			-
	Minimum	13.3	-	31.1	46.7	33	20	13	-
	Maximum	-	-	-	-	-	-	-	-
	Average	-	-	-	-	-	-	-	-
	Std. dev.	-	-	-	-	-	-	-	-
GP	Data #	2	-	2		-			-
	Minimum	4.50	-	33.50	35.90	-	-	-	-
	Maximum	13.20	-	48.80	41.40	-	-	-	-
	Average	8.85	-	41.15	38.65	-	-	-	-
	Std. dev.	6.15	-	10.82	3.89	-	-	-	-
W <sub>n</sub> :	Water content								
γ <sub>n</sub> :	Natural unit weight								
q <sub>u</sub> :	Unconfined compressive strength								

In addition to drilling, a number of geophysical applications were also conducted in Ankara University Scientific Research Project to identify the dynamic properties of subsurface soils as well as their horizontal and vertical distribution at the site. Resistivity surveys were carried out with 100 m investigation depth (Figure 4.4). The Schlumberger technique was applied using Mc-Phar type deep resistivity instrument.

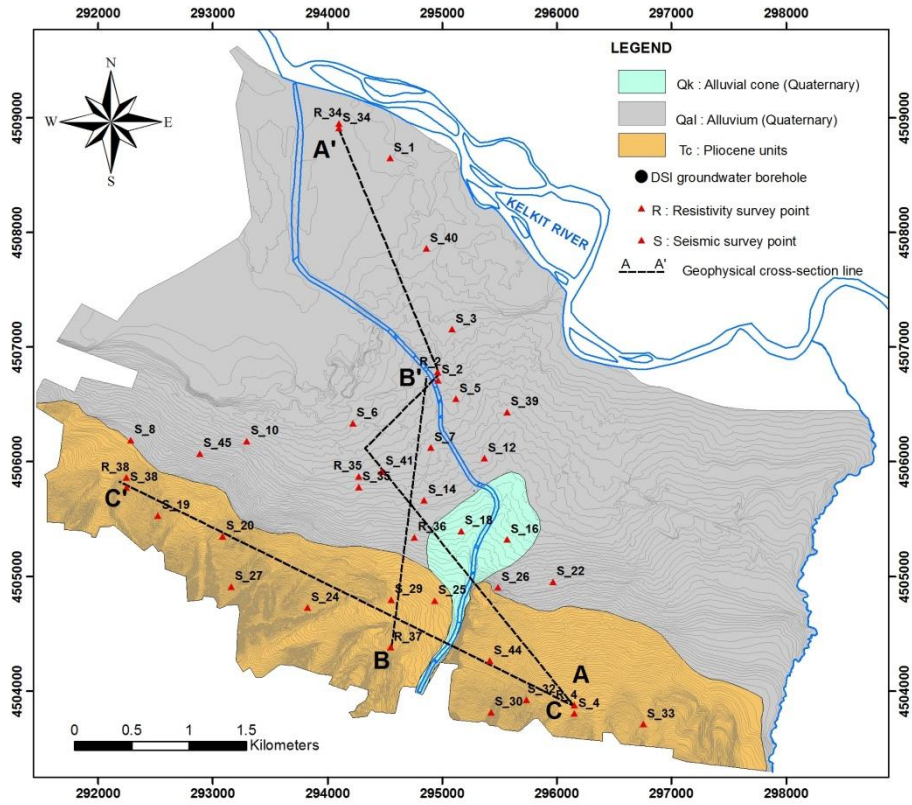


Figure 4.4. Distribution of geophysical survey points in Ankara University Scientific Research Project (modified from Canik and Kayabalı, 2000)

The soil layers in the study area were defined as mostly sand, clayey gravel and gravelly clay with respect to resistivity measurements by Canik and Kayabalı (2000) as given in Table 4.3.

Table 4.3. General results of the resistivity measurements in Ankara University Scientific Research Project (Canik and Kayabali, 2000)

Resistivity Location	Soil Type	Thickness (m)	Apparent Resistivity ( $\Omega$ m)
R-2	Gravel-sand	5	220
	Clayey sandy clay	25	50
	Sandy gravel	18	80
	Clayey gravel	-	55
R-4	Sandy clay	1.3	21
	Clayey gravel	13.7	50
	Clay	5	14
	Clayey gravel	26	43
	Gravelly clay	-	20
R-34	Coarse gravelly sand	5.5	180
	Silty clayey sand	18.5	9
	Clayey sandy gravel	-	55
R-35	Slightly sandy clay	5	17
	Clayey sandy gravel	15	80
	Clayey gravel	40	40
	Slightly gravelly clay	-	13
R-36	Clayey gravel	3	36
	Gravelly clay	5.5	23
	Clayey sandy gravel	15.5	90
	Clayey gravel	24	36
	Gravelly clay	-	23
R-37	Clayey sandy gravel	1.4	60
	Clayey gravel	2	37
	Gravelly clay	17.6	21-27
	Clayey gravel	7	55
	Gravelly clay	-	30
R-38	Slightly sandy clay	6.5	20
	Clayey gravel	4.5	40
	Gravelly clay	54	23
	Clay	-	25

As a result of the interpretation of the resistivity measurements, Pliocene (Neogene) units are very thick at the site, and the basement rock could not be encountered until 100 m depth (Canik and Kayabali, 2000). The resistivity cross sections of Ankara University Scientific Research Project are presented in Figures 4.5, 4.6, and 4.7.

Figure 4.5. A-A' resistivity cross-section of Ankara University Scientific Research Project (modified from Canik and Kayabali, 2000)





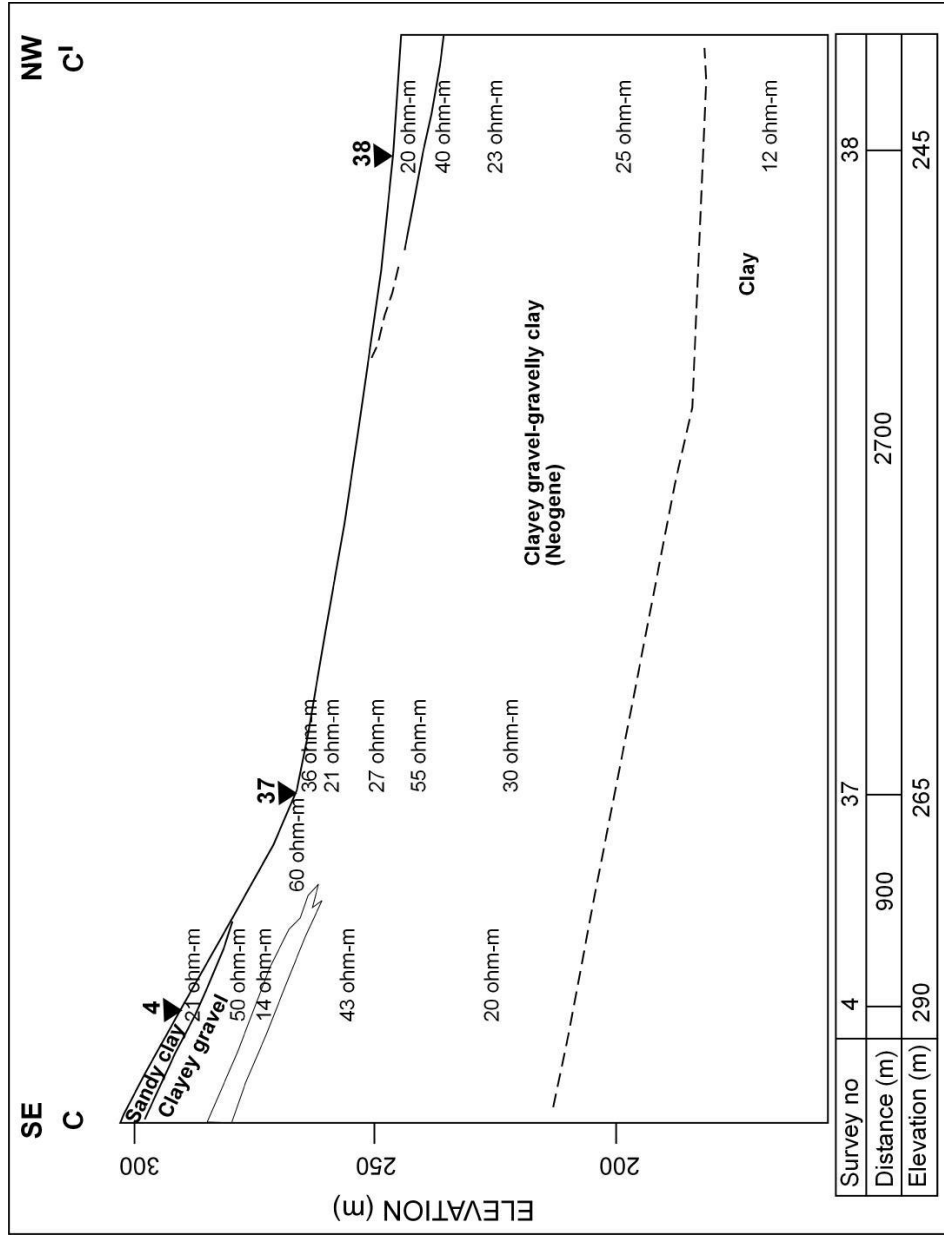


Figure 4.7. C-C' resistivity cross-section of Ankara University Scientific Research Project (modified from Canik and Kayabali, 2000)

In addition to resistivity surveys, seismic refraction measurements were also performed at the site within Ankara University Scientific Research Project (Figure 4.4). For each survey location, 6 seismic refraction measurements were completed and a total of 204 seismic measurements were performed. The results of 34 seismic refraction scanline surveys were summarized in Table 4.4.

Table 4.4. General results of the seismic refraction measurements in Ankara University Scientific Research Project (Canik and Kayabali, 2000)

Scanline No	New BH No*	1 <sup>st</sup> layer (m)**	2 <sup>nd</sup> layer (m)**	3 <sup>rd</sup> layer (m)**	1 <sup>st</sup> layer Vp*** (m/s)	2 <sup>nd</sup> layer Vp*** (m/s)	3 <sup>rd</sup> layer Vp*** (m/s)	1 <sup>st</sup> layer Vs*** (m/s)	2 <sup>nd</sup> layer Vs*** (m/s)	3 <sup>rd</sup> layer Vs*** (m/s)	Period**** T <sub>0</sub> (sec)
1	AU-92	-			600			217			0.89
2	AU-78	8	-		550	900		208	280		0.75
3	AU-80	7	-		400	2000		190	416		0.56
4	AU-52	0.5	7	-	300	600	850	-	227	294	0.71
5	AU-81	5	-		450	800		208	294		0.71
6	AU-74	2	9	-	250	550	1100	-	227	294	0.69
7	AU-64	9	-		400	800		178	255		0.84
8	AU-70	10.5	-		550	900		210	280		0.76
9	AU-60	11.2	-		450	1600		192	345		0.68
10	AU-53	8.5	-		500	1900		208	384		0.59
11	AU-50	6	-		500	1600		195	357		0.61
12	AU-87	12	-		500	1550		210	350		0.66
13	AU-51	7	-		400	2000		190	416		0.56
14	AU-88	4	-		400	1700		166	357		0.62
15	AU-49	3	-		350	1900		150	384		0.57
16	AU-82	4	-		400	1500		166	344		0.63
17	AU-54	8	-		450	1325		192	312		0.71
18	AU-55	12	-		500	1500		200	344		0.68
19	AU-62	14	-		500	1900		200	385		0.65
20	AU-66	3.9	-		400	800		172	280		0.75
21	AU-73	9	-		500	200		200	280		0.77
22	AU-77	14.5	-		600	1100		227	280		0.77
23	AU-78	8.5	-		400	900		160	277		0.81
24	AU-51	7	-		850	1400		254	357		0.59
25	AU-72	9	7	-	250	750	1000	-	250	280	0.71
26	AU-75	6	-		450	1050		190	294		0.73
27	AU-68	7	-		550	1575		208	345		0.63
28	AU-67	3	-		400	1450		184	330		0.64
29	AU-86	2	5	-	300	825	1200	-	277	294	0.66
30	AU-56	9	-		700	1500		250	357		0.6
31	AU-93	9.5	-		550	1300		227	294		0.72
32	AU-58	12.5	-		500	1500		217	357		0.65
33	AU-89	11	-		475	1800		208	370		0.63
34	AU-83	8.4	-		500	1100		195	290		0.74

\*Nearest borehole to scanline location is indicated, \*\*The measurement levels are divided into sublayers

\*\*\*The velocity of P and S waves for different sublayers, \*\*\*\*Period of soil layers

P- and S-wave velocities for 3 different sublayers are presented in Table 4.4. The average P and S wave velocities for 3 different sublayers are found to be 467, 1281, 1038 m/s; and 200, 321, 291 m/s, respectively. After seismic investigations, the dominant period of subsurface layers were evaluated. The dominant period is ranging between 0.5 and 0.9 seconds in the study area according to the study conducted by Canik and Kayabalı (2000).

#### 4.2.3 Geotechnical investigations for industrial area and water treatment plant

Two different geotechnical investigations were carried out for industrial area by Akademi Geotechnical Company in 2002 (Akademi, 2002) and water treatment plant by Metropol Geotechnical Company in 2005 (Metropol, 2005). The coordinates, depth and groundwater level of boreholes in industrial area and water treatment plant projects are summarized in Table 4.5 and the distribution of these boreholes are depicted in Figure 4.3.

Table 4.5. General properties of boreholes in the industrial area and water treatment plant projects

Old BH No	New BH No	Coordinates		Depth (m)	Depth to GWL (m)
		Easting	Northing		
Industrial area					
1	OS-95	293483	4507970	6.45	1.0
2	OS-96	293520	4508229	6.45	0.9
3	OS-97	293383	4508523	6.45	0.8
4	OS-98	293580	4508600	6.45	0.9
5	OS-99	293538	4508823	6.45	1.2
6	OS-100	293310	4508933	6.45	1.2
7	OS-101	293404	4509310	4.95	1.1
8	OS102	293647	4509144	6.45	1.0
Water treatment plant area					
1	ART-103	293493	4509060	12.5	1.2
2	ART-104	293559	4509311	8.00	0.9

The industrial area in Erbaa is located on the left embankment of Kelkit River. The geotechnical investigations in industrial area were performed by means of 8 boreholes in 2002. The depth of those boreholes is quite shallow. Furthermore, the water treatment plant is in the close vicinity of the industrial area and the geotechnical investigation was conducted in 2005 in accordance with 2 boreholes.

According to the reports of these two studies (Akademi, 2002; Metropol, 2005), low plastic clay and loose sand with silty intercalations were generally observed in this area with a shallow groundwater depth (0.8 m to 1.2 m). The combined laboratory test results of industrial area and water treatment plant projects are summarized in Table 4.6.

Table 4.6. Summary of the laboratory test results of the industrial area and water treatment plant projects

Soil type		$W_n$ (%)	$\gamma_n$ (kN/m <sup>3</sup> )	Sieve analyses (%)		Atterberg limits (%)		
				Sieve #4	Sieve #200	LL	PL	PI
CL	Data #	12	2	12		12		
	Minimum	34	18.3	0	50.3	25	11	14
	Maximum	37	18.7	16.8	95.7	40	25	17
	Average	35.5	18.5	3.22	69.40	32.6	18	15.8
	Std. dev.	1.17	0.28	3.77	12.42	5.1	5.2	1
SM	Data #	16	1	16		-		
	Minimum	11	20.7	0.00	20.70	NP	NP	NP
	Maximum	15	-	28.60	49.90			
	Average	13.1	-	10.65	40.02			
	Std. dev.	1.47	-	5.75	7.56			

### 4.3 Recent Field Studies

Having selected Erbaa for the study area, 3 new borehole locations were determined to investigate the site conditions as a preliminary research in 2006 within the context of Turkish Prime Ministry State Planning Organization (DPT) Project (Tatar et al., 2009). A total of 45 additional boreholes were drilled in the study area between 2007 and 2008. The boundary of the study area was defined in accordance with the Municipality plans. The general properties and the distribution of recent boreholes drilled in this study are given in Table 4.7 and Figure 4.8, respectively. It should be noted that the previous boreholes are also indicated in Figure 4.8. The data of 104 boreholes in Figure 4.8 will be considered in the evaluation stage of this study. Besides, the distribution of depth to groundwater level map is given in Figure 4.9.

Table 4.7. General properties of recent boreholes drilled in this study

BH No	Coordinates		Elevation (m)	Depth (m)	Depth to GWL (m)	# of SPT samples	# of UD samples
	Eastings	Northings					
BH-1	291886	4507274	199	30.0	1.55	29	2
BH-2	291976	4506299	238	25.5	13.00	21	6
BH-3	292744	4506495	215	24.0	9.10	23	11
BH-4	293605	4508079	198	26.0	1.00	25	5
BH-5	293672	4507425	200	27.0	2.00	26	3
BH-6	292809	4507464	200	26.5	2.00	26	2
BH-7	293846	4509138	198	30.2	1.50	30	10
BH-8	294951	4508438	200	21.0	1.55	20	2
BH-9	294594	4508132	200	30.5	2.05	30	2
BH-10	294287	4507288	201	27.5	4.00	27	4
BH-11	293900	4507035	200	30.2	4.55	30	1
BH-12	292817	4505764	243	21.5	DRY	20	8
BH-13	293478	4505902	219	25.5	14.50	25	15
BH-14	294054	4505139	248	30.0	DRY	30	4
BH-15	294226	4506222	210	29.5	9.00	28	15
BH-16	294448	4506488	208	29.55	10.00	29	9
BH-17	294893	4507427	204	23.0	5.00	22	2
BH-18	295710	4507782	200	30.5	2.10	30	3
BH-19	295400	4507049	209	30.5	9.55	30	5
BH-20	295200	4506579	213	30.5	10.00	30	10
BH-21	294766	4506125	214	28.5	10.00	28	5
BH-22	294850	4505582	224	30.5	15.20	30	9
BH-23	295701	4504798	241	30.1	19.00	30	18
BH-24	295481	4504056	294	30.1	DRY	30	11
BH-25	295826	4504865	238	30.0	18.05	30	10
BH-26	295368	4505789	223	30.0	10.10	30	9
BH-27	295802	4506138	219	30.2	10.00	30	9
BH-28	296105	4506604	211	30.5	2.55	30	5
BH-29	296436	4506260	213	30.5	12.00	30	11
BH-30	296014	4505861	220	31.0	13.50	30	12
BH-31	296330	4505145	230	30.0	15.35	30	18
BH-32	297464	4505271	232	30.5	15.55	30	18
BH-33	296422	4504016	281	28.5	DRY	28	4
BH-34	296862	4504466	254	30.2	13.50	30	18
BH-35	297467	4503997	264	30.0	DRY	30	1
BH-36	293853	4507220	200	29.5	1.50	29	-
BH-37	293367	4507112	200	30.5	2.10	30	-

Table 4.7. continued

BH-38	294373	4507626	202	30.0	3.25	30	-
BH-39	298211	4505593	225	29.5	9.15	29	4
BH-40	298076	4505146	231	29.5	8.10	29	3
BH-41	298273	4506111	214	29.5	9.75	29	3
BH-42	298200	4506249	211	29.5	3.20	29	1
BH-43	297205	4506174	215	29.5	2.05	29	3
BH-44	295165	4508110	200	29.5	1.85	29	-
BH-45	293675	4507808	200	29.5	1.80	29	5
BH-46*	294972	4506829	209	30.20	9.05	28	6
BH-47*	295013	4507433	204	30.45	1.10	19	1
BH-48*	297336	4506295	212	30.11	1.70	25	9

\* Drilled in 2006

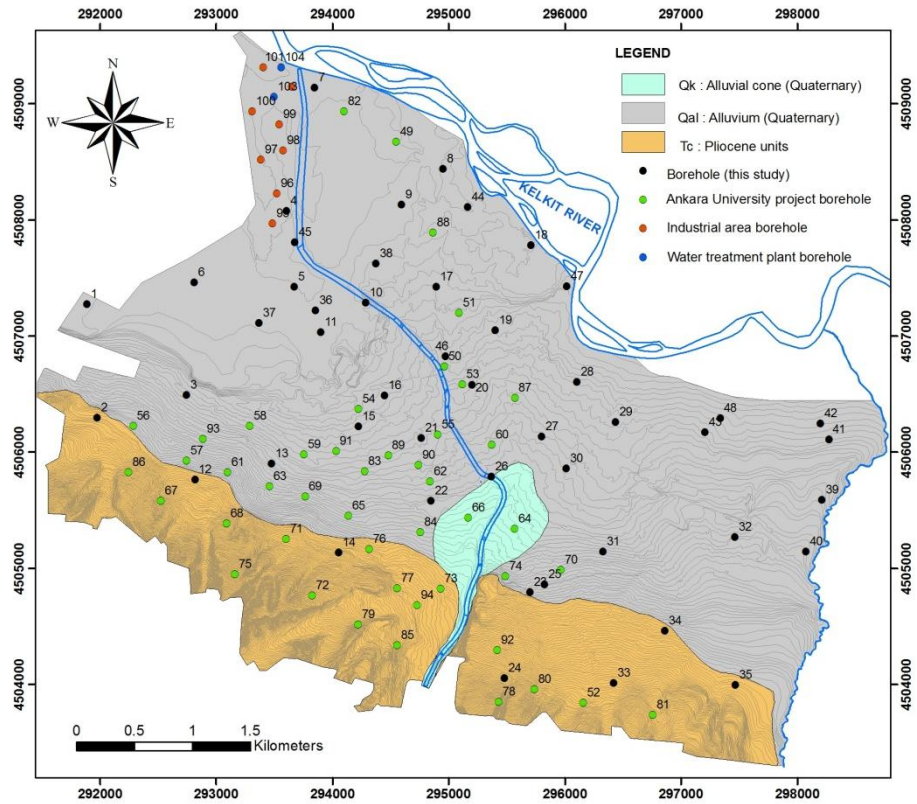


Figure 4.8. General distribution of recent and previous borehole locations considered in this study

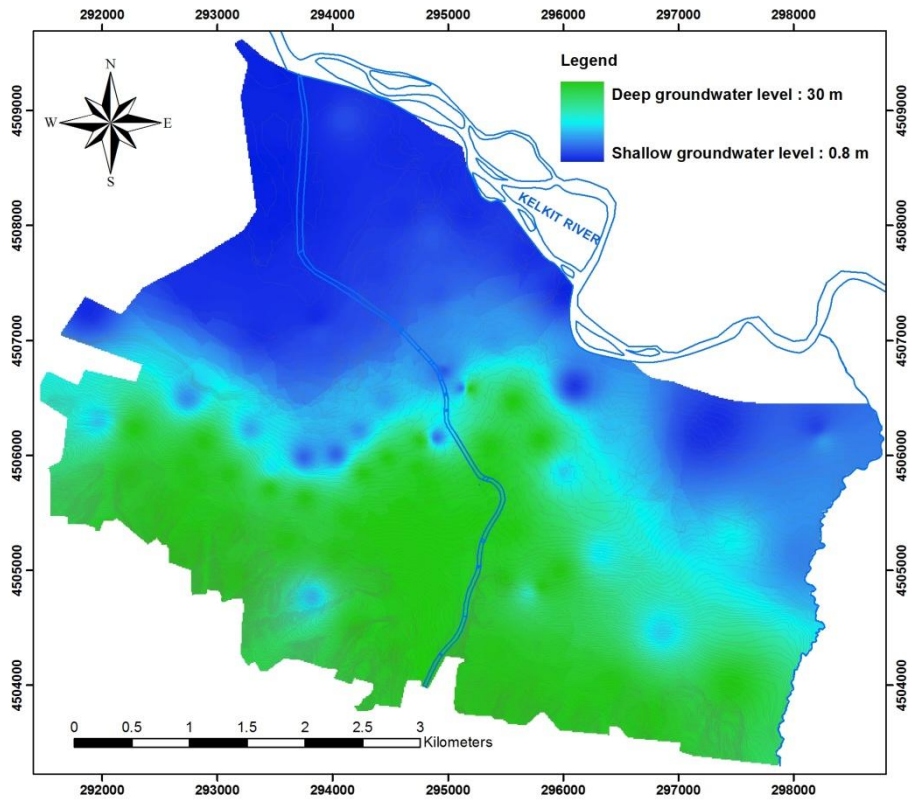


Figure 4.9. Depth to groundwater level map

Boreholes were drilled using Atlas-Copco, Craelius D750 rotary drilling rigs (Figure 4.10). A different systematic sampling interval was concerned in this study. In general, Standard Penetration Tests (SPT) are performed at every 1.5 m and undisturbed samples are acquired at every 3 meters in accordance with ASTM D 1586-92 (1998). However, an intensive testing and sampling program was preferred instead of the standard approach in this study. It was aimed to distinguish the possible problems that may occur due to variable soil characteristics. In addition, it is important to get a continuous geotechnical data from the soil profile. For this reason, SPT tests were performed at every 1 m and undisturbed samples (UD) were taken at every 1 m (if possible) in order to obtain a continuous soil profile as much as possible. Moreover, it was planned to drill 30 m deep boreholes to use SPT- $N_{30}$  blow count values for the correlation of shear wave velocity ( $V_s$ ). However, some boreholes could not reach the desired depth due to soil conditions (e.g. intensive gravelly layers). The SPT- $N_{30}$  -  $V_s$  correlations were employed to estimate the shear wave velocity profiles up to 30 meters depth in possible areas in the further sections.





Figure 4.10. A general view of drilling application in the study area

A total depth of 1386.81 m drilling was performed in this study, and 1341 SPT and 312 UD samples were obtained. General views from SPT applications can be seen in Figure 4.11. The groundwater level (GWL) in the boreholes was measured after drilling. The GWL at the study area varies between 1 and 19 m. There are a few dry boreholes in the Pliocene units as well. The GWL in the Pliocene unit is deeper (13-19 m) than in alluvium. The alluvium unit has very shallow GWL (1-2 m) towards the Kelkit River (Figure 4.9).

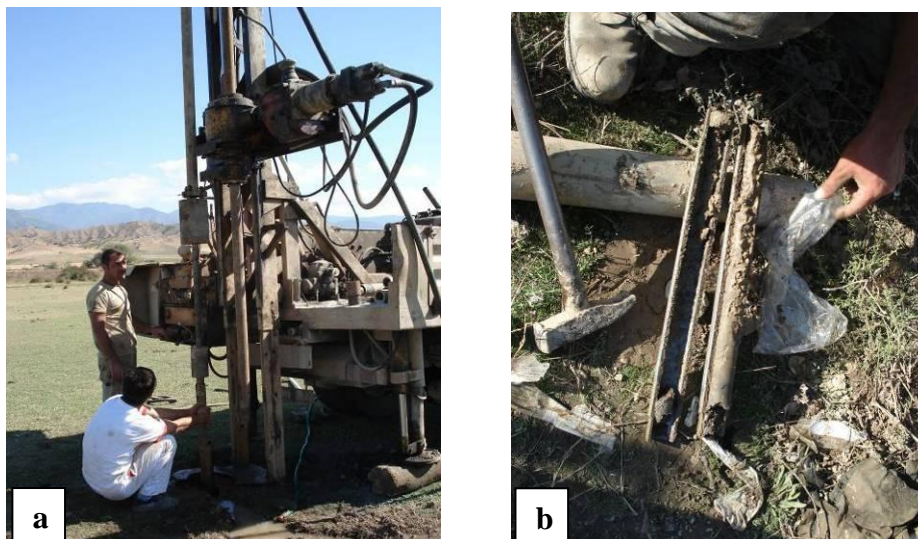


Figure 4.11. General views from SPT application (a) and SPT disturbed sample (b)

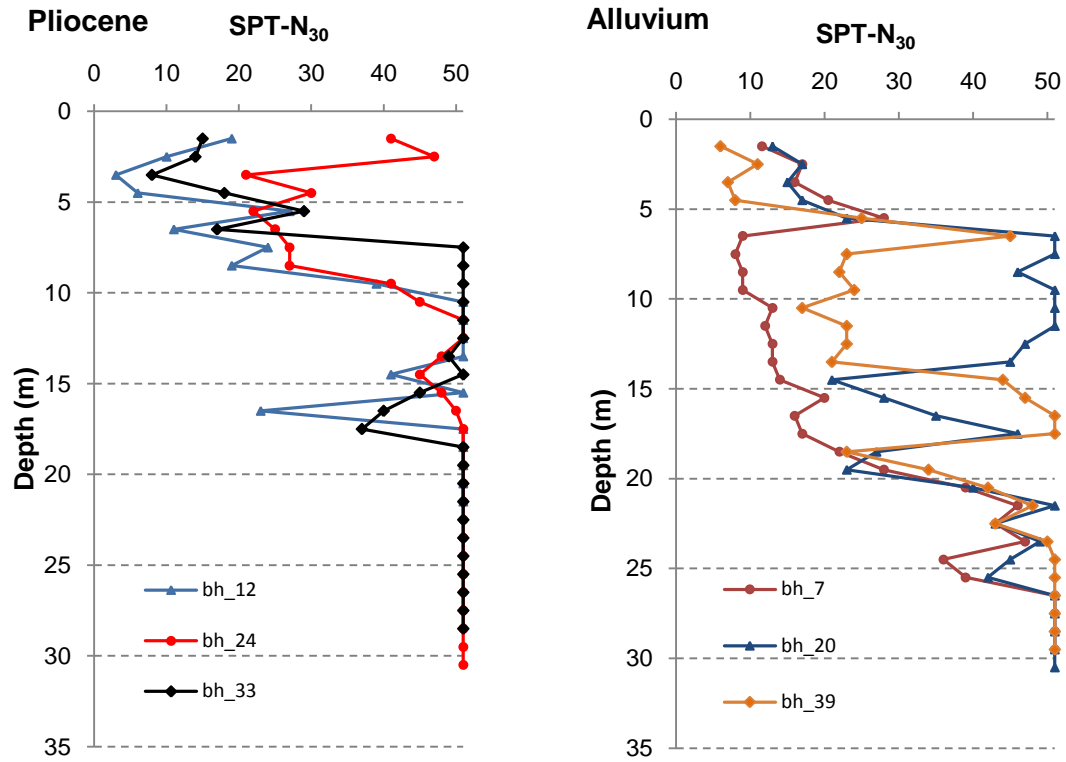


Figure 4.12. Variation of SPT- $N_{30}$  blow counts in alluvial and Pliocene layers based on the data from six boreholes

SPT- $N_{30}$  values were evaluated in terms of different geological units. The variation of SPT- $N_{30}$  values in several representative boreholes (Pliocene boreholes 12, 24, 33 and alluvium boreholes 7, 20, 39) from each geological unit is illustrated in Figure 4.12. The alluvial sequence has generally lower SPT- $N_{30}$  values ( $N_{30} < 20$ ) than Pliocene unit indicating a medium dense-loose sedimentation. Refusal SPT- $N_{30}$  blow counts were mostly obtained in gravelly layers of the alluvium. In addition, the Pliocene units mostly reveal refusal SPT- $N_{30}$  values after 10-15 m depth.

The geological and geotechnical properties of the study area were investigated in two dimensional scale and an overall evaluation was performed with respect to field studies. Five different cross-sections along the study area are illustrated in Figures 4.14 - 4.18. The alignment of the cross-sections can be seen in Figure 4.13. Four of the cross-sections are drawn from south to north while one cross section represents the variation of subsurface layers along east - west direction.

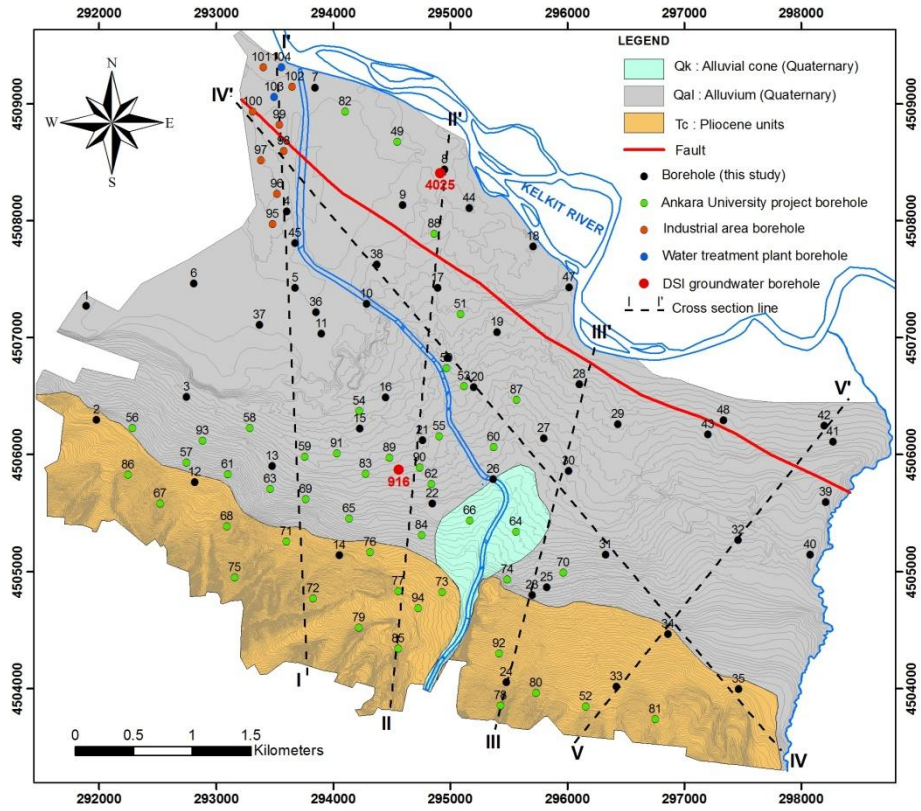


Figure 4.13. Alignment of cross section lines (I-I', II-II', III-III', IV-IV', V-V')

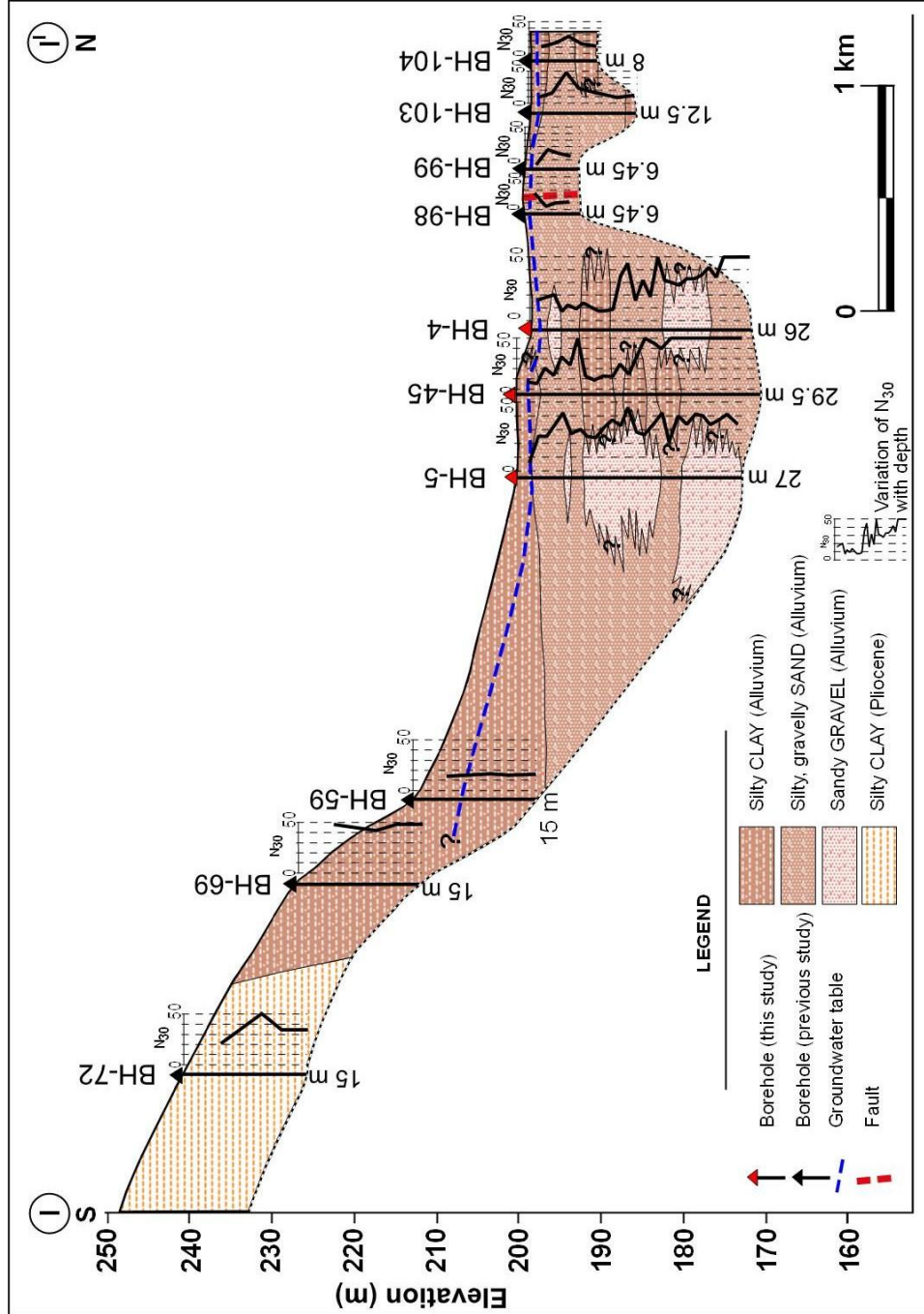


Figure 4.14. Cross section I-I'



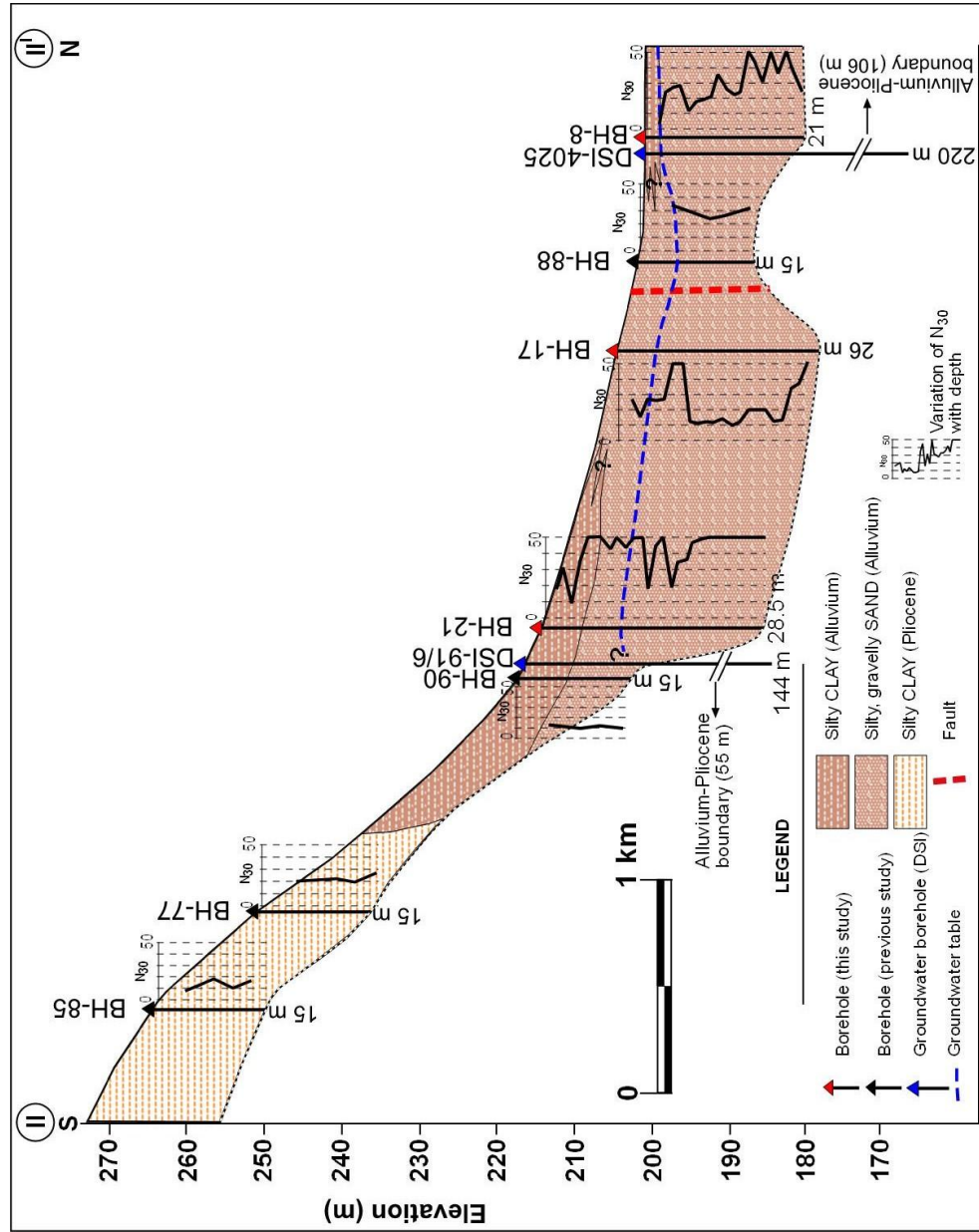


Figure 4.15. Cross section II-II'

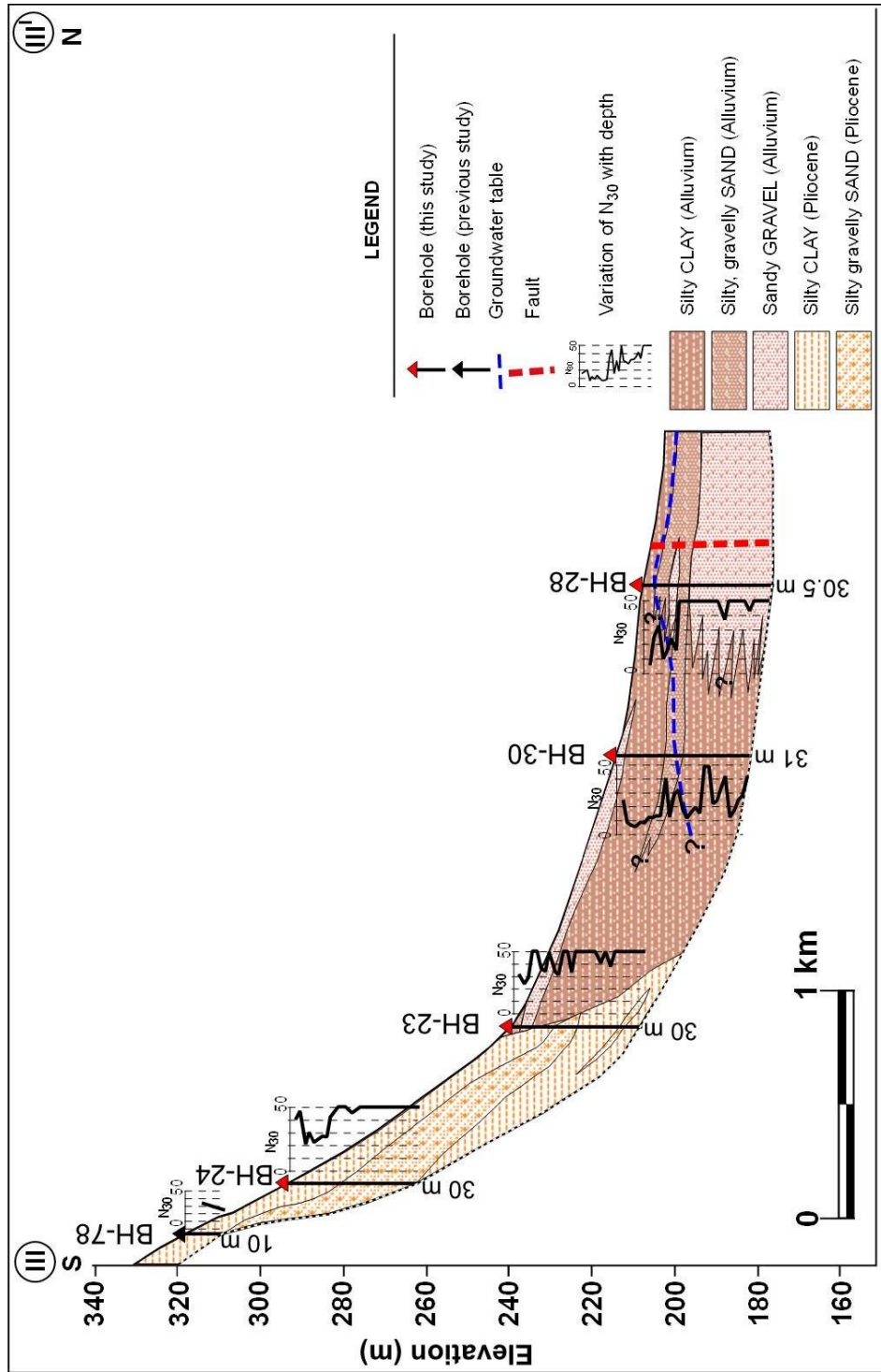


Figure 4.16. Cross section III-III'

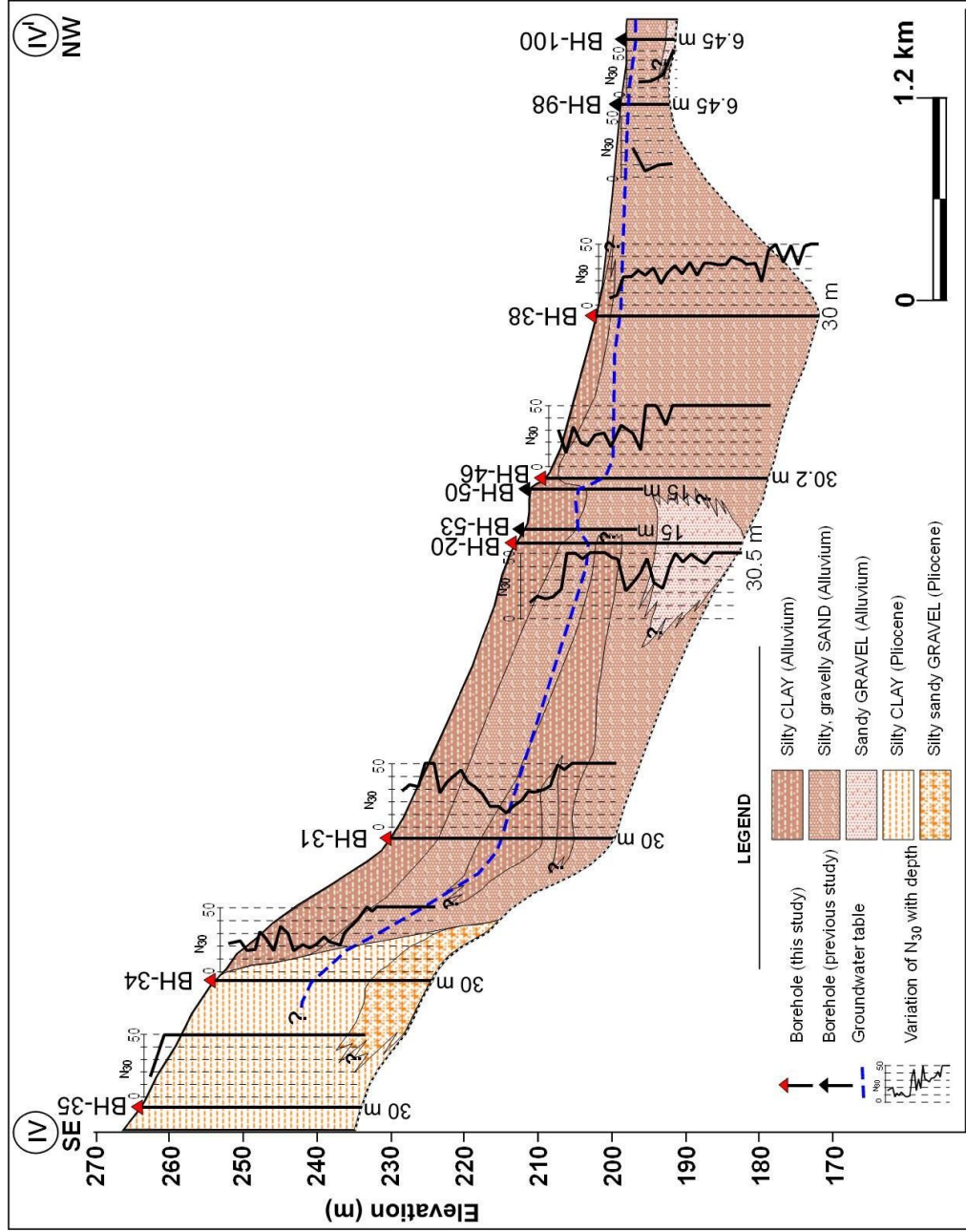
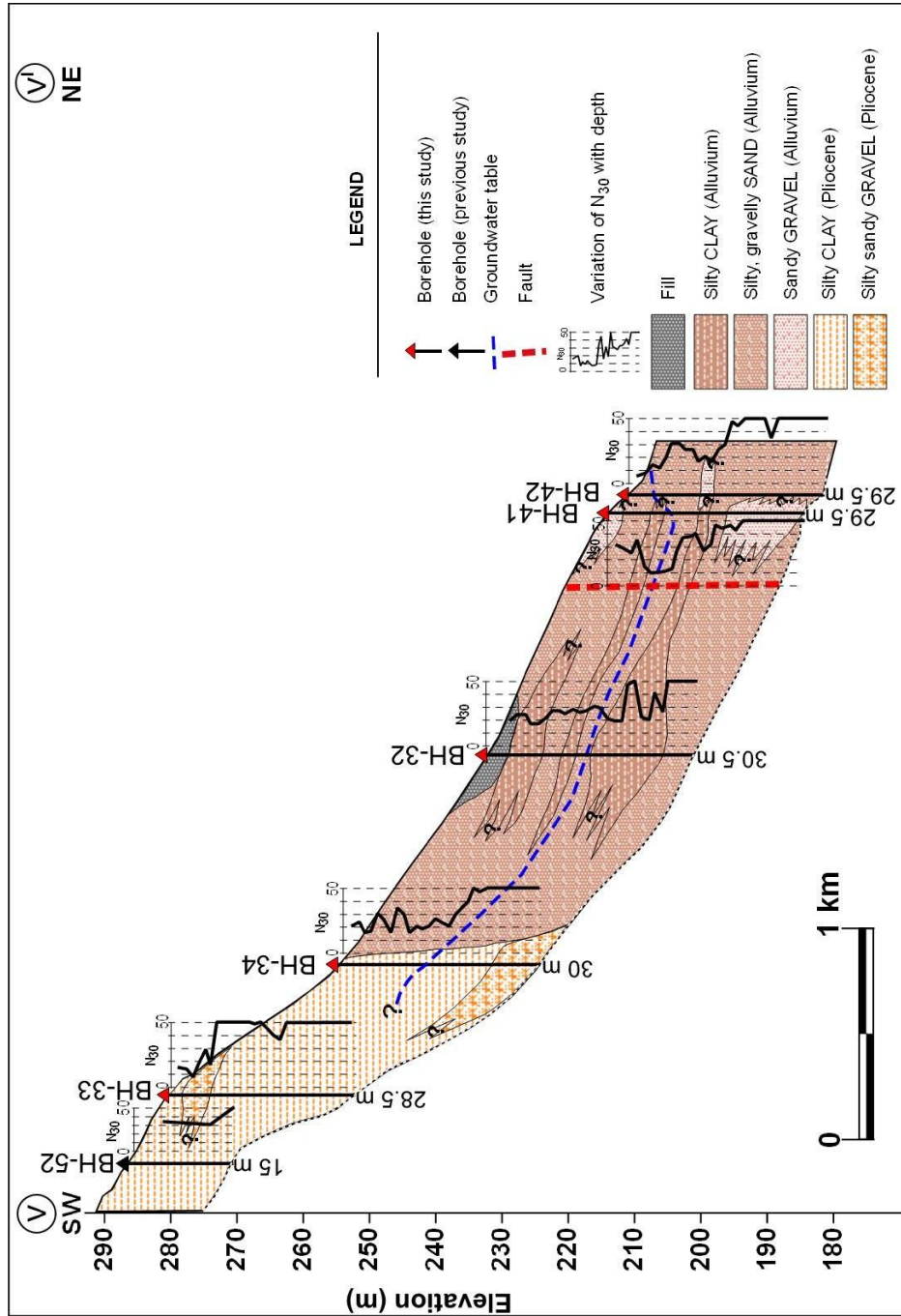


Figure 4.17. Cross section IV-IV'





#### 4.4 Recent Laboratory Studies

Laboratory tests were performed on 880 SPT (disturbed) and 110 undisturbed samples to determine the index and mechanical properties of the soils (particle size distribution, water content, Atterberg limits, triaxial compressive strength, and consolidation) (Figure 4.19). Based on the test results, soil samples were classified according to Unified Soil Classification System (USCS). The laboratory test results are summarized in Tables 4.8-4.12. On undisturbed (UD) samples, 125 water content, 102 Atterberg Limits, 123 particle size distribution, 83 natural unit weight, 76 specific gravity, 80 hydrometer, 11 triaxial, and 5 consolidation tests were performed. Furthermore, 564 water content, 455 Atterberg Limits, and 950 particle size distribution tests were performed on disturbed samples. The particle size distribution of the samples was determined by sieve analyses and hydrometer tests in accordance with ASTM-D-422 (2000). The sieve analysis was used to determine the particle size distribution for particles larger than the No.200 sieve (0.075mm) and the hydrometer analysis was used for particles finer than the No.200 sieve. Atterberg limits were also distinguished by means of liquid limit and plastic limit tests. Triaxial tests (UU and CU) and consolidation tests were carried out to reveal the mechanical properties of plastic soils.



Figure 4.19. A close-up view of UD and SPT samples

After laboratory tests, the results were separately evaluated for two main soil types (Alluvium and Pliocene) in the study area. The statistical distribution of water content for two different units is summarized in Table 4.8. Accordingly, gravelly and sandy layers have less water content than silty and clayey layers in alluvium unit. Additionally, the average water content of clay layers in the Pliocene units is lower than the alluvial ones. The water content of samples varies between 1.1% and 63.9% for alluvium, and 4% and 31.6% for Pliocene unit.

Table 4.8. Statistical distribution of water content for alluvium and Pliocene soils

Soil type		Total number of samples	Water content (%)			
			Minimum	Maximum	Average	Standard deviation
Alluvium	GC-GM-GP	102	1.5	20.1	6.5	3.5
	SC-SM-SP-SW	297	1.1	34.9	12.3	5.6
	ML-MH	21	7.1	51.8	22.4	10.2
	CL-CH	189	3.3	63.9	21.2	7.8
Pliocene	GC-GM	11	4.0	20.6	10.0	4.6
	SC	12	4.7	27.5	12.4	6.1
	CL-CH	58	7.9	31.6	18.9	5.7

On the basis of grain size distributions, most of the soil samples in alluvium unit are represented by silty, clayey sand and clean sand (SC, SM, SW, and SP). In addition, there is a significant amount of clayey (CL-CH) and gravelly (GC-GM-GP) layers in alluvium units. The grain size distribution of the soil layers is summarized in Table 4.9 and the grain size distribution graphs from six representative alluvium and Pliocene boreholes are presented in Figure 4.20 and Figure 4.21.

Table 4.9. Statistical distribution of grain size for alluvium and Pliocene soils

Soil type	Total number of samples	Sieve no	Grain size (%)			
			Minimum	Maximum	Average	Standard deviation
Alluvium	GC-GM-GP	4	0	88.4	55.7	14
		200	0.1	49.2	9.9	9.6
	SC-SM-SP-SW	4	0	48.9	28	13
		200	0.2	49.8	15.9	11.6
	ML-MH	4	0	13	2.3	3.9
		200	50	94	67	12.3
	CL-CH	4	0	9.8	2.1	1.9
		200	50.2	96.4	69.6	10.7
Pliocene	GC-GP-GM	4	32.3	64.2	43.7	10.9
		200	8.3	35.8	24.9	10
	SC	4	0	33.5	16.1	11.6
		200	14.2	49.2	35.9	9
	CL-CH	4	0	14.6	3.1	3.5
		200	51.1	85.9	66.8	8.2

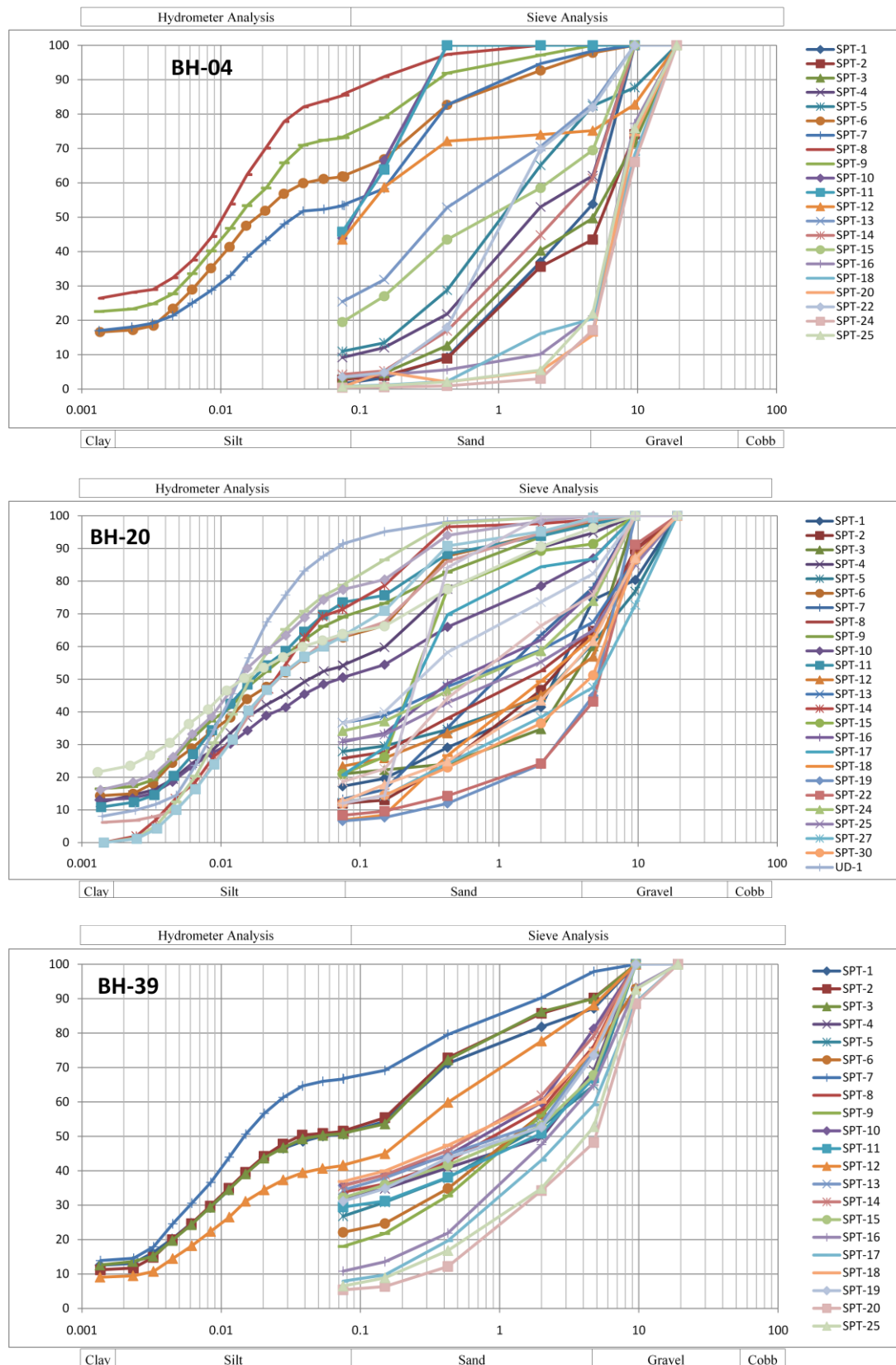


Figure 4.20. Examples of sieve and hydrometer analyses graphics for alluvium soil samples from BH-4, BH-20, and BH-39

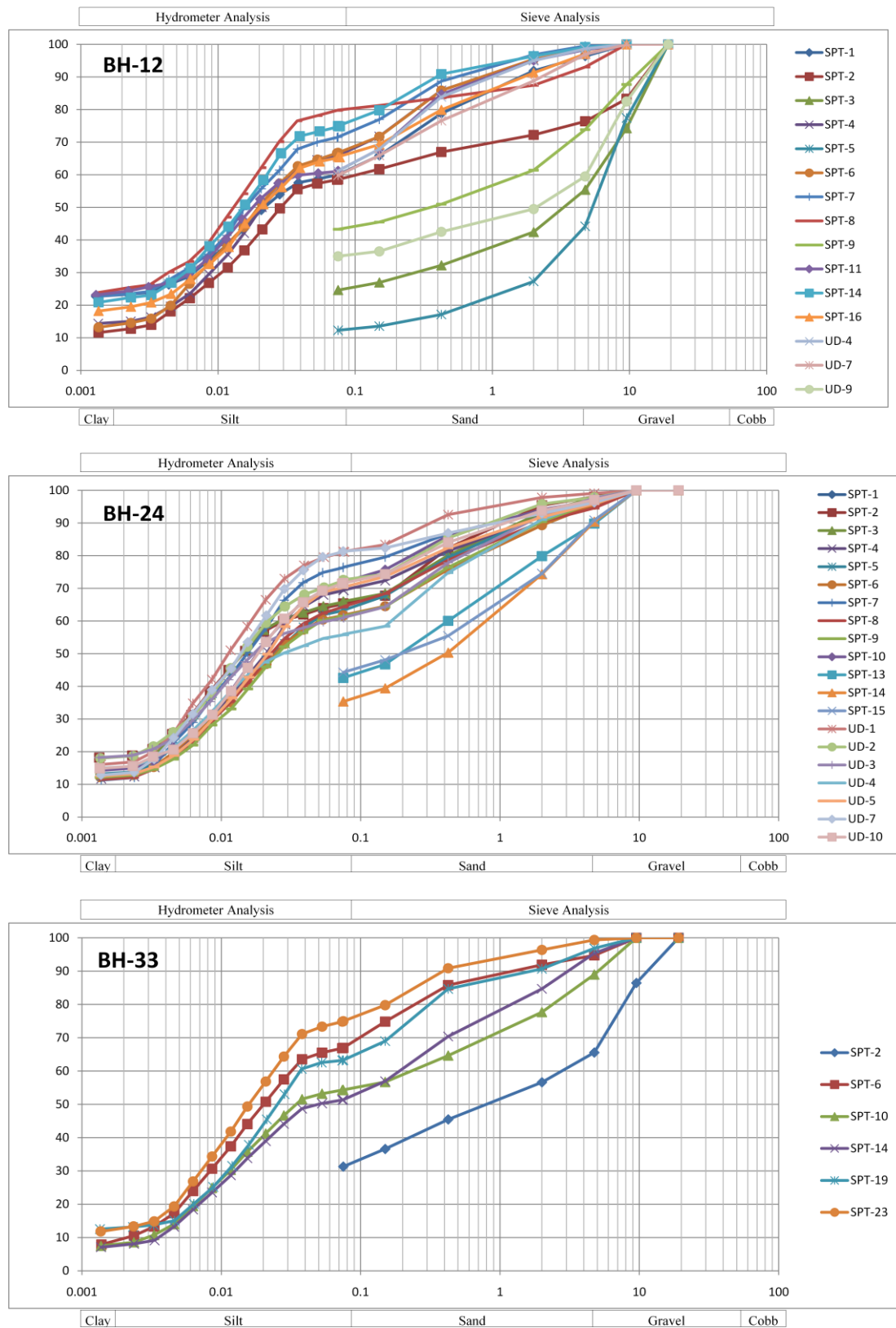


Figure 4.21. Examples of sieve and hydrometer analyses graphics for Pliocene soil samples from BH-12, BH-24, and BH-33

The plasticity of soil samples were evaluated by means of Atterberg limits tests based on ASTM (1994) standards (Table 4.10). The sandy layers (SM and SP-SW) in alluvium are found to be generally non-plastic according to test results. The only plastic unit in sand deposits is clayey sand (SC) and it has considerably low plasticity. The clayey gravel (GC) unit shows a similar plasticity with SC. Moreover, the silty layers (ML) in alluvium are commonly non-plastic as well. There are only a few high plastic silt (MH) samples. Based on Atterberg limits, the alluvial clay is mostly low plastic (CL). On the other hand, Pliocene gravel unit is usually accompanied by clay particles with respect to sieve analysis. The clayey gravel unit (GC) is low-plastic. Furthermore, the sandy layers are represented by clayey sand (SC) in Pliocene and the SC samples are typically low plastic. The clayey deposits (CL-CH) in Pliocene unit are also generally low plastic.

Table 4.10. Statistical distribution of Atterberg limits for alluvium and Pliocene soils

Soil type	Total number of samples		Atterberg limits (%)			
			Minimum	Maximum	Average	Standard deviation
Alluvium	GC-GM-GP	LL	NP - 20.4	44.4	30.3	6.3
		PL	NP - 13.6	28.6	17.4	3.1
		PI	NP - 5.6	22.8	12.8	4.7
	SC-SM-SP-SW	LL	NP - 20.6	43.7	30.1	5.6
		PL	NP - 11.1	21.6	16.7	2.2
		PI	NP - 5.5	22.7	13.4	3.9
	ML-MH	LL	NP - 35.0	57.3	49.2	12.4
		PL	NP - 24.8	30.9	28.4	3.2
		PI	NP - 10.2	26.4	20.8	9.2
	CL-CH	LL	22.6	71.3	37.8	7.6
		PL	10.7	30	19.2	3.1
		PI	6.4	42.9	18.7	5.2
Pliocene	GC-GM-GP	LL	NP - 20.4	40.4	30.5	4.9
		PL	NP - 15.3	19.1	16.9	1.1
		PI	NP - 6.7	22.5	13.6	4.8
	SC	LL	22.3	41.4	30.0	6.0
		PL	11.1	23.1	16.7	3.3
		PI	9.2	21.9	13.3	3.9
	CL-CH	LL	26.4	57.1	40.0	6.2
		PL	15.3	25	20.2	2.3
		PI	10.2	34.8	20.0	4.6

The plasticity properties of alluvium and Pliocene deposits are depicted on plasticity charts (Figure 4.22 and 4.23). According to the plasticity charts, clay with low plasticity (CL) is more common than clay with high plasticity (CH) in the study area and all clay samples are above the A line. Additionally, the plasticity properties of alluvium and Pliocene clay seem to be very similar with respect to the plasticity distribution on the plasticity charts.

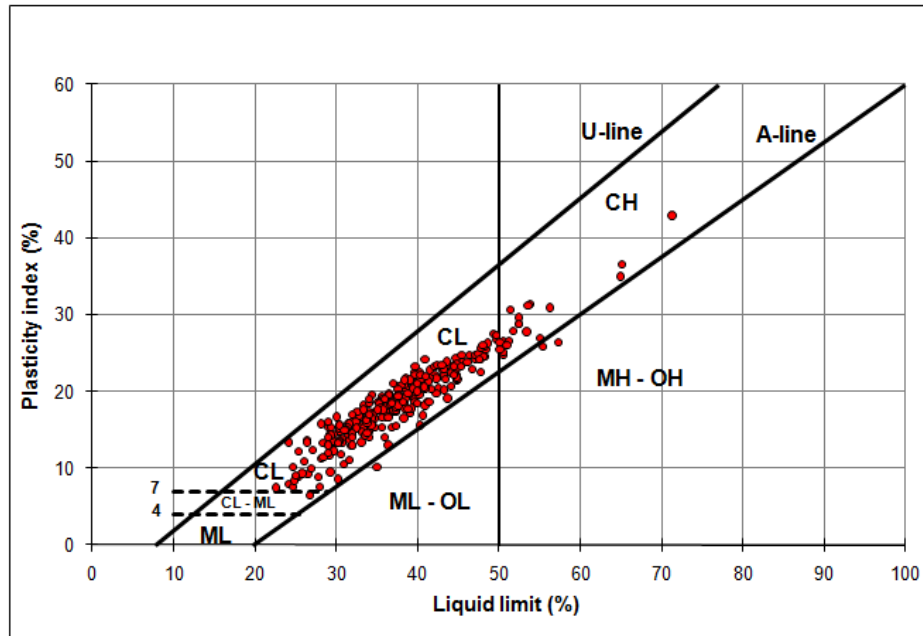


Figure 4.22. Plasticity chart for alluvial soils

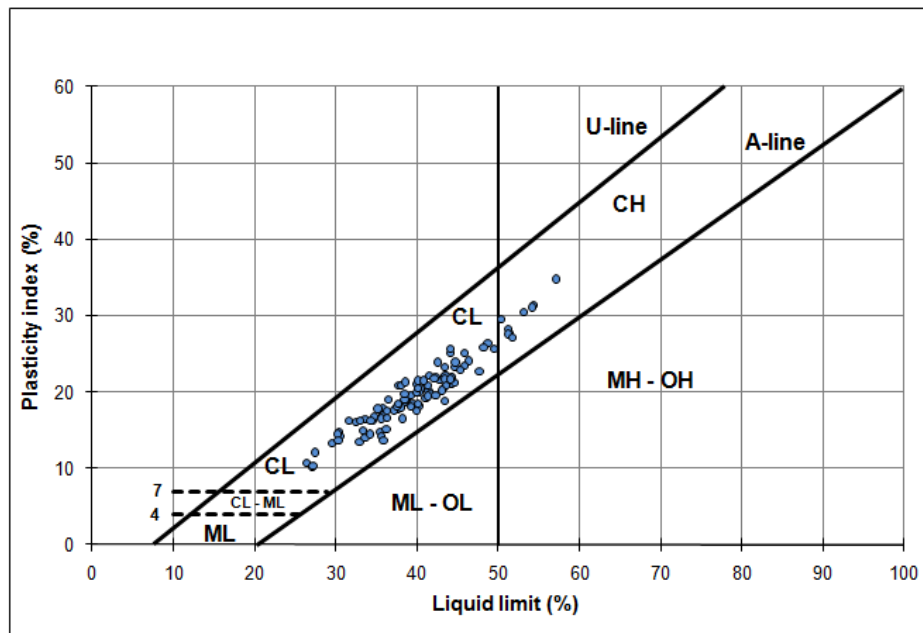


Figure 4.23. Plasticity chart for Pliocene soils

A number of physical and mechanical properties of alluvial and Pliocene plastic soils were determined on undisturbed (UD) samples. The natural unit weight, dry unit weight, specific gravity, void ratio, porosity, and saturation ratio of alluvium soils is presented in Table 4.11 while shear strength and consolidation parameters (cohesion, internal friction angle, swelling ratio, and swelling pressure) of alluvium unit is given in Table 4.12. In addition, the natural unit weight, dry unit weight, specific gravity, cohesion, and internal friction angle of Pliocene deposits are summarized in Table 4.13. The natural unit weight ( $\gamma_n$ ) of alluvium clay varies between 17.6 and 21.8 kN/m<sup>3</sup> with an average of 19.4 kN/m<sup>3</sup>. Based on the test results, the average  $\gamma_n$  of Pliocene clay (18.3 kN/m<sup>3</sup>) is found to be quite lower than that of alluvium clay. Besides, the other soil types in alluvium have typically lower  $\gamma_n$  than 19 kN/m<sup>3</sup>. Furthermore, the dry unit weight of alluvium clay is higher than Pliocene clay as well. The means of specific gravity of alluvium and Pliocene clay are 2.69 and 2.65, respectively. The alluvium silt, sand, and gravel units have typically lower specific gravity than alluvium clay. The average void ratio and porosity of alluvium clay is 0.63% and 0.38%. As a conclusion, the physical properties of alluvium clay generally indicate a stiff soil material.

Table 4.11. Statistical distribution of natural unit weight, dry unit weight, specific gravity, void ratio, porosity, and saturation ratio for alluvium soils

Soil type		Natural unit weight ( $\gamma_n$ ) (kN/m <sup>3</sup> )	Dry unit weight ( $\gamma_d$ ) (kN/m <sup>3</sup> )	Specific gravity (Gs)	Void ratio (e) (%)	Porosity (n) (%)	Saturation ratio (S <sub>r</sub> ) (%)
CL-CH	# of data	47	47	53	32	30	5
	Minimum	17.6	13.6	2.61	0.40	0.29	72.6
	Maximum	21.8	19.0	2.78	0.84	0.44	76.2
	Average	19.4	16.2	2.69	0.63	0.38	74.0
	Std. dev.	1.26	1.19	0.04	0.10	0.04	1.46
ML-MH	# of data	3	3	5	-	-	-
	Minimum	17.6	15.1	2.65	-	-	-
	Maximum	17.7	16.5	2.68	-	-	-
	Average	17.7	15.8	2.67	-	-	-
	Std. dev.	0.06	0.73	0.01	-	-	-
SC-SM	# of data	7	7	5	2	-	-
	Minimum	18.2	13.5	2.59	0.51	-	-
	Maximum	18.7	18.0	2.65	0.90	-	-
	Average	18.5	16.9	2.62	0.71	-	-
	Std. dev.	0.15	1.62	0.03	0.28	-	-
GM	# of data	2	2	1	-	-	-
	Minimum	18.7	17.9	2.50	-	-	-
	Maximum	18.8	18.4	-	-	-	-
	Average	18.8	18.2	-	-	-	-
	Std. dev.	0.06	0.38	-	-	-	-

The average undrained (UU) cohesion and internal friction angle of alluvium and the average drained (CD) cohesion and internal friction angle of Pliocene clay with low plasticity (CL) are 58 kPa, 6° and 57 kPa and 19°, respectively. The high internal friction angle in Pliocene clay is attributed to the amount of coarse grained material in the content. Moreover, the alluvial clay in the study area has low swelling potential with respect to swelling ratio and pressure. The maximum swelling pressure of the alluvial clay was found to be 11 kPa after free swell oedometer tests.

Table 4.12. Statistical distribution of undrained cohesion and internal friction angle, swelling ratio, and swelling pressure for alluvial soils

Soil type		Cohesion (c) (kPa)	Internal friction angle ( $\phi$ ) (°)	Swelling ratio (%)	Swelling pressure (kPa)
CL	# of data	5	5	5	5
	Minimum	55	4	0.85	9
	Maximum	60	7	1.05	11
	Average	58	6	0.96	10
	Std. dev.	0.02	1.22	0.08	0.01
SC	# of data	1	1	-	-
	Minimum	16	15	-	-
	Maximum	-	-	-	-
	Average	-	-	-	-
	Std. dev.	-	-	-	-

Table 4.13. Statistical distribution of natural unit weight, dry unit weight, specific gravity, effective cohesion and internal friction angle for Pliocene soils

Soil type		Natural unit weight ( $\gamma_n$ ) (kN/m <sup>3</sup> )	Dry unit weight ( $\gamma_d$ ) (kN/m <sup>3</sup> )	Specific gravity (Gs)	Cohesion (c') (kPa)	Internal friction angle ( $\phi'$ ) (°)
CL	# of data	26	23	11	3	3
	Minimum	17.7	14.4	2.64	46	18
	Maximum	20.5	16.3	2.66	70	20
	Average	18.3	15.3	2.65	57	19
	Std. dev.	0.79	0.42	0.01	12	1.0
SC	# of data	1	1	-	-	-
	Minimum	18.3	16.7	-	-	-
	Maximum	-	-	-	-	-
	Average	-	-	-	-	-
	Std. dev.	-	-	-	-	-



## 4.5 Recent Geophysical Studies

In order to correlate the characteristics of soil layers with other field and laboratory studies, several geophysical applications were performed at the site. Within the context of geophysical applications, 21 resistivity, 20 seismic refraction, 3 downhole, 10 uphole surveys, and a total of 517 microtremor measurements, 6 Multichannel Analysis Surface Waves (MASW) - Refraction microtremor (REMI) surveys were carried out. The total number of each application is given in Table 4.14. A number of 3 new boreholes were drilled to apply downhole applications and additional measurements (refraction microtremor, microtremor, resistivity, seismic refraction) were conducted near these boreholes as shown in Table 4.14. The aforementioned downhole boreholes are named as DBH-1, 2, and 3 in the following figures.

Table 4.14. Total number of geophysical applications

Geophysical tests applied in the study area	Number of locations
Resistivity survey	21
Seismic refraction	20
SPT-based uphole	10
Microtremor	517
REMI-MASW	6
Downhole boreholes	3 (DBH-1, 2, and 3)
Refraction microtremor*	3
Microtremor*	3
Resistivity*	3
Seismic refraction*	3

\*In addition to the general test applications, additional tests were applied at downhole boreholes.

In these geophysical tests, it is aimed to distinguish subsurface layers and to obtain dynamic soil parameters (e.g. shear wave velocity). The distribution of resistivity, seismic refraction, and other survey points as well as geophysical cross section lines are shown in Figure 4.24.

### 4.5.1 Resistivity survey

In general, electrical resistivity is applied to determine the location of saltwater boundaries, clean granular and clay strata, rock depth, and underground mines by measured anomalies (Hunt, 2007). Resistivity surveys were performed at 24 (21+3) points along 3 profiles in Erbaa to differentiate the subsurface geology and the bedrock depth (Figure 4.24).

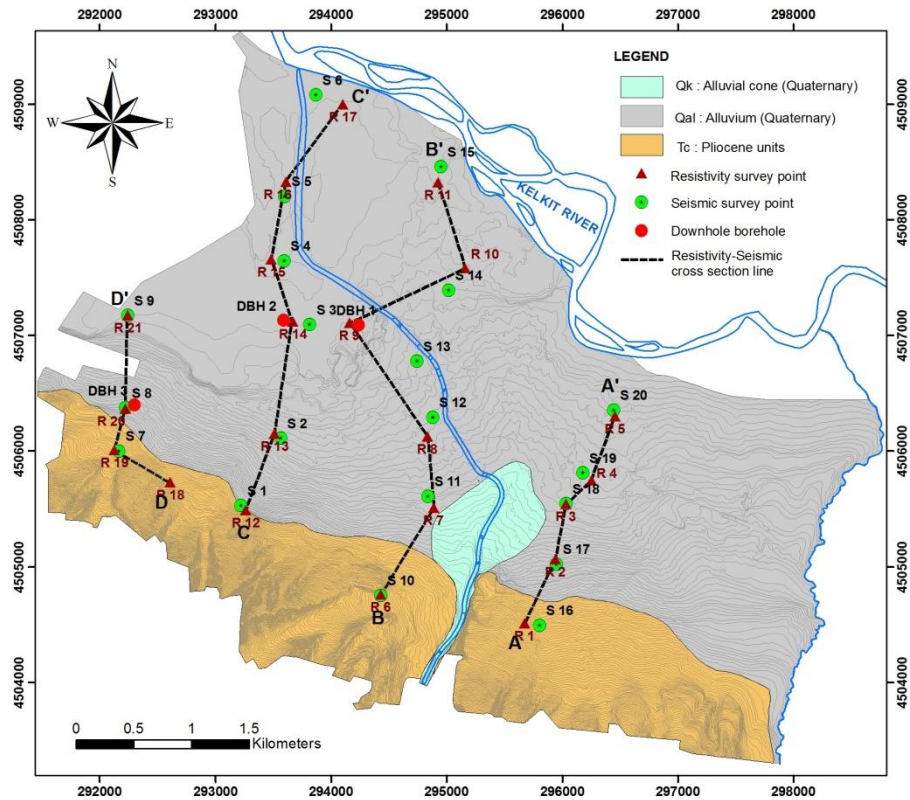


Figure 4.24. Distribution of geophysical survey points

Schlumberger method was applied during resistivity measurements and a total of 150 m depth was investigated (Figures 4.25 and 4.26). A low frequency original resistivity instrument working with an alternative current was employed in resistivity surveys.

The resistivity device involves three main units; transmitter, receiver, and source. The properties of these three units are summarized below:

- a. Transmitter
  - Output voltage: 400 Volt max
  - Output current: 1,2,10,20,50,100,200,500 mA
- b. Receiver
  - Input impedance: 10 M\_Ω
  - Measured potential: 25 mV, 250 mV, 2500 mV
  - Resolution: 1 microV
  - Stack count: 1,4,16,64
  - Time of one measurement cycle: 3.7 seconds
- c. Source : 12 V accumulator

The Schlumberger electrode configuration was utilized in the resistivity applications and the gradient value of potential function was measured. In this measurement system, the undesired shattering effect of horizontal formations is minimized and the effective penetration depth is increased. In the Schlumberger electrode configuration system, a total of four electrodes are aligned with respect to a zero point on a linear alignment (Figure 4.25). As seen in Figure 4.25, the A and B points are the current electrodes, whereas M and N points are the potential electrodes. The potential gradient of electrical field generated by the application of an electrical current (I) in soil layers using current electrodes is measured by potential electrodes.

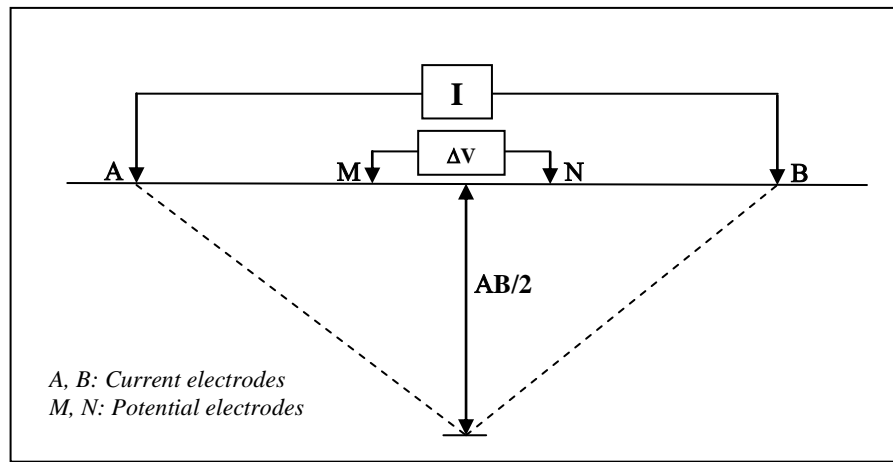


Figure 4.25. Schlumberger electrode configuration

The apparent resistivity is calculated by dividing the measured potential difference by the input current and multiplying by a geometric factor specific to the array being used and the electrode spacing (Equation 4.1). The measurement depth varies according to the resistivity, thickness, and deposition order of the soil layers. This depth is considered as  $AB/2$  in the Schlumberger Electrode Configuration.

$$\rho_a = K \cdot \Delta V / I \quad (4.1)$$

- $\rho_a$  : Apparent resistivity (Ohm.m)  
 $K$  : Geometric factor (m)  
 $\Delta V$  : Measured potential difference (mV)  
 $I$  : Input current (electrical current) (mA)



Figure 4.26. Application of resistivity measurement in the study area

The depth, thickness, and resistivity of subsurface layers were evaluated using WinSev 6 software in accordance with the data gathered from 21 resistivity points. The resistivity cross section lines are illustrated in Figure 4.24 and the summary of resistivity survey results is given in Table 4.15. Four different geophysical cross sections are presented in Figures 4.27 to 4.30.

Table 4.15. Summary of the resistivity survey results

Resistivity Location	X	Y	Z (m)	Lithological Unit	Thickness (m)	Apparent Resistivity ( $\Omega m$ )
R-1	4504511	295677	257	Residual soil	7	70
				Gravel	7	50
				Marn-Sandstone	-	20
				Marn-Sandstone	-	30
				Marn-Sandstone	-	30
R-2	4505064	295943	242	Residual soil	10	110
				Gravel	22	65
				Marn-Sandstone	-	20
R-3	4505545	296034	213	Residual soil	3	36
				Clay	13	15
				Sand	81	40
				Marn-Sandstone	-	20
R-4	4505747	296253	221	Residual soil	7	70
				Clay	22	18
				Gravel-sand	92	40
				Marn-Sandstone	-	30

Table 4.15 (continued)

R-5	4506304	296460	211	Residual soil	7	65
				Residual soil	7	130
				Gravel-sand	25	50
				Gravel	62	80
				Marn-Sandstone	-	20
R-6	4504762	294432	260	Sandy clay	7	50
				Gravel	26	170
				Marn-Sandstone	-	15
R-7	4505511	294890	223	Sandy clay	7	30
				Gravel	40	120
				Marn-Sandstone	-	12
R-8	4506127	294837	216	Gravel	18	40
				Gravel	41	200
				Gravel	-	70
R-9	4507108	294163	202	Gravel-sand	9	100
				Sand-gravel	50	50
				Marn-Sandstone	-	12
R-10	4507583	295161	200	Gravel-sand	10	140
				Gravel	14	60
				Sand-gravel	25	100
				Sand-gravel	-	50
R-11	4508327	294926	202	Gravel-sand	5	85
				Gravel	58	120
				Sand-gravel	-	75
R-12	4505490	293261	243	Residual soil	4	34
				Gravel-sand	4	100
				Marn-Sandstone	-	40
R-13	4506154	293511	216	Residual soil	4	30
				Gravel-sand	24	70
				Marn-Sandstone	-	22
R-14	4507122	293668	199	Residual soil	6	18
				Gravel-sand	25	70
				Marn-Sandstone	-	22
R-15	4507660	293484	200	Residual soil	2	15
				Gravel-sand	36	60
				Marn-Sandstone	-	20
R-16	4508330	293611	200	Gravel	8	100
				Gravel	62	120
				Sandstone	-	40
R-17	4509001	294102	198	Gravel	8	140
				Gravel	-	130
R-18	4505730	292608	246	Sand-gravel	8	34
				Gravel	28	100
				Marn-Sandstone	-	34
R-19	4506010	292127	246	Sand-gravel	19	34
				Gravel	17	100
				Marn-Sandstone	20	22
				Marn-Sandstone	-	28
R-20	4506867	291522	215	Sand-gravel	6	19
				Sand-gravel	46	44
				Marn-Sandstone	-	16
R-21	4507178	292240	196	Sand-gravel	102	25
				Marn-Sandstone	-	8

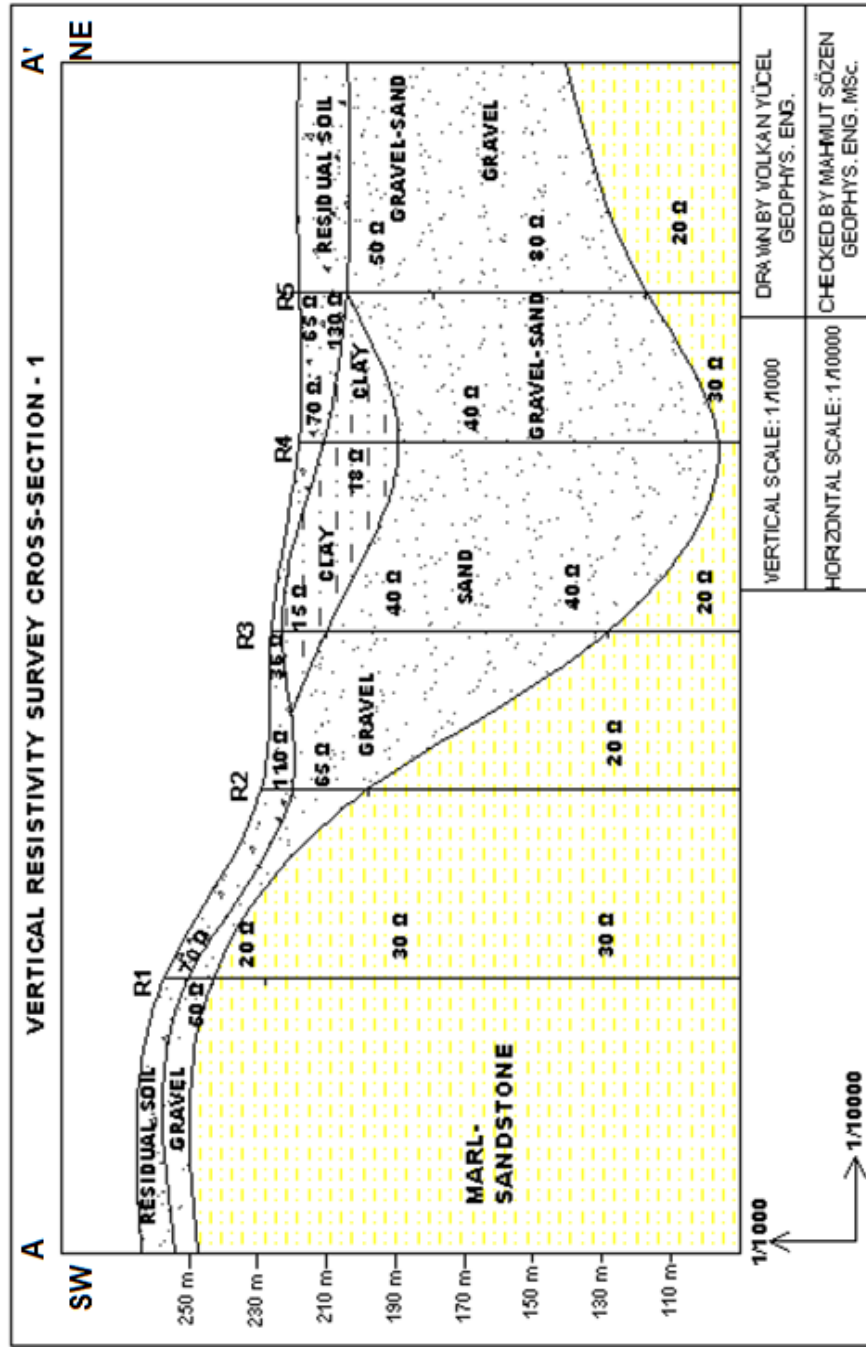


Figure 4.27. A-A' resistivity cross section

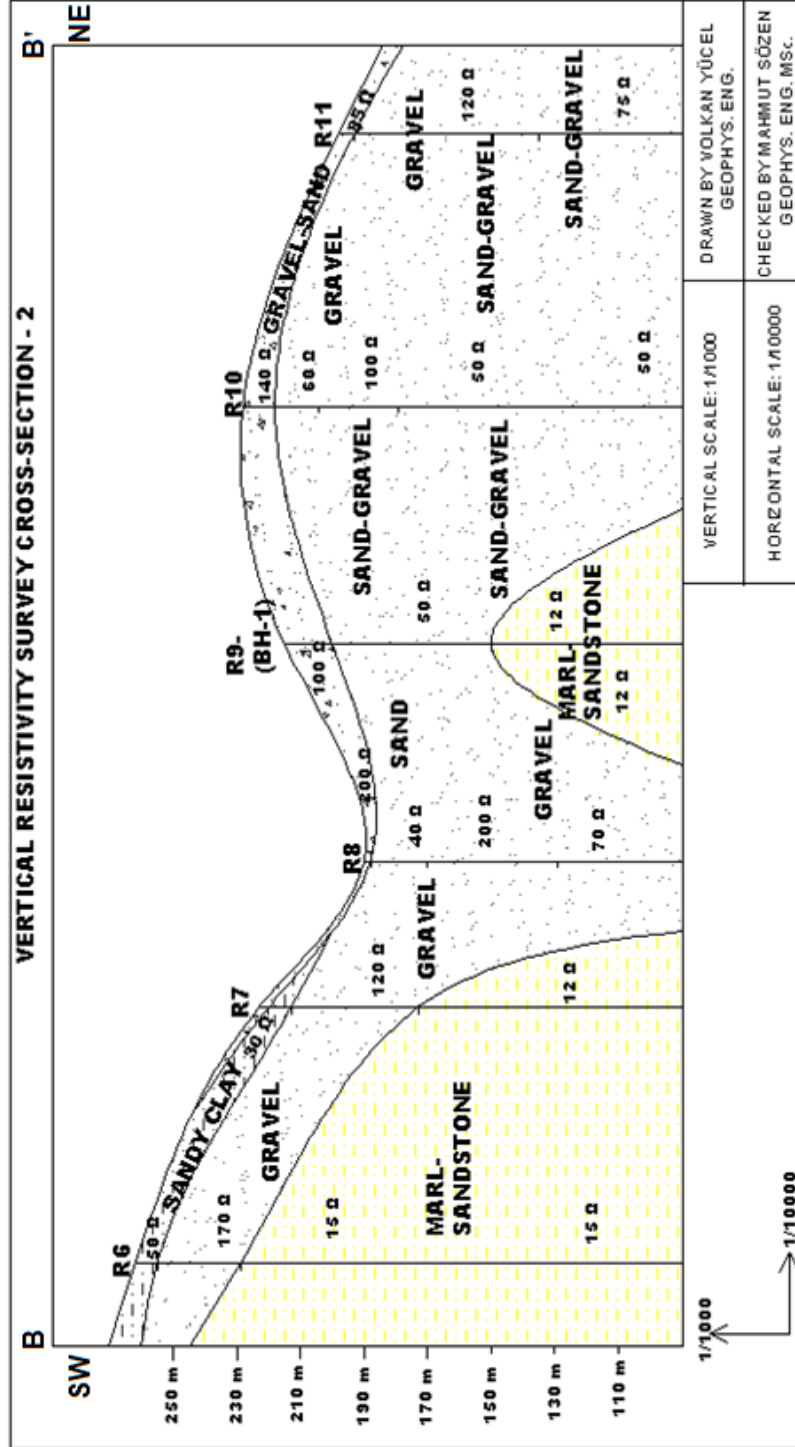


Figure 4.28. B-B' resistivity cross section

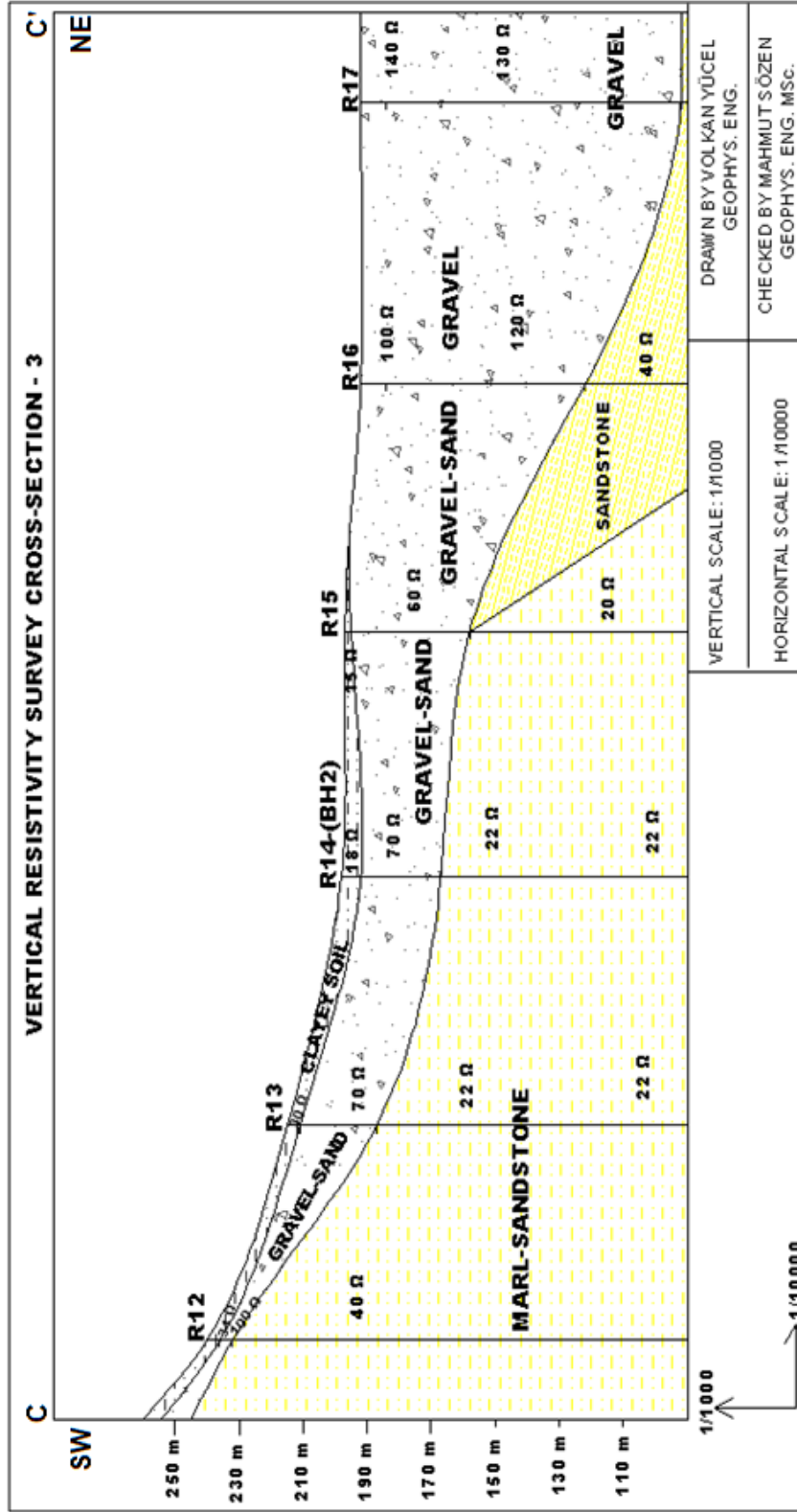


Figure 4.29. C-C' resistivity cross section



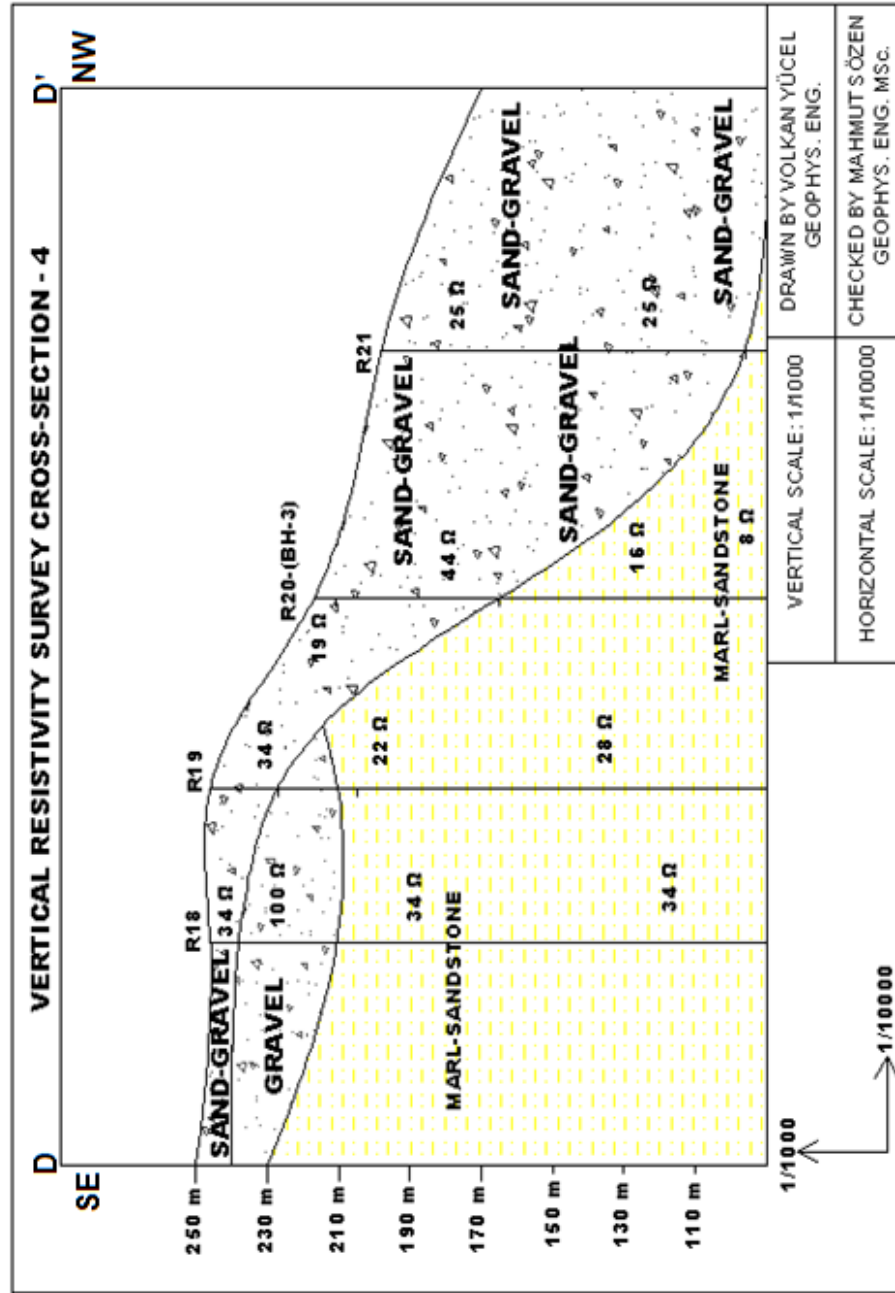


Figure 4.30. D-D' resistivity cross section

#### 4.5.2 Seismic refraction

The seismic refraction test involves the measurement of travel times of P- and/or S-waves from an impulse source to a linear array of points along the ground surface at different distances (ASTM D 5777-00, 2006) (Figure 4.31).

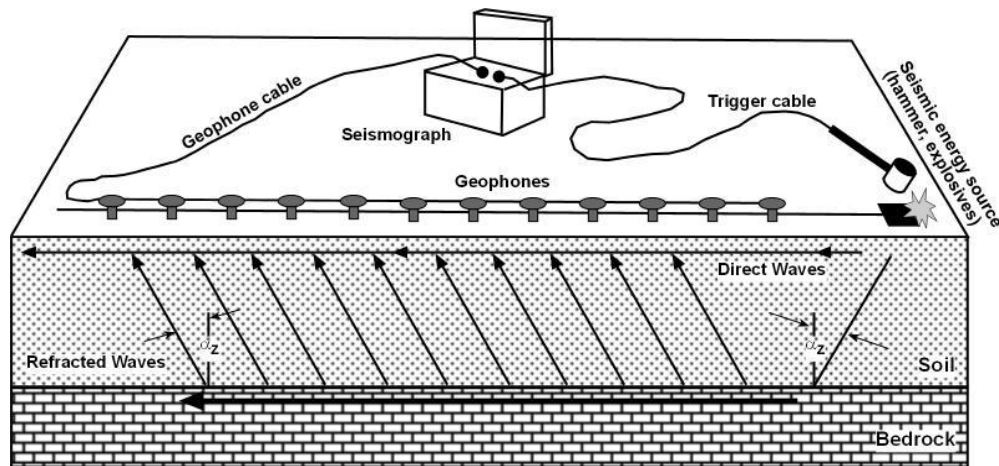


Figure 4.31. Seismic refraction test (modified from ASTM D 5777-00, 2006)

This technique was firstly employed for deep oil explorations and became more popular for relatively shallow depth ranges in the geotechnical applications (Stam, 1962; Richart et al., 1970; Redpath, 1973). The refracted waves travel faster in stiff layers. If the velocity increases with depth, the refracted waves travelling along layer boundaries will arrive to the surface. The limitation of this method is the failure of identifying slow layers below fast layers as well as thin layers with sharp velocity contrasts (Redpath, 1973; Kramer, 1996; Luna and Jadi, 2000; McGillivray, 2007). Basic equipment of this method includes an energy source (hammer), seismometers, geophones, and a recording seismometer. Seismic refraction is generally used for determining the depth of very hard layers, such as bedrock.

Seismic refraction measurements were performed at 23 (20+3) locations to obtain the subsurface geologic conditions in Erbaa. A Seistronix brand, American made digital seismograph with 24 byte A/D resolution and 12 channels was utilized in seismic refraction surveys (Figure 4.32). This seismograph is a stack count type and can record by stacking each track of strike. The results were evaluated by means of RAS-24 software. The software

on seismograph (RAS-24) can also filter the surrounding undesired noises. However, digital filtering was not applied in this project to any of the seismic records. Therefore, raw seismic data were preserved.



Figure 4.32. Application of seismic refraction survey at the field

The compressional wave (P wave) was generated by vertically striking a plate with a 10 kg weigh hammer in seismic refraction survey. A splash and cable with 5 m interval and 12 channel take-out was employed in P-wave seismic survey. A total of 5 strikes were performed. The distance between each strike was 30 meters. The arrival times and P wave velocity was determined by SEISOPT@2D software. The Multichannel Analysis Surface Waves (MASW) method was employed for the determination of shear wave (S<sub>wave</sub>) - depth distribution. The field data were recorded using a 12\_channel RAS 24 digital seismograph with a 3 m geophone interval. The offset distance between source point and first geophone was selected as 18 meters to reach a 30 m investigation depth. A number of 2 surface waves were recorded on the splash. One and two dimensional S wave velocity depth variation was retrieved by SURFSEIS\_1.5 surface wave dispersion analysis software.

As a result, seismic refraction survey with 5 m vertical P wave and 12 channel output (takeout) was recorded. Seismic refraction surveys were carried out along 3 sections to obtain shear wave velocity profile. Table 4.16 presents the results of seismic refraction surveys. The geological cross sections produced according to seismic survey measurements are illustrated in Figures 4.33 - 4.36. Totally, 3 different layers were defined with respect to seismic measurements.

Table 4.16. Results of seismic refraction surveys

	Seismic Refraction Survey #	LAYER 1					LAYER 2				LAYER 3		
		X	Y	Z	Depth (m)	Vs-1 (m/sec)	Vp-1 (m/sec)	Depth (m)	Vs-2 (m/sec)	Vp-2 (m/sec)	Depth (m)	Vs-3 (m/sec)	Vp-3 (m/sec)
DBH 2	S1	4505531	37 293219	240	0-1	55	212	1-16	196	590	>16	392	790
	S2	4506113	37 293565	215	0-9	110	443	>9	279	887			
	S3	4507097	37 293817	198	0-1	138	350				>1	519	1660
	S4	4507648	37 293594	197	0-4	80	385				>4	350	1544
	S5	4508205	37 293601	192	0-2	143	340				>2	447	1500
DBH 3	S6	4509083	37 293870	193	0-3	87	365				>3	216	1170
	S7	4506003	37 292164	246	0-14	373	419				>14	691	1645
	S8	4506877	37 291521	217	0-13	352	566				>13	734	1486
	S9	4507175	37 292242	198	0-1	292	381				>1	?	1811
	S10	4504755	37 294432	263	0-11	254	481				>11	?	1196
DBH 1	S11	4505612	37 294839	223	0-9	294	421	9>	526	824			
	S12	4506295	37 294881	192	0-4	228	357	4-10	?	654	>10	?	1201
	S13	4506780	37 294742	217	0-10	?	340	10>	350	700			
	S14	4507393	37 295019	230	0-10	?	285	10>	306	485			
	S15	4508462	37 294953	198	0-4	?	265	4-14	272	595	>14	?	1102
	S16	4504497	37 295805	257	0-2	72	270	2-12	431	616	>12	703	829
	S17	4505026	37 295951	229	0-6	209	435	6-60	352	654			
	S18	4505548	37 296036	226	0-3	158	446	3-12	354	570	>12	460	1229
	S19	4505815	37 296181	218	0-10	334	382				>10	460	927
	S20	4506358	37 296447	220	0-12	255	452				>12	336	986

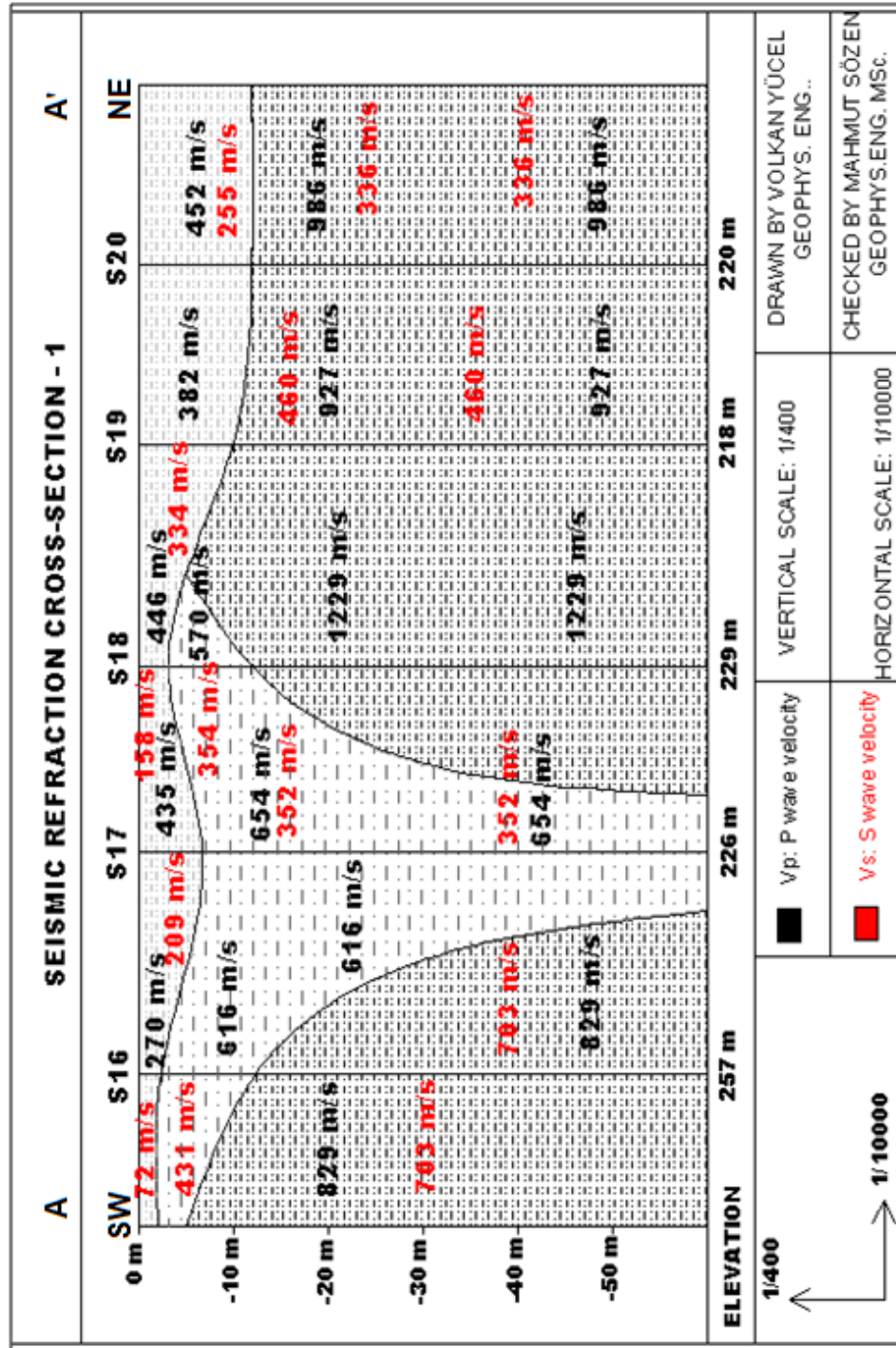


Figure 4.33. A-A' seismic refraction cross section



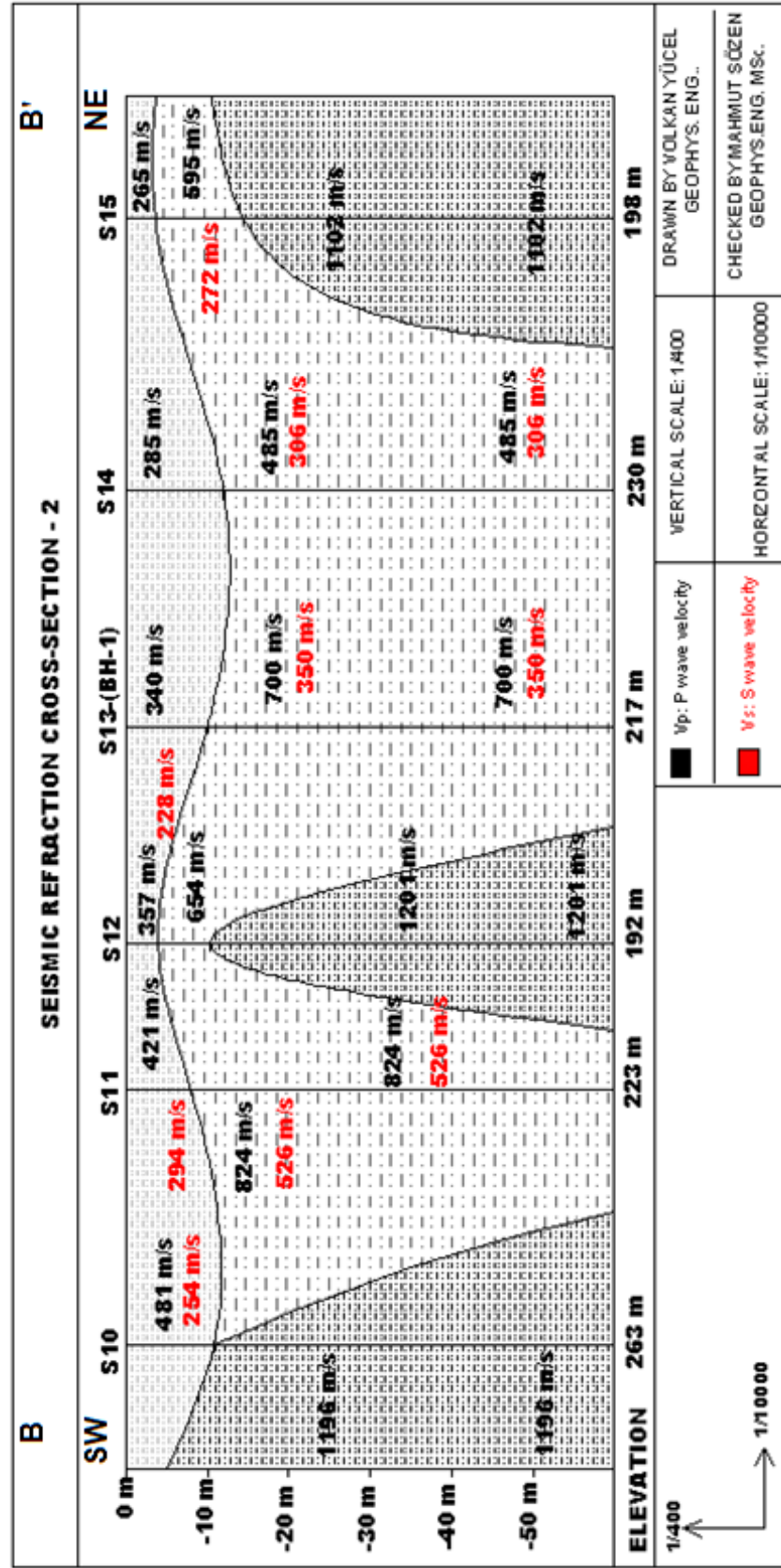


Figure 4.34. B-B' seismic refraction cross section

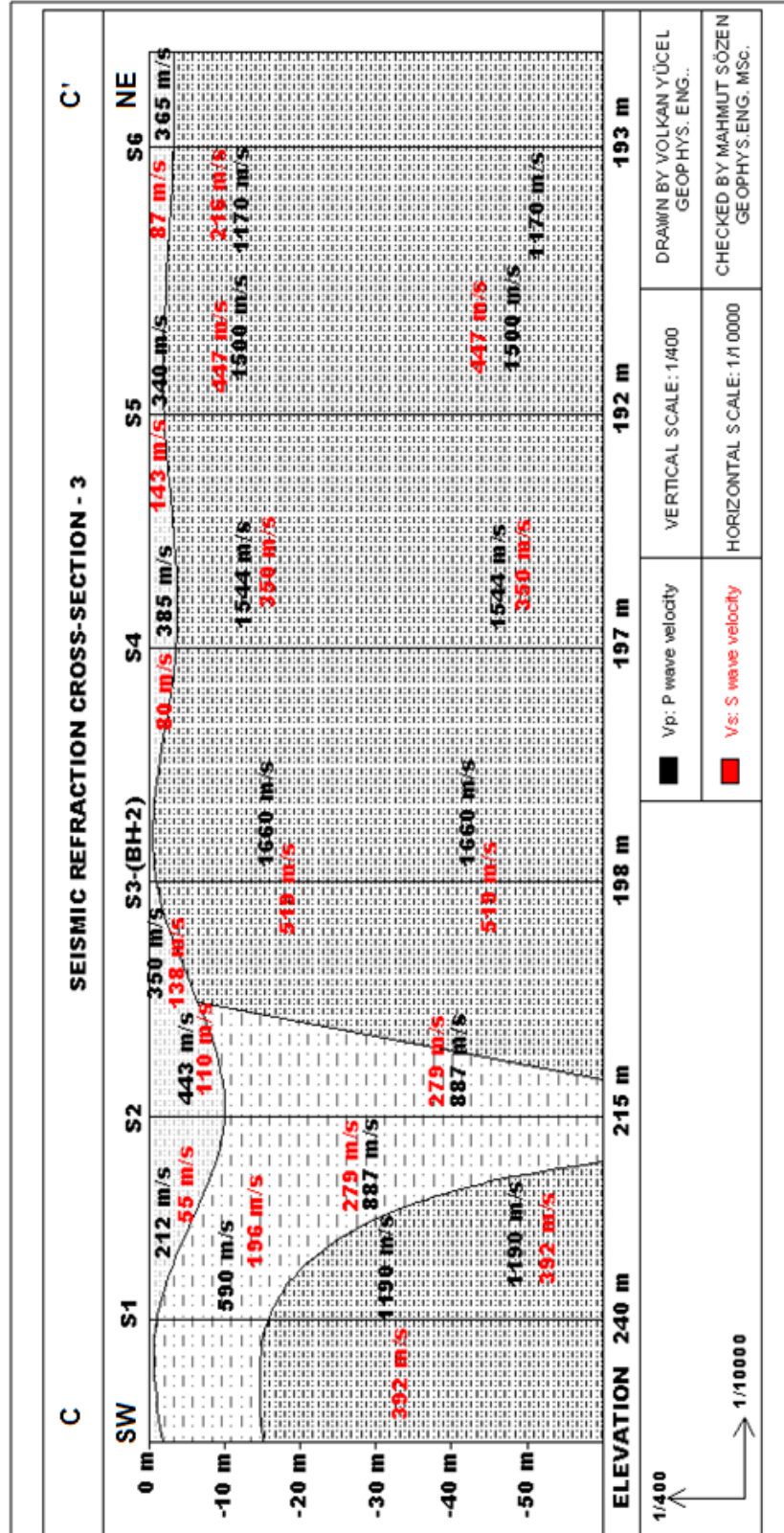


Figure 4.35. C-C" seismic refraction cross section

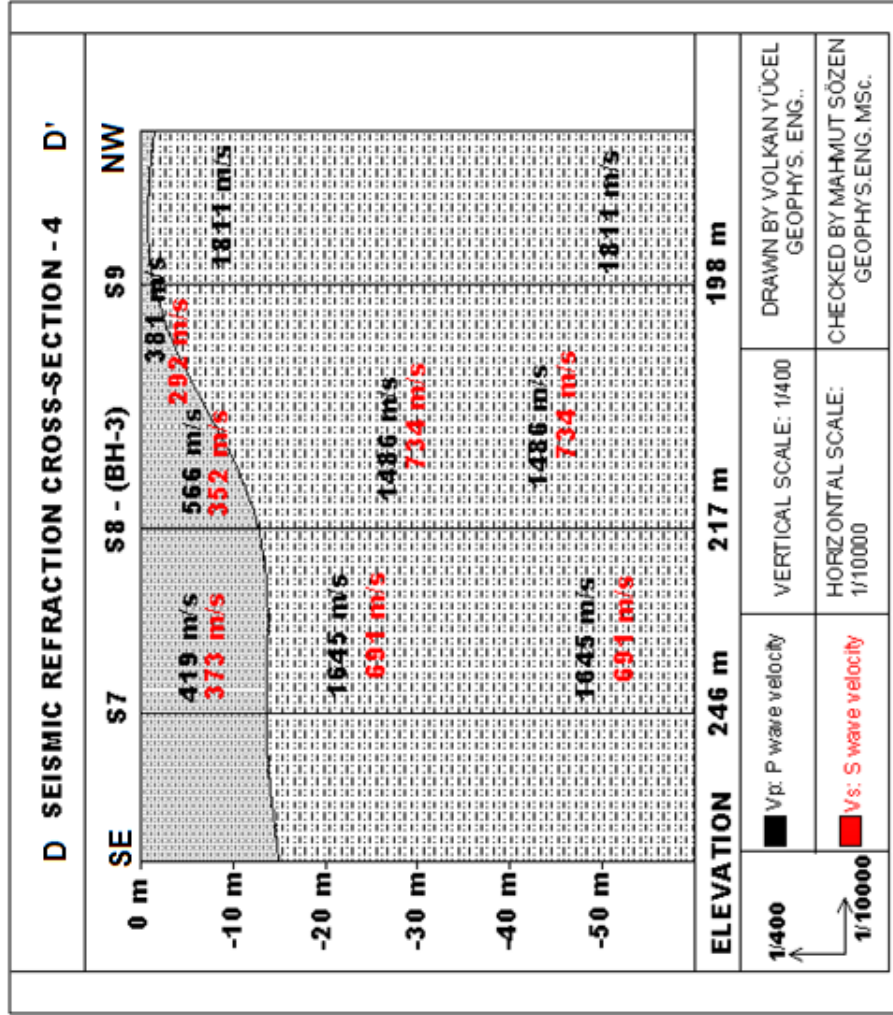


Figure 4.36. D-D' seismic refraction cross section



#### 4.5.3 SPT (Standard Penetration Test)-based uphole

The SPT-based uphole method which uses the impact energy of the split spoon sampler in SPT test as a source was firstly introduced by Ohta et al. (1978b). An experimental study was carried out to develop a technique to measure shear wave velocity simultaneously with the standard penetration test. The obtained shear wave velocities were compared with  $N$  values from the standard penetration test (SPT) and specific resistivity measurements. In addition, Ohta et al. (1978b) mentioned that the gathered data are consistent and the shear wave velocity measurement can precisely be conducted during a routine work of a SPT in future works. After Ohta et al. (1978b), Bang and Kim (2007) used the same method by interpreting the test results. They introduced the SPT-based uphole test as a combination of low and high-strain tests. The SPT-based uphole test is a modified version of the seismic uphole method. Moreover, it is a field seismic test that uses a number of receivers (geophones) inserted on the ground surface to obtain the shear wave velocity ( $V_s$ ) profile of a site.

The impact energy generated by SPT test can be used as a source for the uphole method (Kim et al., 2004; Bang and Kim, 2007). In this method, it is aimed to record the shear waves during SPT test without any additional explosives or mechanical sources. A schematic diagram of the SPT based uphole method is shown in Figure 4.37. A significant amount of compression and shear waves caused by the tip and side stresses ( $\sigma_t$  and  $\sigma_s$  in Figure 4.37) are generated when the split spoon sampler is penetrated into the soil through hammering at the ground surface (Bang and Kim, 2007).

The testing procedure can be briefly described as follows: the surface geophones are placed on the ground surface at the selected intervals from the boring point. A minimum of two receivers are required and at least five receivers are recommended since using more receivers provide better results. During the interpretation stage, the site is assumed to be horizontally layered and the close receivers to the boring machine should be preferred for accurate results. However, the close receivers can be easily affected from the engine noise of boring machine. Therefore, it is advised to drop the hammer manually after turning off the engine in order to reduce the machine noise. Generally, the SPT is performed at 1 or 1.5 m intervals. After drilling until a certain depth, SPT-based uphole method can be performed with SPT simultaneously. In order to check the repeatability, signal traces should be obtained by hammering more than twice at each testing depth. Measuring the exact source depth is also

important, and the distance from the tip of split spoon sampler to the ground surface should be measured at each hammering and recording of the signals. After drilling to the next testing depth, the same steps should be repeated until the end of borehole (Bang and Kim, 2007).

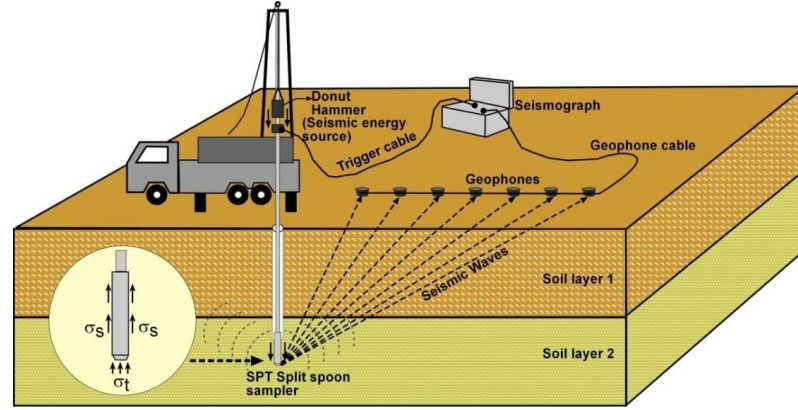


Figure 4.37. A schematic diagram of SPT-based uphole method (after Bang and Kim, 2007)

The SPT-based uphole method was firstly used in Turkey as a part of this study. Accordingly, this method was applied in newly drilled 10 boreholes (BH 4, 6, 8, 10, 12, 18, 23, 28, 30, 33) to obtain shear wave velocity. A total of 7 geophones with 2 m interval were placed on the ground surface and the measurements were recorded during hammering in SPT applications. The application procedure and a sample recording can be seen in Figures 4.38, 4.39, and 4.40. As recommended, two-component (radial, horizontal, and vertical) geophones were preferred in order to obtain better travel time information. Two recordings were conducted during SPT application (Akin et al., 2009).

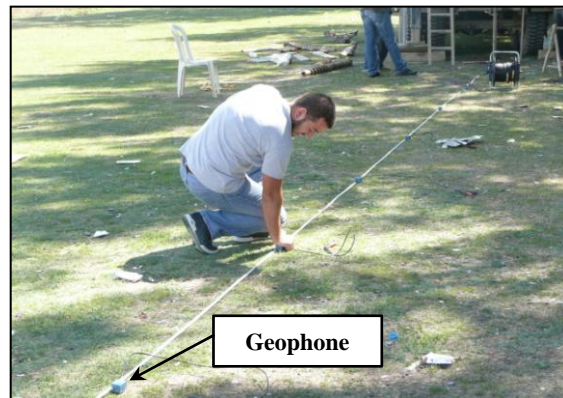


Figure 4.38. Installation of geophones before SPT-based uphole application



Figure 4.39. Installation of trigger cable below the hammer anvil

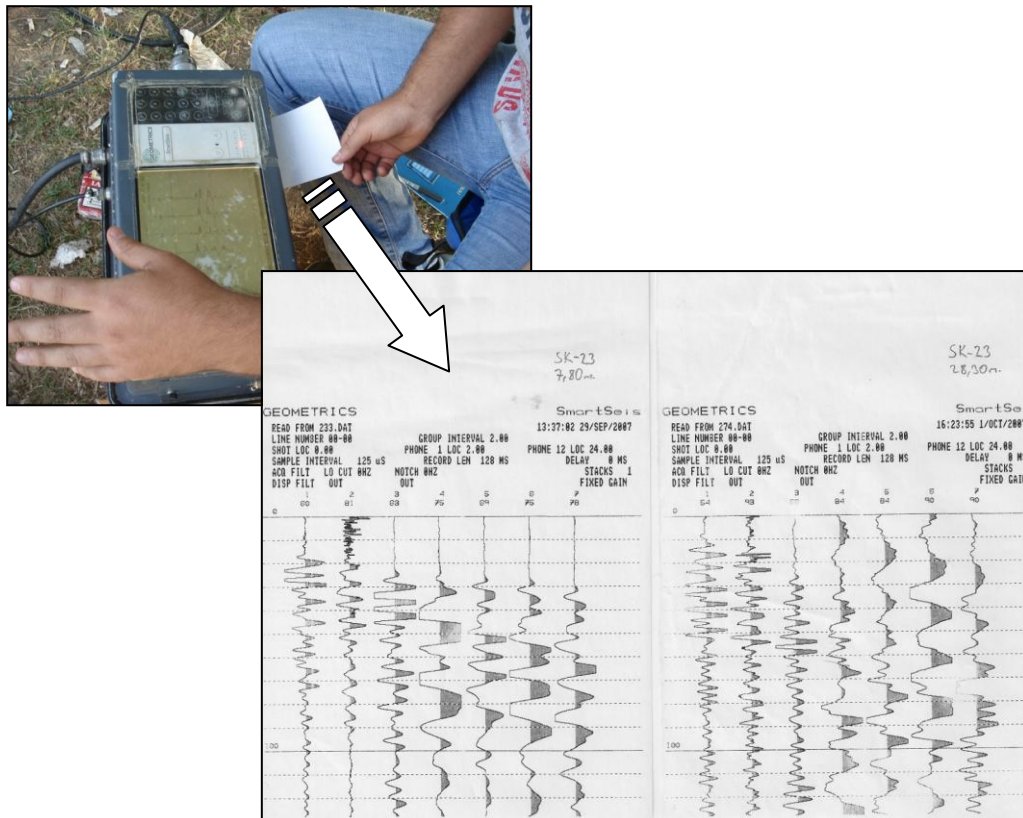


Figure 4.40. A sample SPT-based uphole record including 7 different geophones

#### 4.5.4 Microtremor measurements

The microtremor measurements were firstly employed by Kanai et al. (1954); Kanai and Tanaka (1961) to obtain dynamic properties of soil layers. The periods below 1 sec (above 1 Hz) and the microtremor sources related to traffic, human effects, factory machines, etc. are defined as short-period microtremors. Moreover, the periods above 1 sec (below 1 Hz) and the microtremor sources related to natural hazards such as wind and atmospheric effects, etc. are defined as long-period microtremors (Okada, 2003). The short period related microtremors have been widely used in the literature (Kanai and Tanaka, 1961).

It is very simple to perform microtremor measurements at the site. The main instruments needed for microtremor records are:

- a) High sensitive, long and wide band sensor with 3 components (velocity or acceleration measurement)
- b) Recorder
- c) Battery
- d) GPS
- e) Compass
- f) Notebook

In general, three main techniques were proposed for microtremor analysis (Ojeda and Escallon, 2000):

1. Direct interpretation of the Fourier transform (or autocorrelation spectrum) called as Fourier Analysis.
2. Spectral ratios relative to a reference site called as Kagami technique (Kagami et al., 1986).
3. Spectral ratios of horizontal relative to vertical components called as Nakamura technique (Nakamura, 1989).

Ojeda and Escallon (2000) mentioned that the microtremor analysis using the Nakamura technique is a valuable tool to verify the dominant periods of vibration of shallow soft soils and plastic behavior. In addition, the seismic zones with typical dynamic behaviors can be determined by the obtained microtremor results which become very important in microzonation studies for urban areas as mentioned in the same study.

Within the content of DPT project, Dikmen et al. (2009) carried out microtremor measurements at 517 points considering traffic and noise effects to obtain the period and amplification of subsurface layers. Moreover, the microtremor measurements were evaluated using Nakamura (1989) technique. The predominant period and seismic amplification at each microtremor measurement point are depicted in Figures 4.41 and 4.42.

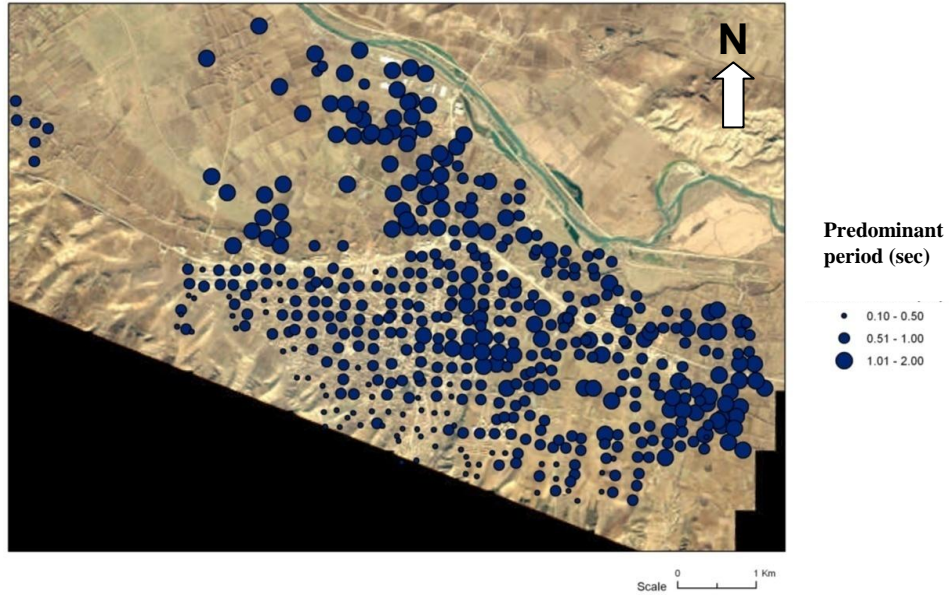


Figure 4.41. Predominant period values at microtremor measurement locations (after Dikmen et al., 2009)

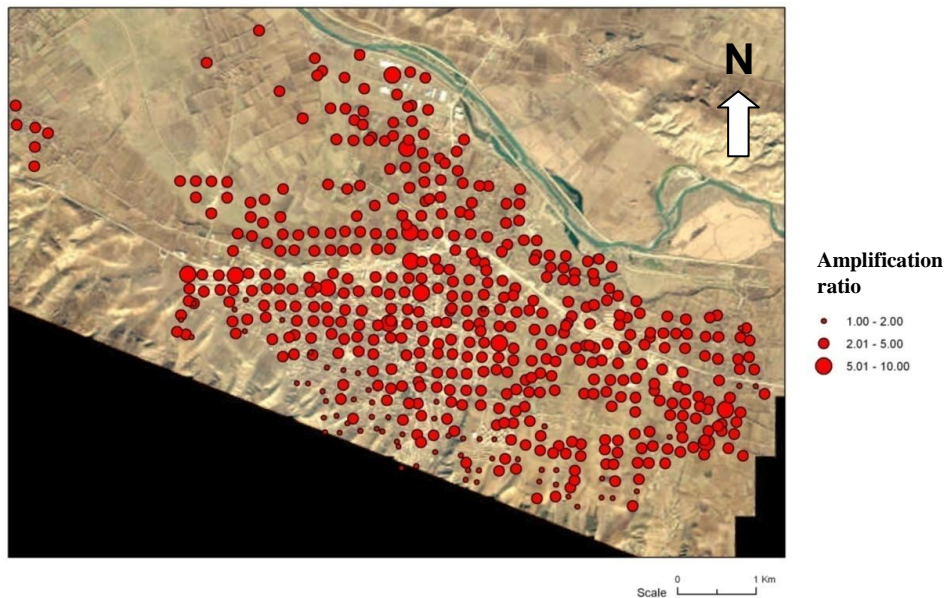


Figure 4.42. Amplification ratios at microtremor measurement locations (after Dikmen et al., 2009)



In addition, the active and passive source shear waves were also obtained at the field along depth by the application of Multichannel Analysis Surface Waves (MASW) and Refraction Microtremor (REMI) methods. The REMI method is based on the analysis of surface waves generated by environmental noise, characterized by low frequency content, usually comprised between 10Hz and 15Hz (Louie, 2001). The REMI method does not allow determining an accurate shear wave velocity profile within the first 30 m. However, the combination of MASW-REMI provides a more reliable shear wave velocity profile. These two methods were applied together at 5 points in the study area. The distribution of these REMI-MASW points and microtremor measurements can be seen in Figure 4.43. It should be noticed that some microtremor and REMI-MASW points are out of the study area boundary. During measurements, Geometrics -GEODE brand, American made digital seismograph with 24 channel resolution was used. Obtained records were evaluated using software developed by Ankara University Geophysical Engineering Department. The obtained shear wave profiles from REMI-MASW surveys are depicted in Figure 4.44.

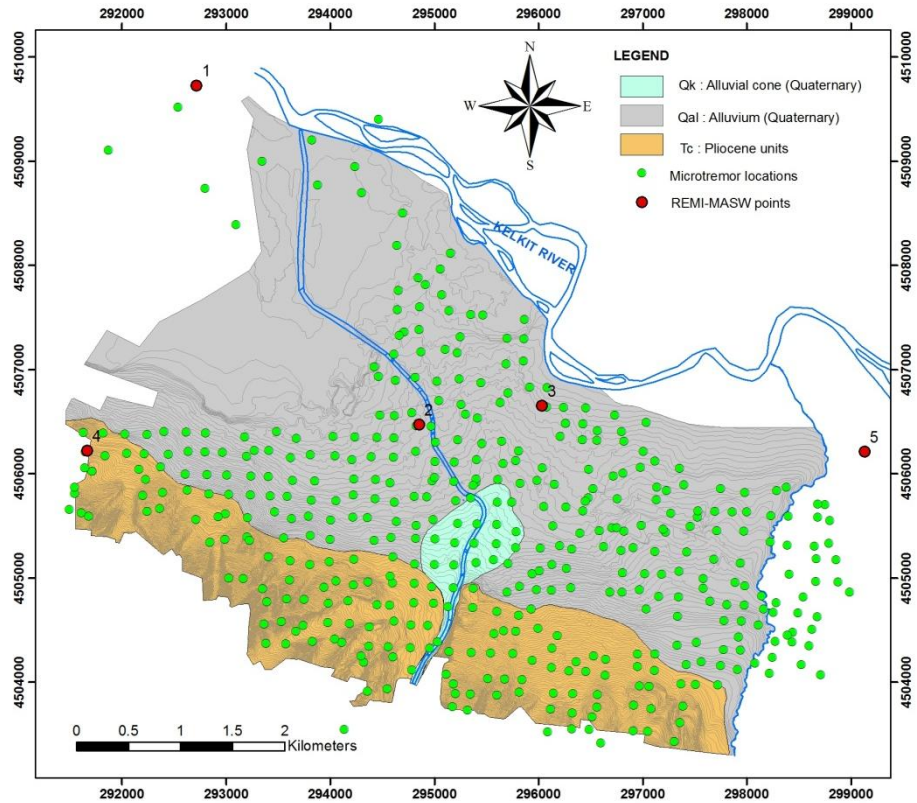


Figure 4.43. Location of REMI-MASW and microtremor measurement points

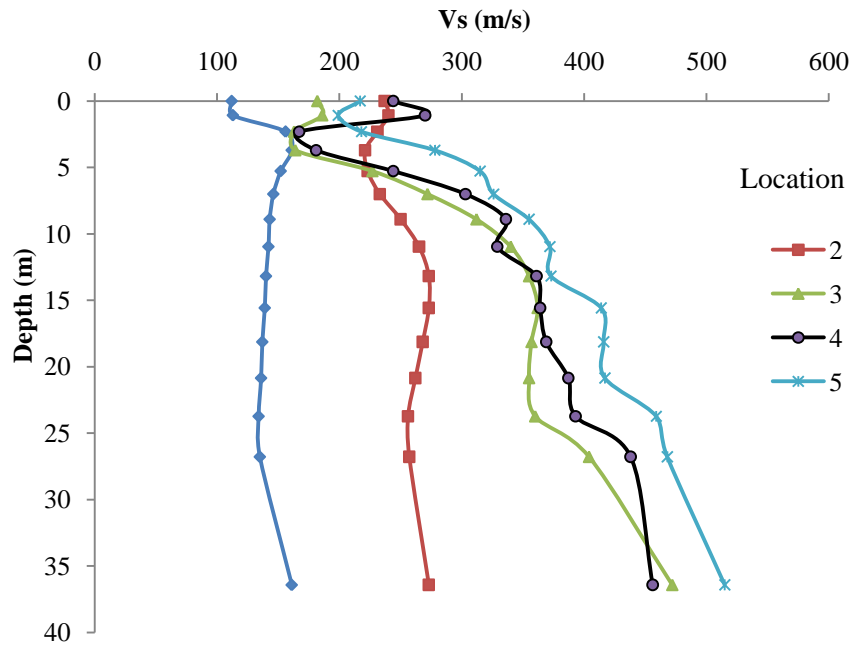


Figure 4.44.  $V_s$  values obtained from REMI-MASW measurements

#### 4.5.5 Downhole measurements

The objective of downhole test is to measure the travel time of P- and/or S-waves from the energy source to the receiver(s) (Figure 4.45). It is easier to generate S waves in downhole test than in uphole test. In addition, downhole test is more commonly used in microzonation applications (Mancuso et al., 1989). Seismic downhole test is very practical for obtaining P- and/or S-wave records after drilling.

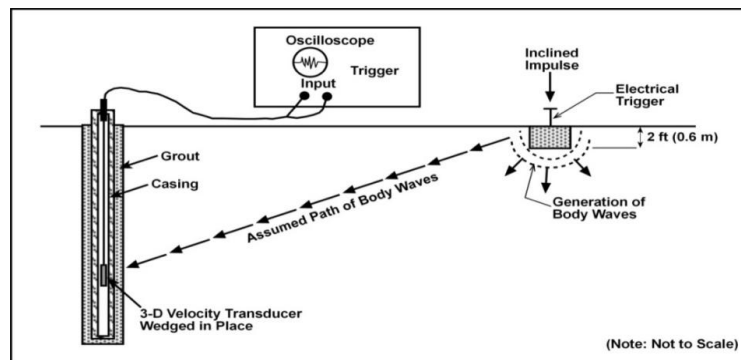


Figure 4.45. A schematic diagram of seismic downhole test

Seismic downhole tests were performed at three different locations in this study. Accordingly, P- and S-wave velocities were measured by means of straight and reverse strikes from top to bottom in downhole boreholes DBH-1, 2 and 3 as shown in Figure 4.24. These borehole locations were also considered in the resistivity and seismic refraction surveys. The plate on which the seismic wave was produced was placed 3 m away from the borehole. Additionally, the geophones were lowered in the borehole and fixed into the borehole walls in certain depths (Figure 4.46). The seismic downhole survey results at three downhole borehole locations as well as the dominant period and amplification of soils are summarized in Table 4.17 and Table 4.18, respectively.



Figure 4.46. Seismic downhole measurement at the field, a) geophone, b) lowering of geophone into borehole

Table 4.17. Seismic downhole survey results

Location	Easting	Northing	Total depth (m)	V <sub>P1</sub> (m/s)	V <sub>P2</sub> (m/s)	V <sub>S1</sub> (m/s)	V <sub>S2</sub> (m/s)	V <sub>S30</sub> (m/s)	Site Class
DBH-1	294076	4506448	28	459	561	165	209	415	C
DBH-2	292752	4506341	19	556	559	226	157	561	C
DBH-3	296151	4505881	19	410	574	188	297	356	C

Table 4.18. Dynamic properties of soils obtained from seismic downhole survey

Location	Dominant period (sec)	Amplification
DBH-1	0.5-1	4-5
DBH-2	0.5-1	3
DBH-3	0.2-0.5	5



As a result, a C type site class was determined in the study area with respect to  $V_{s30}$  measurements and the site classification of NEHRP (2003). The depth versus travel time graphics for three downhole boreholes is given in Figure 4.47. According to the obtained travel time values, the variation of P and S wave (shear wave) velocity along depth was calculated (Figure 4.48). The variation of Young's modulus, shear modulus, Poisson's ratio, and bulk modulus along depth are presented in Figures 4.49, 4.50, 4.51, and 4.52, respectively. It should be noted that limited data were obtained from downhole surveys since the maximum downhole borehole depth is 26 m.

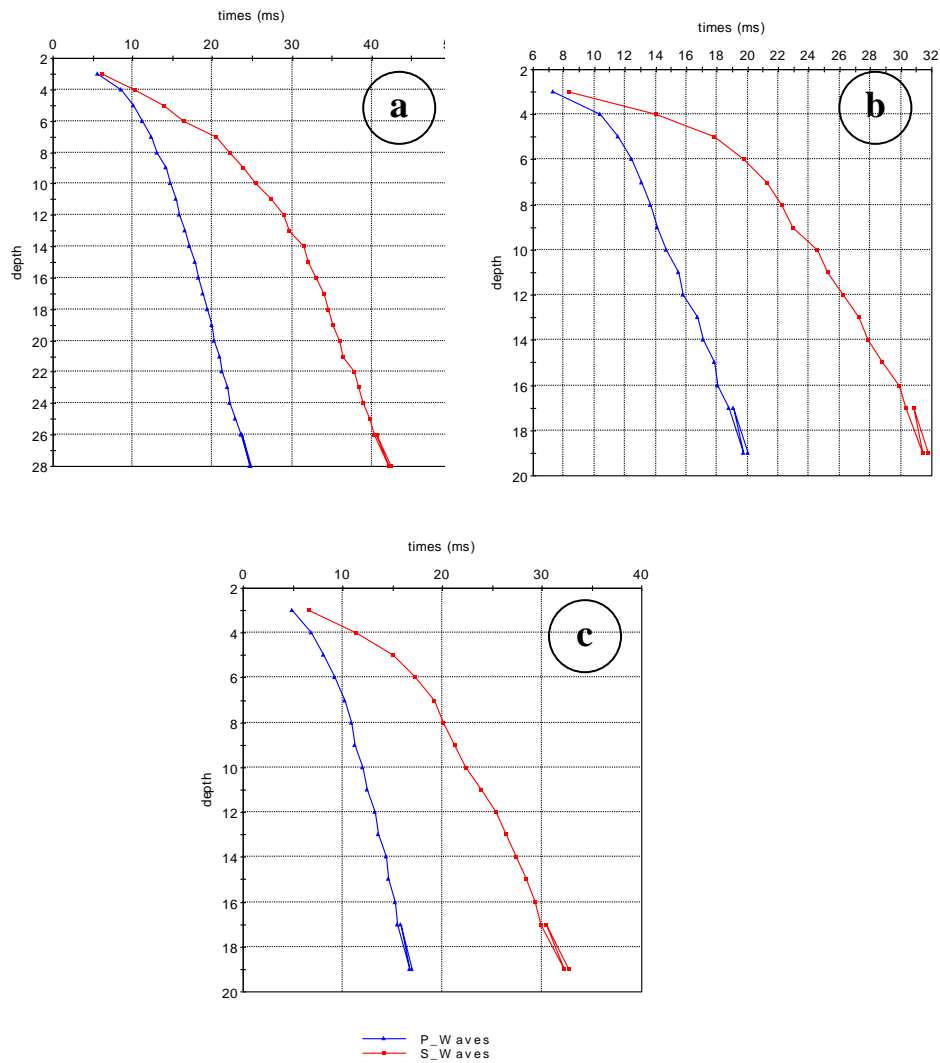


Figure 4.47. Depth versus travel time graphics for (a) DBH-1 (b) DBH-2 (c) DBH-3 downhole boreholes

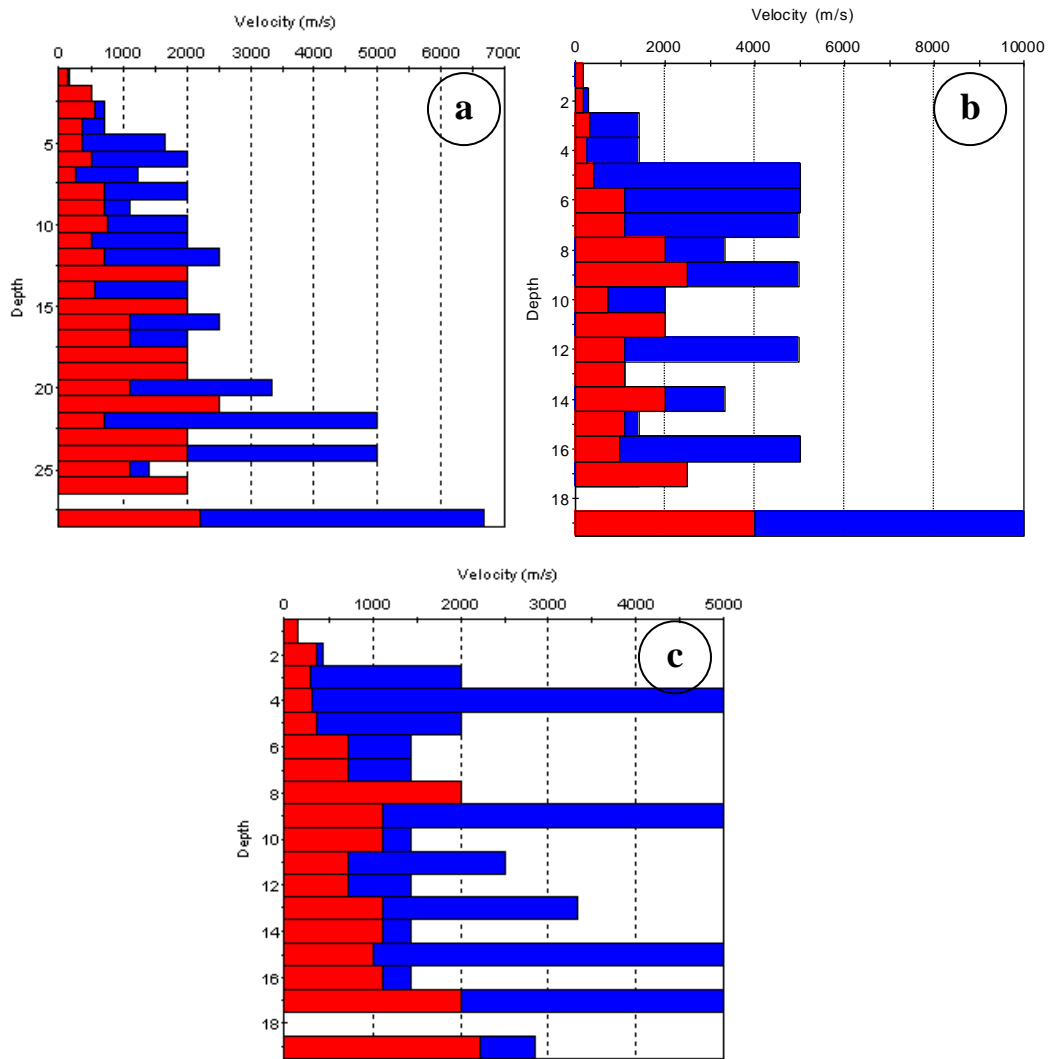


Figure 4.48. Variation of P and S wave velocity in (a) DBH-1 (b) DBH-2 (c) DBH-3 downhole boreholes (Note: red color represents S waves, blue color represents P waves)

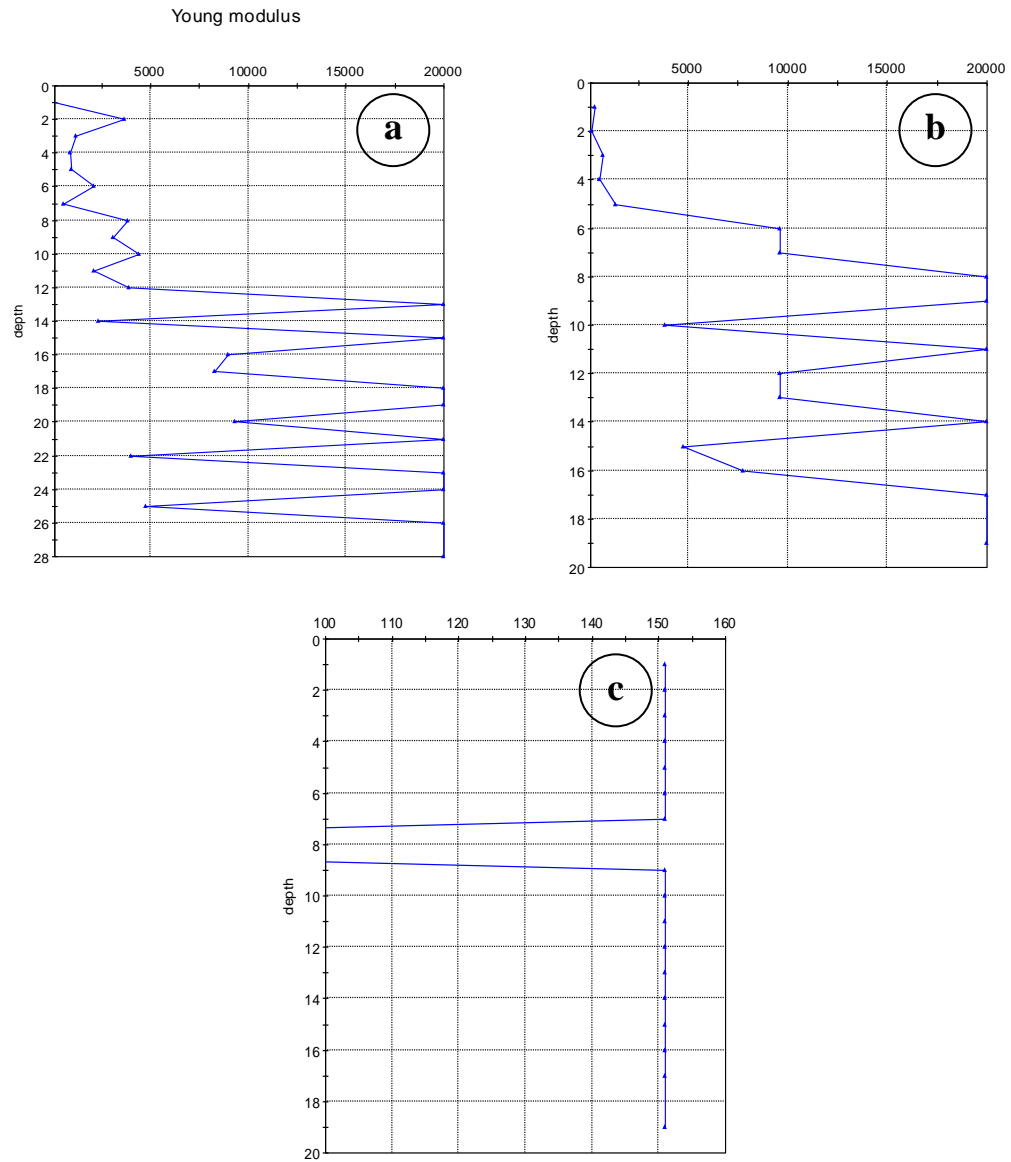


Figure 4.49. Variation of Young's modulus (in kPa) in (a) DBH-1 (b) DBH-2 (c) DBH-3 downhole boreholes

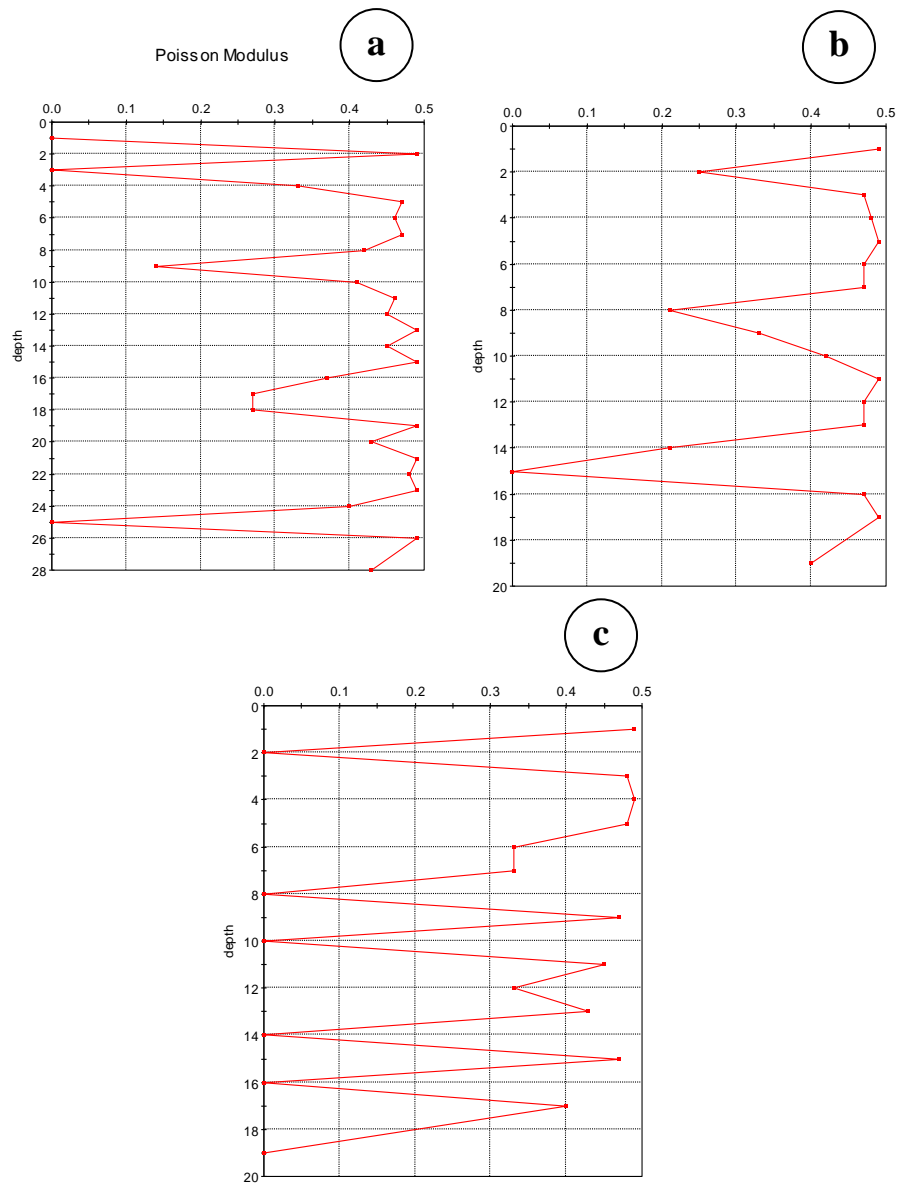


Figure 4.50. Variation of Poisson's ratio in (a) DBH-1 (b) DBH-2 (c) DBH-3 downhole boreholes

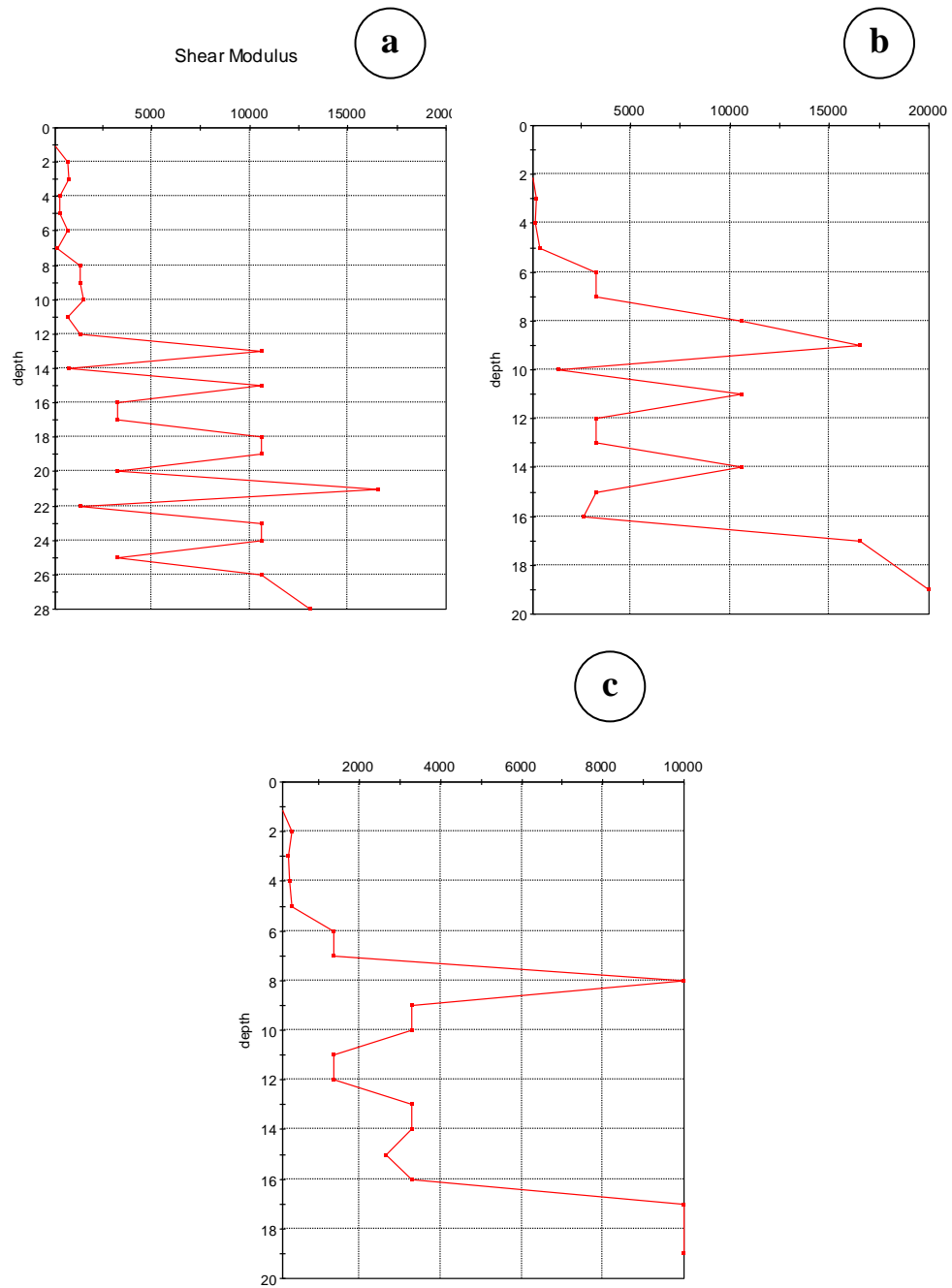


Figure 4.51. Variation of shear modulus (in kPa) in (a) DBH-1 (b) DBH-2 (c) DBH-3 downhole boreholes

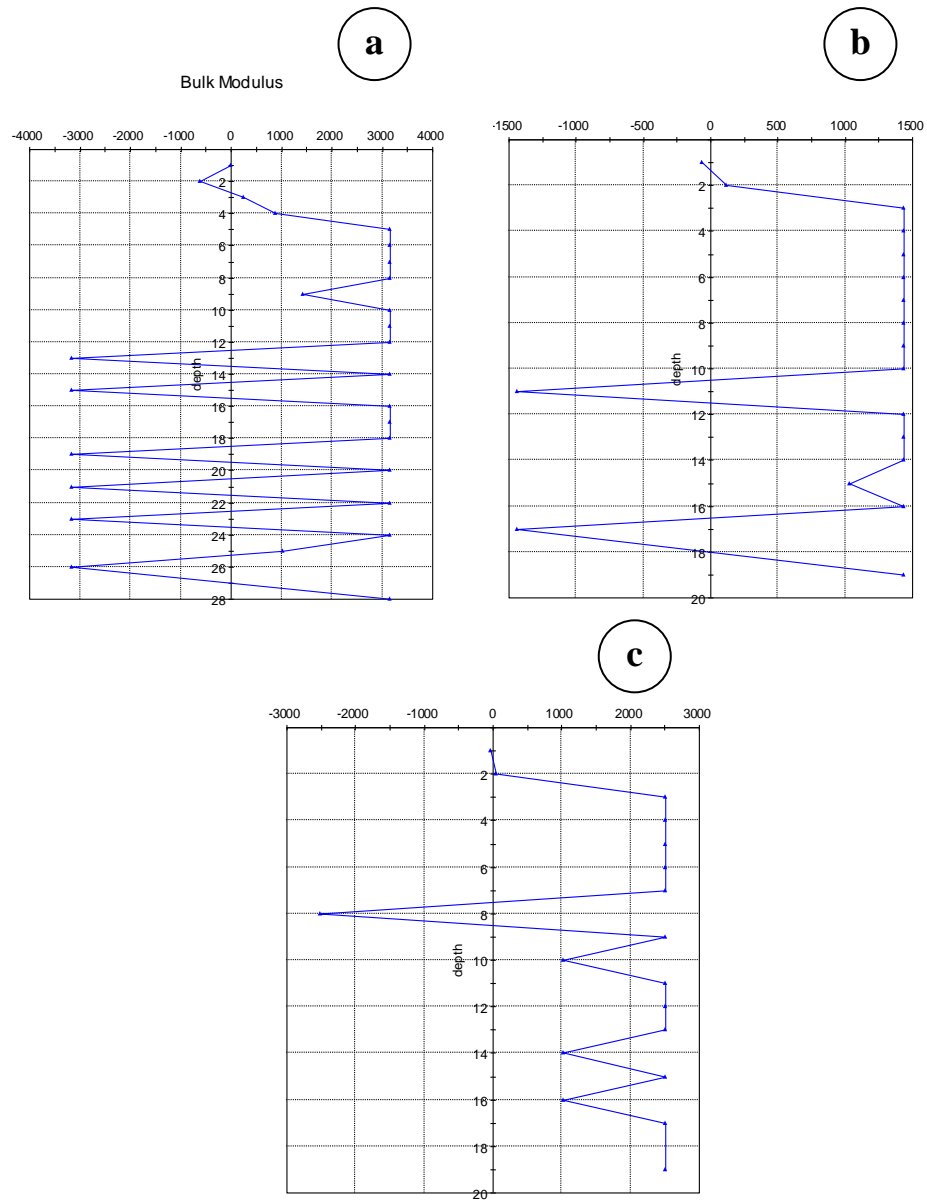


Figure 4.52. Variation of bulk modulus (in kPa) in (a) DBH-1 (b) DBH-2 (c) DBH-3 downhole boreholes

#### 4.5.5.1 Refraction microtremor survey at 3 downhole borehole locations

The refraction microtremor (REMI) method is proposed to overcome the problems related to the sources in noisy urban settings or specialized independent recorders in an extensive array (Louie, 2001). This method is based on the use of standard P-wave recording equipment and ambient noise to produce average one-dimensional shear-wave profiles down to 100 m

depth. It is the combination of simple recording with no source, a wavefield transformation data processing technique, and an interactive Rayleigh-wave dispersion modeling tool which has the most effective aspects of the microtremor, spectral analysis of surface wave (SASW), and multichannel analysis of surface wave (MASW) techniques (Louie, 2001).

In this study, refraction microtremor (REMI) was conducted without using any energy source to determine  $V_{s30}$  value in the close vicinity of three downhole boreholes (DBH-1, 2 and 3). In REMI measurements, 10 Hz. vertical geophones were used to retrieve P wave arrival times. Furthermore, a similar instrument with seismic refraction survey was employed. This equipment consists of a seismograph, geophones placed in an array, and a seismic source. Rayleigh waves are generated from seismic sources described to be active (i.e. from a sledge hammer striking on a plate), passive (i.e. highway traffic, construction equipment working in a distance) or a combination of both. Several recordings (usually 15 to 60 seconds long) were captured and stored for analysis. The software SEISOPT@REMI was employed to determine the  $V_{s30}$  value based on the field data. The variation of  $V_{s30}$  value along depth is illustrated in Figures 4.53, 4.54, and 4.55 and summarized in Table 4.19 for three downhole borehole locations.

Table 4.19. Summary of REMI results for 3 downhole borehole locations

Location No	Thickness (m)	Vs (m/s)	Density (gr/cm <sup>3</sup> )	V <sub>s30</sub> (m/s)
DBH-1	13	242	2.0	415
	27	1000	2.0	
	-	689	2.0	
DBH-2	30	561	2.0	561
	44	680	2.0	
	-	589	2.0	
DBH-3	14.5	214	2.0	356
	28.5	982	2.0	
	-	616	2.0	

### DBH-1 REMI

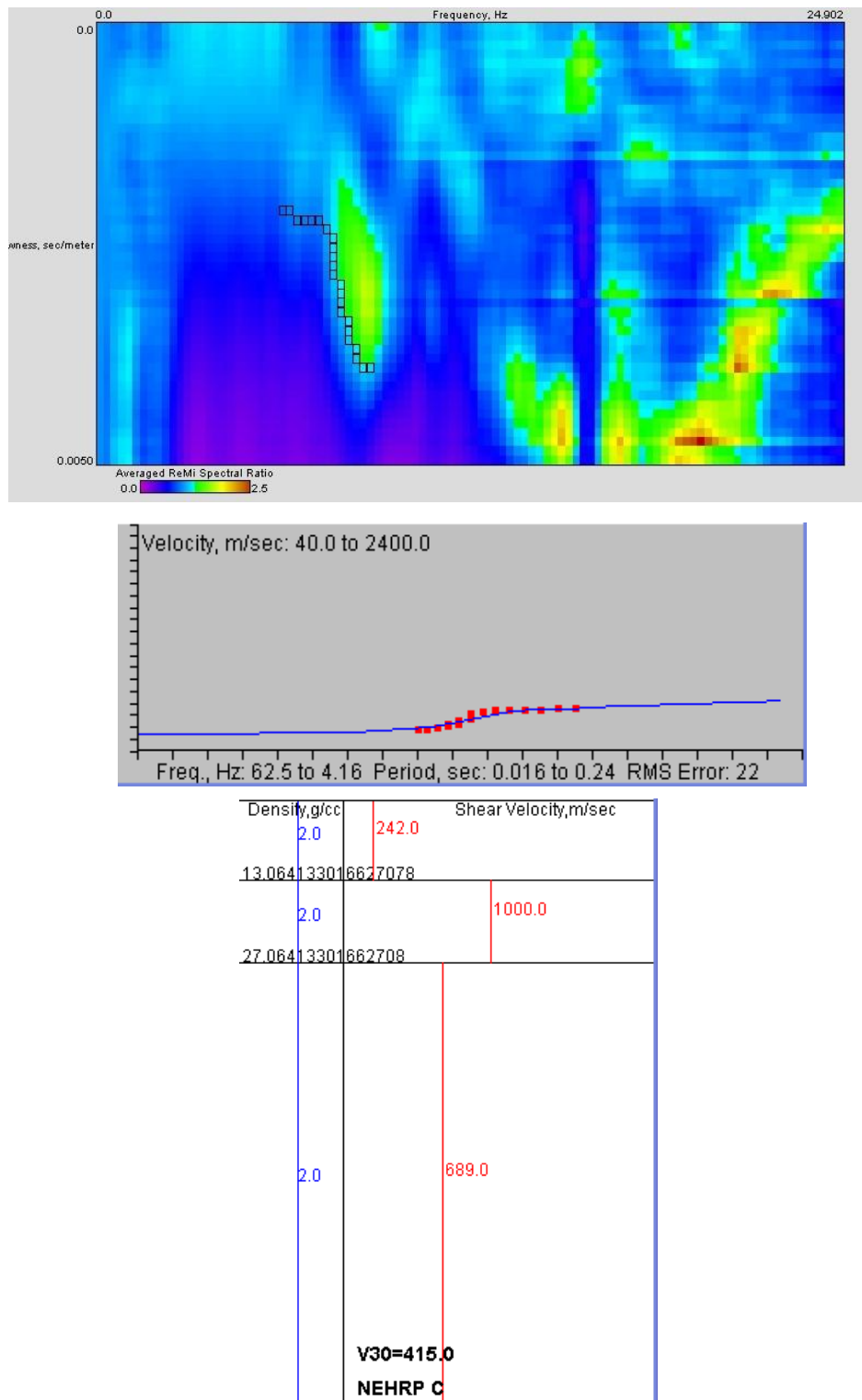
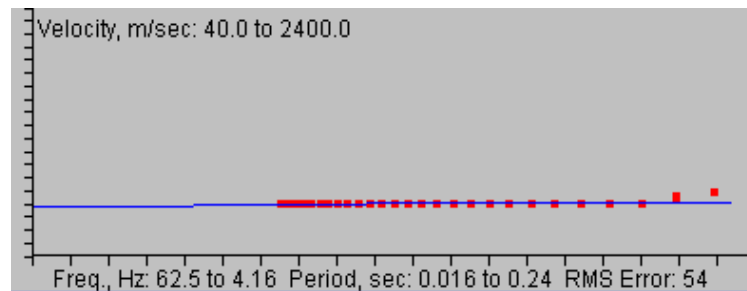
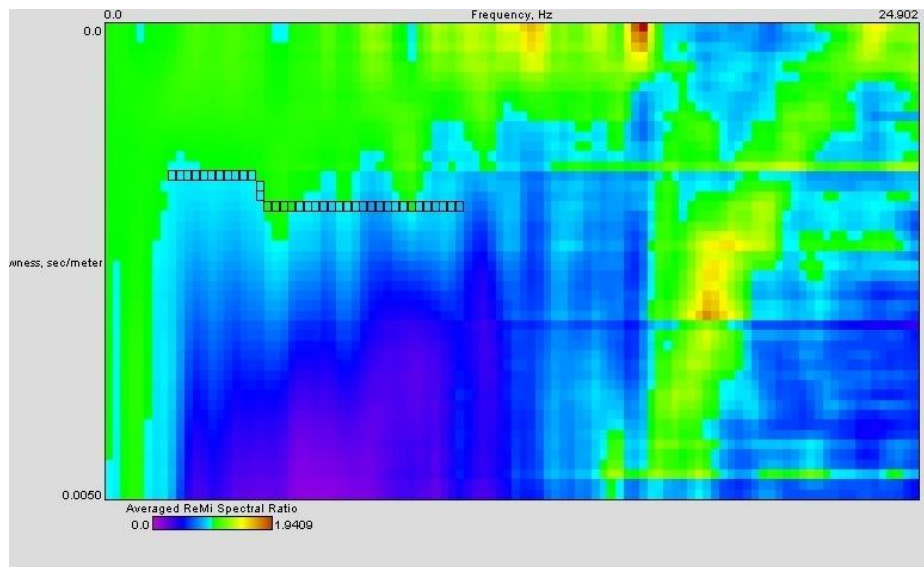


Figure 4.53. Variation of shear wave velocity based on REMI measurement for DBH-1 downhole borehole location



## DBH-2 REMI



Density, g/cc	Shear Velocity, m/sec
2.0	561.0
30.0	680.0
44.0	589.0
2.0	
V30=561.0 NEHRP C	

Figure 4.54. Variation of shear wave velocity based on REMI measurement for DBH-2 downhole borehole location

### DBH-3 REMI

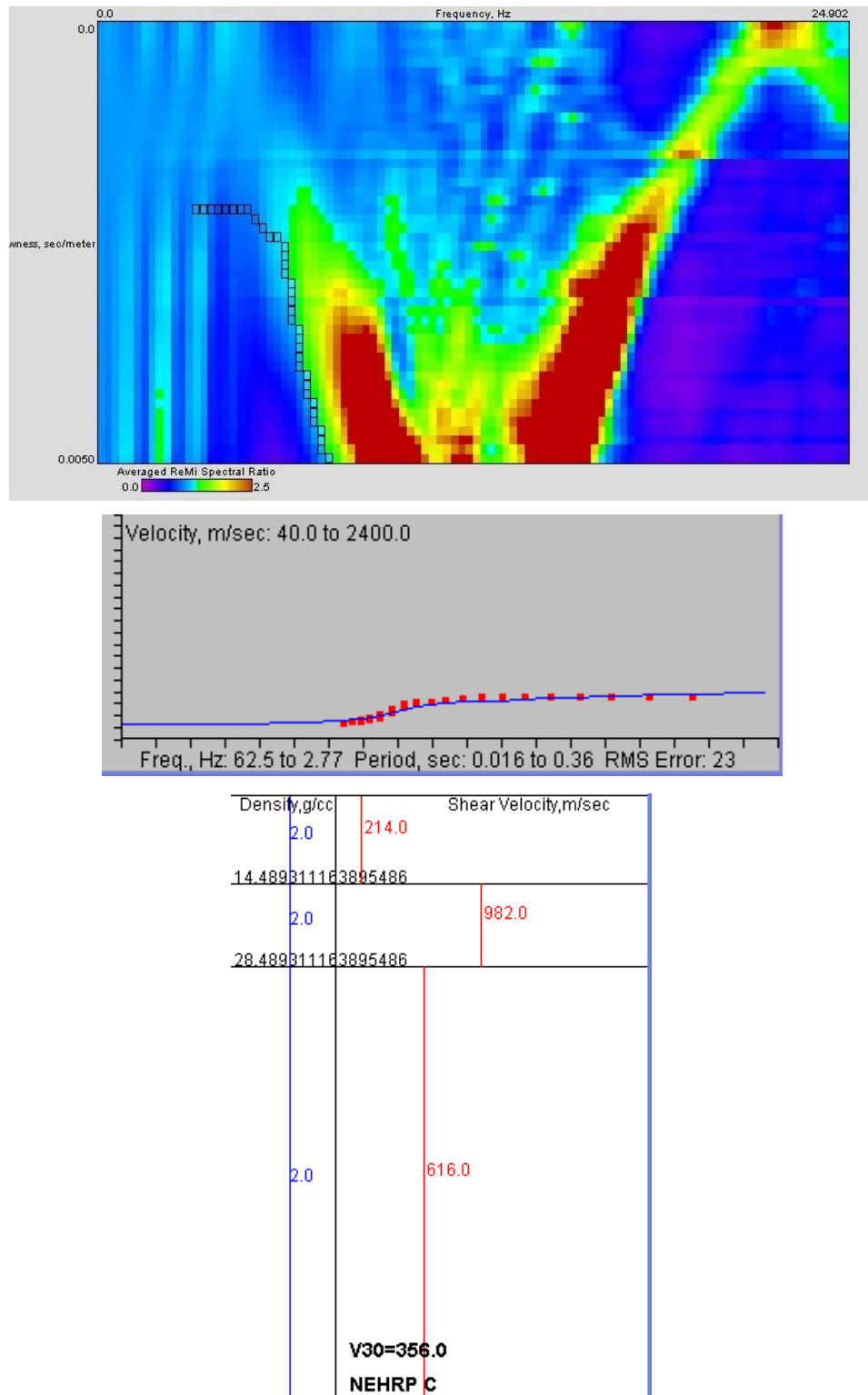


Figure 4.55. Variation of shear wave velocity based on REMI measurement for DBH-3 downhole borehole location

#### **4.5.5.2 Microtremor survey at 3 downhole borehole locations**

Additional microtremor measurements were performed using a GEOSIG GBV\_316 type seismograph to obtain amplification values in these three downhole borehole locations. The technical properties of microtremor device are as follows:

- a. Internal velocity sensor (geophone)
- b. Data memory 64 MB
- c. 16 byte/ 96 dB dynamic ratio
- d. Recording sensor with a velocity seismometer including three (X,Y,Z) components

The obtained results are given in Figures 4.56, 4.57, and 4.58. The amplification ratios were defined by spectral ratio method in these microtremors for different periods.

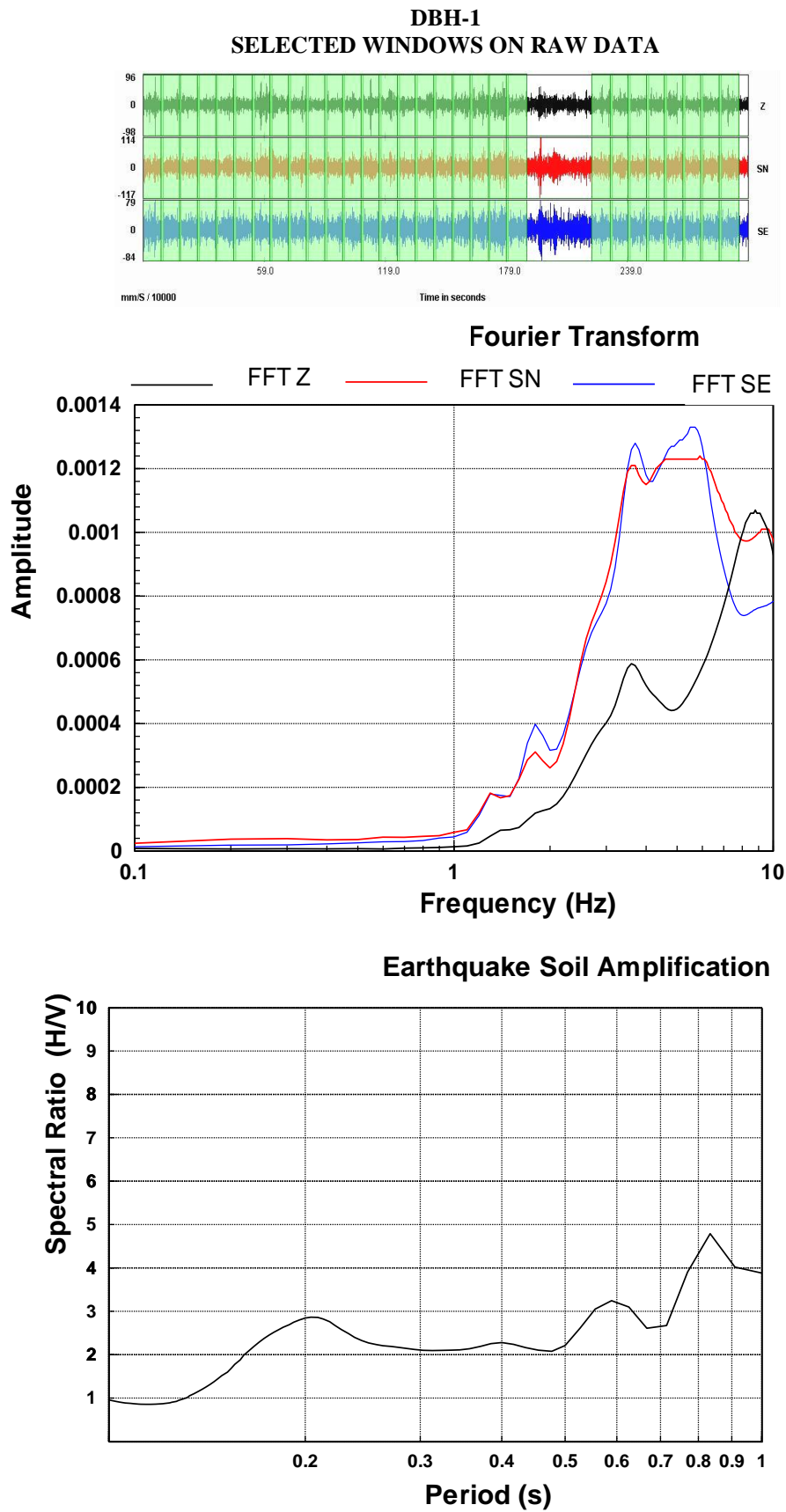


Figure 4.56. Microtremor measurement results for DBH-1 location

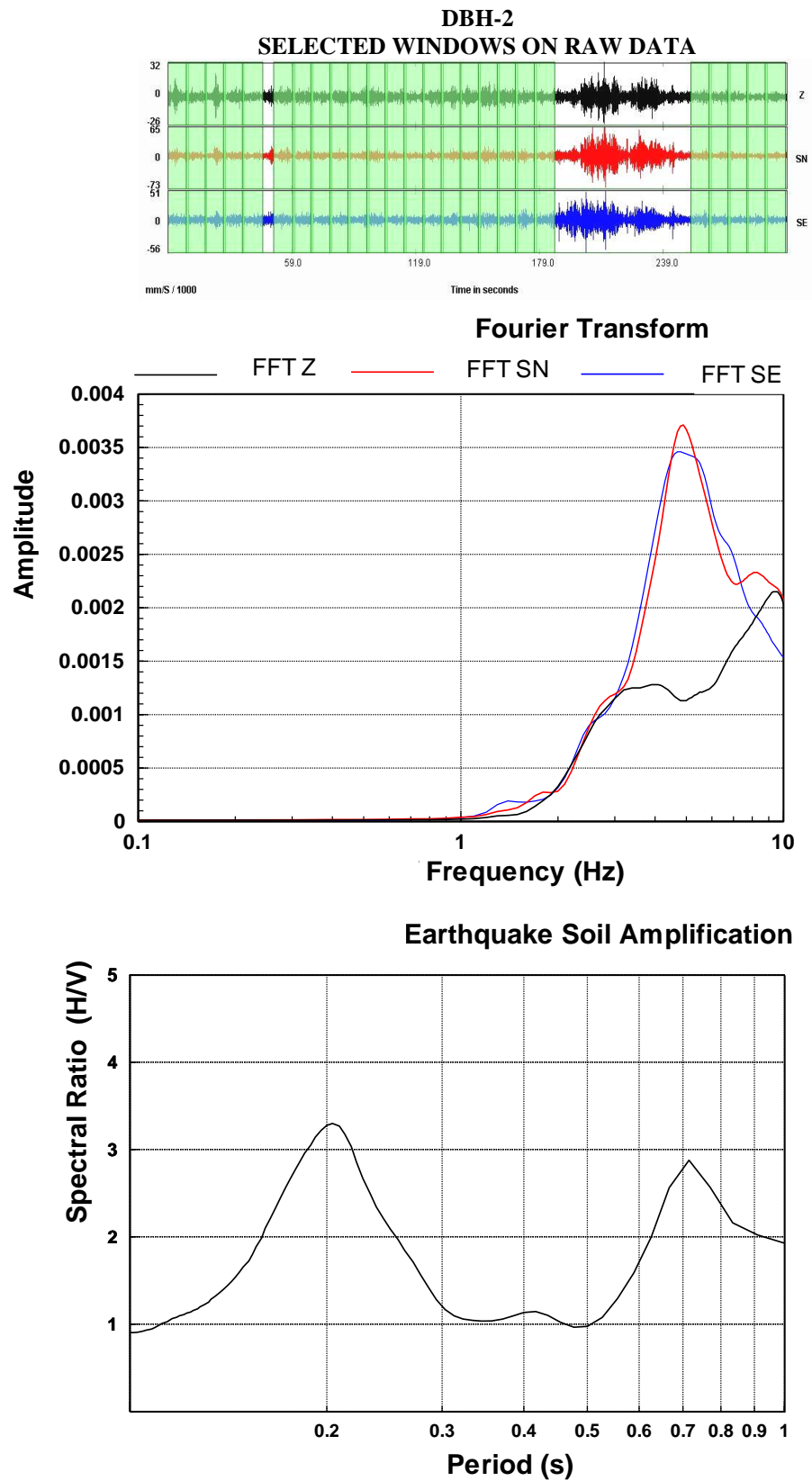


Figure 4.57. Microtremor measurement results for DBH-2 location

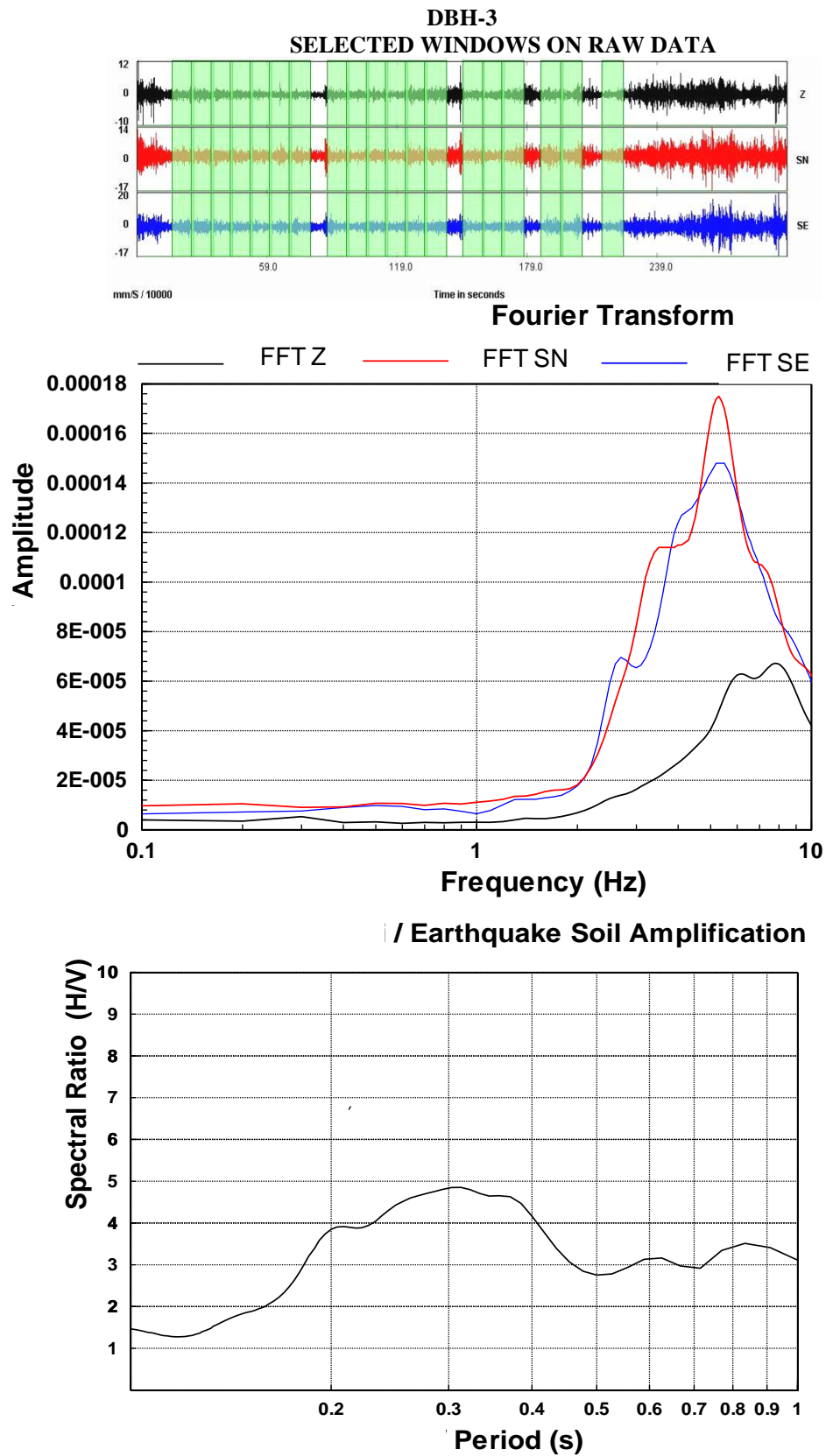


Figure 4.58. Microtremor measurement results for DBH-3 location

#### 4.5.5.3 Resistivity survey at 3 downhole borehole locations

A total of three additional resistivity measurements were executed near 3 downhole borehole locations. The additional resistivity survey results are given in Figures 4.59, 4.60, and 4.61.

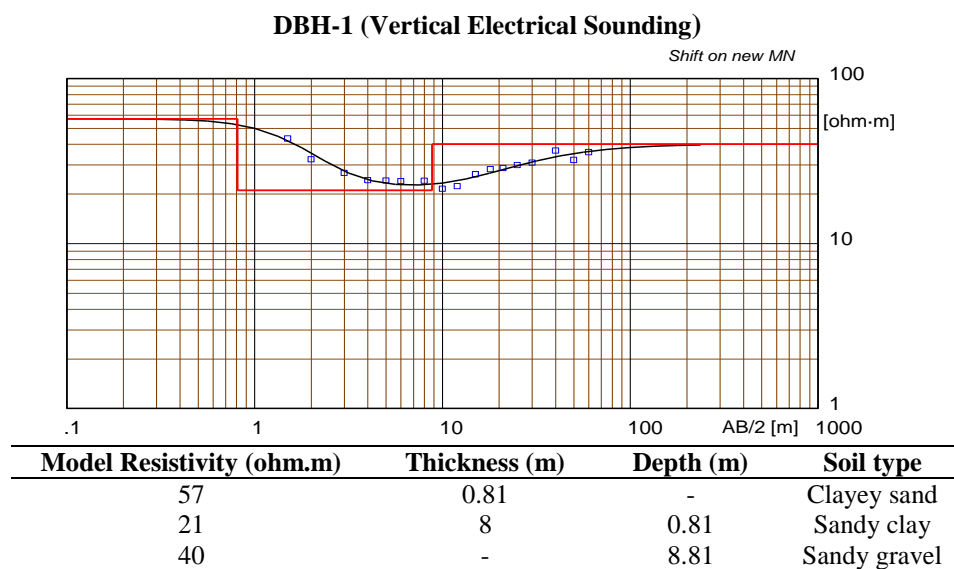


Figure 4.59. Resistivity survey result for DBH-1 location

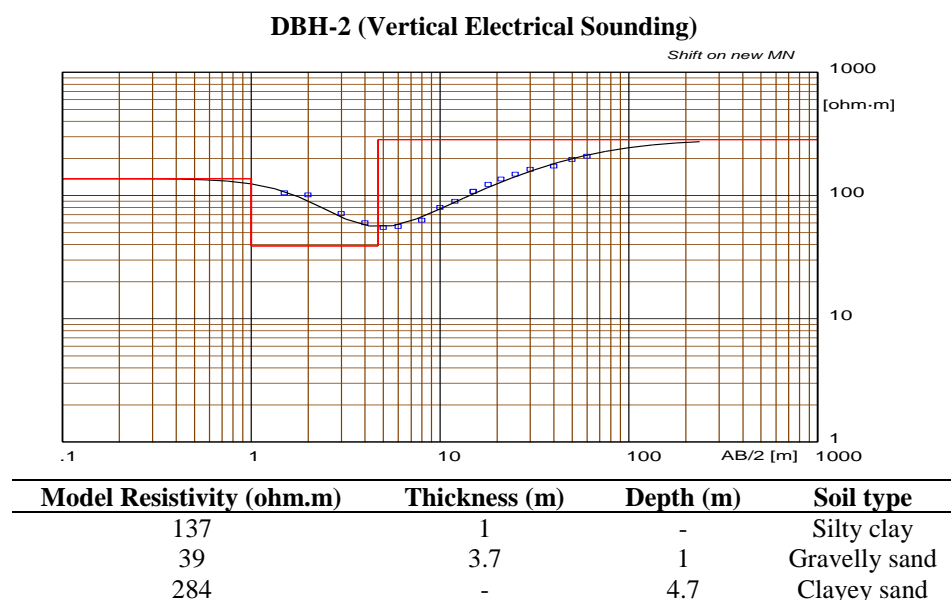


Figure 4.60. Resistivity survey result for DBH-2 location

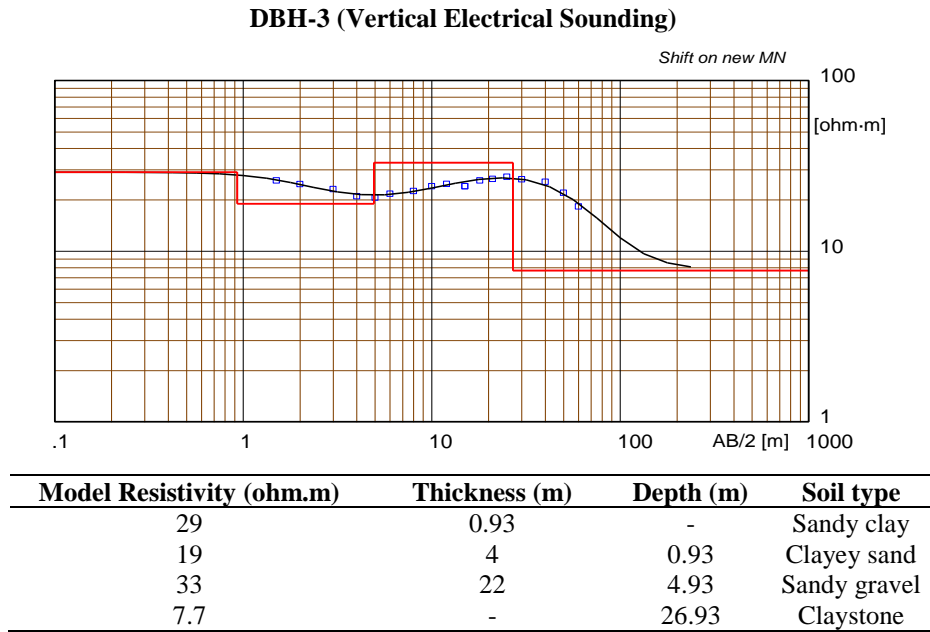


Figure 4.61. Resistivity survey result for DBH-3 location

The soil layers in the study area were distinguished as mostly sandy clay, clayey gravel, gravelly clayey sand, sandy clay with respect to resistivity measurements. Additionally, a claystone layer was defined after 27 m depth at DBH-3 location based on resistivity surveys.

#### 4.5.5.4 Seismic refraction survey at 3 downhole borehole locations

Seismic refraction measurements were also performed near 3 downhole boreholes. The results are depicted in Table 4.20.



Table 4.20. Seismic refraction measurements near 3 downhole boreholes

BH No	Layer	Depth (m)	V <sub>p</sub> (m/s)	V <sub>s</sub> (m/s)	V <sub>p</sub> /V <sub>s</sub>	Density (gr/cm <sup>3</sup> )	Shear Modulus (kg/cm <sup>2</sup> )	Elasticity Modulus (kg/cm <sup>2</sup> )	Poisson Ratio	Bulk Modulus (kg/cm <sup>2</sup> )
1	1	1.39	458	160	2.85	1.43	367.84	1052.05	0.43	250.58
	2	3.12	459	165	2.79	1.43	388.42	1107.89	0.43	250.05
	3	5.29	507	232	2.19	1.47	788.81	2157.52	0.37	271.53
	4	8.00	561	204	2.75	1.51	627.64	1787.14	0.42	390.41
	5	-	866	319	2.71	1.68	1712.42	4867.73	0.42	1030.93
2	1	0.87	345	168	2.05	1.33	377.98	1015.86	0.34	108.38
	2	1.95	345	168	2.05	1.33	377.04	1013.71	0.34	108.51
	3	3.31	334	81	4.11	1.32	87.30	256.41	0.47	135.97
	4	5.00	633	226	2.80	1.55	792.42	2261.59	0.43	516.44
	5	-	556	157	3.54	1.50	370.79	1080.20	0.46	415.20
3	1	3.12	321	110	2.90	1.31	159.72	457.65	0.43	113.23
	2	7.02	410	188	2.18	1.39	492.60	1346.08	0.37	167.81
	3	11.90	574	297	1.93	1.51	1335.93	3518.29	0.32	320.07
	4	18.00	694	341	2.04	1.59	1847.28	4953.93	0.34	518.86
	5	-	1087	441	2.46	1.78	3461.39	9701.03	0.40	1638.45

#### 4.6 SCPTU Applications

The piezocone (CPTU) is an extension of cone penetration test (CPT). The standard cone penetrometer consists of a 35 mm diameter rod with a 60° conical shaped tip to obtain tip resistance and local friction during the test. The piezocone (CPTU) has also another component to measure pore water pressure (Robertson and Campanella, 1983; Lunne et al. 1997). A schematic view can be seen in Figure 4.62.

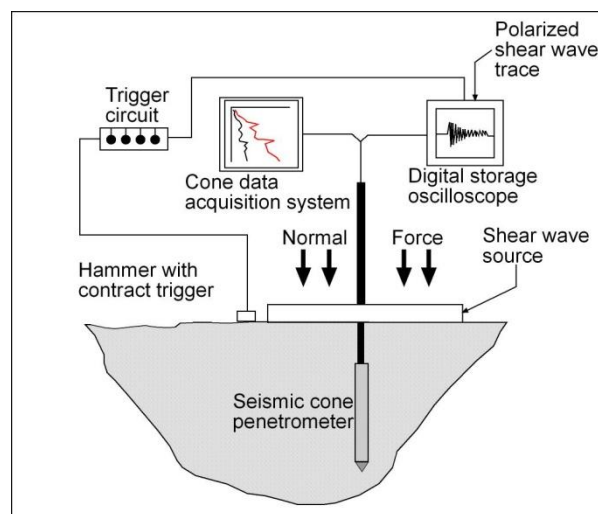


Figure 4.62. A schematic view of SCPTU system

In addition, the modified CPT cone containing a built in seismometer to measure compression and shear wave velocities in addition to the standard piezocone parameters ( $q_c$ ,  $f_s$ , and  $u_2$ ) (Rowe, 2001). Therefore, four independent readings are compiled with depth in a single sounding with SCPTU.

A total of 30 SCPTU (seismic cone penetration test with pore pressure measurement) measurements were performed with varying depths in accordance with ASTM D5778-95 (2000) standards. The performance of the CPT apparatus was significantly affected by gravelly layers in the study area. Therefore, a limited number of CPT tests could be performed in shallow depths. The minimum and maximum investigation depths are 0.4 and 11.4 m. An example of SCPTU recording is shown in Figure 4.63. The location and depth of SCPTU tests are summarized in Table 4.21. Moreover, the distribution of the SCPTUs in the study area is also presented in Figure 4.64.

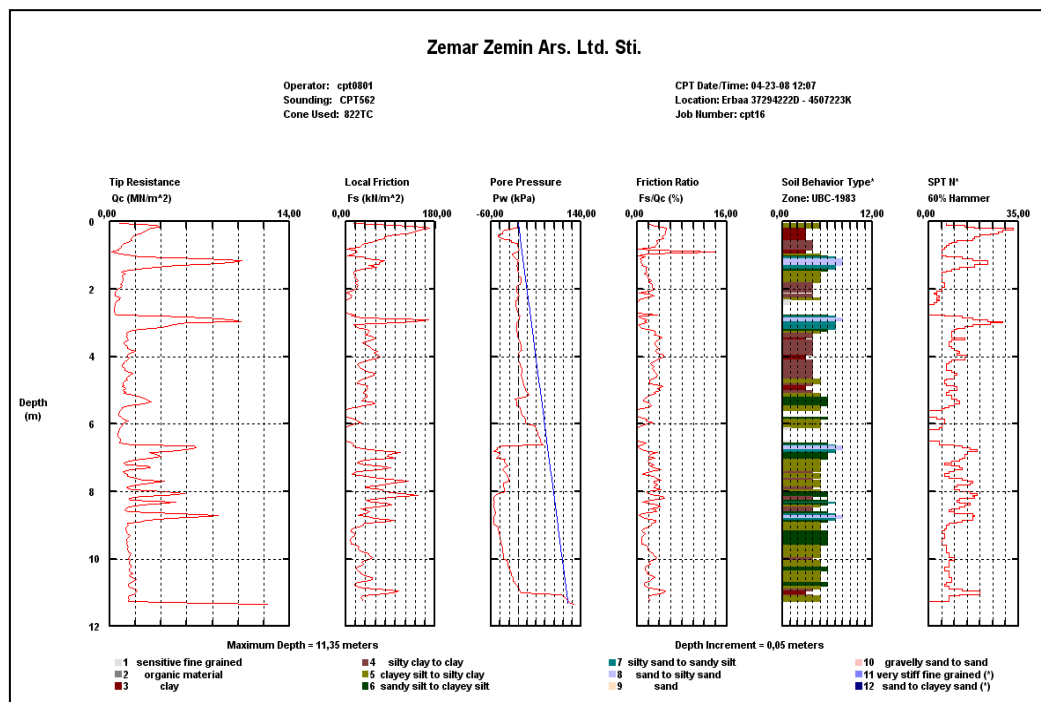


Figure 4.63. An example record of SCPTU (CPT-16)

Table 4.21. General properties of SCPTU locations in the study area

SCPTU No	Total Depth (m)	Coordinates	
		Easting	Northing
1	3.5	291954	4507327
3	4.5	292764	4506498
4	2.5	292787	4507456
6	2.0	293657	4508043
7	0.5	294964	4508430
8	2.5	294955	4508429
10	3.5	294222	4507223
12	3.0	292789	4505751
14	2.0	294060	4505144
16	11.4	294222	4507223
17	2.8	294890	4507423
18	3.0	295663	4507823
20	2.0	295203	4506575
21	5.9	294767	4506132
22	1.8	294832	4505609
23	2.4	294605	4504638
27	3.3	295800	4506136
28	3.4	296118	4506599
29	8.4	296430	4506261
30	10.2	296099	4505862
32	1.5	297466	4505281
33	2.2	296403	4503983
36	3.0	293850	4507218
38	6.9	294404	4507396
39	4.9	298212	4505594
40	1.7	298345	4505174
41	2.7	298267	4506116
42	0.4	298198	4506280
43	3.9	297195	4506174
44	2.5	295169	4508112

Seismic records obtained from every 1 m depth were also evaluated for each CPT point. An example of a seismic record is presented in Figure 4.65 as well. In the evaluation stage, the distribution of shear wave velocity along depth was obtained as shown in Figure 4.66. The available CPT data were only used for correlations (especially for SPT-based uphole boreholes) as SCPTU recordings could be retrieved from limited depths.

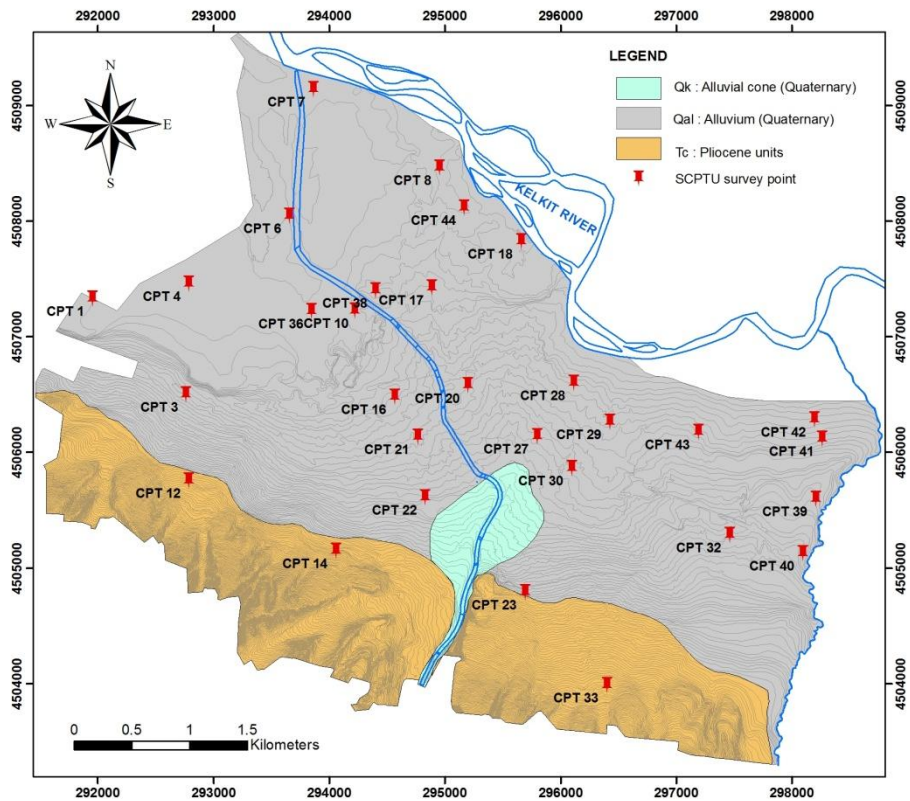


Figure 4.64. Distribution of the SCPTU locations in the study area

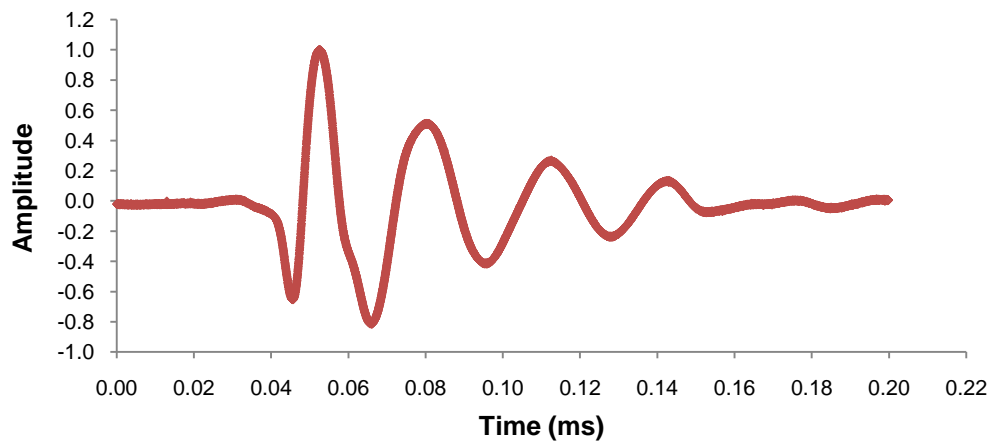


Figure 4.65. An example of seismic record for a certain depth (CPT-30, 9 meter depth)

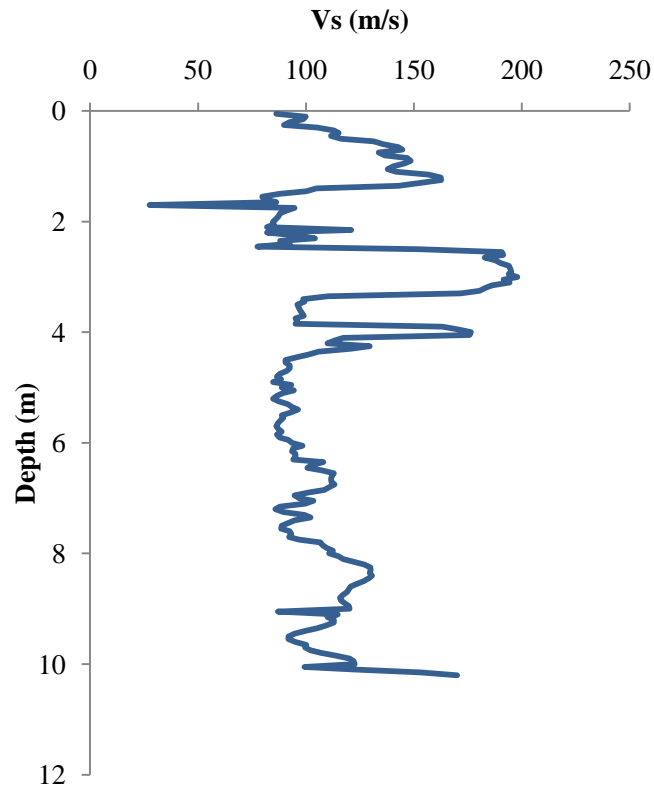


Figure 4.66. An example of evaluated seismic record, depth versus shear wave velocity ( $V_s$ ) (CPT-30)

#### 4.7 Concluding Remarks

As a conclusion, the southern part of Erbaa is mostly settled on Pliocene units. However, the northern part is generally characterized by gravelly and sandy alluvial units. Additionally, the intercalations of clayey and silty layers are also probable in alluvium. According to laboratory test results obtained in this study, soils in Erbaa contain mostly clay with low plasticity (CL), poorly-well graded sand (SP-SW), clayey sand (SC) and silt with low plasticity (ML) and occasionally sandy silty gravel layers (GM-GC). Groundwater table is shallow in the northern part of Erbaa in alluvial deposits. The main reason for high groundwater level is the Kelkit River and low topographic level. In addition, the direction of groundwater flow is also towards Kelkit River. In contrast, groundwater level is deep in the Pliocene deposits. The groundwater level was only recorded in a few Pliocene boreholes. The field and laboratory test studies including geophysical applications are summarized in this chapter. The test results will be evaluated in the following chapters.

## CHAPTER 5

### SEISMIC HAZARD ANALYSIS AND GROUND MOTION PREDICTION

#### 5.1 Introduction

Seismic hazard analysis involves the quantitative estimation of ground shaking hazards in a regional area or at a particular site. Seismic hazard can be analyzed deterministically considering a particular earthquake scenario, or probabilistically considering the uncertainties involved in earthquake size (magnitude or intensity), location, effects, and the rate of occurrence (Ward, 1994; Frankel, 1995; Kramer, 1996; Chen and Scawthorn, 2002; Kramer, 2009a). The most common objective of a seismic hazard analysis is the determination of Peak Ground Acceleration (PGA) and/or spectral acceleration ( $S_a$ ) for an area (Reiter, 1990). Spectral acceleration is usually preferred for the design of civil engineering structures. It is conventional in earthquake engineering practice to develop design response spectra for different types of foundation materials such as rock, hard and soft soils. In many cases, prediction of a response spectrum alone is sufficient for design or evaluation of structures and facilities. The generated spectrum can be used as a target for the identification and scaling of real earthquake ground motions. In site response analyses, the ground motions used as input motions should also be well defined since the results are very sensitive to input motions (Kramer, 1996; 2009a). Moreover, seismic hazard analysis is the major component of seismic microzonation for seismic hazard and risk in such projects (Slemmons, 1982; Ansal et al., 2004b; Nath, 2004; 2007; Sitharam and Anbazhagan, 2007; 2008).

Prediction of the effects of earthquakes requires estimation of ground motions parameters. It has been well known that earthquake source conditions, source to site transmission path properties, and site conditions all affect earthquake ground motions. The source conditions consist of source size, depth, the size of rupture area, rupture directivity, rupture pattern, distribution of asperities, and fault types. The crustal velocity structure and damping parameters of the rock are the main properties of transmission path. The local site properties

and the topography of site directly control the site conditions (Kramer, 1996; Erdik and Durukal, 2004).

Considering the fact that essential seismic hazard analyses have not been performed for the study area (Erbaa) in previous studies, seismic hazard analyses are executed for Erbaa in this study and input ground motions are evaluated. The results of these analyses are proposed to be used in further site response analyses.

## **5.2 Seismic Hazard Analysis**

Seismic hazard analysis is to predict the influence of a future earthquake of certain magnitude on an interested site. The difficulties in seismic hazard assessment mainly deal with the selection of representative earthquake in the region.

The assessment of seismic hazard analysis includes three main steps (Veneziano et al., 1984; Wang and Law, 1994; Cramer et al., 1996; Cao et al., 1996).

1. To identify the potential seismic source or sources surrounding the site and to determine their activity.
2. To establish the path of seismic wave propagation and its attenuation characteristics.
3. To apply a suitable model for seismic hazard analysis.

Furthermore, there are two main approaches for seismic hazard analysis.

- a. Probabilistic Hazard Analysis (PSHA)
- b. Deterministic Hazard Analysis (DSHA)

### **5.2.1 Probabilistic seismic hazard analysis (PSHA)**

Probabilistic seismic hazard analysis (PSHA) is based on the identification of seismic hazard in terms of ground motion intensity considering a probability of exceedance recurrence within a definite period of time (NRC, 1988; Wang and Law, 1994). The PSHA is the most commonly used approach to evaluate the seismic design load for important engineering projects. PSHA method was initially developed by Cornell (1968) and a couple of softwares were developed by McGuire (1976 and 1978) and Algermissen and Perkins (1976). Algermissen and Perkins (1976) proposed a computer program called SEISRISK III.

Earthquake ground motions can be estimated for the selected values of probability of ground motion exceedance in the design period of structures or return period for ground motion exceedance (Sitaharam and Anbazhagan, 2007). Probabilistic seismic hazard maps were prepared to show the hazard potential in many studies (Erdik et al., 1985; Gulkan et al., 1993; Main, 1995; McGuire, 1995; Kebede and Eck, 1997; Kijko and Graham, 1998, 1999; Lindholm and Bungum, 2000; Ayday et al., 2001; Harajli et al., 2002; Kayabali, 2002; Mantyniemi et al., 2003; Genc, 2004; Petersen et al., 2004; Boncio et al., 2004; Koravos et al., 2006; Das et al., 2006; Kalkan et al., 2009). These maps account for uncertainties in the size and location of earthquakes and the resulting ground motions that can affect a particular area. They can be defined in terms of probability of exceeding a certain ground motion. For instance, a ground motion with 10% probability of exceedance in 50 years map represents an annual probability of approximately 1 in 475 of being exceeded each year. This level of ground shaking has preferably been used for designing buildings in high seismic areas (Sitaharam and Anbazhagan, 2007).

The methodology of PSHA has been commonly used in many projects. This method has four main steps in the applications (Cornell, 1968).

1. Identifying the active faults and seismic areas
2. Characterizing the recurrence rates of earthquakes of different magnitudes in each source
3. Selecting an appropriate attenuation relationship
4. Computing the hazard curve which shows the probability in a given level of ground motion intensity with an exceedance in a certain period of time.

The occurrence of earthquakes in a seismic source is assumed to be described accurately by the Poisson distribution (Cornell, 1968; McGuire, 1976). The probability distribution is defined by the annual rate of exceeding the ground motion considering all possible magnitude and epicentral distance scenario events (Sitaharam and Anbazhagan, 2007).

PSHA assumes many scenarios taking into account different magnitudes, distances and all effects. The uncertainty is described in terms of location, size, recurrence and effects of earthquakes using the combination of probabilities for different levels of shaking (Kramer, 1996; 2009a).



### **5.2.2 Deterministic seismic hazard analysis (DSHA)**

Deterministic Seismic Hazard Analysis (DSHA) was developed prior to PSHA mainly for nuclear power industry applications. It is still used for some significant structures such as nuclear power plants, large dams, large bridges, hazardous waste containment facilities or as “cap” for probabilistic analyses (Kramer, 1996; 2009a). This method produces a deterministic assessment of the seismic hazard of a site. It typically involves the assumption of a “worst case scenario” for an earthquake in a particular area. The largest possible magnitude earthquake is assumed to occur at the shortest possible distance for each seismic source in DSHA (Kramer, 1996). The expected motions from each scenario are then compared to determine which scenario should control design.

According to Corps of Engineers Regulation (1995), DSHA approach considers the known seismic sources sufficiently close to the site and available historical seismic and geological data to generate a ground motion model at the site. One or more earthquakes are usually specified by magnitude and location with respect to the site. The site ground motions are estimated deterministically by means of a given magnitude, source-to-site distance, and site condition in this approach.

Krinitzsky (2005) mentioned that a Deterministic Seismic Hazard Analysis (DSHA) employ geology and seismic history to identify earthquake sources and to interpret the strongest earthquake. Each source is considered as able to produce seismic activity regardless of time. As a quantitative approach, the Maximum Credible Earthquakes (MCEs) are the largest earthquakes that can realistically be estimated in the analyses. The deterministic approach basically requires the determination of the maximum magnitude of an active fault or seismo tectonic zone. DSHA consists of four primary steps (Reiter, 1990; Wang and Law, 1994; Kramer, 1996):

1. Identification and characterization of all seismic sources: It considers all the potential seismic sources geographically related to the site based on the historical and postulated events. The maximum magnitude that can be produced by each source is determined.
2. Selection of source-site distance parameter: The minimum source-to-site distance for each source is determined.

3. Selection of "controlling earthquake" by comparing the motions produced by the maximum magnitude occurring at the shortest distance for each source. Attenuation relationships are used to predict the ground motions.

4. Definition of hazard using controlling earthquake: It is essential to define the expected ground motion parameters by appropriate attenuation relationships. Attenuation relationships can account for ground motion uncertainty; design or evaluation ground motions may be specified as median or 84<sup>th</sup> percentile parameters.

Deterministic seismic hazard maps were proposed using seismic source characterization and its geometry (linear, point or area), and maximum earthquake magnitudes in hazardous areas (Balassanian et al. 1997b; Alvarez et al., 1999; Akin (Kivanc), 2001; Muço et al., 2002; Kayabalı and Akin, 2003; Sitharam et al., 2006; Gullu et al., 2008).

DSHA provides a basic framework to evaluate the worst earthquake case for a specific area. On the contrary, it does not provide any information regarding the occurrence of the controlling earthquake and the probability of expected earthquake. Both probabilistic and deterministic analyses are compared in Figure 5.1 to illustrate the degree of suitability for different projects (McGuire, 1995).

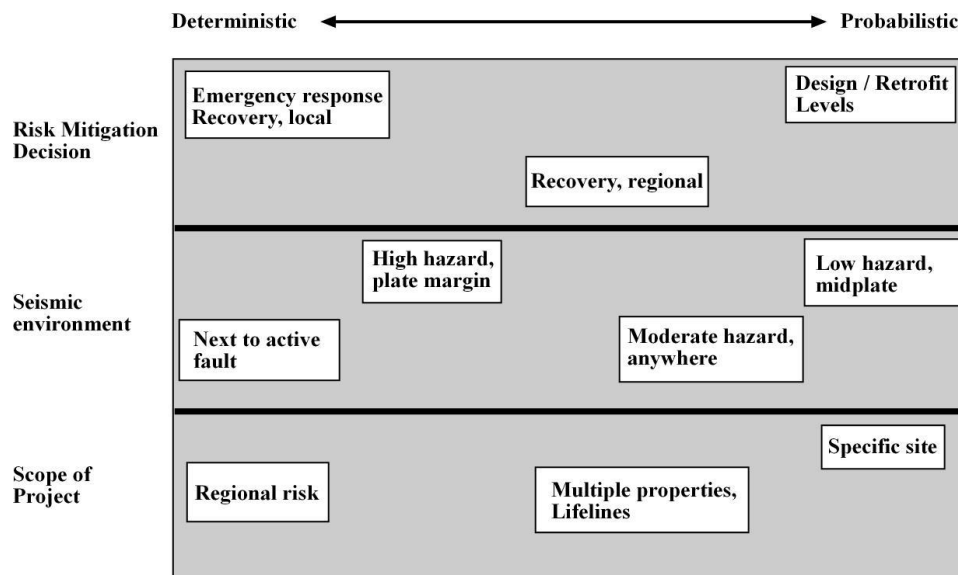


Figure 5.1. Comparison of deterministic and probabilistic approaches for different projects (after McGuire, 1995)

In general, tectonic faults and unidentified seismic sources contribute to the seismic hazard and risk at a site. The analysis of a specific site usually requires a probabilistic approach, but a deterministic approach can also be applied before the final decision or vice versa depending on the scope of the project (Figure 5.1).

Romeo and Prestininzi (2000) proposed a procedure to select design earthquakes for site-specific studies regarding the siting of critical and strategic structures (power plants, waste disposals, large dams, fire stations, military commands, hospitals, etc.) or for seismic microzonation studies matching the results of probabilistic seismic hazard analyses. This methodology encompassed the entire spectrum including the selected design earthquake. Deterministic seismic events are selected as a reference on a probabilistically-based procedure in this study.

Both deterministic and probabilistic methods should be evaluated individually according to the study conducted by Krinitzsky (2003). In addition, Krinitzsky (2003) also mentioned that DSHA is more logical and appropriate for the engineering design requirements than PSHA. It is hard to combine or neglect one of the procedures in earthquake hazard evaluations. Therefore, the policy maker or major project constructors should clarify the framework of the possible options.

### **5.2.3 Seismic hazard analysis for Erbaa**

Seismic hazard analysis was performed to estimate ground shaking hazards in Erbaa. An evaluation was made to estimate seismic hazard at rock level in terms of peak ground acceleration (PGA) and spectral acceleration ( $S_a$ ) using DSHA. DSHA has been carried out considering past earthquakes and their observed fault rupture lengths in Erbaa region. The seismic hazard analysis method was selected considering the degree of suitability approach proposed by McGuire (1995). The main reason for the selection of DSHA approach is that the study area is in the close vicinity of an active fault zone (NAFZ). Therefore, it is aimed to consider the worst case earthquake scenario for Erbaa. The most important and destructive earthquake in the study area occurred in 1942 with a moment magnitude of 7.2 (Ozmen et al., 1997, Tatar et al., 2006). A summary of historical earthquakes in the vicinity of the study area is given in Table 5.1. Accordingly, 7.2 moment magnitude is accepted as the Maximum Credible Earthquake (MCE) for the study area with respect to the important seismotectonic activities around Erbaa.

The MCE is the expected earthquake along a recognized fault under presently known or accepted tectonic activity which will cause the most destructive consequences at the site. In addition to the determination of the MCE from historical data, an empirical approach was also employed to find out the largest earthquake around the study area. To estimate the expected magnitude of an earthquake related to North Anatolian Fault Zone (NAFZ), Wells and Coppersmith (1994) relation (Equation 5.1) was utilized.

$$M = a + b \cdot \log (SRL) \quad (5.1)$$

where

M = Magnitude

a = coefficient (5.16 for strike slip fault)

b = coefficient (1.12 for strike slip fault)

SRL = Surface rupture length in km (70 km for the study area)

Table 5.1. Historical earthquakes around Erbaa

Year	Location	Magnitude (M≥5.5)	Year	Location	Magnitude (M≥5.5)
1543 <sup>(1)</sup>	Tokat and Erzincan	Unknown	1939 <sup>(2)</sup>	Erzincan (325 km to Erbaa)	7.9
1688 <sup>(1)</sup>	Amasya-Niksar	Unknown	1940 <sup>(2)</sup>	Erbaa & its vicinity	6.2
1909 <sup>(2,4)</sup>	Erbaa & its vicinity	6.3	1941 <sup>(2,4)</sup>	Erbaa & its vicinity	5.7
1909 <sup>(2)</sup>	Erbaa & its vicinity	5.8	1942 <sup>(2)</sup>	Niksar-Erbaa	7-7.2
1909 <sup>(2,4)</sup>	Erbaa & its vicinity	5.7	1943 <sup>(2,3,4)</sup>	Tosya-Ladik	7.2-7.3
1916 <sup>(2,4)</sup>	Tokat	7.1	1943 <sup>(2)</sup>	Erbaa & its vicinity	5.6
1923 <sup>(2)</sup>	Erbaa & its vicinity	5.9	1944 <sup>(2)</sup>	Erbaa & its vicinity	5.5
1929 <sup>(2,3,4)</sup>	Erbaa & its vicinity	6.1	1960 <sup>(2,4)</sup>	Erbaa & its vicinity	5.9
1935 <sup>(2,3)</sup>	Erbaa & its vicinity	5.5	1992 <sup>(1,2,3)</sup>	Erzincan (325 km to Erbaa)	6.8
1939 <sup>(2)</sup>	Erbaa & its vicinity	5.7	1992 <sup>(2,4)</sup>	Erzincan (325 km to Erbaa)	5.8

References:

1) Ambraseys and Finkel (2006)

2) Özmen et al. (1997)

3) Ayhan et al. (1984)

4) İnan et al. (1996)

The expected surface rupture length of NAFZ in the study area was determined from historical earthquake data. The surface rupture length of NAFZ around Erbaa was expressed as 70 km by Ambraseys (1970), Can (1974), and Barka (1981). Moreover, Barka et al. (2000) mentioned a 65 km surface rupture. Accordingly, a 70 km surface rupture length is used in Equation 5.1 to predict earthquake magnitude for the study area. The earthquake magnitude determined from Equation 5.1 is 7.2. The obtained result is consistent with the magnitude of the destructive 1942 Niksar-Erbaa earthquake (M = 7.2). As a conclusion, an

earthquake with 7.2 moment magnitude ( $M_s$ ) is considered to be the most appropriate scenario earthquake for the study area in further analyses.

Since the 1970s, strong ground motions have been recorded and used as well in seismic hazard analyses. However, there are no recorded ground motions from destructive earthquakes in the Erbaa region since the destructive earthquakes occurred there in 1940s. Therefore, the PGA for Erbaa is estimated using expected magnitude and different attenuation relationships as explained in the ground motion prediction section.

One of the main surface ruptures of the NAFZ is observed in the northern part of Erbaa (Barka, 1981; Barka et al., 2000; Tatar et al., 2006). The surface rupture in the northern part (Figure 5.2) is accepted as the seismic source area for Erbaa. Accordingly, the study area is divided into 2 km long parallel zones with respect to the abovementioned surface rupture (Figure 5.2). Therefore, site-source distance is evaluated precisely for ground motion prediction.

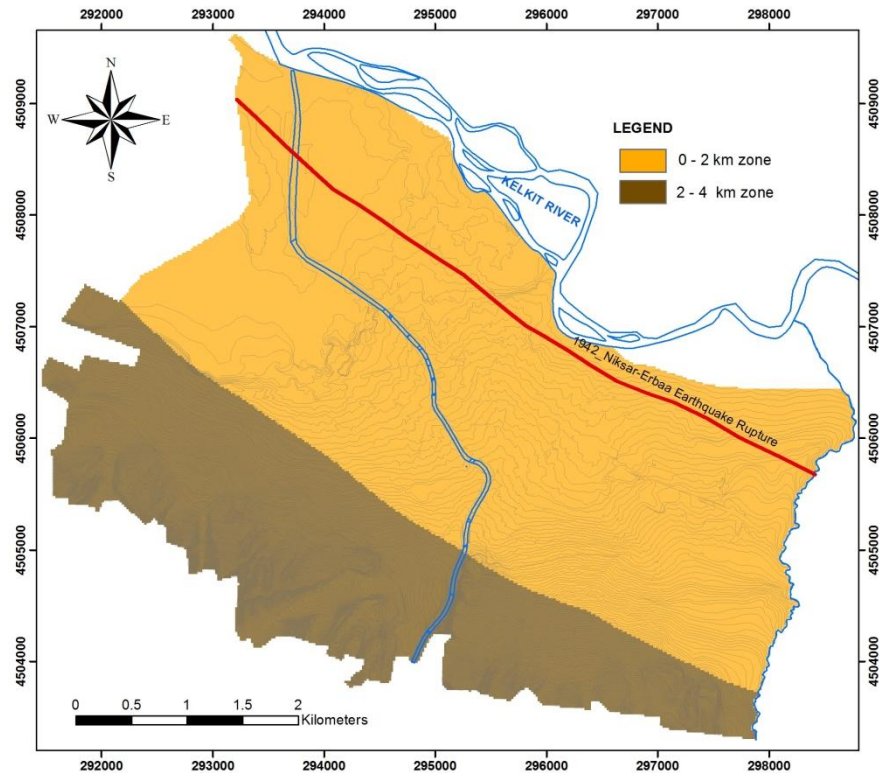


Figure 5.2. Parallel zonation with respect to fault surface rupture in the study area

### 5.3 Ground Motion Prediction

The earthquake resistant structures are subjected to different levels of earthquake effects in earthquake-prone areas. The estimation methods of these earthquake effects require specification of ground motion parameters for a proper design (Kramer, 1996).

In general terms, the prediction of ground motions for seismic sources resulting high PGA is evaluated by means of two methods:

1. Using attenuation equation and the controlling earthquake scenario identified in the DSHA.
2. Using attenuation equation and expected maximum magnitude derived by assuming surface rupture length.

Ground motion parameters can be obtained by predictive relationships as well. These relationships were proposed to characterize the geologic conditions of site, earthquake source mechanism, and the distance to the source. The obtained relationships, known as ground motion model or attenuation relationships were developed on the basis of regression analyses using recorded strong ground motion data.

Peak ground acceleration (PGA), velocity (PGV) and displacement (PGD) are the most common time domain parameters of strong ground motion (Kramer, 1996). The characteristics of ground motion which are significant in earthquake engineering applications are:

1. Amplitude, which can be explained in terms of peak ground motion (peak ground acceleration-PGA, peak ground velocity-PGV, and peak ground displacement-PGD),
2. Frequency content,
3. Duration of strong motion.

Each of these characteristics influences the response of a structure. Peak ground motion significantly affects the vibration amplitudes. Duration of strong motion has a pronounced effect on the number of load reversals imposed on the structure. A ground motion with moderate peak acceleration and a long duration may cause more damage than a ground motion with a larger acceleration and a shorter duration (Elnashai and Sarno, 2008).

The frequency content of ground motion can be scrutinized by the transformation of motion from a time domain to a frequency domain through a Fourier transform. In the frequency domain, Fourier amplitude and phase spectra, power spectrum, and response spectra can all be used to define and characterize the frequency content of strong ground motion (Naeim, 2001). Response spectra present the maximum amplitude of response of a single degree freedom system (SDOF) either at each frequency or each period. There are acceleration, velocity, and displacement spectra and they are related to each other through as relative displacement ( $S_d$ ), relative velocity ( $S_v$ ), absolute acceleration ( $S_a$ ), pseudo-relative velocity (PSV), and pseudo-relative acceleration (PSA).

The frequency content of the response spectrum can be described using the Predominant or Mean Period with a link to the spectral acceleration at 5% damping (Erdik and Durukal, 2004). Frequency content strongly affects the response characteristics of a structure. In a structure, ground motion is extremely amplified when the frequency content of motion and the natural frequency of structure are close to each other.

Other ground motion parameters reflect multiple ground motion characteristics. The “rms acceleration”, which is a single parameter, includes the effects of amplitude and frequency content of a strong ground motion record. The “Arias intensity”, which is similar to rms acceleration, can be obtained by integrating over the duration of the motion. The “cumulative absolute velocity” (CAV) is another ground motion parameter that can be used to correlate structural damage potential. The “response spectrum intensity” developed by Housner (1959) can be applied to capture important aspects of the amplitude and frequency content in a single parameter. The “velocity and acceleration spectrum intensity” parameters were also suggested to characterize strong ground motion in different analysis. The “effective peak velocity (EPV) and acceleration (EPA)” were proposed to be used in the specification of smoothed design response spectra in building codes as an alternative. The summary of ground motion parameters and related ground motion characteristics are presented in Table 5.2 (Kramer, 1996).

The estimation of ground motion parameters can be performed by attenuation relationships (predictive relationships) which are a function of magnitude, distance, and other variables such as hanging wall, depth etc. (Kramer, 1996).

### 5.3.1 Ground motion models (attenuation relationships)

Measured ground motions are compiled in a database to facilitate development of predictive relationships for strong ground motion parameters. The prediction of ground motion parameters were commonly conducted by empirical attenuation relationships. The “attenuation” of earthquake ground motions is an important factor in estimating ground motion parameters for assessment and design purposes. Ground motion models (or attenuation relationships) are analytical expressions describing ground-motion variation with magnitude, source distance, and site condition as well as considering the energy loss of seismic waves. Ground motion attenuation relationships are derived either empirically through utilizing earthquake records or theoretically through employing seismological models to generate synthetic ground motions (Elnashai and Sarno, 2008).

Table 5.2. Summary of ground motion parameters and related characteristic (after Kramer, 1996)

Ground motion parameters	Ground motion characteristics		
	Amplitude	Frequency content	Duration
Peak acceleration-PHA, PHD and PHV	X		
Predominant period		X	
Power spectrum intensity	X	X	X
Duration			X
rms acceleration	X	X	
Arias Intensity	X	X	X
Cumulative absolute velocity (CAV)	X	X	X
Response, velocity and acceleration spectrum intensity	X	X	
Effective peak acceleration (EPA)	X	X	
Effective peak velocity (EPV)	X	X	

Attenuation relationships are empirical descriptions providing the median and standard deviation of various intensity measures of strong ground motion assumed to be log normally distributed in terms of earthquake size, distance, source mechanism and site conditions (Erdik and Durukal, 2004). Douglas (2001) made a comprehensive worldwide summary of strong ground motion attenuation relationships from 1969 to 2000. The compilation of attenuation relationships by Douglas (2001) is modified and presented in Table 5.3.

Previous attenuation relationships typically presented by the natural logarithm of a ground shaking parameter such as acceleration or spectral acceleration as a function of magnitude



were proposed for a particular soil condition (e.g. rock, soft soil, deep stiff soil and shallow stiff soil) (Trifunac and Brady, 1976; Idriss, 1978; Boore and Joyner, 1982; Campbell, 1985; Sabetta and Pugliese, 1987; Joyner and Boore, 1988; 1996; Ambraseys and Bommer, 1995; Campbell and Bozorgnia, 2000; 2003).

Table 5.3. Summary of attenuation relationships in literature (modified from Douglas, 2001)

Location	References for attenuation relationships
West and North USA	Milne and Davenport (1969), Esteva (1970), Esteva and Villaverde (1973), Trifunac and Brady (1975), Trifunac (1976), Trifunac and Brady (1976), McGuire (1977), Milne (1977), Donovan and Bornstein (1978), Cornell et al. (1979), Joyner and Boore (1981), Bolt and Abrahamson (1982), Joyner and Fumal (1984), Joyner and Boore (1988), Campbell (1989), Ambraseys (1990), Boore et al. (1994), Boore et al. (1997), Chapman (1999), and Tao (2000)
California	Orphal and Lahoud (1974), Blume (1977), Abrahamson and Litehiser (1989), Sadigh et al. (1993), Sadigh et al. (1997), Crouse and McGuire (1996), Ohno et al. (1996), Sadigh and Egan (1998)
Europe-Middle East	Ambraseys (1975), Chiaruttini and Siro (1981), Petrovski and Marcellini (1988), Ambraseys and Bommer (1991), Ambraseys and Bommer (1992), Ambraseys (1995), Ambraseys et al. (1996), Simpson (1996), Ambraseys et al. (2005a), (2005b), Akkar and Bommer (2007)
Japan	Kawashima et al. (1985), Yamabe and Kanai (1988), Fukushima et al. (1988), Fukushima and Tanaka (1990), Fukushima et al. (1994), Fukushima et al. (1995), Molas and Yamazaki (1995), Kobayashi et al. (2000), Si and Midorikawa (2000)
Himalayas	Sharma (1998), Jain et al. (2000), Sharma (2000)
Italy- Greece	Faccioli (1978), Tento et al. (1992), Sabetta and Pugliese (1987), Theodulidis and Papazachos (1994), Rinaldis et al. (1998)
Worldwide	Aptikaev and Kopnichev (1980), Campbell (1993), Sarma and Srbulov (1996), Campbell (1997), Campbell and Bozorgnia (1994), Sarma and Srbulov (1998), Ambraseys and Douglas (2000), (2003), Bozorgnia et al. (2000), Campbell and Bozorgnia (2000), (2003)
Turkey	Inan et al. (1996), Aydan et al. (1996), Aydan (1997), Kalkan and Gulkan (2004), Ulusay et al. (2004), Ozbey et al. (2004), Gullu and Ercelebi (2007)

Recent and significant addition to the strong ground motion literature are the “Next Generation Attenuation” models generated in a specific project called “Pacific Earthquake Engineering Research Center’s Next Generation Attenuation (PEER NGA)” (Boore and Atkinson, 2007; Campbell and Bozorgnia, 2007; Chiou et al. 2008; Power et al., 2008). As a part of the PEER NGA project, five different groups of researchers developed new ground motion prediction equations (GMPEs) (Abrahamson and Silva, 2008 (AS08); Boore and Atkinson, 2008 (BA08); Campbell and Bozorgnia, 2008 (CB08); Chiou and Youngs, 2008

(CY08); and Idriss, 2008 (I08)). The main aim of PEER NGA project was to develop empirical GMPEs to allow a range of interpretations. The source of strong ground motion data for the development of the GMPEs in that study was a comprehensive and consistent database compiled in the PEER NGA project (Chiou et al. 2008). The strong ground-motion data were summarized in a spreadsheet known as the “NGA Flatfile” in the same project.

The model parameters used by each group are summarized in Table 5.4. The I08 model, which was only developed for rock sites, has the parameters of magnitude, distance, and style of faulting. The  $V_{s30}$  and input rock motion parameters were added to model nonlinear site response in addition to magnitude, distance, and style of faulting in the BA08 model. The AS08, CB08, and CY08 models include a number of additional parameters as part of the models such as hanging-wall (HW), rupture-depth, and soil/sediment depth. All of these models except I08 use the average shear wave velocity in the top 30 m,  $V_{s30}$ , as the primary site parameter.

Table 5.4. Parameters used in the NGA models

Parameter	AS08	BA08	CB08	CY08	I08
Moment magnitude	M	M	M	M	M
Depth to top of rupture (km)	$Z_{TOR}$		$Z_{TOR}$	$Z_{TOR}$	
Reverse style of faulting flag	$F_{RV}$	RS	$F_{RV}$	$F_{RV}$	$F_{RV}$
Normal style of faulting flag	$F_N$	NS	$F_N$	$F_N$	
Strike-slip style of faulting flag		SS			
Unspecified style of faulting flag		US			
Aftershock flag	$F_{AS}$			AS	
Dip (degrees)	$\delta^a$		$\delta^a$	$\delta^a$	
Down-dip rupture width (km)	$W^a$				
Closest distance to the rupture plane (km)	$R_{rup}$		$R_{rup}$	$R_{rup}$	$R_{rup}$
Horizontal distance to the surface projection of the rupture (km)	$R_{jb}^a$	$R_{jb}^a$	$R_{jb}^a$	$R_{jb}^a$	
Horizontal distance to the top edge of the rupture measured perpendicular to strike (km)	$R_x^a$			$R_x^a$	
Hanging wall flag	$F_{HW}$			$F_{HW}$	
Average shear wave velocity in the top 30 m (m/s)	$V_{s30}$	$V_{s30}$	$V_{s30}$	$V_{s30}$	
Depth to $V_s = 1.0$ km/s (km)	$Z_{1.0}$			$Z_{1.0}$	
Depth to $V_s = 2.5$ km/s (km)			$Z_{2.5}$		
Rock motion PGA for nonlinear site response	$PGA_{1100}$	$Pga4nl$	$A_{1100}$		
Rock motion $S_a$ for nonlinear site response				$y_{ref}(T)$	
$V_{s30}$ of rock motion used for nonlinear site response (m/s)	1100	760	1100	1130	

<sup>a</sup>Used for HW scaling only

AS08: Abrahamson and Silva (2008)

BA08: Boore and Atkinson (2008)

CB08: Campbell and Bozorgnia (2008)

CY08: Chiou and Youngs (2008)

I08: Idriss (2008)

Furthermore, AS08, BA08, CB08, and CY08 models include site effects that incorporate nonlinear site response. The BA08 model defines the input rock motion with respect to  $V_{s30}=760$  m/s whereas the other three models use a  $V_{s30}$  of about 1100 m/s. Three models, AS08, CB08, CY08, include the soil depth as an additional site parameter. Accordingly, the AS08 and CY08 models use the depth to  $V_s=1.0$  km/s while the CB08 model applies the depth to  $V_s=2.5$  km/s. These parameters are thought to provide improved representation of basin effects.

All of the proposed models for the NGA project use different style of faulting factors (Table 5.5). However, there is no distinction between strike-slip and normal fault earthquakes in I08 model. All of the models are based on moment magnitude and two different distance measures are used. The BA08 model uses the closest horizontal distance to the surface projection of the rupture plane,  $R_{JB}$ . The other four models, AS08, CB08, CY08, I08, use the closest distance to the rupture plane,  $R_{rup}$ . Eventually, Boore and Atkinson (2008) (BA08) and Campbell and Bozorgnia (2008) (CB08) models are considered in this research to determine target spectra.

Table 5.5. Style of faulting class for the NGA models (after Abrahamson and Silva, 2008)

Style of faulting class	AS08	BA08	CB08	CY08	I08
Normal (NML)	NML	NML and NML/oblique	NML and NML/oblique	NML	-
Strike-slip (SS)	SS and NML/oblique	SS	SS	SS and NML/OBL	SS, NML/OBL and NML
Reverse (RV)	RV and RV/oblique	RV and RV/oblique	RV and RV/oblique	RV and RV/oblique	RV and RV/oblique

AS08: Abrahamson and Silva (2008)  
BA08: Boore and Atkinson (2008)  
CB08: Campbell and Bozorgnia (2008)  
CY08: Chiou and Youngs (2008)  
I08: Idriss (2008)

### 5.3.1.1 Boore and Atkinson (2008) NGA relationship

Boore and Atkinson (2008) proposed ground motion equations (GMPEs) for average horizontal component ground motions as a function of earthquake magnitude, distance from source to site, local average shear wave velocity and fault type. The equations are for peak ground acceleration (PGA), peak ground velocity (PGV), and 5% damped pseudo - absolute acceleration spectra (PSA) at the periods between 0.01 s and 10 s. These equations are

applicable for  $M=5-8$ ,  $R_{JB}<200$  km and  $V_{S30}=180-1300$  m/s. The equation for predicting ground motions are given below with employed coefficients.

$$\ln Y = F_M(M) + F_D(R_{JB}, M) + F_S(V_{S30}, R_{JB}, M) + \varepsilon \sigma_T \quad (5.2)$$

- $F_M$  : magnitude scaling function  
 $F_D$  : distance function  
 $F_S$  : site amplification function  
 $M$  : moment magnitude  
 $R_{JB}$  : Joyner-Boore distance (defined as the closest distance to the surface projection of the fault which is approximately equal to the epicentral distance for the events of  $M<6$ ),  
 $V_{S30}$  : the inverse of the average shear wave slowness from the surface to a depth of 30 m.  
 $\varepsilon$  : the fractional number of standard deviations of a single predicted value of  $\ln Y$  (e.g.,  $\varepsilon=-1.5$  would be 1.5 standard deviations smaller than the mean value)

$\sigma_T$  is computed using the Equation 5.3:

$$\sigma_T = \sqrt{\sigma^2 + \tau^2} \quad (5.3)$$

- $\sigma$  : the intra-event aleatory uncertainty  
 $\tau$  : the inter-event aleatory uncertainty

The coefficients in the related equations are given in Tables 5.6 - 5.10. It should be noted that these coefficients are for  $\ln Y$  where  $Y$  is in “g” unit for PSA (peak spectral acceleration) and PGA (peak ground acceleration), and “cm/s” unit for PGV (peak ground velocity). The units of distance and velocity are “km” and “m/s”, respectively (Boore and Atkinson, 2008).

The distance function ( $F_D$ ) is expressed by:

$$F_D(R_{JB}, M) = (c1 + c2 (M - M_{ref})) \ln (R/R_{ref}) + c3 (R - R_{ref}) \quad (5.4)$$

$$\text{where } R = \sqrt{R_{JB}^2 + h^2} \quad (5.5)$$

- $M_{ref}$  : reference magnitude ( $M_{ref} = 4.5$ )  
 $R_{ref}$  : reference distance ( $R_{ref} = 1$  km)  
 $c1, c2, c3$  and  $h$  are the coefficients to be determined in the analysis (Table 5.7).

Table 5.6. Aleatory uncertainties for different periods for Boore and Atkinson GMPE ( $\sigma$ : intra-event uncertainty;  $\tau$ : inter-event uncertainty;  $\sigma_T$ : combined uncertainty,  $\text{SQRT}(\sigma^2 + \tau^2)$ ; subscripts U and M for fault type unspecified and specified)

Period (T) (s)	$\sigma$	Unspecified fault type		Specified fault type	
		$\tau_U$	$\sigma_{TU}$	$\tau_M$	$\sigma_{TM}$
<b>PGV</b>	0.500	0.286	0.576	0.256	0.560
<b>PGA</b>	0.502	0.265	0.566	0.260	0.564
<b>0.01</b>	0.502	0.267	0.569	0.262	0.566
<b>0.02</b>	0.502	0.267	0.569	0.262	0.566
<b>0.03</b>	0.507	0.276	0.578	0.274	0.576
<b>0.05</b>	0.516	0.286	0.589	0.286	0.589
<b>0.08</b>	0.513	0.322	0.606	0.320	0.606
<b>0.10</b>	0.520	0.313	0.608	0.318	0.608
<b>0.15</b>	0.518	0.288	0.592	0.290	0.594
<b>0.20</b>	0.523	0.283	0.596	0.288	0.596
<b>0.25</b>	0.527	0.267	0.592	0.267	0.592
<b>0.30</b>	0.546	0.272	0.608	0.269	0.608
<b>0.40</b>	0.541	0.267	0.603	0.267	0.603
<b>0.50</b>	0.555	0.265	0.615	0.265	0.615
<b>0.75</b>	0.571	0.311	0.649	0.299	0.645
<b>1.00</b>	0.573	0.318	0.654	0.302	0.647
<b>1.50</b>	0.566	0.382	0.684	0.373	0.679
<b>2.00</b>	0.580	0.398	0.702	0.389	0.700
<b>3.00</b>	0.566	0.410	0.700	0.401	0.695
<b>4.00</b>	0.583	0.394	0.702	0.385	0.698
<b>5.00</b>	0.601	0.414	0.730	0.437	0.744
<b>7.50</b>	0.626	0.465	0.781	0.477	0.787
<b>10.00</b>	0.645	0.355	0.735	0.477	0.801

Table 5.7. Distance-scaling coefficients ( $M_{ref}=4.5$  and  $R_{ref}=1.0$  km for all periods, except  $R_{ref}=5.0$  km for pga4nl)

Period (T) (s)	c1	c2	c3	h
<b>PGV</b>	-0.87370	0.10060	-0.00334	2.54
<b>PGA</b>	-0.66050	0.11970	-0.01151	1.35
<b>0.01</b>	-0.66220	0.12000	-0.01151	1.35
<b>0.02</b>	-0.66600	0.12280	-0.01151	1.35
<b>0.03</b>	-0.69010	0.12830	-0.01151	1.35
<b>0.05</b>	-0.71700	0.13170	-0.01151	1.35
<b>0.08</b>	-0.72050	0.12370	-0.01151	1.55
<b>0.10</b>	-0.70810	0.11170	-0.01151	1.68
<b>0.15</b>	-0.69610	0.09884	-0.01113	1.86
<b>0.20</b>	-0.58300	0.04273	-0.00952	1.98
<b>0.25</b>	-0.57260	0.02977	-0.00837	2.07
<b>0.30</b>	-0.55430	0.01955	-0.00750	2.14
<b>0.40</b>	-0.64430	0.04394	-0.00626	2.24
<b>0.50</b>	-0.69140	0.06080	-0.00540	2.32
<b>0.75</b>	-0.74080	0.07518	-0.00409	2.46
<b>1.00</b>	-0.81830	0.10270	-0.00334	2.54
<b>1.50</b>	-0.83030	0.09793	-0.00255	2.66
<b>2.00</b>	-0.82850	0.09432	-0.00217	2.73
<b>3.00</b>	-0.78440	0.07282	-0.00191	2.83
<b>4.00</b>	-0.68540	0.03758	-0.00191	2.89
<b>5.00</b>	-0.50960	-0.02391	-0.00191	2.93
<b>7.50</b>	-0.37240	-0.06568	-0.00191	3.00
<b>10.00</b>	-0.09824	-0.13800	-0.00191	3.04

The magnitude scaling ( $F_M$ ) is calculated by:

a)  $M \leq M_h$

$$F_M(M) = e_1U + e_2SS + e_3NS + e_4RS + e_5(M-M_h) + e_6(M-M_h)^2 \quad (5.6.1)$$

b)  $M > M_h$

$$F_M(M) = e_1U + e_2SS + e_3NS + e_4RS + e_7(M-M_h) \quad (5.6.2)$$

Table 5.8. Magnitude-scaling coefficients

<b>Period (T) (s)</b>	<b>e<sub>1</sub></b>	<b>e<sub>2</sub></b>	<b>e<sub>3</sub></b>	<b>e<sub>4</sub></b>	<b>e<sub>5</sub></b>	<b>e<sub>6</sub></b>	<b>e<sub>7</sub></b>
<b>PGV</b>	5.00121	5.04727	4.63188	5.08210	0.183220	-0.12736	0.00000
<b>PGA</b>	-0.53804	-0.50350	-0.75472	-0.50970	0.288050	-0.10164	0.00000
<b>0.01</b>	-0.52883	-0.49429	-0.74551	-0.49966	0.288970	-0.10019	0.00000
<b>0.02</b>	-0.52192	-0.48508	-0.73906	-0.48895	0.251440	-0.11006	0.00000
<b>0.03</b>	-0.45285	-0.41831	-0.66722	-0.42229	0.179760	-0.12858	0.00000
<b>0.05</b>	-0.28476	-0.25022	-0.48462	-0.26092	0.063690	-0.15752	0.00000
<b>0.08</b>	0.00767	0.04912	-0.20578	0.02706	0.011700	-0.17051	0.00000
<b>0.10</b>	0.20109	0.23102	0.03058	0.22193	0.046970	-0.15948	0.00000
<b>0.15</b>	0.46128	0.48661	0.30185	0.49328	0.179900	-0.14539	0.00000
<b>0.20</b>	0.57180	0.59253	0.40860	0.61472	0.527290	-0.12964	0.00102
<b>0.25</b>	0.51884	0.53496	0.33880	0.57747	0.608800	-0.13843	0.08607
<b>0.30</b>	0.43825	0.44516	0.25356	0.51990	0.644720	-0.15694	0.10601
<b>0.40</b>	0.39220	0.40602	0.21398	0.46080	0.786100	-0.07843	0.02262
<b>0.50</b>	0.18957	0.19878	0.00967	0.26337	0.768370	-0.09054	0.00000
<b>0.75</b>	-0.21338	-0.19496	-0.49176	-0.10813	0.751790	-0.14053	0.10302
<b>1.00</b>	-0.46896	-0.43443	-0.78465	-0.39330	0.678800	-0.18257	0.05393
<b>1.50</b>	-0.86271	-0.79593	-1.20902	-0.88085	0.706890	-0.25950	0.19082
<b>2.00</b>	-1.22652	-1.15514	-1.57697	-1.27669	0.779890	-0.29657	0.29888
<b>3.00</b>	-1.82979	-1.74690	-2.22584	-1.91814	0.779660	-0.45384	0.67466
<b>4.00</b>	-2.24656	-2.15906	-2.58228	-2.38168	1.249610	-0.35874	0.79508
<b>5.00</b>	-1.28408	-1.21270	-1.50904	-1.41093	0.142710	-0.39006	0.00000
<b>7.50</b>	-1.43145	-1.31632	-1.81022	-1.59217	0.524070	-0.37578	0.00000
<b>10.00</b>	-2.15446	-2.16137	-2.53323	-2.14635	0.403870	-0.48492	0.00000

The site amplification ( $F_S$ ) equation is determined by:

$$F_S = F_{LIN} + F_{NL} \quad (5.7)$$

$F_{LIN}$  : linear term

$F_{NL}$  : nonlinear term

The linear term ( $F_{LIN}$ ) is given by:

$$F_{LIN} = b_{lin} \ln (V_{S30}/V_{ref}) \quad (5.8)$$

$b_{lin}$  : a period-dependent coefficient

$V_{ref}$  : the specified reference velocity (=760 m/s) corresponding to NEHRP B/C boundary site conditions

The nonlinear term ( $F_{NL}$ ) is given by:

a)  $pga_{4nl} \leq a_1$ :

$$F_{NL} = b_{nl} \ln(pga\_low/0.1) \quad (5.9.1)$$

b)  $a_1 < pga_{4nl} \leq a_2$ :

$$F_{NL} = b_{nl} \ln(pga\_low/0.1) + c(\ln(pga_{4nl}/a_1))^2 + d(\ln(pga_{4nl}/a_1))^3 \quad (5.9.2)$$

c)  $a_2 < pga_{4nl}$ :

$$F_{NL} = b_{nl} \ln(pga_{4nl}/0.1) \quad (5.9.3)$$

$a_1$  : 0.03g threshold levels for linear amplification

$a_2$  : 0.09g threshold levels for nonlinear amplification

$pga\_low$  : 0.06 g

$pga_{4nl}$  : the predicted PGA in g for  $V_{ref}=760$  m/s as given in Equation 5.1 with  $FS=0$  and  $\varepsilon=0$  as presented in Table 5.8.

Equation 5.9.2 is determined by:

$$c = 3\Delta y - b_{nl}\Delta x / \Delta x^2 \quad (5.10)$$

$$d = -(\Delta 2y - b_{nl}\Delta x) / \Delta x^3 \quad (5.11)$$

where

$$\Delta x = \ln(a_2/a_1) \quad (5.12)$$

$$\Delta y = b_{nl} \ln(a_2/pga\_low) \quad (5.13)$$

The nonlinear slope  $b_{nl}$  is a function of both period and  $V_{S30}$  as given by:

a)  $V_{S30} \leq V_1$ :

$$b_{nl} = b_1 \quad (5.14.1)$$

b)  $V_1 < V_{S30} \leq V_2$ :

$$b_{nl} = (b_1 - b_2) \ln(V_{S30}/V_2) / \ln(V_1/V_2) + b_2 \quad (5.14.2)$$

c)  $V_2 < V_{S30} < V_{ref}$ :

$$b_{nl} = b_2 \ln(V_{S30}/V_{ref}) / \ln(V_2/V_{ref}) \quad (5.14.3)$$

d)  $V_{ref} \leq V_{S30}$ :

$$b_{nl} = 0.0 \quad (5.14.4)$$

$V_1=180$  m/s,  $V_2=300$  m/s, and  $b_1$  and  $b_2$  are period-dependent coefficients, and  $b_{nl}$  is a function of period as well as  $V_{S30}$ .



Table 5.9. Period-independent site-amplification coefficients

Coefficient	Value
$a_1$	0.03 g
$pga_{low}$	0.06 g
$a_2$	0.09 g
$V_1$	180 m/ s
$V_2$	300 m/ s
$V_{ref}$	760 m/ s

Table 5.10. Period-dependent site-amplification coefficients

Period	$b_{lin}$	$b_1$	$b_2$
PGV	-0.600	-0.500	-0.06
PGA	-0.360	-0.640	-0.14
0.010	-0.360	-0.640	-0.14
0.020	-0.340	-0.630	-0.12
0.030	-0.330	-0.620	-0.11
0.050	-0.290	-0.640	-0.11
0.075	-0.230	-0.640	-0.11
0.100	-0.250	-0.600	-0.13
0.150	-0.280	-0.530	-0.18
0.200	-0.310	-0.520	-0.19
0.250	-0.390	-0.520	-0.16
0.300	-0.440	-0.520	-0.14
0.400	-0.500	-0.510	-0.10
0.500	-0.600	-0.500	-0.06
0.750	-0.690	-0.470	0.00
1.000	-0.700	-0.440	0.00
1.500	-0.720	-0.400	0.00
2.000	-0.730	-0.380	0.00
3.000	-0.740	-0.340	0.00
4.000	-0.750	-0.310	0.00
5.000	-0.750	-0.291	0.00
7.500	-0.692	-0.247	0.00
10.000	-0.650	-0.215	0.00

### 5.3.1.2 Campbell and Bozorgnia (2008) NGA relationship

Campbell and Bozorgnia (2008) (CB08) presented a new empirical ground motion model for PGA, PGV, PGD and 5% damped linear elastic response spectra for periods ranging from 0.01–10 s. The developed equations are valid for magnitudes ranging from 4.0 to 7.5–8.5 (depending on fault mechanism) and for distances ranging from 0–200 km. The Campbell and Bozorgnia (2008) ground motion model includes magnitude saturation, magnitude-dependent attenuation, style of faulting, rupture depth, hanging-wall geometry, linear and nonlinear site response, 3-D basin response, and inter-event and intra-event variability.

The ground motion model can be calculated by Equation 5.15:

$$\ln Y = f_{\text{mag}} + f_{\text{dis}} + f_{\text{flt}} + f_{\text{hng}} + f_{\text{site}} + f_{\text{sed}} \quad (5.15)$$

the magnitude term is expressed by:

$$f_{\text{mag}} = \begin{cases} c_0 + c_1 M; & M \leq 5.5 \\ c_0 + c_1 M + c_2 (M - 5.5); & 5.5 < M \leq 6.5 \\ c_0 + c_1 M + c_2 (M - 5.5) + c_3 (M - 6.5); & M > 6.5 \end{cases} \quad (5.16)$$

the distance term is expressed by:

$$f_{\text{dis}} = (c_4 + c_5 M) \ln (\sqrt{R_{\text{RUP}}^2 + c_6^2}) \quad (5.17)$$

the style of faulting (fault mechanism) term is expressed by:

$$f_{\text{flt}} = c_7 F_{\text{RV}} f_{\text{flt,Z}} + c_8 F_{\text{NM}} \quad (5.18)$$

$$f_{\text{flt,Z}} = \begin{cases} Z_{\text{TOR}}; & Z_{\text{TOR}} < 1 \\ 1; & Z_{\text{TOR}} \geq 1 \end{cases} \quad (5.19)$$

the hanging-wall term is expressed by:

$$f_{\text{hng}} = c_9 f_{\text{hng,R}} f_{\text{hng,M}} f_{\text{hng,Z}} f_{\text{hng,\delta}} \quad (5.20)$$

$$f_{\text{hng},R} = \begin{cases} 1; & R_{JB} = 0 \\ (\max(R_{RUP}, \sqrt{R_{JB}^2 + 1}) - R_{JB}) / \max(R_{RUP}, (\sqrt{R_{JB}^2 + 1})); & R_{JB} > 0, Z_{TOR} < 1 \\ (R_{RUP} - R_{JB}) / R_{RUP}; & R_{JB} > 0, Z_{TOR} \geq 1 \end{cases} \quad (5.21)$$

$$f_{\text{hng},M} = \begin{cases} 0; & M \leq 6.0 \\ 2(M - 6.0); & 6.0 < M < 6.5 \\ 1; & M \geq 6.5 \end{cases} \quad (5.22)$$

$$f_{\text{hng},Z} = \begin{cases} 0; & Z_{TOR} \geq 20 \\ (20 - Z_{TOR}) / 20; & 0 \leq Z_{TOR} < 20 \end{cases} \quad (5.23)$$

$$f_{\text{hng},\delta} = \begin{cases} 1; & \delta \leq 70 \\ (90 - \delta) / 20; & \delta > 70 \end{cases} \quad (5.24)$$

the shallow site response\_term is expressed by:

$$f_{\text{site}} = \begin{cases} c_{10} (\ln V_{S30}/k_1) + k_2 (\ln(A_{1100} + c(V_{S30}/k_1)^n) - \ln(A_{1100} + c)); & V_{S30} < k_1 \\ (c_{10} + k_2 n) \ln(V_{S30}/k_1); & k_1 \leq V_{S30} < 1100 \\ (c_{10} + k_2 n) \ln(1100/k_1); & V_{S30} \geq 1100 \end{cases} \quad (5.25)$$

the basin response term is expressed by:

$$f_{\text{sed}} = \begin{cases} c_{11} (Z_{2.5} - 1); & Z_{2.5} < 1 \\ 0; & 1 \leq Z_{2.5} \leq 3 \\ c_{12} k_3 e^{-0.75} (1 - e^{-0.25(Z_{2.5}^3 - 3)}); & Z_{2.5} > 3 \end{cases} \quad (5.26)$$

where

- Y: the median estimate of the geometric mean horizontal component (GMRotI50) of PGA (g), PGV (cm/s), PGD (cm) or PSA (g)
- M: moment magnitude
- $R_{RUP}$ : the closest distance to the coseismic rupture plane (km)
- $R_{JB}$ : the closest distance to the surface projection of the coseismic rupture plane (km)
- $F_{RV}$ : an indicator variable representing reverse and reverse-oblique faulting, where  $F_{RV}=1$  for  $30^\circ < \lambda < 150^\circ$ ,  $F_{RV}=0$  otherwise
- $\lambda$ : rake defined as the average angle of slip measured in the plane of rupture between the strike direction and the slip vector
- $F_{NM}$ : an indicator variable representing normal and normal-oblique faulting, where  $F_{NM}=1$  for  $-150^\circ < \lambda < -30^\circ$ , and  $F_{NM}=0$  otherwise

- $Z_{TOR}$ : the depth to the top of the coseismic rupture plane (km)  
 $\delta$ : the dip of the rupture plane ( $^{\circ}$ )  
 $V_{S30}$ : the time-averaged shear wave velocity in the top 30 m of the site profile (m/s)  
 $A_{1100}$ : the median estimate of PGA on a reference rock outcrop ( $V_{S30}=1100$  m/s) from Equation 5.25 (g)  
 $Z_{2.5}$ : the depth to 2.5 km/s shear wave velocity horizon referred to basin or sediment depth (km)

The empirical coefficients  $c_{1-12}$  are listed in Table 5.11 and the theoretical coefficients  $c$ ,  $n$ , and  $k_{1-3}$  are listed in Table 5.12. The formula for standard deviation is given below:

$$\alpha = \alpha f_{site} / \ln A_{1100} = k_2 A_{1100} ((A_{1100} + c(V_{S30}/k_1)^n)^{-1} - (A_{1100} + c)^{-1}) \quad V_{S30} < k_1$$

$$0 \quad V_{S30} \geq k_1 \quad (5.27)$$

The related coefficients for standard deviation formula are listed in Table 5.12. The researchers considered their previous studies to develop the new NGA model (Campbell 1997; Campbell and Bozorgnia 2003). The new model will be valid if the following cases are considered:

1.  $M > 4.0$
2.  $M < 8.5$  for strike-slip faulting,  $M < 8.0$  for reverse faulting, and  $M < 7.5$  for normal faulting
3.  $R_{RUP} = 0-200$  km
4.  $V_{S30} = 150-1500$  m/s or alternatively NEHRP site classes B, C, D and E
5.  $Z_{2.5} = 0-10$  km
6.  $Z_{TOR} = 0-15$  km
7.  $\delta = 15-90^{\circ}$

Table 5.11. Coefficients for Campbell and Bozorgnia (2008) NGA model ( $c_1$ - $c_{12}$ )

$T(s)$	$c_0$	$c_1$	$c_2$	$c_3$	$c_4$	$c_5$	$c_6$	$c_7$	$c_8$	$c_9$	$c_{10}$	$c_{11}$	$c_{12}$
0.010	-1.715	0.500	-0.530	-0.262	-2.118	0.170	5.60	0.280	-0.120	0.490	1.058	0.040	0.610
0.020	-1.680	0.500	-0.530	-0.262	-2.123	0.170	5.60	0.280	-0.120	0.490	1.102	0.040	0.610
0.030	-1.552	0.500	-0.530	-0.262	-2.145	0.170	5.60	0.280	-0.120	0.490	1.174	0.040	0.610
0.050	-1.209	0.500	-0.530	-0.267	-2.199	0.170	5.74	0.280	-0.120	0.490	1.272	0.040	0.610
0.075	-0.657	0.500	-0.530	-0.302	-2.277	0.170	7.09	0.280	-0.120	0.490	1.438	0.040	0.610
0.10	-0.314	0.500	-0.530	-0.324	-2.318	0.170	8.05	0.280	-0.099	0.490	1.604	0.040	0.610
0.15	-0.133	0.500	-0.530	-0.339	-2.309	0.170	8.79	0.280	-0.048	0.490	1.928	0.040	0.610
0.20	-0.486	0.500	-0.446	-0.398	-2.220	0.170	7.60	0.280	-0.012	0.490	2.194	0.040	0.610
0.25	-0.890	0.500	-0.362	-0.458	-2.146	0.170	6.58	0.280	0.000	0.490	2.351	0.040	0.700
0.30	-1.171	0.500	-0.294	-0.511	-2.095	0.170	6.04	0.280	0.000	0.490	2.460	0.040	0.750
0.40	-1.466	0.500	-0.186	-0.592	-2.066	0.170	5.30	0.280	0.000	0.490	2.587	0.040	0.850
0.50	-2.569	0.656	-0.304	-0.536	-2.041	0.170	4.73	0.280	0.000	0.490	2.544	0.040	0.883
0.75	-4.844	0.972	-0.578	-0.406	-2.000	0.170	4.00	0.280	0.000	0.490	2.133	0.077	1.000
1.0	-6.406	1.196	-0.772	-0.314	-2.000	0.170	4.00	0.255	0.000	0.490	1.571	0.150	1.000
1.5	-8.692	1.513	-1.046	-0.185	-2.000	0.170	4.00	0.161	0.000	0.490	0.406	0.253	1.000
2.0	-9.701	1.600	-0.978	-0.236	-2.000	0.170	4.00	0.094	0.000	0.371	-0.456	0.300	1.000
3.0	-10.556	1.600	-0.638	-0.491	-2.000	0.170	4.00	0.000	0.000	0.154	-0.820	0.300	1.000
4.0	-11.212	1.600	-0.316	-0.770	-2.000	0.170	4.00	0.000	0.000	0.000	-0.820	0.300	1.000
5.0	-11.684	1.600	-0.070	-0.986	-2.000	0.170	4.00	0.000	0.000	0.000	-0.820	0.300	1.000
7.5	-12.505	1.600	-0.070	-0.656	-2.000	0.170	4.00	0.000	0.000	0.000	-0.820	0.300	1.000
10.0	-13.087	1.600	-0.070	-0.422	-2.000	0.170	4.00	0.000	0.000	0.000	-0.820	0.300	1.000
0 (PGA)	-1.715	0.500	-0.530	-0.262	-2.118	0.170	5.60	0.280	-0.120	0.490	1.058	0.040	0.610
-1 (PGV)	0.954	0.696	-0.309	-0.019	-2.016	0.170	4.00	0.245	0.000	0.358	1.694	0.092	1.000
-2 (PGD)	-5.270	1.600	-0.070	0.000	-2.000	0.170	4.00	0.000	0.000	0.000	-0.820	0.300	1.000

Table 5.12. Coefficients for Campbell and Bozorgnia (2008) NGA model ( $k_1$ - $\rho$ )

T (s)	$k_1$	$k_2$	$k_3$	$c$	n	Standard Deviation for $V_{s30} \geq k_1$				Correlation coefficient	
						$\sigma_{\text{ln}F}$	$\sigma_{\text{ln}F}$	$\sigma_{\text{ln}F}$	$\sigma_C$	$\rho$	
0.010	865	-1.186	1.839	1.88	1.18	0.478	0.219	0.300	0.166	1.000	1.000
0.020	865	-1.219	1.840	1.88	1.18	0.480	0.219	0.300	0.166	0.999	0.999
0.030	908	-1.273	1.841	1.88	1.18	0.489	0.235	0.300	0.165	0.989	0.989
0.050	1054	-1.346	1.843	1.88	1.18	0.510	0.258	0.300	0.162	0.963	0.963
0.075	1086	-1.471	1.845	1.88	1.18	0.520	0.292	0.300	0.158	0.922	0.922
0.10	1032	-1.624	1.847	1.88	1.18	0.531	0.286	0.300	0.170	0.898	0.898
0.15	878	-1.931	1.852	1.88	1.18	0.532	0.280	0.300	0.180	0.890	0.890
0.20	748	-2.188	1.856	1.88	1.18	0.534	0.249	0.300	0.186	0.871	0.871
0.25	654	-2.381	1.861	1.88	1.18	0.534	0.240	0.300	0.191	0.852	0.852
0.30	587	-2.518	1.865	1.88	1.18	0.544	0.215	0.300	0.198	0.831	0.831
0.40	503	-2.657	1.874	1.88	1.18	0.541	0.217	0.300	0.206	0.785	0.785
0.50	457	-2.669	1.883	1.88	1.18	0.550	0.214	0.300	0.208	0.735	0.735
0.75	410	-2.401	1.906	1.88	1.18	0.568	0.227	0.300	0.221	0.628	0.628
1.0	400	-1.955	1.929	1.88	1.18	0.568	0.255	0.300	0.225	0.534	0.534
1.5	400	-1.025	1.974	1.88	1.18	0.564	0.296	0.300	0.222	0.411	0.411
2.0	400	-0.299	2.019	1.88	1.18	0.571	0.296	0.300	0.226	0.331	0.331
3.0	400	0.000	2.110	1.88	1.18	0.558	0.326	0.300	0.229	0.289	0.289
4.0	400	0.000	2.200	1.88	1.18	0.576	0.297	0.300	0.237	0.261	0.261
5.0	400	0.000	2.291	1.88	1.18	0.601	0.359	0.300	0.237	0.200	0.200
7.5	400	0.000	2.517	1.88	1.18	0.628	0.428	0.300	0.271	0.174	0.174
10.0	400	0.000	2.744	1.88	1.18	0.667	0.485	0.300	0.290	0.174	0.174
0 (PGA)	865	-1.186	1.839	1.88	1.18	0.478	0.219	0.300	0.166	1.000	1.000
-1 (PGV)	400	-1.955	1.929	1.88	1.18	0.484	0.203	0.300	0.190	0.691	0.691
-2 (PGD)	400	0.000	2.744	1.88	1.18	0.667	0.485	0.300	0.290	0.174	0.174

### 5.3.2 Ground motion models for Erbaa

The effect of distance on the shape and amplitudes of earthquake response spectra have been evaluated in many studies (e.g. Akkar and Bommer, 2007; Convertito et al., 2008). Mohraz (1992) divided the ground motion records into three sections:

- a. near-field (distance less than 20 km)
- b. mid-field (distance between 20 to 50 km)
- c. far-field (distance greater than 50 km)

It was determined that the amplifications for the near-field are substantially smaller than those for mid- or far-field for periods longer than 0.5 sec in rock sites. On the contrary, the amplifications for the near-field are larger in shorter periods.

The NGA models consider a number of input parameters describing an earthquake scenario and provide estimates of the distribution of expected ground-motion values. A very large range of ground motions can be observed for any earthquake scenario with a particular magnitude, source-to-site distance, and the nature of ground at the site (Campbell and Bozorgnia, 2008).

As mentioned before, the recently proposed Boore and Atkinson (2008) (BA08) and Campbell and Bozorgnia (2008) (CB08) attenuation relationships are used to obtain ground motion models for Erbaa. Both of these newly developed ground motion equations (GMPEs) for average horizontal component ground motions are used to predict the ground motions for the Erbaa scenario event.

The study area is divided into parallel zones with respect to the fault surface rupture as previously indicated in the seismic hazard analysis discussion. The division is performed considering a 2 km distance interval towards the seismic source as seen in Figure 5.2. Subsequently, rock PGA values were calculated by means of two different NGA relationships for different distance zones. The parameters used in the calculations for obtaining target spectra are given in Table 5.13. Moreover, the obtained rock PGA values from BA08 and CB08 NGA relationships for different distance zones are presented in Table 5.14.

Table 5.13. Parameters employed in NGA relationships

Coefficient	Value	Coefficient	Value
$a_1$	0.03 g	M (moment)	7.2
$pga_{low}$	0.06 g	$R_{JB}$ (km)	0 - 2- 4- 6
$a_2$	0.09 g	$M_{ref}$	4.5
$V_1$ (m/s)	180 m/s	$R_{ref}$ (km)	1
$V_2$ (m/s)	300 m/s	$Z_{TOR}$ - Depth to top of coseismic rupture (km)	0
$V_{ref}$ (m/s)	760 m/s	$Z_{2.5}$ - Depth of 2.5 km/s shear wave velocity horizon (km)	2
$V_{s30}$ (m/s) (bedrock)	760 m/s	$\delta$ - Average dip of rupture plane (degrees)	90

Table 5.14. Calculated rock PGA values from NGA relationships for different distance zones in the study area

Distance to surface rupture (km)	PGA (BA08)	PGA (CB08)
0	0.549	0.481
2	0.445	0.457
4	0.361	0.402
6	0.316	0.345

These calculations can also be used to define a target spectrum for the Erbaa scenario event. Additionally, the calculated results are compared and used to scale real earthquake ground motions as will be explained in the subsequent scaling section. The target spectrum graphics of each calculation are compared in each method separately. The graphics based on the Boore and Atkinson (2008) and Campbell and Bozorgnia (2008) attenuation models are depicted in Figures 5.3 and 5.4, respectively.



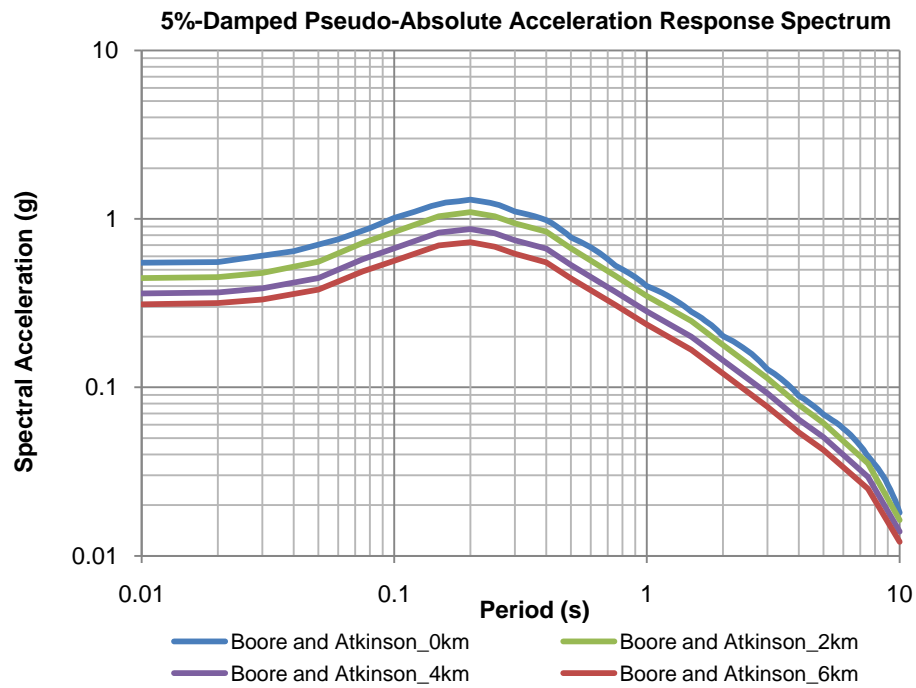


Figure 5.3. Boore and Atkinson (2008) target spectrum model for different distances

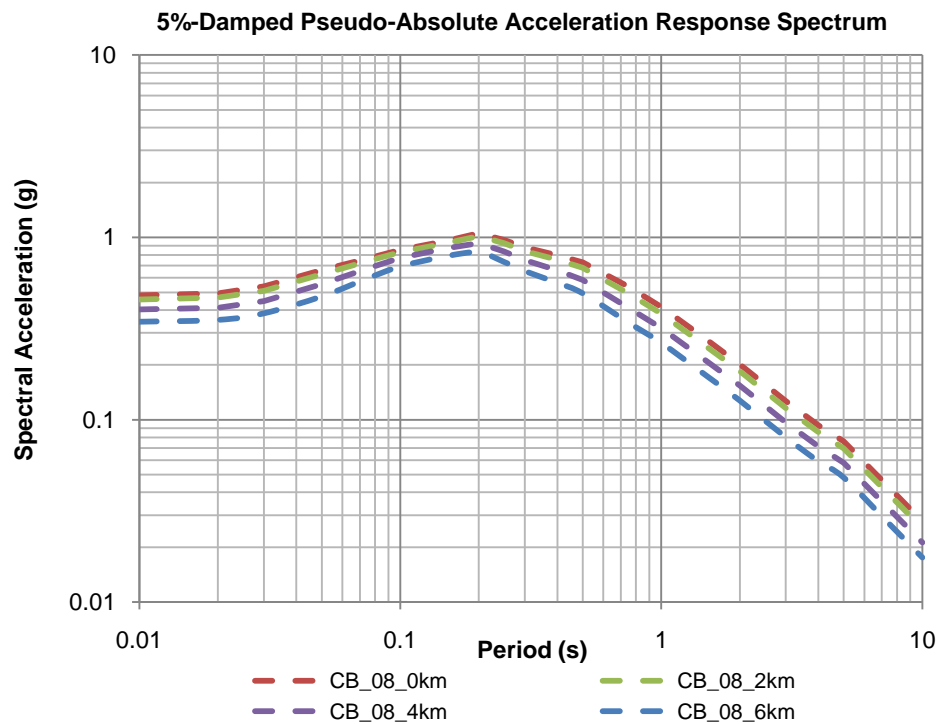


Figure 5.4. Campbell and Bozorgnia (2008) target spectrum model for different distances

The ground motion attenuation relationships and various intensity correlations with PGV, PGA, and Response Spectrum are also evaluated. Acceleration varies with different distances to surface rupture as seen in Figures 5.3 and 5.4. Besides, the same calculations are performed using Boore and Atkinson (2008) model. When compared to Campbell and Bozorgnia (2008), the Boore and Atkinson (2008) relation tends to exhibit higher PGA values for close distances (Figure 5.5).

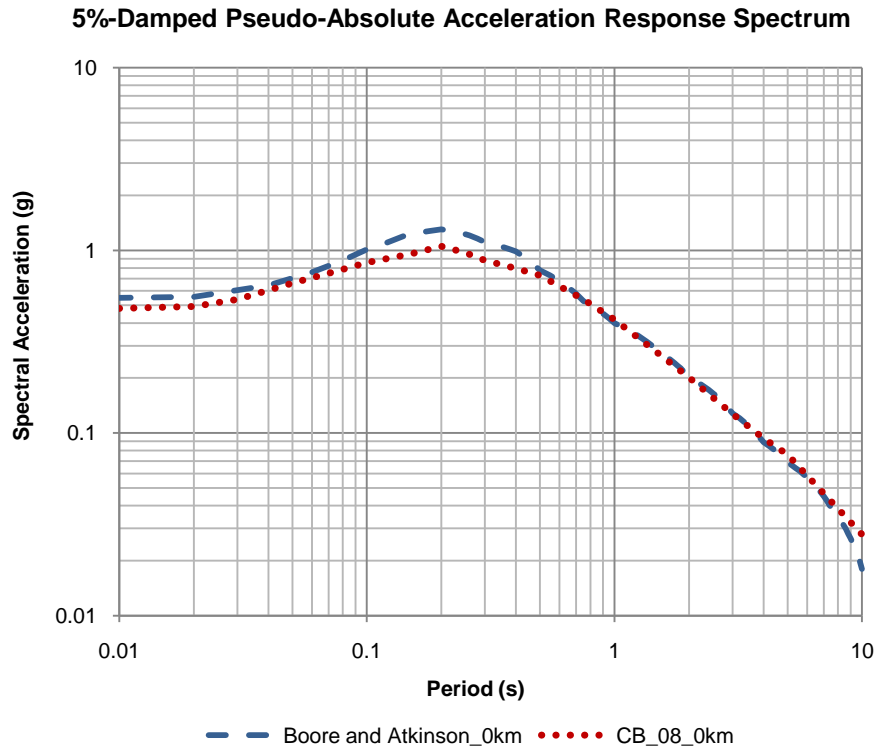


Figure 5.5. Comparison of BA08 and CB08 models for 0 km distance

### 5.3.3 Selection of real earthquake records for Erbaa

A selection criterion for strong ground motion to be used for the analysis of site response is to obtain motions generated with identical conditions to those of the seismic design scenario. The design earthquake is usually defined based on a few parameters. Therefore, it is difficult to determine if the selected records directly match with the characteristics of design earthquake at the source, throughout the path, and on the site surface (Elnashai and Sarno,

2008). The selection process is also related to the objective of collecting strong ground motion records. There are different approaches for selecting earthquakes in the literature (Naeim et al., 2004; Iervolino and Cornell, 2005; Elnashai and Sarno, 2008)

Ground motions during earthquakes have been measured by strong motion instruments since the 1970s. However, there has been no record for the previous strong earthquakes that have occurred in Erbaa to date. Therefore, existing strong ground motion records from similar types of earthquakes are reviewed. Accordingly, the PEER database (PEER Strong Motion Database, 2009) and near fault ground motion databases (Baker, 2007) are examined to obtain earthquake ground motions for the study area.

The PEER Strong Motion Database contains 1557 records of 143 earthquakes from tectonically active regions and it is processed by Dr. Walt Silva of Pacific Engineering using available data from some providers of strong motion data. The PEER NGA Database includes a large set of records, more extensive meta-data, and some corrections about information on this web-site (PEER Strong Motion Database, 2009). Each record in the data files consists of acceleration, velocity, and displacement components. Acceleration, velocity, displacement, and response spectra are presented as separate files in the database.

Baker (2007) proposed a method for quantitatively identifying ground motions containing strong velocity pulses caused by near-fault directivity. This approach uses wavelet analysis to extract the largest velocity pulse from a given ground motion. The extracted pulse is used to provide a quantitative criterion to classify the original ground motion as a “pulse-like” motion. The Baker (2007) approach is beneficial for probabilistic seismic hazard analysis, ground motion prediction (attenuation) models, and nonlinear dynamic analysis of structures. The ground motion library of “The Next Generation Attenuation (NGA) Project” was considered by Baker (2007) and a total of 91 large-velocity pulses were selected from the fault normal components of approximately 3500 strong ground motion recordings. Furthermore, it was also mentioned in the same study that these identified pulses are caused by near-fault directivity effects. For both strike-slip and dip-slip faults, forward directivity typically occurs in the fault normal direction. Accordingly, the results from the fault normal components of ground motions are emphasized by Baker (2007).

Before the elimination of ground motion records from Baker (2007) database, selection criteria were defined considering the earthquake related parameters in the study area (Table 5.15) (Kramer, 2009b).

Table 5.15. Selection criterion of ground motions from Baker (2007) database

<b>Parameter</b>	<b>Criterion</b>
Earthquake	Any
Mechanism	Strike-slip
Magnitude (range)	6.5-7.5
Distance (km)	0-20 km
Site classification	D – 180-360 m/s

A total of 42 suitable strong ground motions were selected based on the criteria mentioned in Table 5.15. After the selection process, these ground motions were compared and scaled with the target spectra from two attenuation models. The selected strong ground motions with acceleration, velocity and distance time history, and response spectra are illustrated in Table 5.16.

Table 5.16. Selected earthquake ground motion records from Baker (2007) database

Assoc. number in this study	Assoc. number by Baker (2007)	Record Sequence Number	EQ ID	EarthquakeName	Year	StationName	CtsID (km)	PGA (g)	PGV (cm/sec)	PGD (cm)
1	1	77	0030	San Fernando	1971	Pacoima Dam (upper left abut)	1.81	1.1644	75.55	18.06
2	2	150	0048	Coyote Lake	1979	Gilroy Array #6	3.11	0.4038	37.67	6.15
3	3	158	0050	Imperial Valley-06	1979	Aeropuerto Mexicali	0.34	0.3438	30.39	7.62
4	4	159	0050	Imperial Valley-06	1979	Agrarias	0.65	0.2903	33.85	9.47
5	5	161	0050	Imperial Valley-06	1979	Bravley Airport	10.42	0.1933	39.86	16.02
6	6	170	0050	Imperial Valley-06	1979	EC County Center FF	7.31	0.2165	50.98	28.04
7	7	171	0050	Imperial Valley-06	1979	EC Meloland Overpass FF	0.07	0.3092	79.79	28.13
8	8	173	0050	Imperial Valley-06	1979	El Centro Array #10	6.17	0.2069	47.07	21.80
9	9	174	0050	Imperial Valley-06	1979	El Centro Array #11	12.45	0.3746	38.41	17.72
10	10	178	0050	Imperial Valley-06	1979	El Centro Array #3	12.85	0.2552	40.84	20.98
11	11	179	0050	Imperial Valley-06	1979	El Centro Array #4	7.05	0.3745	73.86	43.20
12	12	180	0050	Imperial Valley-06	1979	El Centro Array #5	3.95	0.4481	71.18	49.59
13	13	181	0050	Imperial Valley-06	1979	El Centro Array #6	1.35	0.4273	83.49	44.38
14	14	182	0050	Imperial Valley-06	1979	El Centro Array #7	0.56	0.4200	79.15	40.83
15	15	183	0050	Imperial Valley-06	1979	El Centro Array #8	3.86	0.5379	56.80	32.99
16	16	184	0050	Imperial Valley-06	1979	El Centro Differential Array	5.09	0.4310	55.32	33.04
17	17	185	0050	Imperial Valley-06	1979	Holtville Post Office	7.65	0.2476	47.65	29.42
18	18	250	0061	Mammoth Lakes-06	1980	Long Valley Dam (Upr L Abut)		0.6293	35.21	5.50
19	19	292	0068	Irpinia, Italy-01	1980	Stunco	10.84	0.2898	46.86	21.51
20	20	316	0073	Westmorland	1981	Parachute Test Site	16.66	0.2193	36.06	19.66
21	21	407	0080	Coalinga-05	1983	Oil City		0.7241	34.17	3.80
22	22	415	0080	Coalinga-05	1983	Transmitter Hill		0.9482	40.61	5.91
23	23	418	0082	Coalinga-07	1983	Coalinga-14th & Elm (Old CHP)		0.5813	31.45	3.64

Table 5.16. Continued

24	24	451	0090	Morgan Hill	1984	Coyote Lake Dam(SW Abut)	0.53	0.9652	68.35	10.21
25	25	459	0090	Morgan Hill	1984	Gihoy Array #6	9.86	0.2814	23.53	3.85
26	26	503	0100	Taiwan SMARTI(40)	1986	SMARTI C00		0.1997	25.11	5.69
27	27	508	0100	Taiwan SMARTI(40)	1986	SMARTI M07		0.2146	30.00	7.21
28	28	529	0101	N. Palm Springs	1986	North Palm Springs	4.04	0.5903	49.65	8.37
29	29	568	0108	San Salvador	1986	Geotech Investing Center	6.30	0.6493	47.36	12.06
30	32	723	0116	Superstition Hills-02	1987	Parachute Test Site	0.95	0.4509	77.19	37.19
31	33	738	0118	Loma Prieta	1989	Alameda Naval Air Stn Hanger	71.00	0.2435	33.42	9.86
32	34	766	0118	Loma Prieta	1989	Gihoy Array #2	11.07	0.3529	35.10	8.54
33	35	783	0118	Loma Prieta	1989	Oakland-Outer Harbor Wharf	74.26	0.2804	41.86	9.60
34	36	802	0118	Loma Prieta	1989	Saratoga - Aloha Ave	8.50	0.3821	48.52	20.25
35	37	821	0121	Erzincan, Turkey	1992	Erzincan	4.38	0.4886	72.95	24.79
36	38	828	0123	Cape Mendocino	1992	Petrolia	8.18	0.6236	69.21	25.72
37	39	838	0125	Landers	1992	Barstow	34.86	0.1193	21.58	16.95
38	40	879	0125	Landers	1992	Lucerne	2.19	0.7214	111.05	188.32
39	41	900	0125	Landers	1992	Yermo Fire Station	23.62	0.2234	36.89	28.58
40	53	1119	0129	Kobe, Japan	1995	Takanazuka	0.27	0.7069	75.88	23.13
41	54	1120	0129	Kobe, Japan	1995	Takatori	1.47	0.6528	117.14	33.06
42	55	1161	0136	Kocaeli, Turkey	1999	Gebze	10.92	0.1833	38.30	33.69

#### **5.3.4 Spectral matching (scaling) of ground motions**

Seismic design codes generally classify ground shaking in terms of a response spectrum and allow using response spectrum compatible time history records in linear and nonlinear time history analyses. These records can be obtained from natural earthquake records or synthetic/artificial records. Although the use of natural earthquake records has many advantages, there could be insufficient records to fulfill seismological and geological conditions consistent with those of the scenario earthquake. Synthetic records can be generated in the time or frequency domains by means of well-matched response spectra to target design response spectra. Matching techniques can be preferably applied to match a target design spectrum by scaling the selected time history in time domain or elementary wavelets added or subtracted from the real time history (Gasparini and Vanmarcke, 1976; Silva and Lee, 1987; Carballo and Cornell, 2000; Hancock et al. (2006); Fahjan and Ozdemir, 2008; Kramer, 2009a).

All existing approaches for the processes of selecting earthquake ground motions and their scaling to match with the design spectrum are separate and dissimilar. Initially, one or more time histories are selected. Then, proper scaling techniques for spectrum matching are applied as expressed in Naeim et al. (2004).

There are two common approaches to scale ground motions for consistency with a target spectrum (Kramer, 2009a):

1. Simulation-using single spectrum with compatible ground motion: There are two common approaches in this approach; Time domain (wavelets) and Frequency domain (Fourier analysis).
2. Scaling- suite of motions with matching ensemble average: Actual recorded motions can be identified and scaled so that their average is consistent with a target spectrum over some desired range of periods.

The required information for proper scaling techniques should include both target spectrum and the essential fundamental period of structure for these approaches. The motions should be chosen for scaling methods to obtain mean/median response or to indicate the variability of response.

Fahjan and Ozdemir (2008) classified the spectral matching methods into three main topics:

- a. Ground motion scaling in time domain
- b. Spectral matching in frequency domain
- c. Spectral matching in time domain

**a. Ground motion scaling in time domain:**

In this approach, the recorded motions is scaled up or down by a constant scaling factor equivalently to produce the best match with the target spectrum over the period range of interest. The procedure aims to minimize the difference between the scaled motion's response spectrum and target spectrum (Figure 5.6). The proposed methodology based on the difference concept was evaluated by the integral (Nikolau, 1998). It was defined in Equation 5.28 (Fahjan and Ozdemir, 2008).

$$\text{Difference} = \int_{T_A}^{T_B} [\alpha S_a^{\text{actual}}(T) - S_a^{\text{target}}(T)]^2 dT \quad (5.28)$$

$S_a^{\text{actual}}$  : acceleration spectrum of the given time history  
 $S_a^{\text{target}}$  : target acceleration response spectrum  
 $\alpha$  : scaling factor  
 $T$  : period of oscillator  
 $T_A$  : lower period of scaling  
 $T_B$  : upper period of scaling

In order to minimize the difference, the first derivative of difference function with respect to the scaling factor has to be zero.

A separate form of scaling factor is given in Equation 5.29.

$$\min \text{Difference} \quad \frac{d(\text{Difference})}{d\alpha} = 0 \quad \alpha = \frac{\sum_{T=T_A}^{T_B} (S_a^{\text{actual}}(T) - S_a^{\text{target}}(T))}{\sum_{T=T_A}^{T_B} (S_a^{\text{actual}}(T))^2} \quad (5.29)$$



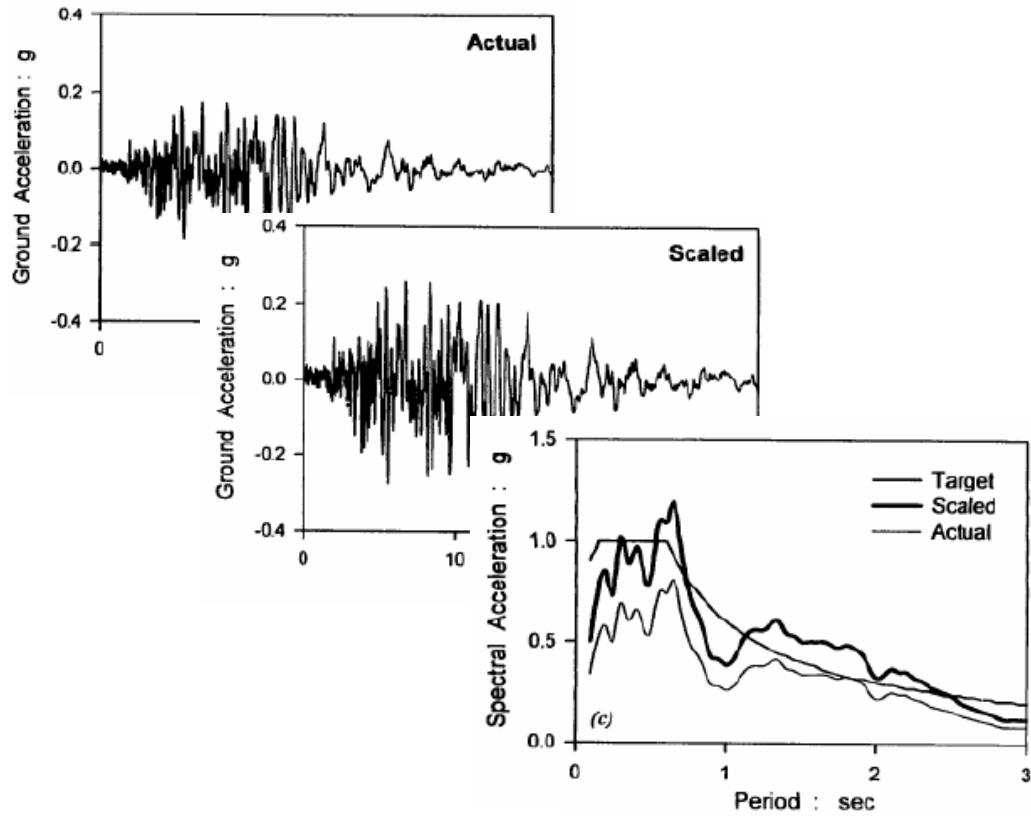


Figure 5.6. Ground motion scaling in time domain (Nikolaou, 1998)

#### **b. Spectral matching in frequency domain:**

An actual record is used to match a target (design) spectrum in this methodology. The actual motion is filtered in frequency domain by its spectral ratio with the target spectrum. Fourier spectral amplitudes of an input motion are modified while the Fourier phases remain unchanged during the entire procedure. This technique is repeated until the desired matching is achieved for a definite range of periods. Succeeded iterations result in enhanced compatibility with the target spectrum (Ozdemir and Fahjan, 2007; Fahjan and Ozdemir, 2008).

#### **c. Spectral matching in time domain:**

The last approach for spectral matching is adjusting the original record in time domain to reach specified target acceleration response spectrum by inserting wavelets depending on the period ranges and limited durations of input time history. The resulting records have an

elastic response spectrum that is consistent (within a desired tolerance) with the target spectrum. RSPMATCH software developed by Abrahamson (1992) is widely used to create spectrum-compatible ground motions that are more realistic than conventional methods that operate in the frequency domain.

### **5.3.5 Scaling and prediction of ground motion for Erbaa**

In this study, the spectral matching method named as “Ground motion scaling in time domain” by Fahjan and Ozdemir (2008) was used to obtain proper ground motions. A total of 42 selected motions were scaled up and down by a constant scaling factor to maximize consistency with each target spectrum (for different distances). One of the scaling graphics is presented in Figure 5.7 as an example for BA08-0 km distance to the seismic source.

During scaling application, the spectral acceleration values are adjusted to make the spectral accelerations equal to the proposed target spectrum at the same periods using Equation 5.28.  $T_A$  and  $T_B$  values, which are the lower and upper boundaries of periods, could not be specified as a constant during comparison and calculation. In other words, instead of considering certain  $T_A$  and  $T_B$  boundaries, the minimum error concept is implemented in Equation 5.28. Therefore, the considered minimum error for each motion is the total least squares error between the individual scaled spectra and the target spectrum. The scaling factor resulting in the lowest error was chosen for each ground motion (Kramer, 2009b).

The scaling factors used to fit the 42 motions varied between 0.81 and 1.02. Therefore, a total of seven earthquake records with a scaling factor around 1.00 out of 42 motions are found to be suitable for the study area (Table 5.17). The time histories of the seven original earthquake records are given in Figures 5.8 - 5.14. Furthermore, two target spectra obtained from BA08 and CB08 NGA models are evaluated separately. Although there are 8 target spectra in total, three different distance zones (0, 2, 4 km) are considered as seen in Table 5.14. It should be noted that the fourth distance zone (6 km) is not considered since it is out of the study boundary.

Moreover, the scaled motions of the seven records with the target spectrum which obtained from BA-08 NGA model with 0 km zone are depicted in Figure 5.15. It should be noted that the properties of the ground motions shown from Figures 5.8 to 5.15 are listed in Table 5.18 according to their ground motion number.

Table 5.17. Selected earthquake records with minimum scaling factors from Baker (2007) database

Associated number in this study	Associated number by Baker (2007)	Record Sequence Number	Earthquake Name	Year	Magnitude	ClstD (km)	PGA (g)	PGV (cm/sec)	PGD (cm)	Tp (s)	Scaling factor					
											Boore and Atkinson (2008)			Campbell and Bozorgnia (2008)		
											0 km	2 km	4 km	0 km	2 km	4 km
9	9	174	Imperial Valley-06	1979	6.5	12.45	0.37	38.41	17.72	7.40	0.84	0.88	0.88	0.87	0.86	0.82
10	10	178	Imperial Valley-06	1979	6.5	12.85	0.26	40.84	20.98	5.20	0.84	0.89	0.92	0.84	0.84	0.84
16	16	184	Imperial Valley-06	1979	6.5	5.09	0.43	55.32	33.04	5.90	0.88	0.86	0.88	0.84	0.91	0.87
19	19	292	Irpinia, Italy-01	1980	6.9	10.84	0.29	46.86	21.51	3.10	1.02	0.95	0.99	0.88	0.94	0.95
34	36	802	Loma Prieta	1989	6.9	8.50	0.38	48.52	20.25	4.50	0.94	0.96	0.97	0.88	0.92	0.87
40	53	1119	Kobe, Japan	1995	6.9	0.27	0.71	75.88	23.13	1.40	0.89	0.93	0.82	0.83	0.86	0.96
42	55	1161	Kocaeli, Turkey	1999	7.5	10.92	0.18	38.30	33.69	5.90	0.84	0.90	0.83	0.82	0.85	0.81

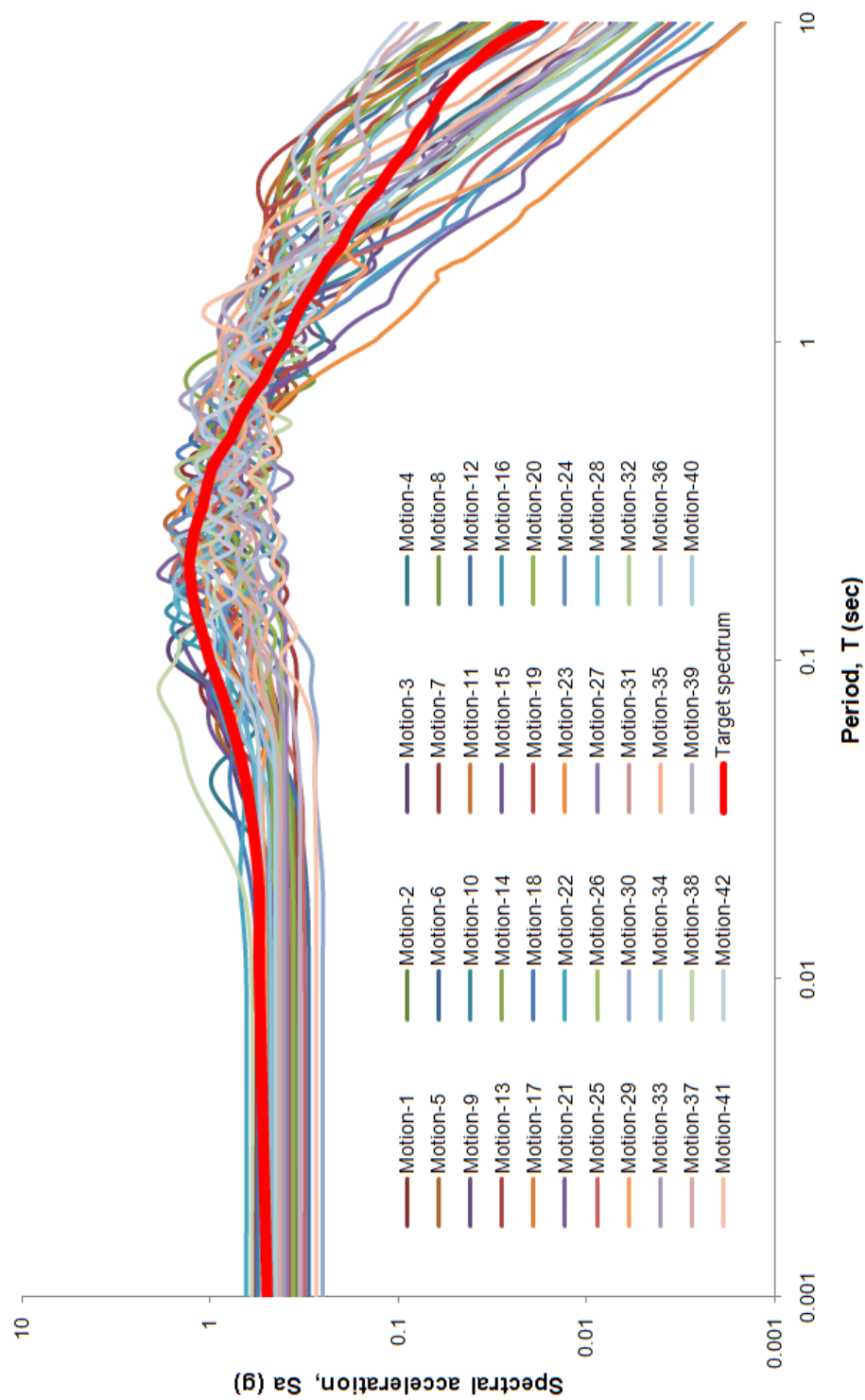


Figure 5.7. Example of scaling of 42 motions with a target spectrum

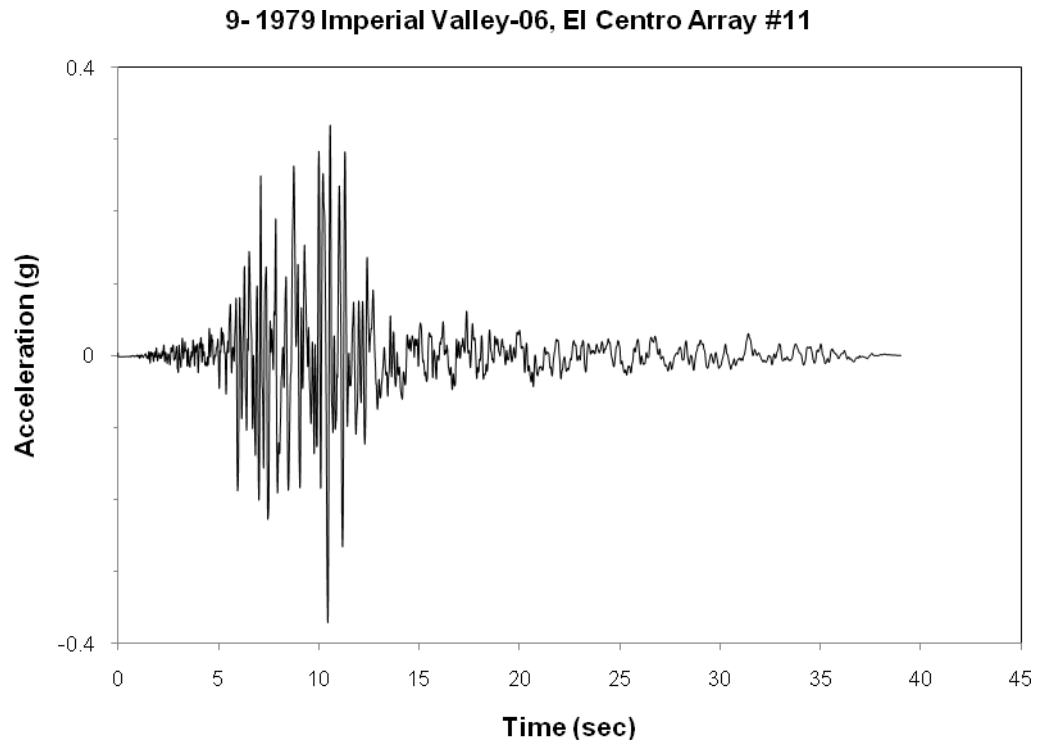


Figure 5.8. Time history of ground motion 9

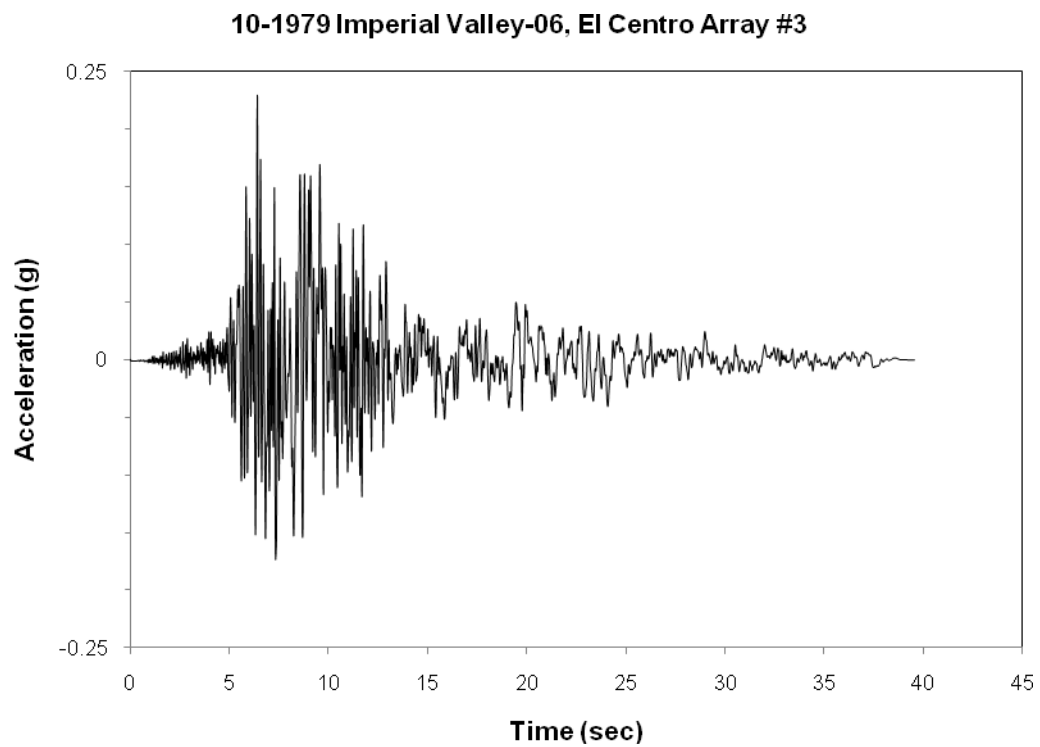


Figure 5.9. Time history of ground motion 10

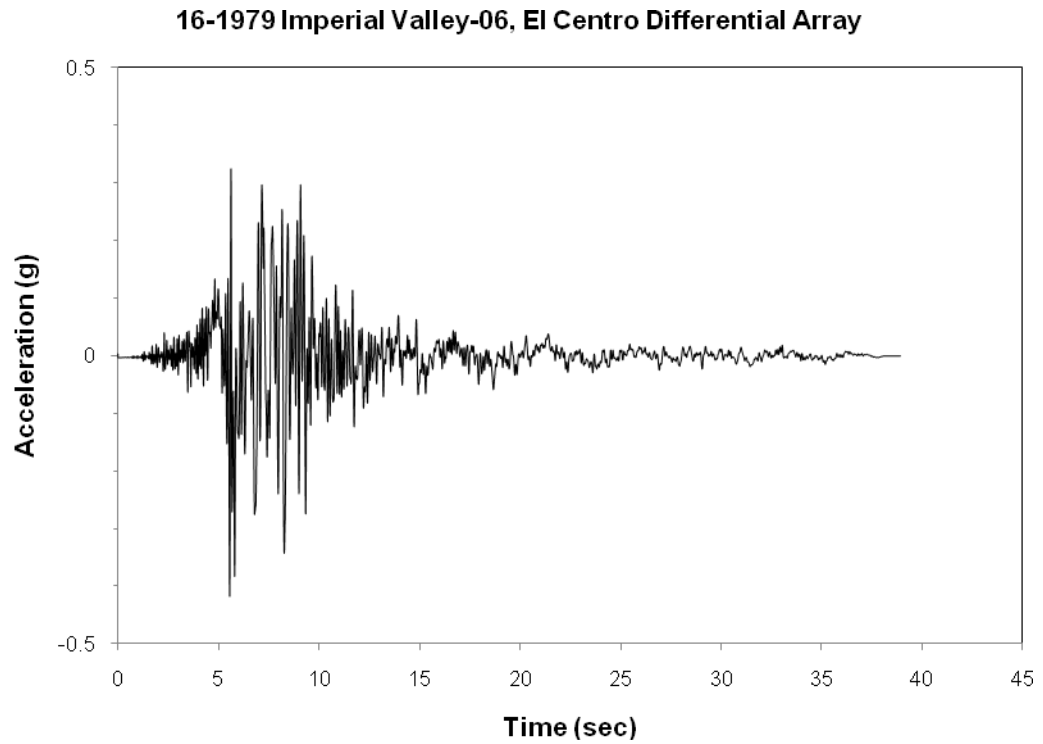


Figure 5.10. Time history of ground motion 16

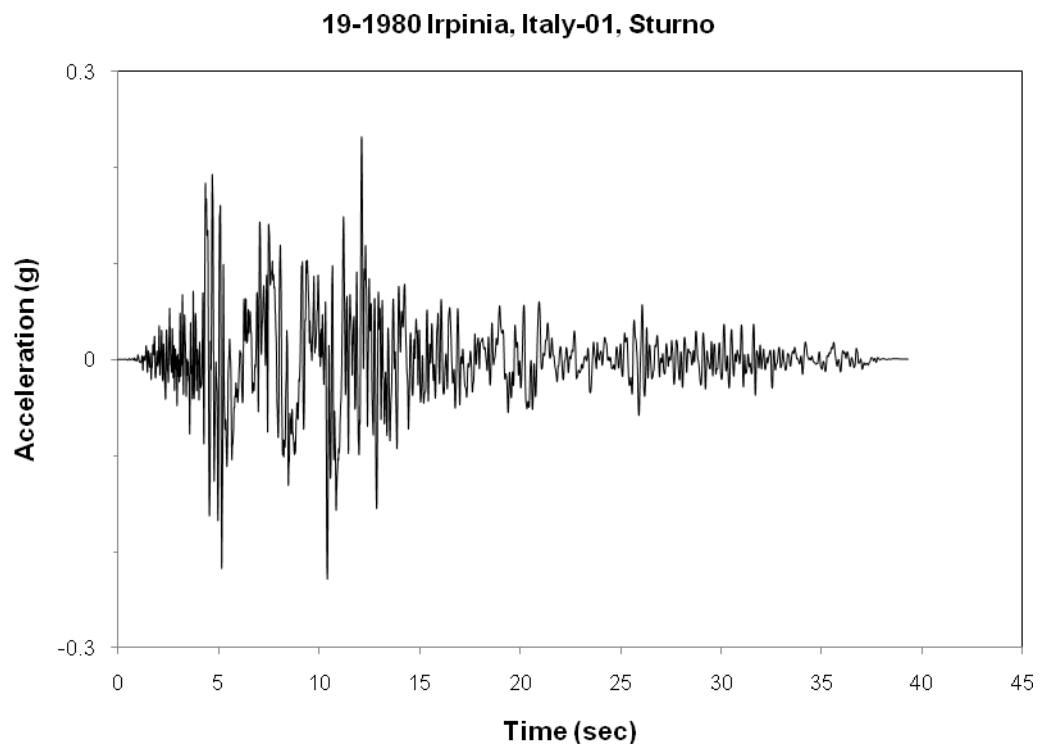


Figure 5.11. Time history of ground motion 19

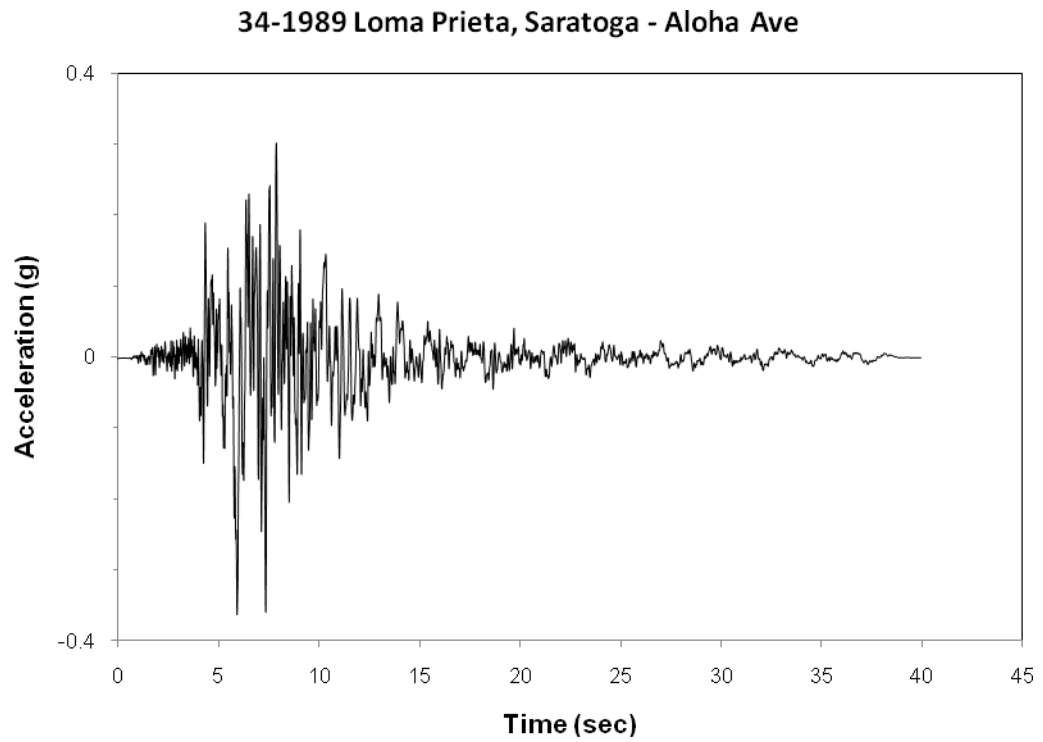


Figure 5.12. Time history of ground motion 34

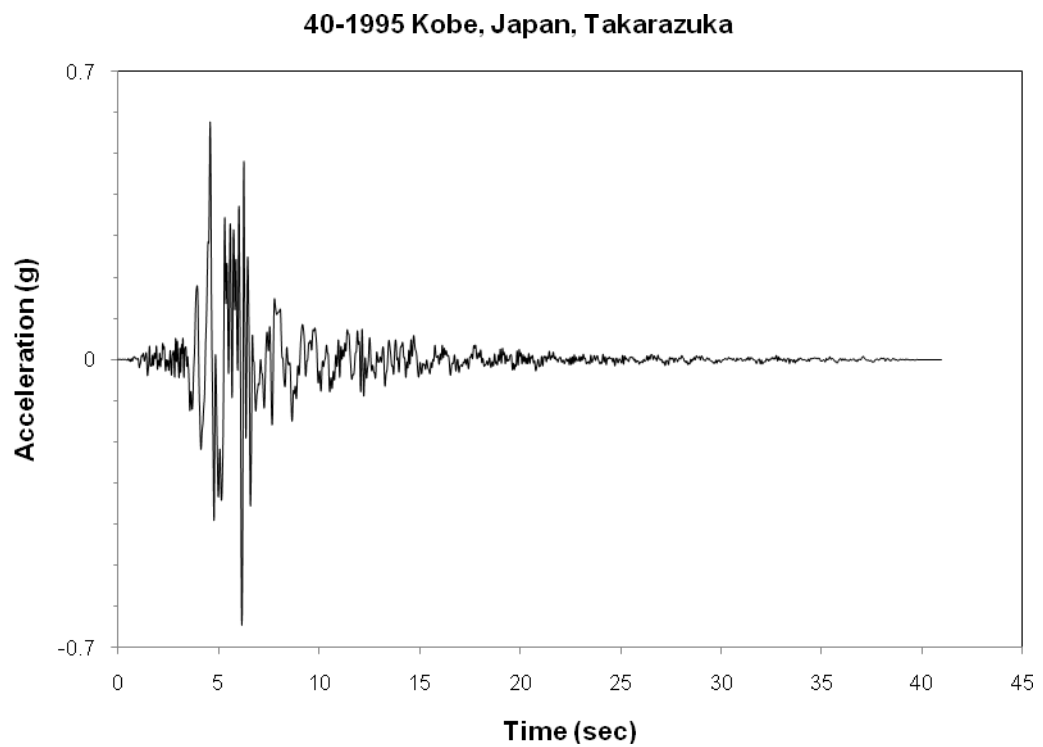


Figure 5.13. Time history of ground motion 40

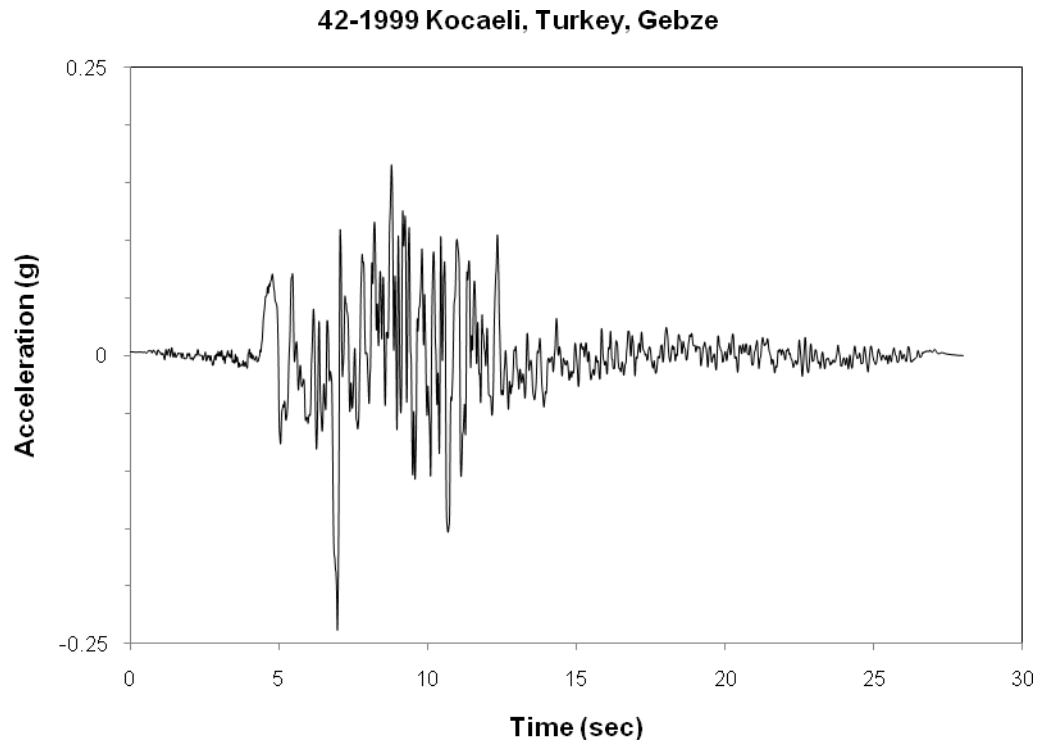


Figure 5.14. Time history of ground motion 42

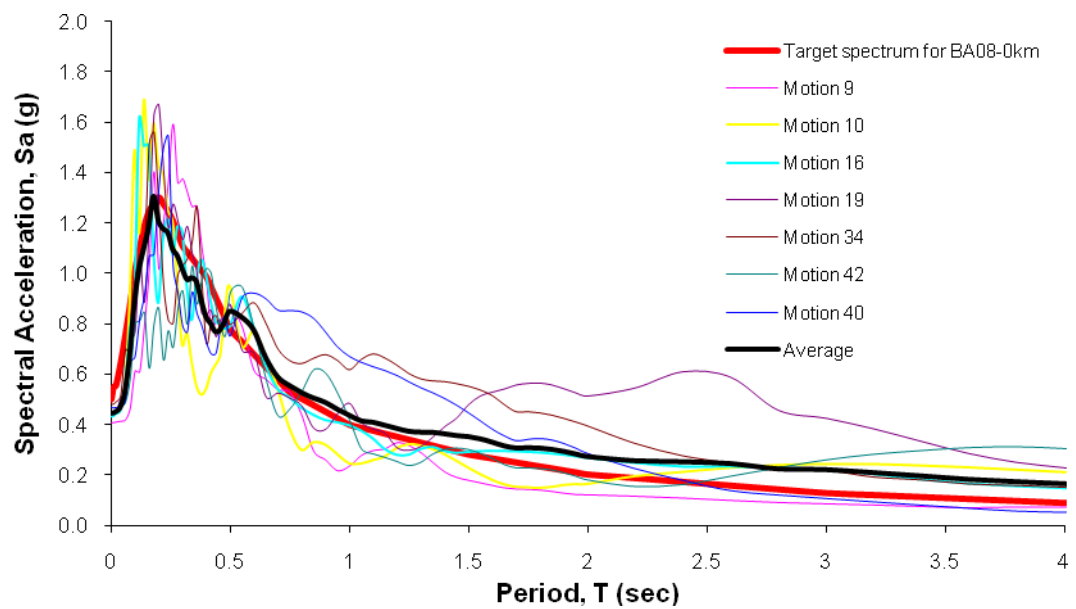


Figure 5.15. Scaled ground motions with target spectrum (for BA-08 with 0 km zone) and the average ground motion



After scaling process, the peak ground acceleration values are determined for site response analyses. The PGA values for the above mentioned ground motions determined from two different NGA relationships are shown in Table 5.18 regarding to the source distance.

Table 5.18. Distance dependent PGA values for different earthquake ground motions

Ground Motion No	Peak Ground Acceleration					
	Boore and Atkinson (2008)			Campbell and Bozorgnia (2008)		
	0 km	2 km	4 km	0 km	2 km	4 km
9	0.4076	0.3486	0.2754	0.3519	0.3297	0.2892
10	0.4522	0.3754	0.3016	0.3774	0.3543	0.3208
16	0.4332	0.3713	0.2911	0.3434	0.3493	0.3023
19	0.4464	0.3799	0.2984	0.3713	0.3508	0.3145
34	0.4827	0.4003	0.3201	0.4021	0.3836	0.3379
40	0.4669	0.4007	0.3133	0.4000	0.3973	0.3296
42	0.4505	0.4587	0.3556	0.4430	0.4242	0.3811

Consequently, the entire time history of the selected ground motions is scaled using the peak ground acceleration values given in Table 5.18 within the framework of site response analyses.

#### 5.4 Concluding Remarks

The essential seismic hazard analyses are performed for Erbaa in this study since such types of analyses were not conducted in previous projects. Seismic hazards are evaluated using a deterministic seismic hazard analysis that considered different earthquake scenarios. Peak Ground Acceleration (PGA) and response acceleration (spectral acceleration, PSA) are determined to obtain proper ground motion scenarios for Erbaa. The newly updated NGA attenuation relationships are used to obtain target spectra for the study area. A suite of ground motions is identified and scaled to be consistent with target response spectrum. The obtained motions are proposed to be used in further site response analyses.

## CHAPTER 6

### DYNAMIC SOIL PROPERTIES, SITE RESPONSE, AND AMPLIFICATION

#### 6.1 Introduction

Dynamic soil properties play a crucial role in site response analyses. Soil materials are mostly represented by different material characteristics in site response models. The behavior of soils under cyclic loading can be explained by dynamic soil properties. Site response and ground failure are mostly affected by the behavior of soils under cyclic loading conditions. Site response controlling by wave propagation is influenced by the stiffness and damping properties of soils. Besides, the shear strength of soil is also an additional parameter controlling ground failure (Kramer, 1996; Kramer and Stewart, 2004). Shear wave velocity ( $V_s$ ), dynamic shear modulus ( $G$ ), damping ratio and their variations with shear strain are regarded as the dynamic stress-strain properties of soils (Dobry and Vucetic, 1987). The variation of stiffness with strain can be defined by modulus reduction ( $G/G_{\max}$ ) and damping ( $\xi$ ) curves. These stiffness and damping characteristics of soil are preferably used in the evaluation stage of earthquake related problems (Kramer, 1996).

Site response analysis is applied to determine the effect of soil conditions during earthquake and to estimate ground response spectra for the design purposes. The response of a soil deposit depends on the ground motion characteristics and the geometry and material properties of soils above bedrock (Sitharam and Anbazhagan, 2007).

Site amplification is one of the most important cases that may occur due to soil conditions and seismic energy. It is a type of site response effect and occurs during the travelling of seismic waves from bedrock to the surface (Stewart et al., 2003).

The dynamic soil properties of the study area including maximum shear modulus, damping ratio and shear wave velocity are summarized in this section. The essential parameters used in site/ground response analyses are firstly determined. Then, the measured and empirically

calculated results are compared. Furthermore, the one-dimensional equivalent site response model of the study area is evaluated. Additionally, amplification values determined from the created model are also presented in this section.

## 6.2 Dynamic Soil Properties

Shear wave velocity ( $V_s$ ) is an important parameter for the design of geotechnical works in seismically active areas. The  $V_s$  value commonly reflects geological setting and engineering properties regarding the stiffness and density of soil layers. It is also an important parameter for design and site response purposes. The  $V_s$  is commonly employed in the evaluation of foundation stiffness, earthquake site response, liquefaction potential, soil density, site classification, soil stratigraphy and foundation settlement (Richart et al., 1970; Schnabel et al., 1972; Sykora and Stokoe, 1983; Burland, 1989; Sasitharan et al., 1994; Shibuya et al., 1995; Kramer, 1996; Andrus and Stokoe, 1997; Wills and Silva, 1998; Mayne et al., 1999; Dobry et al., 2000; Lehane and Fahey, 2002; Seed et al., 2003; Stewart et al., 2003; McGillivray and Mayne, 2004; Holzer et al., 2005).

Shear wave velocity (or shear modulus at low strain levels) is one of the most important dynamic soil parameters to be used in the analysis of earthquake engineering problems. At different strain levels, the stiffness and damping characteristics of a soil can be described by different types of material models. Propagation of seismic waves causes elastic behavior at small strain levels which can lead to permanent deformations, and cyclically induced inelastic behavior, at high strain levels (Brandes, 2003). Therefore, it is essential to use different techniques or empirical approaches including laboratory and field tests to obtain the dynamic properties of soils (Kramer, 1996; Towhata, 2008). A number of different techniques for the determination of dynamic soil properties are summarized in Table 6.1.

Shear modulus ( $G$ ), damping ratio ( $D_s$ ) and shear wave velocity ( $V_s$ ) are important and commonly used dynamic soil properties in site response analyses. The main characteristic of high strain level can be represented by nonlinear inelastic behavior which takes the form of reduced stiffness and increased damping. In the presence of initial (static) shear stresses, nonlinear, inelastic behavior can lead to the development of permanent deformations. The low strain level properties include stiffness, damping, Poisson's ratio and density (Kramer, 1996). It is also broadly accepted that the shear modulus and damping ratio of soils are functions of amplitude of shear strain under cyclic loading. In addition, modulus reduction

and damping curves of local soils are fundamental inputs to perform ground response analysis using equivalent linear technique (Hanumantharao and Ramana, 2008).

Table 6.1. Different techniques for the determination of dynamic soil properties (after Brandes, 2003)

Conditions	Test	Parameters
Field-low strain	Seismic reflection	$V_p$ , thickness of major soil units
	Seismic refraction	$V_s$ , $V_p$ , thickness of major soil units
	Suspension logging	$V_s$ , $V_p$
	Spectral analysis of surface waves (SASW)	$V_R$ , wave length, $V_s$
	Seismic crosshole test	$V_s$ , $V_p$ , damping ratio
	Seismic downhole or uphole test	$V_s$ , $V_p$ , thickness of major soil units
	Refraction microtremor - REMI	
	Bottom shear modulus profiler	$V_s$ , $V_p$
Field-high strain	Standard penetration test (SPT)	Density, stiffness, strength
	Cone penetration test (CPT)	Density, stiffness, strength, soil type, pore pressure
	Dilatometer test	Stiffness
	Seismic cone penetrometer	
Lab-low strain	Resonant column	Stress-strain, strength
	Piezoelectric bender element test and shear plates	$V_s$
	Ultrasonic pulse test	
Lab-high strain	Cyclic triaxial test	Stress-strain, strength, pore pressure
	Cyclic direct simple shear test	Stress-strain, strength, pore pressure
	Cyclic torsional shear test	Stress-strain, strength, pore pressure
	Shaking table tests	Forces and displacements, pore pressure
	Centrifuge tests	Forces and displacements, pore pressure

Note:  $V_s$ = shear wave velocity,  $V_p$ = compressional wave velocity,  $V_R$ = Rayleigh wave phase velocity.

Maximum shear modulus ( $G_{max}$ ) can be computed from shear wave velocity ( $V_s$ ) using the expression:

$$G_{max} = \rho \times V_s^2 \quad (6.1)$$

where  $\rho$  is the mass density of the soil and  $V_s$  is shear wave velocity.

The measured shear wave velocity is generally considered as the most reliable parameter to obtain  $G_{max}$  for a soil deposit (Kramer, 1996). The  $G_{max}$  is commonly used for advanced soil modeling and the dynamic response of soil-structure interactions. When  $V_s$  measurements are not available, the dynamic shear modulus can be estimated from correlations to the

standard penetration test, plasticity index, and grain size distributions (Vucetic and Dobry, 1991; Idriss et al., 1980; Kramer, 1996). In addition, maximum shear modulus ( $G_{\max}$ ) can be calculated by different empirical formulas as shown in the following equations (Kramer, 1996).

a) From available laboratory test data:

$$G_{\max} = 625 F(e) (\text{OCR})^k P_a^{1-n} (\sigma'_m)^n \quad (6.2)$$

$F(e)$  : function of void ratio

OCR : overconsolidation ratio

$k$  : an overconsolidation ratio exponent based on plasticity index

$\sigma'_m$  : the mean principal effective stress

$P_a$  : the atmospheric pressure

The overconsolidation ratio exponent ( $k$ ) can be determined from Table 6.2 based upon the plasticity index of soil layer.

Table 6.2. Overconsolidation ratio exponent ( $k$ ) (after Hardin and Drnevich, 1972)

Plasticity index	$k$
0	0.00
20	0.18
40	0.30
60	0.41
80	0.48
$\geq 100$	0.50

b) From different formulas for specific soil types (such as sands):

$$G_{\max} = 1000 K_{2,\max} (\sigma'_m)^{0.5} \quad (6.3)$$

$K_{2,\max}$ : determined from the void ratio or relative density

$\sigma'_m$  : the mean principal effective stress

c) Table 6.3 can be used for fine-grained soils (e.g. clays) (based on OCR and Plasticity index):

Table 6.3.  $G_{\max}/s_u$  value based on OCR and plasticity index (after Weiler, 1988)

Plasticity index	Overconsolidation Ratio, OCR		
	1	2	3
15-20	1100	900	600
20-25	700	600	500
35-45	450	380	300

The maximum shear modulus ( $G_{\max}$ ) can also be determined from in-situ tests (Kramer, 1996). The results of SPT (Standard Penetration Test), CPT (Cone Penetration Test), DMT (Dilatometer Test), and PMT (Pessuremeter Test) can also be employed to obtain shear wave velocity or shear modulus values. For instance, a widely used empirical formula for estimating  $G_{\max}$  from  $N_{1,60}$  blow count is given in Equation 6.4 (Ohta and Goto, 1976; Seed et al., 1986).

$$G_{\max} = 20000 (N_1)_{60}^{0.333} (\sigma'_m)^{0.5} \quad (6.4)$$

$G_{\max}$  and  $\sigma'_m$  : in lb/ft<sup>2</sup>

Soils show nonlinear, inelastic stress-strain behavior under cyclic loading conditions. The stiffness of a soil is highest and the damping is lowest at low strain levels. The impacts of nonlinearity and inelastic behavior increase at higher strain levels. Accordingly, a stress-strain model classification was made for geotechnical earthquake engineering analyses. Therefore, the stress-strain models were classified into three main topics: equivalent linear models, cyclic nonlinear models and advanced constitutive models (Kramer, 1996).

In the equivalent linear model, a soil behaves like a linear visco-elastic material and the nonlinearity of the soil is characterized by strain-dependent shear modulus values to represent stiffness and by damping ratio values to represent damping behavior. Nonlinear models reflect the nonlinear, inelastic behavior of a soil using a backbone curve and rules that govern loading-unloading behavior. Advanced constitutive models consider the basic principles of mechanics to describe soil behavior for different stress-strain conditions.

Maximum shear modulus and shear modulus evaluated by modulus reduction ( $G/G_{\max}$ ) curves can be affected by soil plasticity and effective confining pressure. Modulus reduction curves have been studied by several researchers in the literature (Dobry and Vucetic, 1987;

Vucetic and Dobry, 1989; Sun et al., 1988; Darendeli, 2001). In general, the shape of modulus reduction and damping curves depend mostly on the plasticity of the fine-grained soils. However, the modulus reduction curves can be prepared for both coarse and fine-grained soils separately as introduced by the abovementioned researchers.

Damping ratio ( $D$ ) is an important parameter in site response analyses. The damping ratio vs. shear strain relationships for different type of soils are described in the literature (Seed et al., 1984; Sun et al., 1988; Luna and Jadi, 2000). The damping ratio describes the dissipation of hysteretic energy by the soil (Kramer, 1996; Luna and Jadi, 2000). The plasticity index has a significant influence on damping ratio (Vucetic and Dobry, 1991). Highly plastic soils have lower damping ratios at the same cyclic strain amplitude. The damping ratio can be affected by effective confining pressure, void ratio, geologic age, and cyclic strain (Dobry and Vucetic, 1987; Kramer, 1996; Darendeli, 2001) (Table 6.4).

The modulus reduction ( $G/G_{\max}$ ) curve describes the manner in which the shear modulus varies with shear strain amplitude. The shape of modulus reduction curve indicates how nonlinear the material is. A linear material would have a horizontal modulus reduction curve, i.e., the modulus reduction factor would be 1.0 at all strains. The plasticity index has also a considerable influence on modulus reduction curves (Vucetic and Dobry, 1991). In general, soil nonlinearity increases with decreasing plasticity index. A number of investigators studied the modulus reduction behavior of different soils and proposed standard modulus reduction curves for those soils (e.g. Dobry and Vucetic, 1987; Darendeli, 2001). The modulus reduction curve can also be affected by effective confining pressure, void ratio, geologic age, and cyclic strain may cause as given in Table 6.4 (Dobry and Vucetic, 1987; Kramer, 1996; Darendeli, 2001).

Various modulus reduction and material damping curves are presented in Figures 6.1 and 6.6 with the essential formulas. The Hardin and Drnevich (1972) relationship was mostly used as a simple hyperbolic law which can be described as the stress-strain curves for small strains. According to hyperbolic relation introduced by Hardin and Drnevich (1972), the equations can be estimated from curves shown in Figure 6.1.

Table 6.4. Effect of various factors on  $G/G_{\max}$  and  $D$  of normally consolidated and moderately overconsolidated clays (Dobry and Vucetic, 1987)

Increasing factor	$G_{\max}$	$G/G_{\max}$	Damping ratio
Confining pressure, $\sigma$	Increases with $\sigma$	Stays constant or increases with $\sigma$	Stays constant or decreases with $\sigma$
Void ratio, $e$	Decreases with $e$	Increases with $e$	Decreases with $e$
Geological age, $t_g$	Increases with $t$	May increase with $t_g$	Decreases with $t_g$
Cementation, $c$	Increases with $c$	May increase with $c$	May decrease with $c$
Overconsolidation, OCR	Increases with OCR	Not affected	Not affected
Plasticity index, PI	Increases with PI if OCR>1; stays about constant if OCR=1	Increases with PI	Decreases with PI
Cyclic strain, $\gamma_c$		Decreases with $\gamma_c$	Increases with $\gamma_c$
Strain rate, $\gamma$	Increases with $\gamma'$	$G$ increases with $\gamma'$ but $G/G_{\max}$ probably not affected if $G$ and $G_{\max}$ are measured at same $\gamma\dot{\epsilon}$	Stays constant or may increase with $\gamma\dot{\epsilon}$
Number of loading cycles, $N$	Decreases after $N$ cycles of large $\gamma_c$ but recovers later with time	Decreases after $N$ cycles of large $\gamma_c$ but recovers later with time	Not significant for moderate $\gamma_c$ and $N$

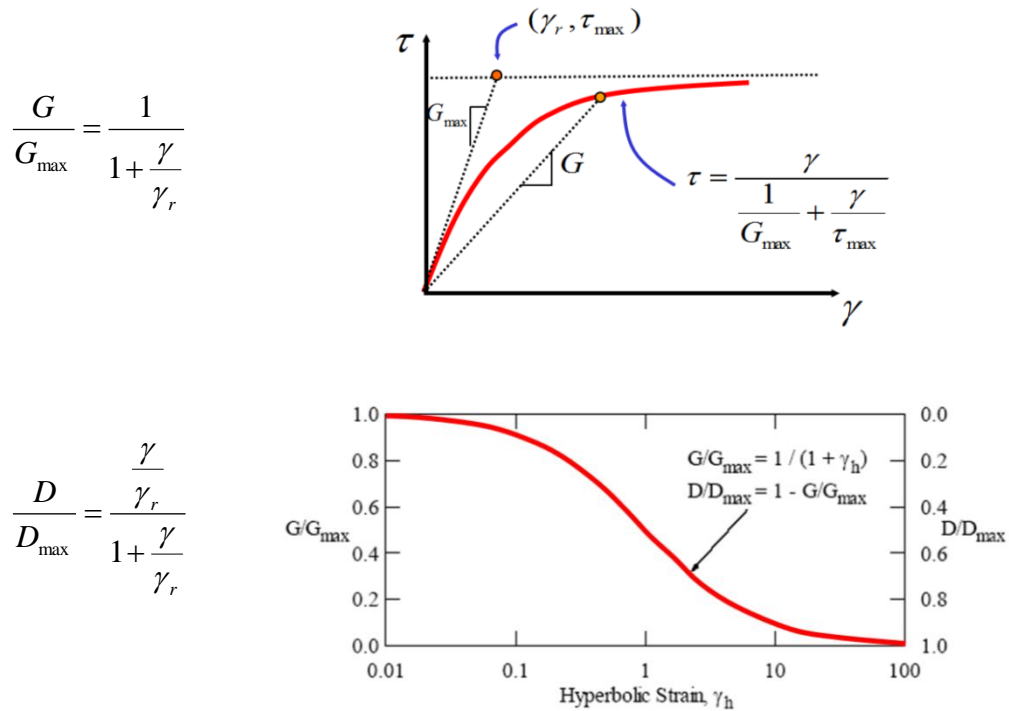


Figure 6.1. Modulus reduction and damping curves based on the hyperbolic relation of Hardin and Drnevich (1972)



Furthermore, material behaviors obtained by experimental curves of Idriss (1990) for shear modulus and damping ratio versus shear strain are depicted in Figure 6.2. Vucetic and Dobry (1991) mentioned that the cyclic shear parameters depend on the plasticity index (PI). The curves were proposed to show the effects of PI on  $G/G_{\max}$  versus cyclic shear strain  $\gamma_c$ , and on the material damping ratio  $D$  versus  $\gamma_c$  (Figure 6.3). It was concluded that PI is the main factor controlling modulus reduction and damping for various soils. The Vucetic-Dobry model describes modulus reduction (and damping) behavior as a function of plasticity index as seen in Figure 6.3.

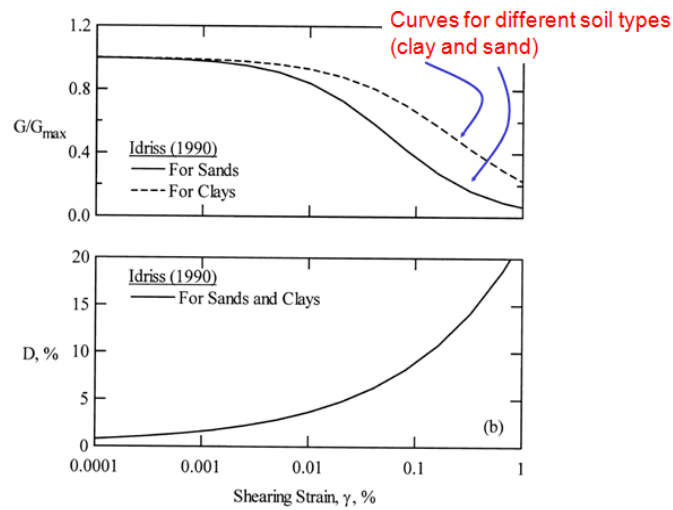


Figure 6.2. Modulus reduction and damping curves based on the experimental study of Idriss (1990)

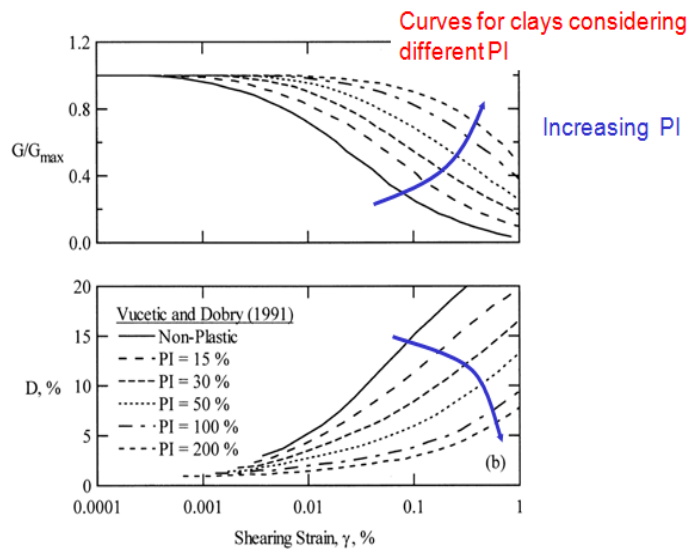


Figure 6.3. Empirical curves for modulus reduction and damping (Vucetic and Dobry, 1991)

Table 6.5. Depth ranges for dynamic curves and the representative depth (EPRI, 1993)

Depth range (ft)	Depth range (m)	Representative depth (m)
0-20	0-6	3
20-50	6-12	9
50-120	12-25	18.5
120-250	25-50	32.5
250-500	50-100	75
500-750	100-200	150
>750	>200	>250

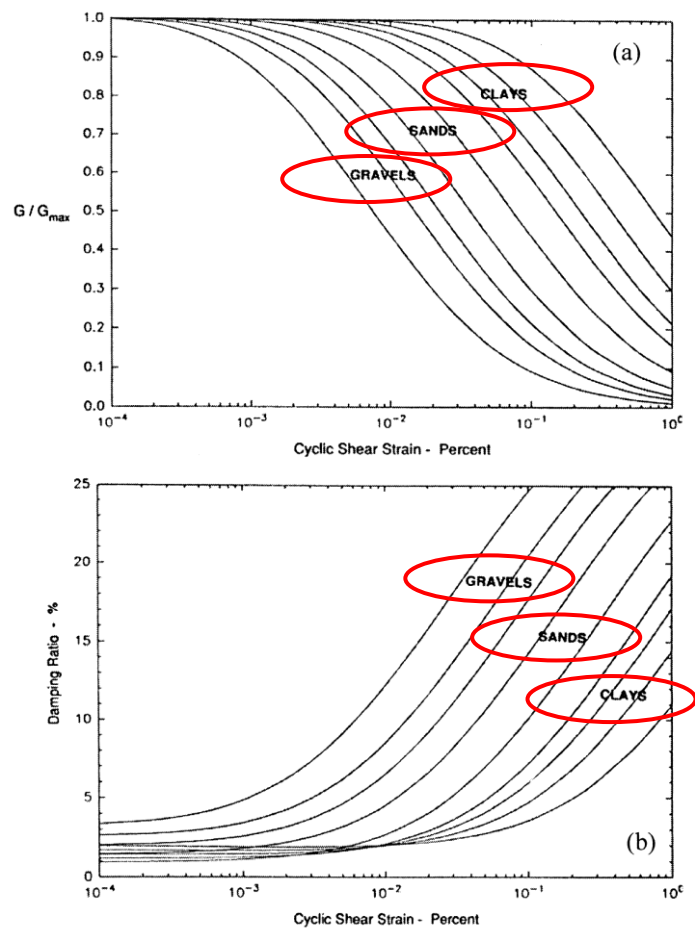


Figure 6.4. Empirical modulus reduction (a) and damping curves (b) for different soil types (EPRI, 1993)

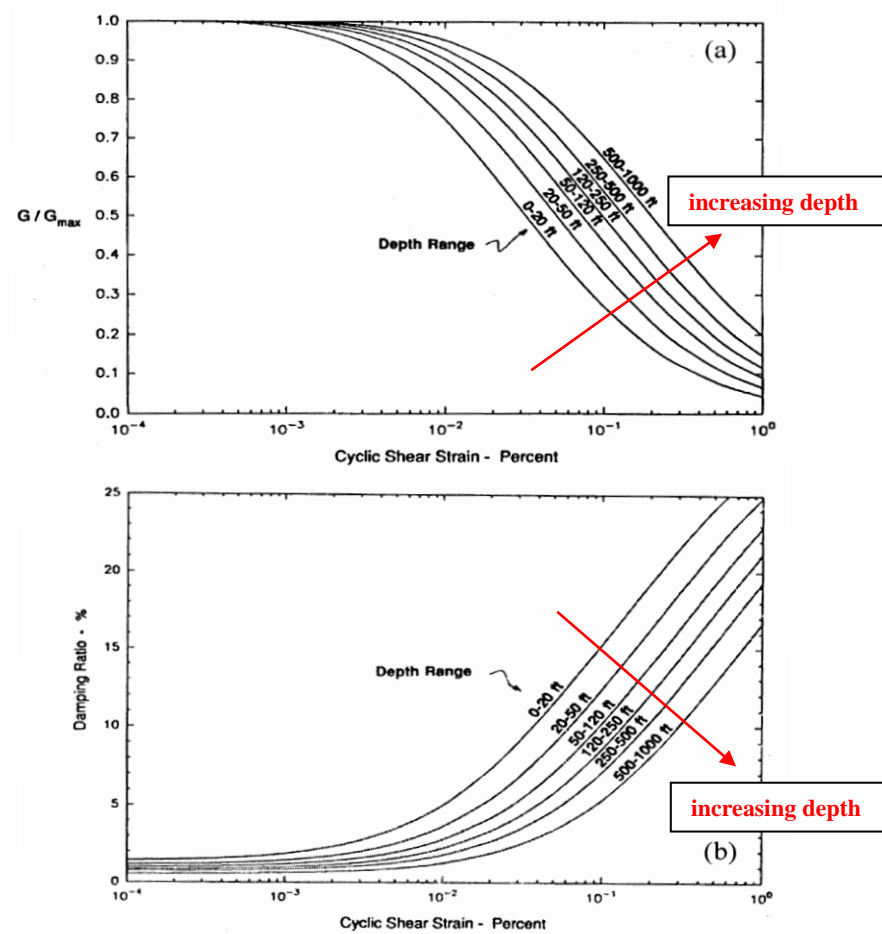


Figure 6.5. Empirical modulus reduction (a) and damping curves (b) for different confining pressures (EPRI, 1993)

Darendeli (2001) proposed a new model based on a modified hyperbolic form of a backbone curve. The introduced curve shows strain-stress relationship and the curve shape depends on the initial (low strain) stiffness and (high strain) shear strength of soil. The response of soil under cyclic conditions during loading-unloading cases can be illustrated by the behavior on the backbone curve.

The modulus reduction and damping versus cyclic strain curves are developed for the Erbaa soils using the model proposed by Darendeli (2001) in this study. The process of modulus reduction and damping curve construction will be explained in the following sections. Moreover, the following equations for different soils are considered for modulus reduction and damping curves in accordance with Darendeli (2001) model. In addition, the essential coefficients in the formulas are shown in Table 6.6.

Modulus reduction ( $G/G_{\max}$ );

$$\frac{G}{G_{\max}} = \frac{1}{1 + \left(\frac{\gamma}{\gamma_r}\right)^a} \quad (6.5)$$

Damping ( $\xi$ );

$$\xi = b \left( \frac{G}{G_{\max}} \right)^{0.1} \quad \xi_{\text{masing}} + \xi_{\min} \quad (6.6)$$

where:

$$a = \phi_5 \quad (6.5.1)$$

$$\gamma_r = (\phi_1 + \phi_2 * \text{PI} * \text{OCR}^{\phi_3}) * \text{SIGo}^{\phi_4} \quad (6.5.2)$$

$\gamma_r$  : reference strain

PI : plasticity index

OCR : overconsolidation ratio

SIGo : initial effective stress

$$b = \phi_{11} + \phi_{12} \ln(N) \quad (6.6.1)$$

$$\xi_{\text{masing}} = c_1 \xi_{\text{masing}, a=1} + c_2 \xi_{\text{masing}, a=1}^2 + c_3 \xi_{\text{masing}, a=1}^3 \quad (6.6.2)$$

$$\xi_{\text{masing}, a=1} = \frac{1}{\pi} \frac{\gamma - \gamma_r \ln\left(\frac{\gamma_r + \gamma}{\gamma_r}\right) - \frac{1}{2} \frac{\gamma^2}{1 + \frac{\gamma}{\gamma_r}}}{\frac{\gamma^2}{\gamma + \gamma_r}} - 2 \quad (6.6.2.1)$$

$$c_1 = -1.1143a^2 + 1.8618a + 0.2523 \quad (6.6.2.1.1)$$

$$c_2 = 0.0805a^2 - 0.0710a - 0.0095 \quad (6.6.2.1.2)$$

$$c_3 = -0.0005a^2 + 0.0002a + 0.0003 \quad (6.6.2.1.3)$$

$$\xi_{\min} = (\phi_6 + \phi_7 * \text{PI} * \text{OCR}^{\phi_8}) * \text{SIGo}^{\phi_9} (1 + \phi_{10} \ln f) \quad (6.6.3)$$

N : number of loading cycles

f : frequency

Table 6.6. Coefficients for Darendeli (2001) model

Prediction mean values	
$\Phi_1 = 0.0352$	$\Phi_7 = 0.0129$
$\Phi_2 = 0.0010$	$\Phi_8 = -0.1069$
$\Phi_3 = 0.3246$	$\Phi_9 = -0.2889$
$\Phi_4 = 0.3483$	$\Phi_{10} = 0.2919$
$\Phi_5 = 0.9190$	$\Phi_{11} = 0.6329$
$\Phi_6 = 0.8005$	$\Phi_{12} = -0.0057$

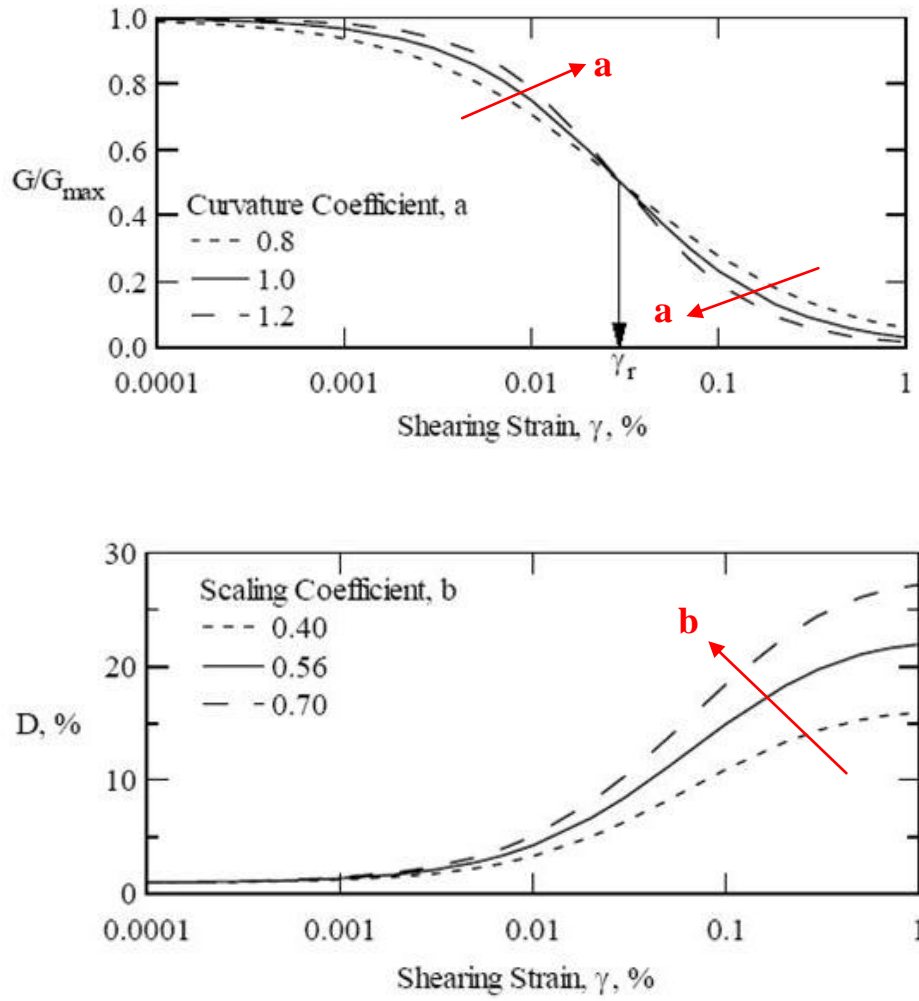


Figure 6.6. Modulus reduction and damping curves based on Darendeli model (2001)

Poisson's ratio ( $\nu$ ) is commonly used in engineering practice. The Poisson's ratio varies between 0.2 and 0.5 for different soils and can be calculated by Equation 6.7 which is based on laboratory tests at low strains (Kramer, 1996; Luna and Jari, 2000).

$$\nu = E / (2G - 1) \quad (6.7)$$

### 6.3 Estimation of $V_s$ for Erbaa

Shear wave velocity values obtained from geophysical tests and empirical correlations are evaluated in this section. Furthermore, several SPT-based empirical correlations are also employed to compare results for the database of ground response analyses.

### 6.3.1 Measured shear wave velocity ( $V_s$ )

As previously described in Chapter 4, several geophysical tests (21 resistivity, 20 seismic refraction, 3 downhole, 10 uphole surveys, and a total of 517 microtremor measurements, 6 Multichannel Analysis Surface Waves (MASW) - Refraction microtremor (REMI), and 30 SCPTU with limited depth are applied to obtain shear wave velocity in the study area. As an example, the shear wave velocity determined from CPT, SCPTU, seismic refraction, and SPT-based uphole is compared in Figure 6.7 for BH-10 location.

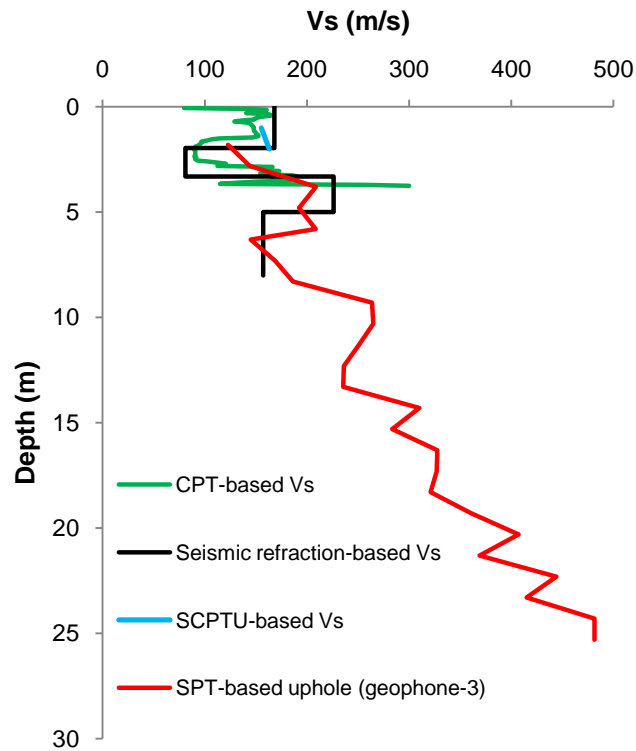


Figure 6.7. Comparison of shear wave velocity determined from CPT, SCPTU, seismic refraction, and SPT-based uphole for BH-10 location

As seen in Figure 6.7, a continuous shear wave velocity profile until 25 m depth can only be obtained from SPT-based uphole test for BH-10 location. It should be noted that the parameters used in site response analyses should be defined as comprehensively as possible for the sensitivity of analyses. For this reason, SPT-based uphole test results are taken into consideration in the evaluation stage of shear wave velocity for the Erbaa soils. In addition, the microtremor results are utilized in the evaluation of soil amplification.

The measurement of shear wave velocity by in-situ field tests is commonly used in practice. A combination of low strain (e.g. seismic refraction, seismic crosshole and downhole-uphole tests) and high strain (e.g. standard penetration, cone penetration) tests were applied in the study of Bang and Kim (2007). The SPT-based uphole method was proposed for the determination of shear wave velocity using the impact energy generated by SPT test as a source (Kim et al., 2004; Bang and Kim, 2007). As previously mentioned in Chapter 4, the shear wave velocity of the Erbaa soils was determined from SPT-based uphole method at ten different boreholes (BH-4, 6, 8, 10, 12, 18, 23, 28, 30, 33). The measurement results of ten SPT-based uphole boreholes with seven geophones are evaluated. The distribution of shear wave velocity along depth in BH-4 for seven different geophones and the average of all geophones are illustrated in Figure 6.8.

At the beginning of the shear wave velocity measurements from the SPT-based uphole tests, time delay measurements from all seven geophones were evaluated. However, it was realized that the two closest geophones (g-1 and g-2) to seismic source (boring machine) give unrealistically high results since they were affected from near-source relationship (Figure 6.8). Geophones 1 and 2 were placed on the ground surface with 2 and 4m distance to the boring machine and the inappropriate high results were caused by the boring machine noise. On the other hand, the more distant geophones (4, 5, 6, and 7) were also significantly affected from refraction-influenced path irregularities and revealed lower shear wave velocities at various testing depths when compared to the calculated empirical results. Moreover, it was determined that the shear wave velocity obtained from 3<sup>rd</sup> geophone is more appropriate with respect to empirical calculations. As a result, the shear wave velocity achieved from geophone 3 (g-3) is considered for the final shear wave velocity profiles. The shear wave velocity profiles obtained from SPT-based uphole tests are depicted in Figure 6.9 for alluvial and Pliocene soils of Erbaa.

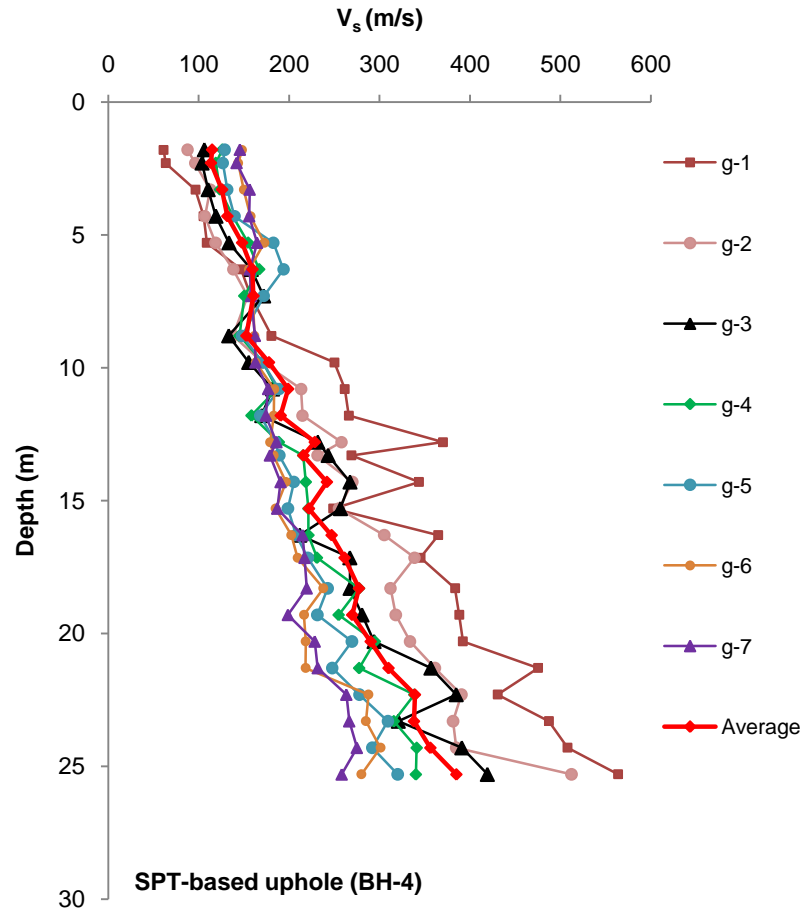


Figure 6.8. Shear wave velocity distribution for all geophones (BH-4)

### 6.3.2 Empirical calculations of the shear wave velocity

The measured shear wave velocities can also be used in the calculation of  $G_{\max}$  (Kramer, 1996) as given in Equation 6.1. When shear wave velocity measurements are not available,  $G_{\max}$  can be estimated using different approaches or empirical formulas. SPT-based  $G_{\max}$  and/or  $V_s$  relationships are most commonly used in the literature (Ohta and Goto, 1976; Seed et al., 1986). For different soil types, SPT-N and  $V_s$  relationships were proposed by different researchers (Ohba and Toriumi, 1970; Imai and Yoshimura, 1970; Fujiwara, 1972; Ohsaki and Iwasaki, 1973; Imai, 1977; Ohta and Goto, 1978; Seed and Idriss, 1981; Imai and Tonouchi, 1982; Sykora and Stokoe, 1983; Jinan, 1987; Lee, 1990; Sisman, 1995; Iyisan, 1996; Kayabali, 1996; Jafari et al., 1997; Pitilakis et al., 1999; Kiku et al., 2001; Jafari et al., 2002; Andrus et al., 2006; Hasançebi and Ulusay, 2007; Hanumantharao and Ramana, 2008;



Dikmen, 2009). In these relationships, SPT  $N_{30}$  blow count is mostly considered, but some relations were derived using energy corrected SPT blow count ( $N_{60}$ ). A summary of the empirical relationships between SPT-N and  $V_s$  in the literature is presented in Table 6.7 for different soil types.

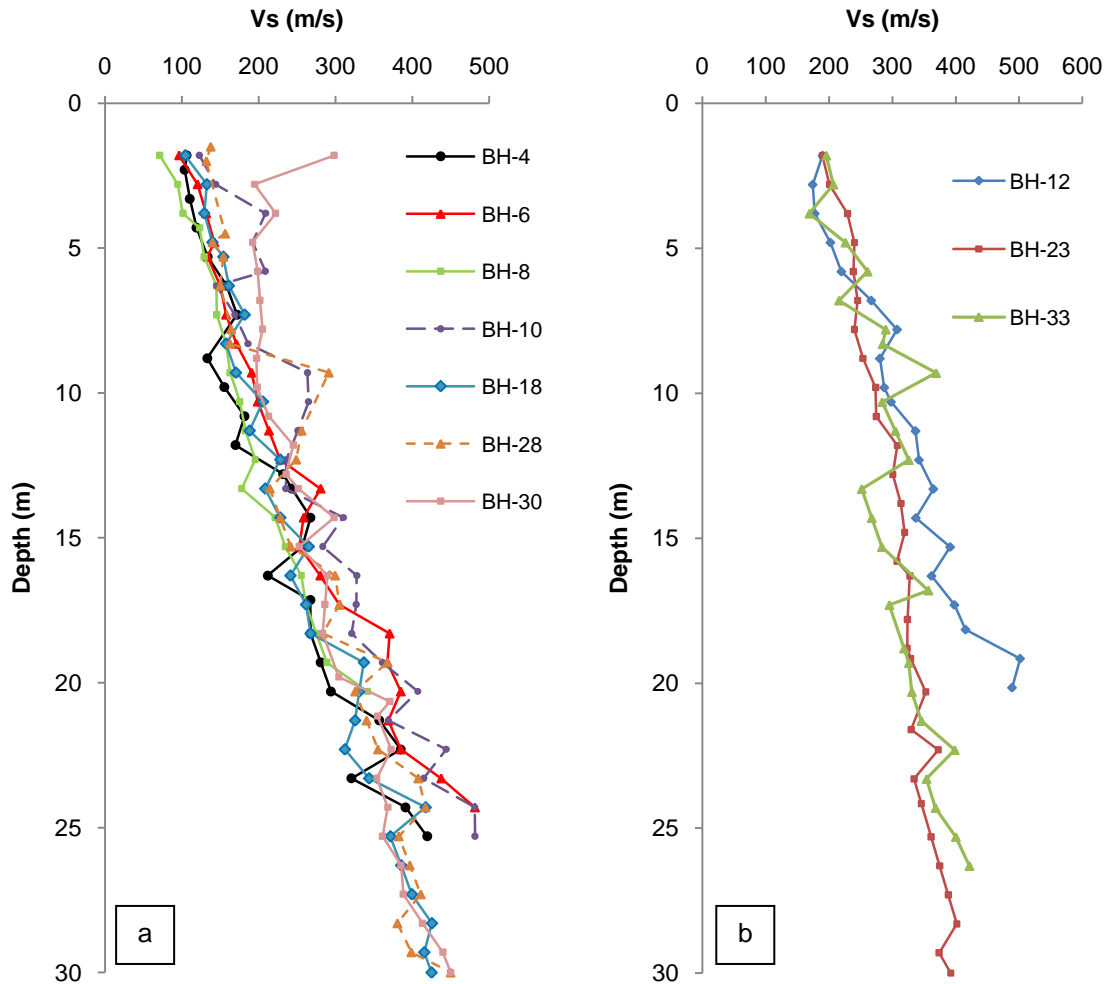


Figure 6.9. Shear wave velocity profiles obtained from SPT-based uphole tests; a: alluvial soils, b: Pliocene soils

The SPT-N values obtained from Erbaa soils are used in these equations to empirically determine shear wave velocity ( $V_s$ ) for each borehole. An example of the empirical  $V_s$  calculations for BH-2 is depicted in Figure 6.10.

A wide range of variation in values obtained from SPT and  $V_s$  correlations can be observed in Figure 6.10. The distribution of  $V_s$  values at a particular depth from the different

relationships is quite broad. Therefore, the selection of most proper SPT-N -  $V_s$  correlation for a study area may be questionable.

Table 6.7. Summary of empirical correlations based on SPT-N vs.  $V_s$

Researcher(s)	$V_s$ (m/s)		
	All soils	Sands	Clays
Kanai (1966)	$V_s = 19N^{0.6}$	-	-
Imai and Yoshimura (1970)	$V_s = 76N^{0.33}$	-	-
Ohba and Toriumi (1970)	$V_s = 84N^{0.31}$	-	-
Fujiwara (1972)	$V_s = 92.1N^{0.337}$	-	-
Shibata (1970)	-	$V_s = 32N^{0.5}$	-
Ohta et al. (1972)	-	$V_s = 87N^{0.36}$	-
Ohsaki and Iwasaki (1973)	$V_s = 81.4N^{0.39}$	$V_s = 59.4N^{0.47}$	-
Imai et al. (1975)	$V_s = 89.9N^{0.341}$	-	-
Imai (1977)	$V_s = 91N^{0.337}$	$V_s = 80.6N^{0.331}$	$V_s = 102N^{0.292}$
Ohta and Goto (1978)	$V_s = 85.35N^{0.348}$	-	-
Seed and Idriss (1981)	$V_s = 61.4N^{0.5}$	-	-
Imai and Tonouchi (1982)	$V_s = 97N^{0.314}$	-	-
Seed et al. (1983)	-	$V_s = 56.4N^{0.5}$	-
Sykora and Stokoe (1983)	-	$V_s = 100.5N^{0.29}$	-
Tonouchi et al. (1983)	$V_s = 97N^{0.314}$	-	-
Fumal and Tinsley (1985)	-	$V_s = 152+5.1N^{0.27}$	-
Jinan (1987)	$V_s = 116.1(N+0.3185)^{0.202}$	-	-
Okamoto et al. (1989)	-	$V_s = 125N^{0.3}$	-
Lee (1990)	-	$V_s = 57N^{0.49}$	$V_s = 114N^{0.31}$
Yokota et al. (1991)*	$V_s = 121N^{0.27}$	-	-
Kalteziotis et al. (1992)	$V_s = 76.2N^{0.24}$	-	-
Pitilakis et al. (1992)	-	$V_s = 162N^{0.17}$	-
Athanasopoulos (1995)	$V_s = 107.6N^{0.36}$	-	-
Raptakis et al. (1995)	-	$V_s = 100N^{0.24}$	-
Sisman (1995)	$V_s = 32.8N^{0.51}$	-	-
Iyisan (1996)	$V_s = 51.5N^{0.516}$	-	-
Kayabali (1996)	-	$V_s = 175+(3.75N)$	-
Jafari et al. (1997)	$V_s = 22N^{0.85}$	-	-
Pitilakis et al. (1999)	-	$V_s = 145(N_{60})^{0.178}$	$V_s = 132(N_{60})^{0.271}$
Kiku et al. (2001)	$V_s = 68.3N^{0.292}$	-	-
Jafari et al. (2002)	-	-	$V_s = 27N^{0.73}$
Hasançebi and Ulusay (2007)	$V_s = 90N^{0.308}$	$V_s = 90.82N^{0.319}$	$V_s = 97.89N^{0.269}$
Hanumantharao & Ramana (2008)	$V_s = 82.6N^{0.43}$	$V_s = 79N^{0.434}$	-
Dikmen (2009)	$V_s = 58N^{0.39}$	$V_s = 73N^{0.33}$	$V_s = 44N^{0.48}$

\*Adopted from Jafari et al. (2002)

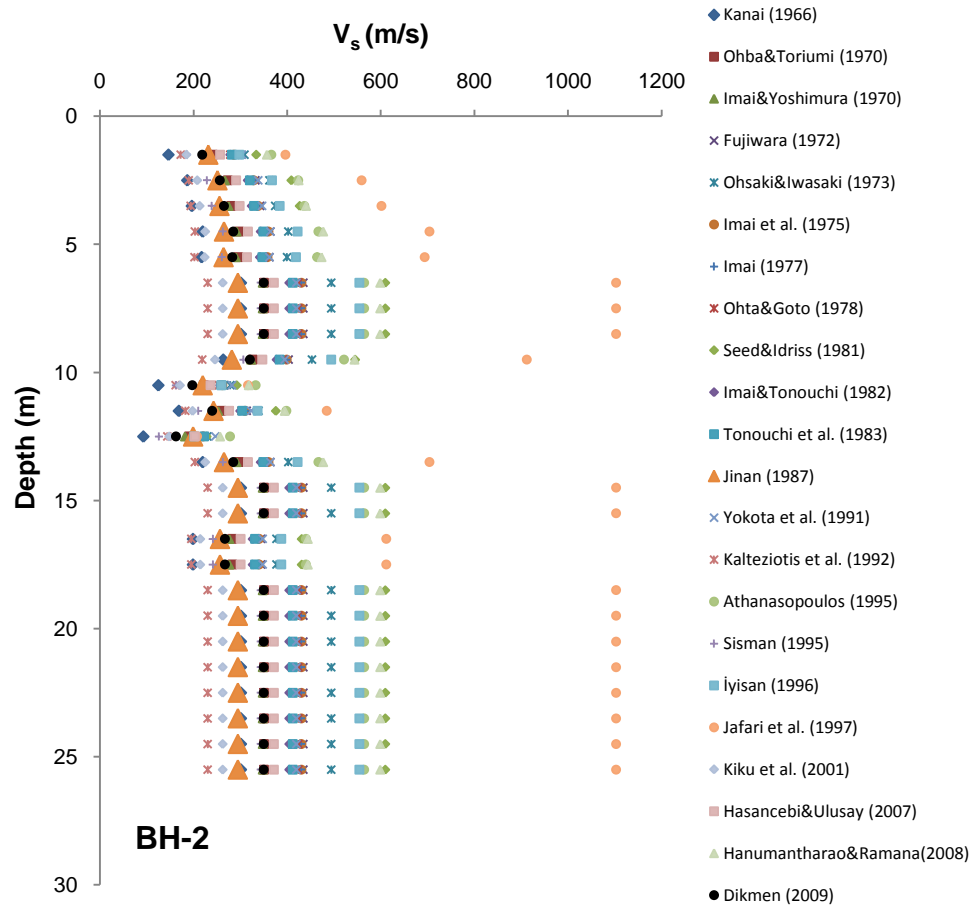


Figure 6.10. SPT-N and  $V_s$  correlations for all soils in BH-4 with respect to different researchers

The shear wave velocities obtained from SPT-based uphole tests (measured shear wave velocity) are compared to empirical results for different soil types in this study. The SPT-N and  $V_s$  correlations of the Erbaa soils with respect to the aforementioned relationships are presented with the shear wave velocities determined from the SPT-based uphole results (based on 3<sup>rd</sup> geophone) in Figures 6.11 - 6.16. The distribution of the shear wave velocity data with respect to SPT-N value at the same uphole testing depth and the power relationship are shown together with other equations in the same figures. It should be noted that the relationships are classified into three main groups according to three main soil types: for all soils, for sand, and for clay. Moreover, alluvial and Pliocene soils are evaluated separately to consider the geologic age factor in this study. Consequently, new empirical relationships between SPT-N and  $V_s$  are proposed for different alluvial and Pliocene soils in the study area in accordance with the SPT-based uphole measurements.

The relationships proposed for all Erbaa alluvial and Pliocene soils (red dashed line in Figures 6.11 and 6.14) are quite compatible with the equations introduced by Hasançebi and Ulusay (2007), Imai and Tonouchi (1982), and Ohba and Toriumi (1970). On the other hand, the Jafari et al. (1997) relationship reveals a very different trend from all other equations (Figures 6.11 and 6.14). Furthermore, the relationship proposed for the Erbaa alluvial sand (red dashed line in Figure 6.12) presents similarities with Dikmen (2009) and Raptakis et al. (1995) correlations. For sandy soils, Okamoto et al. (1989) and Hanumantharao and Ramana (2008) relations provide higher velocities than all other equations (Figure 6.12). The new developed relation for the Pliocene sands shows similarities with Imai (1977) and Hasançebi and Ulusay (2007) relations (Figure 6.15). The Lee (1990) relationship for alluvial clay type soils is consistent with the correlation developed in this study (Figure 6.13). Besides, Imai (1977) relationship is quite relevant to the relation suggested for the Pliocene clay in the study area (Figure 6.16).

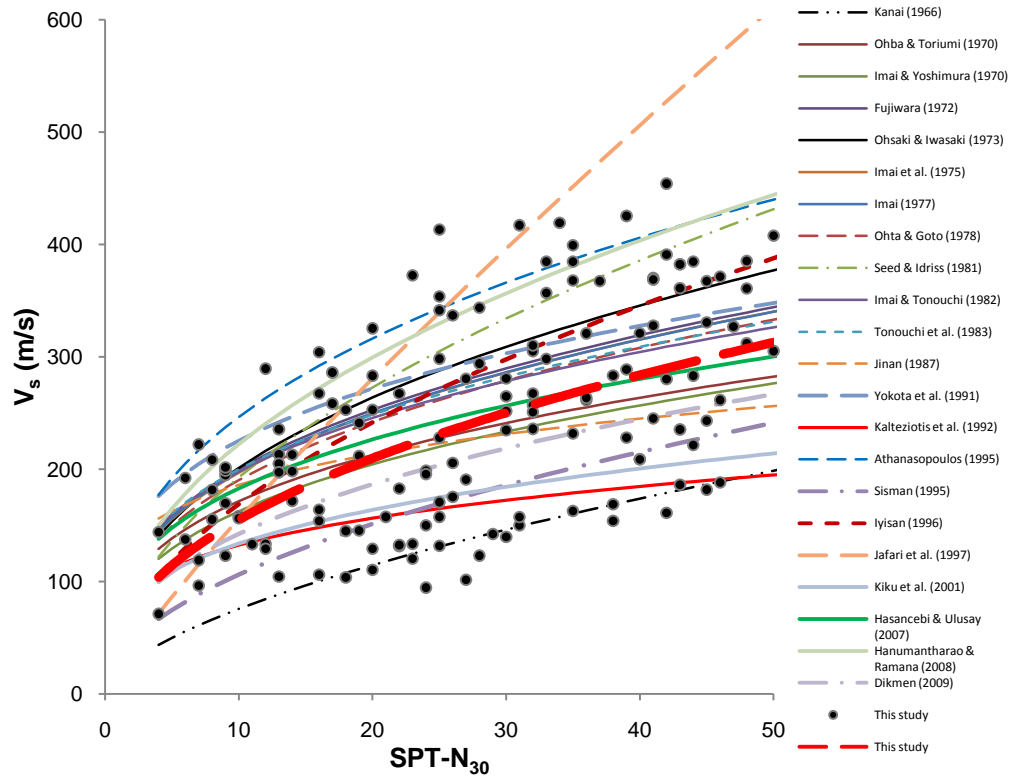


Figure 6.11. SPT-N and  $V_s$  empirical relations for all alluvial soils in Erbaa

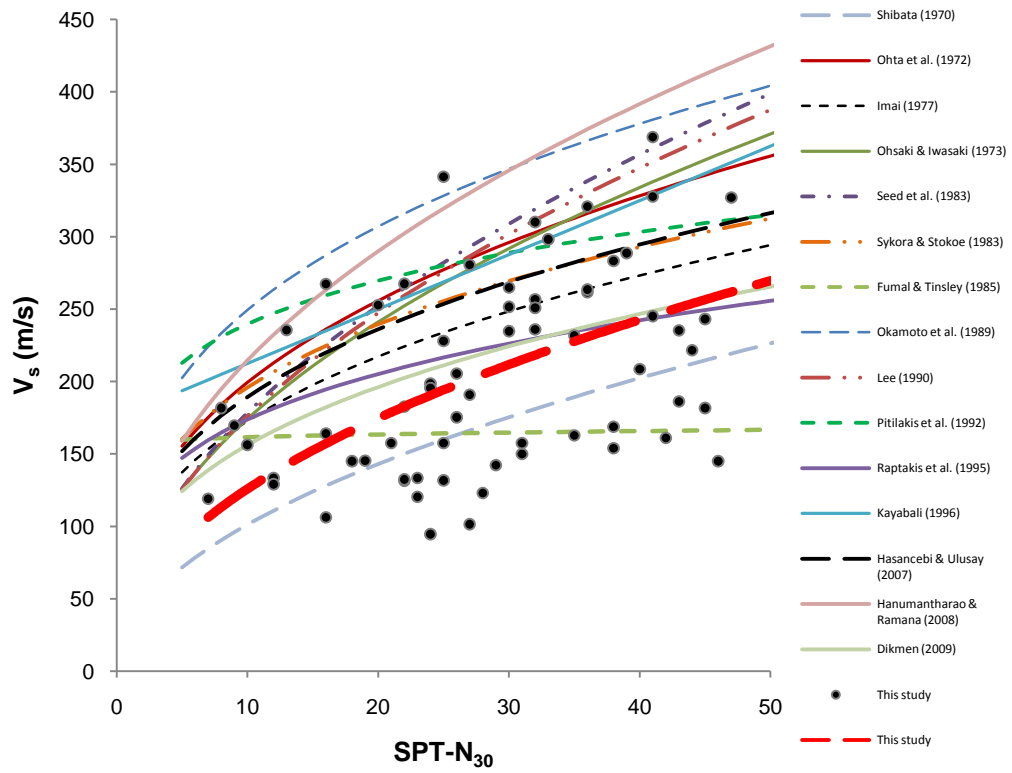


Figure 6.12. SPT-N and  $V_s$  empirical relations for alluvial sand in Erbaa

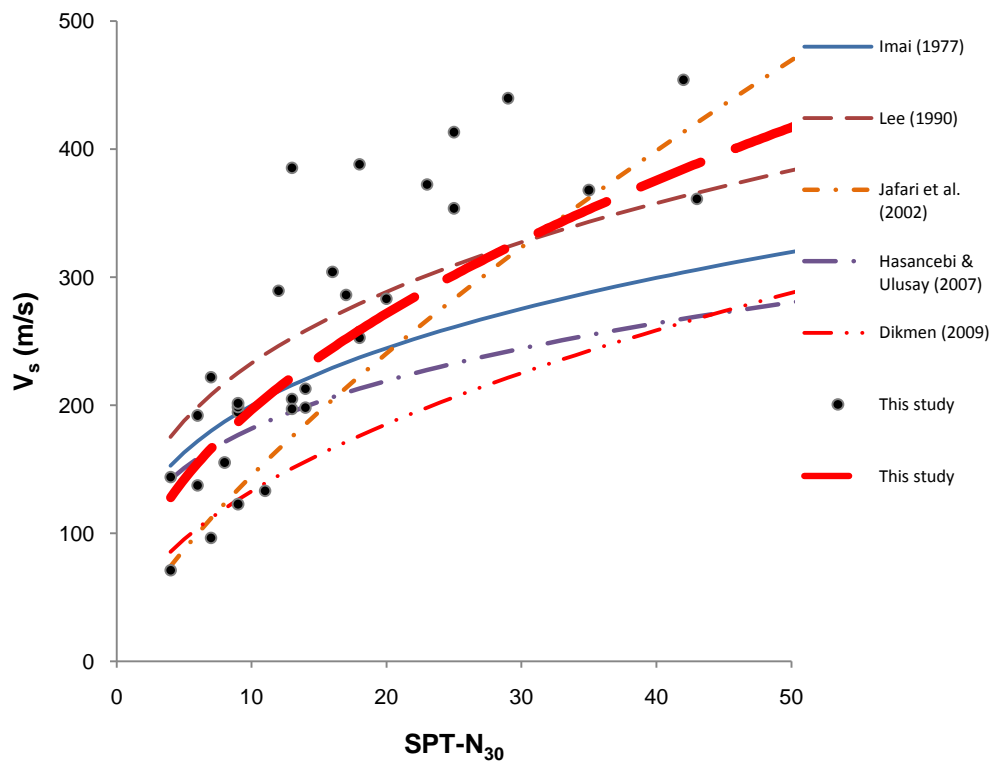


Figure 6.13. SPT-N and  $V_s$  empirical relations for alluvial clay in Erbaa

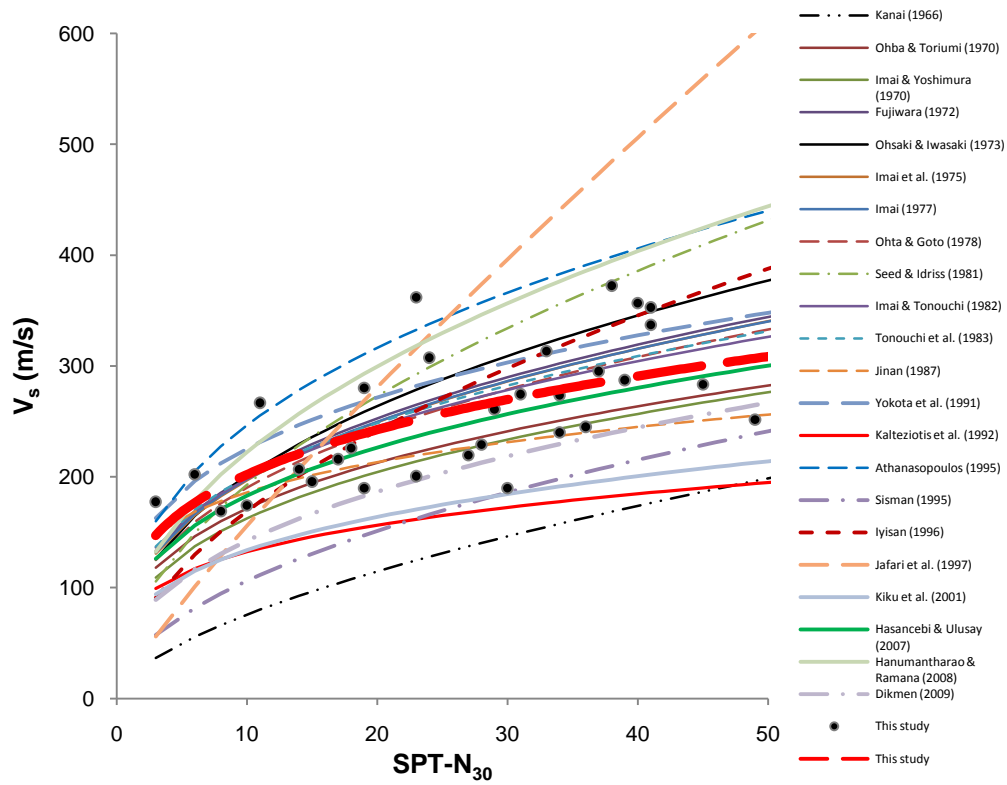


Figure 6.14. SPT-N and  $V_s$  empirical relations for all Pliocene soils in Erbaa

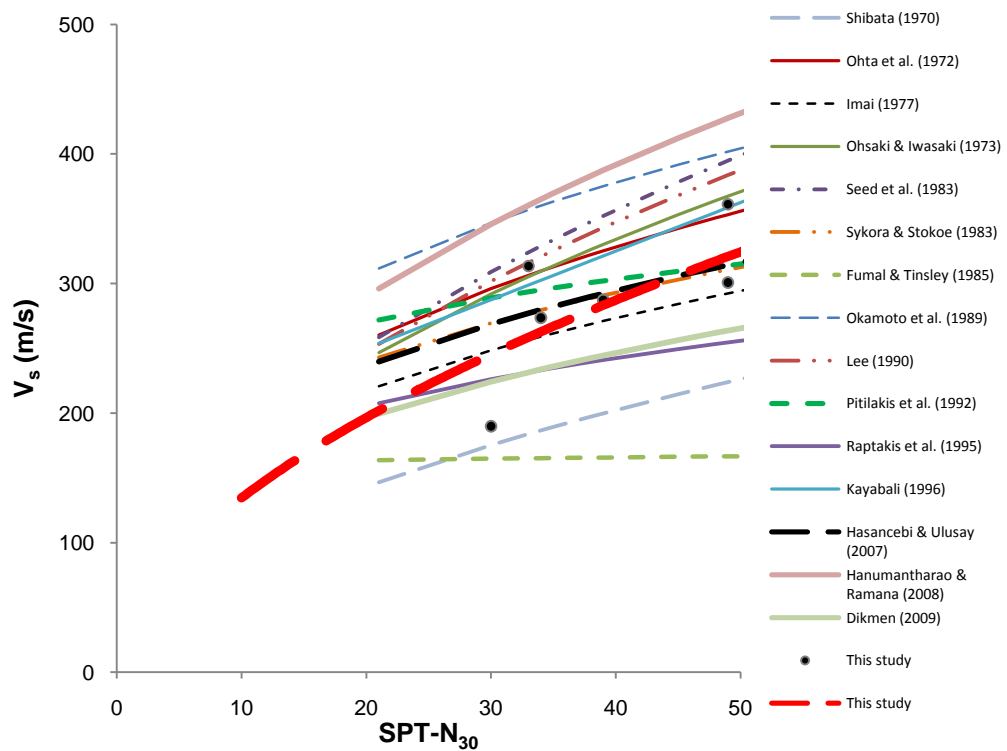


Figure 6.15. SPT-N and  $V_s$  empirical relations for Pliocene sand in Erbaa

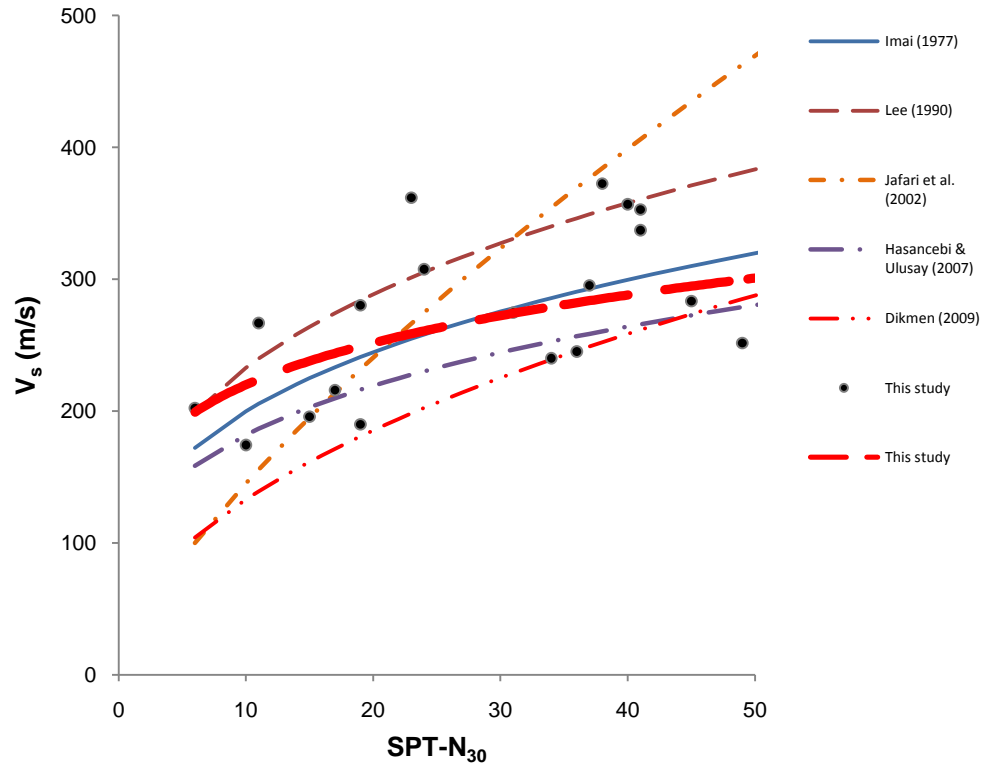


Figure 6.16. SPT-N and  $V_s$  empirical relations for Pliocene clay in Erbaa

As aforementioned, the shear wave velocity determined from SPT-based uphole test and SPT- $N_{30}$  blow count at the same testing depth are considered during the construction of empirical relationships. The following relationships are proposed between  $V_s$  (m/s) and SPT- $N_{30}$  for different soil categories in the study area.

$$V_s = 56.69 N^{0.44} \quad \text{for all alluvial soils} \quad r=0.66 \quad (6.8)$$

$$V_s = 42.28 N^{0.47} \quad \text{for alluvial sand} \quad r=0.70 \quad (6.9)$$

$$V_s = 66.94 N^{0.47} \quad \text{for alluvial clay} \quad r=0.79 \quad (6.10)$$

$$V_s = 110.26 N^{0.26} \quad \text{for all Pliocene soils} \quad r=0.81 \quad (6.11)$$

$$V_s = 38.17 N^{0.55} \quad \text{for Pliocene sand} \quad r=0.90 \quad (6.12)$$

$$V_s = 140.46 N^{0.02} \quad \text{for Pliocene clay} \quad r=0.68 \quad (6.13)$$

The empirical relationships between SPT- $N_{30}$  and shear wave velocity for different soil types are depicted in Figures 6.17, 6.19, 6.21, 6.23, 6.25, and 6.27. In addition, the measured shear wave velocities (from SPT-based uphole tests) are compared to the predicted shear wave velocities (from proposed empirical relations) in Figures 6.18, 6.20, 6.22, 6.24, 6.26, and 6.28.

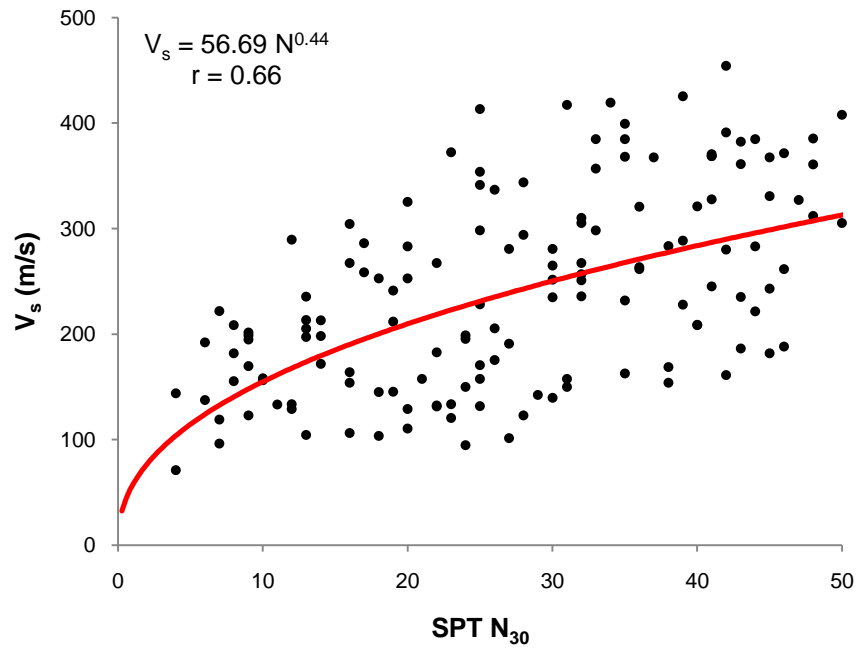


Figure 6.17. Proposed relationship for all alluvial soils in Erbaa

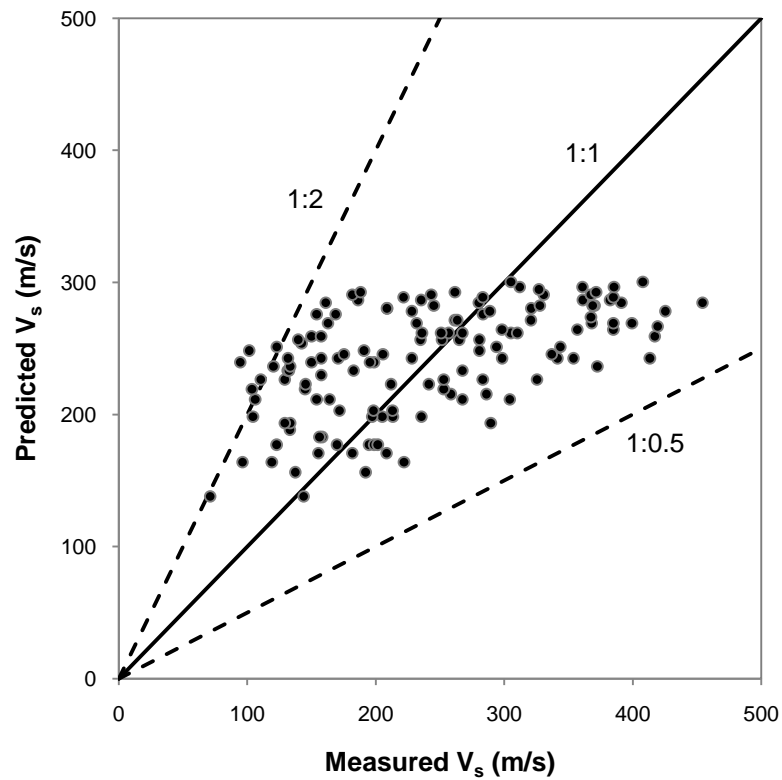


Figure 6.18. Comparison of measured and predicted shear wave velocity for all alluvial soils



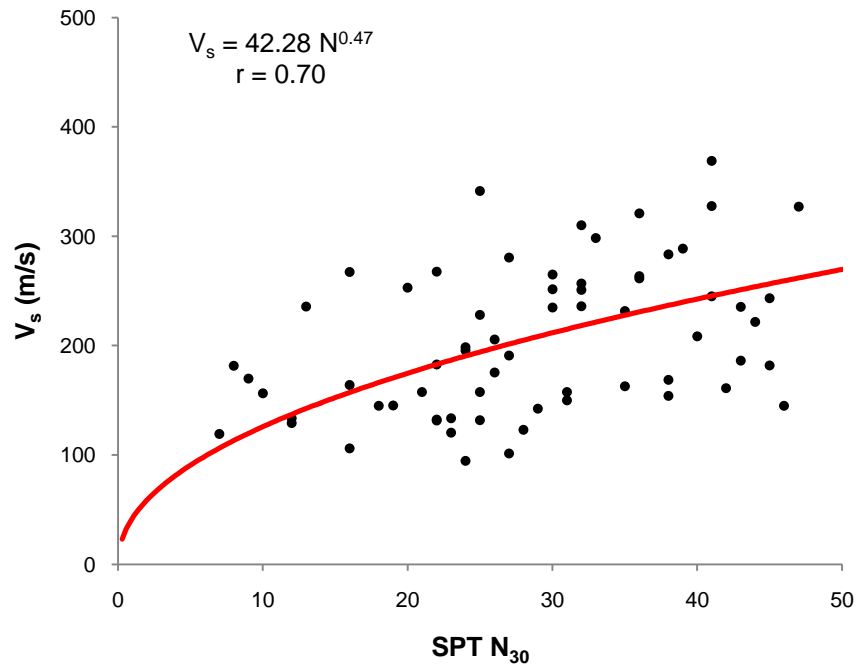


Figure 6.19. Proposed relationship for alluvial sand in Erbaa

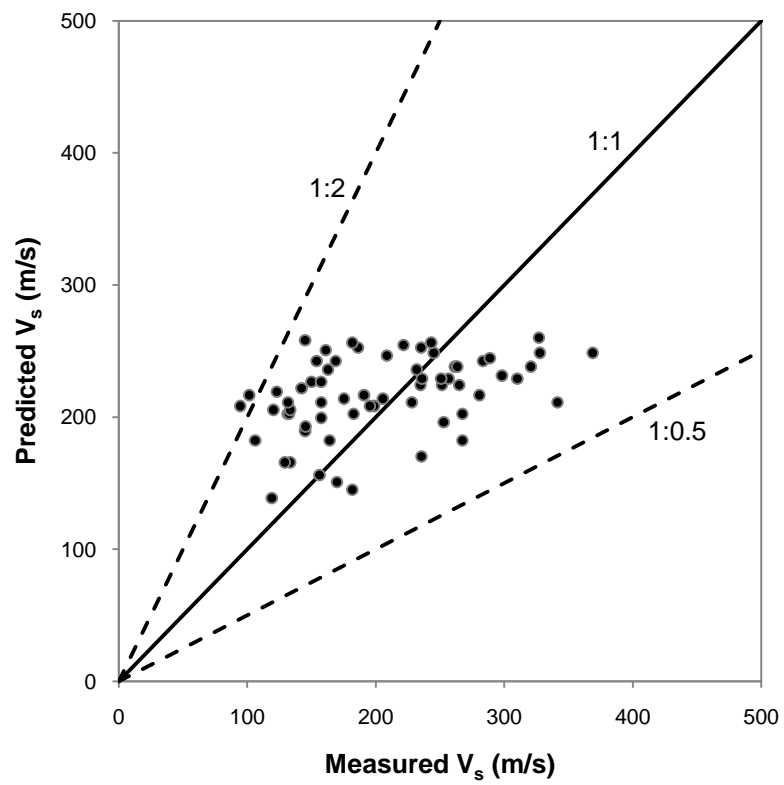


Figure 6.20. Comparison of measured and predicted shear wave velocity for alluvial sand

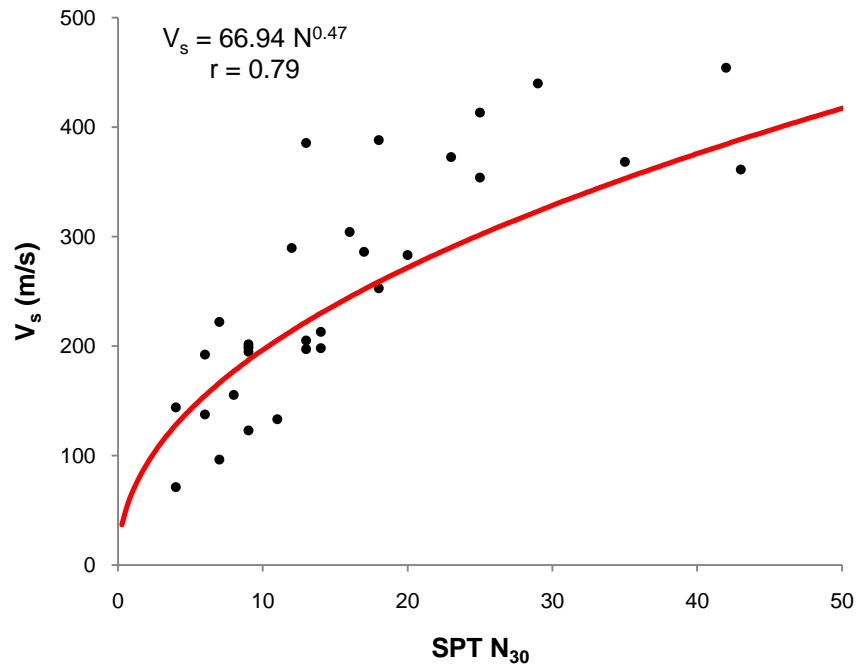


Figure 6.21. Proposed relationship for alluvial clay in Erbaa

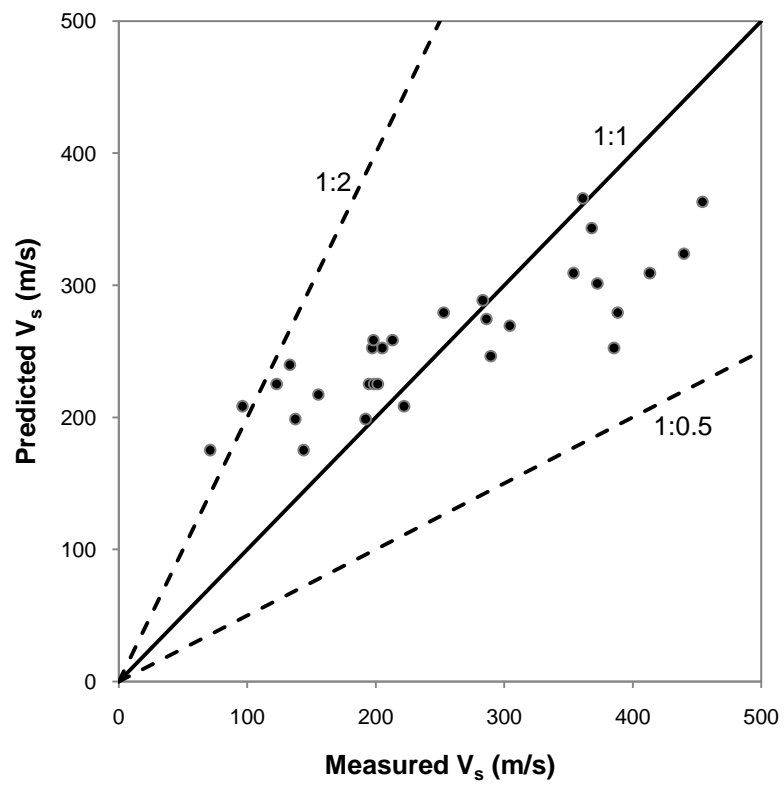


Figure 6.22. Comparison of measured and predicted shear wave velocity for alluvial clay

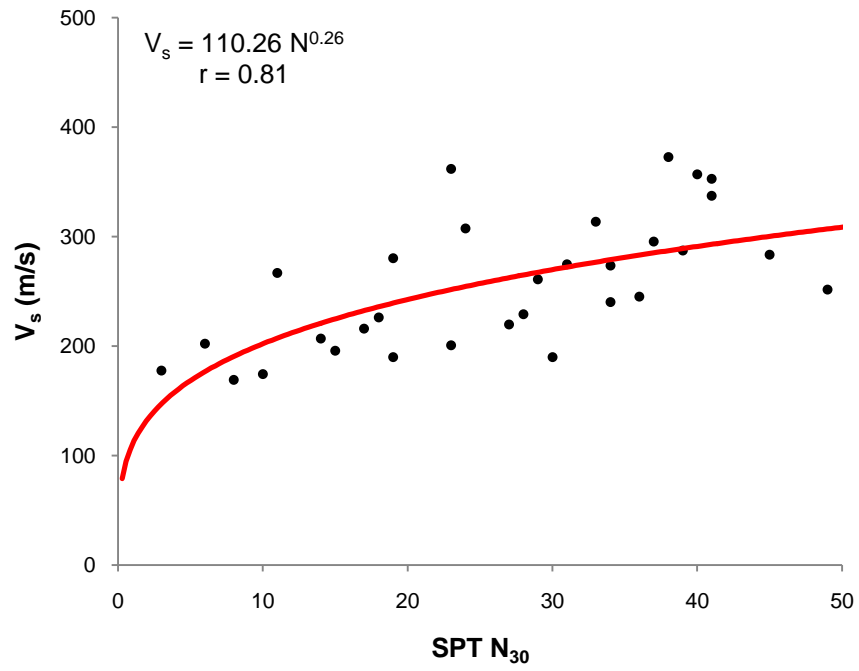


Figure 6.23. Proposed relationship for all Pliocene soils in Erbaa

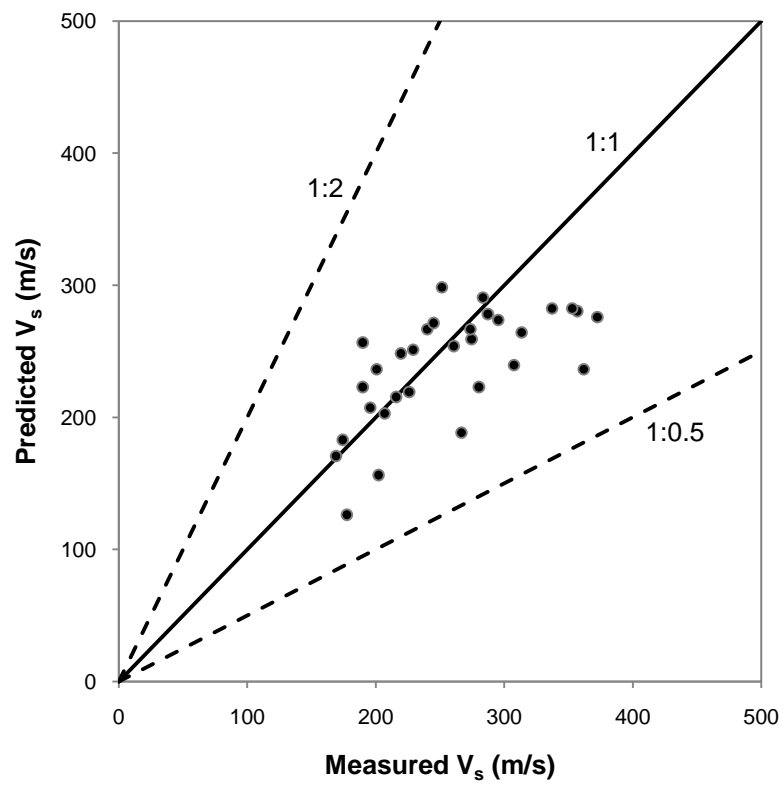


Figure 6.24. Comparison of measured and predicted shear wave velocity for all Pliocene soils

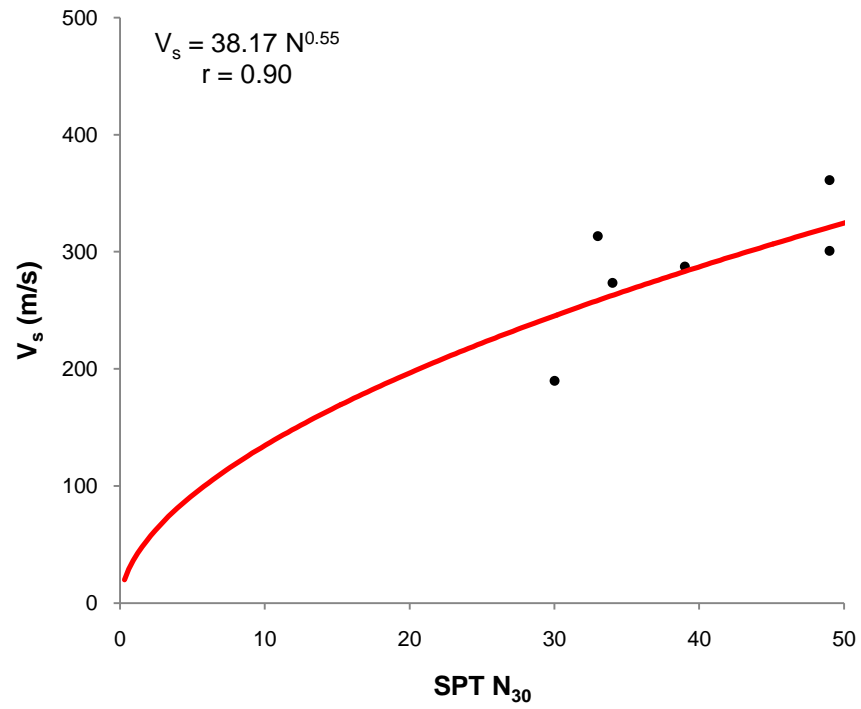


Figure 6.25. Proposed relationship for Pliocene sand in Erbaa

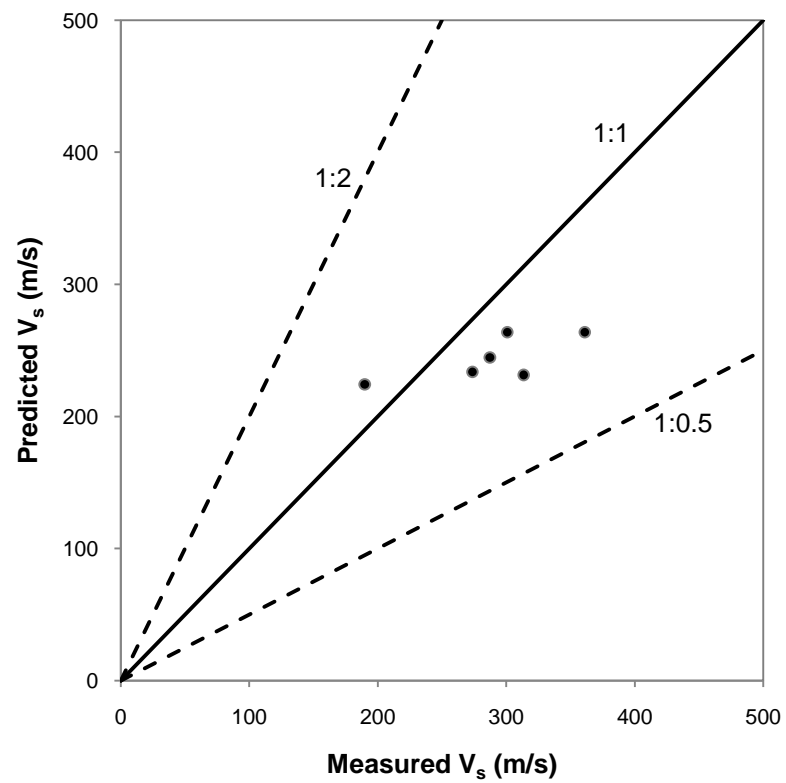


Figure 6.26. Comparison of measured and predicted shear wave velocity for Pliocene sand

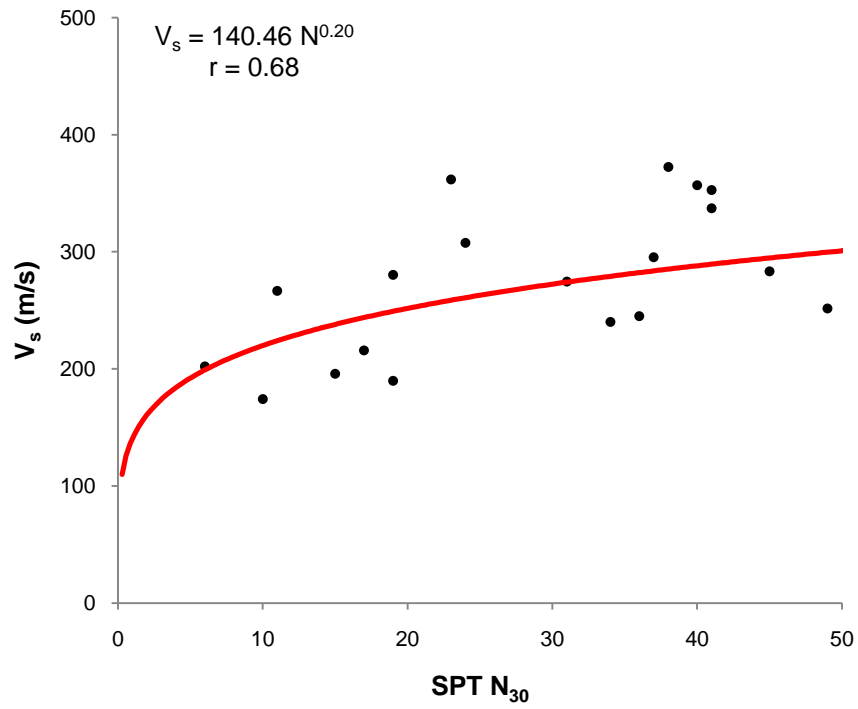


Figure 6.27. Proposed relationship for Pliocene clay in Erbaa

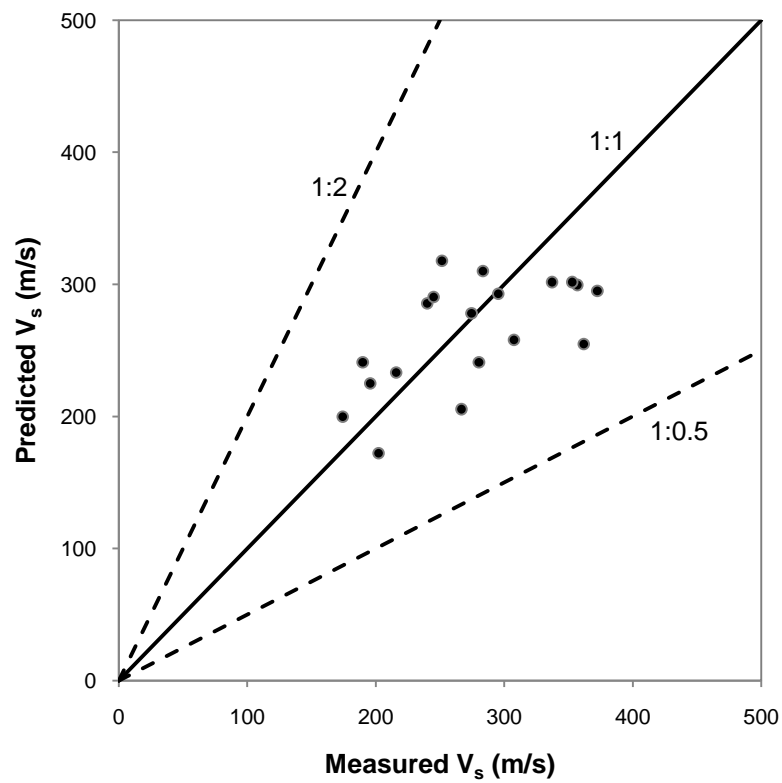


Figure 6.28. Comparison of measured and predicted shear wave velocity for Pliocene clay

The empirical relations for alluvial and Pliocene soils are illustrated in Figures 6.29 and 6.30 to express the effect of different soil types on the proposed relations.

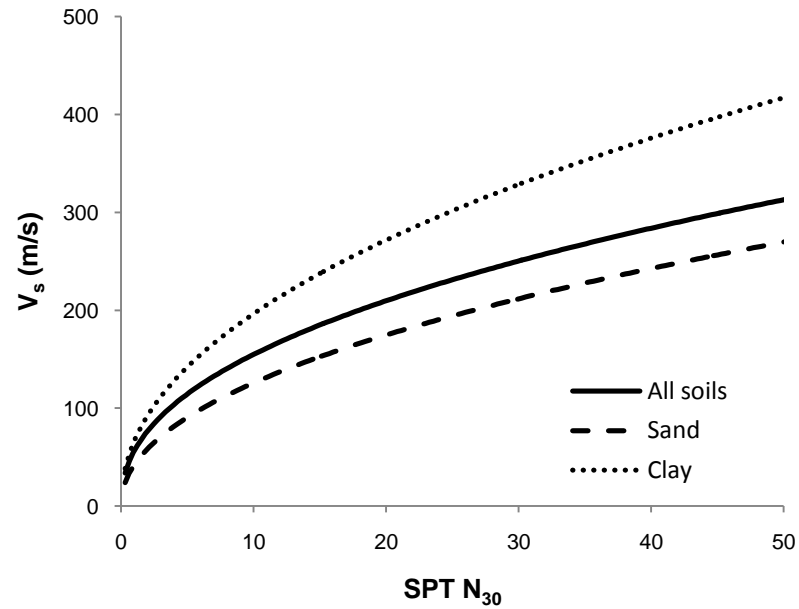


Figure 6.29. Effect of soil type on SPT- $N_{30}$ - $V_s$  relationships for alluvial soils in Erbaa

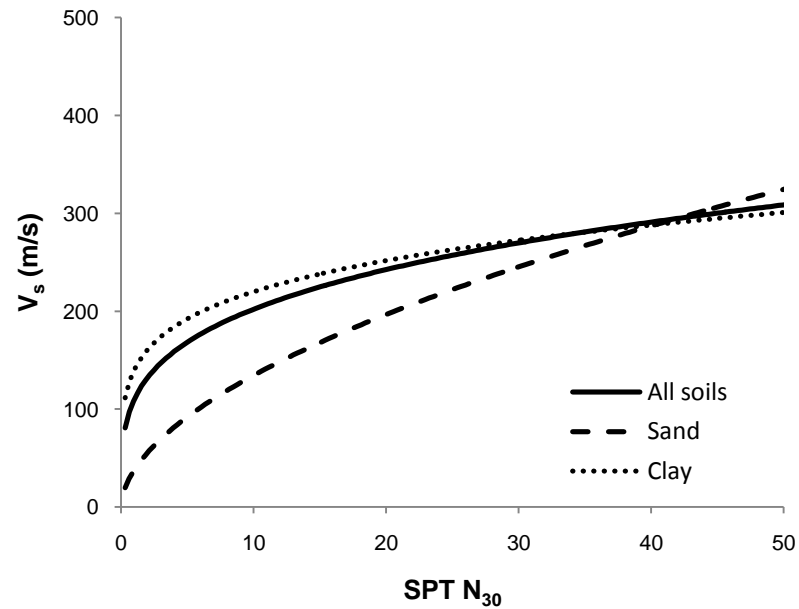


Figure 6.30. Effect of soil type on SPT- $N_{30}$ - $V_s$  relationships for Pliocene soils in Erbaa

Besides, the proposed empirical relationships between  $V_s$  (m/s) and SPT- $N_{30}$  are also evaluated considering the depth ( $z$ ) effect. The following power-law expressions including depth (in meters) based on multiple regressions are obtained for different soil categories. It should be noted that the proposed equations (6.14 to 6.19) are valid up to 25 m depth.

$V_s = 59.44 N^{0.109} z^{0.426}$	for all alluvial soils	$r=0.89$ (6.14)
$V_s = 38.55 N^{0.176} z^{0.481}$	for alluvial sand	$r=0.94$ (6.15)
$V_s = 78.1 N^{0.116} z^{0.35}$	for alluvial clay	$r=0.92$ (6.16)

$V_s = 121.75 N^{0.101} z^{0.216}$	for all Pliocene soils	$r=0.94$ (6.17)
$V_s = 52.04 N^{0.359} z^{0.177}$	for Pliocene sand	$r=0.98$ (6.18)
$V_s = 140.61 N^{0.049} z^{0.232}$	for Pliocene clay	$r=0.89$ (6.19)

Similar correlations between  $V_s$  and energy corrected SPT-N ( $N_{60}$ ) for silts, sands, and clays were proposed by Pitilakis et al. (1999). Accordingly, SPT-N value was corrected by 60% energy ratio to get the average ratio of the actual energy delivered by safety hammers to the theoretical free-fall energy. Pitilakis et al. (1999) mentioned that the proposed correlation for clays is compatible with the existing relationships (Imai, 1977 and Lee, 1992). However, the relationship proposed for silts and sands reveal quite dissimilar results when compared to the existing relations. The reason for dissimilarity was explained by the saturation of  $V_s$  at 400 m/s depending upon the employed dataset. Furthermore, Hasaebi and Ulusay (2007) stated that the proposed equations based on uncorrected SPT-N values provide a somewhat better fit than the equations based on energy corrected SPT-N values. The use of equation for all soils based on uncorrected blow-counts (SPT-N) is applicable for the indirect estimations of  $V_s$  (Hasaebi and Ulusay, 2007).

On the contrary, there are a few SPT-N and shear wave velocity relations using the energy corrected SPT-N blow count ( $N_{1,60}$ ). Ohta and Goto (1976) and Seed et al. (1986) empirical SPT-based relationships are considered in this study to estimate the shear wave velocity for sandy layers.  $G_{max}$  is calculated by means of corrected N-blow count ( $N_1$ )<sub>60</sub> and effective stress with a constant coefficient as given in Equation 6.4 in this approach. Then  $V_s$  can be determined by Equation 6.1. The distribution of shear wave velocity in BH-10 determined by Ohta and Goto (1976) relation is given in Figure 6.31.

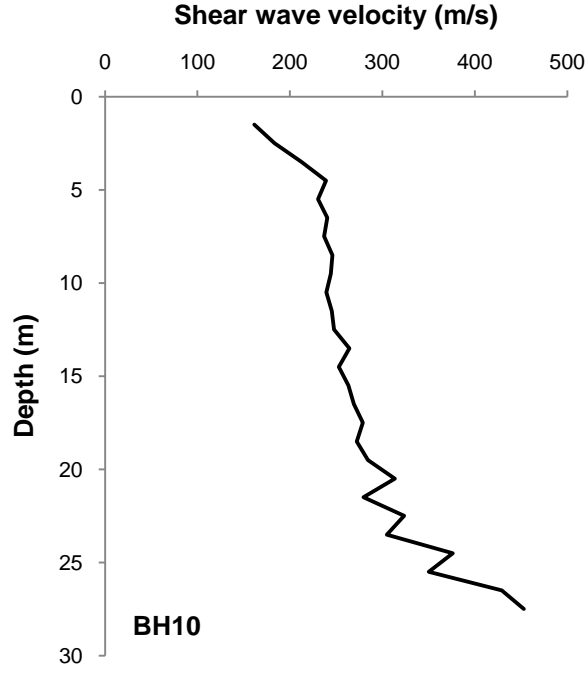


Figure 6.31. Distribution of  $V_s$  determined by Ohta and Goto (1976) relationship

Furthermore, SPT-N blow-counts were corrected to achieve  $(N_1)_{60}$  values using Equation 6.20 for Erbaa. The NCEER Working Group (NCEER, 1997) recommendations were considered for  $C_R$ ,  $C_S$ ,  $C_B$ , and  $C_E$  corrections. The depth of ground water table and the unit weight of the soils were also considered.

$$(N_1)_{60} = N \cdot C_N \cdot C_R \cdot C_S \cdot C_B \cdot C_E \quad (6.20)$$

where  $C_R$  : correction for rod length,  
 $C_S$  : correction for sampler configuration,  
 $C_B$  : correction for borehole diameter, and  
 $C_E$  : correction for hammer energy efficiency (60%).

Idriss and Boulanger's (2006) overburden correction factor ( $C_N$ ) was used for the consideration of overburden pressure in the corrections (Equation 6.21-6.22).

$$C_N = (P_a / \sigma'_v)^\beta \leq 1.7 \quad (6.21)$$

$$\beta = 0.784 - 0.0768 \sqrt{(N_1)_{60}} \quad (6.22)$$



Moreover, different approaches were applied for clayey layers during the empirical calculation of the shear wave velocity. Firstly, Pliocene and alluvial clays were explored separately and alluvial clay units were evaluated on the basis of Equation 6.2 (Kramer, 1996). Besides, the  $G_{\max}$  of Pliocene clay layers were evaluated in accordance with overconsolidation ratio and plasticity index as given in Table 6.3 since there is limited number of CU type triaxial compression test results. After  $G_{\max}$  calculations for different layers,  $V_s$  values are determined for each layer.

### 6.3.3 Comparison of measured and empirical shear wave velocity

The proposed SPT-N and  $V_s$  relation in this study is also correlated with different researchers' relationships. Additionally, empirically determined shear wave velocities are also compared to the measured shear wave velocities. Therefore, it is aimed to correlate measured shear wave velocities with SPT-N based  $V_s$  (from empirical formulas) within the framework of this study. However, available SPT-based uphole results are more coherent to the suitable parameters and related correlations for the study area. The measured SPT-uphole based results are compared to SPT- $N_{1,60}$  based  $V_s$  formulas.

Furthermore, the comparison is made for different soil types in the study area. Firstly, the soil units are classified into four main groups: alluvium clay (A-1), alluvium sand (A-2), Pliocene clay (P-1), and Pliocene sand (P-2). Then,  $G_{\max}$  value is calculated with respect to different approaches using Ohta and Goto (1976)-Seed et al. (1986) formula for sands (given in Equation 6.4). Afterwards, calculated results are compared to  $G_{\max}$  values retrieved from uphole-based shear wave velocities. A comparison between measured and empirical shear wave velocity for BH-4 is shown in Figure 6.32.

The measured  $V_s$  from SPT-based uphole test and empirically calculated  $V_s$  from Ohta and Goto (1976) relation for alluvial and Pliocene sands are statistically evaluated. The linear relationships between measured and empirically calculated  $V_s$  for alluvial (A-2) and Pliocene (P-2) sand are shown in Figures 6.33 and 6.34, respectively.

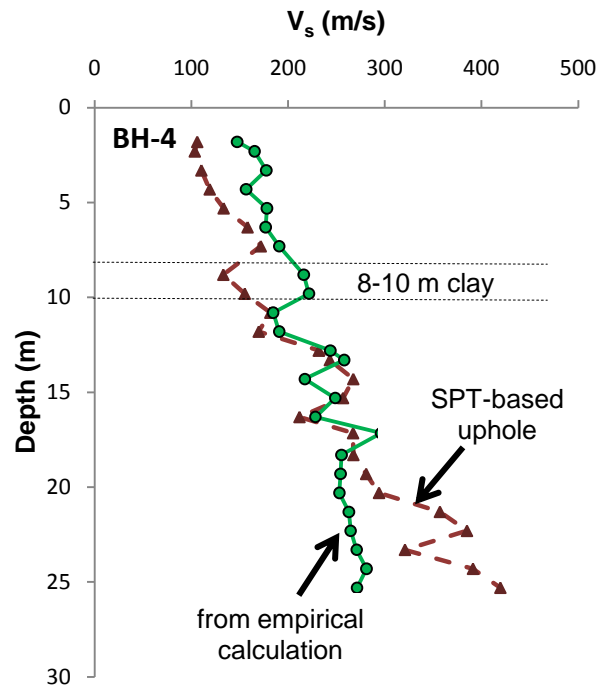


Fig.6.32. Comparison between measured and empirical  $V_s$  for BH-4

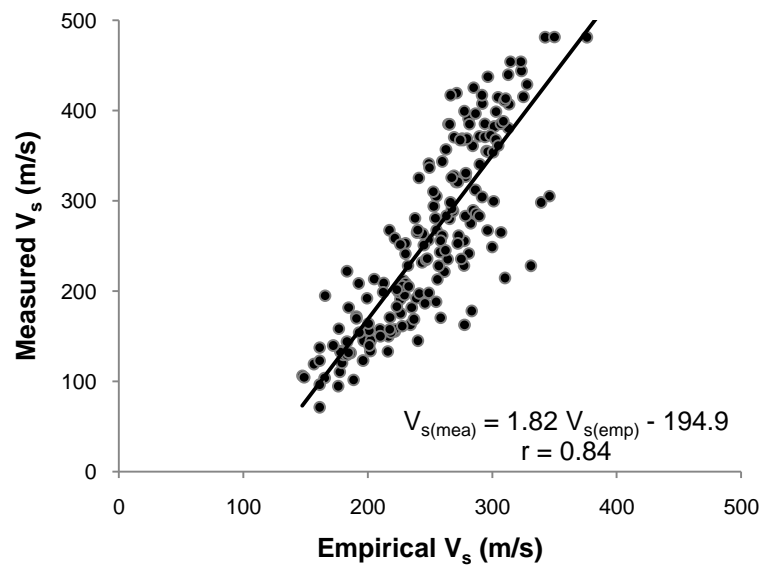


Figure 6.33. Linear relationship between measured and empirically calculated  $V_s$  for alluvial sand (A-2)

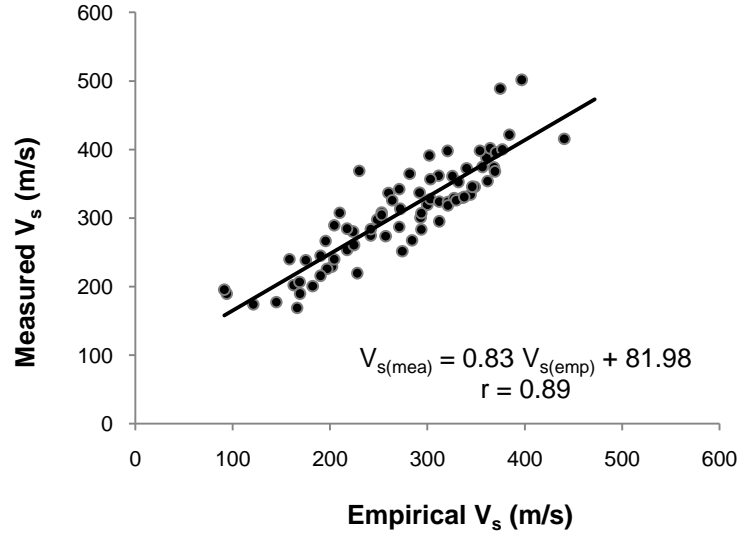


Figure 6.34. Linear relationship between measured and empirically calculated  $V_s$  for Pliocene sand (P-2)

All available SPT-based uphole test results from 10 boreholes are evaluated using the same procedure. As seen in Figure 6.31, some empirical calculations at different depths may not exactly fit to the measured  $V_s$  in BH-4. Therefore, the empirical calculations are re-performed using  $G_{\max}$ - $V_s$  relationship and a site-specific version of Equation 6.4 (Ohta and Goto, 1976; Seed et al., 1986) is proposed for the study area. During the development of a site-specific formula, a new  $\alpha$  coefficient is defined for each soil type instead of 20000 value for sandy layers in Equation 6.4.

$$G_{\max} = \alpha (N_1)_{60}^{0.333} (\sigma'_m)^{0.5} \quad (6.23)$$

The variation of  $\alpha$  coefficient with depth is plotted in Figures 6.35 and 6.36 for alluvial and Pliocene sands. It should be noted that the exponent of  $\sigma'_m$  <sup>(0.5)</sup> is not changed and it would be consistent with the laboratory data for uncemented sandy soils. The new  $\alpha$  coefficient may be affected from in-situ effects such as different cementation, grain-size distribution, overconsolidation, and/or site-specific conditions for different type of sandy soils. Therefore, the new depth-dependent coefficient may not be universally applicable.

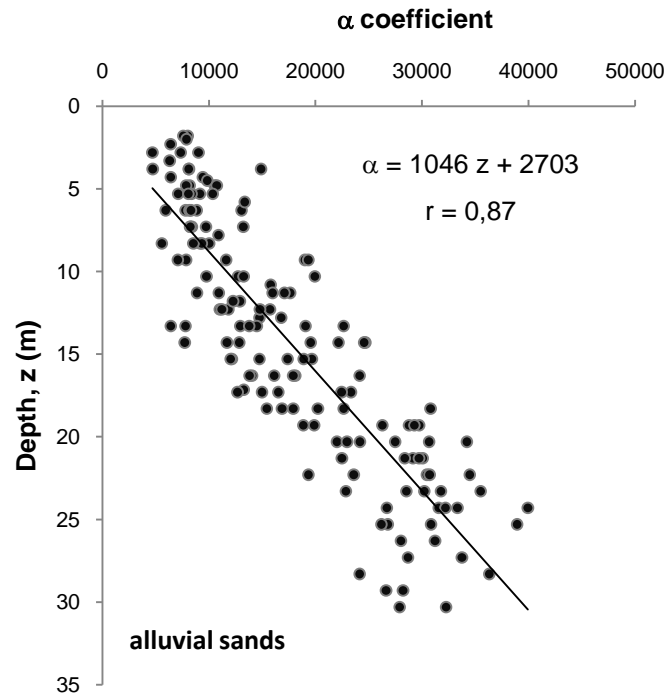


Figure 6.35. Variation of new  $\alpha$  coefficient with depth for alluvial sands

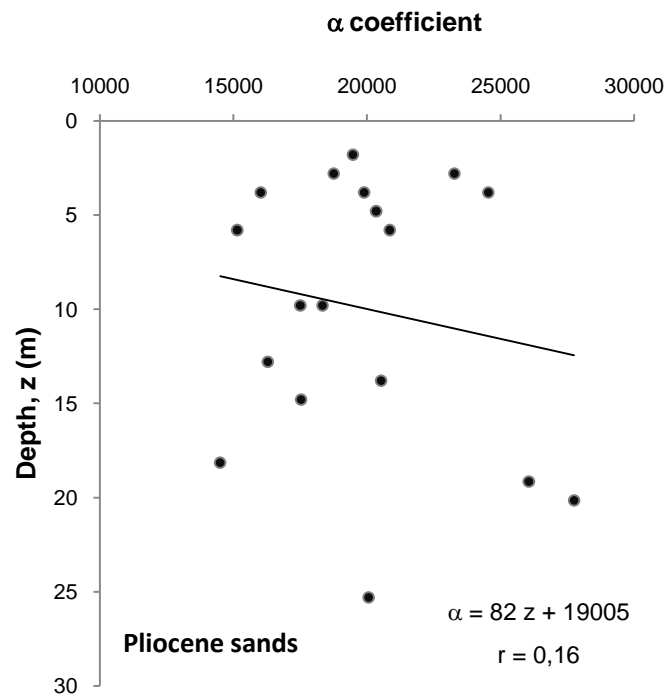


Figure 6.36. Variation of new  $\alpha$  coefficient with depth for Pliocene sands

As seen from Figure 6.35, the relation between new  $\alpha$  coefficient and depth presents a higher correlation coefficient ( $r=0.87$ ) for the Erbaa alluvial sands. However, a significant pattern cannot be obtained for Pliocene sands since the variation of  $\alpha$  is limited between 14000 and 27000. The low correlation coefficient for Pliocene sands may be attributed to the fact that the Pliocene unit in Erbaa dominantly contains clay and silt with a few sandy layers. Therefore, limited data are available for Pliocene sand. It should also be noted that the refusal SPT-N blow counts were mostly obtained from Pliocene layers. Additionally, the groundwater level in Pliocene is deeper than in alluvium. The abovementioned factors may cause the scattering of new  $\alpha$  coefficient for Pliocene sand (Figure 6.36).

The variation of vertical effective stress ( $\sigma_v'$ ) is also investigated using constant and variable  $\alpha$  coefficients as well. The distribution of effective stress throughout depth for constant and variable  $\alpha$  coefficient is depicted in Figures 6.37 and 6.38.

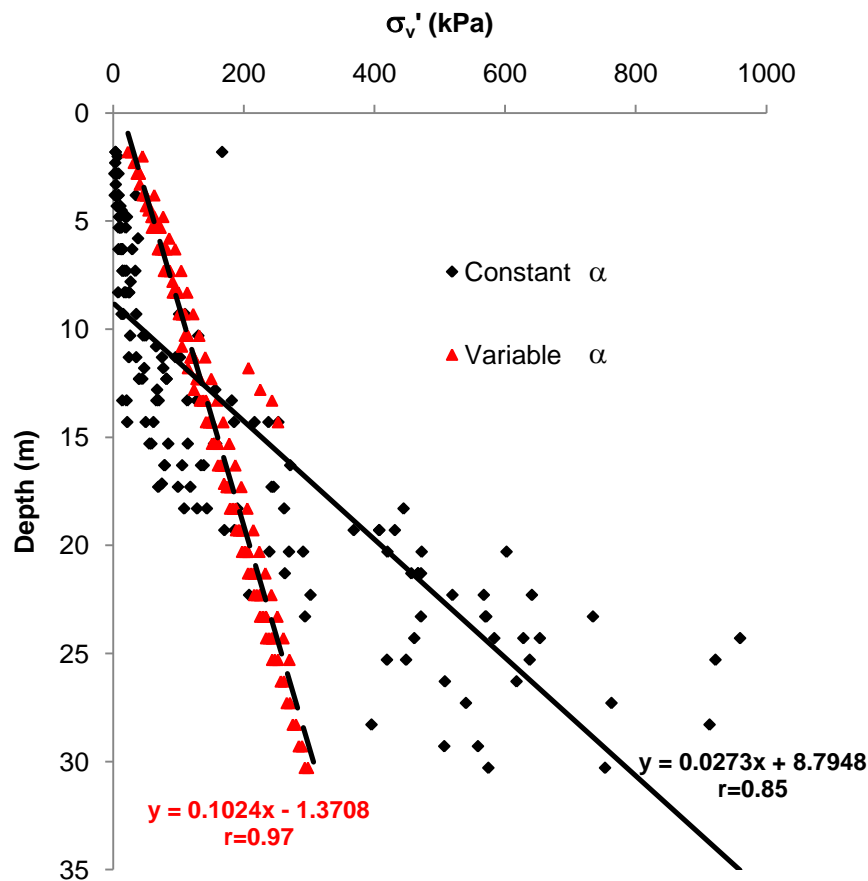


Figure 6.37. Variation of vertical effective stress using constant and variable  $\alpha$  coefficients for alluvial sands

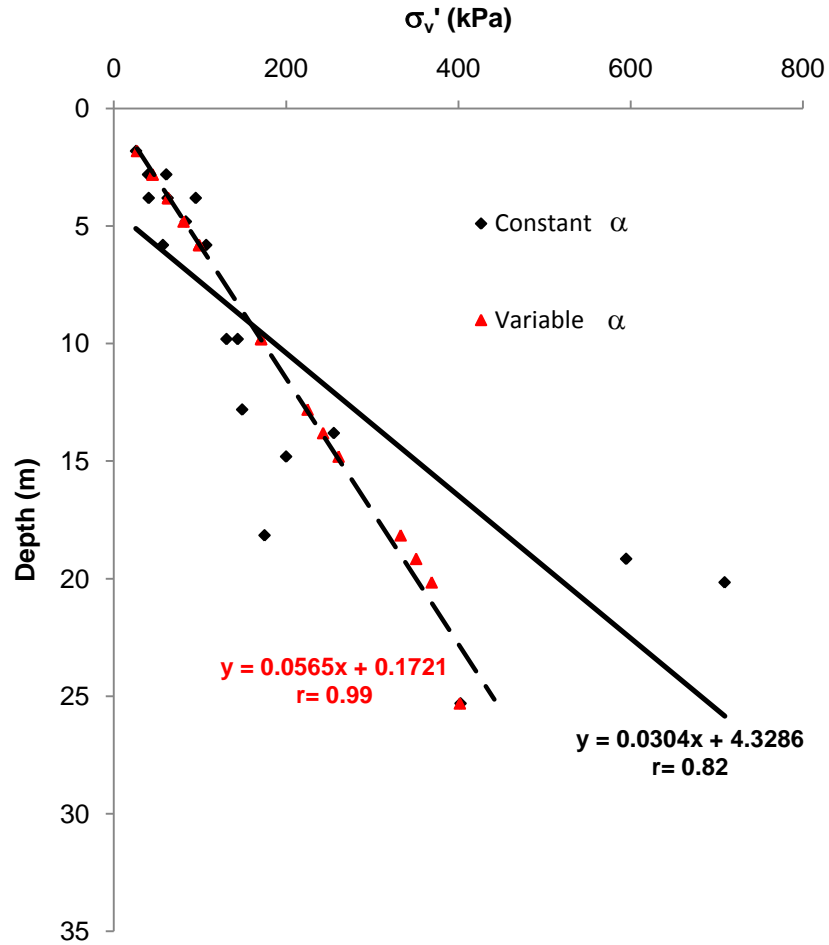


Figure 6.38. Variation of vertical effective stress using constant and variable  $\alpha$  coefficients for Pliocene sands

The proposed variable  $\alpha$  coefficient provides a good fit to the vertical effective stress data as can be seen in Figures 6.37 and 6.38. Therefore, the use of proposed variable  $\alpha$  coefficient approach for Erbaa soils is appropriate regarding the the regression coefficient of the linear relationships.

Furthermore, after the construction of new  $\alpha$  coefficient for Erbaa alluvial sands, the calculations are modified using the site-specific equation (Equation 6.23) with a new proposed  $\alpha$  coefficient. The updated calculation for BH-4 is given in Figure 6.39.

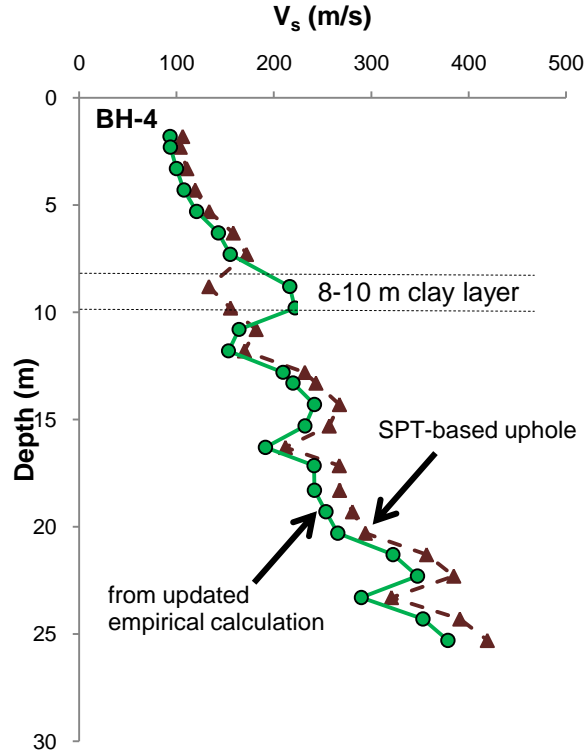


Figure 6.39. Comparison between measured and empirically calculated  $V_s$  with new  $\alpha$  coefficient for BH-4

The updated results reveal that the calculations are well-correlated with the measurements. As seen in Figure 6.39, the updated empirical calculations reflect quite similar results with the measured shear wave velocity. Additionally, the comparisons between measured and the updated version of empirically calculated  $V_s$  with the new  $\alpha$  coefficient are also modified.  $G_{\max}$  values are re-calculated using Equation 6.23. Then, calculated results are compared to  $G_{\max}$  values retrieved from uphole-based shear wave velocities (Figures 6.40 and 6.41).

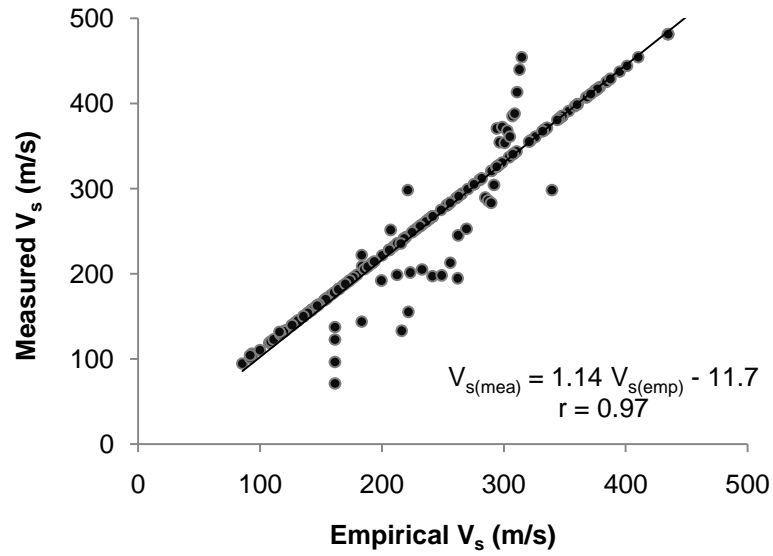


Figure 6.40. Linear relationship between measured and empirically calculated  $V_s$  with new  $\alpha$  coefficient for alluvial sand (A-2)

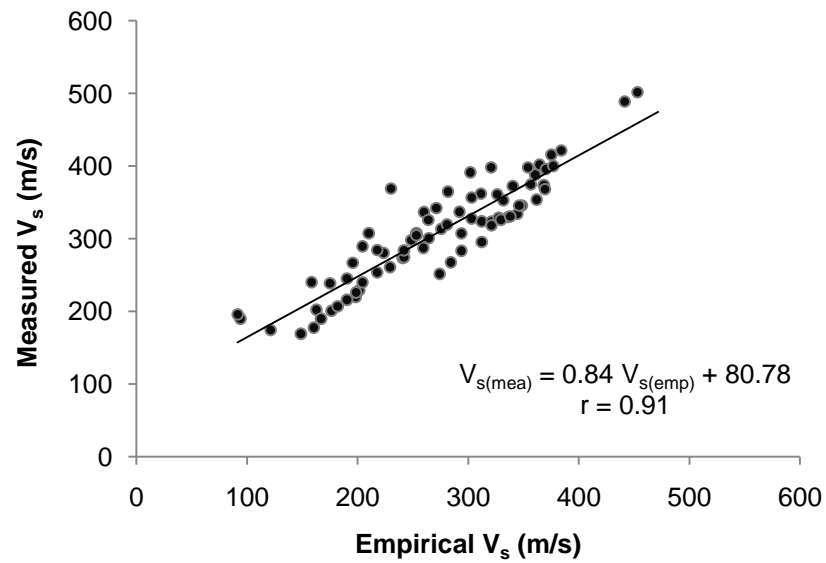


Figure 6.41. Linear relationship between measured and empirically calculated  $V_s$  with new  $\alpha$  coefficient for Pliocene sand (P-2)

The modified site-specific empirical equation for shear wave velocity exhibits significantly better results when compared to the measured shear wave velocities in Erbaa. After the application of new  $\alpha$  coefficient, the relationship is particularly improved for alluvial sands.



Consequently, the measured shear wave velocity profiles for alluvial sand and Pliocene sand are considered for further site response analyses.

Additionally, the empirical correlations are evaluated and an overall comparison for  $V_s$  calculations is performed including newly proposed SPT- $N_{30}$  based formulas. The difference between the shear wave velocities determined from SPT-N ( $N_{30}$ ) and SPT ( $N_{1,60}$ ) values can be seen in Figure 6.42. As a result, corrected SPT-N ( $N_{1,60}$ ) based empirical  $V_s$  estimations reveal more reasonable results than those obtained from SPT- $N_{30}$  especially for sandy layers with respect to SPT-based uphole results. It is also important to develop sensitive approaches since SPT- $N_{1,60}$  values exhibit logical results for sandy layers considering the depth effects, confining pressure, and SPT corrections. Therefore, indirect SPT- $N_{1,60}$  -  $V_s$  relationships should be preferred.

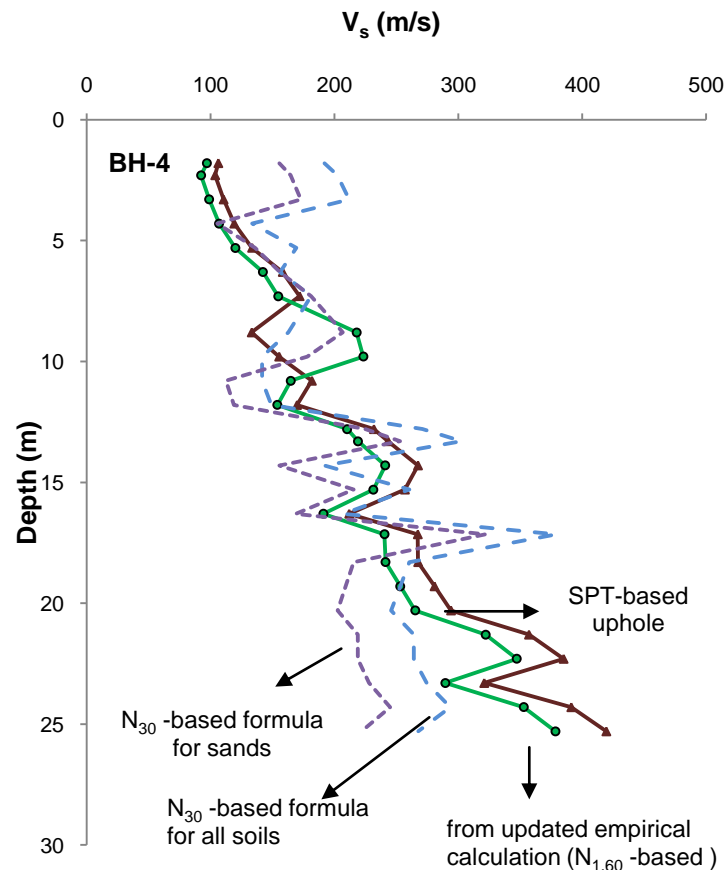


Figure 6.42. Comparison of SPT  $N_{30}$  and  $N_{1,60}$  based empirical formulas with measured  $V_s$  values

Moreover, the empirical calculation of shear wave velocity for clay layers is explained previously. Accordingly, alluvial clay units are evaluated on the basis of Equation 6.2. Besides, Pliocene clay layers are evaluated in accordance with overconsolidation ratio and plasticity index as given in Table 6.2. Therefore, the clay layers are tried to be compared separately. On the contrary, due to the limited number of data from Pliocene and alluvium clays, the calculations are considered merely for further site response analyses.

#### 6.3.4 Site classification based on $V_s$ soil profiles and determination of $V_{s30}$ for Erbaa

Amplification behavior can be estimated for different categories of site conditions. Site classification can be based on average shear wave velocity from upper 30 m, surface geology, and geotechnical data including stiffness, depth, and material type (Kramer and Stewart, 2004). The average shear wave velocity for the upper 30 m ( $V_{s30}$ ) is an extensively used parameter for classifying sites to predict amplification potential (Boore, 2004). The value of  $V_{s30}$  is computed by dividing 30 m by the travel time of a shear wave from surface to 30 m depth. Normally, the expression for  $V_{s30}$  is given as:

$$V_{s30} = \sum_{i=1}^n \left( \frac{\Delta Z_i}{V_{si}} \right) \quad (6.24)$$

where  $n$  is the number of soil layers of consistent velocity in the upper 30m,  $\Delta z_i$  is the thickness of the  $i^{\text{th}}$  layer, and  $V_{si}$  is the shear wave velocity of  $i^{\text{th}}$  layer.

It is a significant parameter used for the classification of sites for loss estimation and the development of recent building codes (e.g., Dobry et al., 2000; BSSC, 2001). It was first adopted by Borchardt (1994) based on data from the Western USA. It has also been used to predict amplification in deep basins (Park and Hashash, 2004) or in tectonically active regions (Stewart et al., 2003). Site classification and building code developers have applied shallow shear-wave velocity models in the form of site classification maps to derive strong ground motion prediction equations (Boore et al., 1997; Wills et al., 2000; Boore, 2004; Kanlı et al., 2006). The  $V_{s30}$ -based site classification scheme in the NEHRP provisions is presented in Table 6.8.

Table 6.8. Site categories in NEHRP and CGS Provisions for the design of new structures (Category Description Mean Shear Wave Velocity to 30 m) (Martin, 1994; Dobry et al., 2000) (modified from Bozorgnia and Campbell, 2004)

NEHRP category <sup>a</sup>		Description	Mean shear wave velocity for 30m $V_{s30}$ (m/s)		
Code	CGS		Code	CGS <sup>b</sup>	Nominal <sup>c</sup>
A	A	Hard Rock	> 1500 m/s	>1695	1890
	AB	A-B boundary		1315-1695	1500
B	B	Firm to hard rock	760-1500 m/s	945-1315	1130
	BC	B-C boundary		660-945	760
C	C	Dense soil, soft rock	360-760 m/s	460-660	560
	CD	C-D boundary		315-460	360
D	D	Stiff soil	180-360 m/s	225-315	270
	DE	D-E boundary		165-225	180
E	E	Soft clays	< 180 m/s	<165	150
F	-	Special study soils, e.g., liquefiable soils, sensitive clays, organic soils, soft clays > 36 m thick	-	-	-

<sup>a</sup> National Hazard Reduction Program (NEHRP) site class definitions: Code, as defined in the 1997 Uniform Building Code (UBC) and 2000 International Building Code (IBC); CGS, as defined by the California Geological Survey.

<sup>b</sup> Approximate ranges of  $V_{s30}$  proposed to use in assigning CGS NEHRP site classes when  $V_{s30}$  is known.

<sup>c</sup> Single best estimate of  $V_{s30}$  to use for each NEHRP site class when no other information is available.

Bozorgnia and Campbell (2004) described two different methods that could be used to classify a site in terms of shear wave velocity. The first method was based on  $V_{s30}$ . The second method was based on the effective velocity which was defined as the average value of  $V_s$  over a depth equal to a quarter-wavelength of a ground motion parameter of specified period or frequency. In some cases, shear wave velocity data does not extend to depths as large as 30m. Boore (2004) proposed three different exploration methods to calculate  $V_{s30}$  for the models that do not reach 30 m. As given in Equation 6.25, the time-averaged velocity to depth,  $d$ , can be computed.

$$\tilde{V}_s(d) = d/tt(d) \quad (6.25)$$

where the travel time  $tt(d)$  is given by

$$tt(d) = \int_0^d dz/V_s(z) \quad (6.26)$$

where  $V_s(z)$  is the depth-dependent velocity model

Depending on this assumption, following methods were proposed by Boore (2004);

1. Extrapolation assuming constant velocity below the explored depth : If the velocity model is available only to depth d, an assumption of constant velocity between d and 30 m can be applied to compute an estimate of  $V_{s30}$  using the following equation:

$$\tilde{V}_{s30} = 30/(t(d) + (30-d)/V_s(d)) \quad (6.27)$$

2. Extrapolation based on the velocity profile above depth, d: Regression analysis can be used to evaluate the shear wave velocity profile above depth, d. The resulting expression can then be used to extrapolate to 30m depth.

$$\log V_{s30} = a + b \log V_s(d) \quad (6.28)$$

the a and b regression coefficients can be defined by using Table 6.9.

Table 6.9 Summary of regression coefficients for Equation 6.28

d	a	b	$\sigma$
10	4.2062E - 02	1.0292E + 00	7.1260E - 02
11	2.2140E - 02	1.0341E + 00	6.4722E - 02
12	1.2571E - 02	1.0352E + 00	5.9353E - 02
13	1.4186E - 02	1.0318E + 00	5.4754E - 02
14	1.2300E - 02	1.0297E + 00	5.0086E - 02
15	1.3795E - 02	1.0263E + 00	4.5925E - 02
16	1.3893E - 02	1.0237E + 00	4.2219E - 02
17	1.9565E - 02	1.0190E + 00	3.9422E - 02
18	2.4879E - 02	1.0144E + 00	3.6365E - 02
19	2.5614E - 02	1.0117E + 00	3.3233E - 02
20	2.5439E - 02	1.0095E + 00	3.0181E - 02
21	2.5311E - 02	1.0072E + 00	2.7001E - 02
22	2.6900E - 02	1.0044E + 00	2.4087E - 02
23	2.2207E - 02	1.0042E + 00	2.0826E - 02
24	1.6891E - 02	1.0043E + 00	1.7676E - 02
25	1.1483E - 02	1.0045E + 00	1.4691E - 02
26	6.5646E - 03	1.0045E + 00	1.1452E - 02
27	2.5190E - 03	1.0043E + 00	8.3871E - 03
28	7.7322E - 04	1.0031E + 00	5.5264E - 03
29	4.3143E - 04	1.0015E + 00	2.7355E - 03

The extrapolation based velocity statistics to determine site class which was also described in the study of Boore (2004) was the third method. However, it will not be presented here to give so much detail about the method.

Boore (2004) emphasized that none of the methods mentioned above should be expected to give an exact value of  $V_{s30}$  for a specific site. These statistical procedures can be applied only in regression analysis or unimportant particular sites.

$V_{s30}$  values are calculated for each borehole using the actual  $V_s$  data where it was available. Nevertheless, some boreholes in the study area do not reach to 30 m depth. Considering the smooth curve between the deepest data and 30 m, SPT-based uphole boreholes are evaluated and the relationships of  $V_s$  values are proposed for each borehole to estimate  $V_{s30}$  by extrapolation. One of the relations belong to BH-4 is illustrated in Figure 6.43.

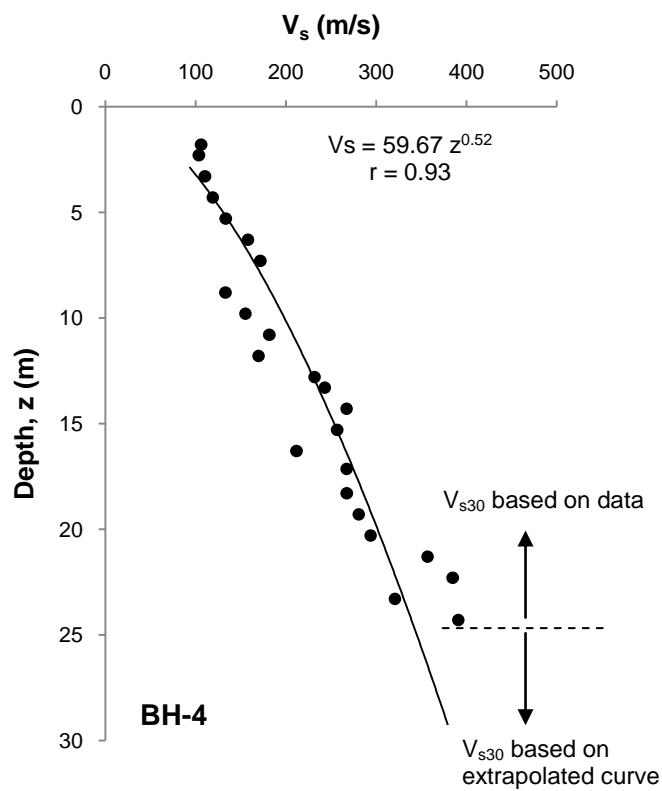


Figure 6.43. Relationship between shear wave velocity and depth for BH-4

The other power-law relationships obtained from SPT-based uphole boreholes are summarized in Table 6.10. These proposed relationships are used for the estimation of  $V_{s30}$  values for boreholes that do not reach to 30 m depth. The closest SPT-based uphole borehole is considered during the extrapolation of shear wave velocity.

Table 6.10. Power-law relationships for SPT-based uphole boreholes

BH No	Power-law relationship	r
4	$V_s = 59.67 z^{0.52}$	0.93
6	$V_s = 53.76 z^{0.62}$	0.96
8	$V_s = 48.73 z^{0.58}$	0.98
10	$V_s = 82.89 z^{0.49}$	0.92
18	$V_s = 67.73 z^{0.49}$	0.95
28	$V_s = 82.43 z^{0.45}$	0.90
30	$V_s = 156.16 z^{0.21}$	0.64
12	$V_s = 112.33 z^{0.45}$	0.95
23	$V_s = 156.78 z^{0.25}$	0.97
33	$V_s = 152.92 z^{0.26}$	0.85

The soil profiles are prepared for site response analyses and the  $V_{s30}$  values are calculated for each borehole on the basis of Equation 6.24. The calculated  $V_{s30}$  values are summarized in Table 6.11.

Moreover, the  $V_{s30}$  soil profiles are also evaluated in terms of NEHRP site classification category. As a result, the  $V_{s30}$  values in the study area range between 180 and 360 m/s representing D type soil in accordance with NEHRP classification. D type soils can be classified as stiff soils. On the contrary, if the CGS (California Geological Survey) classification is considered, the soils in the study area can be distinguished in between C and D soil type.

The distribution of  $V_{s30}$  values in the study area is presented in Figure 6.44. The lowest shear wave velocity zones coincide with loose alluvial layers as shown in Figure 6.44. There also exist several small localized areas indicating C type soils with respect to NEHRP categorization in Pliocene unit at higher altitudes.

Table 6.11. Calculated  $V_{s30}$  values for each borehole in the study area

Borehole	$V_{s30}$	Borehole	$V_{s30}$	Borehole	$V_{s30}$	Borehole	$V_{s30}$
1	231	27	252	53	325	79	331
2	282	28	235	54	256	80	270
3	266	29	261	55	278	81	291
4	195	30	262	56	290	82	285
5	250	31	276	57	290	83	291
6	200	32	260	58	311	84	297
7	241	33	291	59	301	85	351
8	202	34	264	60	279	86	377
9	254	35	279	61	291	87	289
10	257	36	242	62	266	88	277
11	263	37	237	63	308	89	267
12	343	38	256	64	324	90	263
13	282	39	264	65	290	91	302
14	301	40	257	66	311	92	340
15	280	41	277	67	330	93	290
16	275	42	266	68	330	94	298
17	272	43	287	69	306	95	246
18	233	44	243	70	290	96	251
19	255	45	259	71	382	97	241
20	259	46	276	72	340	98	237
21	262	47	287	73	298	99	241
22	267	48	257	74	290	100	245
23	287	49	278	75	367	101	242
24	266	50	314	76	349	102	241
25	271	51	304	77	297	103	252
26	305	52	268	78	317	104	243

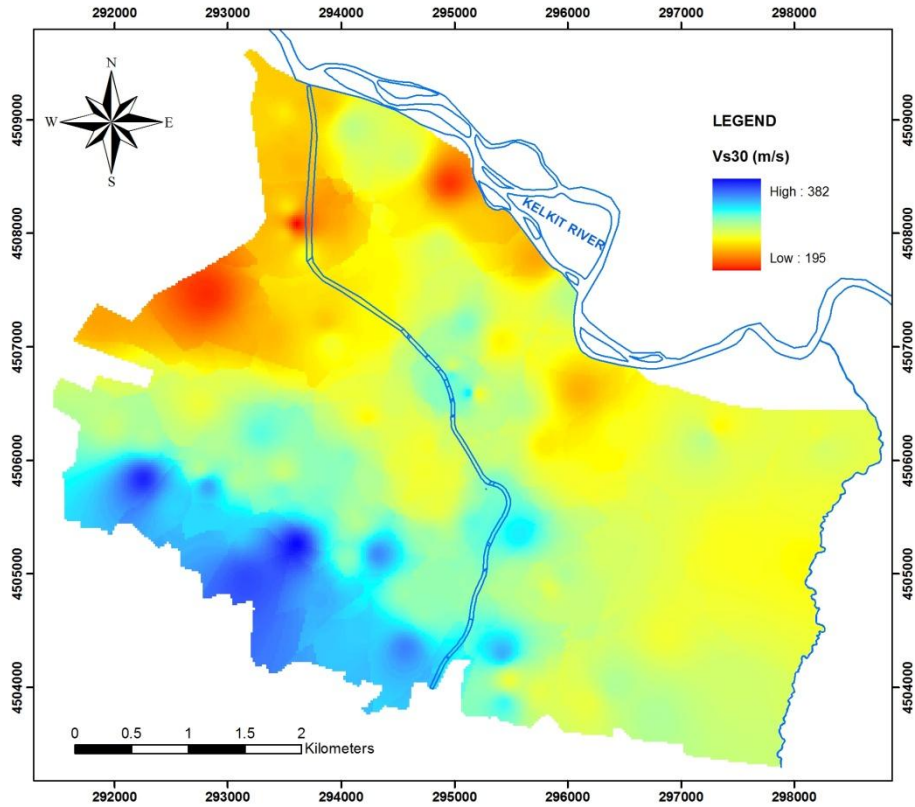


Figure 6.44.  $V_{s30}$  map of the study area

#### 6.4 Site Response Analyses

Site effects were observed in many disastrous seismic events in seismogenic areas such as 1985 Michoacan-Mexico (Seed and Sun, 1989), 1989 Loma Prieta (Seed et al., 1990), 1994 Northridge (Moehle, 1994), 1995 Kobe (Takemiya and Adam, 1997), 1999 Kocaeli (Tezcan et al., 2002; Ergin et al., 2004; Ozel and Sasatani, 2004) and 1999 Chi-Chi earthquakes (Pavlenko, 2008). The previous catastrophic earthquakes proved the importance of geologic and geomorphologic conditions on seismic site response. The 1985 Michoacan earthquake ( $M_s=8.1$ ) particularly caused severe damage in Mexico City inside the Mexico Valley which is approximately 400 km away from the epicenter in the Pacific Ocean. It was one of the great examples to understand the effects of amplification phenomena or the amount of site effects since the seismic waves were incredibly amplified inside the lake-bed zone of the valley (Vucetic and Dobry, 1991; Castro et al., 1990, Humprey and Anderson, 1992).



The variation in ground motions depending on the propagation of seismic waves in soil deposits or the existence of topographic features which contain a direct impact on the response of the structures can be defined as site effects (Phillips and Hashash, 2009). The process by which ground motions occur at a particular site is complex but can be classified into three categories (Figure 6.45).

- a. Source effects
- b. Path effects
- c. Site effects

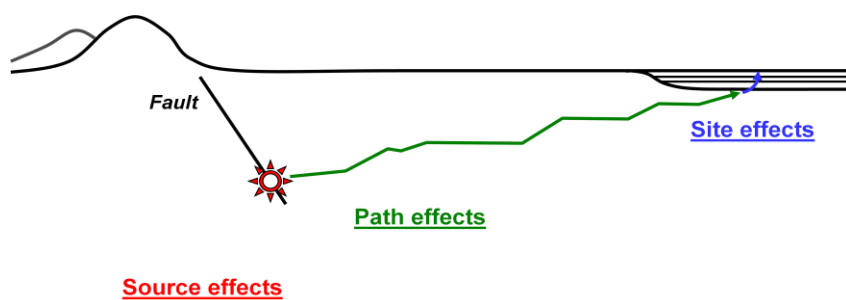


Figure 6.45. Effects of ground motion in soil layers

Source effects may occur randomly. The location of rupture initiation, the distribution of rupture pattern and the slip rate of seismic sources may vary for different faulting mechanisms. The propagation of seismic waves through the crust of the earth between the source and the site can be assigned to path effects. Finally, the change from bedrock motion to surface motion is affected by site effects which may produce amplification or de-amplification or be influenced by topographic effects. Site response analyses are widely used to quantify the effect of soil deposits on propagated ground motion. These methods can be divided into two main categories: (1) frequency domain analyses (including the equivalent linear method) and (2) time-domain analyses (including nonlinear analyses). Frequency domain methods have been more commonly used to estimate site effects with respect to their simplicity, flexibility and less computational requirements (Pitilakis, 2004; Arduino and Kramer, 2009; Phillips and Hashash, 2009). Numerous softwares are used to determine site response for different site conditions (Table 6.12).

Table 6.12. Softwares used for site response analyses (after Arduino and Kramer, 2009)

Dimension	Operating system	Equivalent Linear	Nonlinear
1-D	DOS	Dyneq, Shake91	AMPLE, DESRA, DMOD, FLIP, SUMDES, TESS
	Windows	ShakeEdit, ProSHAKE, Shake2000, EERA	CyberQuake, DeepSoil, NERA, FLAC, DMOD2000
2-D / 3-D	DOS	FLUSH, QUAD4/QUAD4M, TLUSH	DYNAFLOW, TARA-3, FLIP, VERSAT, DYSAC2, LIQCA, OpenSees
	Windows	QUAKE/W, SASSI2000	FLAC, PLAXIS

The simplest approach to evaluate a site response problem is to consider a single horizontal layer with infinite length and uniform characteristics, overlaying a rigid semi-infinite body. Numerical modeling with linear and nonlinear soil properties require quite sophisticated methods in 1-D, 2-D or in 3-D. Moreover, linear modeling might be easier to handle, but must include all kinds of possible propagating waves. For even 1-D nonlinear analysis, a good characterization of the mechanical properties of soil layers is required (Roca et al., 2006).

Most site response analyses solve the wave equations for 1-D wave propagation using equivalent linear analysis. Nonetheless, nonlinear approaches or solutions are also used in some cases in which 1-D equivalent linear analyses cannot represent the nonlinear, inelastic behavior of soil layers with sufficient accuracy (Pitilakis, 2004; Phillips and Hashash, 2009).

Site response analyses can be used to predict ground surface motions, and to evaluate dynamic stresses, strains, and ground failure potential. The results of ground surface motions obtained from site response analyses can be expressed in terms of time histories and response spectra. Liquefaction hazards, foundation loading and the response of retaining structures can be determined within the framework of site response analyses.

#### 6.4.1 1-D equivalent linear site response analyses

One-dimensional site response analyses are based on the assumption that all boundaries are horizontal and the response of a soil deposit is caused by SH-waves propagating vertically from the underlying bedrock. In other words, for 1-D ground response analyses, the soil and

bedrock surface are supposed to extend infinitely in horizontal direction (Kramer, 1996). In this study, software called ProSHAKE (v.1.12) (EduPro Civil Systems) is used to perform 1-D equivalent site response analyses. ProSHAKE (v.1.12) is a powerful, user-friendly computer program for one-dimensional, equivalent linear ground response analysis. The features of this software are highly compatible and allow evaluating modulus reduction and damping models. The graphical display of soil profile and input motion parameters, graphical display of a wide variety of output parameters, and animation of ground response are other advantages of ProSHAKE (v.1.12) software.

#### **6.4.1.1 Soil parameters used for site response analyses**

Firstly, the data from 104 boreholes are evaluated for site response analyses. Then, the shear wave velocity profile for each borehole is defined by dividing the soil profile into 3 m (for  $z < 100$  m) or 5 m (for  $z > 100$  m) sublayers. The laboratory and field test results are considered for employed soil properties as given in Chapter 4. As also previously mentioned, alluvial and Pliocene soil deposits are individually evaluated in four main soil groups: A1-Clay (alluvium clay), A2-Sand (alluvium sand), P1-Clay (Pliocene clay) and P2-Sand (Pliocene sand). The gravelly and silty soil layers are also considered. Instead of using default models, the essential modulus reduction and damping curves are calculated to model the soil units in the study area.

Modulus reduction and damping curves are needed to perform equivalent linear 1-D site response analysis. Hence, proper modulus reduction and damping curves are established using the Darendeli model (Darendeli, 2001) in this study. Accordingly, the model is reformulated with different confining pressures and the curves are similar to the EPRI (Electric Power Research Institute) curves. So, site-specific soil models are established producing modified  $G/G_{\max}$ -shear strain curves in this study (Kramer, 2009b). The  $G/G_{\max}$ -shear strain curves are produced for the four previously defined soil groups. The representative depths (in meters) mentioned in Table 6.5 are taken into consideration during the calculations to reflect different confining pressures. The modified curves are illustrated in Figures 6.46-6.53. In these figures, the symbol of each curve (e.g.  $G/G_{\max}$ -strain\_3) indicates the representative depth in meters (e.g. 3 meters) and the related confining pressure for the same depth.

The default curves are also used for gravel, silt and bedrock layers as defined in ProSHAKE (v.1.12) program. Furthermore, the average unit weight of the soil layers are determined from laboratory test results.

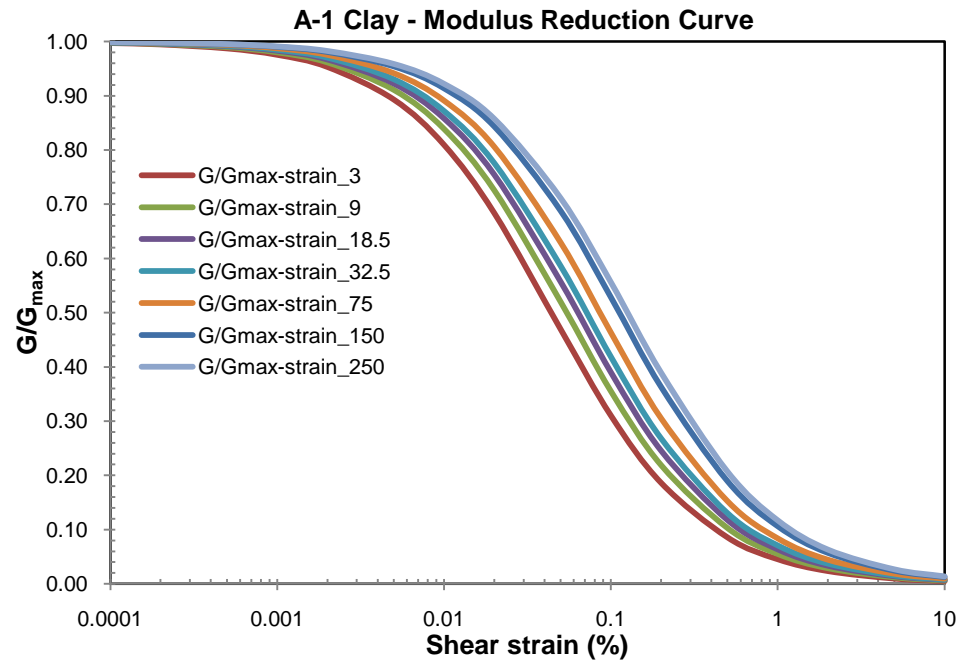


Figure 6.46. Modified modulus reduction curves for alluvium clay (A-1)

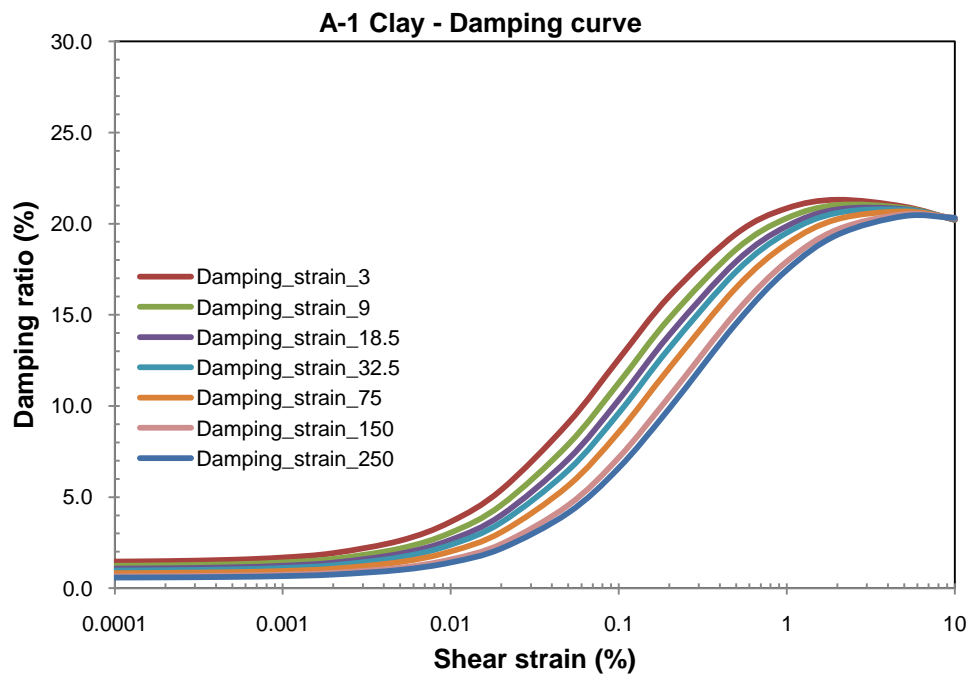


Figure 6.47. Modified damping curves for alluvium clay (A-1)

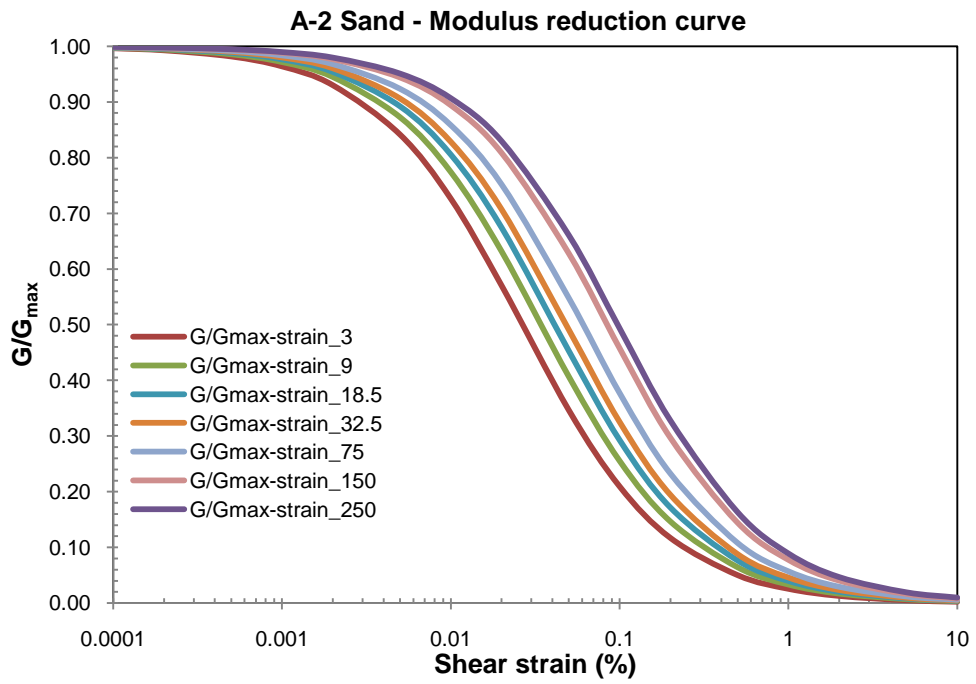


Figure 6.48. Modified modulus reduction curves for alluvium sand (A-2)

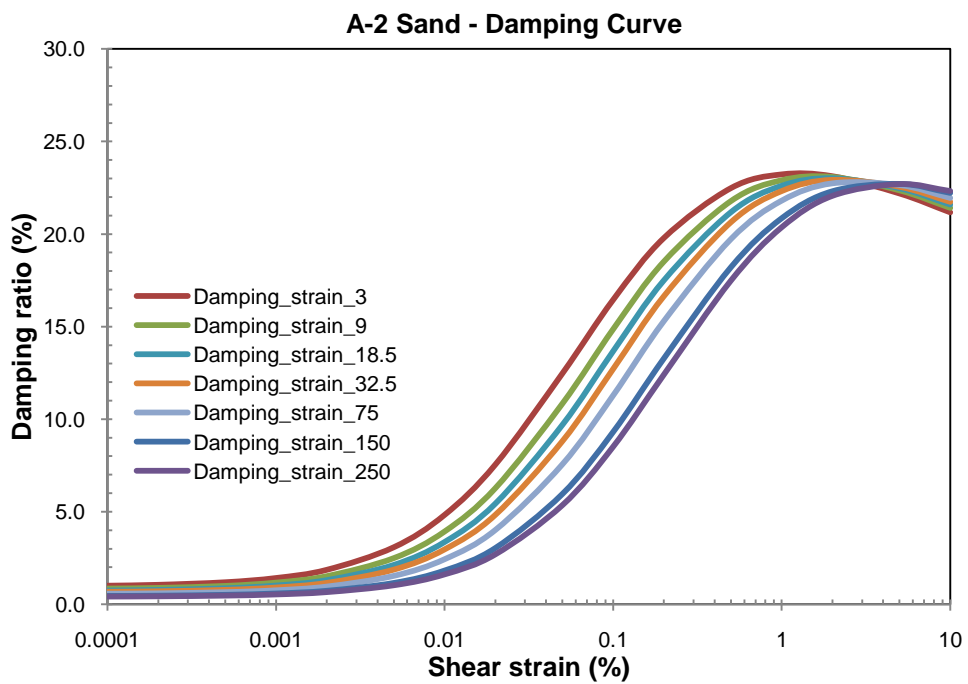


Figure 6.49. Modified damping curves for alluvium sand (A-2)

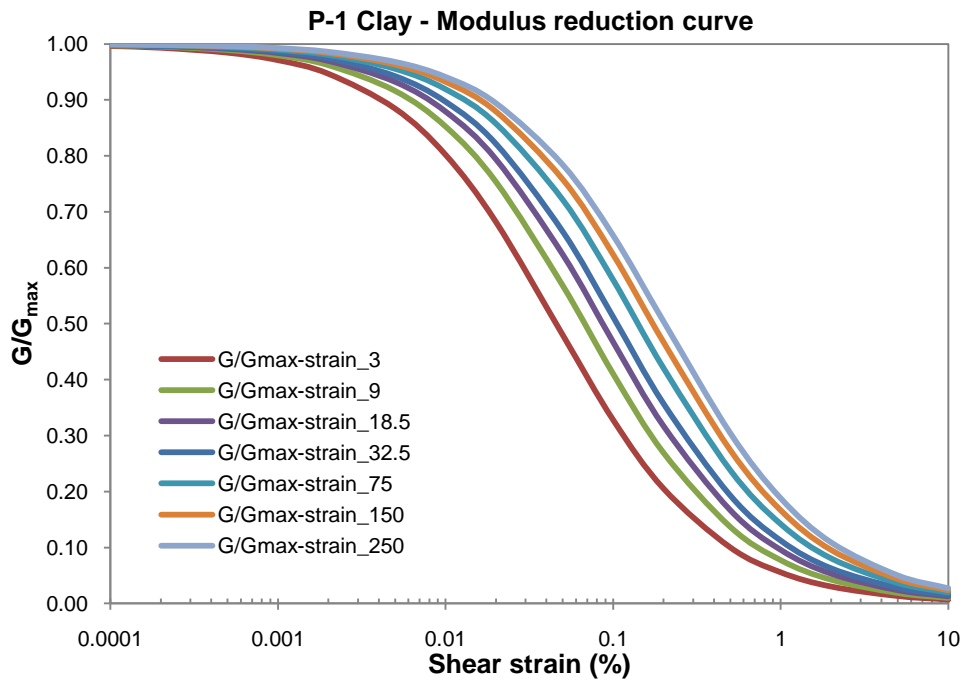


Figure 6.50. Modified modulus reduction curves for Pliocene clay (P-1)

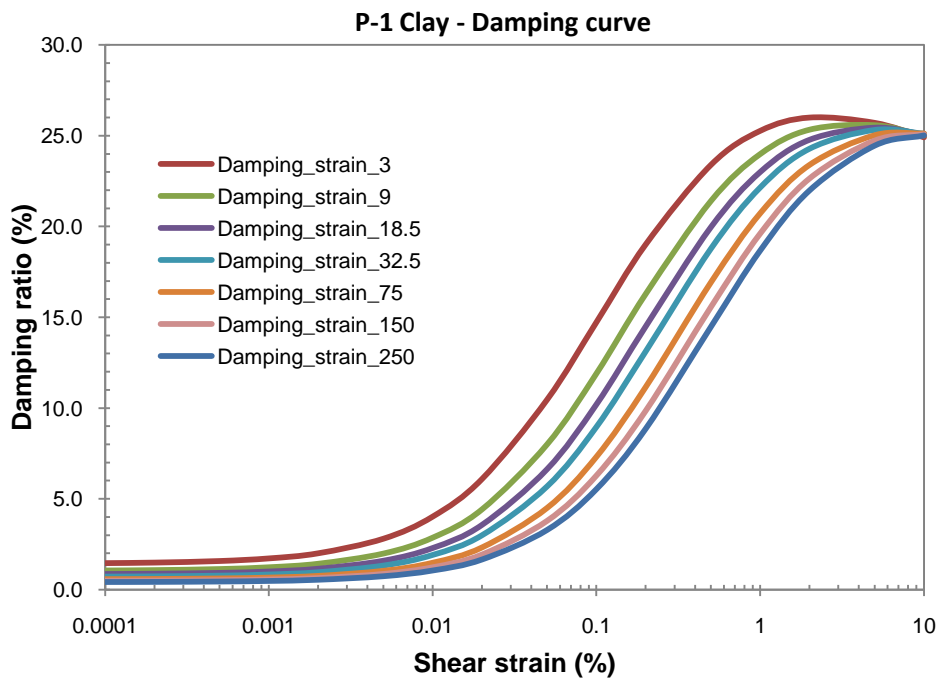


Figure 6.51. Modified damping curves for Pliocene clay (P-1)

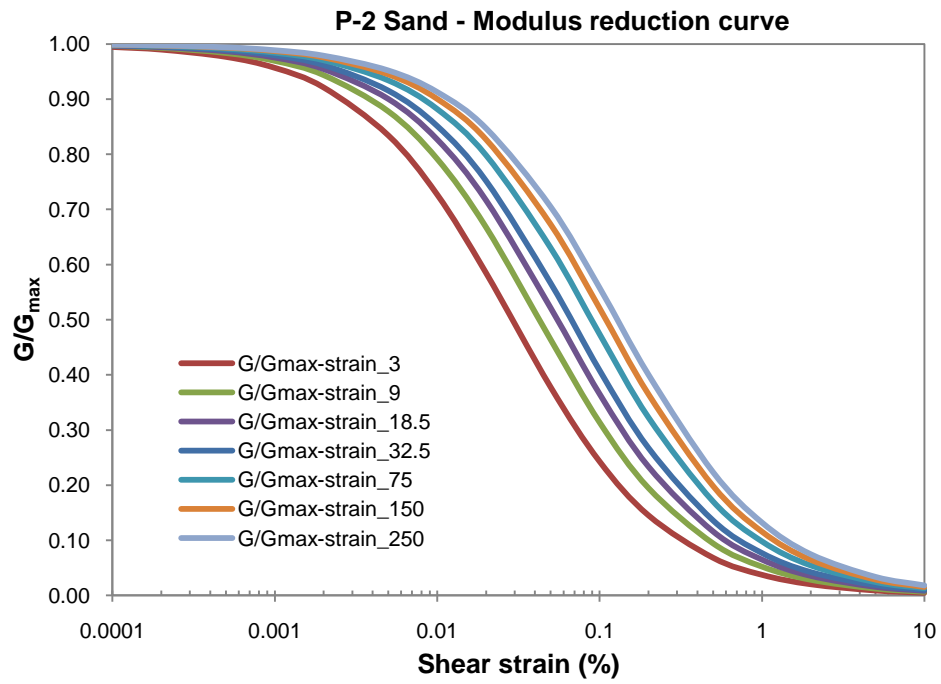


Figure 6.52. Modified modulus reduction curves for Pliocene sand (P-2)

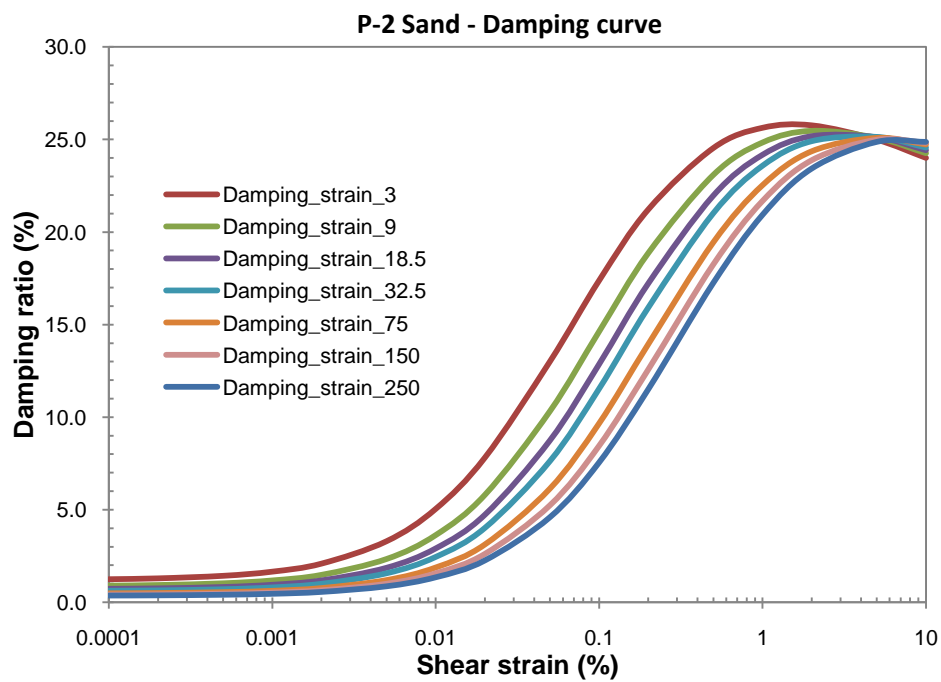


Figure 6.53. Modified damping curves for Pliocene sand (P-2)

#### 6.4.1.2 Modeling of soil profiles for site response analyses

Dividing a study area into grid cells is a common practice in seismic microzonation applications. The dimension of grid cells mostly depends upon the availability of geological, geophysical and geotechnical data for the investigated area. The most common grid sizes in the literature are 500 m x 500 m or 250 m x 250 m. Site characterization can be performed based on grid system using the available data for each cell by some authors (Matsuoka et al., 2006; Erdik et al., 2005; Ansal et al., 2006; Ansal and Tonuk, 2007).

Therefore, the study area, Erbaa settlement, is divided into 500 m x 500 m grid cells and seismic response analysis is performed for each cell. A total of 118 grid cells are formed for the study area (Figure 6.54). Afterwards, the results of representative soil profiles are statistically extrapolated for the entire study area.

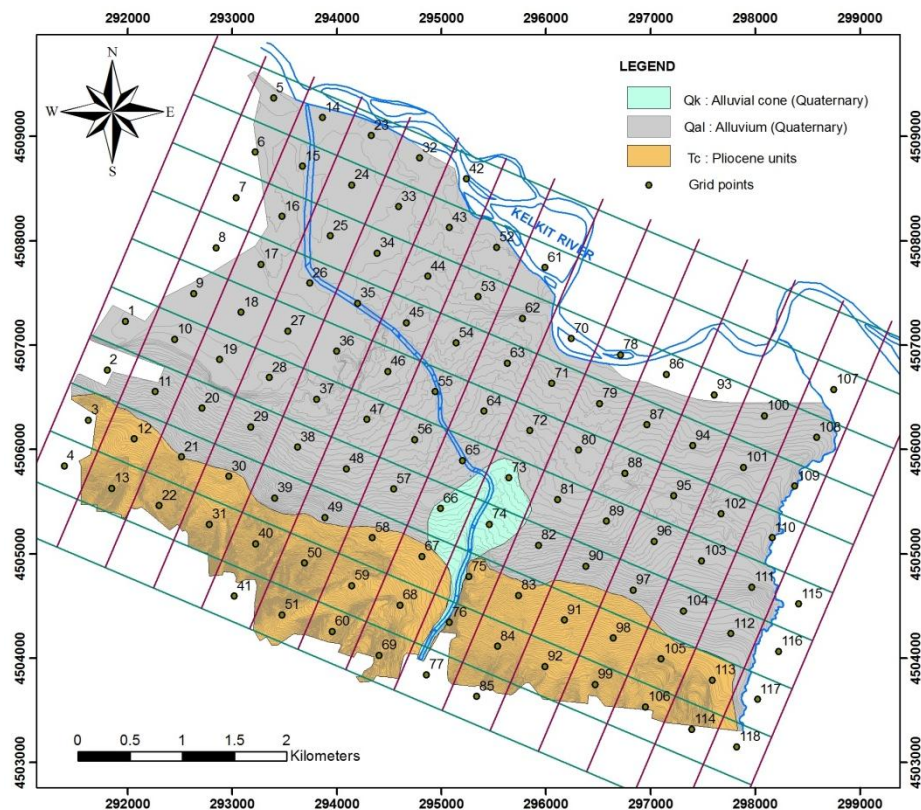


Figure 6.54. Grid system used for site response analysis in this study



The bedrock profiles are determined on the basis of the constant shear wave velocity ( $V_s=760$  m/s). Ansal and Tonuk (2007) mentioned that the shear wave velocity profiles should be established down to the depth of engineering bedrock with an estimated shear wave velocity of 700-750 m/s. However, B and C type soil boundary in NEHRP starts with 760 m/s indicating the boundary value of bedrock shear wave velocity. The same boundary value ( $V_s=760$  m/s) is accepted as bedrock shear wave velocity in Erbaa (Kramer, 2009b).

Accordingly, the soil profiles are extended using the power-law relationships given in Table 6.11 to the depth where the shear wave velocity is 760 m/s for boreholes in which shear wave velocities for rock are unavailable. The available data for each cell is used in site response analysis. For empty cell or unavailable data conditions, the nearest borehole data are used in order to perform site response analysis. As a result, a total of 118 soil profiles are obtained for the site response analyses.

#### **6.4.1.3 Ground motions used for site response analyses**

An earthquake magnitude of 7.2 with a 0-4 km rupture distance is accepted for the regional earthquake hazard analysis as aforementioned. As given in Chapter 5, scaled acceleration time histories are selected on the basis of best match to target spectra obtained from NGA ground motion models. In total, 14 (seven for Boore and Atkinson (2008) and seven for Campbell and Bozorgnia (2008) next generation attenuation relationships (NGA)) scaled acceleration time histories for each cell are defined previously. These 14 ground motions are employed as input motions in site response analyses. During analyses, the essential scaled peak ground acceleration (PGA) values (given in Table 5.18) are assigned for each analysis point.

#### **6.4.1.4 Input and output formats in ProSHAKE (v.1.12) software**

The proposed soil profiles and ground motions are used as inputs for site response analyses using ProSHAKE software. The data entry page of ProSHAKE (v.1.12) software is shown in Figure 6.55. Additionally, a soil profile graph after data entry is given in Figure 6.56. The input motions are assigned in the input motion section of the software (Figure 6.57).

ProShake Input Manager - C:\Program Files\ProShake\ProShake.exe

File Input Manager Solution Manager Output Manager Help

Profile Input Motion Report

Profile Title: BH-18\_final

No. of Layers: 32 Depth to Water Table: 6.6 ft 2.0 m

Summary Data

Layer No	Material Name	Thickness (m)	Unit Weight (kN/m <sup>3</sup> )	Gmax (MPa)	Vs (m/s)	Mod. Reduction Curve	Mod. Parameter	Damping Curve	Damping Parameter
1	Sand	3.8	19.0	28.0	122.0	ALSand	1.8	ALSandD	1.8
2	Sand	2.5	19.0	44.8	152.0	ALSand	5.1	ALSandD	5.1
3	Clay	3.0	19.0	56.0	170.0	ALClay	7.8	ALClayD	7.8
4	Sand	3.0	19.0	83.0	207.0	ALSand	10.8	ALSandD	10.8
5	Sand	3.0	19.0	106.1	234.0	ALSand	13.8	ALSandD	13.8
6	Sand	3.0	19.0	128.0	257.0	ALSand	16.8	ALSandD	16.8
7	Sand	3.0	19.0	212.3	331.0	ALSand	19.8	ALSandD	19.8
8	Sand	3.0	19.0	248.3	358.0	ALSand	22.8	ALSandD	22.8
9	Sand	3.0	19.0	287.2	385.0	ALSand	25.8	ALSandD	25.8
10	Sand	7.7	19.0	300.8	394.0	ALSand	31.2	ALSandD	31.2
11	Sand	5.0	19.0	306.9	398.0	ALSand	37.5	ALSandD	37.5
12	Sand	5.0	19.0	348.3	434.0	ALSand	42.5	ALSandD	42.5
13	Sand	5.0	19.0	387.1	447.0	ALSand	47.5	ALSandD	47.5

Select Output Units: ☐ U.S. ☒ S.I. View Profile

Figure 6.55. Input summary table in ProSHAKE (v.1.12) software

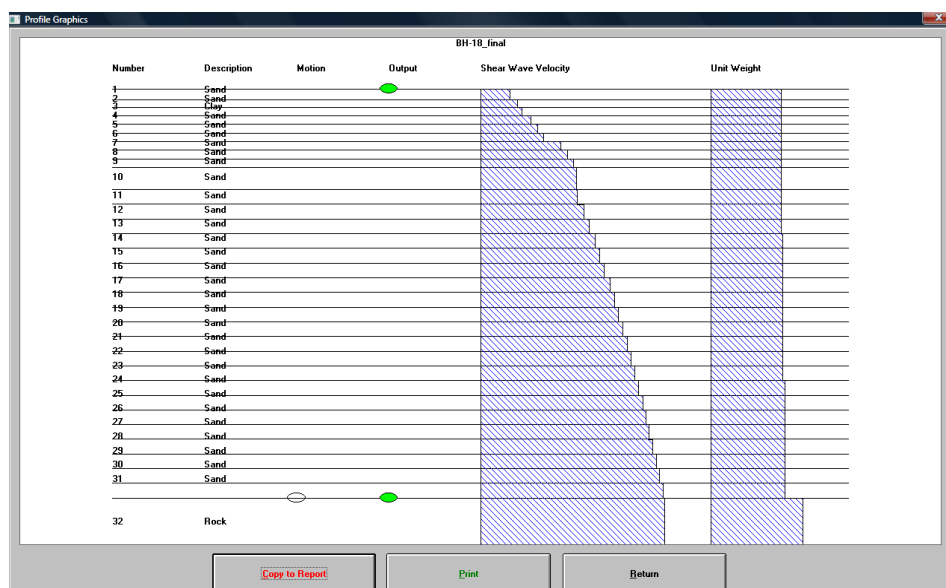


Figure 6.56. A soil profile in ProSHAKE (v.1.12) software

After running the ProSHAKE solution manager, ground surface motions and response spectra can be computed. The variation in motions is shown in Figure 6.58. The yellow color in Figure 6.58 represents the surface motion after site response analyses. The blue colored motion is the bedrock motion assigned as 9<sup>th</sup> earthquake in Table 5.18 in Chapter 5.

Additionally, it is possible to obtain response spectrum for each motion to be used in amplification ratio analyses.

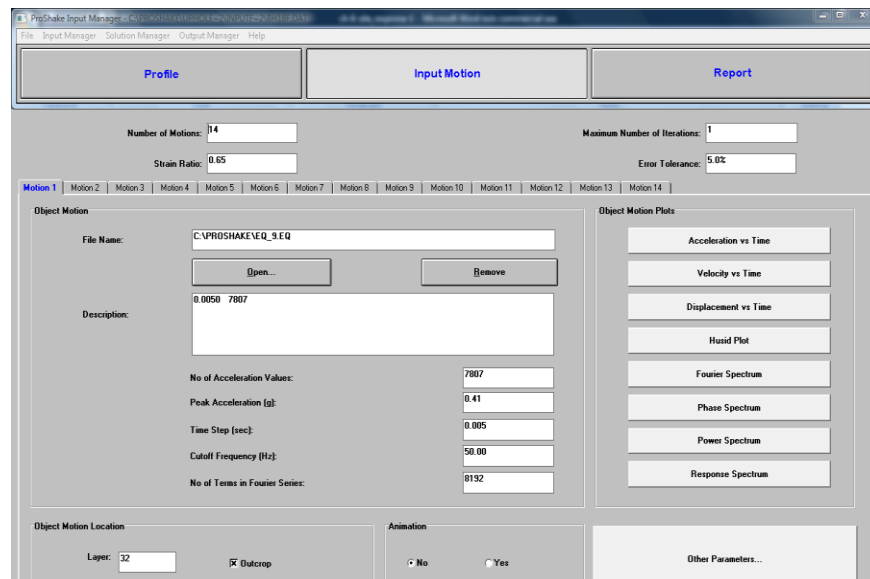


Figure 6.57. Assigning input motions for each profile in ProSHAKE (v.1.12) software



Figure 6.58. Output of ProSHAKE (v.1.12) software representing the variations in motions

## 6.5 Site Effects and Amplification

Site effects control the variation of ground surface motion components (amplitude, frequency content, and duration) caused by the incoming wave field due to properties of soil deposits properties and surface topography (Pitilakis, 2004). The modification of ground motion amplitudes can be expressed in terms of amplification or de-amplification. The amplification of ground motion is schematized in Figure 6.59.

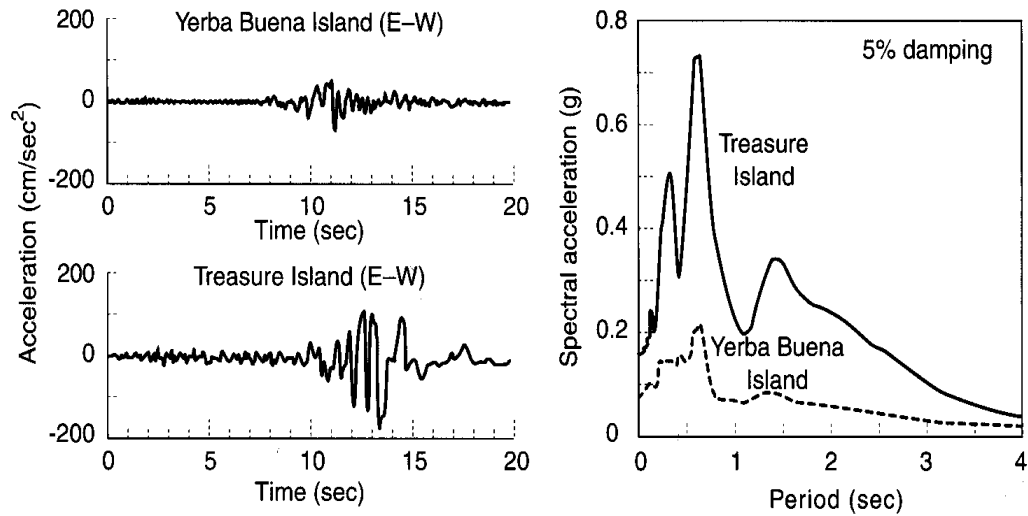


Figure 6.59. An amplification during 1989 Loma Prieta earthquake (after Kramer 2009a)

The amplification case shown in Figure 6.59 is from a site located 97 km from the epicenter of 1989 Loma Prieta earthquake ( $M_w = 7.1$ ). Soft soil conditions in the abovementioned site amplified bedrock motions by a factor of 2-3 as seen in both time history and spectral acceleration for different periods (Kramer, 2009a).

Site effects reflect the influence of local geology on the wavefield propagation. Local geology can influence soil depth, thickness and surface topography. Surface soil layers are responsible for significant amplification and variation of surface ground motion (Figure 6.60). Surface soil units and topography are the main parameters of site effects which are often quantitatively expressed by the amplification factor ( $A$ ) (Pitilakis, 2004).

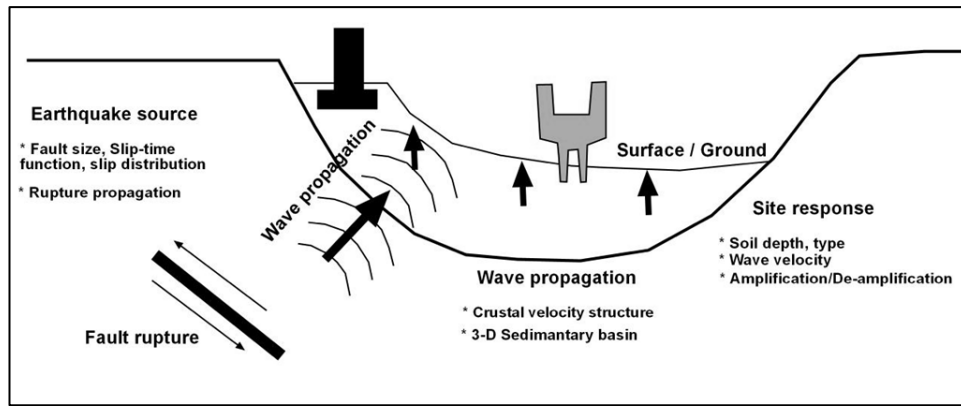


Figure 6.60. An illustration of wave propagation from rupture zone to surface

Site amplification is one of the important factors controlling damage in urban areas during strong earthquakes. Moreover, the attenuation functions and site amplification factors can be employed in the seismic hazard calculations of urban areas. Site amplification factors are appropriate tools for evaluating the effects of site conditions as well as the previously given techniques. Site conditions can be determined by site classifications for ground motion amplification purposes. Site classifications can be determined by means of surface geology, geotechnical data, and/or  $V_{s30}$  values to define amplification factors (Kramer and Stewart, 2004).

The determination of site amplification was performed using different site response estimation techniques. The calculation of the standard spectral ratio based on the spectrum of ground motions of an interested area over the spectrum of a rock site is mostly used to evaluate site effects. The evaluation methods of site effects were grouped into five main topics by Pitilakis (2004).

The methods are summarized in order to give information about these techniques.

1. Experimental-empirical techniques: These can be applied to analyze site effects in frequency domain.

Standard Spectral Ratio Technique (SSR) (Borcherdt, 1970) which depends on the availability of an adequate reference site was defined as the ratio of the Fourier amplitude

spectra of a soil-site record to that of a nearby rock-site record from the same earthquake and component of motion which is mentioned as commonly used technique (Figure 6.61).

Generalized Inversion Scheme Technique (GIS) which presents average amplitude as a function of distance can be estimated by Fourier amplitude spectra from the unknown source and site effects through least square weighted inversion.

Coda wave technique includes the latest part of the recordings (coda waves) where the time is twice of the first S wave arrival.

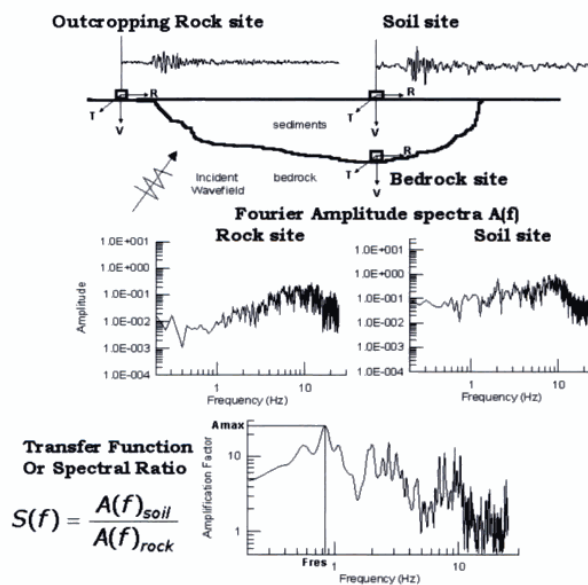


Figure 6.61. General description of the Standard Spectral Ratio Technique (SSR) (after Pitilakis, 2004)

Horizontal to Vertical Spectral Ratio Technique (HVSr) uses the spectral ratio of the horizontal to vertical component ground motion which exhibits similarities with SSR technique (Figure 6.62). HVSr method or H/V ratio known as Nakamura's (1989) technique was used in the microtremor based projects (e.g. Lermo and Chavez-Garcia, 1994; Tokimatsu et al., 1992; Bard et al., 1997; Mirzaoglu and Dikmen, 2003).

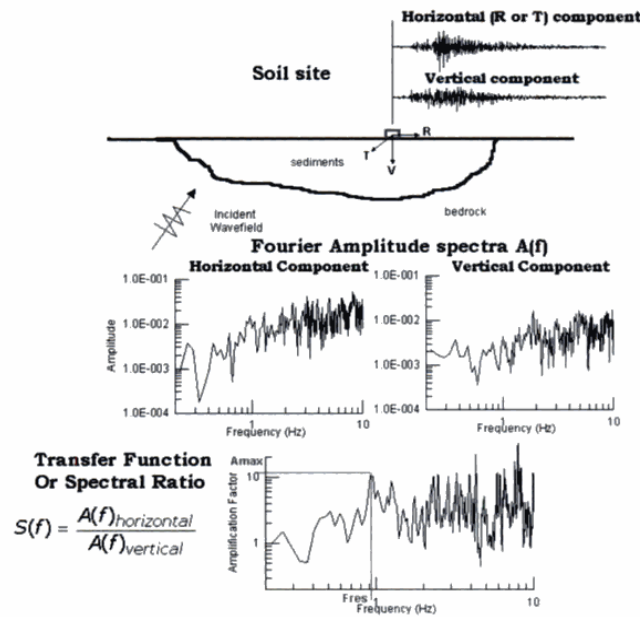


Figure 6.62. Description of the Horizontal to Vertical Spectral Ratio Technique (HVSr) (after Pitilakis, 2004)

2. Empirical techniques: There are a few proposed relationships exhibiting the amplification factors for the peak acceleration and/or average shear wave velocity of the soil profiles (Joyner and Fumal, 1984; Midorikawa, 1987, Borchardt et al., 1991). Moreover, Pitilakis (2004) stated that these empirical techniques should be applied in the preliminary stage or in the simplified evaluation of basic parameters for site amplification.

3. Semi-Empirical techniques: They can provide computing time histories of earthquake motion by the combination of recorded earthquake motions of smaller earthquakes (i.e. Green's functions).

4. Theoretical (Numerical and Analytical) methods: The geological structure of an area and the geotechnical characteristics of the site can be most efficient to calculate site effects thorough theoretical analysis. One of the simple analytical methods based on the fundamental period of the soil and the corresponding amplification factor can be applicable to estimate site effects in an area. This simple method requires soil density, thickness, S-wave velocity, and damping characteristics of soil layers.

5. Hybrid methods: The time histories of earthquake motions can be computed by considering longer and shorter periods separately.

Site response analyses are performed using different approaches in Erbaa. The obtained results from 1-D equivalent linear model using ProSHAKE (v.1.12) software are firstly evaluated. Furthermore, shear wave velocities are used to obtain amplification values using amplification equations in the literature. Afterwards, the site amplification factors based on Stewart et al. (2003) approach are considered. Finally, the period and amplification values gathered by microtremor measurements are compared to amplification values obtained from the site response analysis.

### 6.5.1 Amplification of soil deposits in Erbaa

The time-histories obtained from site response analyses can be used as the representative time-histories of surface motions. The direct use of response spectra of calculated surface motions is generally not preferred in practice. However, it is advantageous to obtain site amplification ratio from ground response analyses. Site amplification ratio is the ratio between response spectra of ground surface motions computed from ground response analyses and the response spectra of corresponding input rock motions. The time-histories obtained from ground response analyses can be used directly to represent ground surface motions, or synthetic time-histories can be developed to match the design ground surface response spectrum (U.S. Army Corps of Engineers, 1999).

In the site response analyses of Erbaa, input ground motions are considered using PGA values as given in Table 5.8. Afterwards, the ratio is calculated on the basis of site amplification ratio method using soil/bedrock ratio (Borcherdt, 1970) as given in Equation 6.29 to obtain amplification ratios (AF) for the study area.

$$AF = \frac{IM_{\text{soil}}}{IM_{\text{rock}}} \quad (6.29)$$

where IM : Intensity Measure

The distribution of selected input ground motions are depicted for BH-4 in Figure 6.63. The surface time histories obtained from the site response analyses are illustrated in Figure 6.64. The calculated amplification ratios are also shown in Figure 6.65 with respect to Boore and Atkinson (2008) (BA08) model as indicated in the previous sections which has been introduced that the input motions are scaled to be compatible with BA08 model. It should be noted that different distance zones are also considered during the site response analysis.



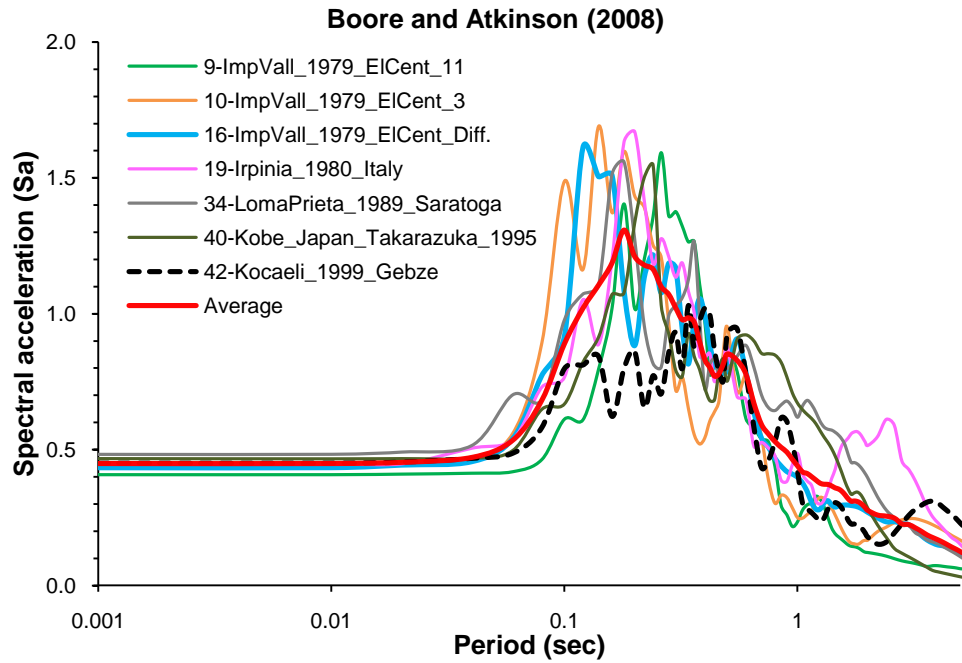


Figure 6.63. Input response spectra of BH-4 based on Boore and Atkinson (2008) model for 0 km distance zone

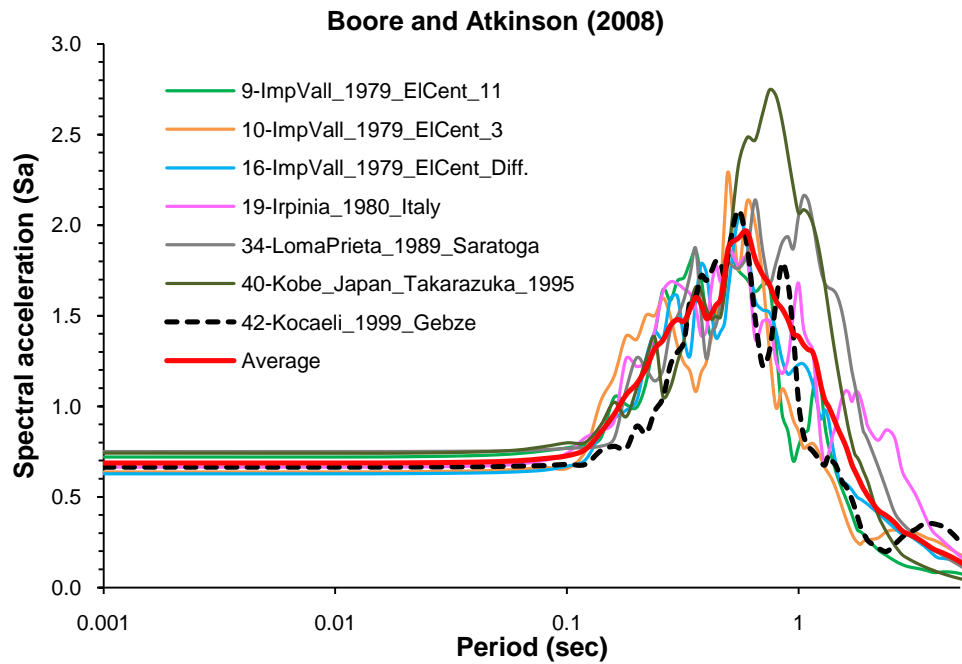


Figure 6.64. Surface response spectra of BH-4 based on Boore and Atkinson (2008) model for 0 km distance zone

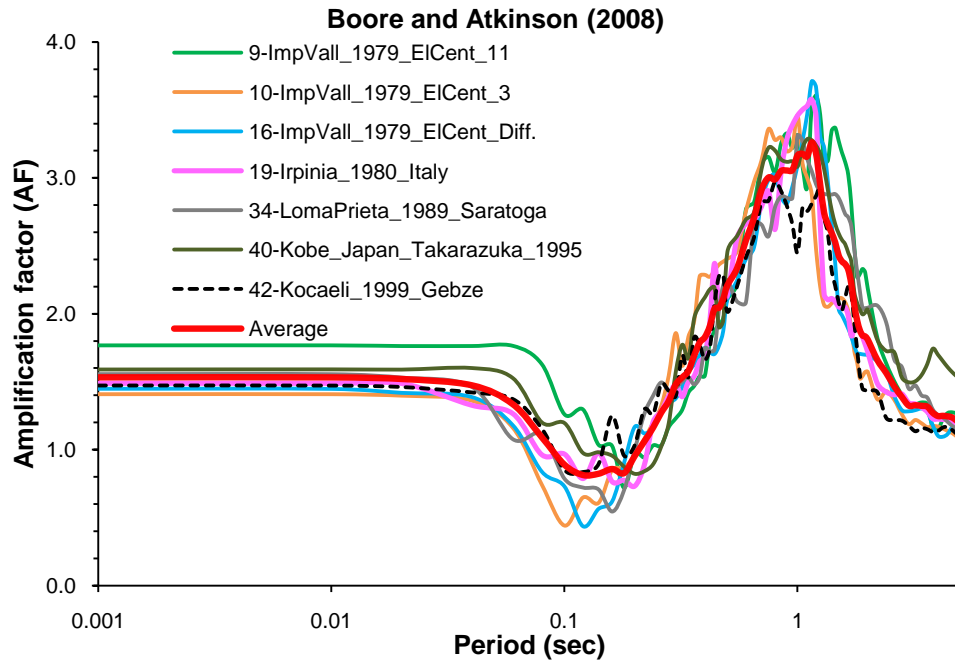


Figure 6.65. Amplification ratio of BH-4 based on Boore and Atkinson (2008) model for 0 km distance zone

A summary of obtained data from the ProSHAKE (v.1.12) analyses for the soil profile of BH-4 is given as an example in Table 6.13 including both of the NGA models.

Table 6.13. Results of site response analysis for BH-4

Ground motion	Maximum Surface PGA (g)		Amplification ratio (AF) (for PGA)	Predominant period (sec) (from ProSHAKE)	Amplification ratio (AF) (for PGA)	Predominant period (sec) (from ProSHAKE)
	BA08 Model	CB08 Model		BA08 Model		CB08 Model
	9	0.721	0.676	1.8	1.21	1.9
10	0.637	0.559	1.4	0.99	1.5	0.99
16	0.627	0.536	1.4	1.28	1.6	0.95
19	0.664	0.596	1.5	0.97	1.6	0.97
34	0.751	0.659	1.5	1.24	1.6	1.24
40	0.741	0.656	1.6	0.87	1.7	0.87
42	0.663	0.687	1.5	1.15	1.5	1.15
Average	0.686	0.624	-	-	-	-

As seen in Table 6.13, the peak ground acceleration varies between 0.34 and 0.48g for different earthquakes in BH-4. Besides, the predominant periods range between 0.8 and 1.2 sec. The amplification ratios are mostly around 1.5 for both NGA models. The results

obtained from both NGA based models reveal that the amplification factors based on BA08 model are slightly less than the factors based on CB08 model. The slight difference can be explained by the consideration of different model parameters. For instance, in the application of the NGA model calculations, BA08 model considers the closest horizontal distance to the surface projection of the rupture plane ( $R_{JB}$ ). However, CB08 model uses the closest distance to the rupture plane ( $R_{rup}$ ). Although there is a slight difference in amplification factors, the PGA values of BA08 model are generally higher than those of CB08 model.

The variation of PGA values along depth with respect to different earthquake motions and different attenuation models is also illustrated in Figures 6.66 and 6.67 for alluvium (BH-9) and Pliocene (BH-14) units.

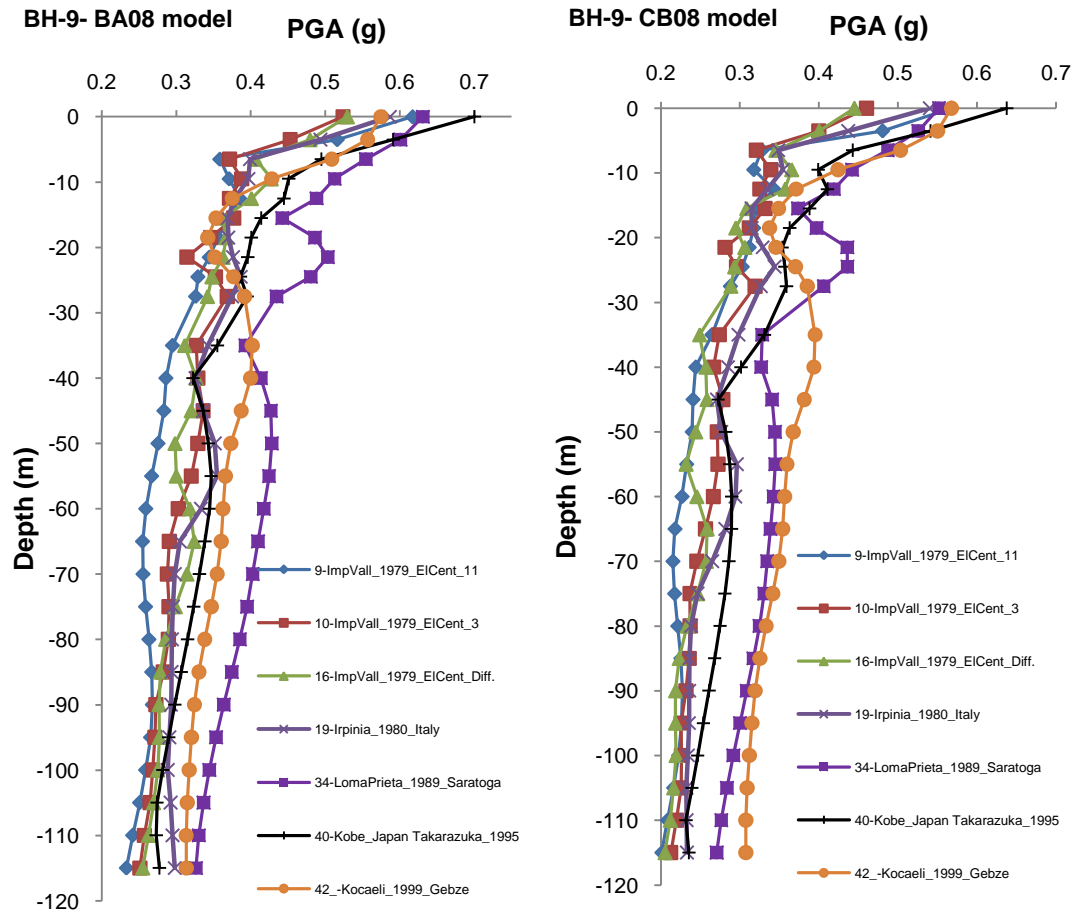


Figure 6.66. Variation of PGA values along depth for alluvium units in BH-9

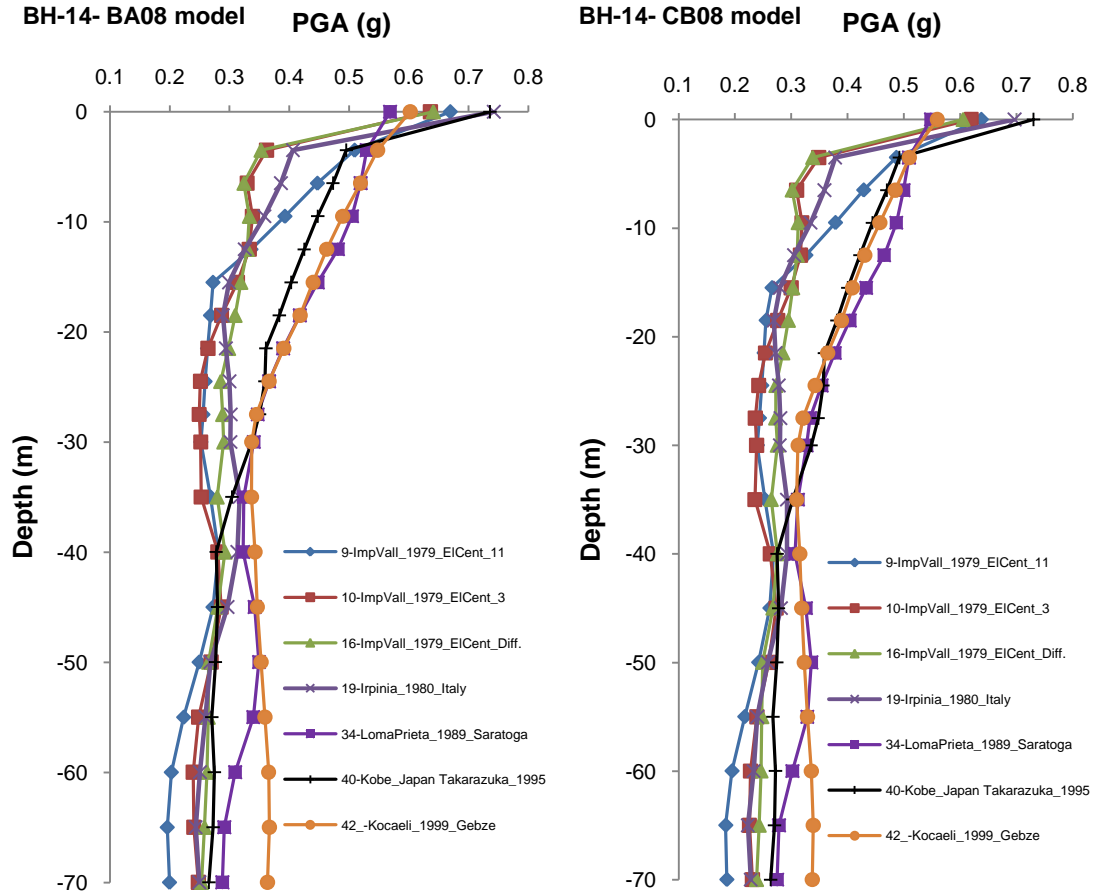


Figure 6.67. Variation of PGA values along depth for Pliocene units in BH-14

The peak ground acceleration (PGA) from surface motions and amplification maps are prepared using the obtained data from the site response analysis based on the aforementioned 118 grid points in the grid system (Figures 6.68, 6.69, 6.70, and 6.71). Moreover, the predominant periods obtained from ProSHAKE results are also spatially illustrated in Figures 6.72 and 6.73 for BA08 and CB08 models.

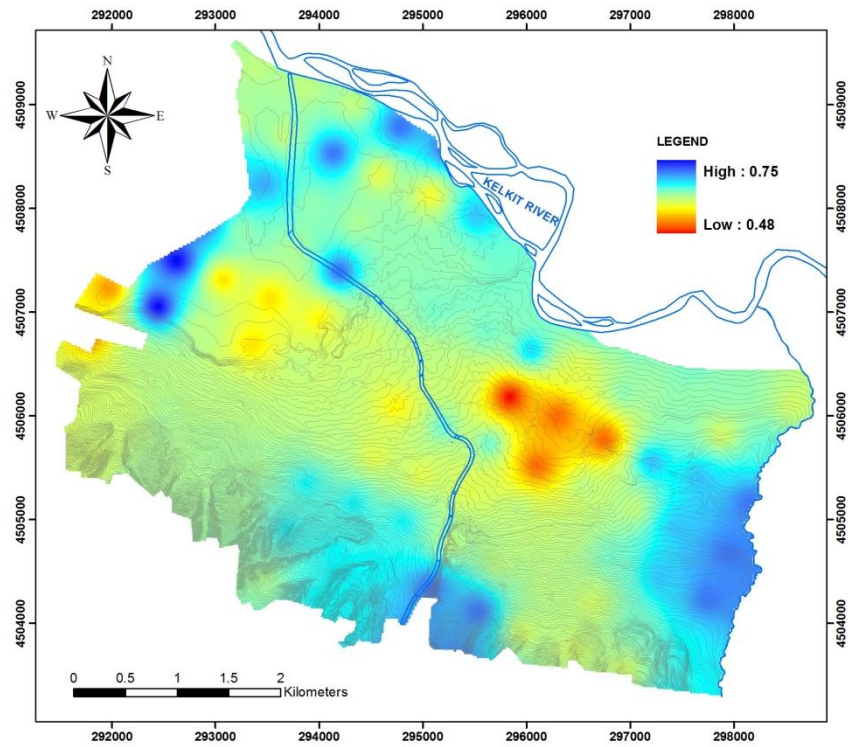


Figure 6.68. Peak ground acceleration (PGA) (surface) map of the study area based on Boore and Atkinson (2008) model

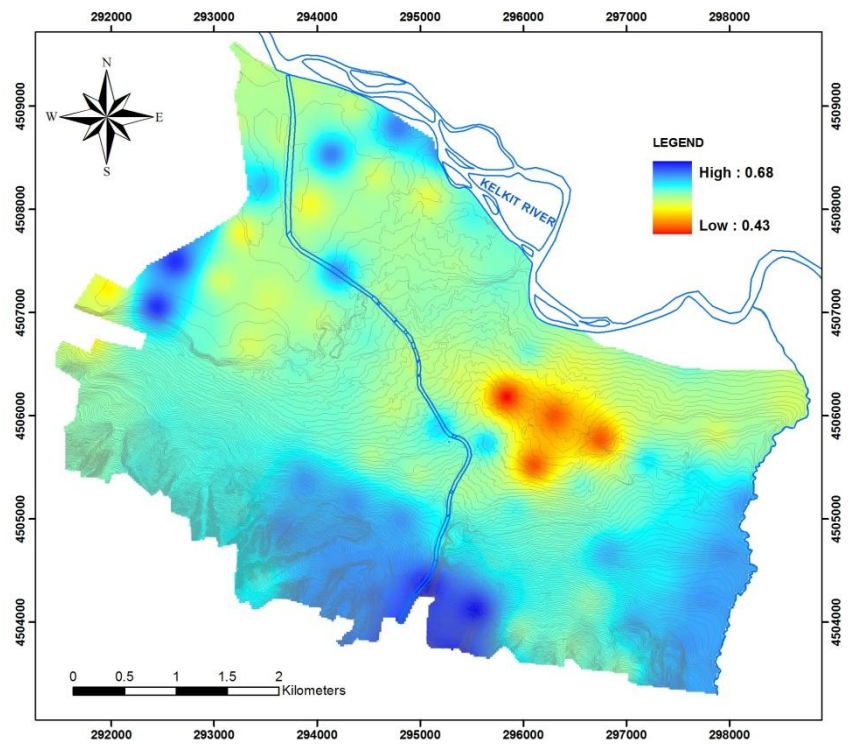


Figure 6.69. Peak ground acceleration (PGA) (surface) map of the study area based on Campbell and Bozorgnia (2008) model

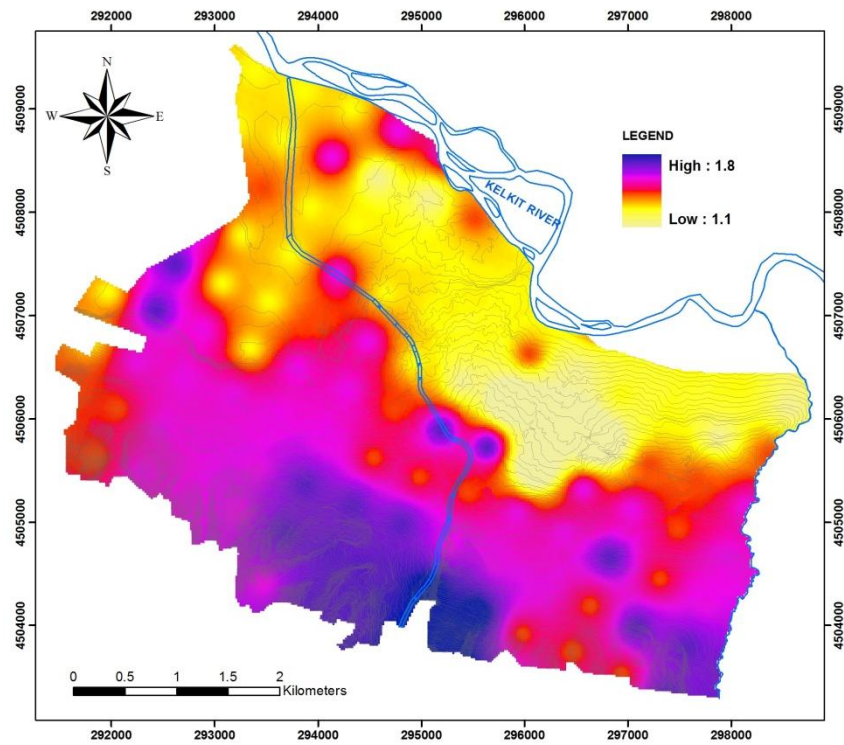


Figure 6.70. Amplification map of the study area based on Boore and Atkinson (2008) model (for 0.001 sec)

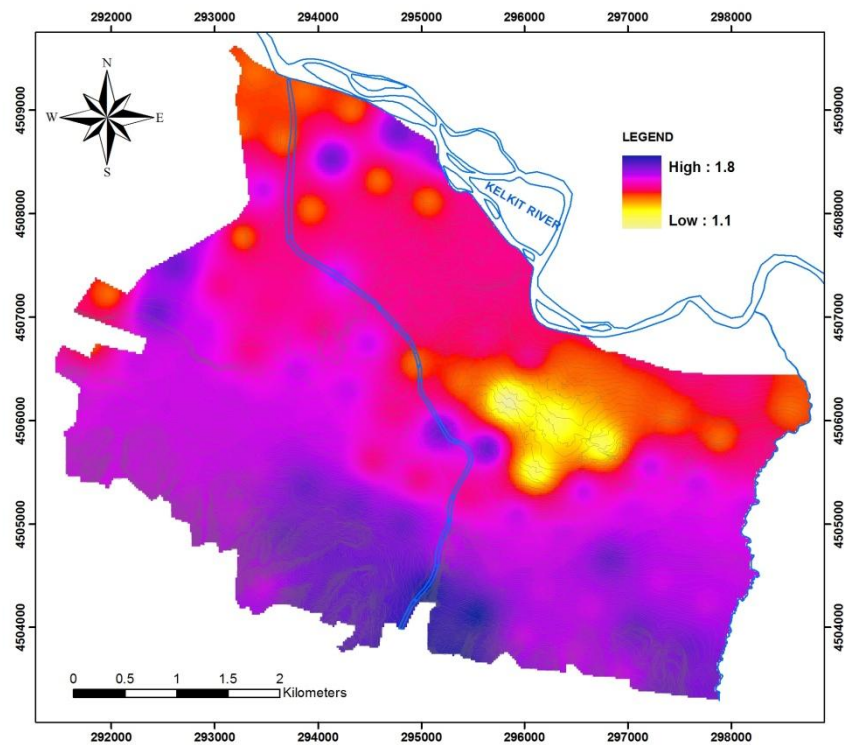


Figure 6.71. Amplification map of the study area based on Campbell and Bozorgnia (2008) model (for 0.001 sec)



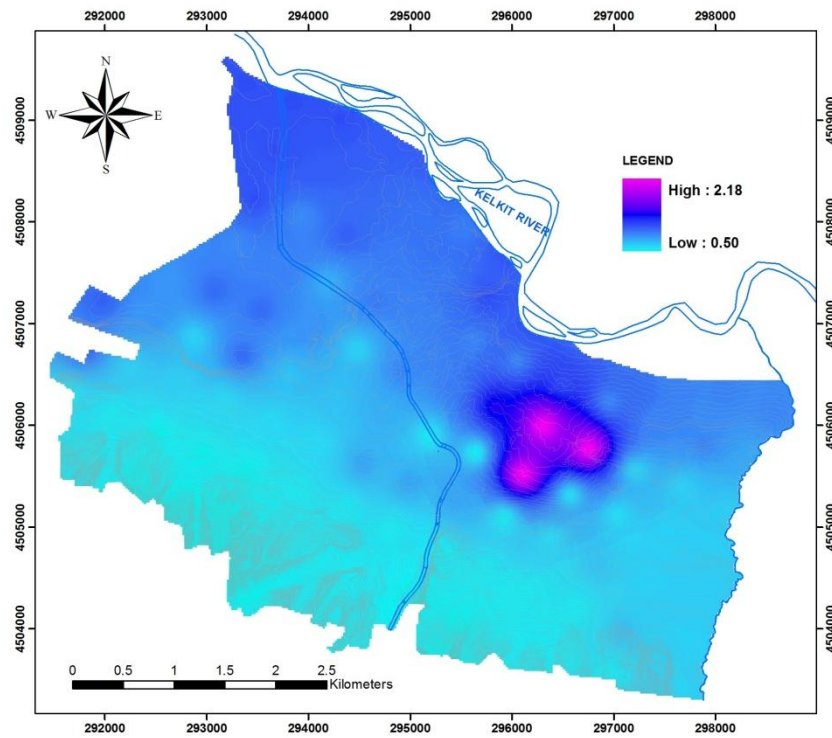


Figure 6.72. Predominant period map of the study area (for BA08 model)

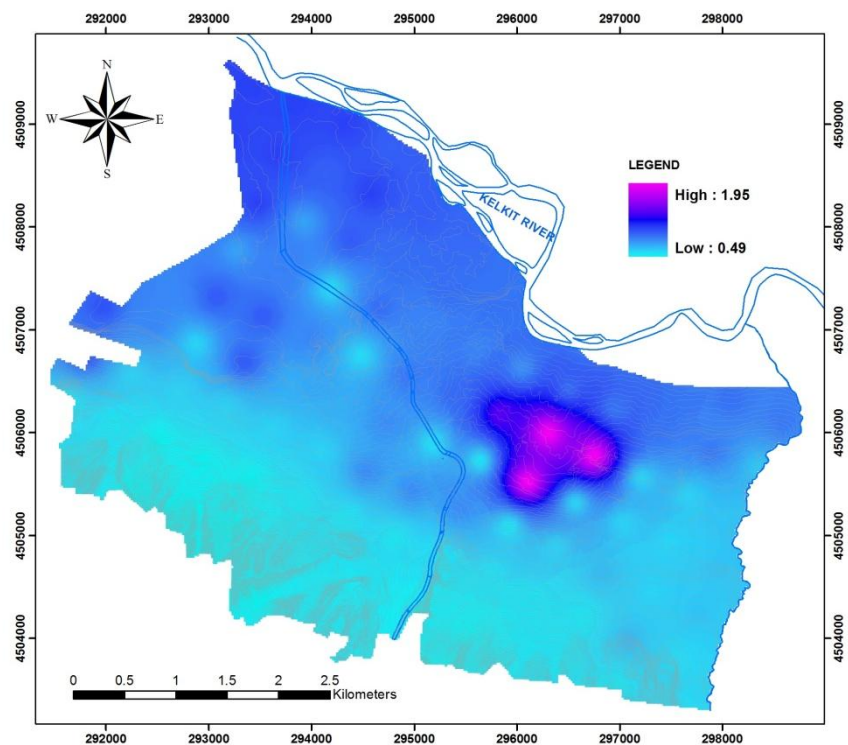


Figure 6.73. Predominant period map of the study area (for CB08 model)

The predominant period varies between 0.48 and 1.85 sec in the study area. The soil units along Kelkit River generally exhibit a period range of 0.961 and 1.23 sec. The Pliocene soil layers relatively have low periods (high frequencies) around 0.48 and 0.76 sec. The highest predominant period is determined in the central part of Erbaa in alluvial units where the soil layers have probably maximum thickness. The amplification values are quite similar for both NGA based models. Furthermore, high amplification values for longer periods (more than 3.5) are locally observed along Kelkit River embankment.

### 6.5.2 Amplification factors determined from shear wave velocity

Shear wave velocity of soil layers can also be used for the evaluation of amplification. There are a number of shear wave velocity based amplification formulas in the literature (Midorikawa, 1987; Joyner and Fumal, 1984 and Borchardt et al., 1991) (Table 6.14). The proposed equations were also evaluated in TCEGE (1999) and an assessment was made showing the comparison of relative amplification factors determined by the equations presented in Table 6.14 (Figure 6.75).

Table 6.14. Correlations of relative amplification factors with average shear wave velocity (after TCEGE, 1999)

Researcher(s)	Equation
Midorikawa (1987)	$A = 68V_1^{-0.6}$ ( $V_1 < 1100\text{m/s}$ )
	$A = 1$ ( $V_1 > 1100\text{m/s}$ )
Joyner and Fumal (1984)	$A = 23V_2^{-0.45}$
Borchardt et al. (1991)	$AHSA = 700/V_1$ (for weak motion)
	$AHSA = 600/V_1$ (for strong motion)

A: Relative amplification factor for peak ground velocity

AHSA: Average horizontal spectral amplification in period range of 0.4 to 2.0 sec.

$V_1$ : Average shear-wave velocity over a depth of 30m (in m/s)

$V_2$ : Average shear-wave velocity over a depth of one-quarter wavelength for a one-second period wave (in m/s)

The equation proposed by Midorikawa (1987) is used for the determination of amplification factors in the study area. The previously proposed  $V_{s30}$  values for Erbaa are used for the calculation of  $V_s$  based amplification factors. The amplification results for each borehole are summarized in Table 6.15.



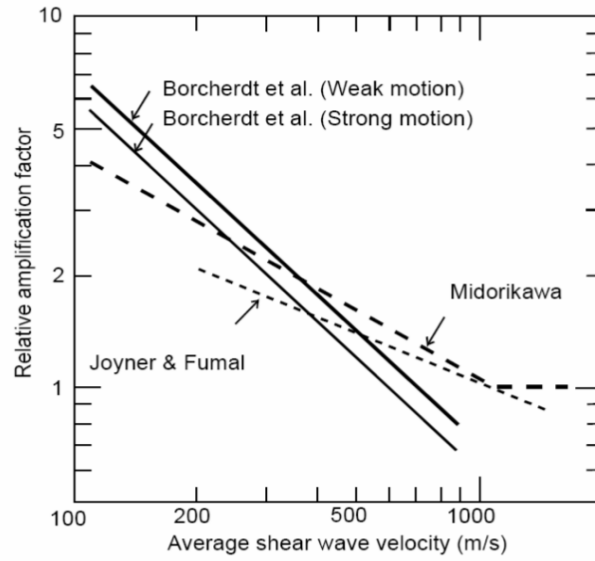


Figure 6.74. Comparison of amplification factors according to different relationships (after TCEGE, 1999)

Table 6.15. Amplification factors based on Midorikawa (1987) shear wave velocity relation

BH-no	Amplification factor	BH-no	Amplification factor	BH-no	Amplification factor	BH-no	Amplification factor
1	2.59	27	2.46	53	2.11	79	2.09
2	2.30	28	2.57	54	2.44	80	2.36
3	2.38	29	2.41	55	2.33	81	2.26
4	2.88	30	2.41	56	2.27	82	2.29
5	2.48	31	2.34	57	2.27	83	2.26
6	2.83	32	2.42	58	2.17	84	2.23
7	2.53	33	2.26	59	2.21	85	2.02
8	2.81	34	2.40	60	2.32	86	1.94
9	2.45	35	2.32	61	2.26	87	2.27
10	2.43	36	2.53	62	2.38	88	2.33
11	2.40	37	2.56	63	2.19	89	2.38
12	2.05	38	2.44	64	2.12	90	2.40
13	2.31	39	2.40	65	2.27	91	2.21
14	2.21	40	2.43	66	2.17	92	2.06
15	2.31	41	2.33	67	2.09	93	2.27
16	2.34	42	2.39	68	2.09	94	2.23
17	2.35	43	2.28	69	2.19	95	2.50
18	2.59	44	2.52	70	2.26	96	2.47
19	2.45	45	2.42	71	1.92	97	2.53
20	2.42	46	2.33	72	2.06	98	2.56
21	2.41	47	2.28	73	2.23	99	2.53
22	2.38	48	2.43	74	2.26	100	2.51
23	2.28	49	2.32	75	1.97	101	2.53
24	2.39	50	2.16	76	2.03	102	2.53
25	2.36	51	2.20	77	2.23	103	2.47
26	2.20	52	2.38	78	2.15	104	2.52

As seen in Table 6.15, the amplification factors range between 1.92 and 2.88 for different boreholes. The mean amplification factor for the study area is found to be 2.34 considering all soil profiles. Furthermore, the mean amplification factor for alluvial and Pliocene soils is 2.38 and 2.17, respectively. The distribution of amplification factors based on Midorikawa (1987) shear wave velocity approach is illustrated in Figure 6.75.

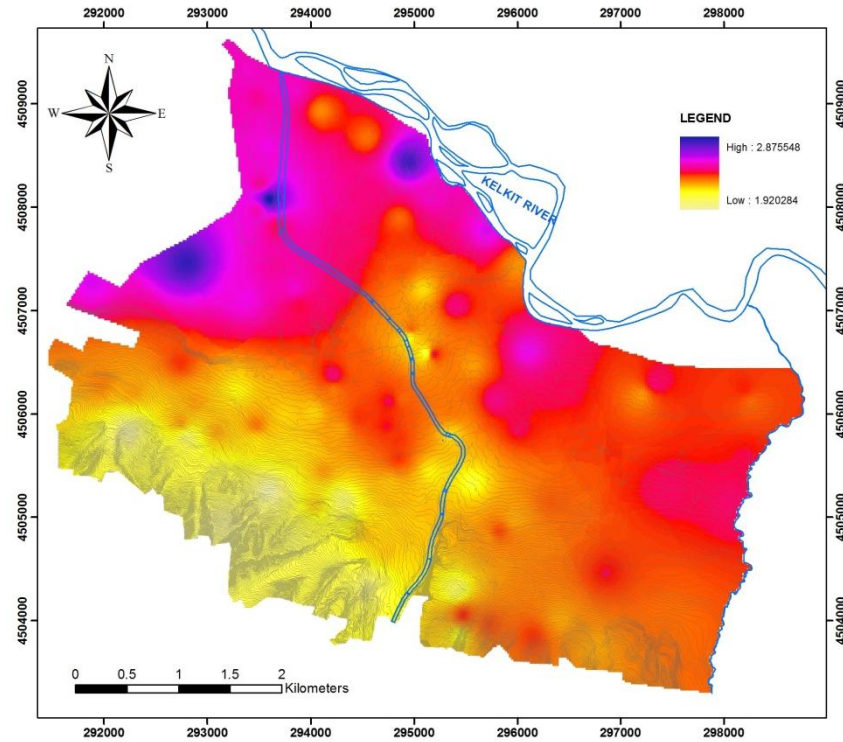


Figure 6.75. Amplification factor map of the study area based on Midorikawa (1987) shear wave velocity relationship

The lowest amplification factors are generally observed in Pliocene soil layers in accordance with Midorikawa (1987) approach. Besides, amplification factor increases towards the northwestern part of the study area.

### 6.5.3 Amplification factors determined from Stewart et al. (2003) equation

Amplification factors are proposed to quantify site effects, ground response effects, 2D and 3D basin effects, and the influence of surface topography by different researchers. Amplification factors can be defined as the ratio of an intensity measure for a specified site condition to the value of intensity measure that would have been expected for a reference site

condition (Kwok and Stewart, 2006). Several empirical relationships have been proposed to predict amplification factors for 5% damped response spectral acceleration as a function of site category by Stewart et al. (2003). Site classification can be performed on the basis of surface geology (age-only, age-depositional environment, and age-material texture), shallow shear-wave velocity (30 m- $V_{s30}$ ), and geotechnical data in the same study. The criteria used for surface geology classification are summarized in Table 6.16 with respect to the classification proposed by Stewart et al. (2003).

Table 6.16. Criteria used for surface geology classification (Stewart et al., 2003)

Age	Depositional Environment	Sediment Texture
Holocene	H. alluvium	Coarse
	Lacustrine/ marine	Fine-mixed
Pleistocene	P. alluvium	
	Lacustrine/ marine	Coarse
	Aeolian	Fine-mixed
	Artificial fill	
Tertiary		
Mesozoic + igneous		

The produced site classifications are evaluated and the most recent geotechnical classification is preferred in amplification factor analyses. In Table 6.17, the recent site classification proposed by Rodriguez-Marek et al. (2001) is depicted.

Table 6.17. Geotechnical site categories proposed by Rodriguez-Marek et al. (2001)

Site	Description	Approximate site period (sec)	Comments
A	Hard rock	0.1	Crystalline bedrock; $V_s \geq 1500$ m/s
B	Competent bedrock	0.2	$V_s \geq 600$ m/s or $< 6$ m of soil
C1	Weathered rock	0.4	$V_s = 300$ m/s increasing to $> 600$ m/s
C2	Shallow stiff soil	0.5	Soil depth $> 6$ m and $< 30$ m
C3	Intermediate Depth Stiff soil	0.8	Soil depth $> 30$ m and $< 60$ m
D1	Deep Stiff Holocene soil	1.4	Depth $> 60$ m and $< 200$ m
D2	Deep Stiff Pleistocene soil	1.4	Depth $> 60$ m and $< 200$ m
D3	Very deep stiff soil	2.0	Depth $> 200$ m
E1	Medium thickness soft clay	0.7	Thickness of soft clay layer 3-12 m
E2	Deep soft clay	1.4	Thickness of soft clay layer $> 12$ m
F	Potentially liquefiable sand	-	Holocene loose sand with high water table ( $< 6$ m)

The shallow shear wave velocity defined as  $V_{s30}$  can also be considered for the classification of NEHRP Provision which was established by Martin (1994) (Table 6.18).

Table 6.18. Site categories in NEHRP Provisions (Martin, 1994)

NEHRP category	Description	Mean shear wave velocity to 30m $V_{s30}$ (m/s)
A	Hard Rock	> 1500 m/s
B	Firm to hard rock	760-1500 m/s
C	Dense soil, soft rock	360-760 m/s
D	Stiff soil	180-360 m/s
E	Soft clays	< 180 m/s
F	Special study soils, e.g., liquefiable soils, sensitive clays, organic soils, soft clays > 36 m thick	-

The recommended function of amplification ratio can be calculated from Equation 6.30 which is proposed in the study of Stewart et al. (2003).

$$\ln(F) = a + b \ln(\text{PHA}_r) + \varepsilon \quad (6.30)$$

where

a and b : regression coefficients

$\text{PHA}_r$ : peak horizontal acceleration for the reference (rock) site condition

$\varepsilon$  : error term (considered as zero for mean residual)

The coefficients in Equation 6.30 for different site classes are given in Tables 6.19 and 6.20. Moreover, the amplification factors can be used for other tectonic regimes as mentioned. Consequently, this amplification factor approach is applied to the study area. The prepared target spectra by two different next generation attenuation (NGA) models (Boore and Atkinson, 2008 and Campbell and Bozorgnia 2008) are accepted to represent reference site conditions for Erbaa. The obtained spectral acceleration values from the NGA models are used in the calculation of amplification factors for different periods. The calculated amplification factors are illustrated in Figures 6.76, 6.77, 6.78, and 6.79. Firstly, Pliocene soils are assigned as Pleistocene in age as shown in Table 6.19. Then, alluvial soils which are shown as Qa in Table 6.19 are given in Figure 6.77 for 0 and 2 km distance zones of BA08 model. As an evaluation of the following figures, geotechnical parameters which are pointed out as NEHRP classification in Table 6.20 are considered. Alluvial soils are previously assigned as D-type of soils; however it is decided that Pliocene soils should be differentiated from the same D class (alluvial soils) to make a comparison. Therefore, depending on the some  $V_{s30}$  results which are placed into C-D boundary for Pliocene soils are accepted as C

type of soils for the calculation of these amplification factors. The graphics based on the geotechnical classification are shown in Figures 6.78 and 6.79 for alluvial and Pliocene soil, respectively. Lastly, the same sequence is followed and then the related figures for CB08 model are proposed (Figures 6.80, 6.81, 6.82, and 6.83).

As seen in the figures the distance has a negligible impact for the distribution amplification factors due to the different periods. Alluvial soils have slightly higher values in terms of amplification factor than Pliocene soils. Especially, for the longer periods there is a considerable change in the trend of the distribution of the amplification. In other words, the longer periods have higher amplification potential due to the given results.

In the sense of geological age-based surface geology and NEHRP provision based geotechnical classification, the amplification values are variable for the same period. For instance, at 1 sec period amplification value becomes 2.4 in the surface geology-based approach on the contrary it changes into 1.7 for the same period in geotechnical evaluation part both for the same NGA model. The amplification factor maps which are based on the NGA models (BA08 and CB08) are depicted in Figures 6.84, 6.85, 6.86 and 6.87. In Figures 6.84 and 6.85 the geological classification is considered for the calculation of amplification ratios. In Figures 6.86 and 6.87, the geotechnical criteria-based results are presented. According to different amplification ratio maps, the geotechnical criteria-based maps represent that the amplification ratios in alluvial soils are higher than in Pliocene soils. On the contrary, the geological-based amplification factors exhibit opposite results in the same units. In other words, the Stewart et al. (2003) geological classification-based approach may reveal dissimilar results. Therefore, the geotechnical classification-based approach is preferred for the interpretations.

Table 6.19. Surface geology categories (modified from Stewart et al., 2003)

Period (sec)	P			Hlm			Qa			Hc			Hm		
	a	b	$\sigma$	a	b	$\sigma$	a	b	$\sigma$	a	b	$\sigma$	a	b	$\sigma$
0.01	0.14	0.02	0.47	-0.59	-0.39	0.47	-0.15	-0.13	0.52	-0.11	-0.10	0.52	-0.50	-0.33	0.51
0.02	0.08	0.00	0.47	-0.55	-0.39	0.48	-0.14	-0.13	0.52	-0.10	-0.10	0.52	-0.48	-0.31	0.52
0.03	0.03	0.00	0.48	-0.57	-0.36	0.49	-0.24	-0.14	0.52	-0.17	-0.10	0.52	-0.51	-0.29	0.52
0.04	-0.19	-0.02	0.48	-0.63	-0.33	0.50	-0.49	-0.14	0.51	-0.39	-0.10	0.53	-0.60	-0.29	0.52
0.05	-0.19	-0.01	0.47	-0.72	-0.34	0.47	-0.47	-0.13	0.51	-0.38	-0.09	0.53	-0.67	-0.27	0.50
0.06	-0.19	-0.03	0.46	-0.70	-0.31	0.45	-0.46	-0.14	0.50	-0.36	-0.08	0.54	-0.66	-0.27	0.50
0.08	-0.20	-0.03	0.45	-0.70	-0.32	0.48	-0.43	-0.12	0.50	-0.29	-0.05	0.54	-0.66	-0.26	0.49
0.09	-0.09	0.01	0.45	-0.67	-0.31	0.52	-0.36	-0.11	0.51	-0.20	-0.01	0.55	-0.64	-0.25	0.49
0.10	-0.07	0.00	0.45	-0.67	-0.29	0.53	-0.35	-0.11	0.52	-0.18	-0.01	0.55	-0.62	-0.23	0.51
0.12	-0.05	0.01	0.45	-0.66	-0.30	0.54	-0.29	-0.10	0.53	-0.14	-0.03	0.55	-0.60	-0.23	0.52
0.15	-0.07	-0.01	0.46	-0.67	-0.33	0.54	-0.29	-0.12	0.53	-0.12	-0.04	0.54	-0.61	-0.27	0.52
0.17	-0.08	-0.03	0.46	-0.66	-0.33	0.54	-0.31	-0.14	0.52	-0.12	-0.05	0.54	-0.61	-0.29	0.52
0.20	-0.02	-0.01	0.47	-0.66	-0.32	0.52	-0.32	-0.15	0.52	-0.12	-0.08	0.54	-0.59	-0.28	0.51
0.24	0.14	0.03	0.48	-0.49	-0.27	0.50	-0.20	-0.12	0.50	-0.11	-0.06	0.53	-0.47	-0.25	0.49
0.30	0.22	0.07	0.48	-0.39	-0.25	0.48	-0.10	-0.11	0.51	-0.08	-0.08	0.53	-0.36	-0.24	0.47
0.36	0.24	0.06	0.50	-0.26	-0.21	0.46	-0.02	-0.10	0.50	-0.01	-0.06	0.51	-0.27	-0.23	0.46
0.40	0.25	0.06	0.50	-0.25	-0.22	0.46	0.00	-0.09	0.51	-0.01	-0.08	0.51	-0.23	-0.25	0.46
0.46	0.25	0.02	0.52	-0.23	-0.21	0.46	0.04	-0.09	0.52	0.02	-0.08	0.51	-0.17	-0.23	0.48
0.50	0.24	0.03	0.53	-0.17	-0.21	0.46	0.09	-0.08	0.53	0.04	-0.07	0.51	-0.10	-0.19	0.49
0.60	0.27	0.03	0.53	-0.13	-0.23	0.49	0.12	-0.09	0.54	0.06	-0.08	0.53	0.00	-0.18	0.53
0.75	0.27	0.03	0.53	-0.02	-0.21	0.49	0.09	-0.11	0.56	0.07	-0.09	0.55	0.05	-0.18	0.56
0.85	0.25	-0.01	0.53	0.01	-0.21	0.48	0.10	-0.10	0.57	0.09	-0.07	0.56	0.07	-0.16	0.56
1.00	0.21	-0.02	0.53	0.03	-0.22	0.45	0.20	-0.06	0.58	0.13	-0.06	0.57	0.10	-0.14	0.56
1.50	-0.12	-0.18	0.52	0.08	-0.21	0.43	0.02	-0.14	0.61	-0.16	-0.18	0.61	0.14	-0.14	0.56
2.00	-0.21	-0.22	0.51	0.09	-0.22	0.49	-0.05	-0.18	0.63	-0.19	-0.20	0.63	0.18	-0.13	0.56
3.00	-0.30	-0.28	0.51	0.10	-0.23	0.48	-0.05	-0.19	0.66	-0.20	-0.21	0.67	0.23	-0.09	0.55
4.00	-0.40	-0.31	0.55	0.10	-0.24	0.48	-0.05	-0.20	0.68	-0.21	-0.23	0.72	0.25	-0.13	0.54
5.00	-0.40	-0.34	0.59	0.10	-0.25	0.48	-0.05	-0.21	0.69	-0.22	-0.25	0.78	0.28	-0.17	0.62

P: Pleistocene, Hlm: Holocene lacustrine/marine, Qa: Quaternary alluvium, Hc: Holocene mixed sediments, Hm: Holocene mixed sediments,  $\sigma$ : Standard error term

Table 6.20. NEHRP and Geotechnical Categories (after Stewart et al., 2003)

Period (sec)	NEHRP B			NEHRP C			NEHRP D			NEHRP E			Geot. B			Geot. C			Geot. D			Geot. E		
	a	b	$\sigma$	a	b	$\sigma$	a	b	$\sigma$	a	b	$\sigma$	a	b	$\sigma$	a	b	$\sigma$	a	b	$\sigma$	a	b	$\sigma$
0.01	0.09	0.05	0.49	-0.06	-0.05	0.55	0.08	-0.07	0.57	-0.62	-0.52	0.48	0.07	0.07	0.56	0.11	-0.04	0.60	-0.02	-0.08	0.56	-0.82	-0.63	0.40
0.02	0.10	0.01	0.50	-0.07	-0.06	0.55	0.06	-0.07	0.57	-0.70	-0.51	0.48	0.09	0.07	0.56	0.10	-0.05	0.60	-0.03	-0.09	0.55	-0.75	-0.61	0.40
0.03	0.10	0.11	0.50	-0.12	-0.04	0.55	0.03	-0.06	0.56	-0.75	-0.51	0.49	0.05	0.09	0.56	0.07	-0.03	0.60	-0.07	-0.08	0.55	-0.74	-0.57	0.42
0.04	0.10	0.12	0.48	-0.31	-0.08	0.55	-0.17	-0.09	0.55	-0.81	-0.51	0.47	-0.05	0.08	0.56	-0.13	-0.07	0.60	-0.23	-0.09	0.53	-0.89	-0.56	0.40
0.05	0.16	0.18	0.45	-0.41	-0.09	0.55	-0.19	-0.07	0.54	-1.04	-0.54	0.44	-0.13	0.07	0.55	-0.18	-0.07	0.60	-0.28	-0.09	0.52	-0.99	-0.55	0.38
0.06	0.21	0.20	0.46	-0.40	-0.09	0.54	-0.20	-0.07	0.54	-1.05	-0.54	0.43	-0.13	0.06	0.55	-0.19	-0.08	0.60	-0.30	-0.08	0.51	-0.98	-0.55	0.38
0.08	0.19	0.17	0.45	-0.40	-0.11	0.54	-0.19	-0.07	0.55	-1.11	-0.54	0.43	-0.18	0.03	0.52	-0.18	-0.07	0.60	-0.30	-0.09	0.53	-1.14	-0.58	0.36
0.09	-0.07	0.06	0.42	-0.39	-0.08	0.55	-0.13	-0.05	0.56	-1.11	-0.54	0.44	-0.23	0.02	0.52	-0.15	-0.06	0.59	-0.23	-0.07	0.55	-1.12	-0.57	0.40
0.1	0.09	0.15	0.43	-0.38	-0.09	0.56	-0.12	-0.05	0.58	-1.05	-0.51	0.45	-0.22	0.02	0.53	-0.15	-0.06	0.60	-0.22	-0.07	0.56	-1.12	-0.54	0.40
0.12	0.16	0.17	0.44	-0.38	-0.10	0.55	-0.11	-0.04	0.58	-0.95	-0.46	0.46	-0.28	0.00	0.54	-0.16	-0.06	0.58	-0.17	-0.05	0.56	-1.12	-0.55	0.35
0.15	0.40	0.22	0.44	-0.38	-0.14	0.57	-0.10	-0.06	0.58	-0.74	-0.43	0.49	-0.19	0.01	0.57	-0.18	-0.11	0.58	-0.15	-0.06	0.55	-1.12	-0.57	0.36
0.17	0.30	0.22	0.46	-0.36	-0.13	0.58	-0.12	-0.10	0.56	-0.70	-0.43	0.50	-0.17	0.03	0.60	-0.24	-0.14	0.57	-0.12	-0.07	0.54	-1.14	-0.61	0.36
0.2	0.36	0.25	0.48	-0.35	-0.13	0.60	-0.12	-0.09	0.55	-0.63	-0.42	0.50	-0.14	0.04	0.62	-0.28	-0.15	0.57	-0.09	-0.05	0.54	-1.08	-0.59	0.36
0.24	0.05	0.16	0.47	-0.30	-0.12	0.61	-0.12	-0.07	0.54	-0.55	-0.41	0.52	-0.10	0.08	0.65	-0.23	-0.15	0.58	-0.02	-0.05	0.52	-0.89	-0.56	0.32
0.3	-0.06	0.08	0.45	-0.22	-0.09	0.64	0.11	-0.04	0.54	-0.45	-0.41	0.54	-0.04	0.15	0.70	-0.10	-0.12	0.62	0.08	-0.04	0.51	-0.83	-0.55	0.36
0.36	-0.12	0.15	0.58	-0.19	-0.09	0.67	0.15	-0.03	0.53	-0.41	-0.40	0.53	-0.02	0.17	0.76	-0.02	-0.11	0.64	0.12	-0.04	0.50	-0.79	-0.54	0.37
0.4	-0.16	0.11	0.61	-0.14	-0.07	0.70	0.16	-0.04	0.51	-0.40	-0.40	0.54	0.00	0.19	0.75	0.01	-0.09	0.65	0.13	-0.04	0.49	-0.78	-0.53	0.39
0.46	-0.30	0.03	0.63	-0.11	-0.07	0.70	0.20	-0.07	0.49	-0.36	-0.40	0.54	0.01	0.18	0.75	0.04	-0.09	0.66	0.18	-0.06	0.48	-0.70	-0.52	0.44
0.5	-0.37	0.00	0.65	-0.07	-0.06	0.70	0.26	-0.04	0.49	-0.31	-0.40	0.54	0.02	0.19	0.76	0.09	-0.07	0.66	0.20	-0.05	0.49	-0.57	-0.52	0.47
0.6	-0.46	-0.02	0.67	-0.06	-0.07	0.72	0.30	-0.03	0.51	-0.25	-0.40	0.50	0.02	0.16	0.75	0.12	-0.06	0.68	0.24	-0.06	0.49	-0.30	-0.48	0.48
0.75	-0.65	-0.14	0.70	0.02	-0.06	0.72	0.40	-0.01	0.49	-0.18	-0.40	0.46	0.06	0.15	0.74	0.15	-0.05	0.70	0.36	-0.03	0.49	-0.20	-0.46	0.45
0.85	-0.70	-0.13	0.77	0.04	-0.05	0.73	0.39	-0.01	0.49	-0.12	-0.39	0.44	0.15	0.20	0.74	0.11	-0.06	0.71	0.38	-0.02	0.49	-0.18	-0.45	0.40
1	-0.72	-0.13	0.78	0.07	-0.03	0.74	0.38	-0.02	0.48	-0.09	-0.39	0.47	0.24	0.25	0.73	0.04	-0.08	0.72	0.41	-0.01	0.49	-0.12	-0.42	0.45
1.5	-0.88	-0.27	0.57	0.04	-0.03	0.77	0.34	-0.04	0.50	-0.02	-0.38	0.48	0.19	0.21	0.70	-0.06	-0.09	0.75	0.42	-0.03	0.51	0.07	-0.33	0.45
2	-1.33	-0.43	0.47	-0.01	-0.04	0.80	0.27	-0.07	0.51	0.03	-0.37	0.48	-0.41	-0.01	0.68	-0.12	-0.09	0.76	0.33	-0.05	0.55	0.14	-0.29	0.45
3	-1.47	-0.50	0.36	-0.08	-0.07	0.87	0.27	-0.09	0.55	0.09	-0.35	0.49	-0.44	-0.08	0.77	-0.12	-0.10	0.79	0.22	-0.10	0.59	0.25	-0.18	0.45
4	-1.55	-0.52	0.33	-0.20	-0.09	0.92	0.27	-0.09	0.57	0.10	-0.32	0.50	-0.47	-0.11	0.82	-0.12	-0.10	0.83	0.15	-0.14	0.65	0.30	-0.15	0.45
5	-1.60	-0.54	0.37	-0.25	-0.10	1.04	0.27	-0.10	0.66	0.12	-0.31	0.50	-0.50	-0.15	0.94	-0.12	-0.10	0.99	0.10	-0.16	0.71	0.33	-0.10	0.40

*$\sigma$ : Standard error term*

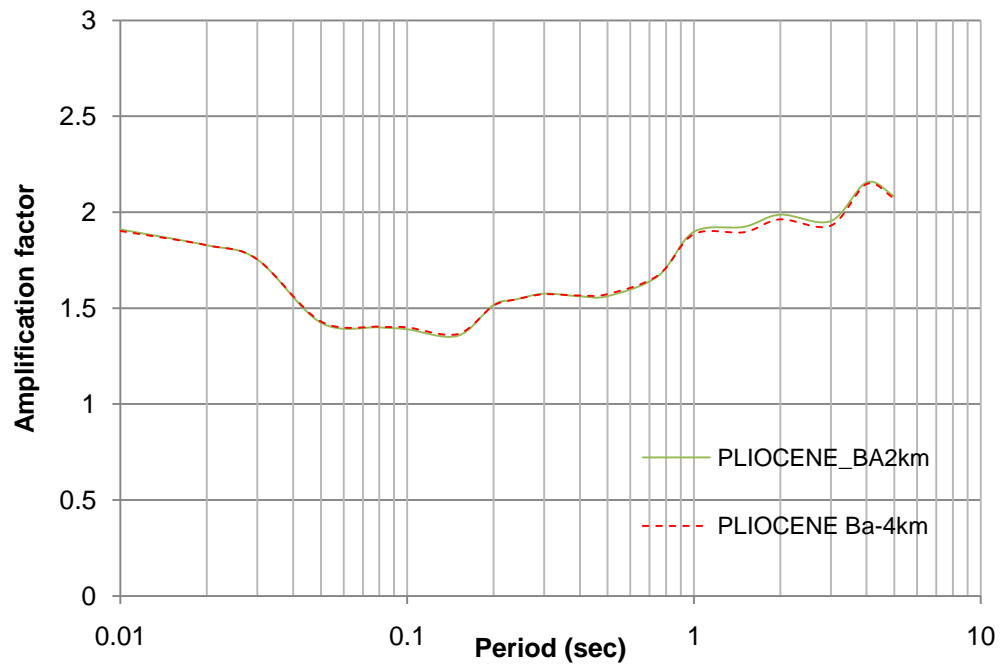


Figure 6.76. Amplification factor based on surface geology for Pliocene soils with BA08 model

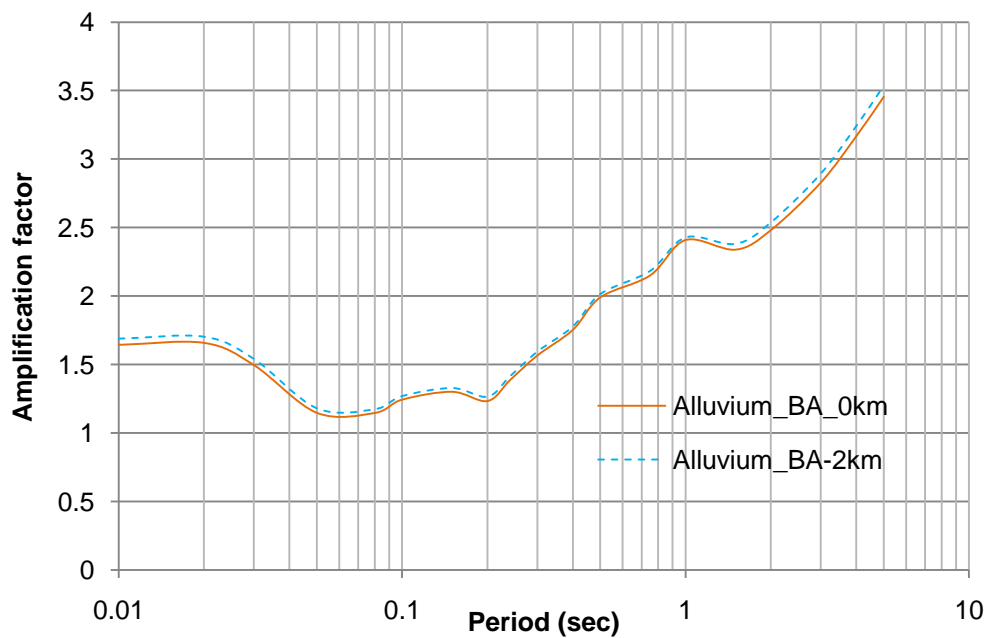


Figure 6.77. Amplification factor based on surface geology for alluvial soils with BA08 model



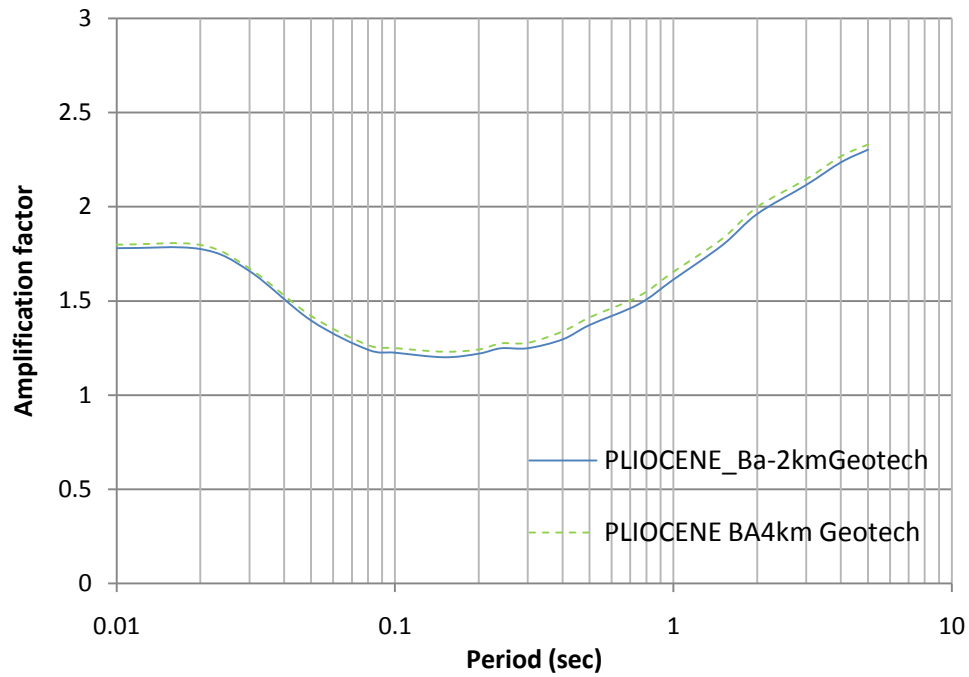


Figure 6.78. Amplification factor based on geotechnical classification for Pliocene soils with BA08 model

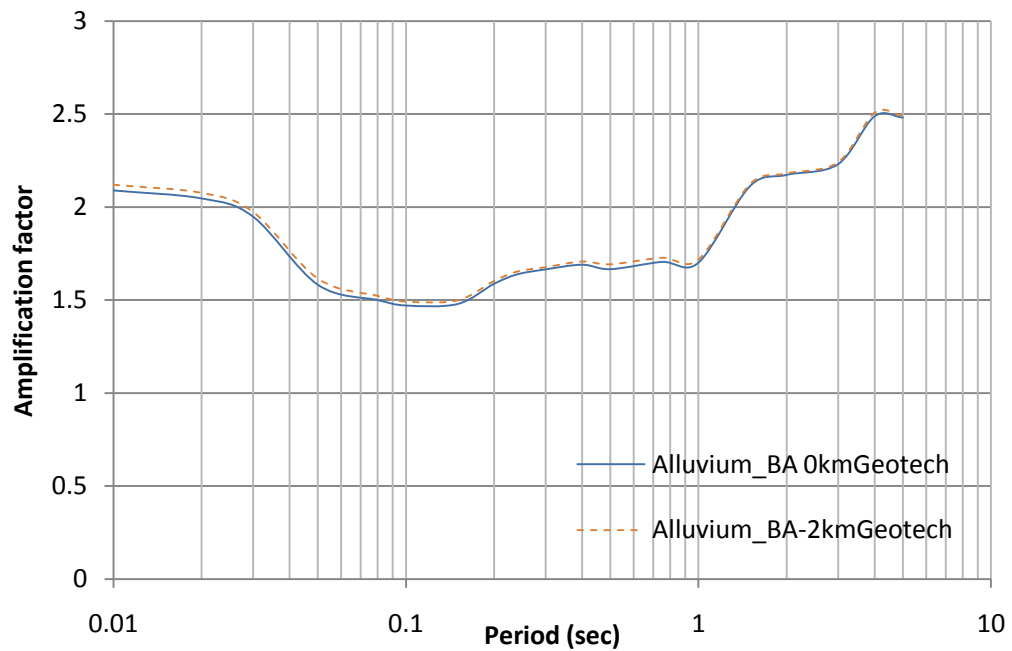


Figure 6.79. Amplification factor based on geotechnical classification for alluvial soils with BA08 model

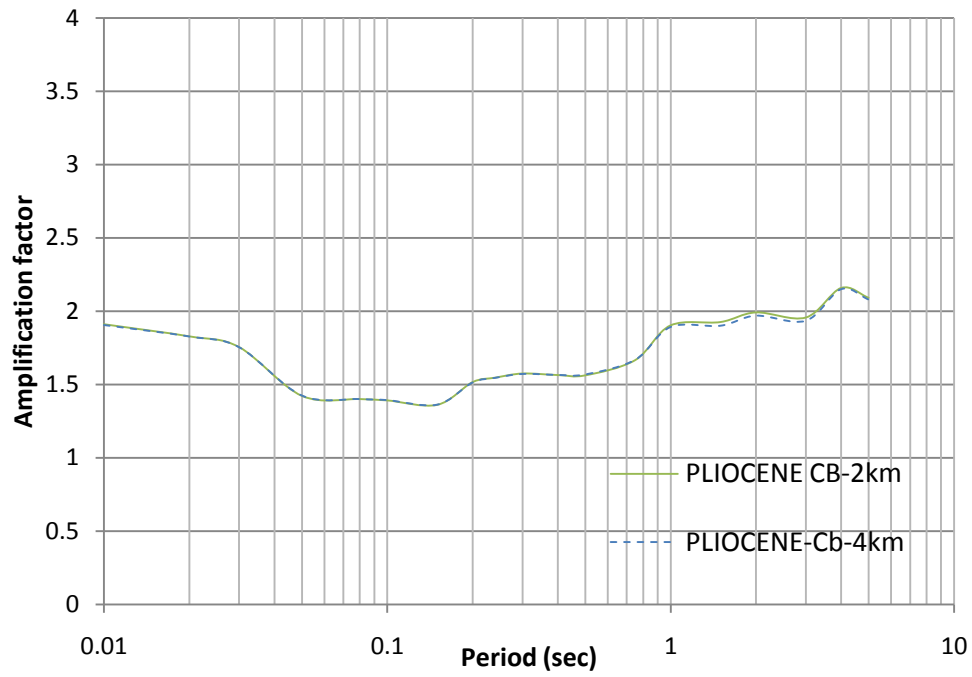


Figure 6.80. Amplification factor based on surface geology for Pliocene soils with CB08 model

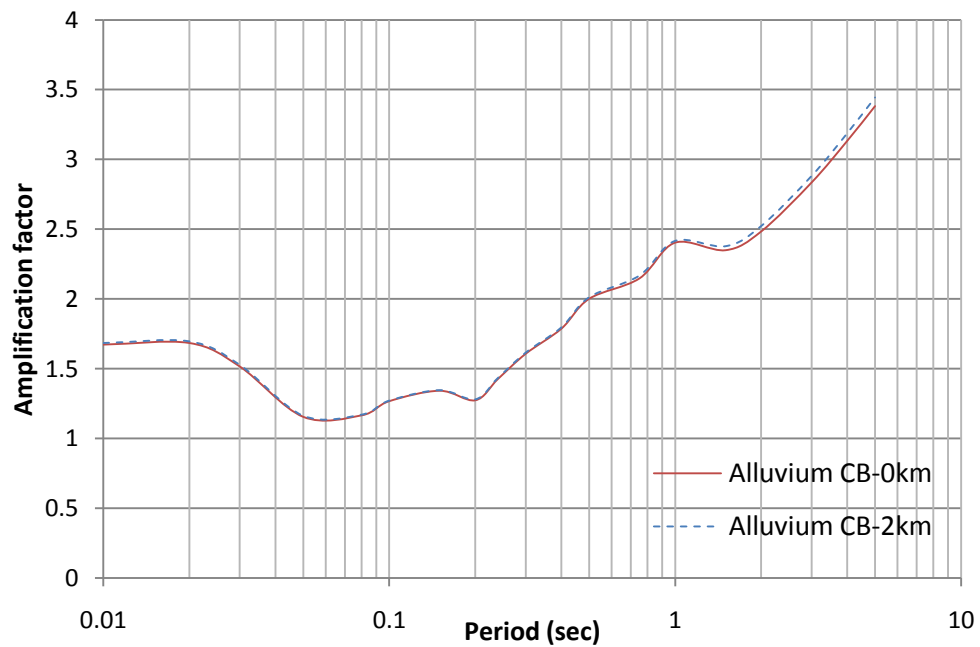


Figure 6.81. Amplification factor based on surface geology for alluvial soils with CB08 model

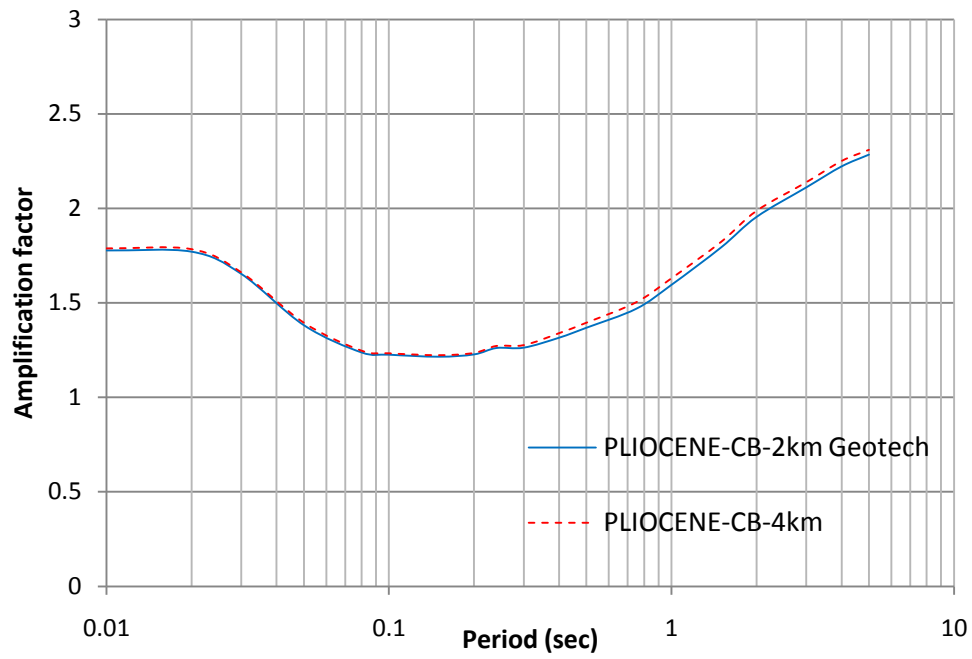


Figure 6.82. Amplification factor based on geotechnical classification for Pliocene soils with CB08 model

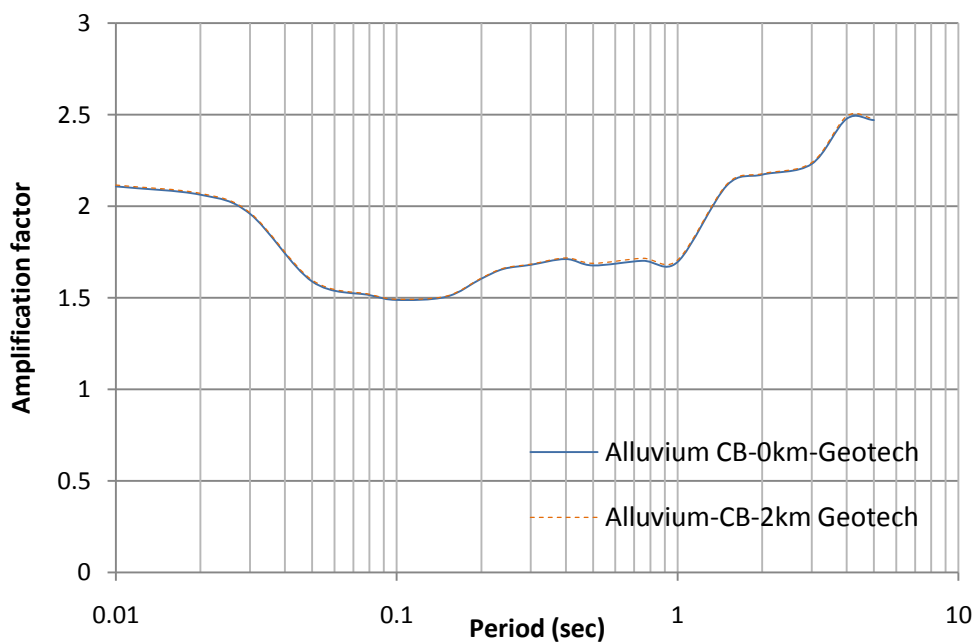


Figure 6.83. Amplification factor based on geotechnical classification for alluvial soils with CB08 model

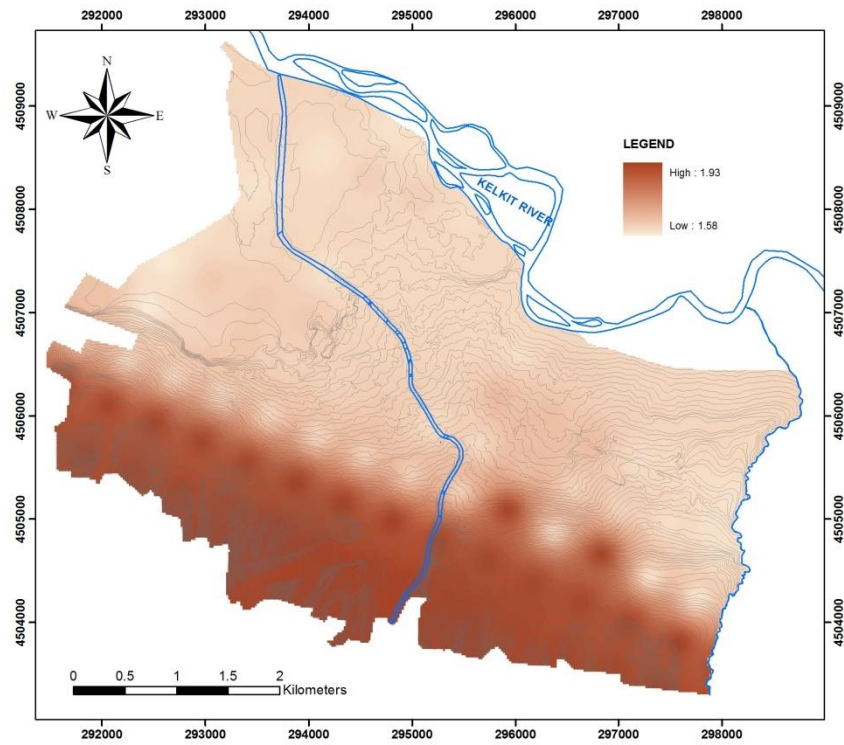


Figure 6.84. Amplification factor map based on geological classification with BA08 model

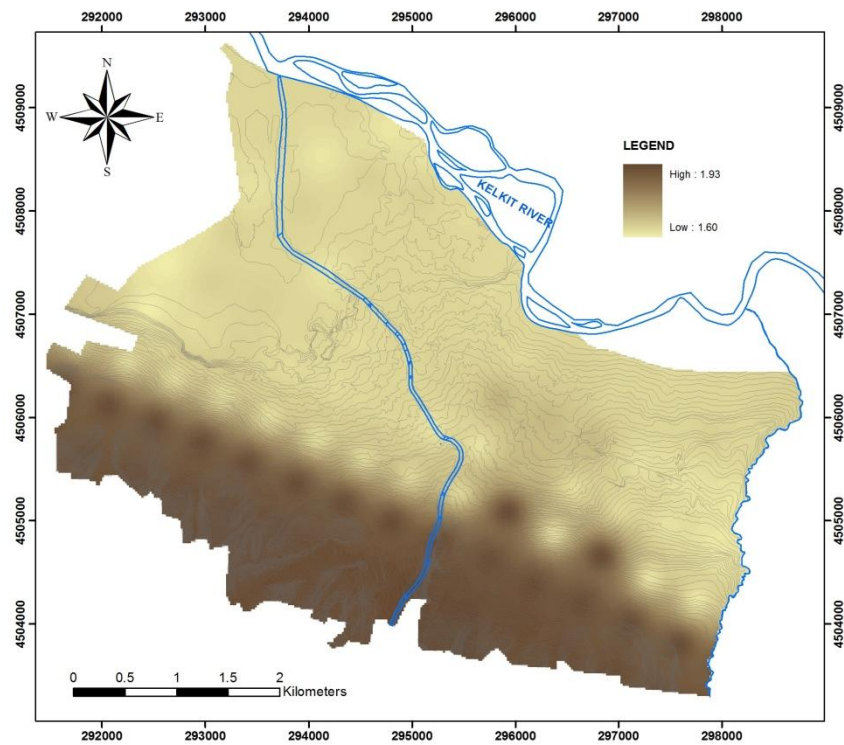


Figure 6.85. Amplification factor map based on geological classification with CB08 model

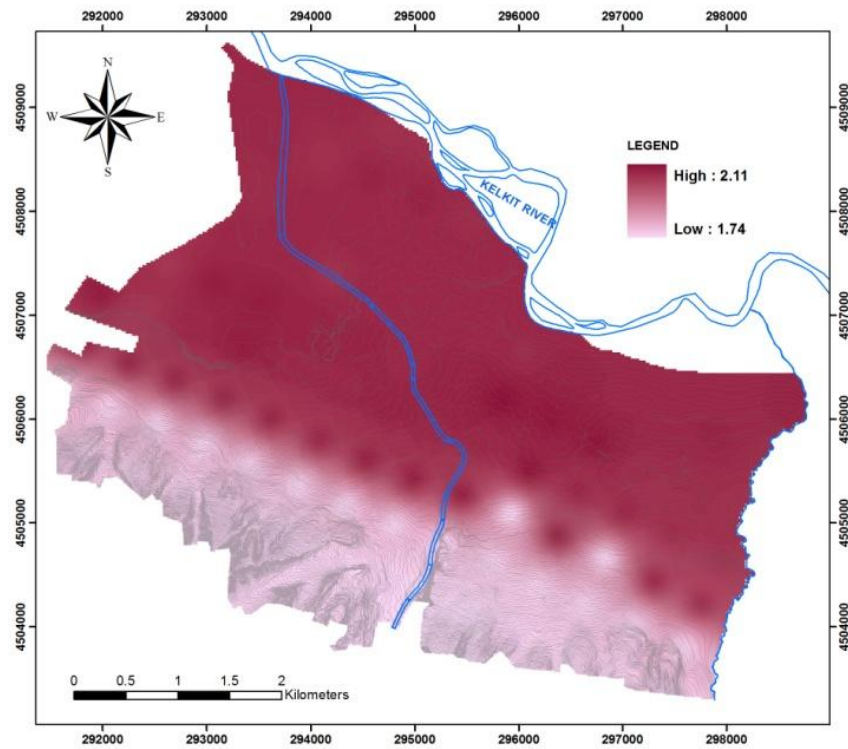


Figure 6.86. Amplification factor map based on geotechnical classification with BA08 model

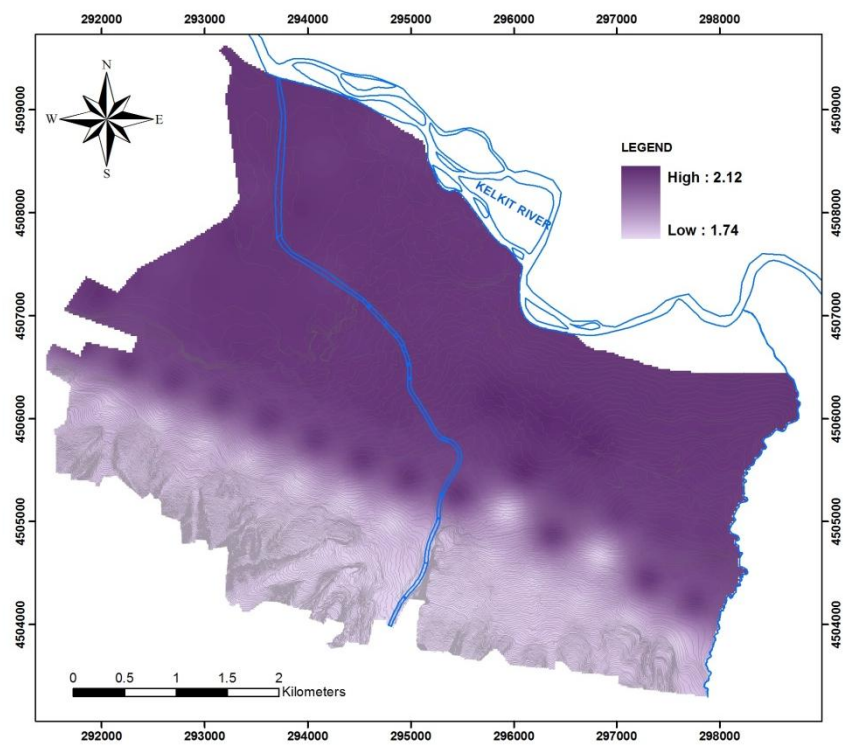


Figure 6.87. Amplification factor map based on geotechnical classification with CB08 model

#### 6.5.4 Amplification values from microtremor measurements

Microtremors are ground vibrations with displacement amplitude about 0.1-1 micron, and velocity amplitude about 0.001-0.01 cm/s that can be recorded by seismograph with high magnification. Within the content of DPT project, Dikmen et al. (2009) carried out microtremor measurements at 517 points as mentioned in previous chapters. The obtained predominant period and seismic amplification at each microtremor measurement point are re-evaluated in this study to compare amplification values determined from different methods. These locations are re-mapped and related maps are re-generated for Erbaa (Figures 6.88 and 6.89).

Within the study area, the predominant period varies between 0.088 and 3.03 based on microtremor measurements. Low periods can be observed in the western part of the settlement. Peak periods are determined towards the eastern boundary with decreasing frequencies. Although the Nakamura based microtremor measurements reveal logical results for the predominant frequencies, the results can hardly be compared with the other predominant period values obtained from different methods due to intense scattering.

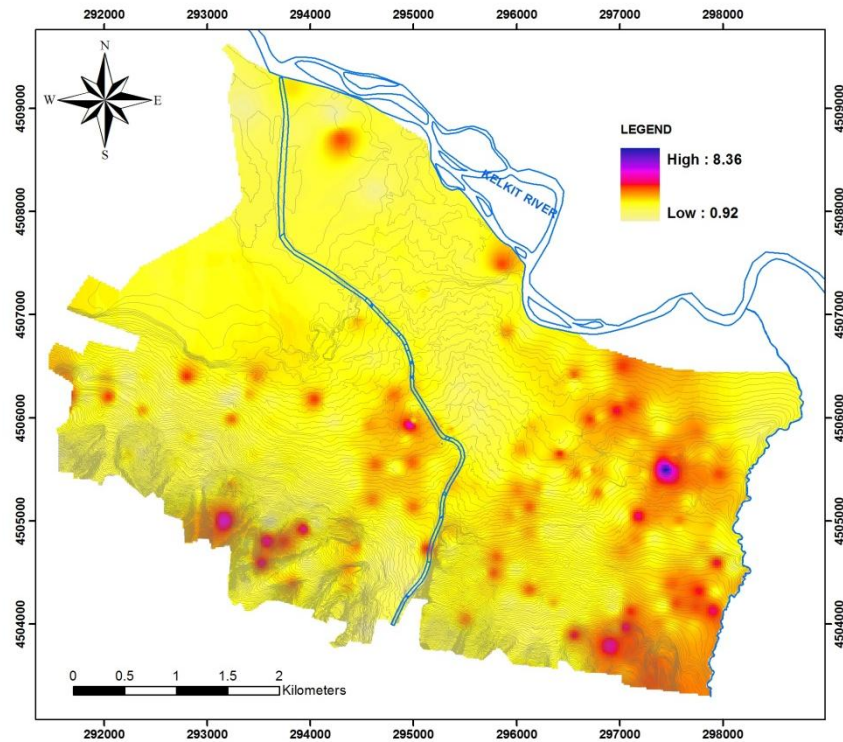


Figure 6.88. Amplification map of the study area based on microtremor results



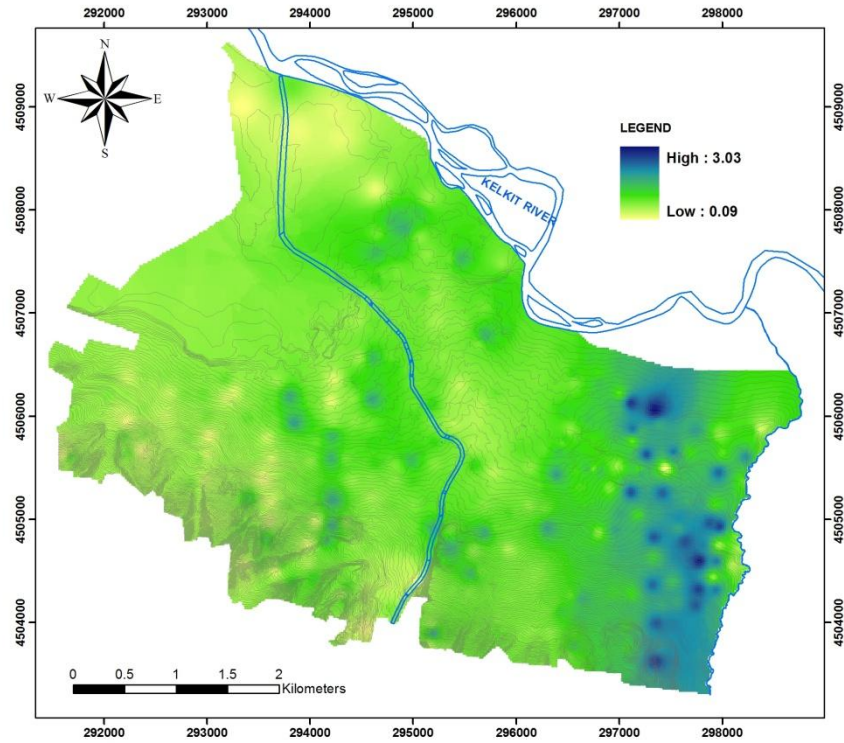


Figure 6.89. Predominant period map of the study area based on microtremor results

#### 6.5.5 Comparison of the estimated site effects for Erbaa based on amplification values

The site amplifications and predominant site periods obtained from three methods are compared in the following paragraphs. Initially, the amplification values obtained from different methods are correlated. The compared results are summarized in Table 6.21 depending on the maximum and minimum values of each parameter.

Moreover, the amplification factors are compared for each borehole. The comparison of amplification values for alluvial and Pliocene soil layers with respect to different approaches is depicted in Figures 6.90 and 6.91, respectively. Afterwards, the produced maps from the amplification factors obtained from  $V_s$ -based empirical equations (Midorikawa, 1987), the amplification factors obtained from 1-D dynamic site response analyses (ProSHAKE (v.1.12) analyses) and the amplification factors obtained from microtremor measurements (within the framework of the DPT project) are compared to provide the differences of amplification values.

Table 6.21. Comparison of amplification and predominant periods based on different methods

Methods		Amplification		Predominant periods	
		min	max	min	max
1-D equivalent linear based (ProSHAKE v.1.12)	BA08 model	1.1	1.8	0.5	2.18
	CB08 model	1.1	1.8	0.5	1.95
V <sub>s</sub> based empirical approach (Midorikawa, 1987)	-	1.92	2.88	-	-
Microtremor measurements	-	0.92	8.36	0.08	3.03
(Geological based)					
Stewart et al. (2003) amplification factor	BA08 model	1.58	1.93	-	-
	CB08 model	1.60	1.93	-	-
	(Geotechnical based)				
	BA08 model	1.74	2.11	-	-
	CB08 model	1.74	2.12	-	-

As seen in Figures 6.90 and 6.91, microtremor measurements indicate higher amplification values than the other methods. The general trend of amplification values which covers most of the study area varies between 2.4 and 4.2 based on the microtremor interpretations. According to the results of Stewart et al. (2003) amplification factor approach, the amplification values vary between 1.5 and 2.2. However, the geological based amplification values expose relatively less amplification in the alluvial soils. Therefore, the geotechnical based calculations seem to be more logical than the geological based approach with respect to the obtained results from other methods. High amplification values can be expected in the alluvial units in the study area as shown in Figures 6.86 and 6.87 in accordance with two different models (BA08 model and CB08 model). Therefore, the amplification effects can be modeled better using the geotechnical based amplification factors proposed by Stewart et al (2003).

Moreover, when the predominant periods obtained from ProSHAKE analyses and microtremor measurement are compared, it can be seen that the predominant periods from site response analyses are smaller in Pliocene layers than in alluvial soils. However, the same conclusion cannot be evidently retrieved from microtremor measurements. As a result, 1-D site response analyses reveal reasonable results considering the soil characteristics of the study area.



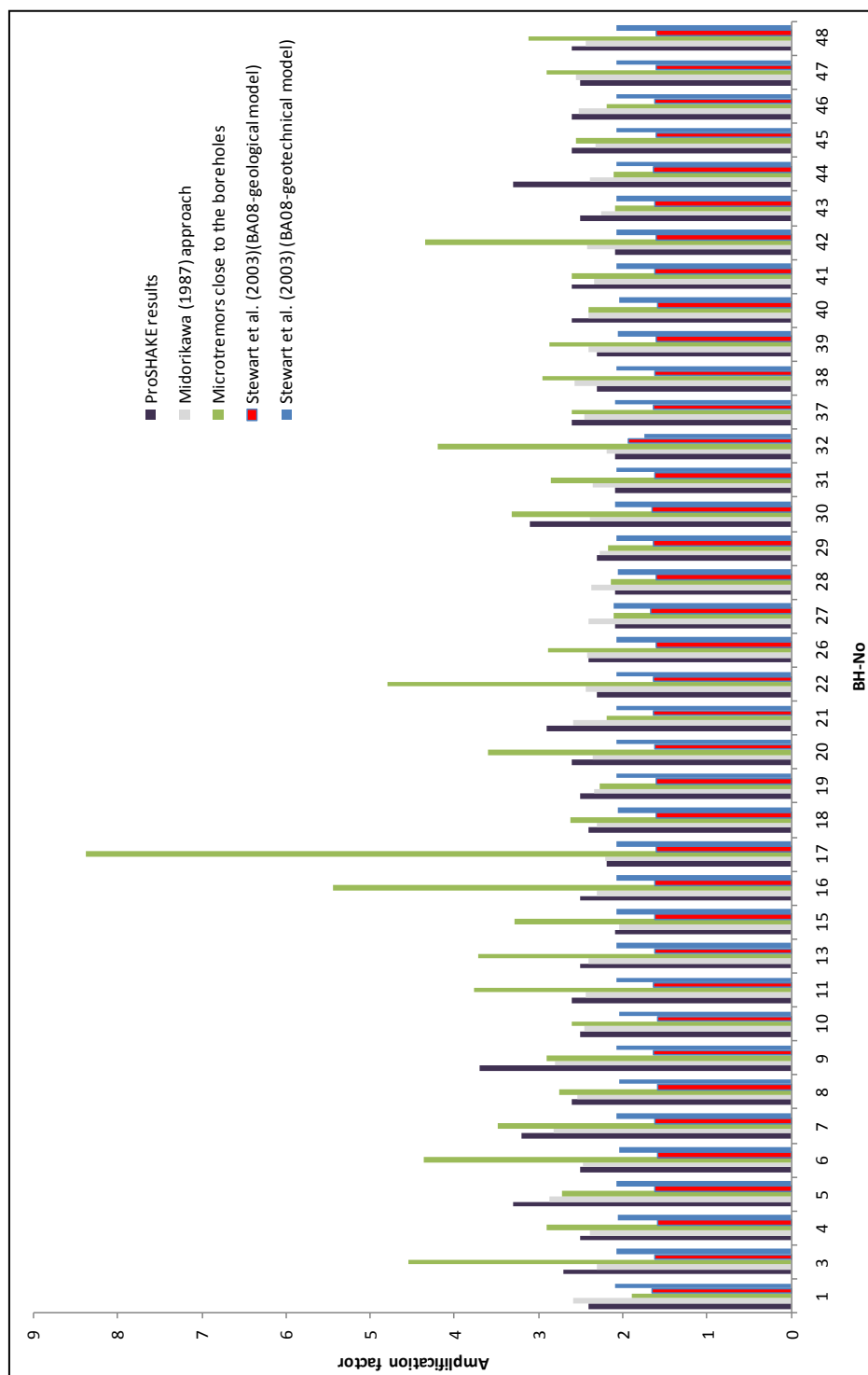


Figure 6.90. Comparison of amplification factors for alluvial soils

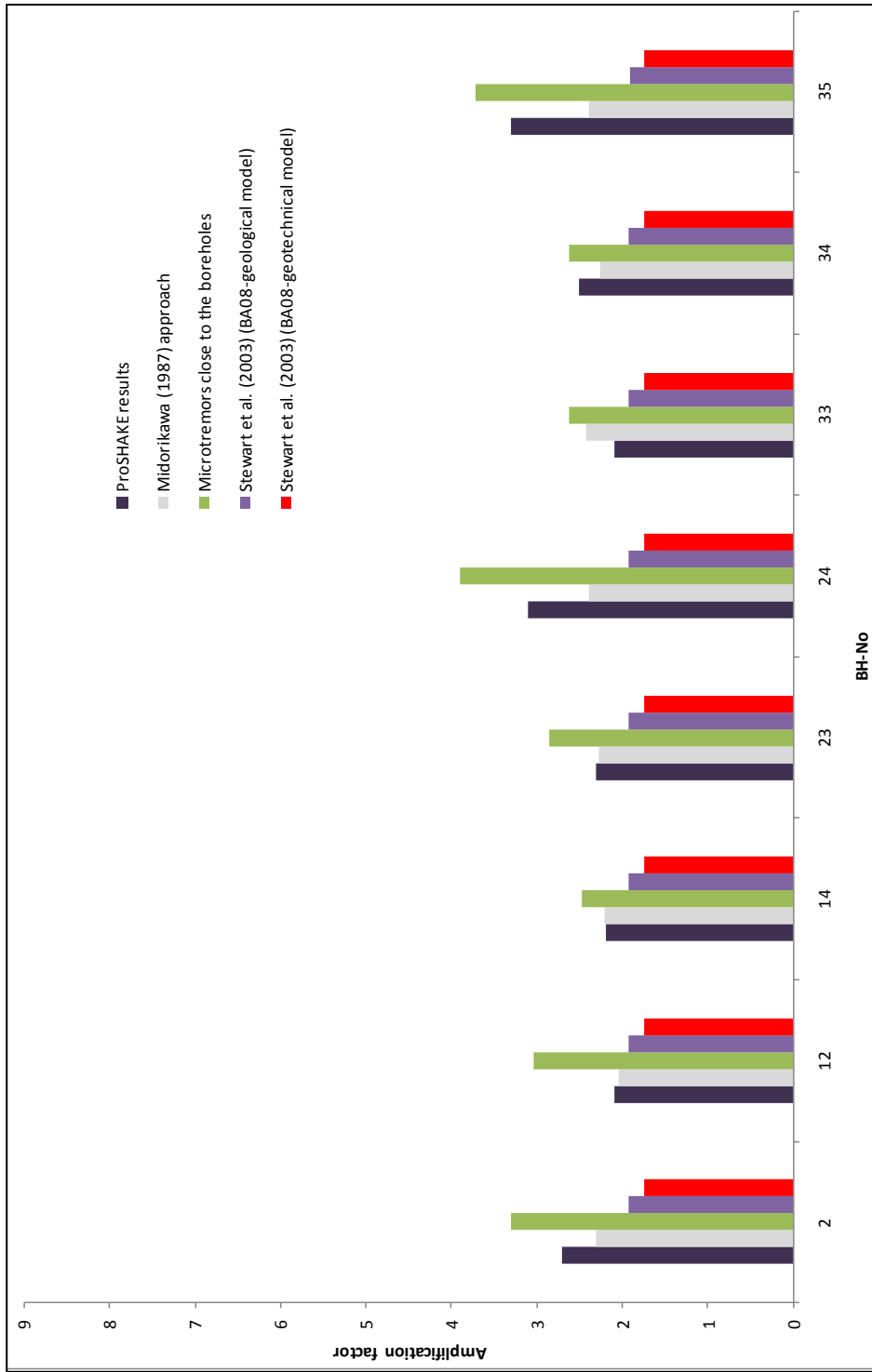


Figure 6.91. Comparison of amplification factors for Pliocene soils

## 6.6 Concluding Remarks

Dynamic properties of Erbaa soils are determined and shear wave velocity profiles are prepared to be used in site response analyses. During this process, empirical based shear wave velocities are calculated and site-specific formulas are proposed.

1-D equivalent linear site response analyses are performed in accordance with site-specific grid model using ProSHAKE (v.1.12) software. In the site response analyses of Erbaa, input ground motions are considered using PGA values as given in Chapter 5. Afterwards, the ratio is calculated on the basis of site amplification method using soil/bedrock ratio to obtain amplification factors (AF) for the study area.

Amplification factors are defined by different empirical approaches. The obtained values are compared to the measured microtremor results. Amplification factors from 1-D site response analyses and from different empirical approaches mostly vary within a range of approximately 1.5-2.5 in the study area. However, the microtremor measurements expose quite high amplifications up to 8.36. Besides, different period ranges should be taken into account for the design of structures. The proposed map derived from geotechnical based amplification factors by Stewart et al (2003) is preferred for the overlay analyses.

## CHAPTER 7

### LIQUEFACTION AND POST-LIQUEFACTION EFFECTS

#### 7.1 Introduction

Liquefaction results from the development of high pore water pressures due to ground shaking and the upward flow of water which may transform the sand into a liquefied condition. This event can also cause the temporary loss of stiffness and strength of saturated loose soils. It may cause many catastrophic failures during and after earthquakes as experienced, for instance, in Adapazarı (after the Kocaeli 1999 earthquake). The concept of liquefaction was first introduced by Casagrande in the late 1930s (Day, 2002). In the middle of this century, liquefaction and its effects were observed by researchers in two important earthquakes. The 1964 Alaska earthquake was followed by the 1964 Niigata earthquake, which both produced spectacular examples of liquefaction-induced damage (Kramer, 1996). During the more recent 1995 Kobe and 1999 Kocaeli earthquakes, many structures were affected by liquefaction and post-liquefaction effects. Post-liquefaction failure took the form of settlement in structures, tilting of buildings, and lateral spreading.

The liquefaction potential of project areas should be defined considering ground shaking hazards and local site conditions. Furthermore, the initiation mechanisms and susceptibility conditions of liquefaction as well as the post-liquefaction effects of seismic areas provide useful information to quantify the potential extent of liquefaction. In the literature, several methodologies have been suggested by various scientists to evaluate liquefaction potential of areas (Seed and Idriss, 1971; 1983; Seed et al., 1985; 2001; Poulos et al., 1985; NCEER, 1997; Youd and Noble, 1997; Youd et al., 2001; Kramer, 1996; Cetin, 2000; Cetin et al., 2004; Idriss and Boulanger, 2006). These methods mostly use SPT, CPT, and/or  $V_s$  measurements to characterize liquefaction resistance at a site. The SPT-based methods are frequently used in the literature since the SPT applications are more practical and cheaper than the other applications and because the geotechnical engineering profession has more experience with it. However, CPT-based (Robertson and Wride, 1998; Toprak, et al., 1999;

Juang et al., 2003; Olsen, 1984; 1997; Moss, 2003; Moss et al., 2006) and  $V_s$ -based (Andrus and Stokoe, 1997; 2000) techniques have distinct advantages and are also gaining popularity for liquefaction potential analyses.

In order to assess liquefaction and post-liquefaction hazards in Erbaa, potentially liquefiable soils are evaluated using existing data for soil profiles as described in the previous chapters. Afterward, post-liquefaction stability and possible deformations are determined. The susceptible layers, initiation models, and post-liquefaction effects are calculated by WSliq (WSDOT Liquefaction Hazard Evaluation System) software which is newly developed by Kramer (2008) to implement several methods for the evaluation of liquefaction and post-liquefaction effects.

## **7.2 Liquefaction Definition**

Liquefaction occurs when saturated, loose sandy or low plasticity cohesive soil loses stiffness and/or strength during earthquakes. These losses occur as effective stresses are reduced as a result of increased pore water pressure. Terzaghi and Peck (1948) described liquefaction as the significant loss of strength due to small disturbance. Mogami and Kubo (1953) mentioned that the liquefaction is triggered by monotonic or cyclic loading causing soil deformations. In the study of Marcuson (1978), liquefaction was also defined as the transformation of a granular soil from a solid to a liquefied state as an outcome of increased pore water pressure and decreased effective stress. Robertson and Wride (1997) indicated that the liquefaction phenomenon can be divided into two main groups: flow liquefaction and cyclic softening. Flow chart for the evaluation of liquefaction is given in Figure 7.1.

After the characterization of soil material, the strain hardening and softening behaviors can be distinguished into two different terms. If a soil is strain softening, flow liquefaction can occur due to the gravitational stresses. The general properties of these two groups, flow-liquefaction and cyclic softening, are summarized in the following paragraphs. The cyclic softening fact is mentioned in cyclic mobility section.

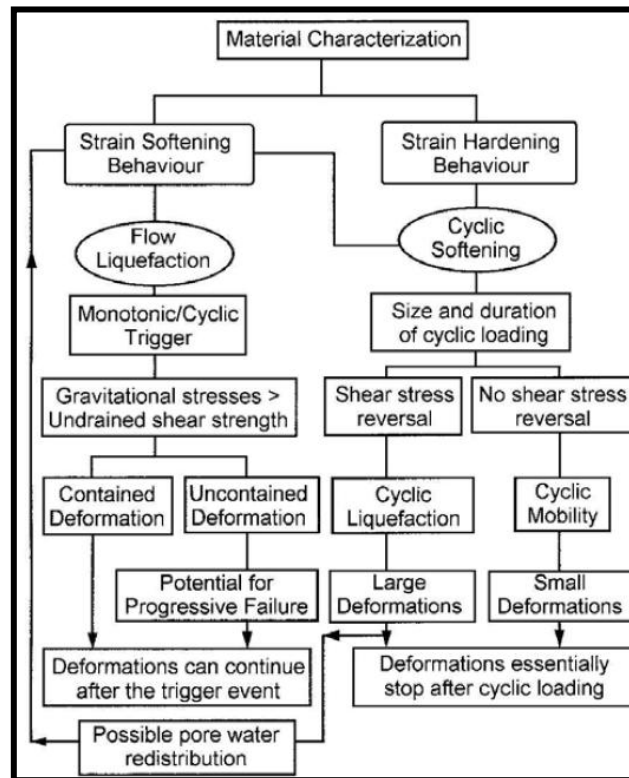


Figure 7.1. Flow chart for evaluation of liquefaction (after Robertson, 1994)

### 7.2.1 Flow liquefaction

Flow liquefaction can occur when the shear stress required for static equilibrium of a soil mass (the static shear stress) is greater than the shear strength of the soil in its liquefied state. The large deformations produced by flow liquefaction are driven by static shear stress. The cyclic stresses may simply shift the soil to an unstable state at which its strength drops adequately to allow the static stresses to produce the flow failure (Kramer, 1996).

Flow liquefaction is illustrated in Figure 7.2. A series of properties were introduced for flow liquefaction by Robertson (2004):

- It applies to only strain-softening soils and it requires a strain-softening response under undrained loading conditions.
- It requires in-situ shear stresses to be greater than the residual or minimum undrained shear strength.
- It can be triggered by monotonic or cyclic loading.

- For failure of a soil structure, such as a slope, to occur a sufficient amount of material must strain soften. The resulting failure can be a slide or a flow depending on the material characteristics and ground geometry.

- It may occur in any metastable saturated soil, such as very loose, fine, cohesionless deposits, very sensitive clays, and loess (silt) deposits.

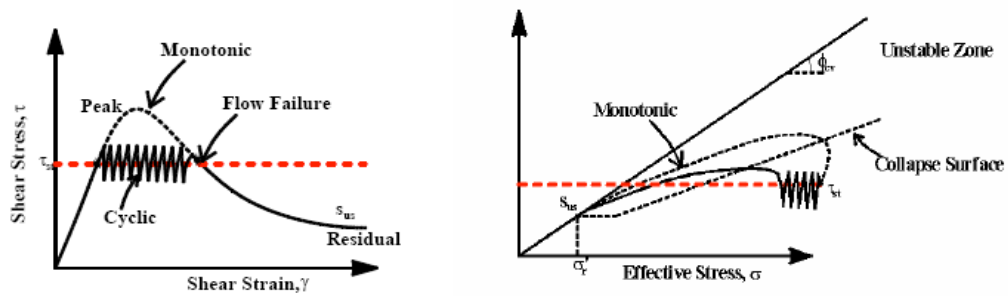


Figure 7.2. Flow liquefaction mechanism

In general, flow liquefaction cases are not very common. A few catastrophic examples of flow liquefaction failures are the Aberfan flow slide in South Wales in 1966 and Stava tailings dam failure in Italy in 1985 (Bishop, 1973).

### 7.2.2 Cyclic mobility

Cyclic mobility, which can be triggered by cyclic loading, can also produce unacceptably large permanent deformations. Deformations due to cyclic mobility develop incrementally because of static and dynamic stresses that exist during an earthquake. In contrast to flow liquefaction, cyclic mobility can occur in soil deposits with static shear stresses lower than the liquefied soil strength (Kramer, 1996).

Several properties of cyclic softening were also indicated by Robertson (2004):

- It requires undrained cyclic loading during which shear stress reversal occurs or zero shear stress can develop and allow effective stresses to reach zero.
- Deformations during cyclic loading can accumulate to large values, but generally stabilize shortly after cyclic loading stops.

- It can occur in almost all saturated sandy soils provided that the cyclic loading is sufficiently large in magnitude and duration.

- Clayey soils generally do not experience cyclic liquefaction and deformations are generally small due to the cohesive nature of the soils. Rate effects (creep) often control deformations in cohesive soils.

According to an NCEER (1997) study, cyclic mobility can be used to define the cyclic softening phenomenon which applies to both strain-softening and strain-hardening materials. The term cyclic softening was divided into two groups as cyclic mobility and cyclic liquefaction. The mechanisms are illustrated in Figures 7.3 and 7.4.

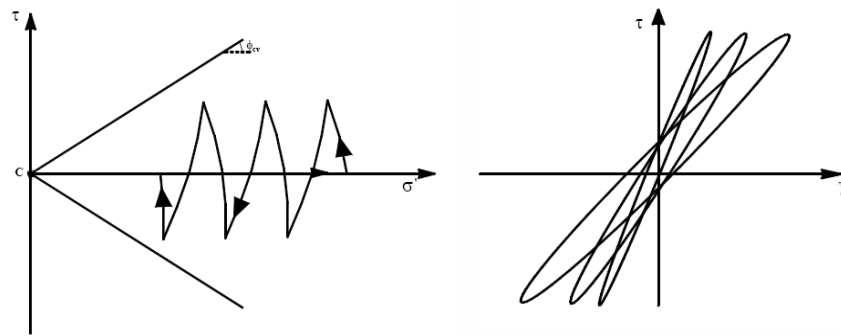


Figure 7.3. Mechanism of cyclic mobility

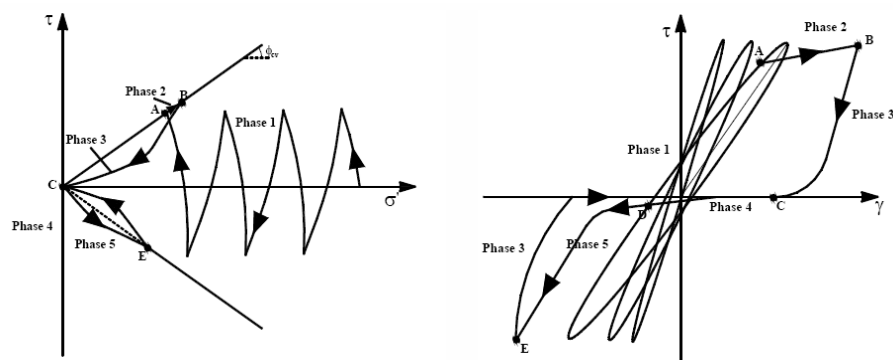


Figure 7.4. Mechanism of cyclic liquefaction



Cyclic softening may occur due to cyclic undrained loading, such as earthquake loading. The amount of deformations depends on the density of soil and the magnitude and duration of cyclic loading. If shear stress reversal occurs, it is possible for the effective stresses to reach zero. Therefore, cyclic liquefaction can take place as seen in Figure 7.4. When the condition of zero effective stress is achieved, large deformations can result in soils. If cyclic loading continues, deformations can progressively increase. If shear stress reversal does not take place, it is generally not possible to reach the condition of zero effective stress and deformations will be smaller and cyclic mobility may occur as seen in Figure 7.3.

Both flow liquefaction and cyclic liquefaction can cause large deformations. Hence, it can be very difficult to identify the correct phenomenon based on observed deformations following earthquake loading. A schematic illustration of the mechanism of cyclic softening combination is given in Figure 7.5. Common examples of cyclic softening were observed in the major earthquakes in Niigata in 1964 and Kobe in 1995 in the form of sand boils, damaged pipelines, lateral spreads, destruction of small embankments, settlements, and ground-surface cracks (Robertson and Wride, 1998).

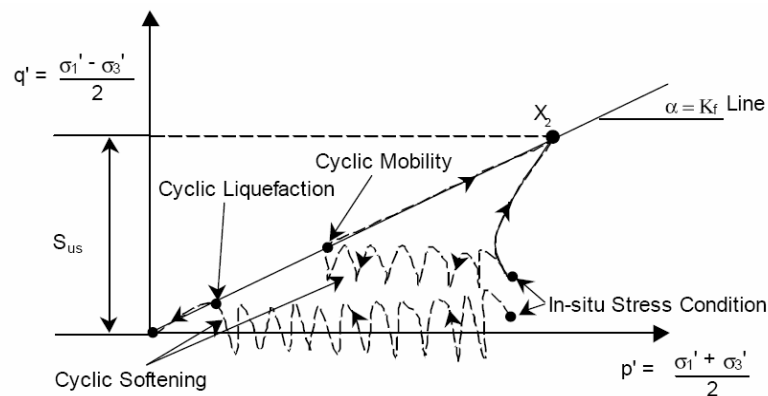


Figure 7.5. Combination of two phenomena in cyclic softening (modified from Rauch, 1997)

### 7.3 Liquefaction Susceptibility

Liquefaction susceptibility criteria generally consider groundwater level conditions, grain size characteristics, and plasticity of the soils at an interested area since liquefaction occurs in saturated soils. The typical subsurface soil condition that is susceptible to liquefaction is

loose sand with a shallow ground water table. The age of the deposit, soil type, particle size distribution, plasticity, groundwater level, and earthquake intensity are some of the main factors affecting the potential of soil against liquefaction. There are some procedures as well as evaluations based on in-situ test techniques such as SPT and CPT to determine liquefaction susceptible areas (Day, 2002).

### 7.3.1 Susceptibility criteria

The age of deposit, soil type, particle size distribution, plasticity, groundwater level, and earthquake intensity are the main criteria used to determine liquefaction susceptibility. In the literature, several procedures have been proposed to define the liquefaction susceptibility of fine-grained soils during earthquakes. The determination of susceptibility for fine-grained soils had been previously performed by Chinese criteria (Wang, 1979). However, recent earthquakes revealed that the Chinese criteria are not reliable to estimate the liquefaction susceptibility of fine-grained soils. As a result, the recently developed procedures are not consistent with the results proposed by Chinese criteria (Boulanger and Idriss, 2005; Bray and Sancio, 2006).

Boulanger and Idriss (2005) defined two types of soil behavior called “sand-like” and “clay-like” on the basis of stress normalization and stress-strain behavior of fine-grained soils. The difference between two behaviors can be distinguished on the basis of plasticity index (PI) and liquid limit (LL) as depicted in the Atterberg limit chart in Figure 7.6.

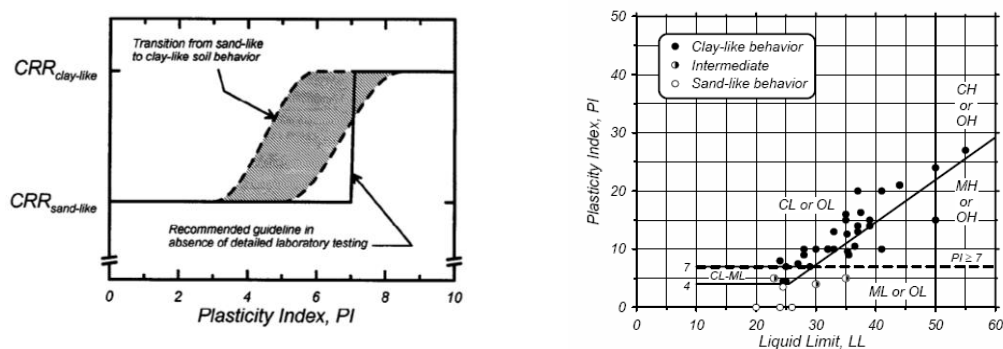


Figure 7.6. Atterberg limits chart showing representative values for soils exhibiting clay-like, sand-like, and intermediate stress-strain behaviors (after Boulanger and Idriss, 2005)

The observed transition “sand-like” and “clay-like” behavior is differentiated with the following criteria. Sand-like soils have a plasticity index (PI) value of less than 3 and clay-like soils have PI value higher than about 8. Thus, it was stated that the soils with sand-like behavior can be considered as susceptible to liquefaction. On the contrary, the soils showing clay-like behavior are not susceptible to liquefaction. This translational behavior was modeled with a susceptibility index ( $S_I$ ) as given in Equation 7.1. This equation was developed by Huang (2008) to approximate the transition shown by Boulanger and Idriss (2005).

$$S_{BI} = [1 + (\ln PI / 1.843)^{11.483}]^{-2.0} \quad (7.1)$$

In the study of Bray and Sancio (2006), new compositional criteria for liquefaction susceptibility evaluation were proposed on the basis of the investigation of fine-grained soils that liquefied during the 1994 Northridge, 1999 Kocaeli, and 1999 Chi-Chi earthquakes. The liquefied soil in those earthquakes was not consistent with the clay-size criterion of the Chinese criteria. Bray and Sancio (2006) mentioned that the amount and type of clay minerals in the soil are the best indicators of liquefaction susceptibility. Thus, the plasticity index-based approach was proposed as an indicator of liquefaction susceptibility. In addition to the plasticity index (PI), it was stated that the ratio of water content to liquid limit ( $w_c/LL$ ) is also another crucial parameter to determine the liquefaction susceptibility. It was concluded that loose soils with  $PI < 12$  and  $w_c/LL > 0.85$  are susceptible to liquefaction, and loose soils with  $12 < PI < 18$  and  $w_c/LL > 0.8$  are systematically more resistant to liquefaction. Soils with  $PI > 18$  tested at low effective confining stresses are not susceptible to liquefaction (Figure 7.7) (Bray and Sancio, 2006). The susceptibility criterion ( $S$ ) in terms of a relation was defined as given in Equation 7.2 and it was developed by Huang (2008).

$$S_{BS} = [1 + (\ln PI / 2.778)^{33.077}]^{-2.0} [1 + (4.401 / (\ln (w_c/LL))^{360.471})]^{-2.0} \quad (7.2)$$

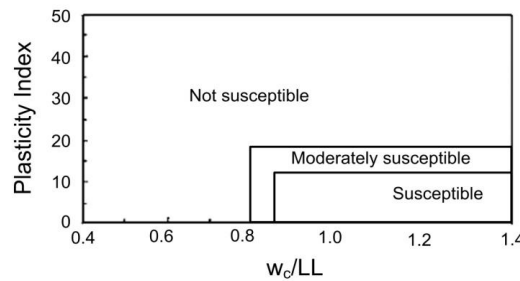


Figure 7.7. Ranges of  $w_c/LL$  and plasticity index for various susceptibility categories according to Bray and Sancio (2006)

### 7.3.2 Liquefaction potential

In order to define liquefaction susceptible areas, Liquefaction Potential Index (LPI) can also be employed as an alternative approach. LPI was originally proposed by Iwasaki et al. (1982). In the study of Iwasaki et al. (1982), the Equation 7.3 was recommended to obtain LPI values.

$$LPI = \int_0^z F(z) W(z) dz. \quad (7.3)$$

where  $z$  is the depth below the ground surface in meters and  $F(z)$  is a function of factor of safety depends on the threshold value of 1.0. The weighting factor,  $W(z)$ , can be calculated as:

$$W(z) = 10 - 0.5z \quad \text{for } z < 20 \text{ m} \quad (7.4)$$

LPI is therefore related to the thickness of liquefiable and non-liquefiable soil layers and to the factor of safety. LPI provides a unique value to quantify the liquefaction potential of liquefiable soil layers. In liquefaction hazard maps, this LPI method has frequently been considered (Sonmez, 2003, Ulusay and Kuru, 2004; Ku and Chi, 2006, Lenz and Baise, 2007). Hence, the LPI was adjusted using SPT and CPT data with the studies in the literature (Sonmez, 2003; Toprak and Holzer, 2003; Sonmez and Gokceoglu, 2005; Juang et al., 2008; Papathanassiou, 2008).

Sonmez (2003) proposed a modified LPI method considering the threshold value of factor of safety ( $F_L$ ) as 1.2. The  $W(z)$  value can also be calculated on the basis of  $F_L$  value using the formulas shown below for different limits. Sonmez (2003) developed the proposed factor of safety limits by re-arranging the sublayers which were proposed by Iwasaki et al. (1982) based on SPT-based approach.

$$LPI = \int_0^z F_L W(z) dz \quad (7.5)$$

which depends on:

$$F_L = 0 \text{ for } FS \geq 1.2 \quad (7.6a)$$

$$F_L = 1 - FS \text{ for } FS < 0.95 \quad (7.6b)$$

$$F_L = 2 \times 10^6 e^{-18.427FS} \text{ for } 1.2 > FS > 0.95 \quad (7.6c)$$

where  $W(z)$  can be calculated from Equation 7.4.

Sonmez and Gokceoglu (2005) suggested Liquefaction Severity Index ( $L_S$ ) which can be used in the preparation of susceptibility maps. This approach has a different threshold value than Sonmez (2003) based method. The upper boundary of the liquefaction was proposed as 1.411. The equations to be used for the determination of liquefaction severity index are given below:

$$L_S = \int_0^{20} P_L W(z) dz \quad (7.7)$$

where  $P_L$  (probability of liquefaction) depends on:

$$P_L(z) = \frac{1}{1 + (F_L/0.96)^{4.5}} \quad \text{for } F_L \leq 1.411 \quad (7.8a)$$

$$P_L(z) = 0 \quad \text{for } F_L > 1.411 \quad (7.8b)$$

where  $W(z)$  can be calculated from Equation 7.4.

Li et al. (2006) proposed the use of liquefaction potential index (IL) which was extended by introducing an empirical formula for assessing the probability of liquefaction-induced ground failure. Besides, the probabilistic-based approach is different than the other two of the deterministic methods (Iwasaki et al., 1982 and Sonmez, 2003). The criteria regarding to the probability is given in Table 7.1 and the formula is given in Equation 7.9.

Table 7.1. Probability of liquefaction-induced ground failure (after Li et al., 2006)

Probability	Description of the risk of liquefaction-induced ground failure
$0.9 < P_G$	extremely high to absolutely certain
$0.7 < P_G < 0.9$	high
$0.3 < P_G < 0.7$	medium
$0.1 < P_G < 0.3$	low
$P_G \leq 0.1$	extremely low to none

$$PL = \frac{1}{1 + \left(\frac{FS}{0.81}\right)^{5.45}} \quad (7.9)$$

Using Equation (7.9), the probability of liquefaction at a given depth can be determined based on calculated FS.

$$F = PL - 0.35 \quad \text{if } PL \geq 0.35 \quad (7.10a)$$

$$F = 0 \quad \text{if } PL < 0.35 \quad (7.10b)$$

Furthermore, Juang et al. (2008) reviewed the entire LPI-based methods and suggested a new model based on piezo-cone test (CPTU) results. Juang et al. (2008) concluded that Iwasaki et al. (1982) criteria cannot be universally applicable since the threshold liquefaction potential values (5 and 15) of Iwasaki et al. (1982) are not compatible with the real liquefaction cases presented in Juang et al. (2008).

The reliability of LPI methods was evaluated by Jha and Suzuki (2009). The effect of parameter uncertainties on the LPI was investigated in terms of the variability in the factor of safety. As a result, it was mentioned that the LPI was defined based on a reliability-based design safety factor as the variability in input parameters increases for a specified level of risk, the LPI also increases in the definition of LPI reliability-based approach. In addition, the liquefaction potential indices proposed by Iwasaki et al. (1982) and Sonmez (2003) can also be used for the preparation of liquefaction maps.

Liquefaction susceptibility can be defined in terms of liquefaction severity index (LSI) (Youd and Perkins, 1987) as a measure of liquefaction severity. The term liquefaction severity was considered in the studies of Sonmez and Gokceoglu (2005) and Yalcin et al. (2008) instead of the liquefaction risk which was suggested by Lee et al. (2003). Yilmaz and Cetin (2004) suggested a new Liquefaction Severity Index (LSI) considering the terms of probability of liquefaction. Moreover, the liquefaction severity index was compared to the liquefaction sensitivity index (LSeI) in the study of Ramakrishna et al. (2006). During the derivation of LSeI, multi-spectral, spatial, and temporal data sets from Indian remote sensing satellite were used depending on the increments of soil moisture after the seismic event since the near infrared and shortwave infrared regions of electromagnetic spectrum were highly absorbed by soil moisture after an earthquake.

### **7.3.3 Liquefaction susceptibility of Erbaa**

The first stage of determining the liquefaction potential of an area is the evaluation of susceptible soil units and site conditions. For this purpose, the WSliq software which was developed at the University of Washington (Huang, 2008; Kramer, 2008) was used to evaluate liquefaction susceptibility in Erbaa. The WSliq software was developed as part of an extended research project supported by the Washington State Department of Transportation (WSDOT) (Figure 7.8). The WSliq software was intended to allow engineers to evaluate liquefaction hazards more accurately, reliably, and consistently (Kramer, 2008).

The program allows deterministic, probabilistic, and performance-based evaluation at liquefaction hazards.

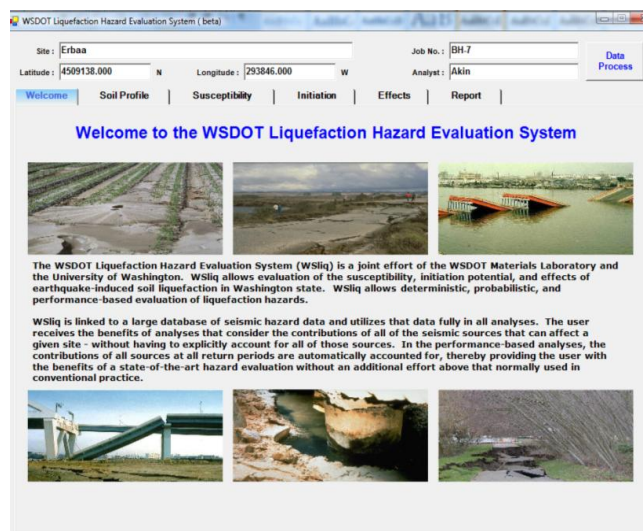


Figure 7.8. Introduction page of WSliq liquefaction evaluation software

The properties of each soil layer are entered in input files as shown in Figure 7.9. Moreover, the measured SPT-N resistance and unit weight of each soil layer are defined. Then, initial vertical stress,  $N_{1,60}$  and  $V_s$  values are calculated.

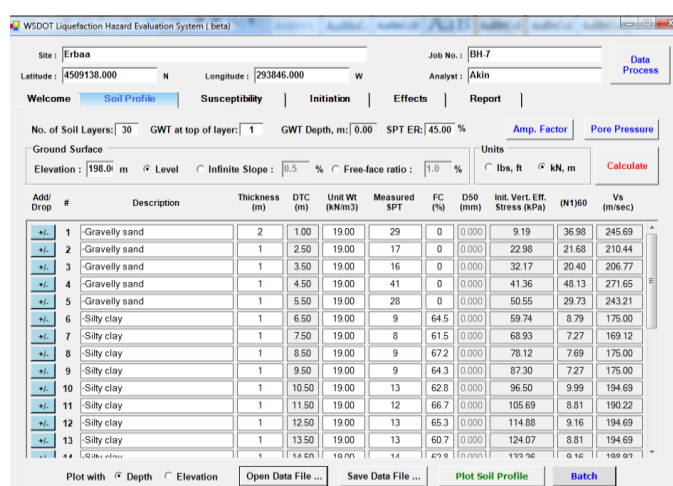


Figure 7.9. Data entry into the input files of WSliq software for BH-7

The liquefaction susceptible soil layers are evaluated using Boulanger and Idriss (2005) and Bray and Sancio (2006) methods in the susceptibility part of the software and an example of the susceptibility part can be seen in Figure 7.10. The susceptibility index defined in the software was proposed by Kramer (2008) which is also explained in the following paragraphs. The susceptibility index (SI) in WSliq software is the combination of the susceptibility models of Boulanger and Idriss (2005) and Bray and Sancio (2006) to provide a single index for liquefaction susceptibility estimation.

The SI provides a quantitative measure of liquefaction susceptibility that allows user to compare the relative susceptibilities of different layers. The SI value is also used in subsequent calculations to account for epistemic uncertainty in liquefaction susceptibility. The final liquefaction susceptibility (SI) is given using a weighted average of both methods in the software.

$$SI = w_1 S_{BI} + w_2 S_{BS} \quad (7.11)$$

where  $w_1$  and  $w_2$  are user-defined weighting factors ( $w_1 + w_2 = 1$ ). The susceptibility index (SI) from Equation 7.11 can range between 0.0 and 1.0 as seen in the lower part of the Figure 7.10.

The user can decide to consider only soil layers judged to be susceptible to liquefaction or to consider all layers with their contributions weighted by the SI value; in that case, the SI value is treated as a subjective probability, or degree of belief, of susceptibility.

The liquefaction susceptible zones in Erbaa are evaluated on the basis of the susceptibility index for each borehole. SI values are taken as 0.5 for each weighting factor to judge whether or not the soil is susceptible to liquefaction. The obtained liquefaction susceptibility map for the study area is presented in Figure 7.11.



WSDOT Liquefaction Hazard Evaluation System (beta)

Site: Erbaa Job No.: BH-7  
 Latitude: 4509138.000 N Longitude: 293846.000 W Analyst: Akim

Welcome | Soil Profile | **Susceptibility** | Initiation | Effects | Report

Layer	Description	DTC	PI	wcLL	Boulanger Idriss	Bray Sancio	Susceptibility Index	Susceptible?
1	Gravelly sand	1.00	N.P.	N.P.	1.00	1.00	1.00	YES
2	Gravelly sand	2.50	N.P.	N.P.	1.00	1.00	1.00	YES
3	Gravelly sand	3.50	N.P.	N.P.	1.00	1.00	1.00	YES
4	Gravelly sand	4.50	N.P.	N.P.	1.00	1.00	1.00	YES
5	Gravelly sand	5.50	N.P.	N.P.	1.00	1.00	1.00	YES
6	Silty clay	6.50	22.5	0.6	0.00	0.01	0.00	NO
7	Silty clay	7.50	19.7	0.45	0.00	0.00	0.00	NO
8	Silty clay	8.50	16.9	0.7	0.00	0.09	0.04	NO
9	Silty clay	9.50	18.7	0.6	0.00	0.02	0.01	NO
10	Silty clay	10.50	22.8	0.6	0.00	0.01	0.00	NO
11	Silty clay	11.50	22.4	0.6	0.00	0.01	0.00	NO
12	Silty clay	12.50	24.2	0.6	0.00	0.01	0.00	NO
13	Silty clay	13.50	21.4	0.6	0.00	0.01	0.01	NO
14	Silty clay	14.50	23.3	0.6	0.00	0.01	0.00	NO
15	Silty clay	15.50	23.2	0.7	0.00	0.02	0.01	NO
16	Silty sand	16.50	N.P.	N.P.	1.00	1.00	1.00	YES
17	Silty sand	17.50	N.P.	N.P.	1.00	1.00	1.00	YES

Threshold SI: 0.5 Weighting Factors: B1 0.50 B5 0.50 B-S Evaluate

Figure 7.10. Liquefaction susceptibility evaluation in WSliq software for BH-7

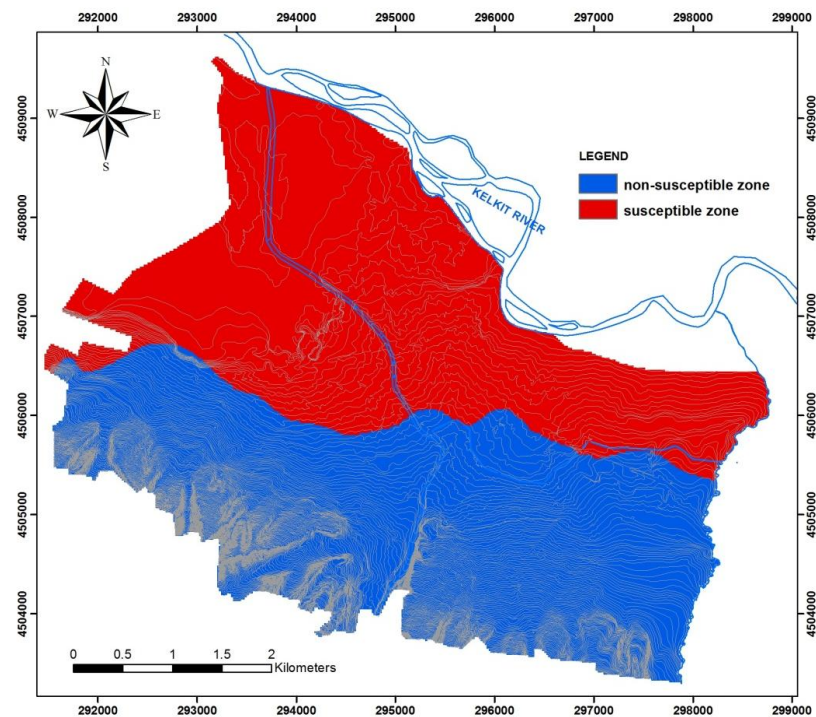


Figure 7.11. Liquefaction susceptibility map of Erbaa

Liquefaction susceptible zones given in Figure 7.11 mostly cover the northern part of the study area. These zones indicate that numerous possible liquefiable layers exist in this area.

### 7.3.4 Liquefaction potential of Erbaa

The LPI methods proposed by Iwasaki et al. (1982); Sonmez (2003) and LSI method proposed by Sonmez and Gokceoglu (2005) are considered to obtain liquefaction potential of Erbaa. Initially, factor of safety (FS) values were determined for each borehole using the Idriss and Boulanger (2008) approach as will be explained in the initiation of liquefaction section. During the determination of factor of safety, different PGA values obtained from site response analyses for each borehole were considered. In other words, instead of using a constant PGA value for the entire study area, borehole and/or grid system specific PGA values were taken into consideration for liquefaction evaluations. Finally, liquefaction potential index (LPI) and liquefaction severity index ( $L_s$ ) values were calculated based on the Iwasaki et al. (1982) and Sonmez (2003), and Sonmez and Gokceoglu (2005) approaches. The liquefaction potential index (LPI) categories proposed by Iwasaki et al. (1982) and Sonmez (2003), and the liquefaction severity index (LSI) categories proposed by Sonmez and Gokceoglu (2005) are summarized in Tables 7.2, 7.3, and 7.4, respectively.

Table 7.2. Liquefaction index categories proposed by Iwasaki et al. (1982)

<b>Liquefaction index (<math>L_i</math>)</b>	<b>Liquefaction potential</b>
0	Very low
$0 < L_i \leq 5$	Low
$5 < L_i \leq 15$	High
$15 > L_i$	Very high

Table 7.3. Liquefaction index categories proposed by Sonmez (2003)

<b>Liquefaction index (<math>L_i</math>)</b>	<b>Liquefaction potential</b>
0	Non-liquefied
$0 < L_i \leq 2$	Low
$2 < L_i \leq 5$	Moderate
$5 < L_i \leq 15$	High
$15 > L_i$	Very high

Table 7.4. Liquefaction index categories proposed by Sonmez and Gokceoglu (2005)

<b>Liquefaction index (<math>L_s</math>)</b>	<b>Liquefaction potential</b>
0	Non-liquefied
$0 < L_s < 15$	Very low
$15 \leq L_s < 35$	Low
$35 \leq L_s < 65$	Moderate
$65 \leq L_s < 85$	High
$85 \leq L_s < 100$	Very high

The liquefaction potential maps of the study area in accordance with three abovementioned methods are presented in Figures 7.12, 7.13, and 7.14.

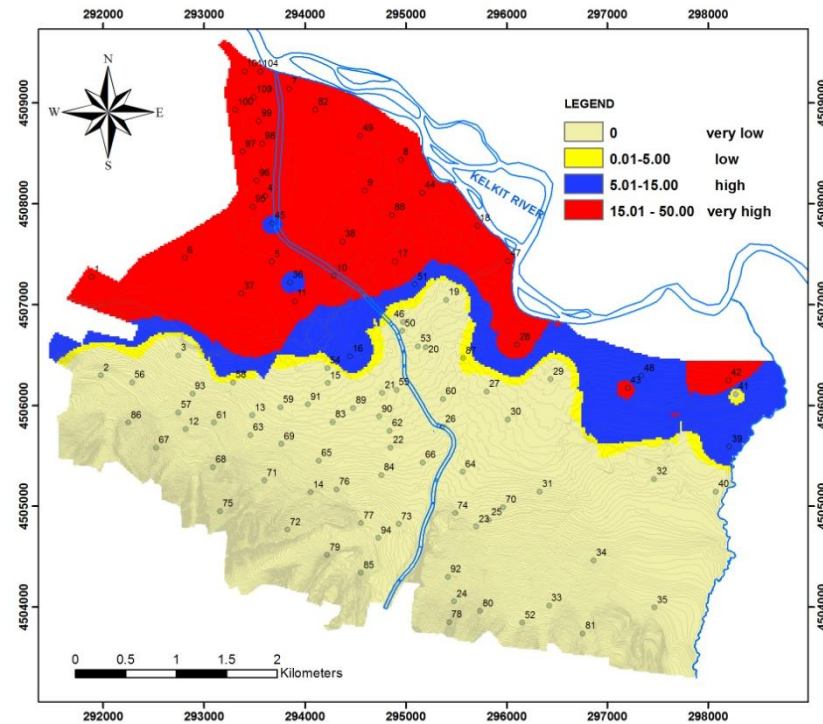


Figure 7.12. Liquefaction potential map of the study area based on Iwasaki et al. (1982) LPI method

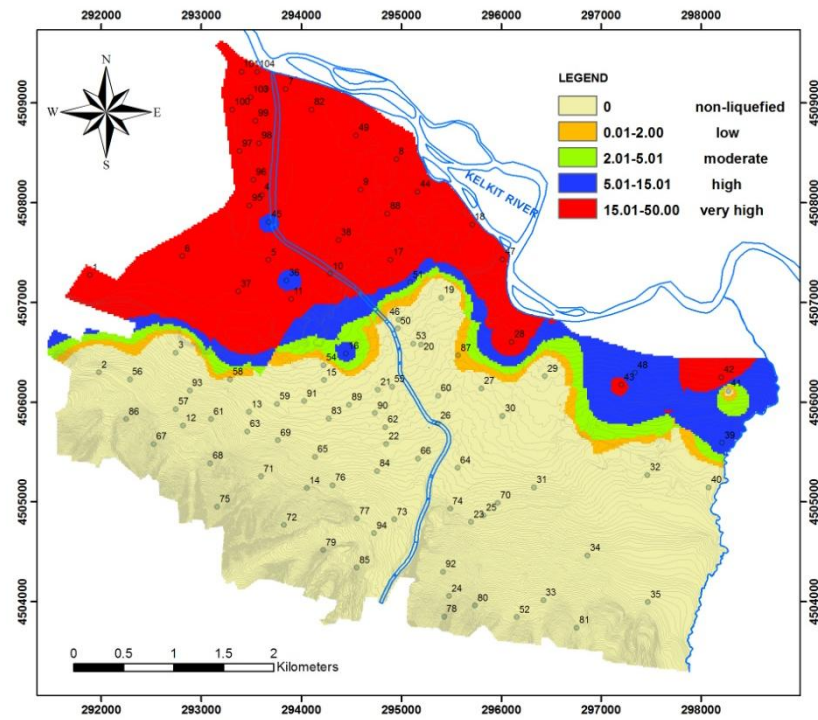


Figure 7.13. Liquefaction potential map of the study area based on Sonmez (2003) LPI method

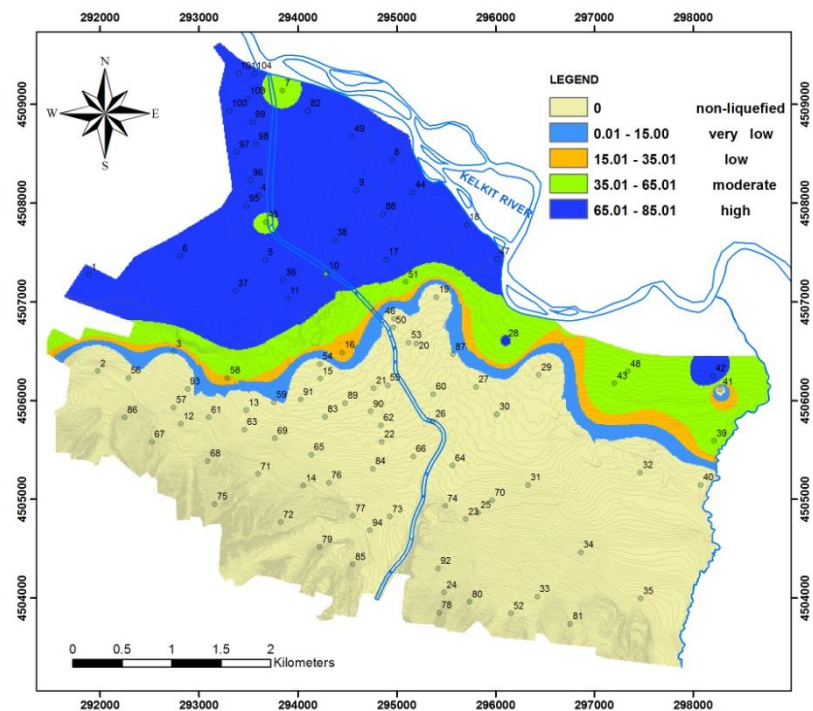


Figure 7.14. Liquefaction potential map of the study area based on Sonmez and Gokceoglu (2005) LSI method

The light yellow areas represent very low LPI values in the liquefaction potential map based on Iwasaki et al. (1982) method (Figure 7.12). This is quite illogical as the non-susceptible Pliocene units are also included in the same zone. Furthermore, the same zone reasonably corresponds to non-liquefiable layers in accordance with the modified LPI method by Sonmez, 2003. Both LPI models (Iwasaki et al., 1982 and Sonmez, 2003) imply a very high liquefaction potential zone (red zone) in the northwestern part of the study area especially in sandy alluvial deposits along Kelkit River. On the contrary, LSI method proposed by Sonmez and Gokceoglu (2005) exhibits high liquefaction severity for the northwestern part of the study area (Figure 7.14).

#### 7.4 Evaluation of Initiation of Liquefaction

A number of approaches to evaluate the potential for the initiation of liquefaction were developed after having understood the liquefaction effects. The most commonly used approach is the cyclic stress approach which considers the loading conditions in terms of cyclic shear stresses. The other, less commonly, used approaches include cyclic strain, energy dissipation, and probabilistic methods.

In the cyclic stress approach, loading is based on the amplitude and the number of cycles of earthquake-induced shear stress (Kramer, 1996). This cyclic shear stress is used in the comparison of liquefaction resistance of soil. The liquefaction resistance of soils can be characterized based on the laboratory and field tests. The necessary parameters to define the liquefaction resistance of susceptible soil layers can be obtained by correlation to the results of in-situ tests including SPT, CPT, and/or  $V_s$  based measurements. Moreover, the empirical approaches are mostly employed on the basis of SPT applications since the SPT is practical and cheap. The SPT-based procedures updated by Youd et al. (2001), Cetin et al. (2004), and Idriss and Boulanger (2006) are derived from the ratio between cyclic resistance ratio (CRR) and the cyclic stress ratio (CSR).

The factor of safety against liquefaction is calculated by Equation 7.12 in all deterministic methods.

$$FS_L = \frac{CRR}{CSR} \quad (7.12)$$

The cyclic stress ratio (CSR) can be estimated by the simplified method;

$$CSR = 0.65 \frac{a_{\max}}{g} \frac{\sigma_{v0}}{\sigma'_{vo}} \frac{r_d}{MSF} \quad (7.13)$$

Different estimations for depth reduction factor ( $r_d$ ) and magnitude scaling factor (MSF) exist in the literature. According to the study of NCEER (Youd et al., 2001),  $r_d$  and MSF can be obtained as follows:

$$r_d = \frac{(1.000 - 0.41113z^{0.5} + 0.04052z + 0.001753z^{1.5})}{(1.000 - 0.4177z^{0.5} + 0.05729z - 0.006205z^{1.5} + 0.001210z^2)} \quad (7.14)$$

$$\begin{aligned} MSF &= (7.5/M_w)^{2.95} & M_w \leq 7.5 \\ MSF &= (7.5/M_w)^{2.56} & M_w > 7.5 \end{aligned} \quad (7.15)$$

According to the study of Idriss and Boulanger (2004),  $r_d$  and MSF can be calculated as follows:

$$\ln(r_d) = \alpha(z) + \beta(z)M \quad (7.16a)$$

$$\alpha(z) = -1.012 - 1.126 \sin((z/11.73) + 5.133) \quad (7.16b)$$

$$\beta(z) = 0.106 + 0.118 \sin((z/11.28) + 5.142) \quad (7.16c)$$

$$MSF = 6.9 \exp(-M/4) - 0.058 \quad (7.17)$$

The cyclic resistance ratio (CRR) can be estimated for a standard vertical effective stress of 1 tsf or 1 atm and can be modified for other effective stress levels by the term  $K_\sigma$ .

$$CRR = CRR_{\sigma=1 \text{ tsf}} K_\sigma \quad (7.18)$$

The  $CRR_{\sigma=1 \text{ tsf}}$  is a function of in-situ parameters based on SPT or CPT resistance. The CRR represents the liquefaction resistance of soils following some essential corrections for the obtained SPT-N blow-counts. The equivalent overburden stress of 100 kPa using the stress normalization correction factor ( $C_N$ ) is one of the most important corrections for the analyses. Several equations for  $C_N$  have been suggested by different researchers (Peck et al., 1974; Seed, 1976; Seed and Idriss, 1983; Tokimatsu and Yoshimi, 1983; Liao and Whitman, 1986; Bowles, 1988; Boulanger and Idriss, 2004). The two most common empirical overburden corrections were proposed by Liao and Whitman (1986) (Equation 7.19) and Idriss and Boulanger (2006) (Equation 7.20a, b).

$$C_N = (1 / \sigma'_v)^{0.5} \quad (7.19)$$

$$C_N = (P_a / \sigma'_v)^\alpha \leq 1.7 \quad (7.20a)$$

$$\alpha = 0.784 - 0.0768 \sqrt{(N_1)_{60}} \quad (7.20b)$$

Other factors (energy correction, hole-diameter, rod-length, and the type of sampler) should also be concerned to calculate the energy corrected SPT N-value,  $(N_1)_{60}$ . The corrections for  $C_R$ ,  $C_S$ ,  $C_B$ , and  $C_E$  can be performed as recommended by the NCEER Working Group (NCEER, 1997).

$$(N_1)_{60} = N C_N C_R C_S C_B C_E \quad (7.21)$$

where

$C_N$ : overburden correction,

$C_R$ : correction for rod length,

$C_S$ : correction for sampler configuration,

$C_B$ : correction for borehole diameter, and

$C_E$ : correction for hammer energy efficiency (60%).

After the determination of normalized SPT resistance, fines content correction and overburden stress correction factors can also be applied. According to the study of NCEER (Youd et al., 2001), the fines content (FC) and overburden stress correction factor ( $K_\sigma$ ) can be determined by;

$$(N_1)_{60, CS} = \alpha + \beta (N_1)_{60} \quad (7.22a)$$

$$\alpha = (\exp (1.76-190/FC^2)) \quad 5\% < FC < 35\% \quad (7.22b)$$

$$\beta = (0.99+FC^{1.5} / 1000) \quad 5\% < FC < 35\% \quad (7.22c)$$

$$K_\sigma = \min (\sigma'_{v0} / P_a)^{f-1} \quad (7.23)$$

In the study of Idriss and Boulanger (2004), the fines content (FC) and overburden stress correction factor ( $K_\sigma$ ) can be determined by;

$$(N_1)_{60, CS} = (N_1)_{60} + \Delta (N_1)_{60} \quad (7.24a)$$

$$\Delta (N_1)_{60} = (\exp (1.63- (9.7/FC)- (15.7/FC)^2)) \quad (7.24b)$$

$$K_\sigma = \min (1- C_\sigma \ln (\sigma'_{v0} / P_a)) \quad (7.25a)$$

$$C_\sigma = 1 / (18.9 -2.55 \sqrt{(N_1)_{60, CS}}) \quad (7.25b)$$

According to the study of NCEER (Youd et al., 2001),  $CRR_{\sigma=1 \text{ tsf}}$  can be determined by the following relations.

$$CRR_{\sigma=1 \text{ tsf}} = \frac{1}{34 - (N_1)_{60, CS}} + \frac{(N_1)_{60, CS}}{135} + \frac{50}{(10 (N_1)_{60, CS} + 45)^2} - \frac{1}{200} \quad (7.26)$$

Idriss and Boulanger (2004) defined CRR as follows:

$$CRR_{\sigma=1 \text{ tsf}} = \exp\left(\frac{(N_1)_{60, CS}}{14.1} + \left(\frac{(N_1)_{60, CS}}{126}\right)^2 - \left(\frac{(N_1)_{60, CS}}{23.6}\right)^3 - \left(\frac{(N_1)_{60, CS}}{25.4}\right)^4 - 2.8\right) \quad (7.27)$$

Cetin et al. (2004) proposed the liquefaction initiation models both for deterministic and probabilistic based methods. The charts in Figure 7.15 were proposed in order to define liquefaction triggering effects from SPT results.

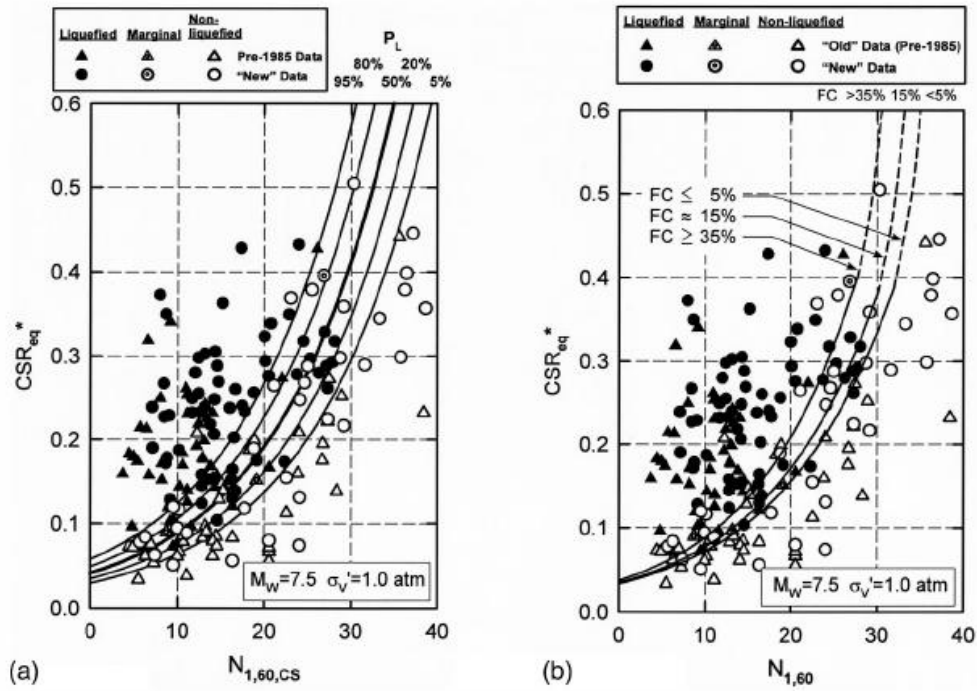


Figure 7.15. (a) Recommended probabilistic standard penetration test-based liquefaction triggering correlation (b) recommended "deterministic" standard penetration test-based liquefaction triggering correlation (after Cetin et al., 2004)

#### 7.4.1 Liquefaction initiation models of Erbaa

The existing borehole data were evaluated in the liquefaction initiation analyses in the preliminary stage of the thesis (Akin and Topal, 2008a; 2008b). Considering the new



borehole data, the proposed liquefaction initiation models of Youd et al. (2001), Cetin et al. (2004), Idriss and Boulanger (2006) are employed in the initiation section for the liquefaction analyses. The single scenario liquefaction analyses are considered in the initiation part of the WSLiq software (Figure 7.16). The loading parameters (earthquake parameters) for the selected scenario event were evaluated in the previous chapters. Moreover, user-defined option in the selection of loading parameters is preferred to consider each PGA surface value obtained from the site response analyses for each borehole. The earthquake magnitude is accepted as 7.2 which was previously mentioned in the seismic hazard analyses part of the dissertation.

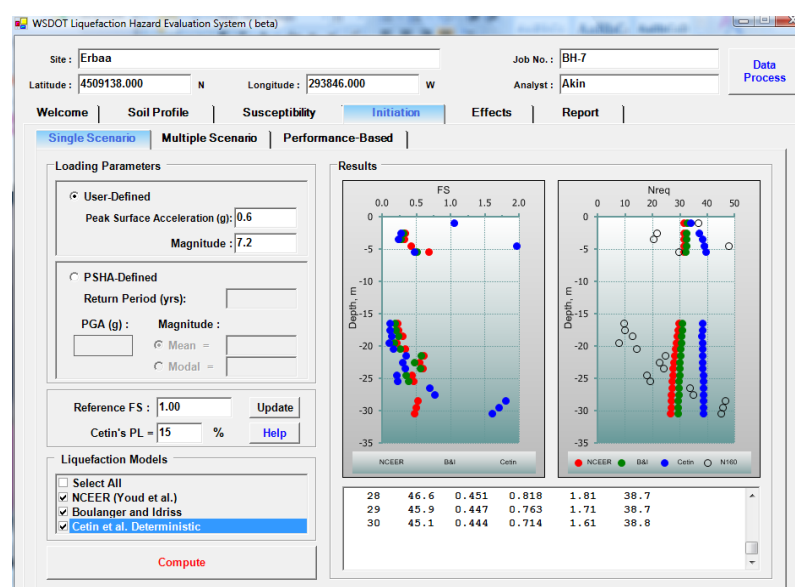


Figure 7.16. Liquefaction initiation models of Erbaa based on NCEER (Youd et al., 2001), Boulanger and Idriss (2006), and Cetin et al. (2004) models

The initiation models of Erbaa involve the distribution of factor of safety values for each borehole data including different methods. The produced results from the initiation models are considered in susceptibility part of this section.

## 7.5 Post-liquefaction Effects

Liquefaction may cause permanent deformations that can significantly affect structures. The severity of liquefaction effects depends on the characteristics of the soil and the loading.

Hence, the determination of post-liquefaction effects generally requires estimation of the level of liquefaction-based deformations. Liquefaction may cause settlement, sinking, bearing capacity failure, lateral movements, and landslides. The two most important post-liquefaction effects are lateral spreading and vertical settlements in soils which may cause permanent deformations in structures. Various schematic examples for post-liquefaction deformations are shown in Figure 7.17.

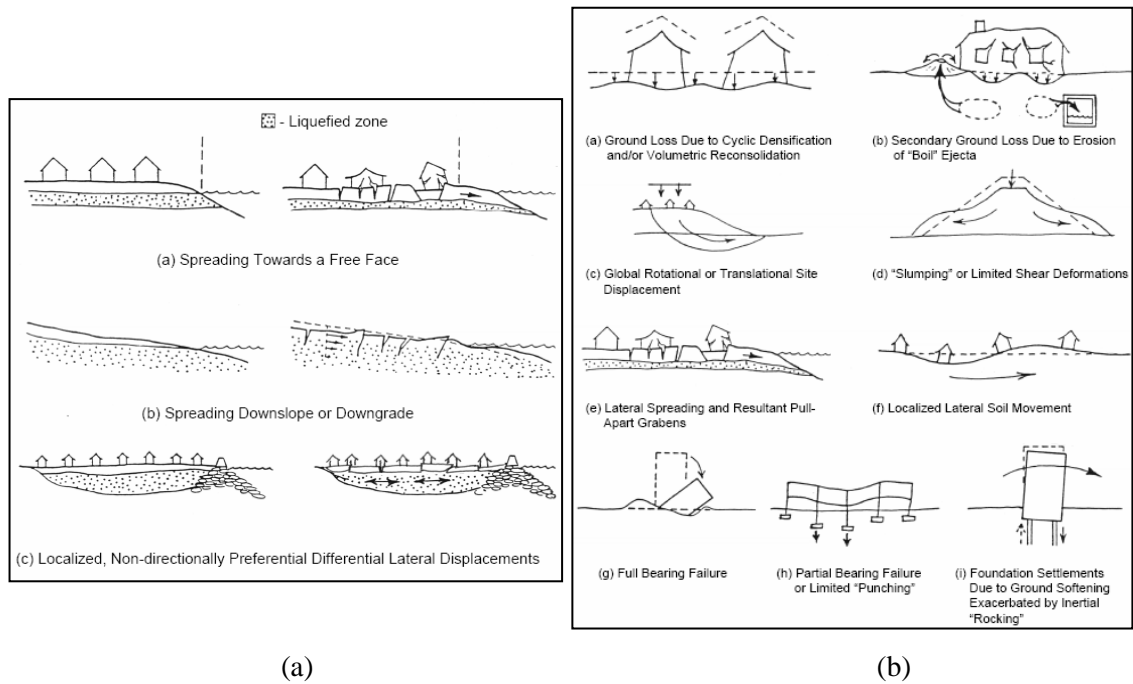


Figure 7.17. Schematic examples of (a) liquefaction-induced lateral translation and (b) liquefaction-induced vertical displacements (after Seed et al., 2001)

### 7.5.1 Lateral spreading displacements

Permanent lateral ground deformation due to liquefaction-induced lateral spreading is a potential source of major damage to structures and lifelines during earthquakes. Lateral spreading can lead to significant permanent deformations in gently sloping ground and in the vicinity of natural and cut slopes. Lateral spreading is one of the ground failures which can be accompanied by flow slides, ground settlements, ground oscillation, and sand boils. Moreover, the liquefaction-induced ground failures, especially lateral spreads, can be observed around gentle slopes or gently inclined ground with a free face (e.g., river banks, road cuts).

The potential of liquefaction-induced lateral spreading displacements should be investigated in microzonation studies. For this aim, several researchers investigated the potential areas and explained the liquefaction-induced damage especially after the 1999 Kocaeli earthquake (Bray et al., 2001; Cetin et al., 2002; Aydan et al., 2004; Kanıbir et al., 2006; Sonmez et al., 2008; Sonmez and Ulusay, 2008; Youd et al., 2009).

The methods proposed to estimate liquefaction-induced lateral ground displacements include numerical models, laboratory tests, and field-based test methods. The proposed empirical methods employ the ground inclination and the thickness of liquefiable ground layer generally through regression analyses (Hamada, 1999; Bardet et al., 1999; Youd et al., 2002; Zhang et al., 2004; Kramer and Baska, 2006; Idriss and Boulanger, 2008). Three empirical lateral spreading models (Youd et al., 2002; Kramer and Baska, 2006; Idriss and Boulanger, 2008) are considered in WSliq software to compute lateral spreading. These methods are briefly summarized in the following sections. In addition to these three lateral spreading models, the lateral spreading model proposed by Zhang et al. (2004) is also explained in the following sections.

#### 7.5.1.1 Youd et al. (2002) lateral spreading model

The multiple linear regression (MLR) procedure proposed by Youd et al. (2002) is widely used for predicting lateral spread displacements. This model requires the mean grain size of the soils with SPT resistances to be less than 15. The characterization of slopes should be done in terms of free face or ground slope condition. The necessary terms are presented in Figure 7.18 for the definition of slope conditions.

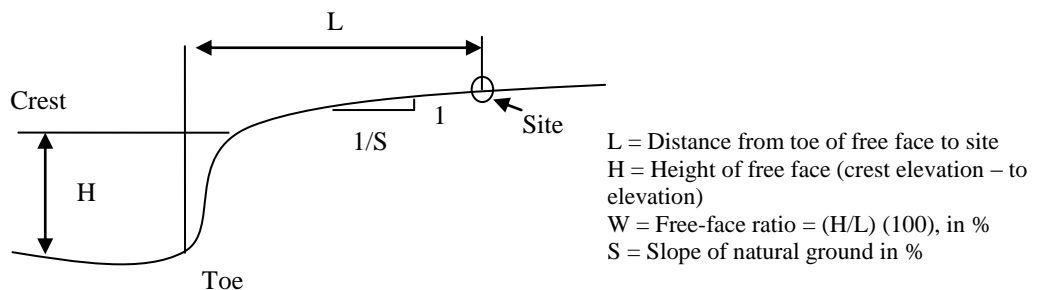


Figure 7.18. Notations for slope geometry (after Youd et al., 2002)

This procedure is expressed in the following equations:

$$\log DH = b_0 + b_1 M_w + b_2 \log R^* + b_3 R + b_4 \log W + b_5 \log S + b_6 \log T_{15} + b_7 \log(100 - F_{15}) + b_8 \log(D50_{15} + 0.1 \text{ mm}) \quad (7.28)$$

where  $DH$  : horizontal displacement in meters and  $R^* = R + 10^{-0.89} M_w^{-5.64}$

$T_{15}$  : cumulative thickness of soil layers with corrected SPT resistance  $(N_1)_{60}$ , less than or equal to 15 for liquefaction susceptible layers

The other recommended variable values for the Youd et al. (2002) predictive equation are given in Figure 7.19. The values of  $W$ ,  $S$ ,  $D50_{15}$  and  $F_{15}$  in the same equation can be found in the same figure. The essential coefficients in Equation 7.28 are summarized in Table 7.5.

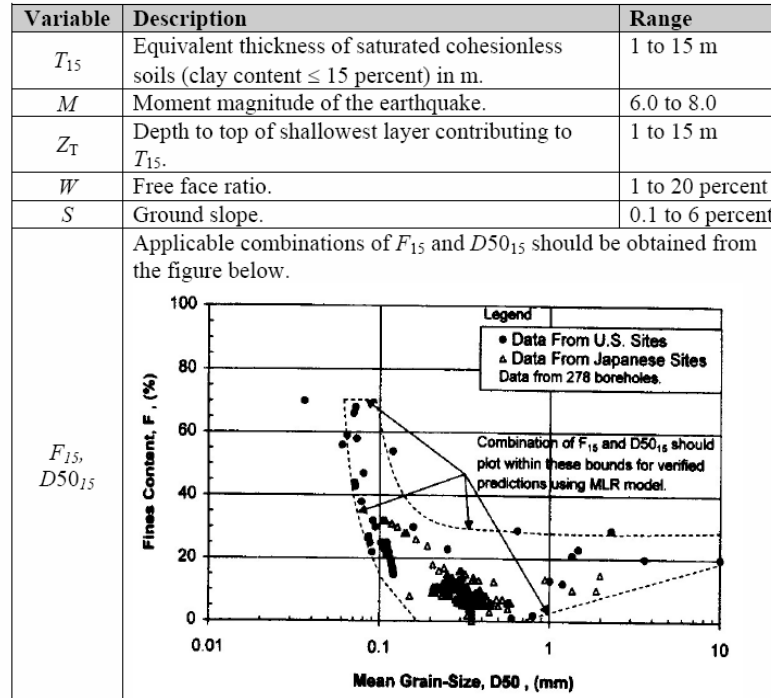


Figure 7.19. Recommended values for the Youd et al. (2002) predictive equation

Table 7.5. Coefficients for Youd et al. (2002) lateral spreading model

Model	$b_0$	$b_1$	$b_2$	$b_3$	$b_4$	$b_5$	$b_6$	$b_7$	$b_8$
Ground slope	-16.213	1.532	-1.406	-0.012	0	0.338	0.54	3.413	-0.795
Free face	-16.713	1.532	-1.406	-0.012	0.592	0	0.54	3.413	-0.795

### 7.5.1.2 Zhang et al. (2004) lateral spreading model

Zhang et al. (2004) proposed a semi-empirical approach to estimate liquefaction-induced lateral displacements using SPT or CPT data. The empirical relationships between relative density and penetration resistance (SPT or CPT) to allow lateral spreading displacement are used for prediction. A lateral displacement index (LDI) obtained by integrating the maximum cyclic shear strains ( $\gamma_{\max}$ ) with depth was proposed in the same study. The lateral displacement index (LDI) can be calculated by Equation 7.29.

$$\text{LDI} = \int_0^{Z_{\max}} \gamma_{\max} dz \quad (7.29)$$

where  $Z_{\max}$  : maximum depth below the entire potential liquefiable layers with a calculated factor of safety (FS) < 2.0.

Ishihara and Yoshimine (1992) initially developed a relationship between  $\gamma_{\max}$  and FS based on laboratory test results on clean sands considering the effect of fines content. Zhang et al. (2004) also applied the effect of fines content on SPT-CPT results to estimate  $\gamma_{\max}$ . Figure 7.20 shows the relation between  $\gamma_{\max}$  and FS for different  $D_r$  (relative density). Eventually, the essential  $\gamma_{\max}$  parameter can be estimated from Figure 7.20 using FS and relative density.

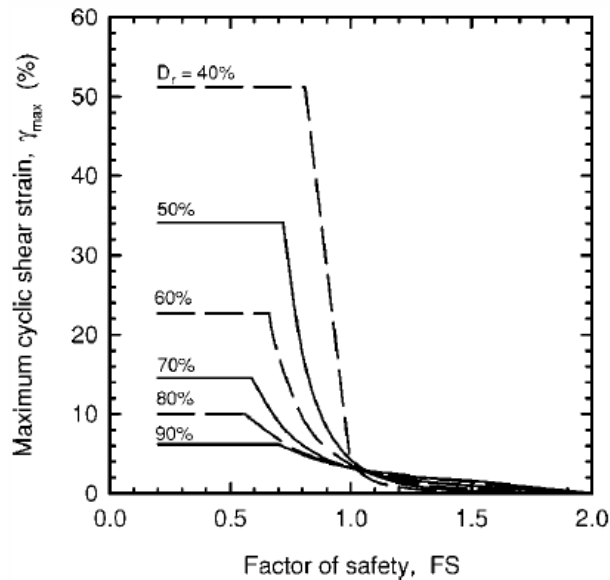


Figure 7.20. Relationship between  $\gamma_{\max}$  and FS for different  $D_r$  for clean sands (after Zhang et al., 2004)

It was aimed to quantify potential lateral displacements for a given soil profile, soil properties, and earthquake characteristics using LDI in the study of Zhang et al. (2004). Moment magnitude of an earthquake ( $M_w$ ) and peak surface acceleration ( $a_{max}$ ) were suggested to be used for the characterization of the earthquake size and the intensity of strong ground motion in this approach.

### 7.5.1.3 Kramer and Baska (2006) lateral spreading model

Kramer and Baska (2006) proposed a model that can be used to predict the probability distribution of lateral spreading displacement. In this model, a series of nonlinear analyses were performed to identify the mechanics of liquefiable soil conditions. According to the study of Kramer and Baska (2006), the median lateral spreading displacement can be calculated using the following equations:

$$\sqrt{DH} = \frac{\beta_1 + \beta_2 T_{gs}^* + \beta_3 T_{ff}^* + 1.231M_w - 1.151\log R^* - 0.01R + \beta_4\sqrt{S} + \beta_5 \log W}{1 + 0.0223 (\beta_2/T_{gs}^*)^2 + 0.0135 (\beta_3/T_{ff}^*)^2} \quad (7.30)$$

where  $R^* = R + 100.89M_w - 5.64$

The definitions of  $\beta$ ,  $T_{gs}^*$  and  $T_{ff}^*$  are explained in the following section. The model-specific  $\beta$  coefficients are given in Table 7.6.

Table 7.6. Coefficients for Kramer and Baska (2006) lateral spreading model

Model	$\beta_1$	$\beta_2$	$\beta_3$	$\beta_4$	$\beta_5$
Ground slope	-7.207	0.067	0.0	0.544	0.0
Free face	-7.518	0.0	0.086	0.0	1.007

The equivalent thickness parameters  $T_{gs}^*$  and  $T_{ff}^*$  for ground slope and free-face sites can be estimated by the following formulas, respectively.

$$T_{gs}^* = 2.586 \sum_{i=1}^n t_i \exp (-0.05N_i - 0.04z_i) \geq 0.001m \quad (7.31a)$$

$$T_{ff}^* = 5.474 \sum_{i=1}^n t_i \exp (-0.08N_i - 0.10z_i) \geq 0.001m \quad (7.31b)$$

where  $N_i : (N_i)_{60,cs}$  for the  $i^{th}$  sublayer

$t_i$  : sublayer thickness (limited to a maximum value of 1 m)

#### 7.5.1.4 Idriss and Boulanger (2008) lateral spreading model

An alternative lateral displacement index (LDI) was proposed by Idriss and Boulanger (2008). The LDI can be computed by integrating the maximum strains over the thickness of the profile. The estimated displacement value from LDI approach supposes that all potentially liquefiable layers attain their respective maximum strain values, and that all of those values are acting in the same direction.

This model considers slopes in loose, saturated soils to move toward a relative density-dependent limiting shear strain upon initiation of liquefaction. Idriss and Boulanger (2008) recommended a limiting shear strain using the curves shown in Figure 7.21. It can be computed as follows:

$$\gamma_{lim} = 1.859 \left( 1.1 - \frac{\sqrt{(N_1)_{60CS}}}{46} \right)^3 \quad (7.32)$$

Then, the maximum expected shear strain for a given level of loading could be related to the density of the soil and the factor of safety against liquefaction using the Equation 7.33.

$$\gamma_{max} = \begin{cases} 0 & \text{if } FS_L \geq 2 \\ \gamma_{lim} & \text{if } FS_L \leq A \\ \min(B, \gamma_{lim}) & \text{if } A \leq FS_L \leq 2 \end{cases} \quad (7.33)$$

where

$$A = 0.535 + 0.398 \sqrt{\max(5.6, (N_1)_{60CS})} - 0.0924 \max(5.6, (N_1)_{60CS})$$

$$B = 0.035 (1-A) \left( \frac{2-FS_L}{FS_L-A} \right) \quad (7.34)$$

With the maximum strain values computed for potentially liquefiable layers in a soil profile, the lateral displacement index, taken as a measure of the potential maximum displacement, can be computed by integrating the maximum strains over the thickness of the profile as given in Equation 7.29. The LDI produces a displacement value that implicitly assumes all potentially liquefiable layers reach their respective maximum strain values, and that all of those values are acting in the same direction (Kramer, 2008).

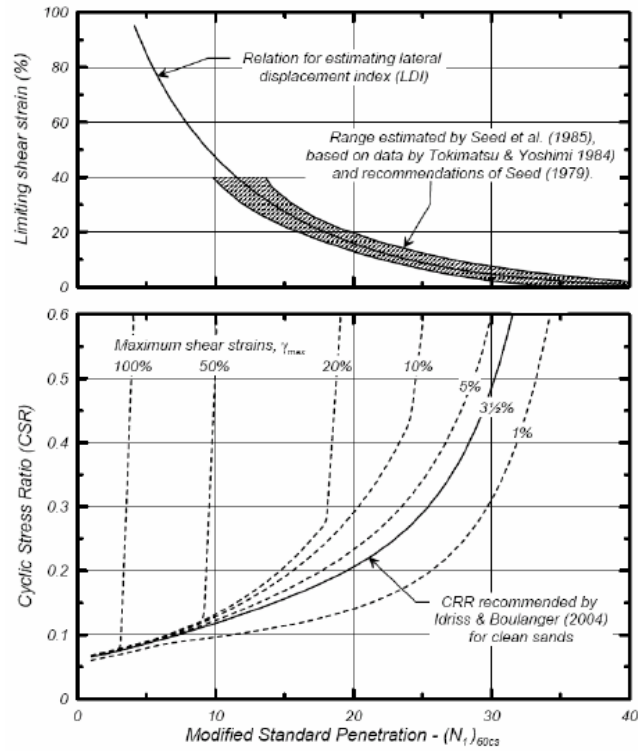


Figure 7.21. Limiting strain curves (after Kramer, 2008)

### 7.5.2 Evaluation of lateral spreading displacements for Erbaa

Lateral spreading can produce significant and damaging lateral displacements of the ground surface. The permanent possible deformations in Erbaa as a post-liquefaction effect are determined using the three empirical approaches (Youd et al., 2002; Kramer and Baska, 2006; Idriss and Boulanger, 2008) summarized in the abovementioned paragraphs. These approaches are implemented in the WSliq software to assess the possible lateral displacements after liquefaction. The potential lateral spreading maps of the study area are prepared after calculations in accordance with three different approaches (Figures 7.22, 7.23, and 7.24).



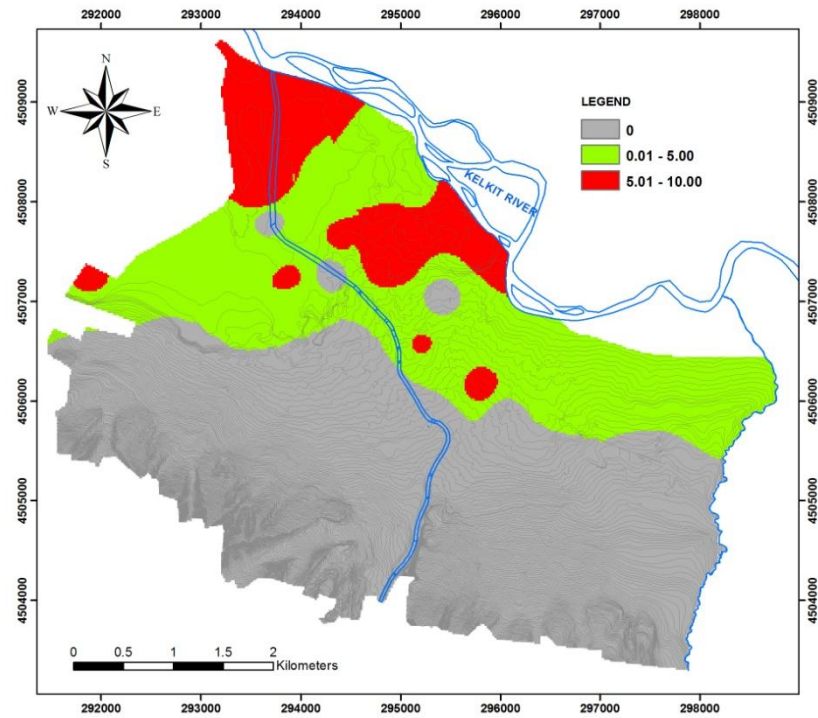


Figure 7.22. Lateral spreading map of the study area based on Youd et al. (2002) method (lateral spreading in meters)

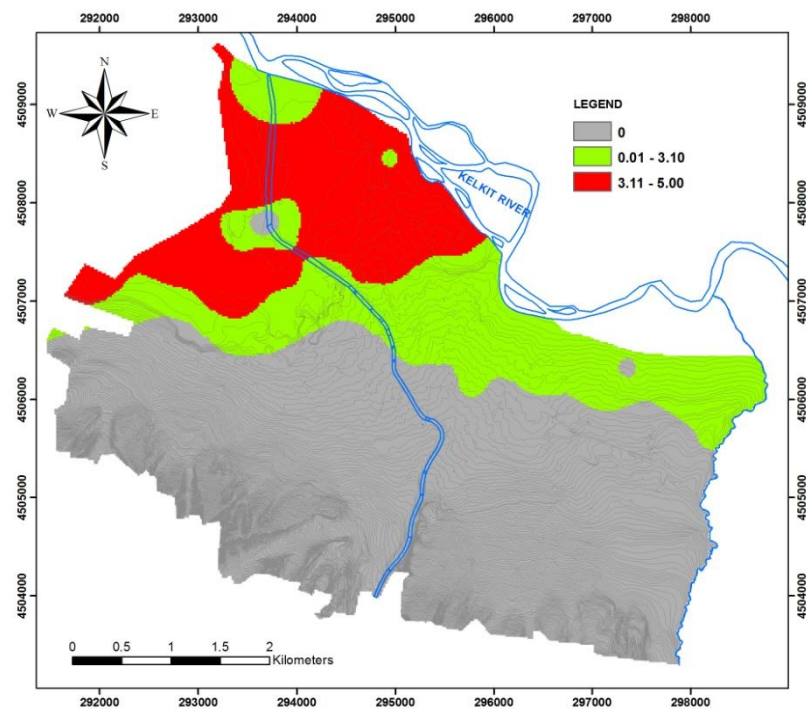


Figure 7.23. Lateral spreading map of the study area based on Kramer and Baska (2006) method (lateral spreading in meters)

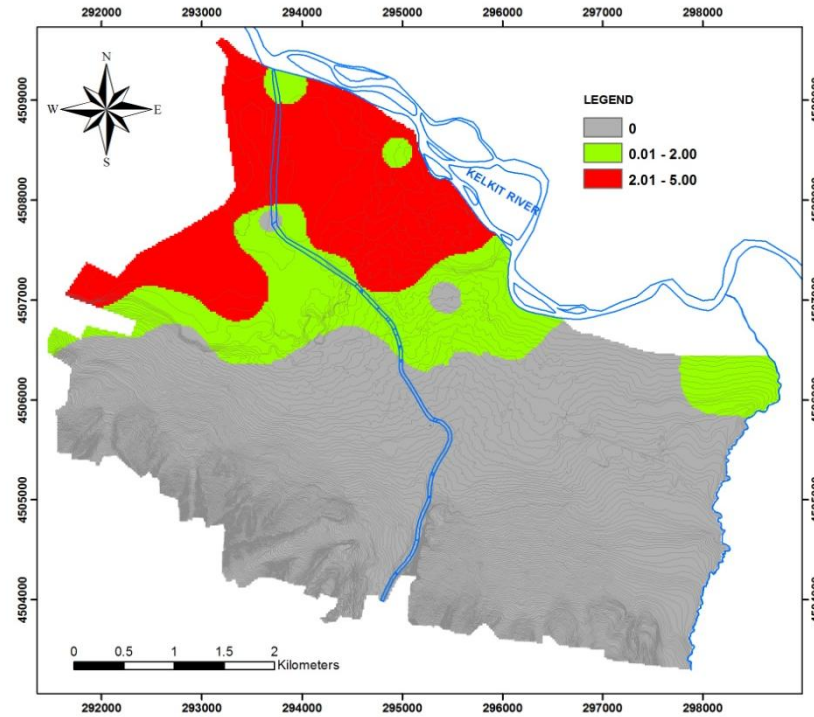


Figure 7.24. Lateral spreading map of the study area based on Idriss and Boulanger (2008) method (lateral spreading in meters)

The presented maps exhibit the quantity of possible lateral spreading displacements. On the basis of Youd et al. (2002) method, the lateral spreading displacement can attain a value of up to 10 m, especially in the close vicinity of the Kelkit River embankment. The Kramer and Baska (2006) and Idriss and Boulanger (2008) approaches present a maximum displacement of around 5 m in the same regions of Erbaa. Eventually, the northwestern part of the study area reveals a higher lateral spreading displacement potential than the rest of the study area considering lateral spreading analyses. The approaches employed in WSliq software can also be weighted for multiple scenario conditions. However, the single scenario based calculations are considered in this study. The lateral spread displacement maps are also taken into account for obtaining the final liquefaction potential map of the study area.

### 7.5.3 Post-liquefaction settlements

The second crucial post-liquefaction effect which may also cause permanent deformation in structures is vertical ground displacement after liquefaction. Post-liquefaction settlement

may occur when the dissipation of excess pore pressure following liquefaction settlement due to bearing capacity failure results from shear strains rather than volumetric strain and it may cause structures to sink into the soil simultaneously. Liquefaction-induced vertical settlements can damage bridges, abutments, and shallow foundations. This type of earthquake-induced vertical settlements has been tried to be modeled by various approaches to estimate the possible effects of settlements. Hence, the available procedures mostly based on the observed soil behavior in laboratory tests and field behavior based on post-earthquake effects was considered in the proposed procedures. The available procedures to predict the settlements are mostly based on semi-empirical models and were developed by Tokimatsu and Seed, 1984; Ishihara and Yoshimine, 1992; Shamoto et al., 1998; Wu and Seed, 2004. The latest model recently developed by Cetin et al. (2009) is based on the probabilistic approach to determine vertical settlements. The available methods in the WSliq software are summarized in the following paragraphs.

#### 7.5.3.1 Tokimatsu and Seed (1984) post-liquefaction settlement model

Tokimatsu and Seed (1984) used a correlation between  $(N_1)_{60}$  and relative density to estimate the shear strain potential of liquefied soil from  $(N_1)_{60}$  and cyclic stress ratio (CSR). The researchers produced a chart based on volumetric strain (Figure 7.25).

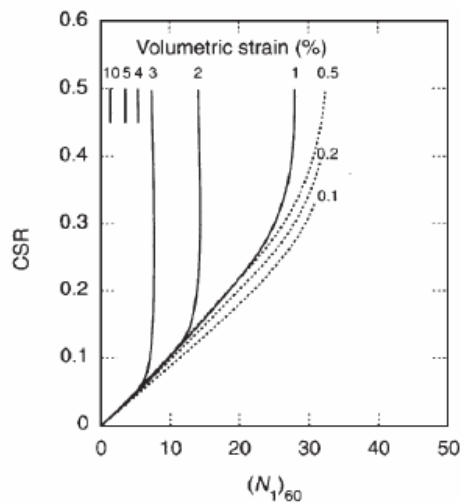


Figure 7.25. Variation of volumetric strain with corrected SPT resistance and cyclic stress ratio (after Tokimatsu and Seed, 1987)

The curves in Figure 7.25 indicate that post-liquefaction volumetric strain increases with increasing loading and decreasing SPT resistance. The Tokimatsu and Seed (1984) model computes ground surface settlement by integrating volumetric strain over the depth of liquefiable layer.

$$\Delta H = \int \varepsilon_v dz \quad (7.35)$$

The soil profile is usually divided into sublayers in the Tokimatsu and Seed model (1984) to calculate the total settlement of the profile. Initially, volumetric strain ( $\varepsilon_v$ ) values can be determined using proposed chart in Figure 7.24 for the sublayers. The obtained volumetric strain values should be multiplied by the layer thicknesses ( $\Delta z$ ) to calculate the settlement as given in Equation 7.35.

### 7.5.3.2 Ishihara and Yoshimine (1992) post-liquefaction settlement model

Ishihara and Yoshimine (1992) proposed an approach to estimate post-earthquake settlements in terms of soil density which can be expressed by relative density, SPT resistance or CPT tip resistance. In order to define the variation of volumetric strain, a chart was proposed by Ishihara and Yoshimine (1992) (Figure 7.26). As shown in Figure 7.26, the volumetric strain is correlated with density and factor of safety against liquefaction.

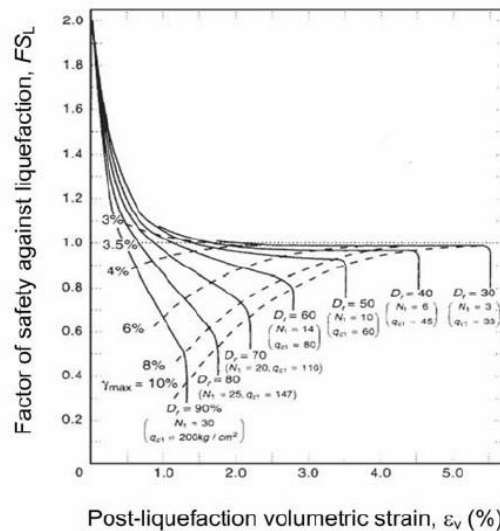


Figure 7.26. Variation of volumetric strain with relative density, SPT or CPT resistance, and factor of safety against liquefaction (after Ishihara and Yoshimine, 1992)

The proposed curves in Ishihara and Yoshimine (1992) model can be used to estimate the volumetric strain value for the sublayers, and then the total settlement can be calculated by Equation 7.35.

### 7.5.3.3 Shamoto et al. (1998) post-liquefaction settlement model

The Shamoto et al. (1998) model is quite similar to that of the Tokimatsu and Seed (1984) approach. However, the volumetric strain model is based on a constitutive model and laboratory torsional shear test results. The chart solutions are also similar to the proposed charts in Tokimatsu and Seed (1984) model (Figure 7.27).

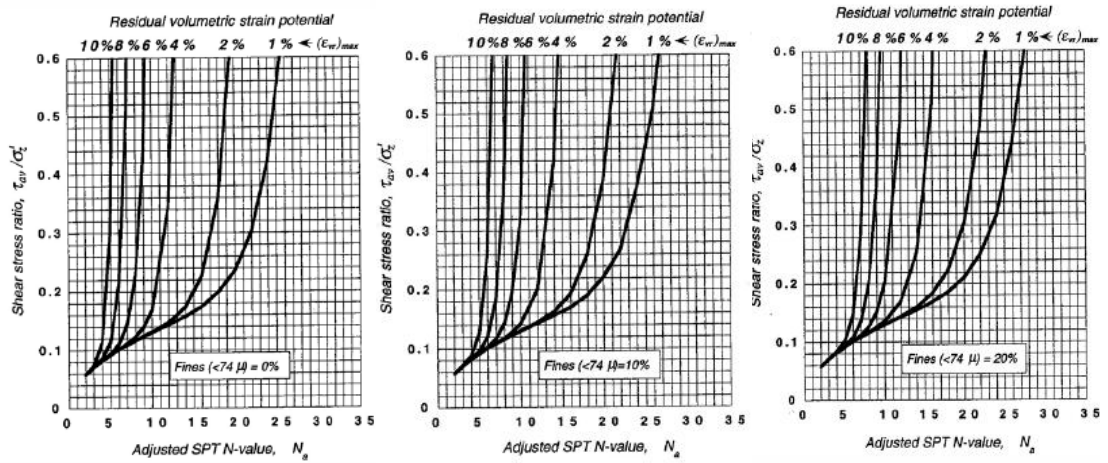


Figure 7.27. Variation of maximum residual volumetric strain with corrected SPT resistance and cyclic stress ratio for sands with different percent fines content (0, 10, 20 %) (after Shamoto et al., 1998)

According to different fines contents percentages of 0, 10 and 20% for sands, residual volumetric strain potential is estimated using the proposed charts (Figure 7.27). Moreover, the volumetric strain can be defined using Equation 7.36 by multiplying a factor of 0.84 based on the case histories from the 1995 Hyogoken-Nambu earthquake.

$$\Delta H = 0.84 \int (\epsilon_v)_{max} dz \quad (7.36)$$

The obtained volumetric strain values from Equation 7.36 should also be multiplied by the layer thicknesses to calculate the total settlement for the soil profile.

#### 7.5.3.4 Wu and Seed (2004) post-liquefaction settlement model

Wu and Seed (2004) recommended a similar method to the Tokimatsu and Seed (1984) and Shamoto et al. (1998) approaches based on cyclic simple shear tests performed on Monterey sands. The values obtained from cyclic simple shear tests were used to develop a relationship between  $(N_1)_{60, CSR}$ , CSR, and volumetric strain (Figure 7.28).

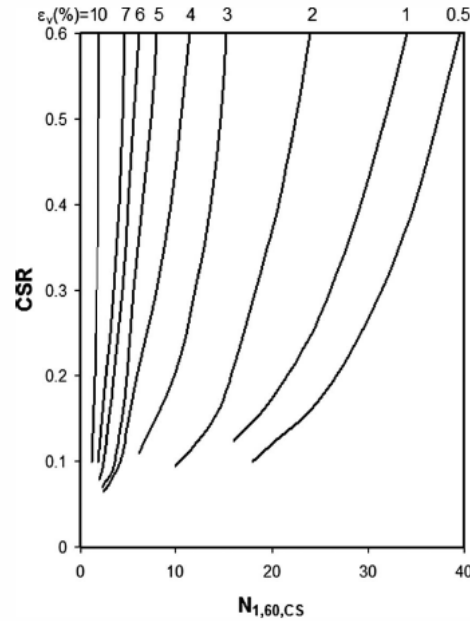


Figure 7.28. Variation of volumetric strain with corrected SPT-N and CSR (after Wu and Seed, 2004)

The settlements can be computed by integrating volumetric strain depending on the thickness of the soil profile as mentioned in Equation 7.35.

#### 7.5.4 Evaluation of post-liquefaction settlements for Erbaa

Liquefaction-induced vertical settlements can cause permanent deformations after an earthquake. The possible permanent deformations in Erbaa as a post-liquefaction effect are determined using four empirical approaches (Tokimatsu and Seed, 1984; Ishihara and Yoshimine, 1992; Shamoto et al., 1998; Wu and Seed, 2004) mentioned in the previous sections. These approaches, also employed in WSliq software, are used to calculate the post-

liquefaction vertical settlements in Erbaa. The produced maps from the calculations are shown in Figures 7.29, 7.30, 7.31, and 7.32.

When the proposed maps for vertical settlements based on the different models are evaluated, the highest post-liquefaction vertical settlement is obtained from Shamoto et al. (1998) model indicating a maximum of 2.5 m settlements for the northwestern part of the study area. Furthermore, Tokimatsu and Seed (1984) model reveals a maximum of 0.48 m settlement for the same region. The other two models (Ishihara and Yoshimine, 1992 and Wu and Seed, 2004) exhibit similar vertical displacements which are found to be maximum 0.7 and 0.8 m, separately. The northwestern part of the study area reveals relatively high vertical settlement risk based on empirical post-liquefaction vertical settlement models. The vertical settlement maps are also considered in the evaluation stage of final liquefaction map with different weight factors.

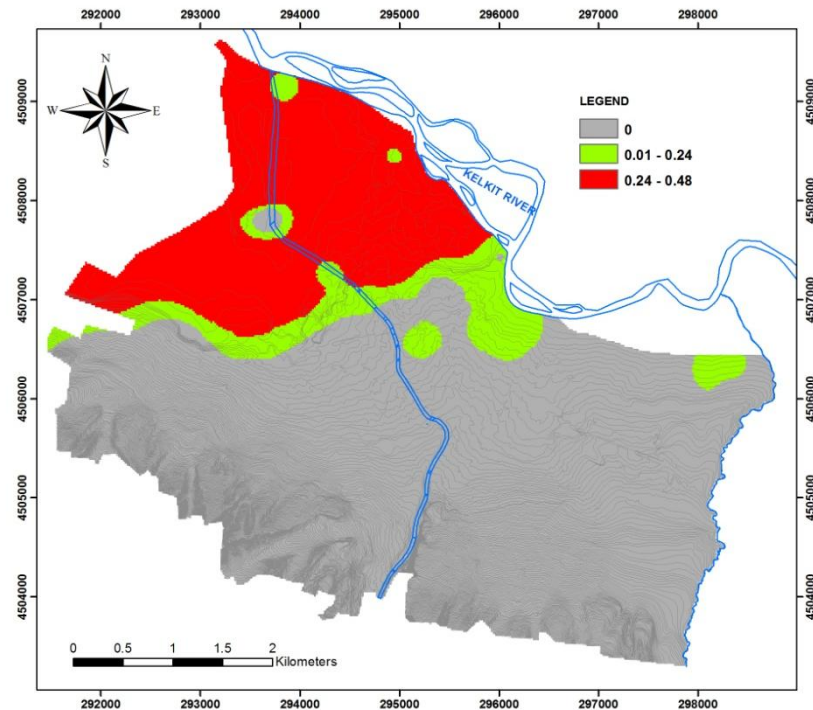


Figure 7.29. Post-liquefaction vertical settlement map of the study area based on Tokimatsu and Seed (1984) method (settlement in meters)



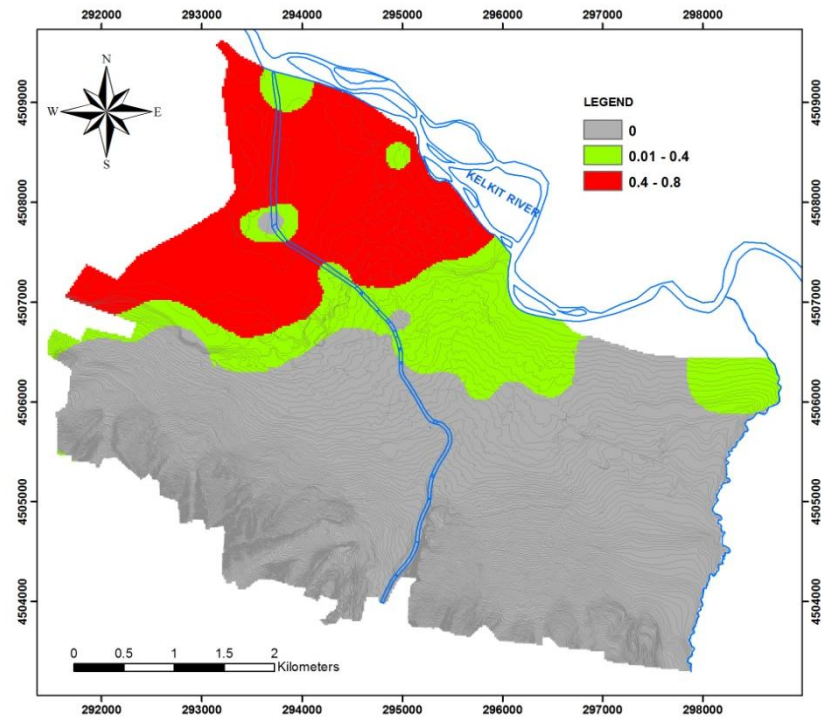


Figure 7.30. Post-liquefaction vertical settlement map of the study area based on Ishihara and Yoshimine, (1992) method (settlement in meters)

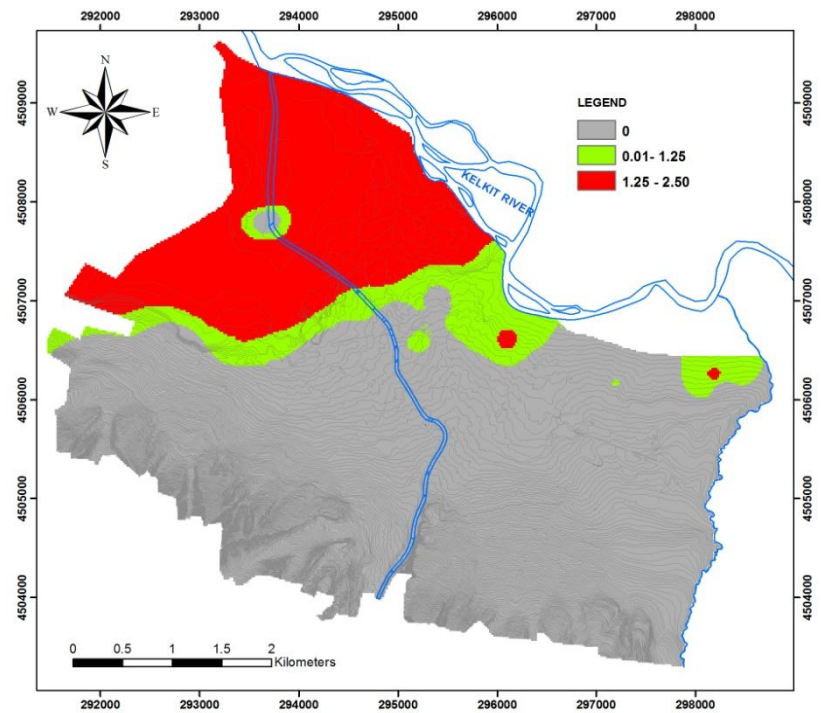


Figure 7.31. Post-liquefaction vertical settlement map of the study area based on Shamoto et al. (1998) method (settlement in meters)



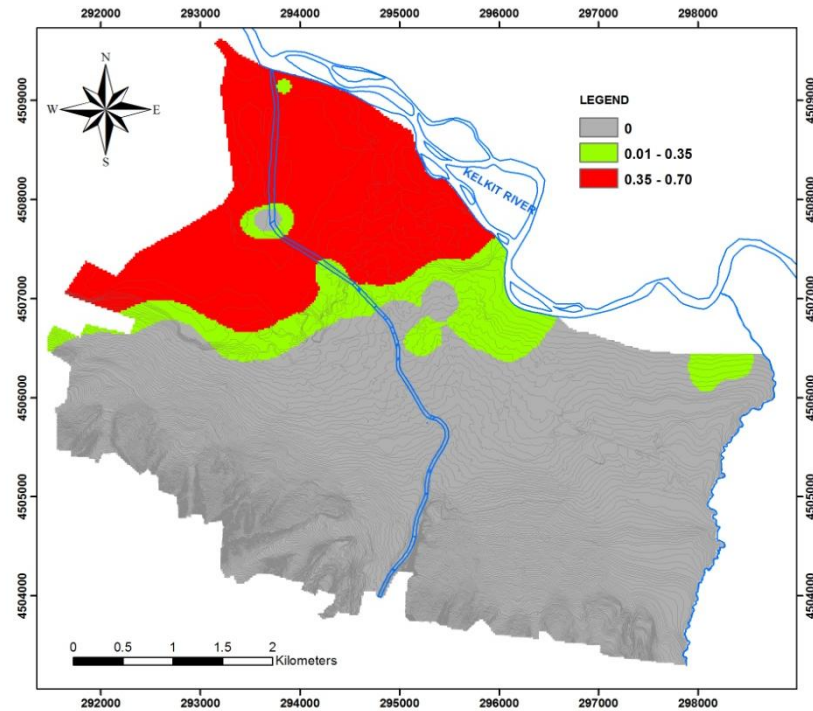


Figure 7.32. Post-liquefaction vertical settlement map of the study area based on Wu and Seed (2004) method (settlement in meters)

Settlement of dry sands, such as those above the water table, is mostly completed at the end of an earthquake. However, saturated sands may need more time to complete their settlement. Therefore, the estimation of the amount and the time of liquefaction-induced settlement are complicated (Kramer, 1996). As a particular note, the WSliq software used for liquefaction-induced settlement calculations cannot compute the settlement of partially saturated or dry sands above the water table. The developers are currently implementing a new volumetric strain model proposed by Cetin et al. (2009) into the software (Kramer, 2009b). Therefore, the settlement of dry sands above the water table is manually calculated in this study by the help of the simplified equation (Equation 7.37).

Dry sand settlements after liquefaction can be estimated by Tokimatsu and Seed (1987) simplified approach. Youd (1972) revealed that the sands at different saturation levels have similar seismic settlement potential. Duku et al. (2008) also proposed that the environmental factors including saturation do not significantly affect seismic vertical settlements in clean sands. The simplified equation proposed by Tokimatsu and Seed (1987) is considered in order to define dry settlements in sands in the study area as mentioned in the previous paragraph.

$$\gamma_{cyc} = 0.65 \frac{a_{max}}{g} \frac{\sigma_v r_d}{G(\gamma_{cyc})} \quad (7.37)$$

when  $G_{max}$  is known,  $\gamma_{cyc}$  can be estimated using the relationships shown in Figure 7.33.

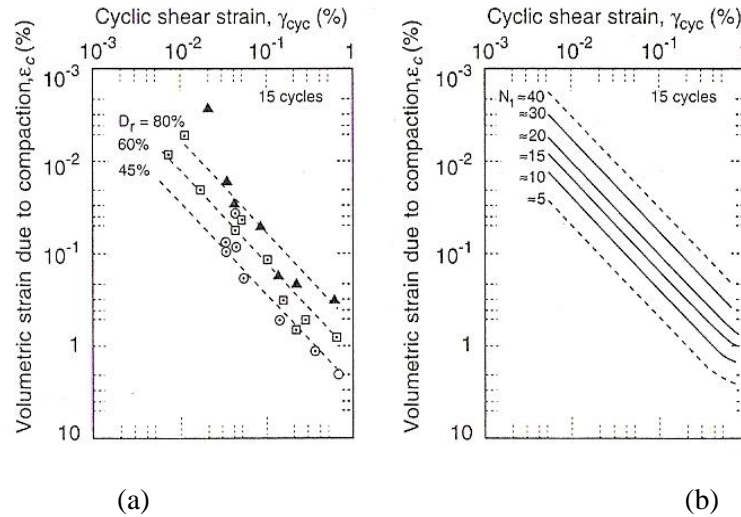


Figure 7.33. Relationship between volumetric shear strain and cyclic shear strain in terms of (a) relative density and (b) standard penetration resistance (after Tokimatsu and Seed, 1987)

The 15 cycles of strain given in Figure 7.33 was assumed to correspond to a  $M=7.5$  earthquake. For other earthquake magnitudes, Tokimatsu and Seed (1987) proposed the volumetric ratio values mentioned in Table 7.7.

Table 7.7. Variation of earthquake magnitude and volumetric strain ratio for dry sands (after Tokimatsu and Seed, 1987)

Earthquake magnitude	Volumetric strain / Volumetric strain for $M=7.5$
5.25	0.4
6	0.6
6.75	0.85
7.5	1.0
8.5	1.25

According to the calculations for existing dry-sand layers above the liquefiable layers, dry sand settlements vary between 1 and 2.5 cm in the study area. The dry settlement in sands is

negligible when compared to the saturated sand settlements calculated in WSliq software for Erbaa. This result is not unexpected given the higher water table and significant thickness of saturated sand.

Finally, the calculated lateral spreading and vertical settlements in Erbaa are compared to the real cases. After the 1999 Kocaeli earthquake ( $M_w=7.4$ ), severe damages due to soil liquefaction and related ground deformations occurred widespread in the eastern Marmara Region. Liquefaction-induced damages were generally observed along the shorelines during 1999 Kocaeli earthquake. One of the typical lateral spreading examples was reported in the study of Kanibir et al. (2006). According to this study, horizontal displacement due to lateral spreading and vertical settlement was reported as 352 cm and 0.3 m, respectively along the shoreline of Lake Sapanca (Sapanca Vakıf Hotel). Therefore, such high liquefaction-related ground deformations can be expected on the basis of the obtained results. It can be concluded that the obtained results in this study seem quite reasonable for Erbaa soils.

#### **7.5.5 Ground deformation models**

Liquefaction-induced ground failures were also studied regarding the relationships between the thickness of liquefiable layers and overlying non-liquefiable soils. Ishihara (1985) proposed a graphical relationship to determine the thickness of overlying layer required to prevent ground level liquefaction-related damage (Figure 7.34). The proposed boundary curves were defined based on the maximum peak accelerations within a range of 0.2-0.5g. Moreover, the boundary curves proposed by Ishihara (1985) were explored in the study of Youd and Garriss (1995). Youd and Garriss (1995) stated that the surface liquefaction effects cannot be correctly defined in the susceptible areas to ground oscillation and lateral spread using Ishihara (1985) boundary curves.

Yuan et al. (2003) studied the Ishihara (1985) boundary curves on the basis of cases occurred in 1999 Taiwan earthquake. The researchers concluded that the limits of boundary curves should be validated by more case studies. In addition, Yuan et al. (2003) also mentioned that the Ishihara's procedure should not be applied in the areas involving lateral spreading potential.

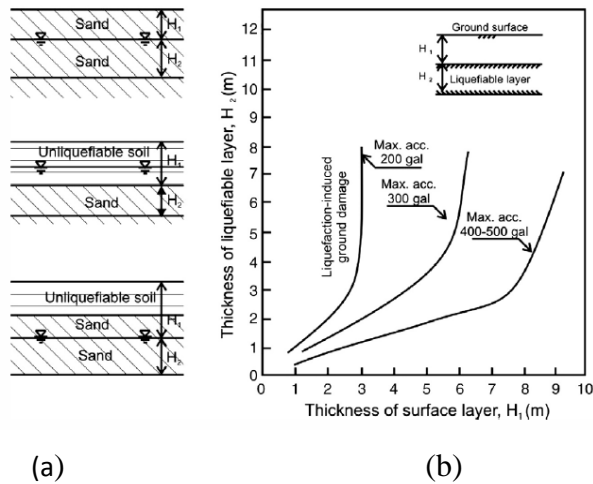


Figure 7.34. (a) the evaluation guide of the thickness of liquefiable layer and overlying liquefiable layer, and (b) the boundary curves for liquefaction induced damage (after Ishihara, 1985)

Sonmez et al. (2008) modified the Ishihara (1985) curves by implementing the data obtained from two different areas (Izmit Bay in Turkey and Yuanlin in Taiwan). Sonmez et al. (2008) mentioned that the liquefaction-induced damage can be predicted by the proposed chart (Figure 7.35). However, the proposed chart needs to be tested in other areas affected from liquefaction-induced ground damage before its application.

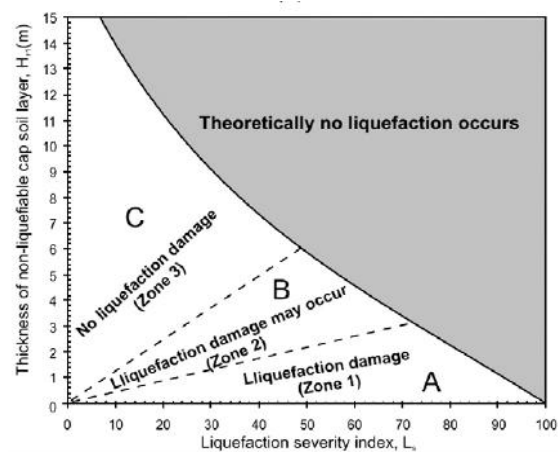


Figure 7.35. The chart proposed for discriminating between occurrence and non-occurrence of surface effects of liquefaction (A (Zone 1): Liquefaction damage, B (Zone 2): Liquefaction damage may occur, and C (Zone 3): No liquefaction damage) (after Sonmez et al., 2008)

### 7.5.6 Evaluation of ground deformation model maps for Erbaa

Liquefaction-induced ground deformation models are considered in order to determine the surface effects of liquefaction for Erbaa. In this study, the abovementioned ground deformation models are implemented in the evaluation part considering their limitations in the areas prone to either sand boiling or lateral spreading and ground oscillation. One of the ground deformation models proposed by Sonmez et al. (2008) is considered to achieve liquefaction-induced ground surface disruption zoning maps of the study area. The related map is shown in Figures 7.36.

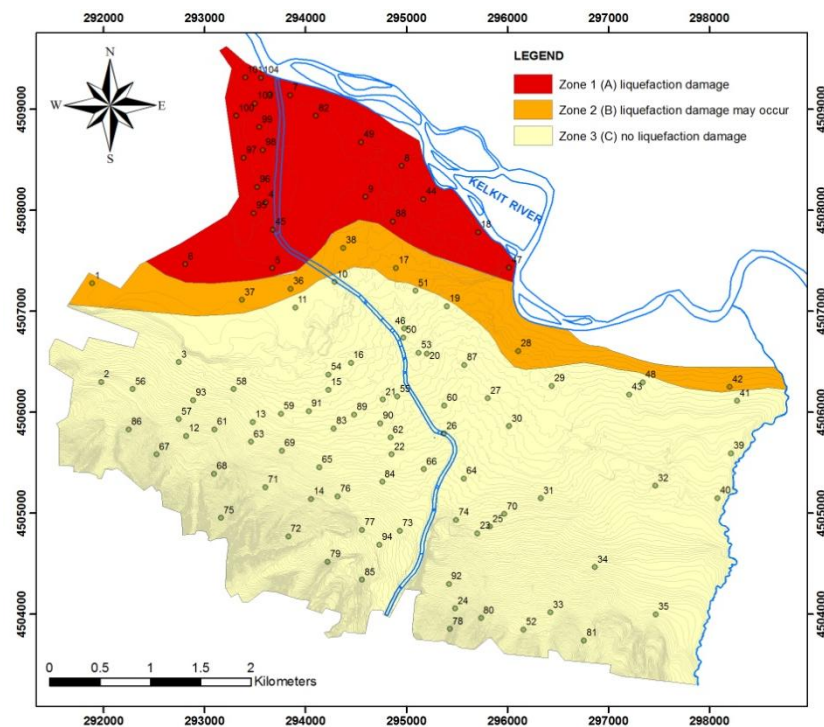


Figure 7.36. Liquefaction-induced ground surface disruption zoning map based on Sonmez et al. (2008) model

The implemented methods for ground deformation models have some limitations during the determination of liquefaction-induced ground deformations. The liquefiable layer thickness is restricted to 12 and 15 m in Ishihara (1985) and Sonmez et al. (2008) methods, respectively. Besides, there is another limitation for the maximum acceleration in Ishihara (1985) method. The study area has high amplification potential values beyond the maximum acceleration boundary (0.4g) proposed in Ishihara (1985) method (Kramer, 1996). Therefore,

the ground deformations are separately modeled in terms of lateral spreading and vertical settlement, since the author of this thesis has detailed data that can be used for the estimation of related ground deformations at every borehole location in the study area.

## 7.6 Evaluation of Liquefaction and Post-Liquefaction Maps of Erbaa

It is aimed to propose a final liquefaction-induced deformation map involving post-liquefaction effects for Erbaa to be used in the evaluation stage of seismic microzonation map of the study area. For this reason, different possible weights are assigned to each class in lateral spreading and vertical settlement maps (Table 7.8).

Table 7.8. Weights assigned to the classes of each layer during the preparation of liquefaction-induced deformation map

Layers	Weight (%)	Weight (%)	Weight (%)	Weight (%)	Weight (%)	Classes
	(a)	(b)	(c)	(d)	(e)	
Lateral spreading	10	20	30	40	50	None Moderate High
Vertical settlement	90	80	70	60	50	None Moderate High

It should be noted that the lateral spreading and vertical settlement maps are reclassified into three classes (none, moderate, high) before assigning the weight ratios. Eventually, the produced liquefaction-induced deformation maps based on different weights (referred with the letters a, b, c, d, e) is shown in Figure 7.37. Before finalizing liquefaction-induced deformation map, the produced maps with respect to different weights are evaluated. It has been found out that maps with different weights reveal very similar results. Therefore, a final liquefaction-induced ground deformation map based upon the weight values of 50% for lateral spreading and 50% for vertical settlement is chosen for the final overlay analyses (Figure 7.38). Although Shamoto et al. (1998) model reflects high post-liquefaction vertical settlements; all four models for vertical settlements are consistent. Ultimately, the employed models for vertical settlement as well as lateral spreading are considered equally during weight assignment.

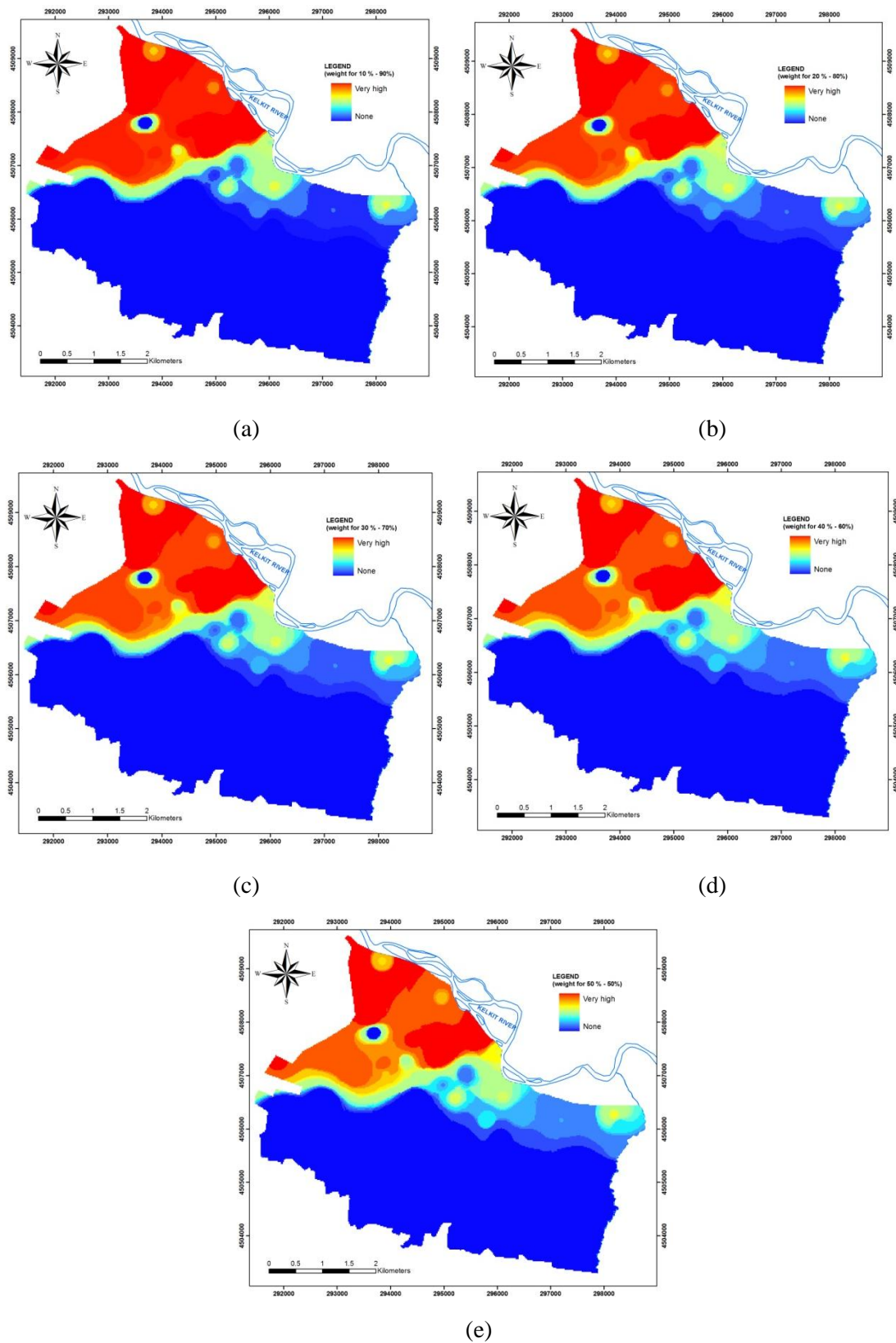


Figure 7.37. Different weight combinations (a, b, c, d, e as given in Table 7.7) for the production of liquefaction-induced ground deformation map



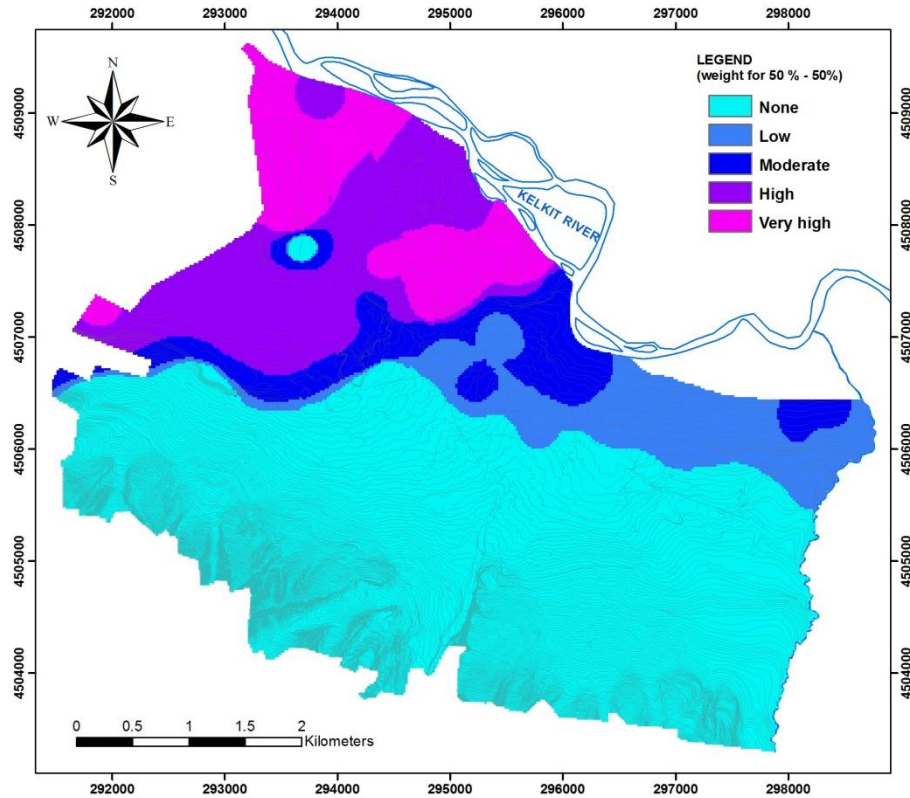


Figure 7.38. Final liquefaction-induced ground deformation map of Erbaa

The reason for the selection of this weight combination (50% for lateral spreading and 50% vertical settlement) for the final liquefaction-based deformation map is to be on the safe side and to consider the importance of vertical settlement after liquefaction. The produced final liquefaction-induced deformation map of the study area has five classes pointing out different degrees of post-liquefaction deformation effects as mentioned in Figure 7.38. These five classes represent the different level of ground deformation in the study area. It can be concluded that the southern part of the study area, where the Pliocene units mostly exist, is not prone to liquefaction-induced ground deformations. However, the northwestern region is highly to very highly susceptible to post-liquefaction ground deformations. There may be some local zones with less deformation in the northwestern part as well. Moreover, the northeastern part of the study area reveals low to moderate susceptibility to liquefaction induced ground deformations probably due to the existence of thick fine-grained intercalations.



Moreover, the ground deformation map based on Sonmez et al. (2008) model and the produced final liquefaction-based deformation map are compared in terms of deformation levels. Both ground deformation maps indicate that the northwestern part of the study area is in the critical zone regarding liquefaction-induced ground deformations. Besides, a transition can be observed between liquefaction damage expected zones in the produced final liquefaction-based deformation map.

## **7.7 Concluding Remarks**

The liquefaction potential of Erbaa is evaluated using different empirical methods and a newly proposed software called WSliq. The seismic parameters (magnitude and PGA) of the study area which are used in liquefaction evaluations are previously determined in seismic hazard and site response analyses sections. Additionally, borehole specific PGA values are taken into account for liquefaction evaluations instead of using a constant PGA value for the whole study area. In the liquefaction susceptibility stage, the soil layers are initially evaluated on the basis of obtained field and laboratory data. The liquefaction susceptibility analyses indicate that the liquefaction-susceptible soils mostly cover the northern part of the study area. In general, Pliocene soils are not susceptible to liquefaction, whereas loose alluvial units with shallow groundwater level dominantly expose liquefaction susceptibility. The liquefaction potential/severity index models based on Iwasaki et al. (1982); Sonmez (2003) and Sonmez and Gokceoglu (2005) designate a high liquefaction potential zone in the northwestern part of Erbaa especially in sandy alluvial deposits along the Kelkit River.

The post-liquefaction effects are evaluated in terms of lateral spreading and vertical settlement. The lateral spreading displacement can attain a maximum value of 5 to 10 m around the Kelkit River embankment in accordance with three different methods. Moreover, the post-liquefaction vertical settlement is quite critical in the northwestern part of Erbaa as well. The settlement calculations performed by four different methods indicate a maximum vertical settlement of 0.48 to 2.5 m. Finally, the produced lateral spreading and vertical settlement maps are re-evaluated by assigning different weights to each layer to obtain a final liquefaction-induced ground deformation map. The final map combines lateral spreading and vertical settlement ground deformations and will be considered in the final overlay analyses representing liquefaction-induced damages.

## **CHAPTER 8**

### **MULTI-CRITERIA DECISION ANALYSES FOR SEISMIC MICROZONATION OF ERBAA**

#### **8.1 Introduction**

The use of different procedures by means of Geographical Information System (GIS) and/or the integration of GIS and Multi-Criteria Decision Analysis (MCDA) are significant techniques to deal with large amounts of complex information and data. In several microzonation applications, GIS-based MCDA techniques are widely used for site selection problems by decision makers and engineers. GIS provides the manipulation of data storage, data analyses, and the presentation of spatial information. Besides, the MCDA techniques supply the algorithm for the combination of spatial data and the preferences of decision makers. The integration of GIS and MCDA can be very functional during the selection of urban areas within the framework of microzonation techniques.

The compilation of spatial data in a database and the data processing with editing capabilities for the generation of multi-layer maps are uncomplicated in GIS-based approaches. Alternatives should be evaluated in a logical manner. Therefore, using MCDA method is of great importance while dealing with multi-layers and decision making. In addition, the necessity of urban planning makes obligatory to use GIS-based MCDA for proper site selection.

In this study, the proposed seismic microzonation maps are generated using GIS-based MCDA techniques. Simple Additive Weighting (SAW) and Analytical Hierarchical Process (AHP), which are the two widely used MCDA methods, are considered for the preparation of seismic microzonation maps. Additionally, the essential layers (maps) are produced by means of GIS methodologies. The process of GIS and MCDA applications and their results are explained in this section. Moreover, the proposed seismic microzonation maps with

respect to two different MCDA methods are compared in order to define the final seismic microzonation map of Erbaa.

## **8.2 Seismic Microzonation Using GIS-Based MCDA**

Multi Criteria Decision Analysis (MCDA) is used to facilitate complex decision making where there are multiple criteria and preferences. Thus, decision-making is performed by simplifying advantages and disadvantages of options under risk or uncertainty (Bello-Dambatta et al., 2009). Furthermore, the main principal of MCDA is to divide the problems into different parts and to analyze them separately, then to integrate these divided parts in a logical order (Malczewski, 1999). In many site selection applications, the GIS-based MCDA procedures are preferably used to make appropriate predictions on various site conditions. The evaluation process in MCDA includes preferences, determination of MCDA methods, calculation of rank and weight values, and preparation of the GIS-based microzonation maps.

MCDA is a powerful tool for environmental decision-making for scientists and practitioners. The application of MCDA methods to environmental decision-making considerably improved the decision process in many engineering projects (Bello-Dambatta et al., 2009). The combination and utilization of the data vary in various MCDA approaches. MCDA approaches are classified with respect to the number of their alternatives (Figure 8.1) (Malczewski, 2006). The main parts of MCDA techniques and their relationships based on decision rules are summarized as follows;

- a) Multi Objective Decision Analysis (MODA) versus Multi Attribute Decision Analysis (MADA)
- b) individual versus group decision-making
- c) decisions under certainty versus decisions under uncertainty

The Multi Attribute Decision Analysis (MADA) is frequently used for problems with simple and distinct alternatives. In contrast, the Multi Objective Decision Analysis (MODA) deals with problems involving large, complex, and continuous number of alternatives. Furthermore, MCDA covers both multi-objective and multi-attribute decision-making. It should be noted that these methods may reveal different results as the success of any method is directly related to the problem and how it is formulated (Bello-Dambatta et al., 2009).

The multi-attribute decision problems are supposed to have a predetermined and limited number of alternatives while the multi-objective problems are more complex. As a result, the best answer can be found anywhere within the region of feasible solutions. Moreover, MADA and MODA can be distinguished according to the evaluation criteria which are the standards of judgments or rules on which the alternatives are ranked due to their popularity (Malczewski, 2006).

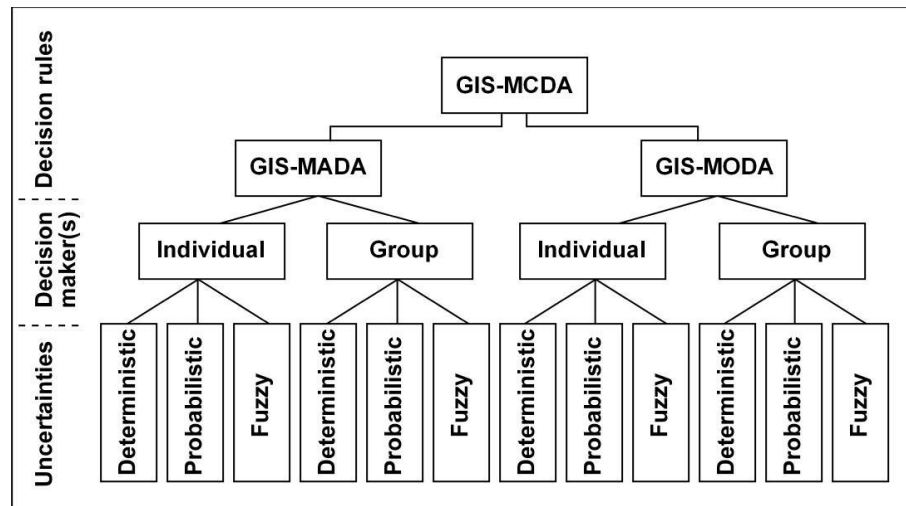


Figure 8.1. Classification of GIS-MCDA (after Malczewski, 2006)

Spatial decisions are generally made by groups rather than individuals. Therefore, group decision-making is more common in practice. The problem is accepted as individual decision making, if there is a single goal preference. The number of decision makers involved in the process is not important. However, if the individual or interest groups have different goal preferences, the problem is considered as group decision making (Malczewski, 1999).

The certainty of the decision depends upon various aspects. If the decision-maker has perfect information of the decision environment and the amount of data available is enough, then the decision is considered as decision under certainty. However, in reality, most decisions involve some aspects that are unknown and difficult to predict which can be classified as decision under uncertainty (Malczewski, 1999). The decision under uncertainty is solved by either probabilistic or fuzzy theory as mentioned in Figure 8.1. The probabilistic decisions are performed by probability theory and statistics. The results are explained as true or false

in this method. The fuzzy set theory is frequently employed if the problem is indefinite and the decision is structured as the degree of how much an event belongs to a class (Zadeh, 1965).

One of the most common advantages of MCDA is its capability to describe similarities and potential areas of conflicts among individuals in group-decision making (Linkov et al., 2005). The current methods of MCDA are summarized below:

- SAW (Simple Additive Weighting)
- MAUT/VT (Multi-Attribute Utility/Value Theory)
- SMART (Simple Multi-Attribute Rating Technique)
- TOPSIS (Technique for Order Preference by Similarity to an Ideal Solution)
- AHP (Analytical Hierarchy Process)
- ELECTRE (Elimination and Choice Expressing Reality)
- PROMETHEE (Preference Ranking Organization Method for Enrichment Evaluations)
- BBNs (Bayesian Belief Networks)

As Simple Additive Weighting (SAW) and Analytical Hierarchy Process (AHP) are considered in this study, these two MCDA methods are briefly explained in the following paragraphs.

### **8.2.1 Simple Additive Weighting (SAW)**

The Simple Additive Weighting (SAW) is an extensively used and simple MADA method based on weighted average. The SAW method is broadly used in environmental sciences in which GIS and spatial processes are utilized (Malczewski, 1999). Different weights are assigned to each thematic map layer with respect to their relative importance. SAW has the capability of weighing criteria on different scales (Bello-Dambatta et al., 2009). SAW method evaluates an alternative  $A_i$  by  $A_i = \sum w_j \cdot x_{ij}$  where  $x_{ij}$  is the score of the  $i^{\text{th}}$  alternative with respect to the  $j^{\text{th}}$  attribute, and  $w_j$  is the normalized weight. A total score is obtained for each alternative by multiplying the importance weight assigned for each attribute by the scaled value given to the alternative on that attribute, and summing the products over all attributes. When the total scores are determined for all alternatives, the alternative with the highest total score is preferred (Malczewski, 1999).

In general, the SAW method has the following steps:

- a) Define the set of map layers and feasible alternatives
- b) Assign rank values to the classes of each layer
- c) Standardize the rank values
- d) Assign the criterion weight values (relative importance weight) to each map layer
- e) Normalize the assigned weight values
- f) Calculate the  $A_i$  score using the aforementioned formula
- g) Evaluate the alternatives based on total score

Moreover, the linearity and additivity of the attributes are the two main assumptions in the SAW method (Malczewski, 1999; Bello-Dambatta et al., 2009). The linearity indicates that the desirability of an additional unit of an attribute is constant for any level of that attribute. Additionally, there is no interaction effect between attributes according to the additivity assumption.

Although the SAW is a simple and widely used method, it may have some disadvantages such as oversimplifying the decision process and misinterpretation (Linkov et al., 2005). Besides, the weights are often obtained subjectively by asking the decision-maker to directly assign numbers to each layer. In other words, the definition of the units of measurement is ignored (Malczewski, 1999).

### **8.2.2 Analytical Hierarchical Process (AHP)**

The Analytical Hierarchical Process (AHP) was firstly developed by Saaty (1977) to produce a ranking of decision alternatives with a mathematical structure. The main goal of AHP is to determine weights using pairwise comparisons of alternatives for each attribute (Marshall and Oliver, 1995; Bello-Dambatta et al., 2009). In AHP, a complex decision problem is divided into simpler decision problems to form a decision hierarchy. Both qualitative and quantitative data is used to form ratio scales between decision elements at each hierarchical level by pairwise comparisons.

The pairwise comparisons are recorded in a comparative matrix  $A$ , which must be both transitive. For instance, if  $i > j$  and  $j > k$  then  $i > k$  where  $i, j$ , and  $k$  are alternatives; for all  $j > k > i$  and reciprocal,  $a_{ij} = 1/a_{ji}$ . Priorities are calculated from the comparison matrix by

normalizing each column of the matrix, to derive the normalized primary right eigen vector, the priority vector, by  $A \cdot w = \lambda_{\max} \cdot w$ ; where  $A$  is the comparison matrix;  $w$  is the principal eigen vector;  $\lambda_{\max}$  is the maximal eigen value of matrix  $A$  (Saaty, 2004).

The pairwise comparison involves the following main steps:

- a) Development of the pairwise comparison matrix
- b) Computation of the criterion weights
- c) Estimation of the consistency ratio

A pairwise comparison matrix is developed using a fundamental scale with values from 1 to 9 to rate the relative preferences for two criteria (Table 8.1). In other words, fundamental rankings for criteria are supplied by pairwise comparisons. Two alternatives and the importance relation between these alternatives of the pairwise comparison are considered.

Table 8.1. Scale for pairwise comparison (after Saaty, 1980)

Intensity of importance	Definition	Explanation
1	Equal importance	Contribute equally to the objective
3	Moderate importance	Slightly favor one objective over another
5	Strong importance	Strongly favor one objective over another
7	Very strong importance	Favored very strongly one objective over another; dominance demonstrated in practice
9	Extreme importance	Evidence favoring one objective over another is of the highest possible order of affirmation
2, 4, 6, 8	For compromise between above values	Sometimes one need to interpolate compromise judgment numerically

The composite weights are determined using a sequence of multiplication after the development of comparison matrix. Firstly, the values in each column of pairwise comparison matrix are summed. Then, each element in the matrix is divided by its column total as the resulting matrix is referred to as the normalized pairwise comparison matrix. Finally, the average of the elements in each row of the normalized matrix is computed and the sum of normalized scores for each row is divided by the number of criteria. The calculated averages supply an estimate of the relative weights of the criteria being compared (Malczewski, 1999).

The decision-makers inconsistency can be calculated by the consistency index (CI) in AHP method to understand whether decisions agree with the transitivity rule. A threshold value of 0.10 is accepted as consistency ratio (CR). The consistency ratio (CR) is calculated by  $CR=CI/RI$ , where RI is the random index. Besides, CI is defined as  $CI = (\lambda_{\max} - n) / (n-1)$  where n is the number of analyzed layers (Malczewski, 1999; Bello-Dambatta et al., 2009). If the CR value is higher than the threshold value of 0.10, the rankings in pairwise comparison matrix should be reconsidered and revised. The RI values according to random matrices are given in Table 8.2.

Table 8.2. RI values with respect to the number of layers (n) (after Saaty, 1980)

n	1	2	3	4	5	6	7	8	9	10	11	12	13	14	15
RI	0.00	0.00	0.58	0.90	1.12	1.24	1.32	1.41	1.45	1.49	1.51	1.48	1.56	1.57	1.59

### 8.3 Data Production and Analyses for Seismic Microzonation

The data are classified as input data and evaluated input data which are both considered in MCDA. Input data include topographical, slope, aspect, lithology, and depth to groundwater table maps. On the other hand, the evaluated input data involves distance to fault,  $V_{s30}$  based site classification, amplification, and liquefaction-induced ground deformation maps. The main reason for the distinction of data is that the evaluated data represent the seismic based layers in the study area which are produced as a result of various analyses.

#### 8.3.1 Input data

##### 8.3.1.1 Elevation map

The elevation data is derived from 1:1.000 scale urban planning maps obtained from General Directorate of Bank of Provinces. The study area involves a total of 53 (1:1.000 scale) maps. Each urban planning map exhibits the elevation contours and urban plans of the settlement. All maps are firstly scanned and then imported to ARCGIS (version 9.2) which is Geographical Information System-based software. Ground control points are imported from the maps in order to make georeferencing. The UTM projection with zone 37, Datum –



European 1950-Mean is used in all maps. The contours with 1 meter interval are digitized and elevation values are entered into an attribute table for further analyses. The digitized contour map of the study area is shown in Figure 8.2.

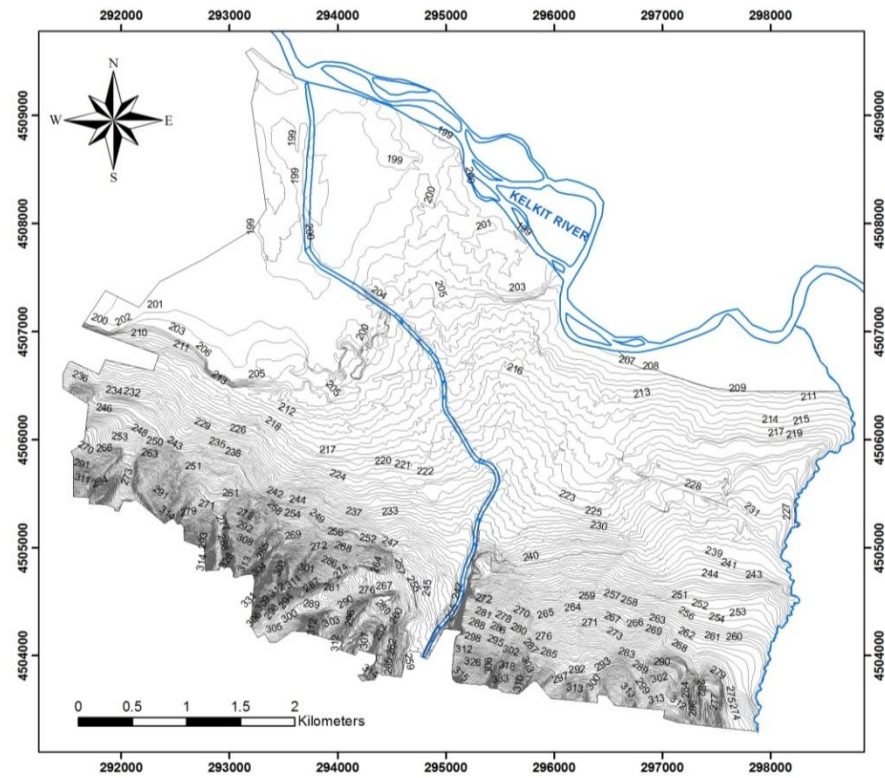


Figure 8.2. Contour map of the study area

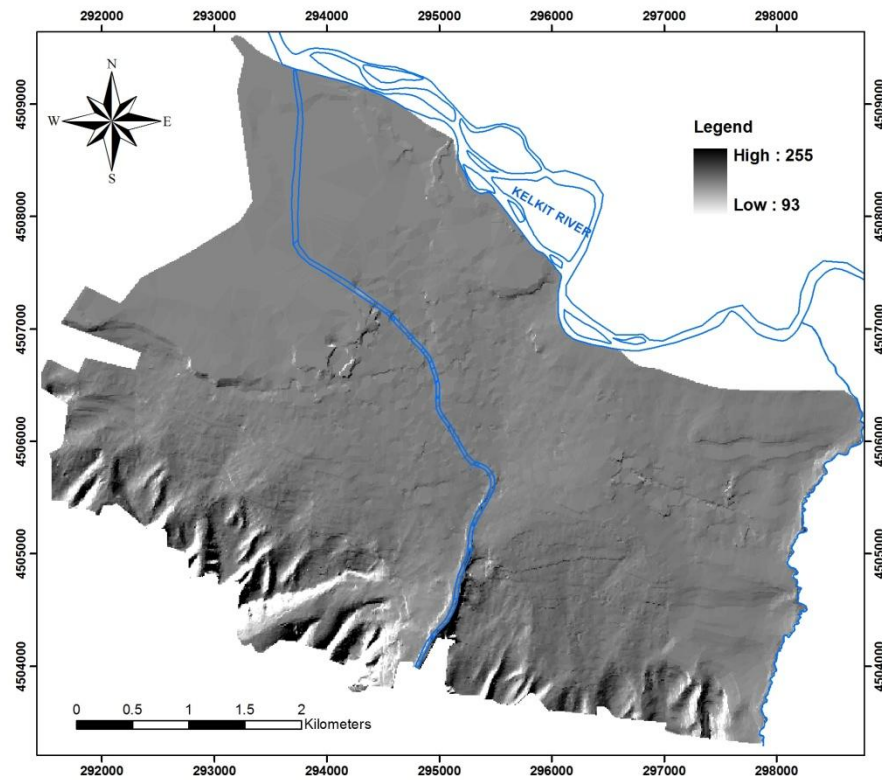


Figure 8.3. Digital Elevation Model (DEM) of the study area

The elevation in Erbaa varies between 198 and 351 m. A gradual elevation decrease can be observed towards the Kelkit River. The elevation map of the study area is used for the production of Digital Elevation Model (DEM) (Figure 8.3) to obtain slope and aspect maps.

#### 8.3.1.2 Slope map

The slope map is an important layer for the determination of susceptibility to landsliding or the ease of engineering construction (Dai et al., 2001). The slope map is generated from Digital Elevation Model (DEM), which is derived from elevation contours. The distribution of slope angle in the study area ranges between 0 and 85° (Figure 8.4). Since there is no serious slope instability problem in the study area, the slope map is not used for the determination of susceptibility to landsliding. However, it contributes to the seismic microzonation map for the delineation of proper settlement areas regarding the ease of constructions and for the estimation of liquefaction-based ground deformations since lateral spreading is typically related to slopes with free faces which are almost horizontal.

The slope angles are subdivided into five main classes. During the classification, the Guidelines for Urban Engineering Geological Investigations proposed by Van Rooy and Stiff (2001) is considered. However, this classification is modified for Erbaa according to the site conditions. The classes for different slope angles are summarized in Table 8.3. As a particular note, a detailed slope class division is performed to emphasize the susceptible layers to lateral spreading. The classified slope map of the study area is given in Figure 8.5.

Table 8.3. Classification of slope angle

Ranking	Slope angle (°) class
5	0-5
4	5-10
3	10-15
2	15-20
1	>20

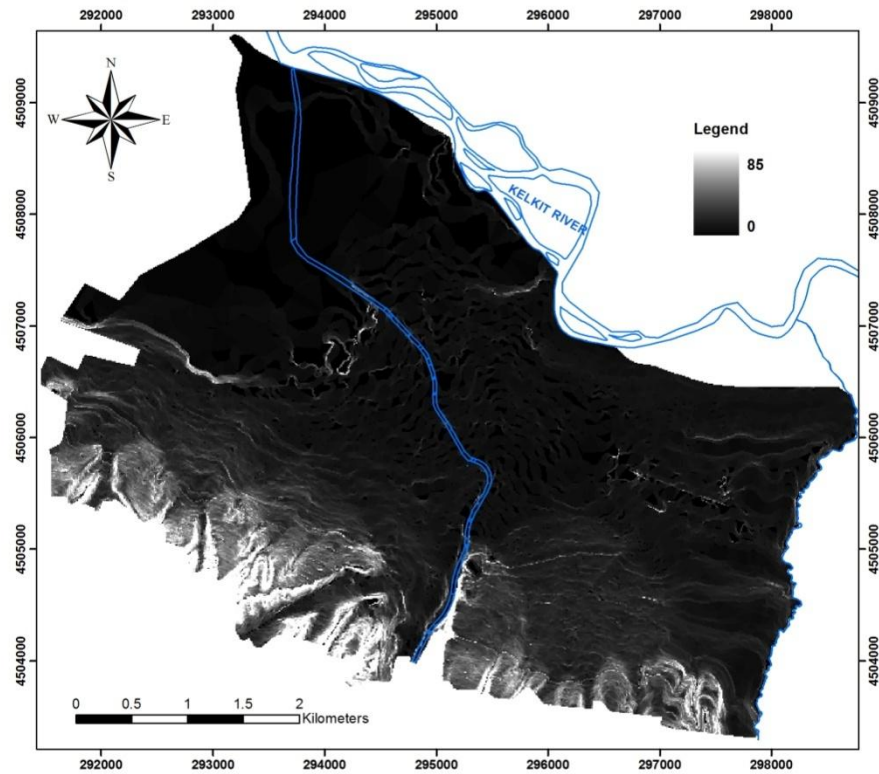


Figure 8.4. Distribution of slope angle in the study area (in degrees)

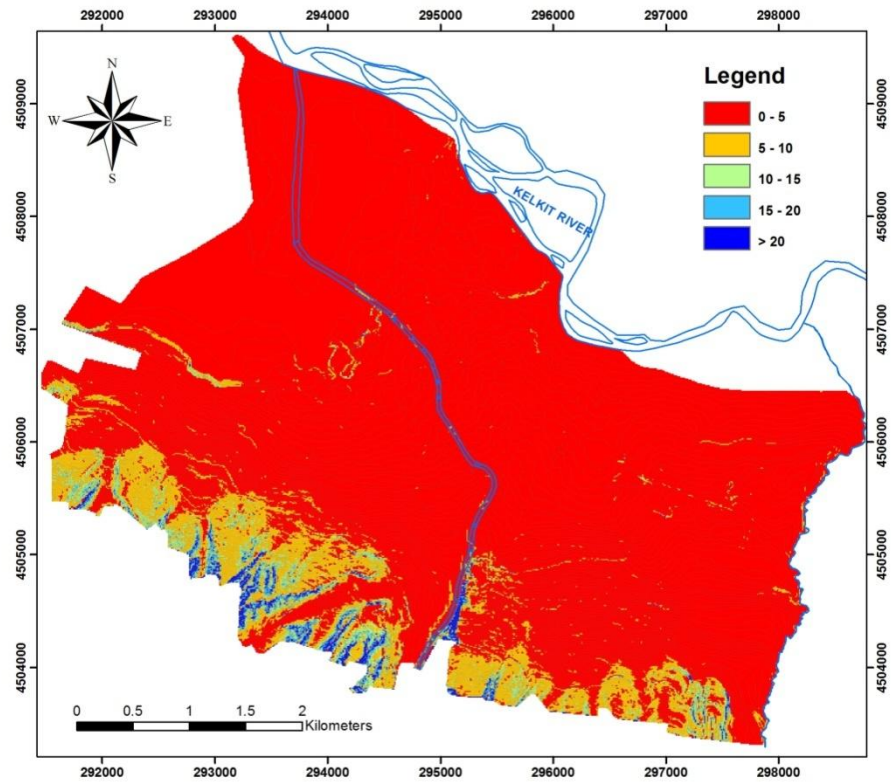


Figure 8.5. Slope map of the study area (in degrees)

### 8.3.1.3 Aspect map

Aspect (direction) map depicted in Figure 8.6 is generated from DEM. The classification of aspect is given in Table 8.4. Aspect map contributes to the final seismic microzonation map with a less weight, but it should definitely be considered in microzonation studies (Figure 8.7).

Table 8.4. Classification of aspect layer

Ranking	Aspect (°)	Direction
5	135-180, 180-225	South
4	225-270, 270-315	West
2	45-90, 90-135	East
1	315-360, 0-45	North



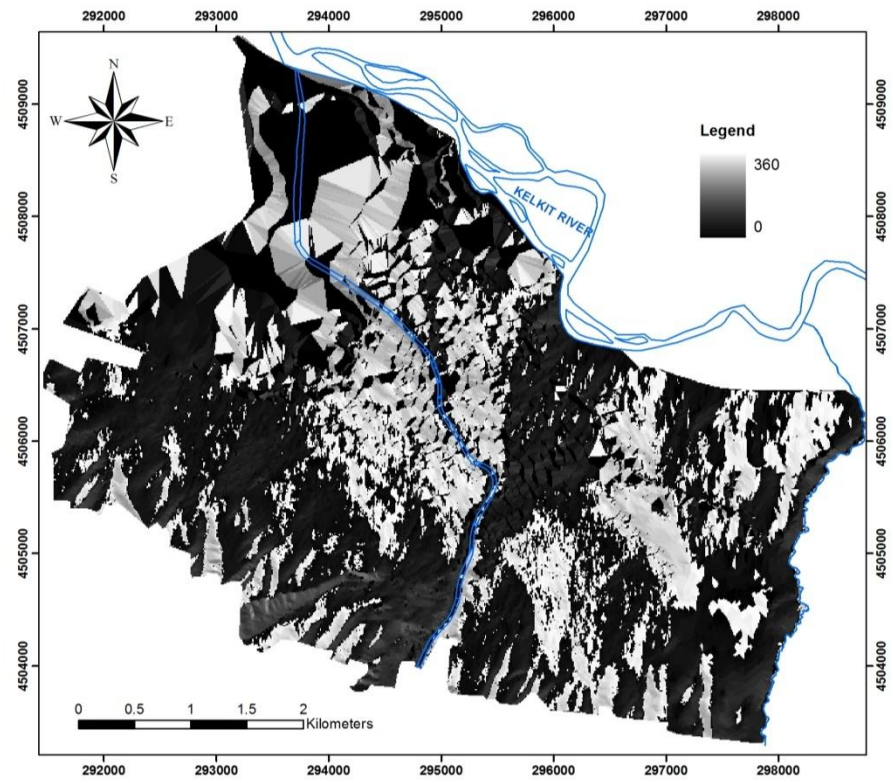


Figure 8.6. Distribution of aspect values in the study area (in degrees)

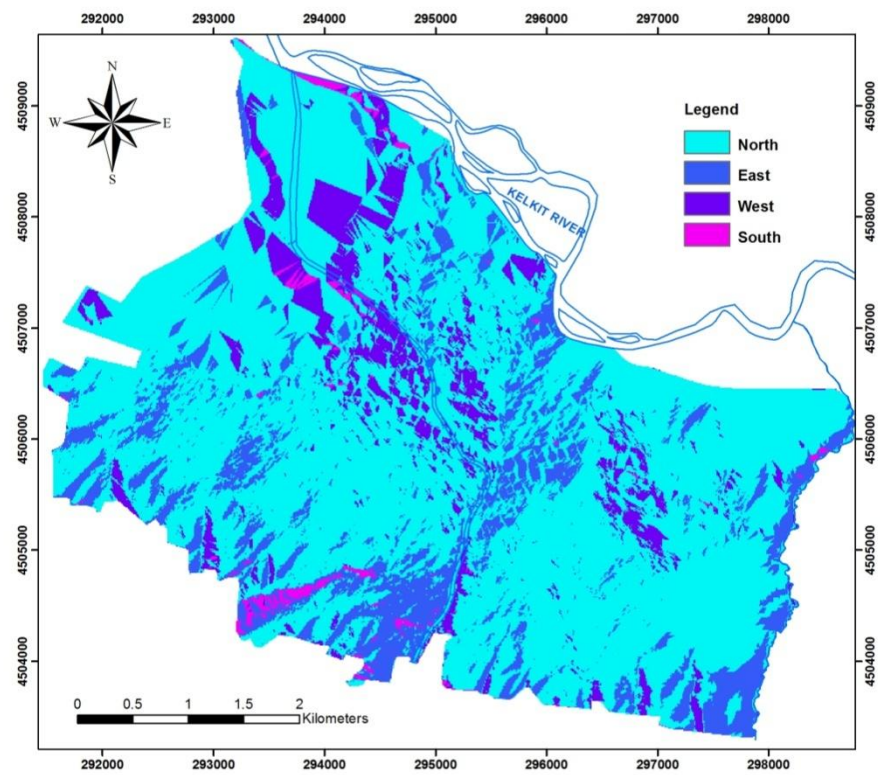


Figure 8.7. Aspect map of the study area

### 8.3.1.4 Lithology map

The lithology map of the study area is derived from the proposed geology map of Erbaa given in Chapter 3. The classified units are presented in Table 8.5. In this study, alluvial and Pliocene units are distinguished for overlay analyses (Figure 8.8). It should be noted that the alluvial cone shown in Figure 3.21 is not considered in GIS analyses since it has similar characteristics with alluvial units.

Table 8.5. Classification of lithological units

Ranking	Definition
1	Alluvial units
2	Pliocene units

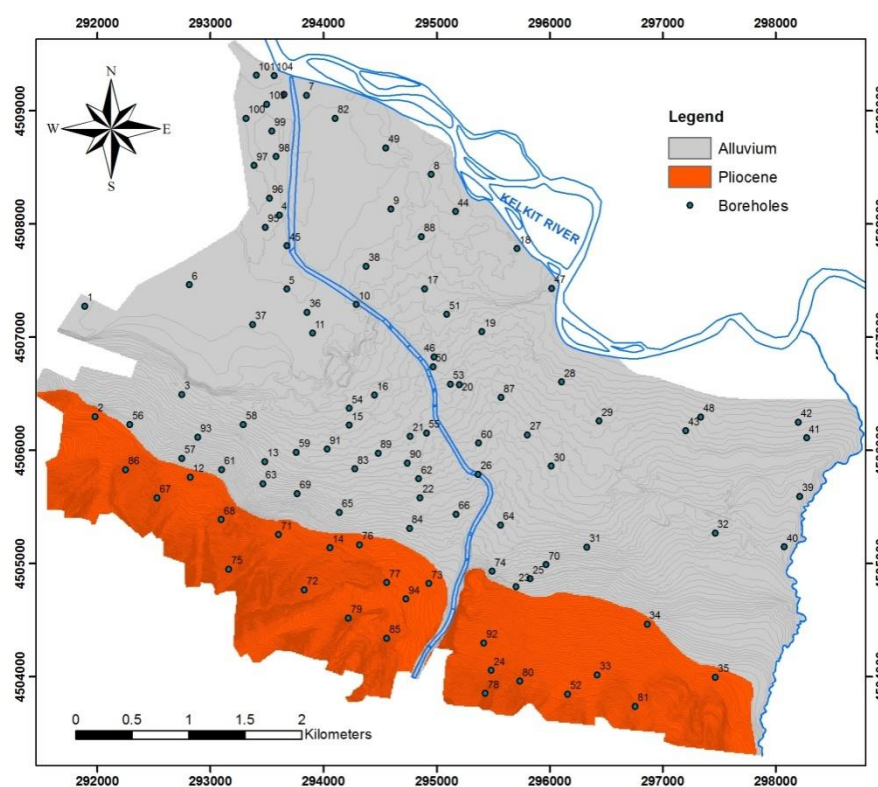


Figure 8.8. Lithology map of the study area

### 8.3.1.5 Depth to groundwater table map

Depth to groundwater table layer is prepared due to its significance on the performance of foundation stability and excavation works. During the preparation of depth to groundwater table map (as given in Figure 4.9), the groundwater levels of May 2008 are considered since precipitation occurs mostly during April - May period in the study area (as depicted in Figure 1.4). The depth to groundwater level map with 5 m contour intervals is prepared considering the previous depth to groundwater level map. Afterwards, the classes for depth to GWL are summarized in Table 8.6 and the related map is shown in Figure 8.9.

Table 8.6. Classification of depth to groundwater level

Ranking	Classes
5	> 20 m
4	10-20 m
2	5-10 m
1	0-5 m

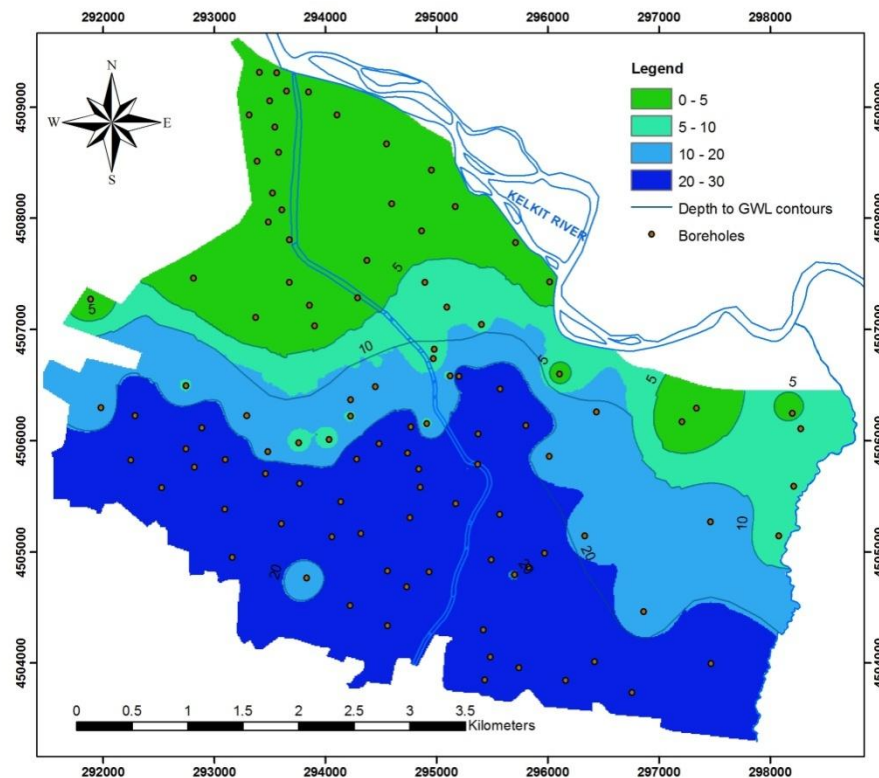


Figure 8.9. Depth to groundwater table map of the study area

### 8.3.2 Evaluated input data

#### 8.3.2.1 Distance to fault map

In order to determine seismic hazard potential of the study area, fault to distance and fault surface rupture with buffer zones are determined in this section. Beforehand, the surface rupture of the 1942 Niksar-Erbaa earthquake is considered for the production of distance to fault map. The surface ruptures generally occur when movement on a fault is observed with an earth breaking surface rupture. Some earthquakes may not result in a surface rupture. For instance, the 1989 Loma Prieta earthquake ( $M_w = 6.9$ ) caused major damage without any surface break. The surface rupture almost follows preexisting faults or break may occur suddenly during an earthquake or slowly within a fault creep. The sudden movements can cause more damage to structures (Bryant and Hurt, 2007).

A specific criterion which is proposed in the study of Bryant and Hurt (2007) is taken into account for the preparation of fault to distance map. According to the study of Bryant and Hurt (2007), the following condition is used within the framework of building structures in earthquake fault zones:

*“No structure for human occupancy shall be permitted to be placed across the trace of an active fault. Furthermore, as the area within fifty (50) feet (~15m) of such active faults shall be presumed to be underlain by active branches of that fault unless proven otherwise by an appropriate geologic investigation and report as suggested in the other regulations in this special publication.”*

Besides, the limitation of constructions in active fault zones is also mentioned by Waltham (1994). The mapping of recognized active faults with displacements should be limited for new buildings within 15 m of known faults (35 m for larger structures) and it should be given an extra 15 m setback on fault for not accurately being traced (Waltham, 1994).

Eventually, a buffer zone of 35 m in both directions is defined for the surface rupture of the 1942 earthquake considering the abovementioned studies since there is no guidance for the mapping of such type of buffer zones in Turkey. Therefore, a total of 70 m buffer zone is obtained for the restricted area of construction along the surface rupture. The assigned rank values to the classes for the preparation of distance to fault map are given in Table 8.7.



Afterwards, the distance to fault map is prepared for the study area with 2000 m intervals (Figure 8.10).

Table 8.7. Classification of distance to fault map

Ranking	Classes
2	2000-4000 m zone
1	0-2000 m zone

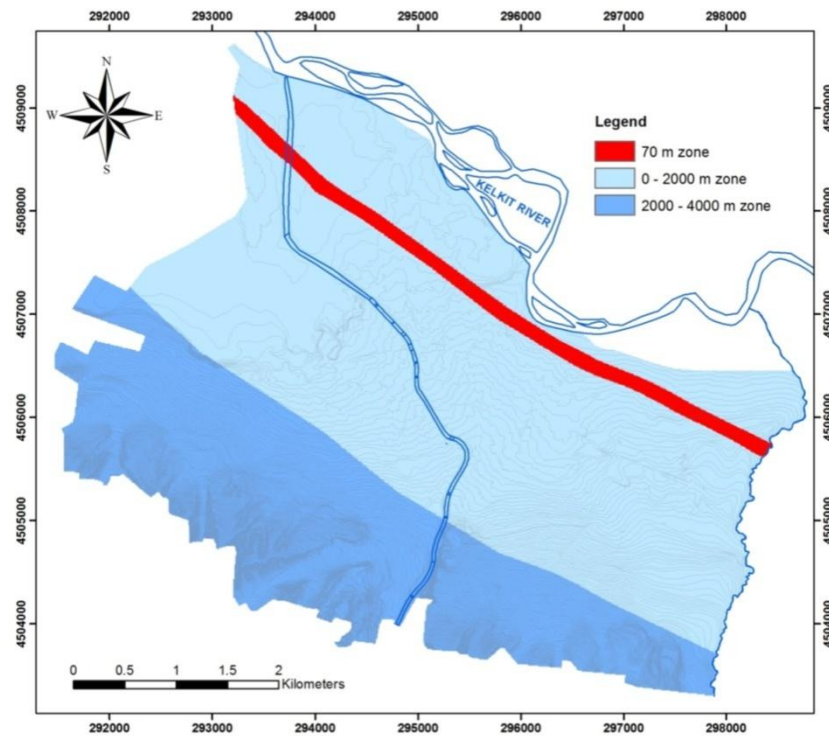


Figure 8.10. Distance to fault map of the study area

### 8.3.2.2 $V_{s30}$ -based site classification map

The distribution of the average of upper 30 m shear wave velocity ( $V_{s30}$ ) is also prepared to be considered in the final seismic microzonation map. The NEHRP (2000) provisions are taken into account for the classification of  $V_{s30}$  in order to evaluate the dynamic parameters of the soil layers. Accordingly, the soil units in the study area are classified as D and C type soils. The C type soils designate dense soils and soft rock. In addition, stiff soils can be

classified as D type soils as mentioned in Table 6.8. The classification of  $V_{s30}$  values in accordance with NEHRP (2000) provision and their areal distribution can be seen in Table 8.8 and Figure 8.11, respectively.

Table 8.8. Classification of  $V_{s30}$ -based site classification map

Ranking	Definition	$V_{s30}$ values
1	D type soils	180-360 m/s
2	C type soils	360-380 m/s

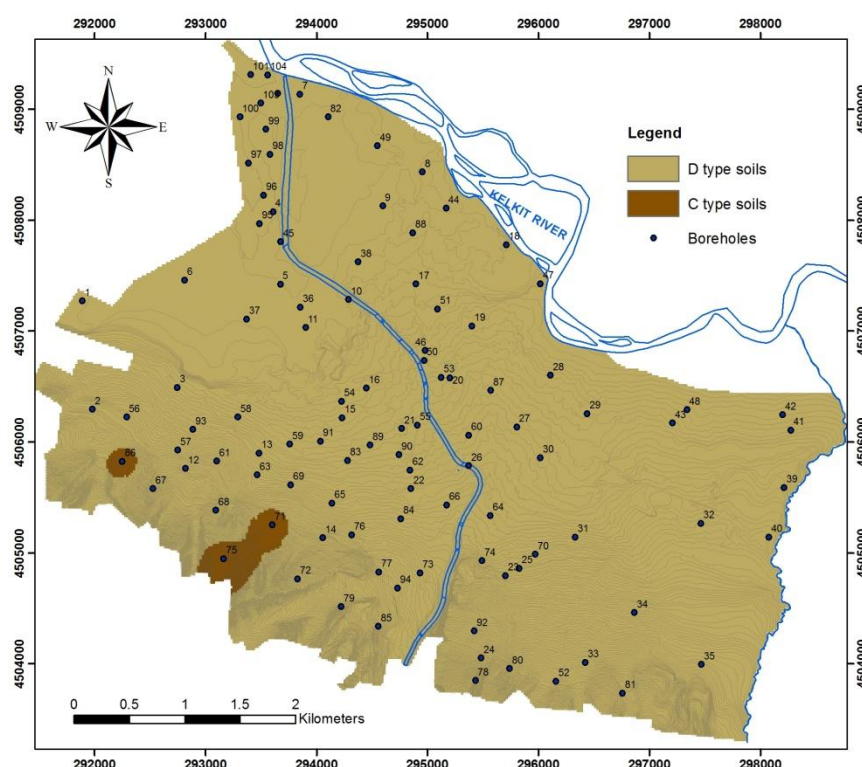


Figure 8.11.  $V_{s30}$ -based site classification map of the study area

As shown in Figure 8.11, D type soils with 180-360 m/s shear wave velocity mostly cover the study area. It is obvious that the Pliocene and alluvial units are generally classified in the same soil class with respect to  $V_{s30}$ -based site classification. The  $V_{s30}$ -based site classification is considered as a separate layer in the analyses since it is necessary to highlight the importance of dynamic soil properties in seismic microzonation.

### 8.3.2.3 Amplification map

The distribution of amplification values is also prepared to be considered in the final seismic microzonation map in order to involve site response effects in the study area. The amplification values determined by the geotechnical based amplification factors model proposed by Stewart et al. (2003) are taken into account during the evaluation stage. Consequently, the amplification factors based on Stewart et al. (2003) model is classified as well. The classification ranges and the amplification factor map are presented in Table 8.9 and Figure 8.12, respectively.

Table 8.9. Classification of amplification factor based map

Ranking	Classes
2	1.74-1.91
1	1.91-2.10

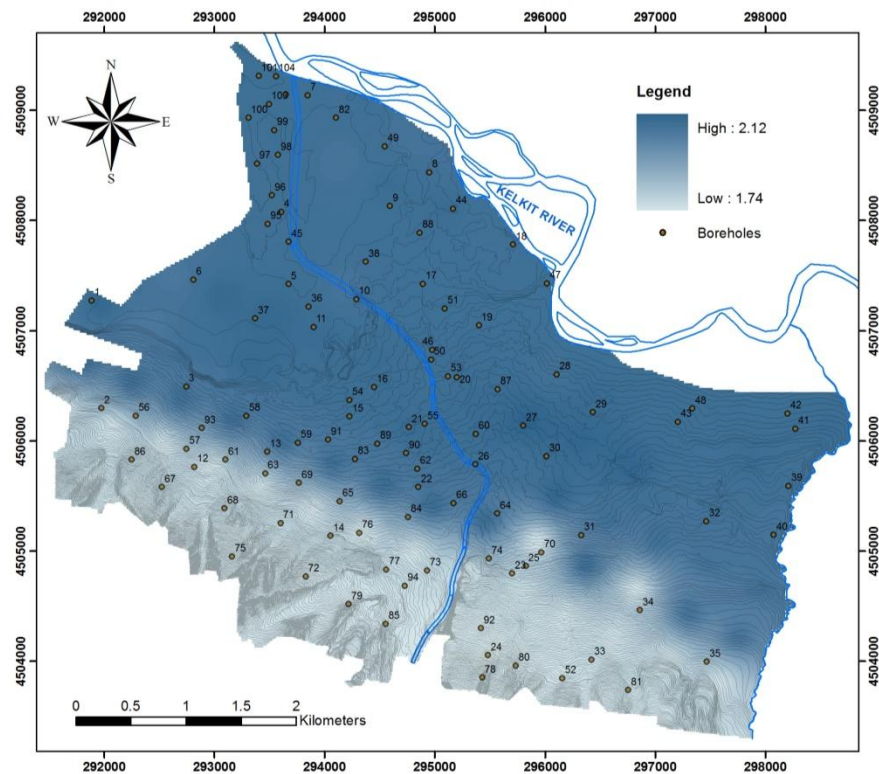


Figure 8.12. Amplification factor based map of the study area

The amplification values obtained from Stewart et al. (2003) model seem to be more logical for 0.001 sec period when compared to other methods. Additionally, the variation of amplification factors with different period ranges should be considered in design and construction stages. In other words, the related period levels of structures should be taken into account in order to determine possible effects of amplification.

#### **8.3.2.4 Liquefaction-induced ground deformation map**

The final liquefaction-induced ground deformation map of the study area with five classes is proposed in Chapter 7. The proposed map is considered for the final seismic microzonation model in order to evaluate the liquefaction and post-liquefaction effects in the study area. The classification of liquefaction-induced ground deformation ranges and the map is given in Table 8.10 and Figure 8.13, respectively.

Table 8.10. Classification of liquefaction-induced ground deformation

<b>Ranking</b>	<b>Classes</b>
1	Very high
2	High
3	Moderate
4	Low
5	None

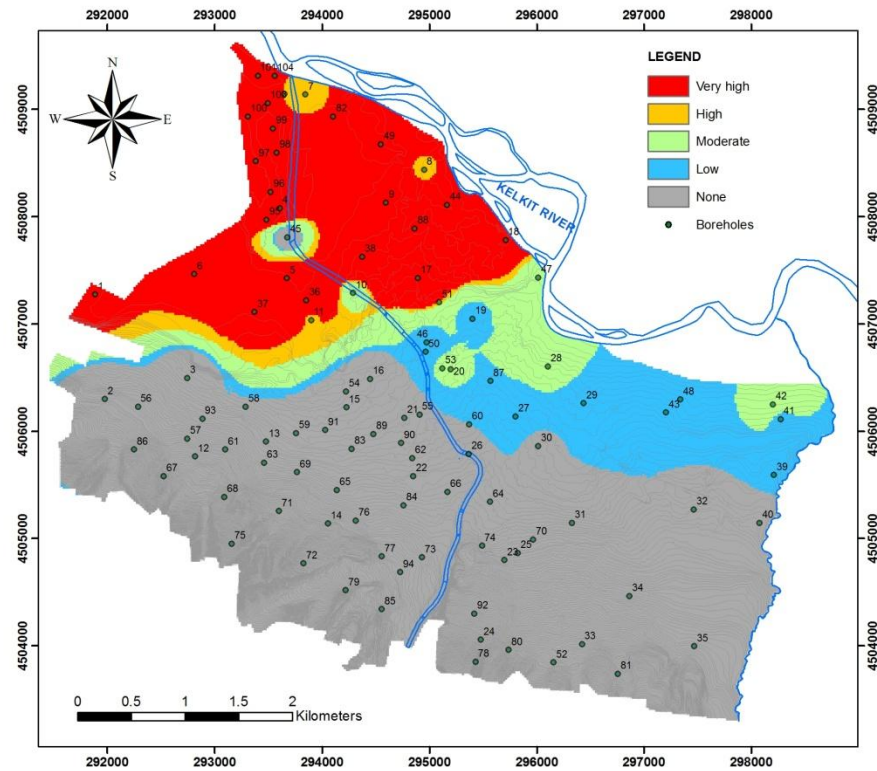


Figure 8.13. Liquefaction-induced ground deformation map of the study area

## 8.4 Multi-Criteria Decision Analyses

### 8.4.1 Classification of settlement zones

The proposed rank and weight values based on two different MCDA methodologies are standardized in order to obtain a common dimensionless unit. Afterwards, the produced maps are grouped into different zones considering the subdivisions which were proposed by General Directorate of Disaster Affairs of Turkey (GDDA, 2000). The residential areas can be defined by these subdivisions (Topal et al., 2003):

- Zone I-Areas suitable for settlement: normal residential developments can be planned without any further precautions.
- Zone II-Provisional settlement areas: development can take place provided certain precautionary measures against heave, excessive settlements, shallow water table, etc. are taken.

- Zone III-Areas requiring detailed geotechnical investigations: conditions are such that individual investigations are required and prescribed standard precautions to be taken against very high heave, very high settlement, very shallow water table, liquefaction, flood, etc.
- Zone IV-Areas not suitable for settlement: no settlement of any kind is allowed in areas where seismicity, landslides, floods, water table at the surface, steep slopes, etc. pose serious risks to residential development. Such areas may be used for recreational purposes.

In order to classify the study area into different zones with respect to proper settlement, four main groups (Suitable area, Provisional area, Detailed geotechnical investigation required area, Unsuitable area) are defined for the microzonation maps of the study area on the basis of GDDA (2000) recommendations. The identified zones can be adapted to the conditions of the study area. The detailed explanation of each zone is given below:

**Suitable area:** Residential developments can be planned without any further precautions on suitable areas. However, various site specific conditions should be considered. One of the specific conditions for new settlements in Erbaa is the earthquake related hazards. The amplification in such type of areas may cause severe damage to structures. Therefore, the soil and structure periods should be well-defined for design purposes. The amplification values proposed in this study for different period levels can be considered for further developments.

**Provisional area:** Development in these areas requires precautions with some mitigation techniques. The topographical conditions and the amplification effects should also be considered especially in structure design in the provisional areas. The variation in groundwater level and soil conditions should be determined in these zones, especially towards the Kelkit River.

**Detailed geotechnical investigation required area:** Possible ground deformations should be investigated in foundation scale in these areas. The ground deformation may highly occur based on the high risk of post-liquefaction effects (lateral spreading and vertical settlement). In addition, groundwater table is very shallow that may cause serious problems during excavations. High amplification can also be expected during a strong earthquake due to the

characteristics of soil profiles. The remedial measures should be determined and applied for site-specific regions with detailed geotechnical investigations.

**Unsuitable area:** Any type of settlements should not be allowed in these areas. The fault rupture zone is the main place where the structures must not be constructed. Additionally, the archeological site in the southern part of the study area is also considered as unsuitable area in Erbaa.

#### 8.4.2 Multi-Criteria Decision Analyses using Simple Additive Weighting (SAW) method

The assigned weight and rank values for the layers/classes of the study area based on the engineering judgment are given in Table 8.11. The most important layer is accepted as the liquefaction-induced ground deformation map. It is followed by the distance to fault, lithology, amplification,  $V_{s30}$ -based site classification, depth to groundwater table, slope, and aspect layers with decreasing importance. Moreover, rank values vary between 1 and 5 indicating an importance increase towards 5. On the other hand, weight values ranges between 1 and 10 indicating an importance increase towards 10.

Table 8.11. Assigned rank and weight values for the layers/classes in SAW method

Layers	Weighting	Classes	Ranking
Slope (°)	2	0-5	5
		5-10	4
		10-15	3
		15-20	2
		> 20	1
Aspect	1	S	5
		W	4
		E	2
		N	1
Lithology	5	Pliocene	2
		Alluvium	1
Depth to groundwater table	4	> 20 m	5
		10-20 m	4
		5-10 m	2
		0-5 m	1
Distance to fault	7	2000 - 4000 m zone	2
		0 - 2000 m zone	1
$V_{s30}$ -based site classification	3	(360-380 m/s)-D type soils	2
		(180-360 m/s)-C type soils	1
Amplification	6	1.74-1.91	2
		1.91-2.10	1
Liquefaction-induced ground deformation	8	None	5
		Low	4
		Moderate	3
		High	2
		Very high	1

The highest weight is assigned to the liquefaction-induced ground deformation layer in SAW method. The ground deformation caused by liquefaction can be quite destructive in the study area. The second highest weight is given to the distance to the fault surface rupture since the study area is in an active fault zone. The order of weight assigning continues with decreasing importance in the study area with respect to the seismic microzonation design purposes. Besides, the assigned rank values are also shown in Table 8.11. During the assignment of rank values to different classes, ‘5’ represents the most valuable class whereas the least valuable class is represented by ‘1’ which means the worst case will have the less value in the ranking part. Afterwards, the proposed rank values of the classes are standardized according to the relative distance between the origin and the maximum rank value using the following formula:

$$X'_{ij} = X_{ij} / X_{j\max} \quad (8.1)$$

where  $X'_{ij}$  is the standardized rank value for the  $i^{\text{th}}$  class for the  $j^{\text{th}}$  layer,  
 $X_{ij}$  is the raw rank value,  
 $X_{j\max}$  is the maximum rank value for the  $j^{\text{th}}$  layer

Additionally, the weight values are normalized by dividing each weight by the weight sums. The sum of the normalized weights should be equal to 1. The standardized rank values and normalized weight values are given in Table 8.12.



Table 8.12. Normalized rank and weight values for the layers/classes in SAW method

Layers	Weighting	Classes	Ranking
Slope (°)	0.056	0-5	1
		5-10	0.8
		10-15	0.6
		15-20	0.4
		> 20	0.2
Aspect	0.028	S	1
		W	0.8
		E	0.4
		N	0.2
Lithology	0.139	Pliocene	1
		Alluvium	0.5
Depth to groundwater table	0.111	> 20 m	1
		10-20 m	0.8
		5-10 m	0.4
		0-5 m	0.2
Distance to fault	0.194	2000 - 4000 m zone	1
		0 - 2000 m zone	0.5
$V_{s30}$ -based site classification	0.083	(360-380 m/s)-D type soils	1
		(180-360 m/s)-C type soils	0.5
Amplification	0.167	1.74-1.91	1
		1.91-2.10	0.5
Liquefaction-induced ground deformation	0.222	None	1
		Low	0.8
		Moderate	0.6
		High	0.4
		Very high	0.2

The overlay analyses are conducted using the weight and rank values of the layers. The normalized weight values assigned for each layer are multiplied by the standardized rank value given to the classes of that layer. The seismic microzonation map prepared in accordance with SAW method is classified into four zones. The division of “detailed geotechnical investigation required area, provisional area, and suitable area” is performed with respect to the histogram of seismic microzonation map. The boundaries of abovementioned classes are depicted on the histogram of the map (Figure 8.14). The “unsuitable area” boundary is determined separately according to the buffer zone criterion. The seismic microzonation map of the study area based on SAW method is presented in Figure 8.15.

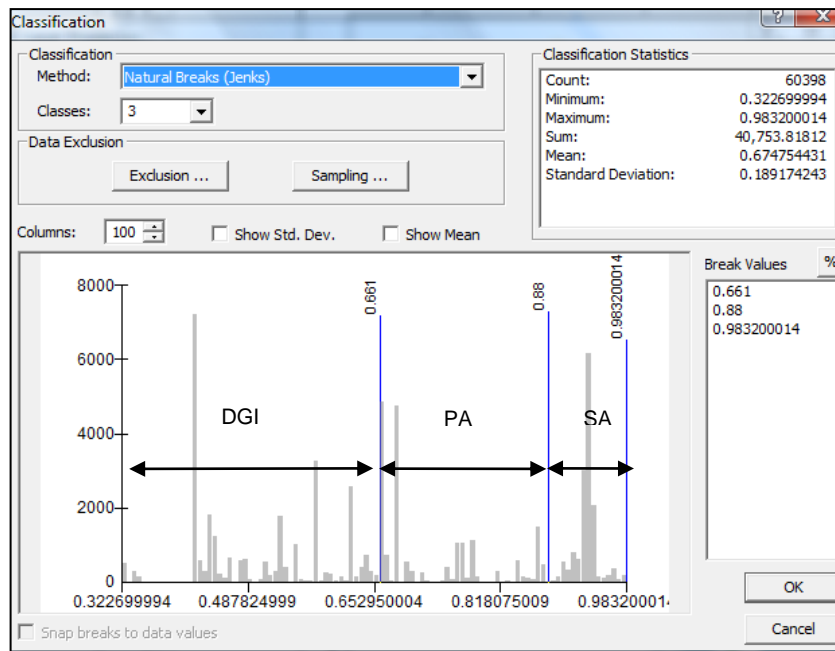


Figure 8.14. Histogram showing the boundaries of three zones of seismic microzonation map based on SAW method (SA: Suitable area; PA: Provisional area; DGI: Detailed geotechnical investigation required area)

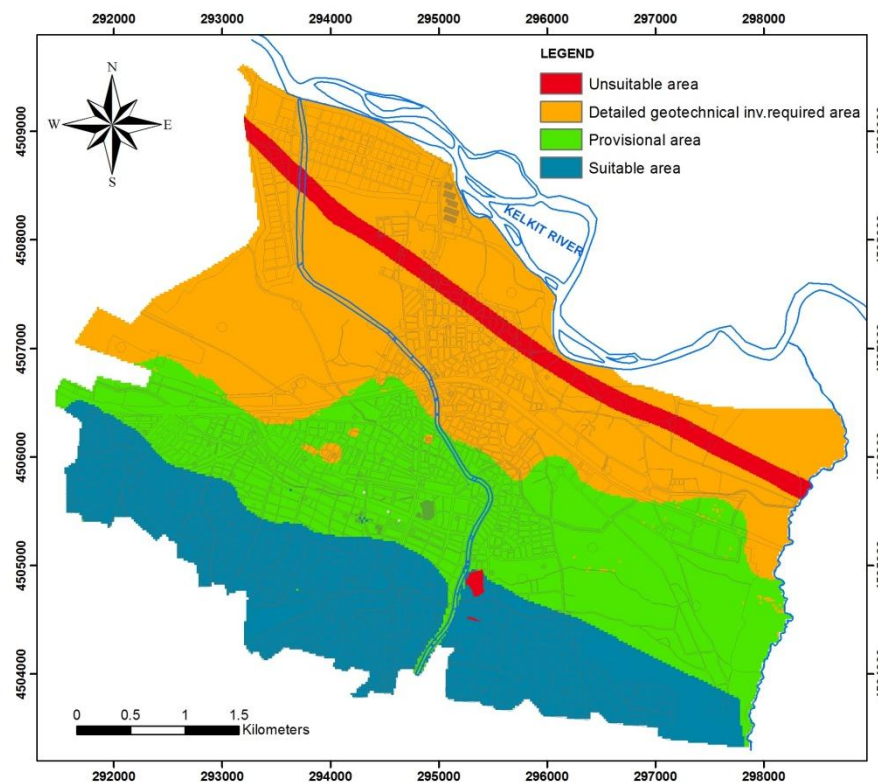


Figure 8.15. Seismic microzonation map of the study area based on SAW method

### 8.4.3 Multi-Criteria Decision Analyses using Analytical Hierarchical Process (AHP) method

A pairwise comparison is performed for AHP method. The weight values assigned to each map are obtained from pairwise comparison. On the contrary, AHP method does not suggest any technique for ranking the layers. Therefore, the applications performed in Kolat (2004) and Sener (2004) is concerned to get ranking values for each layer. In addition, Janssen (1992) stated that the AHP method cannot only be used to asses weights, but it can also be used to assess the performance of alternatives by pairwise comparison. Considering these assumptions, it is decided to apply the pairwise comparison for each separate layer to obtain ranking values. The pairwise comparison matrix developed for eight criteria is shown in Table 8.13.

Table 8.13. Comparison matrix developed for AHP-based seismic microzonation map

AHP calculation criterion	Liquefaction	Distance to fault	Lithology	Amplification	V <sub>s30</sub> -based site classification	Depth to groundwater table	Slope	Aspect
Liquefaction	1	2	2	3	3	5	7	9
Distance to fault	1/2	1	4	2	4	5	8	9
Lithology	1/2	1/4	1	3	4	4	7	9
Amplification	1/3	1/2	1/3	1	2	4	7	9
V <sub>s30</sub> -based site classification	1/3	1/4	1/4	1/2	1	2	8	9
Depth to groundwater table	1/5	1/5	1/4	1/4	1/2	1	6	9
Slope	1/7	1/8	1/7	1/7	1/8	1/6	1	2
Aspect	1/9	1/9	1/9	1/9	1/9	1/9	1/2	1

The assigned weight values for the layers/classes of the study area based on the engineering judgment are given in Table 8.13. The consistency ratio (CR) of the comparison matrix is calculated as 0.095 which is less than the threshold value (0.10). It means the pairwise comparison matrix is acceptable for AHP method.

The most important layer is defined as the liquefaction-induced ground deformation layer, followed by the distance to fault, lithology, amplification, V<sub>s30</sub>-based site classification, depth to groundwater table, slope, and aspect layers with decreasing importance as also mentioned in SAW method.

During the estimation of rank values, a similar pairwise comparison is utilized for each layer separately. The rank values are assigned considering the comparison of layer classes. The obtained ranking values are presented in Table 8.14. An example of pairwise comparison matrix for ranking calculations is given in Table 8.15. In addition, the consistency ratios for each layer are summarized in Table 8.16.

Table 8.14. Assigned weight and rank values to the layers/classes in AHP method

Layers	Weighting	Classes	Ranking
Slope (°)	0.022	0-5	0.401
		5-10	0.258
		10-15	0.179
		15-20	0.123
		> 20	0.040
Aspect	0.016	S	0.548
		W	0.281
		E	0.115
		N	0.056
Lithology	0.177	Pliocene	0.833
		Alluvium	0.167
Depth to groundwater table	0.067	> 20 m	0.542
		10-20 m	0.248
		5-10 m	0.139
		0-5 m	0.070
Distance to fault	0.241	2000 - 4000 m zone	0.857
		0 - 2000 m zone	0.143
V <sub>s30</sub> -based site classification	0.093	(360-380 m/s)-D type soils	0.833
		(180-360 m/s)-C type soils	0.167
Amplification	0.125	1.74-1.91	0.833
		1.91-2.10	0.167
Liquefaction-induced ground deformation	0.259	None	0.415
		Low	0.270
		Moderate	0.182
		High	0.106
		Very high	0.027

Table 8.15. Pairwise comparison matrix for liquefaction-induced ground deformation map

AHP calculation criterion	None	Low	Moderate	High	Very high
None	1	2	3	5	9
Low	1/2	1	2	4	9
Moderate	1/3	1/2	1	3	9
High	1/5	1/4	1/3	1	9
Very high	1/9	1/9	1/9	1/9	1

Table 8.16. Consistency ratios (CR) for each layer

Layers	Consistency Ratio (CR)
Liquefaction-induced ground deformation	0.086
Distance to fault	0.010
Lithology	0.010
Amplification	0.046
V <sub>s30</sub> -based site classification	0.010
Depth to groundwater table	0.096
Slope	0.088
Aspect	0.065

The microzonation map prepared using the AHP method is divided into four zones. The classification procedure of SAW method is also applied in AHP method. The boundaries of map classes except “Unsuitable area” are depicted on the histogram of the map in Figure 8.16. The unsuitable areas involve the fault buffer zone and the archeological site. The resultant seismic microzonation map based on AHP method is also illustrated in Figure 8.17.

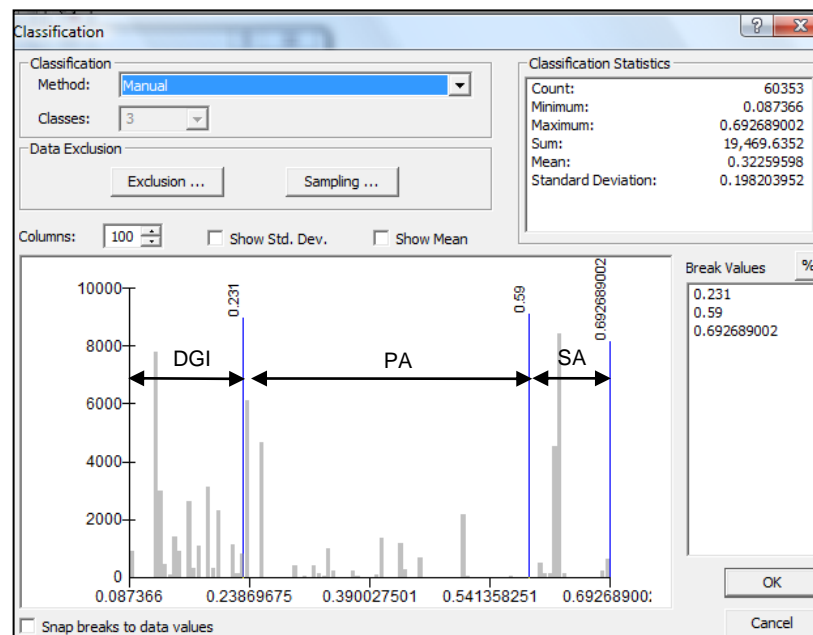


Figure 8.16. Histogram showing the boundaries of three zones of seismic microzonation map based on AHP method (SA: Suitable area; PA: Provisional area; DGI: Detailed geotechnical investigation required area)

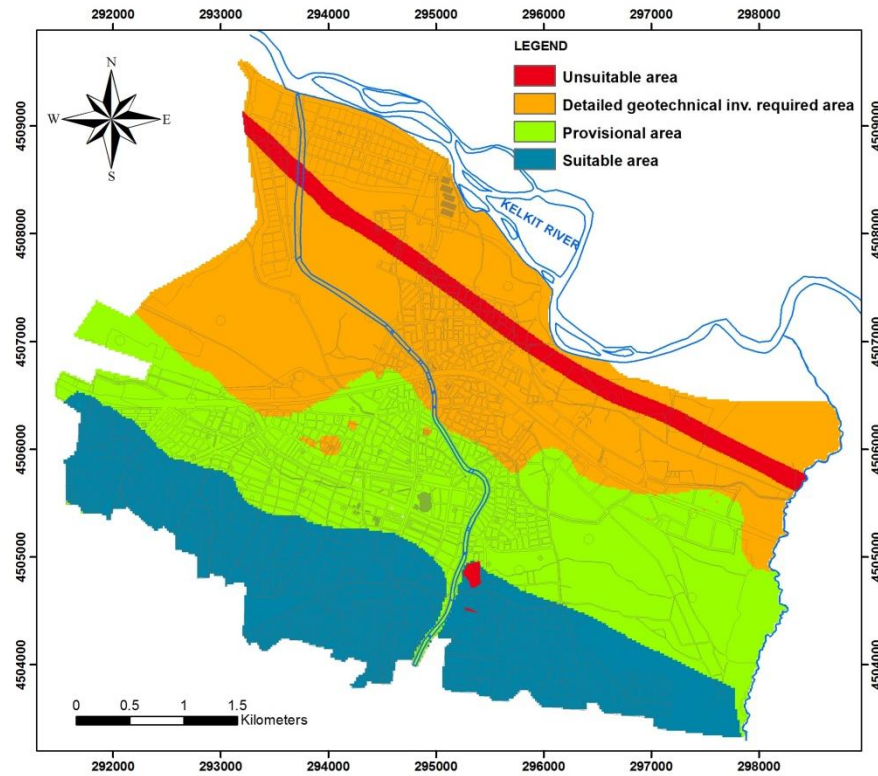


Figure 8.17. Seismic microzonation map of the study area based on AHP method

### 8.5 Comparison of Seismic Microzonation Maps

In the framework of MCDA methods, the decision problem should be truly well-defined. The set of possible alternatives, criteria and limitations should be identified for different cases. Therefore, the seismic microzonation maps are prepared based on two MCDA methods (SAW and AHP) for the study area. In order to compare these seismic microzonation maps, re-classification is performed for two raster maps. Afterwards, the same values are assigned to the classes in two microzonation maps. The comparison is performed to interpret the differences between these maps. Hence, a resultant map showing the difference between for two maps is generated (Figure 8.18). In this resultant map, the red areas indicate non-overlapped areas of two methods. Besides, the light yellow areas show the consistency of the two MCDA methods for the same area.

According to the comparison of two maps, the results are generally compatible with each other. The non-overlapping areas cover provisional and detailed geotechnical investigation required areas in both maps (Figure 8.18). Besides, consistent results are found for suitable areas. Eventually, the seismic microzonation map based on AHP method is accepted to be the final seismic microzonation map of Erbaa as the AHP method is more objective than the SAW method with respect to logical judgment criteria and theoretical foundation. Besides, the pairwise comparison matrix in AHP method provides interrelation assumptions between layers. However, the SAW method only considers the decision maker's assigned weights.

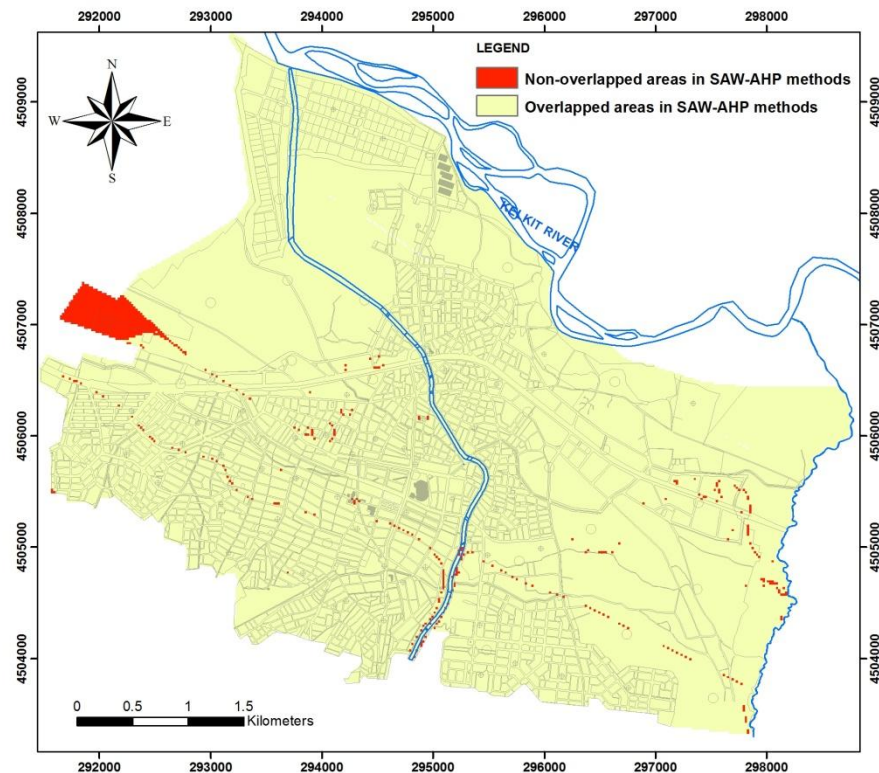


Figure 8.18. Comparison map of SAW and AHP-based seismic microzonation maps

The northern part of the study area generally requires detailed geotechnical investigation according to the final seismic microzonation of the study area presented in Figure 8.17. On the contrary, the Pliocene units in the south represent the suitable areas. A transition zone between north and south is determined where the provisional area exists. It should also be noted that the necessary remedial measurements should be investigated for the previously settled areas in detailed geotechnical investigation required zones and provisional zones.

## 8.6 Concluding Remarks

The Multi-Criteria Decision Analysis (MCDA) is an efficient tool in seismic microzonation projects for site classification. Simple Additive Weighting (SAW) and Analytical Hierarchical Process (AHP) methodologies, which are the two most common MCDA techniques, are exploited to obtain the final seismic microzonation map of Erbaa. Liquefaction-induced ground deformation, distance to fault, lithology, amplification,  $V_{s30}$ -based site classification, depth to groundwater table, slope, and aspect layers are analyzed in GIS environment using different weighting and ranking values.

In general, liquefaction-induced ground deformation map is accepted to be the most significant layer for seismic microzonation whereas aspect map is found to be the least effective. Therefore, the highest weighting is assigned to liquefaction-induced ground deformation layer in both methods. As a result of evaluation process, quite similar results are obtained from SAW and AHP methods. The non-overlapping areas are determined by comparing both methods. The non-overlapping areas exist in detailed geotechnical investigation required and in provisional areas. Both methods reveal almost the same results for suitable areas. The unsuitable areas for settlement are buffered in the study area. Finally, the microzonation map prepared using AHP method is accepted as the final seismic microzonation map of Erbaa.



## CHAPTER 9

### DISCUSSION

In this dissertation, it is intended to prepare a seismic microzonation map using a variety of geological, geotechnical, and geophysical data since such type of a seismic microzonation study for Erbaa was not performed in the past.

The aim of this chapter is to continue step by step through the procedures of seismic microzonation with the discussion of the problems faced during the study. This chapter is divided into two main sections in order to interpret the results.

#### 9.1 Data Production

The utilized field and laboratory data are presented in the data production section. In general, most of the field techniques have some limitations. The important issue is to consider advantages and disadvantages of the used techniques.

The applied sampling technique in this study is different than the usual sampling techniques. In general, SPT is performed at every 1.5 m and undisturbed (UD) samples are taken at every 3 m (if possible) during drilling. In this study, the SPT and UD sampling are executed at every 1 m successively not to neglect very thin sandy layers or other soil units. Hence, a continuous soil profile can be retrieved using a tight sampling program. As a result, the data obtained from sampling and SPT-N resistance are used in order to get sensitive results for the evaluation part. Therefore, it is of great importance to acquire a continuous soil profile by successive sampling with shorter intervals in seismic microzonation studies. In addition, the depth of geotechnical boreholes is very important in such projects. In this study, it is tried to drill down to 30 m. The average shear wave velocity of upper 30 m ( $V_{s30}$ ) can be obtained using various SPT-N –  $V_s$  correlations since  $V_{s30}$  is quite important in terms of site classification. However, in this study, the drilling staff was sometimes forced to interrupt

drilling before 30 m due to gravelly layers. For this reason, some of the boreholes in the study area could not reach the desired depth.

SPT-based uphole technique is firstly applied in Turkey within the framework of this dissertation. The abovementioned method provides the recording of shear wave velocities during SPT test simultaneously. The impact energy produced by the SPT test is used as a source for the uphole method. It is a very practical method which can be easily applied in every geotechnical investigation. Additionally, SPT-N resistance and shear wave velocities can also be correlated as proposed in this study. A number of relations between SPT-N resistance and shear wave velocity are obtained using SPT-based uphole results. Furthermore, the empirically calculated shear wave velocities are also correlated to the measured velocities. In general, the SPT-N resistance is simply considered during shear wave velocity correlations. However, the SPT-N resistance may not be sufficient in order to determine shear wave velocity. The SPT-N-based correlations can only be used for site specific conditions. It should be kept in mind that depth is a crucial parameter for the determination of shear wave velocities as shear wave velocity typically increases with depth. Therefore, the proposed shear wave velocity correlations should include the effect of depth. Eventually, empirical formulas considering depth effect are proposed for different soil types in this dissertation.

Microtremor measurements are commonly preferred in microzonation projects. However, the microtremor measurements are not sufficient due to its limitations in microzonation projects. Hence, they should not be used solely in microzonation projects and the results should be compared to other measurements or approaches. For instance, some inconsistent results are obtained from microtremor surveys when compared to other methods in this study. Microtremor measurements generally reveal higher amplification values than the other methods.

In this study, deterministic seismic hazard analyses are performed to reveal the hazard level in the study area. It may be quite useful to perform probabilistic seismic hazard analyses in order to investigate the probability of hazard level in Erbaa.

The parameters of ground motion prediction are defined for Erbaa as well. The newly proposed NGA (Next Generation Attenuation Models) are applied in order to get earthquake ground motion parameters. There are some site specific attenuation models developed by

several researchers. However, the quantity and the quality of data are the most important aspects during the production of NGA models. The NGA models can be used in the areas located in tectonically active regions. The NGA models are the improved version of the previous ground motion models. Therefore, the new NGA model is selected in this study for its suitability in tectonically active regions such as Erbaa. Additionally, new parameters are proposed in NGA models which are hanging wall effects of the fault, sediment and basin depth effects for the tectonically active regions. As a result, two different NGA models are used in order to consider different attenuation model parameters as abovementioned. It is also aimed to define the dissimilarities in both NGA models.

The dynamic soil parameters are mostly based on shear wave velocity values and are also evaluated in a site-specific region for site response analyses. The average shear wave velocity of upper 30 m as previously mentioned is also calculated for Erbaa. The calculations are correlated with the SPT-N resistance for each borehole in order to define the proper site class using various provisions. If the data is insufficient down to 30 m depth, a classification and a resultant classification map cannot be proposed. Hence, a detailed geotechnical site investigation should be planned in such type of seismic microzonation projects.

In order to model the soil profiles for the entire area, a grid cell system is utilized in this study. Division into grid cells is a common approach used in many seismic microzonation projects. The dimension of grids mostly depends on the size of the area and the available geotechnical data for the investigated area. A 500x500 m grid cell system is preferred for Erbaa. Although the sensitivity of grid system is based on the size of the division, the corresponding available data mostly dominates the results in analyses. In other words, not only the selection of grid cell size is important, but also the distribution of available data is decisive in microzonation projects.

In site response analyses, 1-D equivalent linear method is applied in which all boundaries are assumed to be horizontal. In literature, it is also possible to model in different dimensions (2-D, 3-D). Additionally, non-linear site response analysis is quite common. Although 1-D linear analysis is easy to apply it does not consider all types of waves.

The modulus reduction and damping curves which are both used in 1-D software is modified for the site specific conditions in this study. The modified curves are represented by different confining pressures for different soil types in Erbaa. The site specific models can be

constructive in order to analyze different soil conditions for the investigated area. Therefore, the modified curves are preferred in site response models. However, great care should be taken during the modification process and the site-specific curves should be compared to the default curves not to lead to some illogical results.

The amplification ratios for the study area are obtained from experimental and empirical methods. Additionally, site amplification factors based on different periods are required for design purposes, since the resonance effect should be considered for structures regarding amplification factors.

The proposed final liquefaction map for microzonation layers consists of liquefaction and post-liquefaction effects in Erbaa. Principally, the deterministic based approaches are concerned in the liquefaction analyses. The probabilistic based approach can also be quite useful for the comparison of results obtained from two methods in the liquefaction analyses.

## **9.2 Data Evaluation**

During the evaluation stage, a number of maps showing the distribution of the investigated parameter are prepared. For each subject, several methods are taken into account. Therefore, various maps are prepared for the same theme. For instance, numerous amplification and liquefaction maps are proposed with respect to different methods. For the overlay analyses to produce the final seismic microzonation map of Erbaa, a map is selected from each subject in order to prevent the duplication.

The effects of layers are different in overlay analyses. Therefore, Multi-Criteria Decision Analysis (MCDA) is utilized for decision-making. The main weakness of overlaying is the assignment of weights to each layer. Therefore, two different MCDA methods (SAW and AHP) are applied to correlate the results. The AHP method seems to be more objective for weight assignment since weights are determined through a comparison matrix. Although MCDA methods are accepted as “mutually exclusive” for each parameter, this assumption has to be stretched out because of the connections of the used parameters. Consequently, an interrelation among different layers can be established.

In such microzonation projects, various methods should be taken into account during decision-making. Additionally, the resultant map should be judged according to the obtained

data. The final zonation is performed in accordance with the provisions proposed by GDDA (2000). However, the settlement classes in GDDA (2000) provisions are not very obvious. This uncertainty leads to a limitation for planners and designers during interpretation. The description of each zone should be well-defined by policy makers since it is essential to have distinct provisions for urban planning in tectonically active regions.

## **CHAPTER 10**

### **CONCLUSIONS AND RECOMMENDATIONS**

#### **10.1 Conclusions**

Urban areas with an increasing population require new and suitable residential places. Having understood the role of natural hazards in the selection of proper settlements, newly developed planning techniques are concerned in order to reduce potential risks. Therefore, it is intended to present the development and implementation of different techniques for seismic microzonation concerning different methodologies in this dissertation.

The study area, Erbaa, is located on a very seismically active area (NAFZ). The most destructive earthquake around the study area occurred in 1942 with a magnitude of 7.2. The 1942 hazardous earthquake led to move the settlement towards south on mostly Pliocene units. However, new proper settlements are needed due to rapid development and a significant increase in population.

An appropriate settlement planning for urban areas, especially in the close proximity to seismic zones, requires detailed microzonation studies. Regarding the scope of this research, it is aimed to propose a seismic microzonation map of Erbaa. In this dissertation, it is intended to consider the topographical, geological, and geotechnical conditions as well as the earthquake effects for the selection of proper new settlement areas. Besides, it is highly recommended that the existing settlement area should be re-evaluated to establish safe development strategies in accordance with the proposed seismic microzonation map.

On the basis of the performed analyses following conclusions are drawn in this study:

- The tectonic mechanism of NAFZ and geological setting of the study area dominantly control the earthquake-related hazards. The Erbaa settlement is mainly located on Quaternary alluvial deposits and Pliocene units. Pliocene units generally

consist of uncemented gravel, sand, clay, and occasionally uncompacted sandstone layers. Alluvium is the dominant unit in the study area and is composed of gravelly, sandy, silty, and clayey layers. The grain size variation is due to the different and variable flow regimes of the Kelkit River in the past. The transition of different soil types in horizontal and vertical directions is quite common.

- The SPT-based uphole method, which is recently applied in Turkey in this study, is very functional to determine shear wave velocity in seismic microzonation studies. It provides enormous contribution for the interpretation and comparison of SPT-N resistance for the study area. Empirical relationships between shear wave velocity and SPT-N<sub>30</sub> are proposed considering the depth effect. The following power-law expressions including depth (in meters) based on multiple regressions are obtained for different soil categories.

$V_s = 59.44 N^{0.109} z^{0.426}$	for all alluvial soils
$V_s = 38.55 N^{0.176} z^{0.481}$	for alluvial sand
$V_s = 78.1 N^{0.116} z^{0.35}$	for alluvial clay
$V_s = 121.75 N^{0.101} z^{0.216}$	for all Pliocene soils
$V_s = 52.04 N^{0.359} z^{0.177}$	for Pliocene sand
$V_s = 140.61 N^{0.049} z^{0.232}$	for Pliocene clay

- The alluvial units in the northwestern part of Erbaa are more susceptible to earthquake related ground deformations than the other parts of the study area. According to liquefaction and post-liquefaction analyses, the damage may occur in the close vicinity of the Kelkit River.
- It is also concluded that the northeastern part of the study area where the alluvial units also exist and the Pliocene units in the southern part are found to be less vulnerable to earthquake induced deformations.
- The amplification factors obtained from different methods do not reveal a certain distinction between alluvium and Pliocene deposits in the study area.
- The microzonation map prepared using AHP method is accepted as the final seismic microzonation map. It has been divided into four settlement zones in terms of the settlement suitability.

## 10.2 Recommendations

The performed study on seismic microzonation confirms that a variety of contributions can be done in the future. Hence, the following recommendations should be considered in further projects.

- The soils profiles should be well-defined for site response analyses. Site-specific studies should be considered for seismic microzonation projects. During the ground motion prediction, the newly proposed attenuation models can be preferably used for the investigated areas. The NGA (Next Generation Attenuation) models are proper for seismically active areas.
- Probabilistic seismic hazard analyses can also be performed in order to assess the probability of hazard level in the investigated area. It also supplies a comparison of deterministic and probabilistic based seismic hazard levels.
- The amplification factor should also be provided for the interpretation of site effects. In the design and construction stages, the variation of amplification with respect to different periods should also be considered for possible resonance effects. It is highly suggested to consider the amplification factor associated with the properties of structure. The amplification factors of the soil unit in the study area should also be considered for different periods during the design of constructions to prevent soil and structure resonance.
- It is recommended to use Multi-Criteria Decision Analysis for decision-making in order to assign correct ranks considering the importance of each layer.
- The proposed final seismic microzonation map should be taken into account by the decision makers during urban planning studies in Erbaa. Furthermore, detailed geotechnical investigation required areas should be investigated in terms of the related foundation of the structures.
- Constructions should be avoided on the surface rupture zone of the North Anatolian Fault where soil remediation is not effective during an earthquake rupture.
- Similar seismic microzonation studies should be performed for the settlements in the close vicinity of active fault zones.



## REFERENCES

- Abeki, A., Matsuda, I., Enomoto, T., Shigyo, V., Watanabe, K., Tanzawa, Y., Nakajima, Y., 1995.** A study of seismic microzonation based on the dynamic characteristics of subsurface ground conditions. Proc. 5th International Conference on Seismic Zonation, Nice, France, 3, 2187-2194.
- Abrahamson, N.A., Litehiser, J.J., 1989.** Attenuation of vertical peak acceleration. Bulletin of the Seismological Society of America, 79(3), 549-580.
- Abrahamson, N.A., 1992.** Spatial variation of earthquake ground motion for application to soilstructure interaction, Rept. No. EPRI TR-100463, Electrical Power Research Institute, Palo Alto, California.
- Abrahamson, N.A., Silva, W., 2008.** Summary of the Abrahamson & Silva NGA ground-motion relations. Earthquake Spectra, 24(1), 67-97.
- Akademi Geotechnical Company, 2002.** Erbaa Organize Sanayi Bolgesi Jeoloji-Jeoteknik Etut Raporu, Ankara (unpublished, in Turkish).
- Akin (Kivanc), M., 2001.** Deterministik Yaklaşımla Türkiye'nin Sismik Tehlike Analizi (Seismic Hazard Analysis for Turkey using the Deterministic Approach). M.Sc. thesis. Ankara University, Graduate School of Natural and Applied Sciences, Ankara, Turkey, 74 pp. (in Turkish).
- Akin, M., Topal, T., 2008a.** Assessment of SPT-based liquefaction of Erbaa (Tokat), Turkey. 6th Int. Conference on Case Histories in Geotechnical Engineering, 12-16 August 2008, Arlington, VA.
- Akin, M., Topal, T., 2008b.** Estimation of liquefaction effects of Erbaa (Turkey) by using liquefaction potential index. EUROENGEO 2008, Madrid, Spain.
- Akin, M., Kramer, S.L., Topal, T., 2009.** Comparison of measured and estimated shear wave velocities in a seismically active area (Erbaa, Turkey). Fifth International Conference on "Recent advances in Geotechnical Earthquake Engineering and Soil Dynamics, San Diego, California (in press).
- Akkar, S., Bommer, J.J., 2007.** Empirical prediction equations for peak ground velocity derived from strong-motion records from Europe and the Middle East. Bulletin of the Seismological Society of America, 97(2), 511-530.
- Aktimur, K.T., Tekirli, M.E., Yurdakul, M. E., Ateş, Ş., Ürgün, B.M., Teoman, M.Ş., Keçer, M., Turşucu, A., Genç, S., 1989.** Niksar-Erbaa ve Destek Dolayının Jeolojisi; MTA Rap., 8894, Ankara, (unpublished, in Turkish).
- Aktimur, K.T., Tekirli, M.E., Yurdakul, M. E., Ateş, Ş., Ürgün, B.M., Teoman, M.Ş., Keçer, M., Turşucu, A., Genç, S.,**

**1990a.** 1:100 000 ölçekli açınısma nitelikli Türkiye Jeoloji Haritaları Serisi Tokat D 22 paftası: MTA Yayl., Ankara.

**1990b.** 1:100 000 ölçekli açınısma nitelikli Türkiye Jeoloji Haritaları Serisi Tokat D 23 paftası: MTA Yayl., Ankara.

**1990c.** Sivas-Erzincan Tersiyer havzasının jeolojisi: MTA Derg., 111, 25-36, Ankara (in Turkish).

**Aktimur, T., Ates, S., Yurdakul, E., Tekirli, E., Kecer, M., 1992.** Niksar-Erbaa ve Destek Dolayının Jeolojisi. MTADergisi, 114, 36 pp (in Turkish).

**Algermissen, S.T., Perkins, D.M., 1976.** A probabilistic estimate of maximum acceleration in rock in the contiguous United States. USGS Open File Report 76-416, p-45.

**Allen, C.R., 1969.** Active Faulting in Northern Turkey, Division of Geological Science, California Institute of Technology, Contr. No. 1577, 32 pp.

**Alvarez, L., Vaccari, F., Panza, G.F., 1999.** Deterministic seismic zoning of eastern Cuba. Pure and Applied Geophysics, 156, 469-486.

**Alvarez, L., Vaccari, F., Panza, G.F., Pico, R., 2005.** Seismic microzoning from synthetic ground motion parameters: case study, Santiago de Cuba. Soil Dynamics and Earthquake Engineering, 25, 383-401.

**Ambraseys, N.N., 1970.** Some characteristic features of the North Anatolian fault zone. Tectonophysics 9, 143-165.

**Ambraseys, N.N., Zatopek, A. 1969.** The Mudurnu valley, west Anatolia, Turkey, earthquake of 22 July 1967. Bulletin of the Seismological Society of America, 59 (2), 521-589.

**Ambraseys, N.N., 1970.** Some characteristic features of the Anatolian fault zone. Tectonophysics, 9, 143-165.

**Ambraseys, N.N., 1975.** Trends in engineering seismology in Europe. In: Proceedings of Fifth European Conference on Earthquake Engineering, 3, 39-52.

**Ambraseys, N.N., 1990.** Uniform magnitude re-evaluation of European earthquakes associated with strongmotion records. Earthquake Engineering and Structural Dynamics, 19(1), 1-20.

**Ambraseys, N.N., Bommer, J.J., 1991.** The attenuation of ground accelerations in Europe. Earthquake Engineering and Structural Dynamics, 20(12), 1179-1202.

**Ambraseys, N.N., Bommer, J.J., 1992.** On the attenuation of ground accelerations in Europe. In: Proceedings of Tenth World Conference on Earthquake Engineering, 2, 675-678.

**Ambraseys, N.N., 1995.** The prediction of earthquake peak ground acceleration in Europe. Earthquake Engineering and Structural Dynamics, 24(4), 467-490.

**Ambraseys, N.N., Bommer, J.J., 1995.** Attenuation relations for use in Europe: An overview. In: Elnashai, A. S. (ed), Proceedings of Fifth SECED Conference on European Seismic Design Practice, 67-74.

**Ambraseys, N.N., Simpson, K.A., Bommer, J.J., 1996.** Prediction of horizontal response spectra in Europe. *Earthquake Engineering and Structural Dynamics*, 25(4), 371-400.

**Ambraseys, N., Douglas, J., 2000.** Reappraisal of surface wave magnitudes in the Eastern Mediterranean region and the Middle East. *Geophysical Journal International*, 141(2), 357-373.

**Ambraseys, N., Douglas, J., 2003.** Near-field horizontal and vertical earthquake ground motions. *Soil Dynamics and Earthquake Engineering*, 23, 1-18.

**Ambraseys, N.N., Douglas, J., Sarma, S.K., Smit, P.M., 2005a.** Equation for the estimation of strong ground motions from shallow crustal earthquakes using data from Europe and the Middle East: horizontal peak ground acceleration and spectral acceleration. *Bulletin of Earthquake Engineering*, 3, 1-53.

**Ambraseys, N.N., Douglas, J., Sarma, S.K., Smit, P.M., 2005b.** Equation for the estimation of strong ground motions from shallow crustal earthquakes using data from Europe and the Middle East: vertical peak ground acceleration and spectral acceleration. Imperial College, London.

**Ambraseys, N.N., Finkel, C.F., 2006.** Türkiye'de ve Komşu Bölgelerde Sismik Etkinlikler: Bir Tarihsel İnceleme (1500-1800), TÜBİTAK Akademik Dizi, 252 pp. (in Turkish).

**Anagnostopoulos, S., Providakis, C., Salvaneschi, P., Athanasopoulos, G., Bonacina, G., 2008.** SEISMOCARE: An efficient GIS tool for scenario-type investigations of seismic risk of existing cities. *Soil Dynamics and Earthquake Engineering*, 28, 73-84.

**Anastasiadis, A., Raptakis, D., Pitilakis, K., 2001.** Thessaloniki's detailed microzoning: subsurface structure as basis for site response analysis. *Pure and Applied Geophysics*, 158, 2597-2633.

**Anbazhagan, P., Sitharam, T.G., 2008.** Seismic microzonation of Bangalore, India. *J. Earth Syst. Sci.*, 117(2), 833-852.

**Andrieux, J., Over, S., Poisson, A., Bellier, O., 1995.** The North Anatolian Fault Zone: distributed Neogene deformation in its northward convex part. *Tectonophysics*, 243, 135-154.

**Andrus, R.D., Stokoe, K.H., 1997.** Liquefaction resistance based on shear wave velocity in evaluation of liquefaction resistance of soils. National Center for Earthquake Engineering Research (NCEER) Workshop. Proceedings, Salt Lake, UT, Youd, T. L.; Idriss, I. M., (eds.), 89-128.

**Andrus, R.D., Stokoe, K.H., 2000.** Liquefaction resistance of soils from shear-wave velocity. *Journal of Geotechnical and Geoenvironmental Engineering*, ASCE, 126(11), 1015-1025.

**Andrus, R.D., Fairbanks, C.D., Zhang, J., Camp, W.M., Casey, T. J., Cleary, T. J., Wright, W.B., 2006.** Shear-wave velocity and seismic response of nearsurface sediments in Charleston, South Carolina. *Bulletin of the Seismological Society of America*, 96(5), 1897-1914.

**Ansal, A., İyisan, R., Özkan, M., 1997.** A preliminary microzonation study for the town of Dinar. *Seismic Behaviour of Ground and Geotechnical Structures*, Seco e Pinto (Ed.), Balkema, Rotterdam, 3-9.

**Ansal, A., İyisan, R., Yildirim, H., 2001a.** The cyclic behaviour of soils and effects of geotechnical factors in microzonation, *Soil Dynamics and Earthquake Engineering*, 21, 445-452.

**Ansal, A., İyisan, R., Gullu, H., 2001b.** Microtremor measurements for the microzonation of Dinar. *Pure and Applied Geophysics*, 158, 2525-2541.

**Ansal, A., 2002.** Seismic microzonation methodology. *Proc. of 12th European Conf. on Earthquake Engineering*, Paper No.830, London, UK.

**Ansal, A., Laue, J., Buchheister, J., Erdik, M., Springman, S., Studer, J., Koksall, D., 2004a.** Characterization and site amplification for a seismic microzonation study in Turkey, 11th Intern. Conference on Soil Dynamics and Earthquake Engineering, 3rd Intern. Conf. on Earthquake Geotechnical Engineering, Berkeley, California, USA., 8 pages.

**Ansal, A., Biro, Y., Erken, A., Gülerce, Ü., 2004b.** Seismic microzonation: a case study. In: Ansal, A. (Ed.), *Recent Advances in Earthquake Geotechnical Engineering and Microzonation*. Kluwer Academic Publishers, Dordrecht, The Netherlands, 253-266.

**Ansal, A., Özeydin, K., Erdik, M., Yıldırım, M., Kılıç, H., Adatepe, Ş., Özener, P.T., Tonoroğlu, M., Şeşetyan, K., Demircioğlu, M., 2005.** Seismic microzonation for urban planning and vulnerability assessment. *Proceedings of the International Symposium on Earthquake Engineering Commemorating Tenth Anniversary of the 1995 Kobe Earthquake, Geotechnical Session*, Kobe, Japan.

**Ansal, A., Tonuk, G., Demircioğlu, M., Bayraklı, Y., Sesetyan, K., Erdik, M., 2006.** Ground motion parameters for vulnerability assessment. *Proceedings of the First European Conference on Earthquake Engineering and Seismology*, Geneva, Switzerland, Paper Number: 1790.

**Ansal, A., Tonuk, G., 2007.** Source and site factors in microzonation. In: Pitilakis, K.D. (ed.), *Earthquake Geotechnical Engineering*, 4<sup>th</sup> International Conference on Earthquake Geotechnical Engineering-Invited Lectures, 73-92.

**Antoniou, A.A., Papadimitriou, A.G., Tsiambaos, G., 2008.** A geographical information system managing geotechnical data for Athens (Greece) and its use for automated seismic microzonation. *Natural Hazards*, 47(3), 369-397.

**Aptikaev, F., Kopnichev, J., 1980.** Correlation between seismic vibration parameters and type of faulting. In: *Proceedings of Seventh World Conference on Earthquake Engineering*, 1, 107-110.

**Arduino, P., Kramer, S.L., 2009.** Site response. In: *CEE 526 Geotechnical Earthquake Engineering lecture notes*, University of Washington, Seattle, WA-USA.

**Armijo, R., Meyer, B., Hubert, A., Barka, A., 1999.** Westward propagation of the North Anatolian fault into the northern Aegean: timing and kinematics. *Geology*, 27, 267-270.

**Arpat, E., Şaroğlu, F., 1975.** Türkiye'deki bazı önemli genç tektonik olaylar, TJK Bülteni, 18, 91-101 (in Turkish).

**Arpat E., Herece, E., Komut, T., Şentürk, K., 2001.** 1999 Kocaeli ve Düzce earthquake faults; thier situation within the seismotectonic framework of the Marmara region, 54th Geological Congress of Turkey, May 7-10, 2001, Ankara, Proc. 54-29.

**ASTM, 1994.** Annual Book of ASTM Standarts – Soil and Rock, Building Stones, Section-4, Constructions, V. 04.08. ASTM Publications, 972 pp.

**ASTM D 1586-92, 1998.** Annual book of ASTM standards, Vol. 04.08, Soil and Rock (I) Standard no. D-1586-92, "Standard Test Method for Penetration Test and Split Barrel Sampling of Soils," West Conshohocken, Pa., 137-141.

**ASTM D 422, 2000.** Standard test method for particle size analysis of soil, Annual Book of ASTM Standards.

**ASTM D 5778-95, 2000.** Standard test method for performing electronic friction cone and piezocone penetration testing of soils. ASTM, West Conshohocken, PA.

**ASTM D 5777-00, 2006.** Standard guide for using the seismic refraction method for subsurface investigation. ASTM International, West Conshohocken, PA.

**Athanasopoulos, G.A., 1995.** Empirical correlations Vs-N SPT for soils of Greece: a comparative study of reliability. Proceedings of 7th International Conference on Soil Dynamics and Earthquake Engineering (Chania, Crete) ed A.S.C, Akmak (Southampton: Computational Mechanics), 19-36.

**Aydan, O., Sezaki, M., Yarar, R., 1996.** The seismic characteristics of Turkish earthquakes. 11th World Conference on Earthquake Engineering, Acapulco, Mexico. CD paper no. 1025.

**Aydan, O., 1997.** The seismic characteristics and the occurrence pattern of Turkish earthquakes. Turkish Earthquake Foundation Report No.TDV/TR 97-007, 41 pp.

**Aydan, O., Hamada, M., Bardet, J.P., Ulusay, R., Kanibir, A., 2004.** Liquefaction induced lateral spreading in the 1999 Kocaeli earthquake, Turkey: case study around the Hotel Sapanca. 13th World Conference on Earthquake Engineering. Vancouver, B.C., Canada, Paper No. 2921.

**Ayday, C., Altan, M., Nefeslioğlu, H.A., Canıgür, A., Yerel, S., Tün, M., 2001.** Preparation of Engineering Geological Map of Eskişehir Urban Area, Research Institute of Satellite and Space Sciences, Anadolu University (in Turkish).

**Ayhan, E., Alsan, E., Sancaklı, N., Üçer, S.B, 1984.** Turkish Earthquake Catalogue - Türkiye ve Dolayları Deprem Kataloğu 1881-1980, Boğaziçi Üniversitesi, 126 pp. (in Turkish).

**Ayhan, M.E., Buergermann, R., McClusky, S., Lenk, O., Aktug, B., Herece, E., Reilinger, R.E., 2001.** Kinematic of the Mw=7.2, 12 November 1999, Duzce, Turkey earthquake. Geophysical Research Letters, 28 (2), 367-370.

**Bademli, R., 2001.** Earthquake mitigation and urban planning in Turkey. In: Komut, E. M., Natural Disasters: Designing for safety, Chamber of Architects of Turkey, Ankara, 58-64.

**Baker, J.W., 2007.** Quantitative classification of near-fault ground motions using wavelet analysis. Bulletin of the Seismological Society of America, 97(5), 1486-1501.

**Balassanian S., Pirousian, S., Avanesian, A., Martirosyan, A., Arakelian, A., Eloian, A., Harutunian, H., 1997a.** The catalogue of strong earthquakes in the territory of Armenia and adjacent regions, edited by Giardini D. and Balassanian S., NATO ASI Series, Kluwer Academic Publishers, 28, 313-331.

**Balassanian, S., Mouradian, A., Sahakian, A., Kalinin, S., Babayan, M., Pogossian, A., 1997b.** The investigation of electromagnetic precursors to earthquakes in Armenia. Annali di Geofisica, XL, 209-225.

**Bang, E., Kim, D., 2007.** Evaluation of shear wave velocity profile using SPT-based uphole method, Soil Dynamics and Earthquake Engineering, 27, 741-758.

**Bard, P.Y., Duval, A.M., Lebrun, B., Lachet, C., Riepl, J., Hatzfeld, D., 1997.** Reliability of the H/V technique for site effects measurement: an experimental assessment. Seventh International Conference on Soil Dynamics and Earthquake Engineering, Istanbul, July 19-24.

**Bard, P.Y., 1999.** Microtremor measurements: a tool for site effect estimation, State-of-the-art paper. Second International Symposium on the Effects of Surface Geology on Seismic Motion, Yokohama, Eds., Irikura, Kudo, Okada and Sasatani, Balkema, 3, 1251-1279.

**Bardet, J.P., Mace, N., Tobita, T., Hu, J., 1999.** Large-scale modeling of liquefaction-induced ground deformation: Part I. A four parameter MLR model. Proceedings of the 7th U.S.-Japan Workshop on Earthquake Resistant Design of Lifeline Facilities and Countermeasures against Soil Liquefaction, 155-173.

**Barka, A.A., 1981.** Seismo-tectonic aspects of the North Anatolian fault zone. Ph. D thesis. University of Bristol, 335 pp.

**Barka, A., 1984.** Kuzey Anadolu Fay Zonudaki Bazi Neojen-Kuvanterner Havzalarinin Jeolojisi ve Tektonik Evrimi, Ketin Simpozyumu, 209-227 (in Turkish).

**Barka, A., Hancock, P.L., 1984.** Neotectonic deformation patterns in the convex-northwards arc of the North Anatolian fault zone. In: Dixon, J.E., Robertson, A.H.F. (Eds.), The Geological Evolution of the Eastern Mediterranean. Geol. Soc. London, Spec. Publ. 17, 763-774.

**Barka, A., Kadisky-Cade, K., 1988.** Strike-slip fault geometry in Turkey and its influence on earthquake activity. Tectonics, 7, 663-684.

**Barka, A., Gulen, L., 1989.** New constraints on age and total offset of the North Anatolian Fault Zone: implications for tectonics of the Eastern Mediterranean region, METU. Journal of Pure and Applied Sciences, 21, 39-63.

**Barka, A., 1992.** The North Anatolian Fault Zone. Annal. Tecton., 6, 164-195.

**Barka, A., 1996.** Slip distribution along the North Anatolian fault associated with large earthquakes of the period 1939–1967. *Bulletin of the Seismological Society of America*, 86, 1238-1254.

**Barka, A. A., Akyüz, S. H., Cohen, H. A., Watchorn, F. 2000.** Tectonic evolution of the Niksar and Taşova-Erbaa pull-apart basins, North Anatolian Fault Zone: their significance for the motion of the Anatolian block. *Tectonophysics* 322, 243-264.

**Barka, A.A., Akyuz, H.S., Altunel, E., Sunal, G., Cakir, Z., Dikbas, A., Yerli, B., Armijo, R., Meyer, B., de, C.J.B., Rockwell, T.K., Dolan, J.R., Hartleb, R.D., Dawson, T.E., Christofferson, S.A., Tucker, A., Fumal, T.E., Langridge, R.M., Stenner, H.D., Lettis, W., Bachhuber, J., Page, W.D., 2002.** The surface rupture and slip distribution of the 17 August 1999 Izmit earthquake (M7.4). *North Anatolian Fault. Bulletin of the Seismological Society of America*, 92(1), 43-60.

**Bell, F.G., Cripps, J.C., Culshaw, M.G., O'Hara, M., 1987.** Aspects of geology in planning. In: Culshaw, M.G., Bell, F.G., Cripps, J.C., O'Hara, M. (Eds.), *Planning and Engineering Geology. Geological Society Engineering Geology Special Publication*, 4, 1-38.

**Bell, F.G., 1998.** *Environmental Geology*. Blackwell, Malden, MA. 594 pp.

**Bellier, O., Over, S., Poisson, A., Andrieux, J., 1997.** Recent temporal change in stress state and modern stress field along the North Anatolian Fault Zone (Turkey). *Geophysical Journal. International*, 131, 61-86.

**Bello-Dambatta, A., Farmani, R., Javadi, A.A., Evans, B.M., 2009.** The Analytical Hierarchy Process for contaminated land management. *Advanced Engineering Informatics*, 23, 433-441.

**Belton, V., Stewart, T.J., 2002.** *Multiple Criteria Decision Analysis - An Integrated Approach*. Kluwer Academic Publishers Group, 372 pp.

**Bishop, A.W., 1973.** The stability of tips and spoil heaps. *Quarterly Journal of Engineering Geology*, 6, 335-376.

**Blume, J.A., 1977.** The SAM procedure for site-acceleration-magnitude relationships. In: *Proceedings of Sixth World Conference on Earthquake Engineering*, Vol. I, 416-422.

**Blumenthal, M.M., 1950.** Beitrage zur geologie des landschttten am mittleren und unteren Yeşilirmak (Tokat, Amasya, Havza, Erbaa, Niksar): MTA Yayl., Seri D, no. 4, Ankara (in German).

**Bodde, T., 1992.** Microzoning the likelihood of strong spectral amplification of earthquake motions using MMI surveys and surface geology. *Earthquake Spectra*, 8(4).

**Bolt, B.A., Abrahamson, N.A., 1982.** New attenuation relations for peak and expected accelerations of strong ground motion. *Bulletin of the Seismological Society of America*, 72(6), 2307-2321.

**Bommer, J.J., Scott, S.G., Sarma, S.K., 2000.** Hazard consistent earthquake scenarios. *Soil Dynamics and Earthquake Engineering*, 19(4), 219-231.

**Boncio, P., Lavecchia, G., Pace, B., 2004.** Defining a model of 3D seismogenic sources for seismic hazard assessment applications: The case of central Apennines (Italy). *Journal of Seismology*, 8, 407-425.

**Boore, D. M., Joyner, W.B., 1982.** The empirical prediction of ground motion. *Bulletin of the Seismological Society of America*, 72(6), 43-60.

**Boore, D.M., Joyner, W.B., Fumal, T.E., 1994.** Estimation of response spectra and peak accelerations from western North American earthquakes: An interim report. Part 2. Open-File Report 94-127. U.S. Geological Survey.

**Boore, D.M., Joyner, W.B., Fumal, T.E., 1997.** Equations for estimating horizontal response spectra and peak acceleration from western North American earthquakes: A summary of recent work. *Seismological Research Letters*, 68(1), 128-153.

**Boore, D.M., 2004.** Estimating  $V_{s(30)}$  (or NEHRP Site Classes) from shallow velocity models (depths < 30 m). *Bulletin of the Seismological Society of America*, 94(2), 591-597.

**Boore, D.M., Atkinson, G.M., 2007.** Boore-Atkinson NGA ground motion relations for the geometric mean horizontal component of peak and spectral ground motion parameters, PEER Report 2007/01, Pacific Earthquake Engineering Center, Berkeley, California.

**Boore, D.M., Atkinson, G.M., 2008.** Ground-motion prediction equations for the average horizontal component of PGA, PGV, and 5%-damped PSA at spectral periods between 0.01 s and 10.0 s. *Earthquake Spectra*, 24(1), 99-138.

**Borcherdt, R.D., 1970.** Effects of local geology on ground motion near San Francisco Bay. *Bulletin of the Seismological Society of America*, 60, 29-61.

**Borcherdt, R.D., Glassmoyer, G., Der Kiureghian, A., Cranswick, E., 1989.** Results and data from seismologic and geologic studies following earthquakes of Dec. 7, 1988 near Spitak, Armenia, USSR, USGS Open File Rept., 89-163.

**Borcherdt, R.D., Wentworth, C.M., Janssen, A., Fumal, T., Gibbs, J., 1991.** Methodology for predictive GIS mapping of special study zones for strong ground shaking in the San Francisco Bay Region. *Proceedings of the 4th International Conference on Seismic Zonation*, 3, 545-552.

**Borcherdt, R.D., 1994.** Estimates of site depending response spectra for design methodology and justifications. *Earthquake Spectra*, 10(4), 617-654.

**Boulanger, R.W., Idriss, I. M., 2004.** State normalization of penetration resistance and the effect of overburden stress on liquefaction resistance. *Proc., 11th International Conf. on Soil Dynamics and Earthquake Engineering and 3rd International Conference on Earthquake Geotechnical Engineering*, Univ. of California, Berkeley, CA.

**Boulanger, R. W., Idriss, I. M., 2005.** Evaluating cyclic failure in silts and clays. *Proceedings, Geotechnical Earthquake Engineering Satellite Conference on Performance Based Design in Earthquake Geotechnical Engineering: Concepts and Research*. Prepared by TC4 Committee of ICSMGE, Japanese Geotechnical Society, Tokyo, 78-86.

**Boulanger, R. W., Idriss, I. M., 2006.** Liquefaction susceptibility criteria for silts and clays. *Journal of Geotechnical and Geoenvironmental Engineering*, ASCE, 132(11), 1413-1426.



**Bour, M., Fouissac, D., Dominique, P., Martin, C., 1998.** On the use of microtremor recordings in seismic microzonation. *Soil Dynamics and Earthquake Engineering*, 17, 465-474.

**Bowles, J. E., 1988.** *Foundation Analysis and Design*. McGraw Hill Book Company, Singapore, 4th Edition, 1004 pp.

**Bozkurt E., Kocyigit A., 1995.** Almus Fault Zone: its age, total offset and relation to the North Anatolian Fault Zone, *Turkish Journal of Earth Sciences*, 4, 93-104.

**Bozkurt E., Kocyigit A., 1996.** The Kazova basin: an active negative flower structure on the Almus Fault Zone, a splay fault system of the North Anatolian Fault Zone, Turkey, *Tectonophysics*, 265, 239-254.

**Bozkurt E., 2001a.** Late Alpine evolution of the central Menderes Massif, western Turkey. *International Journal of Earth Sciences*, 89, 728-744.

**Bozkurt, E., 2001b.** Neotectonics of Turkey-a synthesis, *Geodynamica Acta*, 14, 3-30.

**Bozorgnia, Y., Campbell, K.W., Niazi, M., 2000.** Observed spectral characteristics of vertical ground motion recorded during worldwide earthquakes from 1957 to 1995. *Proceedings of 12<sup>th</sup> World Conference on Earthquake Engineering*, Paper No. 2671.

**Bozorgnia, Y., Campbell, K.W., 2004.** Engineering characterization of ground motion. In: Bozorgnia, Y, and Bertero, V.V. (eds.), *Earthquake engineering from engineering seismology to performance-based engineering*, CRC Press, Chapter 5, 74 pp.

**Brandes, H.G., 2003.** Geotechnical and foundation aspects. In: Chen, W-F., Scawthorn, C., (eds.), *Earthquake Engineering Handbook*, CRC Press, Chapter 7, 61 pp.

**Bray, J.D., Sancio, R.B., Youd, L.F., Durgunoglu, T., Onalp, A., Cetin, K.O., Seed, R.B., Stewart, J.P., Christensen, C., Baturay, M.B., Karadayilar, T., Emrem, C., 2001.** Documenting incidents of ground failure resulting from the August 17, 1999 Kocaeli, Turkey Earthquake: Data report characterizing subsurface conditions, PEER. 588 pp.

**Bray, J. D., Sancio, R. B., 2006.** Assessment of the liquefaction susceptibility of fine-grained soils. *Journal of Geotechnical and Geoenvironmental Engineering*, 132(9), 1165-1177.

**Bryant, W.A., Hart, E.W., 2007.** Fault-rupture hazard zones in California: Alquist-Priolo Earthquake Fault Zoning Act with Index to Earthquake Fault Zones Maps. Special Publication 42, California Department of Conservation, California Geological Survey, 42 pp.

**BSSC (Building Seismic Safety Council), 2001.** NEHRP recommended provisions for seismic regulations for new buildings and other structures, 2000 Edition, Part 1: Provisions, prepared by the Building Seismic Safety Council for the Federal Emergency Management Agency (Report FEMA 368), Washington, D.C.

**Burland, J.B., 1989.** Small is beautiful: the stiffness of soils at small strains. *Canadian Geotechnical Journal*, 26(4), 499-516.

**Campbell, K.W., 1985.** Strong motion attenuation relations: A ten-year perspective. *Earthquake Spectra*, 1(4), 759-804.

**Campbell, K.W., 1989.** The dependence of peak horizontal acceleration on magnitude, distance, and site effects for small-magnitude earthquakes in California and eastern North America. *Bulletin of the Seismological Society of America*, 79(5), 1311-1346.

**Campbell, K.W., 1993.** Empirical prediction of near-source ground motion from large earthquakes. In: *Proceedings of the International Workshop on Earthquake Hazard and Large Dams in the Himalaya*. Indian National Trust for Art and Cultural Heritage, New Delhi, India.

**Campbell, K.W., Bozorgnia, Y., 1994.** Near-source attenuation of peak horizontal acceleration from worldwide accelerograms recorded from 1957 to 1993 In: *Proceedings of the Fifth U.S. National Conference on Earthquake Engineering*, Vol. III, 283-292.

**Campbell, K.W., 1997.** Empirical near-source attenuation relationships for horizontal and vertical components of peak ground acceleration, peak ground velocity, and pseudo-absolute acceleration response spectra. *Seismological Research Letters*, 68(1), 154-179.

**Campbell, K.W., Bozorgnia, Y., 2000.** New empirical models for predicting near-source horizontal, vertical, and V/H response spectra: Implications for design. *Proceedings of 6<sup>th</sup> International Conference on Seismic Zonation*, Palm Springs, CA.

**Campbell, K.W., Bozorgnia, Y., 2003.** Updated near-source ground-motion (attenuation) relations for the horizontal and vertical components of peak ground acceleration and acceleration response spectra. *Bulletin of the Seismological Society of America*, 93(1), 314-331.

**Campbell, K.W., Bozorgnia, Y., 2007.** Campbell-Bozorgnia NGA ground motion relations for the geometric mean horizontal component of peak and spectral ground motion parameters, PEER Report No. 2007/02, Pacific Earthquake Engineering Research Center, University of California, Berkeley, 238 pp.

**Campbell, K.W., Bozorgnia, Y., 2008.** NGA ground motion model for the geometric mean horizontal component of PGA, PGV, PGD, and 5% damped linear elastic response spectra for periods ranging from 0.01 to 10 s. *Earthquake Spectra*, 24(1), 139-171.

**Can, R., 1974.** Seismotectonics of the North Anatolian Fault Zone. Unpublished M. Phil, thesis. University of London.

**Canik, B., Kayabali, K., 2000.** Erbaa (Tokat) Zeminlerinin Depremsellik Açısından Değerlendirilmesi, Ankara University, Faculty of Natural Science, Geological Engineering Department Project Report (unpublished, in Turkish).

**Cao, T., Petersen, M.D., Reichle, M.S., 1996.** Seismic hazard estimate from background seismicity in Southern California. *Bulletin of the Seismological Society of America*, 86, 1372-1381.

**Carballo, J. E., Cornell, C. A., 2000.** Probabilistic Seismic Demand Analysis: Spectrum Matching and Design, Department of Civil and Environmental Engineering, Stanford University, Report No. RMS-41.

- Cardona, O.D., Yamin, L.E., 2000.** Seismic microzonation and estimation of earthquake loss scenarios: integrated risk mitigation project of Bogota, Colombia. *Earthquake Spectra*, 14(4), 795-814.
- Carver, S.J., 1991.** Integrating multicriteria evaluation with Geographical Information Systems. *International Journal of Geographical Information Systems* 5(3), 321-339.
- Castro, R.R., Anderson, J.G., Singh, S.K., 1990.** Site response, attenuation and source spectra of S-waves along the Guerrero, Mexico subduction zone. *Bulletin of the Seismological Society of America*, 79, 1481-1503.
- Cetin, K.O., 2000.** Reliability-based assessment of seismic soil liquefaction initiation hazard. Ph.D. dissertation, Univ. of California, Berkeley (unpublished).
- Cetin, K.O., Youd, T.L., Seed, R.B., Bray, J.D., Sancio, R., Lettis, W., Yilmaz, M.T., Durgunoglu, H.T., 2002.** Liquefaction induced ground deformations at Hotel Sapanca during Kocaeli (Izmit) earthquake. *Soil Dynamics and Earthquake Engineering*, 22, 1083-1092.
- Cetin, K.Ö., 2004.** Seismic soil liquefaction assessment methodologies. In: DRM, Seismic Microzonation for Municipalities, Pilot Studies: Adapazarı, Gölcük, İhsaniye and Değirmendere, Chapter 7, 102-119, Republic of Turkey, General Directorate of Disaster Affairs.
- Cetin, K.O., Seed, R.B., Kiureghian, A.D., Tokimatsu, K., Harder L.F., Kayen R.E., 2004.** Standard penetration test-based probabilistic and deterministic assessment of seismic soil liquefaction potential, *Journal of Geotechnical and Geoenvironmental Engineering*, 130(12), 1314-1340.
- Cetin, K.O., Bilge, H.T., Wu, J., Kammerer, A.M., Seed, R.B., 2009.** Probabilistic models for cyclic straining of saturated clean sands. *Journal of Geotechnical and Geoenvironmental Engineering*, 135(3), 371-386.
- Chapman, M.C., 1999.** On the use of elastic input energy for seismic hazard analysis. *Earthquake Spectra*, 15(4), 607-635.
- Chavez-Garcia, F.J., Cuenca, J., 1998.** Site effects and microzonation in Acapulco. *Earthquake Spectra*, 14(1), 75-93.
- Chen, W.F., Scawthorn, C., 2002.** *Earthquake Engineering Handbook*, CRC Press.
- Chiaruttini, C., Siro, L., 1981.** The correlation of peak ground horizontal acceleration with magnitude, distance, and seismic intensity for Friuli and Ancona, Italy, and the Alpide belt. *Bulletin of the Seismological Society of America*, 71(6), 1993-2009.
- Chiou, B., Youngs, R.R., 2008.** An NGA model for the average horizontal component of peak ground motion and response spectra. *Earthquake Spectra*, 24(1), 173-215.
- Chiou, B., Darragh, R., Gregor, N., Silva, W., 2008.** NGA Project Strong-Motion Database. *Earthquake Spectra*, 24(1), 23-44.

**Cid, J., Susagna, T., Goula, X., Chavarria, L., Figueras, S., Fleta, J., Casas, A., Roca, A., 2001.** Seismic zonation of Barcelona based on numerical simulation of site effects. *Pure and Applied Geophysics*, 158, 2559-2577.

**Cioflan, C.O., Apostol, B.F., Moldoveanu, C.L., Panza, G.F., Marmureanu, G.H., 2004.** Deterministic approach for the seismic microzonation of Bucharest. *Pure and Applied Geophysics*, 161, 1149-1164.

**Convertito, V. , Iervolino, I., Zolloc, A., Manfredi, G., 2008.** Prediction of response spectra via real-time earthquake measurements, *Soil Dynamics and Earthquake Engineering* 28, 492–505.

**Cornell, C.A., 1968.** Engineering seismic risk analysis. *Bulletin of the Seismological Society of America*, 58, 1583-1606.

**Cornell, C.A., Banon, H., Shakal, A.F., 1979.** Seismic motion and response prediction alternatives. *Earthquake Engineering and Structural Dynamics*, 7(4), 295-315.

**Corps of Engineers Regulation (USACE), 1995.** Engineering Regulation 1110-2-1806, *Earthquake Design and Analysis for Corps of Engineers Projects*.

**Cramer, C.H., Petersen, M.D., Reichle, M.S., 1996.** A Monte Carlo approach in estimating uncertainty for a seismic hazard assessment of Los Angeles, Ventura, and Orange Counties, California. *Bulletin of the Seismological Society of America*, 86, (Dec. issue).

**Crespellani, T., Madiati, C., Vannucchi, G., Maecellini, A., Maugeri, M., 1997.** Zonation of geotechnical seismic hazards in Tuscany, Italy. *Seismic behavior of Ground and Geotechnical Structures*, Seco e Pinto (Ed.), Balkema, Rotterdam, 11-24.

**Crouse, C.B., McGuire, J.W., 1996.** Site response studies for purpose of revising NEHRP seismic provisions. *Earthquake Spectra*, 12(3), 407-439.

**Çağatay, I., 2005.** Experimental evaluation of buildings damaged in recent earthquakes in Turkey, *Engineering Failure Analysis*, 12, 440-452.

**Dai, F.C., Liu, Y., Wang, S., 1994.** Urban geology: a case study of Tongchuan City, Shaanxi Province, China. *Engineering Geology*, 38, 165-175.

**Dai, F.C., Lee, C.F., Zhang, X.H., 2001.** GIS-based geo-environmental evaluation for urban land-use planning: a case study. *Engineering Geology*, 61, 257-271.

**Darendeli, M.B. 2001.** Development of a new family of normalized modulus reduction and material damping curves. Ph.D. dissertation, University of Texas at Austin, Austin, Tex.

**Dan, M.B., 2005.** Multidisciplinary co-operation in building design according to urbanistic zoning and seismic microzonation. *Natural Hazards and Earth System Sciences*, 5, 397-411.

**Das, S., Gupta, I. D., and Gupta, V. K., 2006.** A Probabilistic Seismic Hazard Analysis of Northeast India. *Earthquake Spectra*, Vol. 22, 1-27.

**Day, R., 2002.** *Geotechnical Earthquake Engineering Handbook*. McGraw Hill Handbook. 700 pp.

**De Mulder, E.F.J., 1996.** Urban geoscience. In: McCall, G.J.H., De Mulder, E.F.J., Marker, B.R. (Eds.), Urban Geoscience. Balkema, Rotterdam, 1-11.

**Demirtaş, R., Yılmaz, R., 1996.** Türkiye'nin Sismotektoniği, Bayındırlık ve İskan Bakanlığı yayınları (in Turkish).

**Dewey, J.W., 1976.** Seismicity of northern Anatolia. Bulletin of the Seismological Society of America, 66, 843-868.

**Destegül, U., 2004.** Sensitivity analysis of soil site response modeling in seismic microzonation for Latitpur, Nepal. M.Sc. thesis, International Institute for Geo-Information Science and Earth Observation (ITC), The Netherlands.

**Dikmen, U., Mirzaoglu, M., 2005.** The seismic microzonation map of Yenisehir-Bursa NW of Turkey by means of ambient noise measurements. Journal of the Balkan Geophysical Society, 8(2), 53-62.

**Dikmen, U., 2009.** Statistical correlations of shear wave velocity and penetration resistance for soils. Journal of Geophysics and Engineering, 6, 61-72.

**Dikmen, U., Pamuk, E., Akın, Ö., Ateş, B., Altuner, B., Demirel, M., Cam, A., 2009.** Kuzey Anadolu Fay Zonu Üzerinde Kelkit Vadisi Boyunca Yer Alan Yerleşim Alanlarının Doğal Afet Risk Analizi ve Afet Bilgi Sisteminin Oluşturulması, Jeofizik İş Paketi, DPT Proje no: CUBAP M-359/DPT 2006K-120220 (in Turkish).

**Dirik K., Göncüoğlu, M.C., 1996.** Neotectonic characteristics of Central Anatolia. Inter. Geol. Rev., 38, 807-817.

**Dirik K., 1993.** Geological history of the northward arched segment of the North Anatolian Transform fault Zone. Geol. J., 28, 251-266.

**Dobry, R., Vucetic, M., 1987.** Dynamic properties and seismic response of soft clay deposits. Proceedings, International Symposium on Geotechnical Engineering of Soft Soils, Mexico City, Published by Sociedad Mexicana de Mecanica de Suelos, A.C., 2, 49-85.

**Dobry, R., Borchardt, R.D., Crouse, C.B., Idriss, I.M., Joyner, W.B., Martin, G.R., Power, M.S., Rinne, E.E., Seed, R.B., 2000.** New site coefficient and site classification system used in recent building code provisions. Earthquake Spectra 16 (1), 41-67.

**Donovan, N.C., Bornstein, A.E., 1978.** Uncertainties in seismic risk analysis. Journal of the Geotechnical Engineering Division, ASCE, 104(GT7), 869-887.

**Douglas, J., 2001.** Engineering Seismology and Earthquake Engineering: A comprehensive worldwide summary of strong-motion attenuation relationships for peak ground acceleration and spectral ordinates (1969 to 2000). ESEE Report No. 01-1, Imperial College of Science, Technology and Medicine Civil Engineering Department, London, pp. 144.

**DRM, 2004.** Seismic Microzonation for Municipalities, Manual. 131 p., Republic of Turkey, General Directorate of Disaster Affairs.

**DSI (Devlet Su İşleri Genel Müdürlüğü), 1971.** Erbaa Ovası Hidrojolojik Etüt Raporu. Ankara, 49 pp (in Turkish).

**Duku, P.M., Stewart, J.P., Whang, D.H., Yee, E., 2008.** Volumetric strains of clean sands subject to cyclic loads. *Journal of Geotechnical and Geoenvironmental Engineering*, ASCE, 134(8), 1073-1085.

**Duval, A.M., Bard, P.Y., Meneroud, J.P., Vidal, S., 1994.** Usefulness of microtremor measurements for site effect studies. *Proceedings of the Tenth European Conference on Earthquake Engineering*, Vienna, Austria, Balkema, Duma Ed., I, 521-528.

**EduPro Civil Systems, Inc.** ProShake version 1.12, Ground Response Analyses Program, Sammamish, Washington, USA.

**Elnashai, A., Sarno L.D., 2008.** *Fundamentals of Earthquake Engineering*. John Wiley & Sons Inc.

**EPRI, 1993.** Guidelines for determining design basis ground motions. Vol. 1: Method and guidelines for estimating earthquake ground motion in eastern North America, Rpt. No. EPRI TR-102293, Palo Alto, California.

**Erbaa, 2007.** [www.erbaa.gov.tr](http://www.erbaa.gov.tr), 21.05.2007.

**Erbaa Municipality, 2007.** [www.erbaa-bld.gov.tr](http://www.erbaa-bld.gov.tr), 21.05.2007.

**Erdik, M., Doyuran, V., Akkas, N., Gulkan, P., 1985.** A Probabilistic assessment of the seismic hazard in Turkey, *Tectonophysics*, 117, 295-344.

**Erdik, M., Durukal, E., 2004.** Seismic microzonation: a case study. In: Ansal, A. (Ed.), *Recent Advances in Earthquake Geotechnical Engineering and Microzonation*. Kluwer Academic Publishers, Dordrecht, The Netherlands, 253-266.

**Erdik, M., Demircioglu, M., Sesetyan, K., Durukal, E., 2005.** Assessment of earthquake hazard for Bakirkoy, Gemlik, Bandırma, Tekirdag and Korfez. WB MEER Project-A3 Component, Microzonation and Hazard Vulnerability Studies for Disaster Mitigation in Pilot Municipalities, Bogazici University, Kandilli Observatory and Earthquake Engineering Research Institute.

**Ergin, M., Ozalaybey, S., Aktar, M., Yakin, M.N., 2004.** Site amplification at Avcilar, Istanbul. *Tectonophysics*, 391, 335-346.

**Esteva, L., 1970.** Seismic risk and seismic design. In: Hansen, R.J. (ed), *Seismic Design for Nuclear Power Plants*. The M.I.T. Press, 142-182.

**Esteva, L., Villaverde, R., 1973.** Seismic risk, design spectra and structural reliability. In: *Proceedings of Fifth World Conference on Earthquake Engineering*, Vol. 2, 2586-2596.

**ESRI, 2006.** ARCGIS version 9.2 Geographic Information System Program, USA.

**Faccioli, E., 1978.** Response spectra for soft soil sites. In: *Proceedings of the ASCE Geotechnical Engineering Division Speciality Conference: Earthquake Engineering and Soil Dynamics*, Vol. I, 441-456.

**Faccioli, E., Pessina, V., Calvi, G.M., Borzi, B., 1999.** A study on damage scenarios for residential buildings in Catania City. *Journal of Seismology*, 3(3), 327-343.

- Faccioli, E., Pessina, V., 2001.** The Catania Project: earthquake damage scenarios for a high risk area in the Mediterranean. CNR-Gruppo Nazionale per la Difesa dai Terremoti, Roma, 225 pp.
- Fah, D., Rüttener, E., Noack, T., Kruspan, P., 1997.** Microzonation of the city of Basel. *Journal of Seismology*, 1, 87-102.
- Fah, D., Kind, F., Lang, K., Giardini, G., 2000.** Earthquake scenarios for the city of Basel. *Soil Dynamics and Earthquake Engineering*, 21(5), 405-413.
- Fahjan, Y..M, Siyahi, B.G., Ansal, A., 2003.** KoeriSlope V1.0: Mikrobolgeleme amaçlı şev stabilitesi hesaplama programı, Bogaziçi Üniversitesi, Deprem Muhendisliği Bölümü, Kandilli, İstanbul (in Turkish).
- Fahjan, Y., Ozdemir , Z., 2008.** Scaling of earthquake accelerograms for non-linear dynamic analyses to match the earthquake design spectra. The 14th World Conference on Earthquake Engineering October 12-17, 2008, Beijing, China.
- Field, E.H., Hough, S.E., Jacob, K.H., 1990.** Using microtremors to assess potential earthquake site response: a case study in Flushing Meadows, New York City. *Bulletin of the Seismological Society of America*, 80(6), 1456-1480.
- Field, E.H., Jacob, K.H., 1995.** A comparison and test of various site-response estimation techniques, including three that are not reference-site dependent. *Bulletin of the Seismological Society of America*, 85(4), 1127-1143.
- Field, E. H., 1996.** Spectral amplification in a sediment-filled valley exhibiting clear basin-edge-induced waves. *Bulletin of the Seismological Society of America*, 86(4), 991-1005.
- Finn, W.D.L., Ventura, C.E., 1995.** Challenging issues in local microzonation. 5<sup>th</sup> International Conference on Seismic Zonation, Nice, France.
- Frankel, A., 1995.** Mapping seismic hazard in the central and eastern United States. *Seismological Research Letters*, 66, 8-21.
- Fujiwara, T., 1972.** Estimation of ground movements in actual destructive earthquakes. *Proceedings of the Fourth European Symposium on Earthquake Engineering*, London, 125-132.
- Fukushima, Y., Tanaka, T., Kataoka, S., 1988.** A new attenuation relationship for peak ground acceleration derived from strong-motion accelerograms. In: *Proceedings of Ninth World Conference on Earthquake Engineering*, Vol. II, 343-348.
- Fukushima, Y., Tanaka, T., 1990.** A new attenuation relation for peak horizontal acceleration of strong earthquake ground motion in Japan. *Bulletin of the Seismological Society of America*, 80(4), 757-783.
- Fukushima, Y., Gariel, J.C., Tanaka, R., 1994.** Prediction relations of seismic motion parameters at depth using borehole data. In: *Proceedings of Tenth European Conference on Earthquake Engineering*, Vol. 1, 417-422.

**Fukushima, Y., Gariel, J.C., Tanaka, R., 1995.** Site-dependent attenuation relations of seismic motion parameters at depth using borehole data. *Bulletin of the Seismological Society of America*, 85(6), 1790-1804.

**Fumal, T.E., Tinsley, J.C., 1985.** Mapping shear wave velocities of near surface geological materials; In: Predicting areal limits of earthquake induced landsliding; In evaluation of earthquake hazards in the Los Angeles region – An earth science perspective (ed.) Ziony T. I, USGS Paper 1360, 127-150.

**Gasparini, D., Vanmarcke, E.H., 1976.** SIMQKE: A Program for Artificial Motion Generation, Department of Civil Engineering, Massachusetts Institute of Technology, Cambridge, MA.

**Gaull, B.A., Kagami, H., M.EERI, Taniguchi, H., 1995.** The microzonation of Perth, Western Australia, using microtremor spectral ratios. *Earthquake Spectra*, 11(2), 173-191.

**GDDA, 1996.** Earthquake zoning map of Turkey. General Directorate of Disaster Affairs. Ministry of Reconstruction and Resettlement of Turkey (in Turkish).

**GDDA, 2000.** Laws and regulations: regulations for the construction of buildings in hazard areas, Ankara, 244-332 (in Turkish).

**Genc, G., 2004.** Probabilistic Seismic Hazard Analysis of Eskisehir. M.Sc. Dissertation, Middle East Technical University, Ankara, Turkey.

**Gencoğlu, S., Özmen, B., Güler, H., 1996,** Yerleşim Birimleri ve Deprem, Türkiye Deprem Vakfı, 80 sayfa, İstanbul (in Turkish).

**General Directorate of Disaster Affairs, 2008.** [www.deprem.gov.tr/indexen.html](http://www.deprem.gov.tr/indexen.html), 01.02. 2008.

**Gizzi, F.T., 2006.** To what degree can historical seismicity records assist in seismic microzonation?. *Engineering Geology*, 87, 1-12.

**Göksu, E., 1960.** 1:500 000 ölçekli Türkiye Jeoloji Haritası, Samsun paftası: MTA Yayınları, Ankara.

**Grasso, S. and Maugeri, M., 2009.** The seismic microzonation of the city of Catania (Italy) for the maximum expected scenario earthquake of January 11, 1693. *Soil Dynamics and Earthquake Engineering*, 29, 953-962.

**Grosser, H., Baumbach, M., Berckhemer, H., Baier, B., Karahan, A., Schelle, H., Krueger, F., Paulat, A., Michel, G., Demirtas, R., Gencoglu, S., Yilmaz, R., 1998.** The Erzincan (Turkey) earthquake (M (subs) 6.8) of March 13, 1992 and its aftershocks sequence. *Pure and Applied Geophysics*, 152(3), 465-505.

**Gulkan, P., Kocigit, A., Yucemen, S.Y., Doyuran, V., Basoz, N., 1993.** Earthquake zoning map of Turkey based on most recent data. METU Earthquake Engineering Research Center, Report No. 93-01. 156 pp., (in Turkish).

**Güllü, H., 2001.** Dinar'ın zemin büyütmelerine göre Coğrafi Bilgi Sistemleri ile mikrobölgelemesi. Ph.D. thesis, Istanbul Technical University Graduate School of Applied Sciences, 289 pp. (in Turkish).



- Gullu, H., Ercelebi, E., 2007.** A neural network approach for attenuation relationships: An application using strong ground motion data from Turkey. *Engineering Geology*, 93, 65-81.
- Gullu, H., Ansal, A.M., Ozbay, A., 2008.** Seismic hazard studies for Gaziantep in South Anatolia of Turkey. *Natural Hazards*, 44, 19-50, DOI 10.1007/s11069-007-9140-3.
- Gutierrez, C., Singh, S.K., 1992.** A site effect study in Acapulco, Guerrero, Mexico: comparison of results from strong motion and microtremor data. *Bulletin of the Seismological Society of America*, 82(2), 642-659.
- Hake, S.S., 1987.** A review of engineering geological and geotechnical aspects of town and country planning with particular reference to minerals and the extractive processes. In: Culshaw, M.G., Bell, F.G., Cripps, J.C., O'Hara, M. (Eds.), *Planning and Engineering Geology*. Geological Society Eng. Geology Special Publication, 4, 69-74.
- Hamada, M., 1999.** Similitude law for liquefied-ground flow. *Proceedings of the 7th U.S.-Japan Workshop on Earthquake Resistant Design of Lifeline Facilities and Countermeasures against Soil Liquefaction*, 191-205.
- Hanumantharao, C., Ramana, G.V., 2008.** Dynamic soil properties for microzonation of Delhi, India. *J. Earth Syst. Sci.*, 117, S2, 719-730.
- Harajli, M., Sadek, S., Asbahan, R., 2002.** Evaluation of seismic hazard of Lebanon, *Journal of Seismology*, 6, 257-277.
- Hardin, B.O., Drnevich, V.P., 1972.** Shear modulus and damping in soils: Design equations and curves. *Journal of Soil Mechanics and Foundations Division, ASCE*. 98(7), 667-692.
- Hasançebi, N., Ulusay, R., 2006.** Evaluation of site amplification and site period using different methods for an earthquake-prone settlement in Western Turkey. *Engineering Geology*, 87, 85-104.
- Hasançebi, N., Ulusay, R., 2007.** Empirical correlations between shear wave velocity and penetration resistance for ground shaking assessments. *Bulletin of Engineering Geology and the Environment*, 66, 203-213.
- Herece, E., 1999.** Kocaeli depremi kırık haritası ve ilgili gözlem noktalarının tanımı. MTA Der. Rep. No, 10230, Ankara (unpublished, in Turkish).
- Herece, E., Uysal, K., 1999.** 12 Kasım 1999 Düzce depremi ön değerlendirme raporu, MTA Der. Rep. No10256, Ankara (unpublished, in Turkish).
- Hitchcock, S.C., Scott C., Lindvall, S.C., Lettis, W.R., John G. Helms., J.G., Randolph, C., Kristin C. Weaver, K.C. & Kada, L., 2000.** "Liquefaction Hazard Mapping, Ventura County, California, 6th Int. Conf. Seismic Zonation.
- Holzer, T.L., Bennett, M.J., Noce, T.E., Tinsley, J.C., 2005.** Shear-wave velocity of surficial geologic sediments in northern California: Statistical distributions and depth dependence. *Earthquake Spectra*, 21, 161-177.
- Hough, S.E., Seeber, L., Rovelli, A., Malagnini, L., 1990.** Ambient noise and weak motion excitation of sediment resonances: results from the Tiber Valley, Italy. A.G.U. Fall Meeting.

**Hough, S. E., Seeber, L., Rovelli, A., Malagnini, L., DeCesare, A., Selveggi, G., Lerner-Lam, A., 1992.** Ambient noise and weak-motion excitation of sediment resonances: results from the Tiber Valley, Italy. *Bulletin of the Seismological Society of America*, 82, 1186-1205.

**Housner, G.W., 1959.** Behavior of Structures during Earthquakes. *Proc. ASCE*. Vol 85, No:EM4, October, 1989.

**Huang, Y., 2008.** Performance-Based Design and Evaluation for Liquefaction-Related Seismic Hazard, PhD Thesis, University of Washington, Seattle, WA.

**Humphrey, J.R., Anderson, J.G., 1992.** Shear wave attenuation and site response in Guerrero, Mexico. *Bulletin of the Seismological Society of America*, 82, 1622-1645.

**Hunt, R.E., 2007.** Geotechnical Investigation Methods: A Field Guide for Geotechnical Engineers, CRC Press, Taylor&Francis Group, 342 pp.

**Idriss, I.M., 1978.** Characteristics of earthquake ground motions. In: *Proceedings of the ASCE Geotechnical Engineering Division Speciality Conference: Earthquake Engineering and Soil Dynamics*, Vol. III, 1151-1265.

**Idriss, I.M., Moriwaki, Y., Wright, S.G., Doyle, E.H., Ladd, R.S., 1980.** Behavior of normally consolidated clay under simulated earthquake and ocean wave loading conditions. *Proceedings, International Symposium on Soils under Cyclic and Transient Loading*, Swansea, United Kingdom, 1, 437-445.

**Idriss, I.M., 1990.** Response of soft soil sites during earthquakes. In: Duncan, J.M. (ed.) *Proceedings of the H. Bolton Seed Memorial Symposium*, Berkeley, Calif., May 1990. BiTech Publishers, Richmond, B.C., 2, 273-289.

**Idriss, I.M., Boulanger, R.W., 2004.** Semi-empirical procedures for evaluating liquefaction potential during earthquakes. *Proceedings 11th ICSD and 3th ICEGE*, 7-9 January 2004, UC Berkeley, California, U.S.A.

**Idriss, I.M., Boulanger, R.W., 2006.** Semi-empirical procedures for evaluating liquefaction potential during earthquakes. *Soil Dynamics and Earthquake Engineering*, 26, 115-130.

**Idriss, I.M., 2008.** An NGA empirical model for estimating the horizontal spectral values generated by shallow crustal earthquakes. *Earthquake Spectra*, 24(1), 217-242.

**Idriss, I. M., Boulanger, R. W., 2008.** Soil liquefaction during earthquakes. Monograph MNO-12, Earthquake Engineering Research Institute, Oakland, CA, 261 pp.

**Iervolino, I., Cornell, C.A. 2005.** Record selection for nonlinear seismic analysis of structures. *Earthquake Spectra*, 21(3), 685-713.

**Imai, T., Yoshimura, Y., 1970.** Elastic wave velocity and soil properties in soft soil. *Tsuchito-Kiso* 18 (1), 17-22 (in Japanese).

**Imai, T., Fumoto, H., Yokota, K., 1975.** The relation of mechanical properties of soil to P- and S- wave velocities in Japan. *Proceedings of 4<sup>th</sup> Japan Earthquake Engineering Symp.*, 89-96, (in Japanese).

**Imai, T., 1977.** P and S wave velocities of the ground in Japan. Proceeding of IX International Conference on Soil Mechanics and Foundation Engineering, 2, 127-132.

**Imai, T., Tonouchi, K., 1982.** Correlation of N-value with S-wave velocity and shear modulus. Proceedings of the 2<sup>nd</sup> European Symposium of Penetration Testing, Amsterdam, 57-72.

**İnan, N., Temiz, H., 1991.** Niksar (Tokat) yöresinde Kretase/Tersiyer geçişinin litostratigrafik ve biyostratigrafik özellikleri. Türkiye Jeoloji Mühendisliği Dergisi (in Turkish).

**Inan, E., Colakoglu, Z., Koc, N., Bayülke, N., Coruh, E., 1996.** Earthquake Catalogs with Acceleration Records from 1976 to 1996. , General Directorate of Disaster Affairs, Earthquake Research Department, Ankara, Turkey, 98 pp (in Turkish).

**İnce, G.Ç., Yıldırım, M, Özaydin, K., Özener, P.T., 2008.** Seismic microzonation of the historic peninsula of İstanbul. Bulletin of Engineering Geology and the Environment, 67, 41-51.

**Irrlitz, W., 1972.** Lithostratigraphie und tektonische Entwicklung des Neogens in Nordostanatolien. Bei. Geol. Jh., 120, 111 pp (in German).

**Irsyam, M., Dangkoa, D.T., Hendriyawan, Hoedajanto, D., Hutapea, B.M., Kertapati, E.K., Boen, T., Petersen, M.D., 2008.** Proposed seismic hazard maps of Sumatra and Java islands and microzonation study of Jakarta city, Indonesia. Journal of Earth System Science, 117(2), 865-878.

**Ishihara, K., Yoshimine, M., 1992.** Evaluation of settlements in sand deposits following liquefaction during earthquakes. Soils and Foundations, 32(1), 173-188.

**ISSMGE-TC4. Manual for Zonation on Seismic Geotechnical Hazards, 1999.** The Technical Committee No. 4 for Earthquake Geotechnical Engineering of the ISSMGE, 1999, Japanese Geotechnical Society of SMGE, Tokyo, 83-99.

**Iwasaki, T., Tokida, K., Tatsuoka, F., Watanabe, S., Yasuda, S., Sato, H., 1982.** Microzonation for soil liquefaction potential using simplified methods. Proceedings of the 3rd International Conference on microzonation, Seattle, 3, 1310-1330.

**Iyengar, R.N., Ghosh, S., 2004.** Microzonation of earthquake hazard in Greater Delhi area. Current Science, 87(9) 1193-1202.

**Iyisan, R., 1996.** Correlations between shear wave velocity and in-situ penetration test results. Chamber of Civil Engineers of Turkey. Teknik Dergi, 7(2), 1187-1199 (in Turkish).

**Jafari, M.K., Asghari, A., Rahmani, I., 1997.** Empirical correlation between shear wave velocity ( $V_s$ ) and SPT-N value for south of Tehran soils. Proceedings of 4th International Conference on Civil Engineering (Tehran, Iran) (in Persian).

**Jafari, M.K., Shafiee, A., Razmkhah, A., 2002.** Dynamic properties of fine grained soils in south of Tehran. Journal of Seismological Earthquake Engineering, 4, 25-35.

**Jain, S.K., Roshan, A.D., Arlekar, J.N. and Basu, P.C., 2000.** Empirical attenuation relationships for the Himalayan earthquakes based on Indian strong ground motion data. In: Proceedings of the Sixth International conference on Seismic zonation.

**Jankowski, P., 1995.** Integrating Geographical Information Systems and multiple criteria decision making methods. *International Journal of Geographical Information Systems*, 9(3), 251-273.

**Janssen, R., 1992.** Multiobjective decision support for environmental management. Dordrecht, The Netherlands, Kluwer Academic.

**Jha, S.K., Suzuki, K., 2009.** Liquefaction potential index considering parameter uncertainties. *Engineering Geology*, 107, 55-60.

**JICA, Japan International Cooperation Agency, 2002.** The study on a disaster prevention/mitigation basic plan in İstanbul including seismic microzonation in the Republic of Turkey, Metropolitan Municipality of Istanbul.

**Jimenez, M.J., Garcia-Fernandez, M., Zona, G., Cella, F., 2000.** Mapping soil effects in Barcelona, Spain, through an integrated GIS environment, *Soil Dynamics and Earthquake Engineering*, 19(4), 289-301.

**Jinan, Z., 1987.** Correlation between seismic wave velocity and the number of blow of SPT and depth. *Selected Papers from the Chinese Journal of Geotechnical Engineering*, 92-100.

**Joyner, W.B., Boore, D.M., 1981.** Peak horizontal acceleration and velocity from strong-motion records including records from the 1979 Imperial Valley, California, earthquake. *Bulletin of the Seismological Society of America*, 71(6), 2011-2038.

**Joyner, W.B., Fumal, T.E., 1984.** Use of measured shear-wave velocity for predicting geologic site effects on strong ground motion. In: *Proceedings of Eighth World Conference on Earthquake Engineering*, Vol. II, 777-783.

**Joyner, W.B., Boore, D.M., 1988.** Measurement, characterization, and prediction of strong ground motion. In: *Proceedings of Earthquake Engineering and Soil Dynamics*, II. Geotechnical Division, ASCE, 43-102.

**Joyner, W.B., Boore, D.M., 1996.** Recent developments in strong motion attenuation relationships. In: *Proceedings of the 28th Joint Meeting of the U.S.-Japan Cooperative Program in Natural Resource Panel on Wind and Seismic Effects*, 101-116.

**Juang, C.H., Yuan, H., Lee D.H., Lin P.S., 2003.** Simplified cone penetration test-based method for evaluating liquefaction resistance of soils. *Journal of Geotechnical and Geoenvironmental Engineering*, 129(1), 66-80.

**Juang, C.H., Liu, C.N., Chen, C.H., Hwang, J.H., Lu, C.C., 2008.** Calibration of liquefaction potential index: a re-visit focusing on a new CPTU model. *Engineering Geology*, 102, 19-30.

**Kagami, H., Duke, C.M., Liang, C.G., Yutaka, O., 1982.** Observation of one to five second microtremors and their application to earthquake engineering. Part II. Evaluation of site effect upon seismic wave amplification due to extremely deep soil deposits. *Bulletin of the Seismological Society of America*, 72, 987-998.

**Kagami, H., Okada, S., Shiono, K., Oner, M., Dravinski, M., Mal, A.K., 1986.** Observation of 1 to 5 second microtremors and their application to earthquake engineering. Part 3: A two dimensional study of site effects in San Fernando Valley. Bulletin of the Seismological Society of America, 76, 1801-1812.

**Kalkan, E., Gulkan, P., 2004.** Site-dependent spectra derived from ground motion records in Turkey. Earthquake Spectra 20 (4), 1111-1138.

**Kalkan, E., Gulkan, P., Ozturk, N.Y., Celebi, M., 2009.** Re-examination of probabilistic seismic hazard in the Marmara Sea Region. Bulletin of Seismological Society of America, 99(4), 2127-2146.

**Kalteziotis, N., Sabatakakis, N., Vassiliou, J., 1992.** Evaluation of dynamic characteristics of Greek soil formations (in Greek). In: Second Hellenic Conference on Geotechnical Engineering, 2, 239-246.

**Kamalian, M., Sohrabi-Bidar, A., Razmkhah, A., Taghavi, A., Rahmani, I., 2008.** Considerations on seismic microzonation in areas with two-dimensional hills. Journal of Earth System Science, 117(2), 783-796.

**Kanai, K., Tanaka, T., Osada, K., 1954.** Measurement of microtremor. I., Bulletin of Earthquake Research Institute, University of Tokyo, 32, 199-209.

**Kanai, K., 1966.** Conf. on Cone Penetrometer The Ministry of Public Works and Settlement (Ankara, Turkey) (presented by Y Sakai, 1968).

**Kanai, K., Tanaka, T., 1961.** On microtremors VIII, Bulletin of the Earthquake Research Institute, 39, 97-114.

**Kanibir A, Ulusay R, Aydan O, 2006.** Assessment of liquefaction and lateral spreading on the shore of Lake Sapanca during the Kocaeli (Turkey) earthquake. Engineering Geology, 83(4), 307-331.

**Kanlı, A.I., Tildy, P., Pronay, Z., Pinar, A., Hermann, L., 2006.** Vs30 mapping and soil classification for seismic site effect evaluation in Dinar region, SW Turkey. Geophysical Journal International, 165(1), 223-235.

**Kaptan, E., 1990.** Findings Related to the History of Mining in Turkey, Mineral Res. Expl. Bull., 111, 75-84.

**Kaymakçı, N. 2000.** Tectono-stratigraphical evolution of the Çankırı Basin (Central Anatolia, Turkey). Ph.D. Thesis, Utrecht University, The Netherlands. Geologica Ultraiectina, no. 190, 248 pp (unpublished).

**Kawashima, K., Aizawa, K., Takahashi, K., 1985.** Attenuation of peak ground motions and absolute acceleration response spectra of vertical earthquake ground motion. Proceedings of JSCE Structural Engineering/Earthquake Engineering, 2(2), 415-422.

**Kayabali, K., 1996.** Soil liquefaction evaluation using shear wave velocity. Engineering Geology, 44(1), 121-127.

**Kayabali, K., 2002.** Modeling of seismic hazard for Turkey using the recent neotectonic data. Engineering Geology, 63, 221- 232.

**Kayabali, K., Akin, M., 2002.** Seismic hazard map of Turkey using the deterministic approach. *Engineering Geology*, 69 (1/2), 127-137.

**Kebede, F., Eck, V.T., 1997.** Probabilistic seismic hazard assessment for the Horn of Africa based on seismotectonic regionalisation. *Tectonophysics*, 270, 221-237.

**Keçer, M., 1990.** Kıtasal alandaki aktif plaka sınırının şekillenmesine bir örnek: Erbaa-Niksar havzası ve jeomorfolojik evrimi, *Jeomorfoloji Dergisi*, 18, 11-18, Ankara (in Turkish).

**Ketin, I., 1948.** Über die tektonisch-mechanischen Folgerungen den grossen anatolischen Erdbeben des letzten Dezenni- sindeki alanin belirlenmesi. In: *ums. Geol. Rundsch.* 36, 77-83 (in German).

**Ketin, I. ve Gümüş, O., 1963.** Sinop-Ayancık arasının III. Bölgeye dahil sahaların jeolojisi: TPAO Rap., 288 (unpublished, in Turkish).

**Ketin, I., 1968.** Relations between general tectonic features and the main earthquake regions of Turkey. *Min. Res. Explor. Inst. Bull.*, 71, 63-67.

**Ketin, I., 1969.** Kuzey Anadolu Fayı Hakkında. *MTA Dergisi* 72, 1-25 (in Turkish).

**Kılıç, H., Özener, P.T., Ansal, A., Yıldırım, M., Özaydın, K., Adatepe, S., 2006.** Microzonation of Zeytinburnu region with respect to soil amplification: a case study. *Engineering Geology*, 86, 238-255.

**Kienzle, A., Hannich, D., Wirth, W., Ehret, D., Rohn, J., Ciugudean, V., Czurda, K., 2006.** A GIS-based study of earthquake hazard as a tool for the microzonation of Bucharest. *Engineering Geology*, 87, 13-32.

**Kijko, A., Graham, G., 1998.** Parametric-historic procedure for probabilistic seismic hazard analysis, Part I: estimation of maximum regional magnitude  $m_{max}$ . *Pure and Applied Geophysics*, 152, 413-442.

**Kijko, A., Graham, G., 1999.** Parametric-historic procedure for probabilistic seismic hazard analysis, Part II: assessment of seismic hazard at specified site. *Pure and Applied Geophysics*, 154, 1-22.

**Kiku, H., Yoshida, N., Yasuda, S., Irisawa, T., Nakazawa, H., Shimizu, Y., Ansal, A., Erkan, A., 2001.** In-situ penetration tests and soil profiling in Adapazari, Turkey. *Proceedings of the ICSMGE/TC4 Satellite Conference on Lessons Learned From Recent Strong Earthquakes*, 259-265.

**Kim, D.S., Bang, E.S., Seo, W.S., 2004.** Evaluation of shear wave velocity profile using SPT-Uphole method. *International site characterization, ISC-2 Porto, Portugal*, 339-344.

**Kiratzis, A.A., 1993.** A study of the active crustal deformation of the North and East Anatolian fault zones. *Tectonophysics*, 225, 191-203.

**Kobayashi, S., Takahashi, T., Matsuzaki, S., Mori, M., Fukushima, Y., Zhao, J.X., Somerville, P.G., 2000.** A spectral attenuation model for Japan using digital strong motion records of JMA87 type. *Proceedings of the 12th World Conference on Earthquake Engineering*, 30 January – 4 February 2000. Auckland, New Zealand.

**Koçkar, M.K., Akgün, H., Rathje, E.M., 2009.** Evaluation of site conditions for the Ankara Basin of Turkey based on seismic site characterization of near-surface geologic materials. *Soil Dynamics and Earthquake Engineering* (in press).

**Koçyiğit, A., Beyhan, A., 1998.** A new intracontinental transcurrent structure: the Central Anatolian Fault Zone, Turkey. *Tectonophysics*, 284, 317-336.

**Koçyiğit, A., Erol, O.A., 2001.** Tectonic escape structure: Erciyes pull-apart basin, Kayseri, Central Anatolia, Turkey. *Geodinamica Acta*, 14, 133-145.

**Koçyiğit, A., 1988.** Basic geological characteristics and total offset of the North Anatolian Fault zone in Süşehri area, NE Turkey. *METU Pure and Applied Sciences*, 22(3), 43-68.

**Koçyiğit, A., 1989.** Susehri basin: an active fault-wedge basin on the North Anatolian Fault Zone, Turkey. *Tectonophysics movements in the Arabia–Africa–Eurasia plate collision zone*. 167, 13-29.

**Koçyiğit, A., 1990.** Tectonic setting of the Golova Basin, total offset of the North Anatolian Fault Zone, Eastern Pontide, Turkey. *Annal. Tecton.* IV(2), 155-170.

**Koçyiğit, A., 1991.** An example of an accretionary forearc basin from Northern central Anatolia and its implications for the history of subduction of Neo-Tethys in Turkey: *Geological Society of America Bulletin*, 103, 22-36.

**Kolat, Ç., 2004.** Geographical Information Systems Based Microzonation Map of Eskişehir Downtown Area. M.Sc. thesis, Middle East Technical University, The Graduate School of Natural and Applied Sciences, Ankara, Turkey, 94 pp.

**Kolat, Ç., Doyuran, V., Ayday, C., Süzen, M.L., 2006.** Preparation of a geotechnical microzonation model using Geographical Information Systems based on Multicriteria Decision Analysis. *Engineering Geology*, 87, 241-255.

**Koravos, C.G., Tsapanos, T.M., Bejaichund, M., 2006.** Probabilistic seismic hazard assessment for Japan. *Pure and Applied Geophysics*, 163, 137-151.

**Kramer, S.L., 1996.** *Geotechnical Earthquake Engineering*. PrenticeHall, Upper Saddle River, New Jersey. 653 pp.

**Kramer, S.L., Stewart, J.P., 2004.** Geotechnical aspects of seismic hazards. In: Bozorgnia, Y, and Bertero, V.V. (eds.), *Earthquake engineering from engineering seismology to performance-based engineering*, CRC Press, Chapter 4, 85 pp.

**Kramer, S.L., Baska, D.A., 2006.** Estimation of permanent displacement due to lateral spreading. *Journal of Geotechnical and Geoenvironmental Engineering*, ASCE, accepted pending revisions.

**Kramer, S.L., 2008.** Evaluation of liquefaction hazards in Washington State. WSDOT Research Report, WA-RD 668.1, Final Research Report Agreement T2695, Task 66.

**Kramer, S.L., 2009a.** CEE 526 Geotechnical Earthquake Engineering lecture notes, University of Washington, Seattle, WA-USA.

**Kramer, S.L., 2009b.** Oral communication. University of Washington, Department of Civil and Environmental Engineering.

**Krinitzsky, E.L., 2003.** How to combine deterministic and probabilistic methods for assessing earthquake hazards. *Engineering Geology*, 70, 157-163.

**Krinitzsky E.L., 2005.** Comment on J.U. Klügel.s: .Problems in the Application of the SSHAC Probability Method for Assessing Earthquake Hazards at Swiss Nuclear Power Plants. *Engineering Geology*, Vol. 82, pp. 66-68.

**Ku, C.S., Chi, Y.Y., 2006.** A study of the CPT-based liquefaction potential index. *Geophysical Research Abstracts*, 8, 01292.

**Kwok, A.O., Stewart, J.P., 2006.** Evaluation of the effectiveness of theoretical 1D amplification factors for earthquake ground-motion prediction. *Bulletin of the Seismological Society of America*, 96(4A), 1422-1436.

**Lachet, C., Hatzfeld, D., Bard, P.Y., Theodulidis, N., Papaioannou, C., Savvaidis, A., 1996.** Site effects and microzonation in the city of Thessaloniki-comparison of different approaches. *Bulletin of the Seismological Society of America*, 86(6), 1692-1703.

**Laue, J., Buchheister, J., Springman, S.M., 2004.** Geotechnical site characterisation - Site response analyses. In: *DRM, Seismic Microzonation for Municipalities, Pilot Studies: Adapazarı, Gölcük, İhsaniye and Değirmendere*, Chapter 5-6, pp. 63-101, Republic of Turkey, General Directorate of Disaster Affairs.

**Lav, A., 1994.** İstanbul ve Erzincan şehirlerinde zemin büyütme etkilerine göre mikrobölgeleme. Ph.D. thesis, ITU Graduate School of Applied Sciences, İstanbul. (in Turkish).

**Lebrun, B., Duval, A.M., Bard, P.Y., Monge, O., Bour, M., Vidal, S., Fabriol, H., 2004.** Seismic microzonation: A comparison between geotechnical and seismological approaches in pointe-à-pitre (French West Indies). *Bulletin of Earthquake Engineering*, 2, 27-50.

**Lee, S.H., 1990.** Regression models of shear wave velocities. *J. Chin. Inst. Eng.*, 13, 519-532.

**Lee, D. H., Ku, C. S., Yuan, H., 2003.** A study of the liquefaction risk potential at Yuanlin. *Taiwan Engineering Geology*, 71, 97-117.

**Lee, W., Kanamori, H., Jennings, P. (Eds.), 2003.** *International Handbook of Earthquake and Engineering Seismology*. IASPEI, Part B.

**Legget, R.F., 1987.** The value of geology in planning. In: *Culshaw, M.G., Bell, F.G., Cripps, J.C., O'Hara, M. (Eds.), Planning and Engineering Geology*. Geological Society Engineering Geology Special Publication, 4, 53-58.

**Lehane, B., Fahey, M., 2002.** A simplified non-linear settlement prediction model for foundations on sand. *Canadian Geotechnical Journal*, 39(2), 293-303.

**Lenz, J.A., Baise, L.G., 2007.** Spatial variability of liquefaction potential in regional mapping using CPT and SPT data. *Soil Dynamics and Earthquake Engineering*, 27, 690-702.



**Lermo, J., Rodriguez, M., Singh, S.K., 1988.** The Mexico earthquake of September 19, 1985-Natural period of sites in the valley of Mexico from microtremor measurements and strong motion data. *Earthquake Spectra*, 4, 805-813.

**Lermo, J., Chavez-Garcia, F.J.,1994.** Are microtremors useful in site response evaluation? *Bulletin of the Seismological Society of America*, 84, 1350-1364.

**Li, D.K., Juang, C.H., Andrus, R.D., 2006.** Liquefaction potential index: a critical assessment using probability concept. *Journal of Geoenvironment, Taiwanese Geotechnical Society*, 1 (1), 11-24.

**Liao, S. C., Whitman R.V., 1986.** Overburden correction factors for SPT in sand. *Journal of Geotechnical Engineering*, 112(3), 373-377.

**Lindholm, C., Bungum, H., 2000.** Probabilistic seismic hazard; a review of the seismological frame of reference with examples from Norway. *Soil Dynamics and Earthquake Engineering*, 20, 27-38.

**Linkov, I., Sahay, S., Kiker, G., Bridges, T., Seager, T.P., 2005.** Multi-criteria decision analysis: a framework for managing contaminated sediments. *Strategic Management of Marine Ecosystems*, 271-297.

**Lorenzo-Martín, F., Roth, F., Wang, R., 2006.** Elastic and inelastic triggering of earthquakes in the North Anatolian Fault zone, *Tectonophysics*, 424, 271-289.

**Louie, J.N., 2001.** Faster, Better: Shear-wave velocity to 100 meters depth from refraction microtremor arrays. *Bulletin of the Seismological Society of America*, 91, 347-364.

**Lu, L., Yamazaki, F., Katayama, T., 1992.** Soil amplification based on seismometer array and microtremor observations in Chiba, Japan. *Earthquake Engineering and Structural Dynamics*, 21, 95-108.

**Luna, R., Jadi, H., 2000.** Determination of Dynamic Soil Properties Using Geophysical Methods. *Proceedings of the First International Conference on the Application of Geophysical and NDT Methodologies to Transportation Facilities and Infrastructure-Geophysics 2000*, Federal Highway Administration, Saint Louis, MO, Paper No. 3-1.

**Lunne, T., Robertson, P.K., Powell, J.J.M., 1997.** *Cone Penetration Testing In Geotechnical Practice*, Blackie Academic & Professional, New York, 312 pp.

**Main, I.G., 1995.** Earthquakes as Critical Phenomena: Implications for Probabilistic Seismic Hazard Analysis. *Bulletin of the Seismological Society of America*, 85:1299-1308.

**Malagnini, L., Rovelli, A., Hough, S.E., Seeber L.,1993.** Site amplification estimates in the Garigliano valley, central Italy, based on dense array measurements of ambient noise. *Bulletin of the Seismological Society of America*, 83, 1744-1744.

**Malczewski, J., 1999.** *GIS and Multicriteria Decision Analysis*. John Willey and Sons Inc. 392 pp.

**Malczewski, J., 2006.** GIS-based multicriteria decision analysis: a survey of the literature. *International Journal of Geographical Information Science*, 20(7), 703-726.

**Mancuso, C., Simonelli, A.L., Vinale, F., 1989.** Numerical analysis of in situ S-wave measurements. In Proceedings of the 12th International conference on Soil Mechanics and Foundation Engineering, Rio de Janeiro, Brazil, 13–18 August 1989. A.A. Balkema, Rotterdam, The Netherlands, 3, 277-280.

**Mantyniemi, P., Marza, V.I., Kijko, A., Retief, P., 2003.** A new probabilistic seismic hazard analysis for the Vrancea (Romania) seismogenic zone. *Natural Hazards*, 29, 371-385.

**Marcellini, A., Bard, P.Y., Iannaccone, G., Meneroud, J.P., Mouroux, P., Romeo, R.W., Silvestri, F., Duval, A.M., Martin, C., Tento, A., 1995.** The Benevento Seismic Risk Project. II- The microzonation. Proc. of 5th International Conference on Seismic Zonation, Nice, France, 1, 810-817.

**Marcellini, A., Daminelli, R., Franceschina, G., Pagani, M., 2001.** Regional and local seismic hazard assessment. *Soil Dynamics and Earthquake Engineering*, 21, 415-429.

**Marcellini, A., Pagani, M., 2004.** Seismic zonation methodologies with particular reference to the Italian situation. In: Ansal, A. (Ed.), *Recent Advances in Earthquake Geotechnical Engineering and Microzonation*, Kluwer Academic Publishers, Dordrecht, The Netherlands, 231-252.

**Marcuson, W.F., 1978.** Definition of terms related to liquefaction. *Journal of Geotechnical Engineering*, ASCE, 104(9), 1197-1200.

**Marinos, P., Bouckovalas, G., Tsiambaos, G., Sabatakakis, N., Antoniou, A., 2001.** Ground zoning against seismic hazard in Athens, Greece. *Engineering Geology*, 62, 343-356.

**Martin, G.M. (Editor), 1994.** Proceedings of the NCEER/SEAOC/BSSC Workshop on Site Response during Earthquakes and Seismic Code Provisions, University of Southern California, Los Angeles, 18-20 November 1992.

**Marshall, K.T., Oliver, R.M., 1995.** *Decision Making and Forecasting*, McGraw-Hill, Inc., 407 pp.

**Masaki, K., Saguchi, K., Sanchez, A., 1998.** On the 1997 Cariaco earthquake and microtremor observation in the Cariaco city. Taller sobre Microzonificación Sísmica en Países Vulnerables, Yokohama, Japon, 9-10 de marzo de 1998, Proceedings. 10 pp.

**Matsuoka, M., Wakamatsu, K., Fujimoto, K., Midorikawa, S., 2006.** Average shear-wave velocity mapping using Japan engineering geomorphologic classification map. *Journal of Structural Mechanics and Earthquake Engineering*, JSCE, 23(1), 57-68.

**Mayne, P.W., Schneider, J.A., Martin, G.K., 1999.** Small- and large strain soil properties from seismic flat dilatometer tests. Proceedings of 2nd Int. Symp. on Pre-Failure Deformation Characteristics of Geomaterials, Torino, 1, 419-427.

**McGillivray, A.V., Mayne, P.W., 2004.** Seismic piezocone and seismic flat dilatometer tests at Treporti. Proceedings of 2nd Int. Conf. on Site Characterization, Porto, 2, 1695-1700.

**McGillivray, A.V., 2007.** Enhanced integration of shear wave velocity profiling in direct-push site characterization systems. Ph.D. thesis, Georgia Institute of Technology, 370 pp.

**McGuire, R.K., 1976.** FORTRAN computer program for seismic risk analysis, Open-File Report 76-67, US Dep. Int, Geological Survey, 90 pp.

**McGuire, R.K., 1977.** Seismic design spectra and mapping procedures using hazard analysis based directly on oscillator response. *Earthquake Engineering and Structural Dynamics*, 5, 211-234.

**McGuire, R.K., 1978.** FRISK computer program for seismic risk analysis, Open-File Report 78-1007, US Dep. Int., 71 pp.

**McGuire, R.K., 1995.** Probabilistic seismic hazard analysis and design earthquakes: closing the loop. *Bulletin of the Seismological Society of America*, 85, 1275-1284.

**McGuire, R.K., 2001.** Deterministic vs. probabilistic earthquake hazards and risks. *Soil Dynamics and Earthquake Engineering*, 21(5), 377-384.

**McKenzie, D., 1972.** Active tectonics of the Mediterranean region. *Geophysical Journal of the Royal Astronomical Society*, 55, 217-254.

**MERM, 2003.** Microzonation Manual, World Institute for Disaster Risk Management.

**Metropol Geotechnical Company, 2005.** Erbaa (Tokat) Sivi-atik Aritma Tesis Sahasinin Jeolojik-Jeoteknik-Jeofizik Etut Raporu, Samsun (unpublished, in Turkish).

**Midorikawa, S., 1987.** Prediction of isoseismal map in the Kanto plain due to hypothetical earthquake. *Journal of Structural Engineering*, 33B, 43-48.

**Milne, W.G., Davenport, A.G., 1969.** Distribution of earthquake risk in Canada. *Bulletin of the Seismological Society of America*, 59(2), 729-754.

**Milne, W.G., 1977.** Seismic risk maps for Canada. In: *Proceedings of Sixth World Conference on Earthquake Engineering*, Vol. I. 2-508, p. 930.

**Mirzaoglu, M., Dikmen, U., 2003.** Application of microtremors to seismic microzoning procedure. *Journal of the Balkan Geophysical Society*, 6(3), 143-156.

**Moehle, J., 1994.** Preliminary report on the seismological and engineering aspects of January 17, 1994 Northridge Earthquake. Univ. of Calif, at Berkeley, Earthquake Engineering Research Center, Report No. UCB/EERC-94/01, 84 pp.

**Moldoveanu, C.L., Radulian, M., Marmureanu, G.H., Panza, G.F., 2004.** Microzonation of Bucharest: State of the Art. *Pure and Applied Geophysics*, 161, 1125-1147.

**Mogami, T., Kubo, K., 1953.** The behaviour of soil during vibration. *Proceedings of the Third International Conference on Soil Mechanics and Foundation Engineering*, 1, 152-153.

**Mohanty, W.K., Walling, M.Y., Nath, S.K., Pal, I., 2007.** First order seismic microzonation of Delhi, India using Geographic Information System (GIS). *Natural Hazards*, 40, 245-260.

**Mohanty, W.K., Walling, M.Y., 2008.** First order seismic microzonation of Haldia, Bengal Basin (India) using a GIS platform. *Pure and Applied Geophysics*, 165, 1325-1350.

**Mohanty, W. K., Walling, M.Y., Vaccari, F., Tripathy, T., Panza, G.F., 2009.** Modeling of SH- and P-SV-wave fields and seismic microzonation based on response spectra for Talchir Basin, India. *Engineering Geology*, 104, 80-97.

**Mohraz, B., 1992.** Recent studies of earthquake ground motion and amplification. *Proc. 10<sup>th</sup> World Conf. Earthquake Eng., Madrid, Spain*, 6695-6704.

**Molas, G.L., Yamazaki, F., 1995.** Attenuation of earthquake ground motion in Japan including deep focus events. *Bulletin of the Seismological Society of America*, 85(5), 1343-1358.

**Moss, R.E.S., 2003.** CPT-based probabilistic assessment of seismic soil liquefaction initiation. Ph.D. Dissertation, University of California, Berkeley, CA.

**Moss, R.E.S., Seed, R.B., Kayen, R.E., Stewart, J.P., Der Kiureghian, A., Cetin, K.O., 2006.** CPT-based probabilistic and deterministic assessment of in-situ seismic soil liquefaction potential. *Journal of Geotechnical and Geoenvironmental Engineering*, 132(8), 1032-1051.

**Motamed, R., Ghalandarzadeh, A., Tawhata, I., Tabatabaei, S.H., 2007.** Seismic microzonation and damage assessment of Bam city, Southeastern Iran. *Journal of Earthquake Engineering*, 11, 110-132.

**Mourabit, T., Cheddadi, A., Talhaoui, A., Seo, K., Vidal, F., 2000.** Microzonage sismique en zones urbaines, m'éthodologie et applications (cas des villes de Grenade en Espagne et d'Al Hoceima au Maroc). *Colloque Scientifique Sur le Thème: Reconstruction de la Ville d'Agadir (1960-2000) Bilans et Perspectives*, Agadir, 1-2 Mars 2000.

**MTA, 1990.** Maden Tektik ve Arama Genel Müdürlüğü, Geologic Map of the Tokat-D23 Quadrangle, 1:100,000 scale, Ankara.

**Mucciarelli, M., 1998.** Reliability and applicability of Nakamura's technique using microtremors: an experimental approach. *Journal of Earthquake Engineering*, 2, 625-638.

**Muço, B., Vaccari, F., Panza, G., Kuka, N., 2002.** Seismic zonation in Albania using a deterministic approach. *Tectonophysics* 344, 277-288.

**Mukhopadhyay, S., Bormann, P., 2004.** Low cost seismic microzonation using microtremor data: an example from Delhi, India. *Journal of Asian Earth Sciences*, 24, 271-280.

**Muller, J.R., Aydin, A., Maerten, F., 2003.** Investigating the transition between the 1967 Mudurnu Valley and the 1999 Izmit earthquakes along the North Anatolian fault with static stress changes. *Geophysical Journal International*, 154(2), 471-482.

**Naeim, F., 2001.** *The Seismic Design Handbook*. Kluwer Academic Publishers, Boston.

**Naeim, F., Alimoradi, A., Pezeshk, S., 2004.** Selection and scaling of ground motion time histories for structural design using genetic algorithms. *Earthquake Spectra*, 20(2), 413-426.

**Nakamura, Y., 1989.** A method for dynamic characteristics estimation of subsurface using microtremor on the ground surface. *Quarterly Report of Railway Technical Research Institute*, 30(1), 25-33.

**Nalbant, S.S., Barka, A.A., Alptekin, Ö., 1996.** Failure stress change caused by the 1992 Erzincan earthquake ( $M_s = 6.8$ ). *Geophysical Research Letters*, 23, 1561-1564.

**Nath, S.K., 2004.** Seismic hazard mapping and microzonation in the Sikkim Himalaya through GIS integration of site effects and strong ground motion attributes. *Natural Hazards*, 31, 319-342.

**Nath, S.K., 2005.** An initial model of seismic microzonation of Sikkim Himalaya through thematic mapping and GIS integration of geological and strong ground motion features. *Journal of Asian Earth Sciences*, 25, 329-343.

**Nath, S.K., 2007.** Seismic Microzonation Framework – Principles & Applications. In *Proceedings of Workshop on Microzonation*, Indian Institute of Science, Bangalore, pp 9-35.

**Nath, S.K., Thingbaijam, K.K.S., Raj, A., 2008.** Earthquake hazard in Northeast India - a seismic microzonation approach with typical case studies from Sikkim Himalaya and Guwahati city. *Journal of Earth System Sciences*, 117(2), 809-831.

**National Center for Earthquake Engineering Research (NCEER) 1997.** Proc. NCEER Workshop on Evaluation of Liquefaction Resistance of Soils, Eds. T. L. Youd and I. M. Idriss, Technical Rep. No. NCEER, 97-022, NCEER, Buffalo, N.Y, 1-40.

**NEHRP, 2000.** Recommended provisions for seismic regulations for new buildings and other structures, Part 1: Provisions, FEMA 368, Building seismic safety council of the National Institute of Building Sciences, USA.

**NEHRP-BSSC, 2003.** NEHRP (National Earthquake Hazard Reduction Program) Recommended Provisions for New Buildings and Other Structures (FEMA 450), 2003 Edition, Building Seismic Safety Council, National Institute of Building Sciences, Washington, D.C.

**Nikolaou, A.S., 1998.** A GIS Platform for Earthquake Risk Analysis. Ph.D.Thesis, State University of New York at Buffalo.

**NRC, 1988.** Probabilistic Seismic Hazard Analysis. Panel on Seismic Hazard Analysis Committee on Seismology Board on Earth Sciences Commission on Physical Sciences, Mathematics, and Resources, National Research Council (U.S), National Academy Press, Washington DC.

**Nunziata, C., 2007.** A physically sound way of using noise measurements in seismic microzonation, applied to the urban area of Napoli. *Engineering Geology*, 93, 17-30.

**Ohba, S., Toriumi, I., 1970.** Dynamic response characteristics of Osaka Plain. *Proceedings of the Annual Meeting*, A. I. J. (in Japanese).

**Ohno, S., Takemura, M., Niwa, M., Takahashi, K., 1996.** Intensity of strong ground motion on prequaternary stratum and surface soil amplifications during the 1995 Hyogo-ken Nanbu earthquake, Japan. *Journal of Physics of the Earth*, 44(5), 623-648.

**Ohsaki, Y., Iwasaki, R., 1973.** On dynamic shear moduli and Poisson's ratio of soil deposits. *Soil Found.*, 13, 61-73.

- Ohta, Y., Goto, N., 1976.** Estimation of s-wave velocity in terms of characteristics indices of soil. *Butsuri-Tanko*, 29(4), 34-41.
- Ohta, Y., Goto, N., 1978.** Empirical shear wave velocity equations in terms of characteristics soil indexes. *Earthquake Engineering and Structural Dynamics*, 6, 167-187.
- Ohta Y., Kagami, H., Goto, N., Sudo, K., 1978a.** Observation of 1 to 5 second microtremors and their application to earthquake engineering. Part I: Comparison with long-period accelerations at the Tokachi-Oki earthquake of 1968. *Bulletin of the Seismological Society of America*, 68.
- Ohta, Y., Goto, N., Kagami, H., Shiono, K., 1978b.** Shear wave velocity measurement during a standard penetration test. *Earthquake Engineering and Structural Dynamics*, 6, 43-50.
- Ojeda, A., Escallon, J., 2000.** Comparison between different techniques for evaluation of predominant periods using strong ground motion records and microtremors in Pereira Colombia. *Soil Dynamics and Earthquake Engineering*, 20, 137-143.
- Ojeda, A., Martinez, S., Bermudez, M., Atakan, K., 2002.** The new accelerograph network for Santa Fe De Bogota, Colombia and implications for microzonation. *Soil Dynamics and Earthquake Engineering*, 22, 791-797.
- Okada, H., 2003.** The Microseismic Survey Method: Society of Exploration Geophysicists of Japan. Translated by Koya Suto, Geophysical Monograph Series No. 12, Society of Exploration Geophysicists.
- Okamoto, T., Kokusho, T., Yoshida, Y., Kusuonoki, K., 1989.** Comparison of surface versus subsurface wave source for P-S logging in sand layer. *Proceedings of 44th Ann. Conf. JSCE*, 3, 996-997, (in Japanese).
- Olsen, R.S., 1984.** Liquefaction analysis using the cone penetrometer test (CPT). *Proc. 8th World Conf. on Earthquake Engrg.*, 3, 247-254.
- Olsen, R.S., 1997.** Cyclic liquefaction based on the cone penetration test. *Proc. NCEER Workshop on Evaluation of Liquefaction Resistance of Soils*, Nat. Ctr. for Earthquake Engrg. Res., State Univ. of New York at Buffalo, 225-276.
- Ordonez, G. A., 2004.** SHAKE2000, A computer program for the 1-D analyses of geotechnical earthquake, *Engineering Problems User's Manual*, 306 pp.
- Orphal, D.L., Lahoud, J.A., 1974.** Prediction of peak ground motion from earthquakes. *Bulletin of the Seismological Society of America*, 64(5), 1563-1574.
- Over, S., Bellier, O., Poisson, A., Andrieux, J., Tutkun, Z., 1993.** Esquisse de l'évolution néogène à actuelle de l'état de contrainte dans la partie centrale de la Faille Nord Anatolienne (Turquie). *C. R. Acad. Sci. Paris II* 317, 827-833 (in French).
- Ozbey, C., Sari, A., Manuel, L., Erdik, M., Fahjan, Y., 2004.** An empirical attenuation relationship for Northwestern Turkey ground motion using a random effects approach. *Soil Dynamics and Earthquake Engineering*, 24, 115-125.

**Ozdemir, Z., Fahjan, Y.M., 2007.** Comparison of time and frequency domain scaling of real accelerograms to match earthquake design spectra. 6th National Conference on Earthquake Engineering (6. Ulusal Deprem Mühendisliği Konferansı), Istanbul, Turkey, October 16-20, 2007.

**Ozel, O., Sasatani, T., 2004.** A site effect study of the Adapazari basin, Turkey, from strong and weak-motion data. *Journal of Seismology*, 8(4), 559-572.

**Özcan, A., Armağan, A., Erkan, A., Keskin, A., Keskin, E., Oral, A., Özer, S., Sümengen, M., Tekeli, O., 1980,** Kuzey Anadolu Fayı ile Kırşehir Masifi arasında kalan alanın temel jeolojisi: MTA Enst. Rapor derleme no. 6722. Ankara (unpublished, in Turkish).

**Özgüç, T., 1964.** New finds from Horoztepe, Anatolia VIII, 1-25.

**Özmen, B., Nurlu, M., Güler, H., 1997.** Coğrafi Bilgi Sistemi ile Deprem Bölgelerinin İncelenmesi, Afet İşleri Genel Müdürlüğü, Deprem Araştırma Dairesi, 89 pp. (unpublished, in Turkish).

**Öztürk, A., 1979.** Ladik-Destek dolayının stratigrafisi: Türkiye Jeo. Kur. Bült., 22/1, 27-34, Ankara (in Turkish).

**Pace, B., Boncio, P., Brozzetti, F., Lavecchia, G., Visini, F., 2008.** From regional seismic hazard to “scenario earthquakes” for seismic microzoning: A new methodological tool for the Celano Project. *Soil Dynamics and Earthquake Engineering*, 28, 866-874.

**Panza, G.F., Vaccari, F., Costa, G., Suhadolc, P., Fäh, D., 1996.** Seismic input modelling for zoning and microzoning. *Earthquake Spectra*, 12(3), 529-566.

**Panza, G. F., Romanelli, F., Vaccari, F., 2001.** Seismic wave propagation in laterally heterogeneous anelastic media: theory and application to seismic zonation, edited by: Dmowska, R., and Saltzman, B., *Advances in Geophysics*, Academic Press, San Diego, USA, 43, 1-95.

**Park, D., Hashash, Y.M.A., 2004.** Soil damping formulation in nonlinear time domain site response analysis. *Journal of Earthquake Engineering*, 8(2), 249-274.

**Papadimitriou, A.G., Antoniou, A.A., Bouckovalas, G.D., Marinou, P.G., 2008.** Methodology for automated GIS-aided seismic microzonation studies. *Computers and Geotechnics*, 35, 505-523.

**Papathanassiou, G., Pavlides, S., Ganas, A., 2005.** The 2003 Lefkada earthquake: Field observations and preliminary microzonation map based on liquefaction potential index for the town of Lefkada. *Engineering Geology*, 82, 12-31.

**Papathanassiou, G., 2008.** LPI-based approach for calibrating the severity of liquefaction-induced failures and for assessing the probability of liquefaction surface evidence. *Engineering Geology*, 96, 94-104.

**Parolai, S., Gottfried G., Wahlström, R., 2007.** Site-specific response spectra from the combination of microzonation with probabilistic seismic hazard assessment - An example for the Cologne (Germany) area. *Soil Dynamics and Earthquake Engineering*, 27, 49-59.

**Parvez, I.A., Vaccari, F., Panza, G.F., 2004.** Site-specific Microzonation Study in Delhi Metropolitan City by 2-D Modelling of SH and P-SV Waves. *Pure and Applied Geophysics*, 161, 1165-1184.

**Pavlenko, O.V., 2008.** Characteristics of soil response in near-fault zones during the 1999 Chi-Chi, Taiwan Earthquake. *Pure and Applied Geophysics*, 165(9-10), 1789-1812.

**Pavoni, N., 1961.** Die Nordanatolische Horizontal-verschnebung. *Geol. Rundsch.* 51, 122-139 (in German).

**Peck, R. B., Hanson, W. E., Thornburn, T. H., 1974.** *Foundation Engineering*. John Wiley and Sons, 312 pp.

**PEER Strong Motion Database, 2009.** <http://peer.berkeley.edu/smcat/>, 15.04.2009.

**Petersen, M.D., Dewey, J., Hartzell, S., Mueller, C., Harmsen, S., Frankel, A.D., Rukstales, K., 2004.** Probabilistic seismic hazard analysis for Sumatra, Indonesia and across the Southern Malaysian Peninsula. *Tectonophysics*, 390, 141-158.

**Petrovski, D., Marcellini, A., 1988.** Prediction of seismic movement of a site: Statistical approach. In: *Proc. UN Sem. on Predict. of Earthquakes*. Lisbon, Portugal, 14-18 November.

**Phillips, C., Hashash, Y.M.A., 2009.** Damping formulation for nonlinear 1D site response analyses. *Soil Dynamics and Earthquake Engineering*, 29(7), 1143-1158.

**Pinar, N., 1953.** Etude géologique et macrosismique du tremblement du terre de Kusurlu (Anatolie septentrionale) du 13 août 1951. *Rev. Fac. Sc. Univ. Istanbul XVIII*, 131-142 (in French).

**Pinar, A., Honkura, Y., Kikuchi, M., 1994.** Rupture process of the 1992 Erzincan earthquake and its implication for seismotectonics in eastern Turkey. *Geophysical Research Letters*, 21(18), 1971-1974.

**Pitilakis, K.D, Anastasiadis, A., Raptakis, D., 1992.** Field and laboratory determination of dynamic properties of natural soil deposits. *Proceedings of 10th World Conf. Earthquake Engineering*, Rotherdam, 1275-1280.

**Pitilakis, K., Raptakis, D., Lontzetidis, K.T., Vassilikou, T., Jongmans, D., 1999.** Geotechnical and geophysical description of Euro-Seistests, using field and laboratory tests, and moderate strong ground motions. *Journal of Earthquake Engineering*, 3, 381-409.

**Pitilakis, K., 2004.** Site effects. In: Ansal, A. (Ed.), *Recent Advances in Earthquake Geotechnical Engineering and Microzonation*. Kluwer Academic Publishers, Dordrecht, The Netherlands, 139-197.

**Poulos, S.J., Castro, G., France, J. W., 1985.** Liquefaction evaluation procedure. *Journal of Geotechnical Engineering*, 111(6), 772-792.

**Power, M., Chiou, B., Abrahamson, N., Bozorgnia, Y., Shantz, T., Roblee, C., 2008.** An Overview of the NGA Project. *Earthquake Spectra*, 24(1), 3-21.

**Priolo, E., 2001.** Deterministic computation of the reference ground motion in Fabriano (Marche-Italy). *Italian Geotechnical Journal*, 35(2).



**Ramakrishnan, D., Mohanty, K.K., Nayak, S.R., Chandran, V., 2006.** Mapping the liquefaction induced soil moisture changes using remote sensing technique: an attempt to map the earthquake induced liquefaction around Bhuj, Gujarat, India. *Geotechnical and Geological Engineering*, 24, 1581-1602.

**Raptakis, D.G., Anastasiadis, S.A.J., Pitilakis, K.D., Lontzetidis, K.S., 1995.** Shear wave velocities and damping of Greek natural soils. *Proceedings of 10th European Conf. Earthquake Engineering*, Vienna, 477-482.

**Rau, J.L., 1994.** Urban and environmental issues in East and Southeast Asian coastal lowlands. *Engineering Geology*, 37, 25-29.

**Rauch, A.F., 1997.** EPOLLS: an empirical method for predicting surface displacements due to liquefaction-induced lateral spreading in earthquakes. Virginia Polytechnic Institute and State University, Blacksburg, VA.

**Redpath, B.B., 1973.** Seismic refraction exploration for engineering site investigations. Technical Report E-73-4, U.S. Army Waterways Experimentation Station, Vicksburg, MS, 60 pp.

**Regnier, M., Moris, S., Shapira, A., Malitzky, A., Shorten, G., 2000.** Microzonation of the expected seismic site effects across Port Vila, Vanuatu. *Journal of Earthquake Engineering*, 4(2), 215-231.

**Reiter, L., 1990.** *Earthquake Hazard Analysis: issues and insights*, Columbia University Press, New York, 254 pp.

**Richart, F.E., Hall, J.R., Woods, R.D., 1970.** *Vibrations of soils and foundations*, Prentice-Hall, 414 pp.

**Richart, F.E., Hall, J.R., Woods, R.D., 1970.** *Vibrations of Soils and Foundations*. Prentice-Hall, Englewood Cliffs, N.J., 414 pp.

**Rinaldis, D., Berardi, R., Theodulidis, N., Margaris, B., 1998.** Empirical predictive models based on a joint Italian & Greek strong-motion database: I, peak ground acceleration and velocity. In: *Proceedings of Eleventh European Conference on Earthquake Engineering*.

**Robertson, P.K., Campanella, R.G., 1983.** Interpretation of cone penetration tests, Part I (Sand); Part II (Clay). *Canadian Geotechnical Journal*, 20(4), 81 pp.

**Robertson, P.K., 1994.** Suggested terminology for liquefaction. 47th Canadian Geotechnical Conference, September 21-23, 1994, Halifax, Nova Scotia, 10 pages.

**Robertson, P.K., Wride (Fear), C.E., 1997.** Evaluation of cyclic liquefaction potential based on the CPT. In: Pinto, P.S.S. (ed.) *Proceedings of the Discussion Special Technical Session on Earthquake Geotechnical Engineering*, 14th International Conference on Soil Mechanics and Foundation Engineering, Hamburg. A.A. Balkema. Rotterdam, The Netherlands, 269-277.

**Robertson, P. K., Wride C. E., 1998.** Evaluating cyclic liquefaction potential using the cone penetration test. *Canadian Geotechnical Journal*, 35(3), 442-459.

**Robertson, P.K., 2004.** Evaluating soil liquefaction and post-earthquake deformations using the CPT. University of Alberta, Dept. of Civil and Environmental Engineering, Edmonton, Canada.

**Roca, A., Oliveira, C.S., Ansal, A., Figueras, S., 2006.** Local site effects and microzonation. In: Oliveira, C.S., Roca, A., Goula, X. (eds.), *Assessing and Managing Earthquake Risk*, 67-89.

**Rodriguez-Marek, A., Bray, J.D., Abrahamson, N.A., 2001.** An empirical geotechnical seismic site response procedure. *Earthquake Spectra*, 17(1), 65-87.

**Rojay, F.B., 1993.** Tectonostratigraphy and neotectonic characteristics of the southern margin of Merzifon-Suluova Basin (Central Pontides, Amasya), Ph.D. Thesis, Middle East Technical University, Ankara (unpublished) .

**Romeo, R., Prestininzi, A., 2000.** Probabilistic versus deterministic seismic hazard analysis: an integrated approach for siting problems. *Soil Dynamics and Earthquake Engineering*, 20, 75-84.

**Romeo, R.W., Bisiccia, C., 2006.** Risk-oriented seismic microzoning study of an urban settlement. *Soil Dynamics and Earthquake Engineering*, 26, 899-908.

**Rovelliet, A., Singh, S.K., Malagnini, L., Amato, A., Cocco, M. 1991.** Feasibility of the use of microtremors in estimating site response during earthquakes: some test cases in Italy. *Earthquake Spectra*, 551-562.

**Rowe, R.K., 2001.** *Geotechnical and Geoenvironmental Engineering Handbook*. Boston-Dodrecht- London: Kluwer Academic Publisher.

**Saaty, T.L., 1977.** A scaling method of priorities in hierarchical structures. *Journal of Mathematical Psychology*, 15(3), 234-281.

**Saaty, T.L., 1980.** *The Analytic Hierarchy Process*. McGraw-Hill, New York.

**Saaty, T.L., 2004.** Decision making-the Analytical Hierarchy and Network Process (AHP/ANP). *Journal of Systems Science and Systems Engineering*, 13(1), 1-35.

**Sabetta, F., Pugliese, A., 1987.** Attenuation of peak horizontal acceleration and velocity from Italian strongmotion records. *Bulletin of the Seismological Society of America*, 77(5), 1491-1513.

**Sadigh, K., Chang, C.Y., Abrahamson, N.A., Chiou, S.J., Power, M.S., 1993.** Specification of long period ground motions: Updated attenuation relationships for rock site conditions and adjustment factors for near-fault effects. In: *Proceedings of ATC-17-1 Seminar on Seismic Isolation, Passive Energy Dissipation, and Active Control*, 59-70.

**Sadigh, K., Chang, C.Y., Egan, J.A., Makdisi, F., Youngs, R.R., 1997.** Attenuation relationships for shallow crustal earthquakes based on California strong motion data. *Seismological Research Letters*, 68(1), 180-189.

**Sadigh, R.K., Egan, J.A., 1998.** Updated relationships for horizontal peak ground velocity and peak ground displacement for shallow crustal earthquakes. In: *Proceedings of the Sixth U.S. National Conference on Earthquake Engineering*.

**Sarma, S. K., Srbulov, M., 1996.** A simplified method for prediction of kinematic soil-foundation interaction effects on peak horizontal acceleration of a rigid foundation. *Earthquake Engineering and Structural Dynamics*, 25(8), 815-836.

**Sarma, S. K., Srbulov, M., 1998.** A uniform estimation of some basic ground motion parameters. *Journal of Earthquake Engineering*, 2(2), 267-287.

**Sasitharan, S., Robertson, P.K., Sego, D.C., Morgenstern, N.R., 1994.** State-boundary surface for very loose sand and its practical implications. *Canadian Geotechnical Journal*, 31, 321-334.

**Schnabel, P.B., Lysmer, J.L., Seed, H.B. 1972.** SHAKE: A computer program for earthquake response analysis of horizontally layered sites. Report EERC-72/12, Earthquake Engineering Research Center (EERC), Berkeley, California.

**Seed, H. B., Idriss, I.M., 1971.** Simplified procedure for evaluating soil liquefaction potential. *J. Soil Mech. Found. Div., American Soc. Civ. Eng.*, 97(9), 1249-1273.

**Seed, H. B., 1976.** Evaluation of soil liquefaction effects on level ground during earthquakes. *Liquefaction problems in Geotechnical Engineering, Proceedings of ASCE Annual Convention and Exposition, Philadelphia*, 1-104.

**Seed, H.B., Idriss, I.M., 1981.** Evaluation of liquefaction potential sand deposits based on observation of performance in previous earthquakes. *ASCE National Convention (MO)*, 481-544.

**Seed, H. B., Idriss, I.M., 1983.** Ground motions and soil liquefaction during earthquakes. *Earthquake Engineering Research Institute, Berkeley, Calif.*, 134 pp.

**Seed, H.B., Idriss, I.M., Arango, I., 1983.** Evaluation of liquefaction potential using field performance data. *J. Geotech. Eng., ASCE*, 109, 458-482.

**Seed, H.B., Wong, R.T., Idriss, I.M., Tokimatsu, K., 1984.** Moduli and damping factors for dynamic analyses of cohesionless soils. *Journal of Geotechnical Engineering, ASCE*, 112(11), 1016-1032.

**Seed, H.B., Tokimatsu, K., Harder, L.F., Chung, R.M., 1985.** Influence of SPT procedures in soil liquefaction resistance evaluations. *Journal of Geotechnical Engineering*, 111(12), 1425-1445.

**Seed, H.B., Wong, R.T., Idriss, I.M., Tokimatsu, K., 1986.** Moduli and damping factors for dynamic analyses of cohesionless soils. *Journal of the Soil Mechanics and Foundations Division, ASCE*, 112 (SM11).

**Seed, H.B., Romo, M.P., Sun, J.I., Jaime, A., Lysmer, J., 1988.** The Mexico earthquake of September 19, 1985-Relationships between soil conditions and earthquake ground motions. *Earthquake Spectra*, 4, 687-729.

**Seed, H.B., Sun, J.H., 1989.** Implication of site effects in the Mexico City earthquake of September 19, 1985 for Earthquake-Resistant Design Criteria in the San Francisco Bay Area of California, Report No. UCB/EERC-89/03, Earthquake Engineering Research Center, University of California, Berkeley.

**Seed, R.B., Dickenson, S.E., Riemer, M.F., Bray, J.D., Sitar, N., Mitchell, J.K., Idriss, I.M., Kayen, R.E., Kropp, A.K., Harder, L.F., Power, M.S., 1990.** Preliminary report on the principle geotechnical aspects of the October 17, 1989 Loma Prieta earthquake, Report No. UCB/EERC-90/05, Earthquake Engineering Research Center, University of California, Berkeley.

**Seed, R.B., Cetin, K.O., Moss, R.E.S., Kammerer, A.M., Wu, J., Pestana, J.M., Riemer, M.F., 2001.** Recent advances in soil liquefaction engineering and seismic site response evaluation. Proc. 4th International Conference on Recent Advances in Geotechnical Earthquake Engineering and Soil Dynamics, San Diego, 1-45.

**Seed, R.B., Cetin, K.O., Moss, R.E.S., Kammerer, A.M., Wu, J., Pestana, J.M., Riemer, M.F., Sancio, R.B., Bray, J.D., Kayen, R.E., Faris, A., 2003.** Recent advances in soil liquefaction engineering: A unified and consistent framework. 26th Annual ASCE Los Angeles Geotechnical Spring Seminar, Long Beach, CA, ASCE, Reston, VA, 71.

**Seht I. M., Wohlenberg, J., 1999.** Microtremor measurements used to map thickness of soft sediment. Bulletin of the Seismological Society of America, 89, 250-259.

**Selçuk, L., Çiftçi, Y., 2007.** Microzonation of the Plio-Quaternary soils: a case study of the liquefaction risk potential in the Lake Van Basin, Turkey. Bulletin of Engineering Geology and the Environment, 66, 161-176.

**Sener, B., 2004.** Landfill site selection by using Geographic Information Systems. M.Sc. thesis, Middle East Technical University, The Graduate School of Natural and Applied Sciences, Ankara, Turkey, 114 pp.

**Seymen, İ., 1975,** Kelkit Vadisi kesiminde Kuzey Anadolu Fay Zonunun Tektonik Özelliği, İstanbul Teknik Üniversitesi Yayınları, Maden Fakültesi, İstanbul, 198 (in Turkish).

**Shamoto, Y., Zhang, J.-M., Tokimatsu, K., 1998.** Methods for evaluating residual postliquefaction ground settlement and horizontal displacement, Soils and Foundations, Special Issue No. 2, 69-83.

**Sharma, M.L., 1998.** Attenuation relationship for estimation of peak ground horizontal acceleration using data from strong-motion arrays in India. Bulletin of the Seismological Society of America, 88(4), 1063-1069.

**Sharma, M.L., 2000.** Attenuation relationship for estimation of peak ground vertical acceleration using data from strong motion arrays in India. 12th World conference on Earthquake Engineering, New Zealand, 1994/ 4 / A, 1-8.

**Sharma, M. L., Wason, H. R., Dimri, R., 2003.** Seismic zonation of the Delhi region for bedrock ground motion. Pure and Applied Geophysics, 160, 2381-2398.

**Shibata, T., 1970.** Analysis of liquefaction of saturated sand during cyclic loading. Disaster Prevention Res. Inst. Bull., 13, 563-570.

**Shibuya, S., Yamashita, S., Mitachi, T., Tanaka, H. 1995.** Effects of sample disturbance on  $G_{max}$  of soils-a case study. 1st International Conference on Earthquake Geotechnical Engineering, Tokyo, Japan, 1, 77.

**Si, H., Midorikawa, S., 2000.** New attenuation relations for peak ground acceleration and velocity considering effects of fault type and site condition. Proceedings of 12th World Conference on Earthquake Engineering, CD-ROM.

**Silva, W., Lee, K., 1987.** State-of-the-art for assessing earthquake hazards in the United States, Report 24, WES RASCAL Code for Synthesizing Earthquake Ground Motions, Miscellaneous Paper S-73-1, U.S. Army Engineer Waterways Experiment Station, Vicksburg, MS.

**Simpson, K.A., 1996.** Attenuation of strong ground-motion incorporating near-surface foundation conditions. Ph.D. thesis, University of London.

**Singh, S. K., Lermo, J., Dominguez, T., Ordaz, M., Espinosa, J. M., Mena, E., Quaas, R., 1988.** The Mexico earthquake of September 19, 1985: a study of amplification of seismic waves in the valley of Mexico with respect to a hill zone site. *Earthquake Spectra*, 4, 653-673.

**Signanini, P., D'intinosante, V., Ferrini, M., Rainone, M.L., 2004.** Evaluation of local amplification in the seismic microzonation: comparison between punctual multidisciplinary integrated studies and macroseismic methods in Fivizzano's area (Toscana, Italy). *Geotechnical and Geological Engineering*, 22, 227-244.

**Sisman, H., 1995.** An investigation on relationships between shear wave velocity, and SPT and pressuremeter test results. MSc Thesis, Ankara University, Geophysical Engineering Department, Ankara, 75 pp (in Turkish).

**Sitharam, G., Anbazhagan, P., Raj, G.K., 2006.** Deterministic seismic hazard analysis and estimation of PHA for Bangalore City. International Conference on Earthquake Engineering, Pakistan, 1-8.

**Sitharam, T.G., Anbazhagan, P., 2007.** Seismic hazard analysis for Bangalore Region, *Journal of Natural Hazards*, 40, 261-278.

**Sitharam, T.G., Anbazhagan, P., 2008.** Seismic microzonation: principles, practices and experiments. *EJGE Special Volume Bouquet 08*. online, <http://www.ejge.com/Bouquet08/Preface.htm>, 61 pp.

**Siyahi, B., Ansal, A., 1993.** Manual for zonation on seismic geotechnical hazard. TC4 Committee of ISSMFE, Japanese Society of Soil Mechanics and Foundation Engineering, 55-57.

**Siyahi, B., Fahjan, Y., 2004.** Landslide hazard. In: DRM, *Seismic Microzonation for Municipalities, Pilot Studies: Adapazarı, Gölcük, İhsaniye and Değirmendere*, Chapter 8, 120-124, Republic of Turkey, General Directorate of Disaster Affairs.

**Slemmons, D.B., 1982.** Determination of design earthquake magnitudes for microzonation. In: Mehmet Sherif (ed.), *Proceedings of the Third International Earthquake Microzonation Conference*, Seattle, WA, U.S. National Science Foundation, Washington, DC, Vol 1, pp 119-130.

**Sonmez, H., 2003.** Modification to the liquefaction potential index and liquefaction susceptibility mapping for a liquefaction-prone area (Inegol-Turkey). *Environmental Geology*, 44(7), 862-871.

**Sonmez, H., Gokceoglu, C., 2005.** A liquefaction severity index suggested for engineering practice. *Environmental Geology* 48, 81-91.

**Sonmez, B., Ulusay, R., 2008.** Liquefaction potential at Izmit Bay: comparison of predicted and observed soil liquefaction during the Kocaeli earthquake. *Bulletin of Engineering Geology and the Environment*, 67, 1-9.

**Sonmez, B., Ulusay, R., Sonmez, H., 2008.** A study on the identification of liquefaction-induced failures on ground surface based on the data from the 1999 Kocaeli and Chi-Chi earthquakes. *Engineering Geology*, 97, 112-125.

**Stam, J.C., 1962.** Modern developments in shallow seismic refraction techniques. *Geophysics*, 27(2), 198-212.

**Stein, R.S., Barka, A., Dieterich, J.H., 1997,** Progressive failure on the North Anatolian Fault since 1989 by earthquake stress triggering. *Geophysical Journal International*, 128, 594-604.

**Stewart, J.P., Liu, A.H., Choi, Y., 2003.** Amplification factors for spectral acceleration in tectonically active regions. *Bulletin of the Seismological Society of America*, 93(1), 332-352.

**Studer, J. and Ansal, A., 2003.** Seismic Microzonation for Municipalities, Manual Research Report for Republic of Turkey, Ministry of Public Works and Settlement, General Directorate of Disaster Affairs prepared by World Institute for Disaster Risk Management.

**Sun, J.I., Goleorkhi, R., Seed, H.B., 1988.** Dynamic Moduli and Damping Ratios for Cohesive Soils. Report No. UCB/EERC-88/15. University of Berkeley, Earthquake Engineering Research Center, California, USA.

**Sun, C.G., Chun, S.H., Ha, T.G., Chung, C.K., Kim, D.S., 2008.** Development and application of a GIS-based tool for earthquake-induced hazard prediction. *Computers and Geotechnics*, 35, 436-449.

**Sykora, D.E., Stokoe, K.H., 1983.** Correlations of in-situ measurements in sands of shear wave velocity. *Soil Dynamics and Earthquake Engineering*, 20, 125-136.

**Şahin, C., 1998.** Erbaa-Niksar havzası ve yakın çevresinin jeomorfolojik etüdü. M.Sc. thesis. Marmara University, Graduate School of Social Sciences, İstanbul, Turkey, 232 pp. (in Turkish).

**Şaroğlu, F., Emre, Ö., Kuscı, I., 1992.** Active fault map of Turkey. Geological Research Department of the General Directorate of Mineral Research and Exploration, Ankara, Turkey.

**Şaroğlu, F., Emre, Ö., Boray, A., 1987.** Türkiye'nin aktif fayları ve depremsellikleri. MTA Rapor no: 8174, 394 s. (unpublished, in Turkish).

**Şengör, A.M.C., 1979.** The North Anatolian transform fault: its age, offset and tectonic significance. *Journal of Geological Society of London*, 136, 269-282.

**Şengör, A. M. C., Görür, N. and Şaroğlu, F., 1985.** Strike-slip faulting and related basin formation in zones of tectonic escape: Turkey as a case study, Strike-slip deformation, basin

formation, and sedimentation, Soc. Econ. Paleont. Min. Spec. Pub. 37 (in honor of J.C. Crowell), 227-264.

**Takemiya, H., Adam, M., 1997.** Seismic wave amplification due to topography and geology in Kobe during Hyogo-Ken Nanbu Earthquake. Journal of Structural Mechanics and Earthquake Engineering. JSCE, 14(2), 129-138.

**Talhaoui, A., Ibrahim, A.I., Aberkan, M., Kasmi, M., Mouraouah, 2004.** Seismic microzonation and site effects at Al Hoceima City, Morocco. Journal of Earthquake Engineering, 8(4), 585-596.

**Tatar, Y., 1975.** Tectonic structures along the North Anatolian fault zone, northeast of Refahiye (Erzincan), Tectonophysics, 29, 401-410.

**Tatar, O., Park, R.G., Temiz, H., Tutkun, S.Z., 1990.** Transtensional and transpressional structures associated with the North Anatolian strike-slip fault zone: the Niksar Basin, Turkey. In: Savascin, M.Y., Eronat, A.H. (Eds.), Proc. Int. Earth Sciences Congress on Aegean Regions, Vol. II., 323-333.

**Tatar, O., Park, R.G., 1992.** Neotectonic extensional and contractional strains within Pliocene basin deposits near the NW margin of the Niksar pull-apart basin, Turkey (abstr.). In: Int. Workshop: Work in Progress on the Geology of Turkey, 9-10 April, Keele University, 65-66.

**Tatar, O., Kavak, K.Ş., Polat, A., Gürsoy, H., Koçbulut, F., Sezen, T.F., Mesci, B.L., Akpınar, Z., Kiratik, L.O., 2006.** Kuzey Anadolu Fay Zonu - 1942 Erbaa-Niksar depremi yüzey kırığı: yeni gözlemler. Aktif Tektonik Araştırma Grubu 10. Toplantısı, Bildiri Özleri Kitabı, s.85, 2-4 Kasım 2006, İzmir (in Turkish).

**Tatar, O., Gürsoy, H., Altunel, E., Akyüz, S., Topal, T., Sezen, T.F., Koçbulut, F., Mesci, B.L., Kavak, K.Ş., Dikmen, Ü., Türk, T., Poyraz, F., Hastaoğlu, K., Ayazlı, E., Gürsoy, Ö., Polat, A., Akın, M., Demir, G., Zabcı, C., Karabacak, V., Çakır, Z., 2007.** Kuzey Anadolu Fay Zonu Üzerinde Kelkit Vadisi Boyunca Yer Alan Yerleşim Alanlarının Doğal Afet Risk Analizi, CBS Tabanlı Afet Bilgi Sistemi (KABİS) Tasarımı: Proje Tanıtımı ve Ön Bulgular. Aktif Tektonik Araştırma Grubu 11. Çalıştayı, TÜBİTAK-MAM, Gebze Kocaeli, Bildiri Özleri Kitabı, s.14 (in Turkish).

**Tatar, O., Gürsoy, H., Altunel, E., Akyüz, S., Topal, T., Sezen, T.F., Koçbulut, F., Mesci, B.L., Kavak, K.Ş., Dikmen, Ü., Türk, T., Poyraz, F., Hastaoğlu, K., Ayazlı, E., Gürsoy, Ö., Polat, A., Akın, M., Demir, G., Zabcı, C., Karabacak, V., Çakır, Z., 2009.** Kuzey Anadolu Fay Zonu Üzerinde Kelkit Vadisi Boyunca Yer Alan Yerleşim Alanlarının Doğal Afet Risk Analizi ve Afet Bilgi Sisteminin Oluşturulması, DPT Proje no: CUBAP M-359/DPT 2006K-120220 (in Turkish, in progress).

**Taymaz, T., Tan, O., Yolsal, Y., 2001.** Active tectonics of Turkey and surroundings and seismic risk in the Marmara Sea Region. The Proceedings of IWAM04, Mizunami, Japan.

**Taymaz, T., Jackson, J., McKenzie, D., 1991.** Active tectonics of the north and central Aegean Sea. Geophysical Journal International, 106, 433-490.

**Taymaz, T. 1990.** Earthquake Source Parameters in the Eastern Mediterranean Region. PhD Thesis, 244 pp, Darwin College-University of Cambridge, England-U.K.

**Taymaz, T., Eyidoğan, H., Jackson, J., 1992.** Source parameters of large earthquakes in the East Anatolian Fault Zone (Turkey), *Geophysical Journal International*, 106, 537-550.

**TCEGE, 1999.** Manual for zonation on seismic geotechnical hazards. Publication of the Japanese Geotechnical Society, Revised Version. 209 pp.

**Tchalenk, J.S., 1977.** A reconnaissance of the seismicity and tectonics of the northern border of Arabian Plate (Lake Van region), *Rev. géog. Phys. géol. Dynm.* 19, 189-208.

**Temiz, H., 1989.** Niksar (Tokat) güneydoğusunda Kuzey anadolu Fay zonunun jeolojik ve tektonik özellikleri. Yüksek Lisans Tezi, Cumhuriyet Üniversitesi, Sivas (unpublished, in Turkish).

**Tento, A., Franceschina, L., Marcellini, A., 1992.** Expected ground motion evaluation for Italian sites. In: *Proceedings of Tenth World Conference on Earthquake Engineering*, Vol. 1, 489-494.

**Teramo, A., Maugeri, M., Bottari, A., Termini, D., 2005.** On a quick seismic microzonation of wide areas. *Pure and Applied Geophysics*, 162, 671-682.

**Terzaghi, K., Peck, R.B. 1948.** *Soil Mechanics in Engineering Practice*, John Wiley and Sons, New York, The second edition by Ralph B. Peck, 1967, The third edition by Ralph B. Peck and Gholamreza Mesri, 1996.

**Teves-Costa, P., Almeida, I.M., Silva, P.L., 2001.** Microzonation of Lisbon: 1-D Theoretical Approach. *Pure and Applied Geophysics*, 158, 2579-2596.

**Tezcan, S.S., Kaya, E., Bal, İ.E., Özdemir, Z., 2002.** Seismic amplification at Avcılar, Istanbul. *Engineering Structures*, 22, 661-667.

**Theodulidis, N.P., Papazachos, B.C., 1994.** Dependence of strong ground motion on magnitude-distance, site geology and macroseismic intensity for shallow earthquakes in Greece: II horizontal pseudovelocity. *Soil Dynamics and Earthquake Engineering*, 13(5), 317-343.

**Tibi, R., Bock, G., Xia, Y., Baumbach, M., Grosser, H., Milkereit, C., Karakisa, S., Zünbül, S., Kind, R., Zschau, J., 2001.** Rupture processes of the 1999 August 17 Izmit and November 12 Düzce (Turkey) earthquakes. *Geophysical Journal International*, 144(2), F1-F7.

**Tokimatsu, K., Yoshimi, Y., 1983.** Empirical correlation of soil liquefaction based on SPT-N value and fines content. *Soil Mechanics and Foundations*, 23(4), 56-74.

**Tokimatsu, K., Seed, H.B., 1984.** Simplified procedures of the evaluation of settlements in clean sands. Rep. No. UCB/GT-84/16, Univ. of California, Berkeley, California.

**Tokimatsu, K., Seed, H.B., 1987.** Evaluation of settlements in sand due to earthquake shaking. *Journal of Geotechnical Engineering*, ASCE, 113(8), 861-878.

**Tokimatsu, K., Miyadera, Y., Kuwayama, S., 1992.** Determination of shear wave velocity structures from spectral analyses of short-period microtremors. *Proceedings of the 10th World Conference on Earthquake Engineering*, Balkema, Rotterdam, 3, 253-258.



**Tonouchi, K., Sakayama, T., Imai, T., 1983.** S wave velocity in the ground and the damping factor. Bull. Int. Assoc. Eng. Geologists, 26-27, 327-333.

**Topal, T., Doyuran, V., Karahanoglu, N., Toprak, V., Suzen, M.L., Yesilnacar, E., 2003.** Microzonation for earthquake hazards: Yenisehir settlement, Bursa, Turkey, Engineering Geology 70, 93-108.

**Toprak, S., Holzer, T.L., Bennett, M.J., Tinsley, J.C., 1999.** CPT- and SPT based probabilistic assessment of liquefaction. Proc., 7th U.S.-Japan Workshop on Earthquake Resistant Design of Lifeline Facilities and Countermeasures Against Liquefaction, Seattle, Multidisciplinary Center for Earthquake Engineering Research, Buffalo, NY, 69-86.

**Toprak, S., Holzer, T.L., 2003.** Liquefaction potential index: field assessment. Journal of Geotechnical and Geoenvironmental Engineering, ASCE 129(4), 315-322.

**Toprak, V., 1989.** Tectonic and stratigraphic characteristics of the Koyulhisar segment of the North Anatolian fault zone (Sivas-Turkey). Unpubl. Ph.d. thesis, Middle East Technical University, Ankara, 121 pp (unpublished).

**Toprak, V., 1994.** Central Kızılırmak Fault Zone: northern margin of Central Anatolian volcanics, Turkish Journal of Earth Sciences, 3, 29-38.

**Tosun, H., Ulusay, R., 1997.** Engineering geological characterization and evaluation of liquefaction susceptibility of foundation soils at a dam site, southwest Turkey. Environmental and Engineering Geoscience, 3(3), 389-409.

**Towhata, I., 2008.** Geotechnical Earthquake Engineering. Springer-Verlag, 684 pp.

**Trifunac, M.D., Brady, A.G., 1975.** On the correlation of peak acceleration of strong motion with earthquake magnitude, epicentral distance and site conditions. In: Proceedings of the U.S. National Conference on Earthquake Engineering, 43-52.

**Trifunac, M.D. 1976.** Preliminary analysis of the peaks of strong earthquake ground motion - dependence of peaks on earthquake magnitude, epicentral distance, and recording site conditions. Bulletin of the Seismological Society of America, 66(1), 189-219.

**Trifunac, M.D., Brady, A.G. 1976.** Correlations of peak acceleration, velocity and displacement with earthquake magnitude, distance and site conditions. Earthquake Engineering and Structural Dynamics, 4(5), 455-471.

**Trifunac, D., Todorovska, M.I., 2000.** Long period microtremors, microseisms and earthquake damage: Northridge, CA, earthquake of 17 January 1994. Soil Dynamics and Earthquake Engineering, 19(4), 253-267.

**Tuladhar, R., Yamazaki, F., Warnitchai, P., Saita, J., 2004.** Seismic microzonation of the greater Bangkok area using microtremor observations. Earthquake Engineering and Structural Dynamics, 33, 211-225.

**Turkish Earthquake Code (TEC), 1998.** Specification for Structures to be Built in Disaster Areas, Part-III: Earthquake Disaster Prevention, Government of Republic of Turkey, Ministry of Public Works and Settlement, Ankara, 84 pp.

**Turkish State Meteorological Service, 2006.** İstatistik ve Yayın Şube Müdürlüğü, Ankara (in Turkish).

**Tutkun, S. Z., Inan, S., 1982.** Niksar-Erbaa (Tokat) yöresinin jeolojisi. Karadeniz Teknik Üniversitesi Yerbilimleri Dergisi, C. 2, 1-2, 51-58 (in Turkish).

**Ulaş, K., Kılıç, R., 2008.** Liquefaction potential of Quaternary alluvium in Bolu settlement area, Turkey, Environmental Geology, 55, 1029-1038.

**Ulusay, R., Kuru, T., 2004.** 1998 Adana-Ceyhan (Turkey) earthquake and a preliminary microzonation based on liquefaction potential for Ceyhan town. Natural Hazards, 32, 59-88.

**Ulusay, R., Tuncay, E., Sonmez, H., Gokceoglu, C., 2004.** An attenuation relationship based on Turkish strong motion data and iso-acceleration map of Turkey. Engineering Geology, 74, 265-291.

**Umutlu, N., Koketsu, K., Milkereit, C., 2004.** The rupture process during the 1999 Düzce, Turkey, earthquake from joint inversion of teleseismic and strong-motion data. Tectonophysics 391, 315-324.

**U.S. Army Corps of Engineers, 1999.** Engineer Manual, EM1110-2-6050, Engineering and Design: Response Spectra and Seismic Analysis for Concrete Hydraulic Structures, 30 June 1999, Washington, DC 20314-1000, 248 pp.

**USGS, 2007.** [http://neic.usgs.gov/neis/eq\\_depot/1999/eq\\_990817/T990817000138.html](http://neic.usgs.gov/neis/eq_depot/1999/eq_990817/T990817000138.html), 23.07.2007.

**USGS, 2008.** [www.usgs.gov](http://www.usgs.gov), 04.09.2008.

**Utkucu, M., Nalbant, S.S., McCloskey, J., Steacy, S., Alptekin, Ö., 2003.** Slip distribution and stress changes associated with the 1999 November 12, Düzce (Turkey) earthquake (Mw=7.1). Geophysical Journal International, 153(1), 229-241.

**Van Rooy, J.L., Stiff, J.S., 2001.** Guidelines for urban engineering geological investigations in South Africa. Bulletin of Engineering and Geological Environment, 59, 285-295.

**Veneziano, D., Cornell, C.A., O'Hara, T., 1984.** Historic method for seismic hazard analysis, Elect. Power Res. Inst., Report, NP-3438, Palo Alto.

**Vucetic, M., Dobry, R., 1989.** Degradation of marine clays under cyclic loading. Journal of Geotechnical Engineering, ASCE, 114(2), 133-149.

**Vucetic, M., Dobry, R., 1991.** Effect of soil plasticity on cyclic response. Journal of Geotechnical Engineering, ASCE, 117: 87-107.

**Walling, M.Y., Mohanty, W.K., 2009.** An overview on the seismic zonation and microzonation studies in India, Earth Science Reviews, 96(1-2), 67-91.

**Waltham, A.C., 1994.** Foundations of Engineering Geology, Blackie Academic Professional, 88 pp.

**Wang, W. S., 1979.** Some findings in soil liquefaction. Water Conservancy and Hydroelectric Power Scientific Research Institute, Beijing, China.

**Wang, J.G.Z.Q., Law, K.T., 1994.** Siting in Earthquake Zones. A.A.Balkema, Rotterdam, The Netherlands, 114 pp.

**Wang, G., Tao, X., 2000.** A new two-stage procedure for fitting attenuation relationship of strong ground motion. In: Proceedings of the Sixth International conference on Seismic zonation.

**Ward, S.N., 1994.** A multidisciplinary approach to seismic hazard in Southern California . Bulletin of the Seismological Society of America, 84, 1293-1309.

**Warnitchai, P., Sangarayakul, C., Ashford, S.A., 2000.** Seismic hazard in Bangkok due to long-distance earthquakes. Proceedings of the 12th World Conference on Earthquake Engineering, Auckland, New Zealand, Paper no. 2145.

**Weiler, W.A., 1988.** Small strain shear modulus of clay. Proceedings, ASCE Conference on Earthquake Engineering and Soil Dynamics II: Recent Advances in Ground Motion Evaluation, Geotechnical Special Publication 20, ASCE, New York, 331-335.

**Wells, D.L., Coppersmith, K.J., 1994.** New empirical relationships among magnitude, rupture length, rupture width, rupture area, and surface displacement. Bulletin of the Seismological Society of America, 84, 974-1002.

**Westaway R., 1998.** Dependence of active normal fault dips on lower-crustal flow regimes, Journal of Geological Society of London, 155, 233-253.

**Wills, C.J., Silva, W., 1998.** Shear wave velocity characteristics of geologic units in California. Earthquake Spectra, 14(3), 533-556.

**Wills, C.J., Petersen, M., Bryant, W.A., Reichle, M., Saucedo, G.J., Tan, S., Taylor, G., Treiman, J., 2000.** A site conditions map for California based on geology and shear wave velocity. Bulletin of the Seismological Society of America, 90, 187-208.

**Wright, T., Fielding, E., Parsons, B., 2001.** Triggered slip; observations of the 17 August 1999 Izmit (Turkey) earthquake using radar interferometry. Geophysical Research Letters, 28(6), 1079-1082.

**Wu, J., Seed, R.B., 2004.** Estimating of liquefaction-induced ground settlement: case studies. Proc. 5th Int. Conf. on Case Histories in Geotechnical Engineering, New York, Paper No. 3.09.

**Yağcı, B., 2005.** Mikrobölgeleme metodolojileri ve Balıkesir için bir uygulama. Ph.D. thesis. Balıkesir University, Graduate School of Applied Sciences, 194 p. (in Turkish).

**Yalcin, A., Gokceoglu, C., Sonmez, H., 2008.** Liquefaction severity map for Aksaray city center (Central Anatolia, Turkey). Natural Hazards and Earth System Sciences, 8, 641-649.

**Yamabe, K., Kanai, K., 1988.** An empirical formula on the attenuation of the maximum acceleration of earthquake motions. In: Proceedings of Ninth World Conference on Earthquake Engineering, Vol. II, 337-342.

**Yamanaka, H., Takemura, M., Ishida, H., Niwa, M., 1994.** Characteristics of long-period microtremors and their applicability in exploration of deep sedimentary layers. Bulletin of the Seismological Society of America, 84, 1831-1841.

**Yılmaz, I., 1998.** Köklüce regülatörü-Erbaa HES iletim hattı güzergahındaki alüvyal zeminlerin şişme ve oturma sorunlarının jeomühendislik değerlendirmesi: Unpubl. Ph.d. thesis, Cumhuriyet University, Sivas, 102 pp. (in Turkish).

**Yılmaz, I., Karacan, E., 2002.** Geotechnical properties of clayey alluvial soils in the Erbaa basin, Turkey. *International Geology Review*, 44, 179-190.

**Yilmaz, Z., Cetin, K.O., 2004.** GIS-based seismic soil liquefaction assessment for Sakarya city after 1999 Kocaeli-Turkey earthquake. *Proceedings of the 11th International Conference on Soil Dynamics and Earthquake Engineering*, U.C. Berkeley, CA, USA, 1, 909-917.

**Youd, T.L., 1972.** Compaction of sands by repeated shear straining. *Journal of Soil Mechanics and Foundation Div.*, 98(7), 709-725.

**Youd, T.L., Perkins, D.M., 1987.** Mapping of liquefaction severity index. *Journal of Geotechnical Engineering*, ASCE, 113(11), 1374-1392.

**Youd, T.L., Garriss, C.T., 1995.** Liquefaction-induced ground surface disruption. *Journal of Geotechnical Engineering*, ASCE 121(11), 805-809.

**Youd, T.L., Noble, S.K., 1997.** Liquefaction criteria based on statistical and probabilistic analyses. *Proc. NCEER Workshop on Evaluation of Liquefaction Resistance of Soils*, National Center for Earthquake Engineering Research, Buffalo.

**Youd T.L., Idriss, I.M., Andrus, R.D., Arango, I., Castro, G., Christian, J.T., Dobry, R., Finn, W.D.L., Harder, J.L.F., Hynes, M.E., Ishihara, K., Koester, J.P., Liao, S.S.C., Marcuson, W.F., Martin, G.R., Mitchell, J.K., Moriwaki, Y., Power, M.S., Robertson, P.K., Seed, R.B., Stokoe, K.H., 2001.** Liquefaction resistance of soils: Summary Report from the 1996 NCEER and 1998 NCEER/NSF Workshops on Evaluation of Liquefaction Resistance of Soils. *Journal of Geotechnical and Geoenvironmental Engineering*, ASCE, 127(10), 817-833.

**Youd, T.L., Hansen, C.M., Bartlett, S.F., 2002.** Revised multilinear regression equations for prediction of lateral spread displacement. *Journal of Geotechnical and Geoenvironmental Engineering*, ASCE, 128(12), 1007-1017.

**Youd, T.L., DeDen, D.W., Bray, J.D., Sancio, R., Cetin, K.O., Gerber, T.M., 2009.** Zero-displacement lateral spreads, 1999 Kocaeli, Turkey, Earthquake. *Journal of Geotechnical and Geoenvironmental Engineering*, 135(1), 46-61.

**Yürüdü, E., 1991.** Erbaa ve Niksar ovalarının fiziki coğrafya özellikleri. M.Sc. thesis. Selçuk University, Graduate School of Social Sciences, Konya, Turkey, 98 pp. (in Turkish).

**Zadeh, L.A., 1965.** Fuzzy sets. *Information and content*, 8(3), 338-353.

**Zhang, G., Robertson, P.K., Brachman, R.W.I., 2004.** Estimating liquefaction-induced lateral displacements using the standard penetration test or cone penetration test. *Journal of Geotechnical and Geoenvironmental Engineering*, ASCE, 130(8), 861-871.

## CURRICULUM VITAE

### PERSONAL INFORMATION

Surname, Name : AKIN, Müge  
Nationality : Turkish (TC)  
Date and Place of Birth : 23 September 1975, Ankara  
Marital Status : Married  
Phone : +90 312 210 26 89  
Fax : +90 312 210 57 50  
Email : [makin@metu.edu.tr](mailto:makin@metu.edu.tr)  
[mugeakink@gmail.com](mailto:mugeakink@gmail.com)

### EDUCATION

Degree	Institution	Year of Graduation
M.Sc.	Ankara University, Geological Engineering	2001
B.Sc.	Ankara University, Geological Engineering	1997
High School	Gaziosmanpasa Anatolian Technical High School (Computer)	1993

### WORK EXPERIENCE

Year	Place	Enrollment
2003-Present	METU, Dept. of Geological Eng.	Research Assistant
2003 (10 months)	Yüzüncü Yıl University	Research Assistant
2001-2002	Gen. Dir. of Mineral Res.& Exploration	Geological Engineer
2000 (5 months)	Jeotasarım 2000 Geotech. Comp.	Geological Engineer
1998-2000	Islem GIS Company	Geological Engineer
1997-1998	Spektra Jeotek A.Ş. Geotech. Company	Geological Engineer

### FOREIGN LANGUAGES

English (advanced level)

### PUBLICATIONS

#### *Journal Papers*

1. Kayabalı, K., **Akin, M.**, 2003. Seismic hazard map of Turkey using the deterministic approach. Engineering Geology, 69(1), 127-137.

2. Topal, T., **Akin, M.**, Ozden, U., 2007. Assessment of rockfall hazard around Afyon Castle, Turkey. *Environmental Geology*, 53(1), 191-200.
3. Topal, T., **Akin, M.**, 2009. Geotechnical assessment of a landslide along a natural gas pipeline for possible remediations (Karacabey-Turkey). *Environmental Geology*, 57, 611–620.
4. Topal, T., **Akin, M.**, 2009. Measures to establish a safe route for new and existing gas pipelines between Turkey and Greece. *Exploration and production-Oil and Gas Review*, 7(1), 102-104.
5. Akin, M., Özsan, A., **Akin, M.**, 2009. Investigation of the macro pore geometry of yellow travertines using the shape parameter approach. *Environmental & Engineering Geoscience*, 15(3), 197-209.

### ***Conference Papers***

1. **Akin, M.**, Kayabalı, K., 2001. Seismic hazard map of Turkey. Active Tectonic Research Group, 5th Meeting, 15-16 November 2001, Ankara, Turkey.
2. Topal, T., **Akin, M.**, Ozden, U., 2005. Possible rockfall problems around Afyonkarahisar Castle. 40th Anniversary Geology Symposium, 27-30 September 2005, Trabzon, Turkey.
3. Akin, M., **Akin, M.**, Özsan A., 2005. Slope stability analysis in rock slopes by using probabilistic approach: A case study. 58th Geological Congress of Turkey, 11-17 April 2005, Ankara, Turkey.
4. **Akin, M.**, Topal, T, Ozden, U., 2006. Kinetic energies of rockfalls. 59th Geological Congress of Turkey, 20-24 March 2006, Ankara, Turkey.
5. Topal, T, **Akin, M.**, Ozden, U., 2006. Evaluation of Afyonkarahisar rockfall problems. Symposium on Recent Application in Engineering Geology, 25-27 May 2006, Denizli, Turkey.
6. Tatar, O., Gürsoy, H., Altunel, E., Akyüz, S., Topal, T.,..., **Akin, M.**, Demir, G., ...., 2006. North Anatolian Fault Zone – settlement areas and database management of hazards. Active Tectonic Research Group – 10th Meeting, 2-4 November-2006, İzmir, Turkey.
7. Topal, T, **Akin, M.**, Ozden, U., 2006. Analysis and evaluation of rockfall hazard around Afyon Castle, Turkey. IAEG 2006-Engineering Geology for Tomorrow's Cities, The 10th IAEG Congress, 6-10 September 2006, Nottingham, UK.
8. Tatar, O., Gürsoy, H., Altunel, E., Akyüz, S., Topal, T., Sezen, T.F., Koçbulut, F., Mesci, B.L., Kavak, K.Ş., Dikmen, Ü., Poyraz, F., Hastaoğlu, K., Türk, T., Ayazlı, E., Gürsoy, Ö., Polat, A., **Akin, M.**, Demir, G., Zabcı, C., Karabacak, V., Çakır, Z., 2007. Kuzey Anadolu Fay Zonu Üzerinde Kelkit Vadisi Boyunca Yer Alan Yerleşim Alanlarının CBS Tabanlı Afet Bilgi Sistemi (KABİS) Tasarımı ve Ön Bulgular.

Çukurova Üniversitesi, Jeoloji Mühendisliği Bölümü 30. Yıl Sempozyumu, 25-27 Ekim 2007, Adana, Bildiri Özleri Kitabı.

9. Tatar, O., Türk, T., Gürsoy, H., Hastaoğlu, K., Ayazlı, E., Poyraz, F., Gürsoy, Ö., Zabcı, C., Demir, G., Dikmen, Ü., **Akin, M.**, Mesci, B.L., Koçbulut, F., Kavak, K.Ş., T., Sezen, T.F., Polat, A., 2007. Kelkit Vadisi Afet Bilgi Sistemi (KABİS) Altyapısının Oluşturulması. TMMOB Harita ve Kadastro Mühendisleri Odası Ulusal Coğrafi Bilgi Sistemleri Kongresi, 30 Ekim–02 Kasım 2007, KTÜ, Trabzon. Bildiri Özleri Kitabı.
10. Tatar, O., Gürsoy, H., Altunel, E., Akyüz, S., Topal, T., Sezen, T.F., Koçbulut, F., Mesci, B.L., Kavak, K.Ş., Dikmen, Ü., Türk, T., Poyraz, F., Hastaoğlu, K., Ayazlı, E., Gürsoy, Ö., Polat, A., **Akin, M.**, Demir, G., Zabcı, C., Karabacak, V., Çakır, Z., 2007. Kuzey Anadolu Fay Zonu Üzerinde Kelkit Vadisi Boyunca Yer Alan Yerleşim Alanlarının Doğal Afet Risk Analizi, CBS Tabanlı Afet Bilgi Sistemi (KABİS) Tasarımı: Proje Tanıtımı ve Ön Bulgular. Aktif Tektonik Araştırma Grubu 11. Çalıştay, TÜBİTAK-MAM, Gebze Kocaeli, Bildiri Özleri Kitabı, s.14.
11. Topal, T., **Akin, M.**, 2008. Investigation of a landslide along a natural gas pipeline (Karacabey-Turkey). 10th Symp on Landslides and Engineered Slopes, 30 June-4 July 2008, Xian, China.
12. **Akin, M.**, Topal, T., 2008. Assessment of SPT-based liquefaction of Erbaa (Tokat), Turkey. 6th Int. Conference on Case Histories in Geotechnical Engineering, 12-16 August 2008, Arlington-VA, USA.
13. **Akin, M.**, Topal, T., 2008. Estimation of liquefaction effects of Erbaa (Turkey) by using liquefaction potential index. EUROENGEO, 15-20 September 2008, Madrid, Spain.
14. Topal, T., **Akin, M.**, Akin, M., 2009. Investigation of rockfall problems around Kastamonu Castle. In: The Proceedings of the 3rd International Conference on New Development in Rock Mechanics and Engineering & Sanya forum for the plan of city and city construction. 24-26 May 2009, Sanya, China, 295-300.
15. Topal, T., **Akin, M.**, Akin, M., 2009. Rockfall potential of Kastamonu Castle. In: Vrkljan, I. (ed.), EUROCK 2009, ISRM Regional Symposium, Rock Engineering in Difficult Ground Conditions, Soft Rocks and Karst. 29-31 October 2009, Dubrovnik, Cavtat, Croatia, 745-748.
16. **Akin, M.**, Kramer, S.L., Topal, T., 2009. Evaluation of shear wave velocity in a seismically active area (Erbaa, Turkey). 5<sup>th</sup> International Conference on Recent Advances in Geotechnical Earthquake Engineering and Soil Dynamics, 24-29 May 2010, San Diego-CA, USA (in press).

## HOBBIES

Swimming, Literature, Traveling, Photography, Geo-tourism